GENETICS AND MECHANISM OF CILIOPATHIES

EDITED BY: Steven L. C. Pei and Brian Hon-Yin Chung

PUBLISHED IN: Frontiers in Genetics

frontiers Research Topics

frontiers

ISSN 1664-8714
ISBN 978-2-83250-755-1
DOI 10.3389/978-2-83250-755-1

About Frontiers

Frontiers is more than just an open-access publisher of scholarly articles: it is a pioneering approach to the world of academia, radically improving the way scholarly research is managed. The grand vision of Frontiers is a world where all people have an equal opportunity to seek, share and generate knowledge. Frontiers provides immediate and permanent online open access to all its publications, but this alone is not enough to realize our grand goals.

Frontiers Journal Series

The Frontiers Journal Series is a multi-tier and interdisciplinary set of open-access, online journals, promising a paradigm shift from the current review, selection and dissemination processes in academic publishing. All Frontiers journals are driven by researchers for researchers; therefore, they constitute a service to the scholarly community. At the same time, the Frontiers Journal Series operates on a revolutionary invention, the tiered publishing system, initially addressing specific communities of scholars, and gradually climbing up to broader public understanding, thus serving the interests of the lay society, too.

Dedication to Quality

Each Frontiers article is a landmark of the highest quality, thanks to genuinely collaborative interactions between authors and review editors, who include some of the world's best academicians. Research must be certified by peers before entering a stream of knowledge that may eventually reach the public - and shape society; therefore, Frontiers only applies the most rigorous and unbiased reviews.
Frontiers revolutionizes research publishing by freely delivering the most outstanding research, evaluated with no bias from both the academic and social point of view. By applying the most advanced information technologies, Frontiers is catapulting scholarly publishing into a new generation.

What are Frontiers Research Topics?

Frontiers Research Topics are very popular trademarks of the Frontiers Journals Series: they are collections of at least ten articles, all centered on a particular subject. With their unique mix of varied contributions from Original Research to Review Articles, Frontiers Research Topics unify the most influential researchers, the latest key findings and historical advances in a hot research area! Find out more on how to host your own Frontiers Research Topic or contribute to one as an author by contacting the Frontiers Editorial Office: frontiersin.org/about/contact

GENETICS AND MECHANISM OF CILIOPATHIES

Topic Editors:
Steven L. C. Pei, Yale University, United States
Brian Hon-Yin Chung, The University of Hong Kong, Hong Kong, SAR China

Citation: Pei, S. L. C., Chung, B. H.-Y., eds. (2022). Genetics and Mechanism of Ciliopathies. Lausanne: Frontiers Media SA. doi: 10.3389/978-2-83250-755-1

Table of Contents

frontiers | Frontiers in Genetics

TYPE Editorial
PUBLISHED 28 October 2022
DOI 10.3389/fgene.2022.1067168

OPEN ACCESS

EDITED AND REVIEWED BY
Maxim B. Freidin,
Queen Mary University of London,
United Kingdom

*CORRESPONDENCE
Steven Lim Cho Pei,
stevenpei@gmail.com
Brian Hon Yin Chung,
bhychung@hku.hk

SPECIALTY SECTION
This article was submitted to Human and Medical Genomics, a section of the journal Frontiers in Genetics

RECEIVED 11 October 2022
ACCEPTED 14 October 2022
PUBLISHED 28 October 2022

CITATION
Pei SLC and Chung BHY (2022), Editorial: Genetics and mechanism of ciliopathies.
Front. Genet. 13:1067168.
doi: 10.3389/fgene.2022.1067168

Editorial: Genetics and mechanism of ciliopathies

Steven Lim Cho Pei[1]* and Brian Hon Yin Chung[2,3]*

[1]Department of Internal Medicine, School of Medicine, Yale University, New Haven, CT, United States, [2]Department of Paediatrics and Adolescent Medicine, School of Clinical Medicine, Li Ka Shing Faculty of Medicine, The University of Hong Kong, Hong Kong, China, [3]Hong Kong Genome Institute, Hong Kong, China

KEYWORDS

cilia, ciliopathies, primary ciliary dyskinesia, exome sequencing, single nucleotide polymorphisms, dynein

Editorial on the Research Topic
Genetics and mechanism of ciliopathies

Cilium is a microtubule-based hair-like organelle found on almost every type of cells in human body. These cilia can be motile (as in the cilia on respiratory tract epithelial cells) or non-motile (as in the cilia in nephrons of kidneys and photoreceptors on the retina of eyes). Meanwhile, single cilium (e.g., nephrons) or multiple copies of the cilia (e.g., epithelial cells in respiratory tract) are possible and observed in human cells. Despite of their highly complex structure, ciliary structure is conserved in vertebrate and consist of over 600 proteins (Fliegauf et al., 2007) orchestrating in a coordinated manner for its proper functions in development, signaling, homeostasis and sensory functions. Despite of its complicated structure, various signaling pathways were found to be involved in cilia formation, assembly and growth. For instance, hedgehog signaling (Huangfu et al., 2003), Wnt signaling (Clevers and Nusse, 2012), G-protein-coupled receptor signaling (Mykytyn and Askwith, 2017) etc. Were the well-known pathways involved in ciliopathies (Waters and Beales, 2011; Reiter and Leroux, 2017).

Since cilia are almost ubiquitously presence in all cell types in human body, it is not surprising that ciliopathies, which refers to any disorders that affects the ciliary function, cilia itself or its sub-structures, exhibit a large spectrum of anomalies in multiple organs and systems, for instance, brain, kidneys, liver, bone and eyes etc. Because of the complexity of proteins and signaling pathways involved in ciliopathies, the exact molecular mechanism is yet to be elucidated but it is certain that genetic variation like single nucleotide polymorphisms (SNPs), missense or nonsense mutations on cilia and/or related genes etc. played a major role in the pathogenesis. Thanks to the technology advancement in biotechnology and genetics on genome-editing, as well as the prevalence and readily available of next generation sequencing technique on exome and genome, the manuscripts included in this Research Topic can facilitate researchers to have a deeper understanding on the genetic variations in ciliopathies and provide ways for further verification of these changes with genome-editing and thus, test on the signaling pathways and molecular mechanism.

This Research Topic is dedicated to including works that explore any novel identification or characterization of genes, signaling pathways, transcriptomic analyses, and mechanisms on ciliary gene(s) and/or protein(s) involved in ciliopathies. Moreover, recent advancement in diagnosis of ciliary and/or cilia-related diseases, integrative analysis of publicly available data on ciliary genes and/or proteins, articles that summarize the existing data on ciliary pathologies were also included. A total of 13 manuscripts were included in this Research Topic.

Among these works, a number of novel studies revealing the causes and potential mechanisms of ciliopathies has been included. For instance, four reports described the novel variants identifications contributing to various manifestation of ciliopathies, such as nephronophthisis and kidney failure (by novel deletion of *Glis2*:c.560_574delACCATGTCAACGATT, p. H188_Y192del)) (Al Alawi et al.), asthenoteratozoospermia (by missense variant RSPH4A:c.2T>C, p. (Met1Thr) and nonsense variant *RSPH4A*:c.1774_1775del, p. (Leu592Aspfs*5) (Wang et al.), dynein axonemal assembly factor (DNAAF) -4 [by *DNAAF4*:c.733C>T, p.(Arg245*)] (Guo et al.), Meckel Gruber Syndrome (by splice site variant *RPGRIP1L*:c.776 + 1G > A/IVS6 + 1G > A) (Moreno-Leon et al.). These novel findings expanded the variants spectrum related to ciliopathies and provide some reference for others subjects who share the same variants in future.

While there are another three reports on variants that affect the renal and hepatic fibrocystic disease (by missense variant *TULP3*: c.1144C>T, p. (Arg382Trp)) (Jafari Khamirani et al.), showing skeletal ciliopathies (by missense variant *IFT140* (NM_014,714.4) r.2765_2768del; p. (Tyr923Leufs*28)) (Walczak-Sztulpa et al.) and primary ciliary dyskinesia (PCD) in respiratory cilia [by missense variant *DNAI2*:c.740G>A; p. (Arg247Gln)] (Al-Mutairi et al.). All these case reports in this Research Topic, together with other previously published reports in the literatures, enhance our current understanding on the genetics variants contributed to ciliopathies.

Apart from the variant case reports, another three papers illustrated the vital tasks of cilia proteins in cilia assembly and functions were also included. For instance, Lennon et al. focused on the function of *Dnaaf-4* and *Dnaaf-6* in outer dynein arm (ODA) and a subset of inner dynein arm (IDA) assembly using *drosophila* model. While Schultz et al. studied the role of *CFAP300* in dynein complex transport in motile cilia and in dynein arm assembly. Moreover, Nazlamova et al. showed in the CRISPR mutated *PRPF6* and *PRPF31* cell lines, patient-derived retinal organoid cultures and siRNA-treated retinal organotypic cultures that, mutation in the pre-mRNA splicing factor would resulted in defected microtubule and centrosome, ultimately leading to retinal degeneration. These works shed light on the potential mechanisms and signaling pathways for the pathogenesis of ciliopathies.

Furthermore, two articles in this Research Topic have highlighted the importance of genetic testing in the diagnosis of ciliopathies. The work of Chau et al. has demonstrated that genetic testing is essential in the diagnosis of early-onset bronchiectasis. While the project of Antony et al. indicated the significance of genetic diagnosis in a cohort of 37 cases laterality defect with defected left-right patterning. Their efforts have demonstrated that genetic diagnosis is key for the proper diagnosis of ciliopathies and would provide a valuable reference for the clinician.

In addition, it was delighted to have Rusterholz et al. to contribute an insightful review focusing on Joubert Syndrome, which is a rare cilia-related disorder characterized by cerebellar and brain stem malformation with other renal, retinal and skeletal manifestations. Their work has summarized and featured on what have been learnt in understanding Joubert Syndrome from different zebrafish models in the literatures.

In conclusion, despite many unknown and challenges in delineating the exact cause and molecular mechanism of ciliopathies, these studies in this Research Topic have greatly extended our current understanding on the genetic of ciliopathies and shed light on potential signaling pathway down to molecular level. A better understanding of the genetic and molecular mechanism of the disease is crucial for early diagnosis, appropriate treatment and improving the prognosis of patients, thus, this Research Topic would be valuable for further research and beneficial to the patients in future.

Author contributions

All authors listed have made a substantial, direct, and intellectual contribution to the work and approved it for publication.

Acknowledgments

We thank all the authors and reviewers for their effort and contributions to this Research Topic.

Conflict of interest

The authors declare that the research was conducted in the absence of any commercial or financial relationships that could be construed as a potential conflict of interest.

Publisher's note

References

Clevers, H., and Nusse, R. (2012). Wnt/β-catenin signaling and disease. *Cell* 149 (6), 1192–1205. doi:10.1016/j.cell.2012.05.012

Fliegauf, M., Benzing, T., and Omran, H. (2007). When cilia go bad: Cilia defects and ciliopathies. *Nat. Rev. Mol. Cell Biol.* 8 (11), 880–893. doi:10.1038/nrm2278

Huangfu, D., Liu, A., Rakeman, A. S., Murcia, N. S., Niswander, L., and Anderson, K. V. (2003). Hedgehog signalling in the mouse requires intraflagellar transport proteins. *Nature* 426 (6962), 83–87. doi:10.1038/nature02061

Mykytyn, K., and Askwith, C. (2017). G-Protein-Coupled receptor signaling in cilia. *Cold Spring Harb. Perspect. Biol.* 9 (9), a028183. doi:10.1101/cshperspect.a028183

Reiter, J. F., and Leroux, M. R. (2017). Genes and molecular pathways underpinning ciliopathies. *Nat. Rev. Mol. Cell Biol.* 18 (9), 533–547. doi:10.1038/nrm.2017.60

Waters, A. M., and Beales, P. L. (2011). Ciliopathies: An expanding disease spectrum. *Pediatr. Nephrol.* 26 (7), 1039–1056. doi:10.1007/s00467-010-1731-7

frontiers in Genetics

CASE REPORT
published: 30 November 2021
doi: 10.3389/fgene.2021.791495

Case Report: A Novel In-Frame Deletion of *GLIS2* Leading to Nephronophthisis and Early Onset Kidney Failure

Intisar Al Alawi[1,2], *Laura Powell*[1], *Sarah J. Rice*[3], *Mohammed S. Al Riyami*[4], *Marwa Al-Riyami*[5], *Issa Al Salmi*[6,7] *and John A. Sayer*[1,8,9]*

[1]Translational and Clinical Research Institute, Faculty of Medical Sciences, Newcastle University, Newcastle upon Tyne, United Kingdom, [2]National Genetic Center, Ministry of Health, Muscat, Oman, [3]Biosciences Institute, Faculty of Medical Sciences, Newcastle University, Newcastle upon Tyne, United Kingdom, [4]Pediatric Nephrology Unit, Department of Child Health, Royal Hospital, Ministry of Health, Muscat, Oman, [5]Department of Pathology, College of Medicine, Sultan Qaboos University, Muscat, Oman, [6]Renal Medicine Department, Royal Hospital, Ministry of Health, Muscat, Oman, [7]Internal Medicine, Oman Medical Specialty Board, Muscat, Oman, [8]Renal Services, Newcastle Upon Tyne Hospitals NHS Foundation Trust, Newcastle upon Tyne, United Kingdom, [9]Newcastle Biomedical Research Centre, NIHR, Newcastle upon Tyne, United Kingdom

Variants in the *GLIS family zinc finger protein 2* (*GLIS2*) are a rare cause of nephronophthisis-related ciliopathies (NPHP-RC). A reduction in urinary concentration and a progressive chronic tubulointerstitial nephropathy with corticomedullary cysts are the major characteristic features of NPHP. NPHP demonstrates phenotypic and genetic heterogeneity with at least 25 different recessive genes associated with the disease. We report a female, from a consanguineous family, who presented age 9 years with echogenic kidneys with loss of cortico-medullary differentiation and progressive chronic kidney disease reaching kidney failure by 10 years of age. A novel homozygous in-frame deletion (NM_032,575.3: c.560_574delACCATGTCAACGATT, p.H188_Y192del) in *GLIS2* was identified using whole exome sequencing (WES) that segregated from each parent. The five amino acid deletion disrupts the alpha-helix of GLIS2 zinc-finger motif with predicted misfolding of the protein leading to its predicted pathogenicity. This study broadens the variant spectrum of *GLIS2* variants leading to NPHP-RC. WES is a suitable molecular tool for children with kidney failure suggestive of NPHP-RC and should be part of routine diagnostics in kidney failure of unknown cause, especially in consanguineous families.

Keywords: nephronophthisis (NPHP), whole exome sequencing, end stage kidney disease (ESKD), consanguinity, ciliopathies

OPEN ACCESS

Edited by:
Steven L. C. Pei,
Yale University, United States

Reviewed by:
James A. Poulter,
University of Leeds, United Kingdom
Julia Hoefele,
Technical University of Munich, Germany

***Correspondence:**
John A. Sayer
john.sayer@ncl.ac.uk

Specialty section:
This article was submitted to Human and Medical Genomics, a section of the journal Frontiers in Genetics

Received: *08 October 2021*
Accepted: *28 October 2021*
Published: *30 November 2021*

Citation:
Al Alawi I, Powell L, Rice SJ, Al Riyami MS, Al-Riyami M, Al Salmi I and Sayer JA (2021) Case Report: A Novel In-Frame Deletion of GLIS2 *Leading to Nephronophthisis and Early Onset Kidney Failure. Front. Genet. 12:791495. doi: 10.3389/fgene.2021.791495*

INTRODUCTION

Nephronophthisis (NPHP) is an autosomal recessive inherited kidney disease that constitutes the most prevalent monogenic causes of kidney failure in the first 3 decades of life and is responsible for 2.4–15% of pediatric patients with kidney failure (Hildebrandt et al., 2009; Luo and Tao 2018). Urine analysis of NPHP patients generally does not illustrate any characteristic urinary abnormalities, as proteinuria and hematuria are often not found until late stages of chronic kidney disease (CKD) (Luo and Tao 2018). A clue to the underlying diagnosis may be finding a loss of urinary concentration

TABLE 1 | Timeline of patient's journey.

	Presentation	Progression	Progression
Age	9 years old	10 years old	11 years old
CKD stage	CKD stage 4	CKD stage 5	CKD stage 5, commenced hemodialysis
eGFR (ml/min/1.73m^2)	24	15	12
Investigations	Bland urine analysis	Renal biopsy showing NPHP	Molecular genetic studies

CKD, chronic kidney disease; eGFR, estimated glomerular filtration rate (Revised Schwartz equation); NPHP, nephronophthisis.

ability (Simms et al., 2009) and kidney ultrasound scan findings of corticomedullary cysts and a loss of corticomedullary differentiation (Srivastava et al., 2017); however, these findings are non-specific.

Therefore, it is difficult to detect NPHP using simple laboratory testing and often the diagnosis is delayed until the advanced stages of CKD. A kidney biopsy may show features which include tubular atrophy, tubular basement defects, and interstitial fibrosis but often do not lead to a precise diagnosis, especially if the patient is approaching kidney failure (Simms et al., 2009). Extra-renal manifestations occur in 15% of cases of NPHP, consistent with it being a ciliopathy syndrome and may include retinal defects, liver fibrosis, skeletal defects, and brain developmental disorders (Srivastava et al., 2017).

Recent advances in genetic analysis show excessive phenotypic and genetic heterogeneity of this disorder (Chaki et al., 2011; Tang et al., 2020) with at least 25 different genes having been linked (Luo and Tao 2018; McConnachie et al., 2021). However, pathogenic variants in known NPHP genes can explain only up to one-third of cases of clinically diagnosed nephronophthisis, suggesting further genes may underlie this phenotype (König et al., 2017; Luo and Tao 2018). Here, we report a case of NPHP associated with early kidney failure caused by a homozygous in-frame deletion of *GLIS2* diagnosed using WES. Pathogenic variants in *GLIS2* remain very rare with only two families previously reported (Attanasio et al., 2007; Halbritter et al., 2013). This case is unique, as it is the first in-frame deletion within *GLIS2* to be reported in association with NPHP and the predicted loss of a motif within the zinc finger domain suggests strongly its pathogenicity.

Case Description

The proband initially presented at 9 years of age to an orthopedic surgeon following a right hip injury. At this stage she was noted to be hypertensive and had evidence of kidney failure, chronic kidney disease (CKD) stage 4 (**Table 1**). Urine analysis was bland. She was commenced on amlodipine and oral sodium bicarbonate to correct a metabolic acidosis. An ophthalmology assessment revealed no evidence of uveitis or retinitis pigmentosa, and hearing was normal. Parental consanguinity was reported (**Figure 1A**).

Kidney ultrasound scanning showed normal sized but echogenic kidneys with loss of cortico-medullary differentiation. A 24-h urine collection did not show significant proteinuria. To intimately investigate the cause of progressive kidney failure, a kidney biopsy was performed which demonstrated tubular injury, tubulointerstitial nephritis, interstitial fibrosis, and tubular atrophy suggesting NPHP (**Figure 1B**). Immunofluorescence studies were negative. Kidney function deteriorated and she reached ESRD by the age of 10 years. We proceeded to investigate the family, following informed consent for genetic studies.

MATERIALS AND METHODS

Patients

The affected patient, her parents and the eldest of the unaffected siblings were recruited from an Omani cohort of patients within the Royal Hospital, Ministry of Health Hospital, Muscat, Oman with suspected inherited renal ciliopathy syndrome. This study was approved by the North-East Newcastle and North Tyneside 1 Research Ethics Committee (18/NE/350). Whole blood (1.5–2.5 ml in EDTA) samples were collected specifically for this study and used for extraction of genomic DNA. DNA samples from affected and other family members were given a pseudo-anonymized sample number. Written and informed consent was obtained from the parents/guardians of each patient, and any family members (including parents and siblings) involved in this study.

Genetic Studies

Genetic analysis using whole exome sequencing (WES) was carried out after obtaining consent from the family. Whole-exome sequencing was performed in the proband and was outsourced to Novogene Co., Ltd. (China) as previously described (Al Alawi et al., 2021). Exomes were captured by SureSelect Human All Exon V6 Enrichment Kit (Agilent Technologies, CA, United States), and high-throughput sequencing was conducted with an Illumina HiSeq platform (Illumina, San Diego, CA). Analyses of raw data (FASTQ format) were achieved together with sequence reads mapping to the human reference genome hg19 using BWA (Li and Durbin 2009), removal of PCR duplicates using Picard (http://broadinstitute.github.io/picard/), alignment refinement using GATK, and coverage analysis and SNP and INDEL calling using GATK's Haplotype Caller (McKenna et al., 2010). SNP and INDEL VCF files were examined using Qiagen QCI Interpret Translational tool for variants filtration and annotation. The approach of data filtering was as follows: (1) non-synonymous SNPs and frameshift/in-frame INDELs with an alternative allele frequency >0.01 in the NHLBI Exome Sequencing Project, Single Nucleotide Polymorphism database (dbSNP), 1000 Genomes Project (1000G), the Genome Aggregation Database

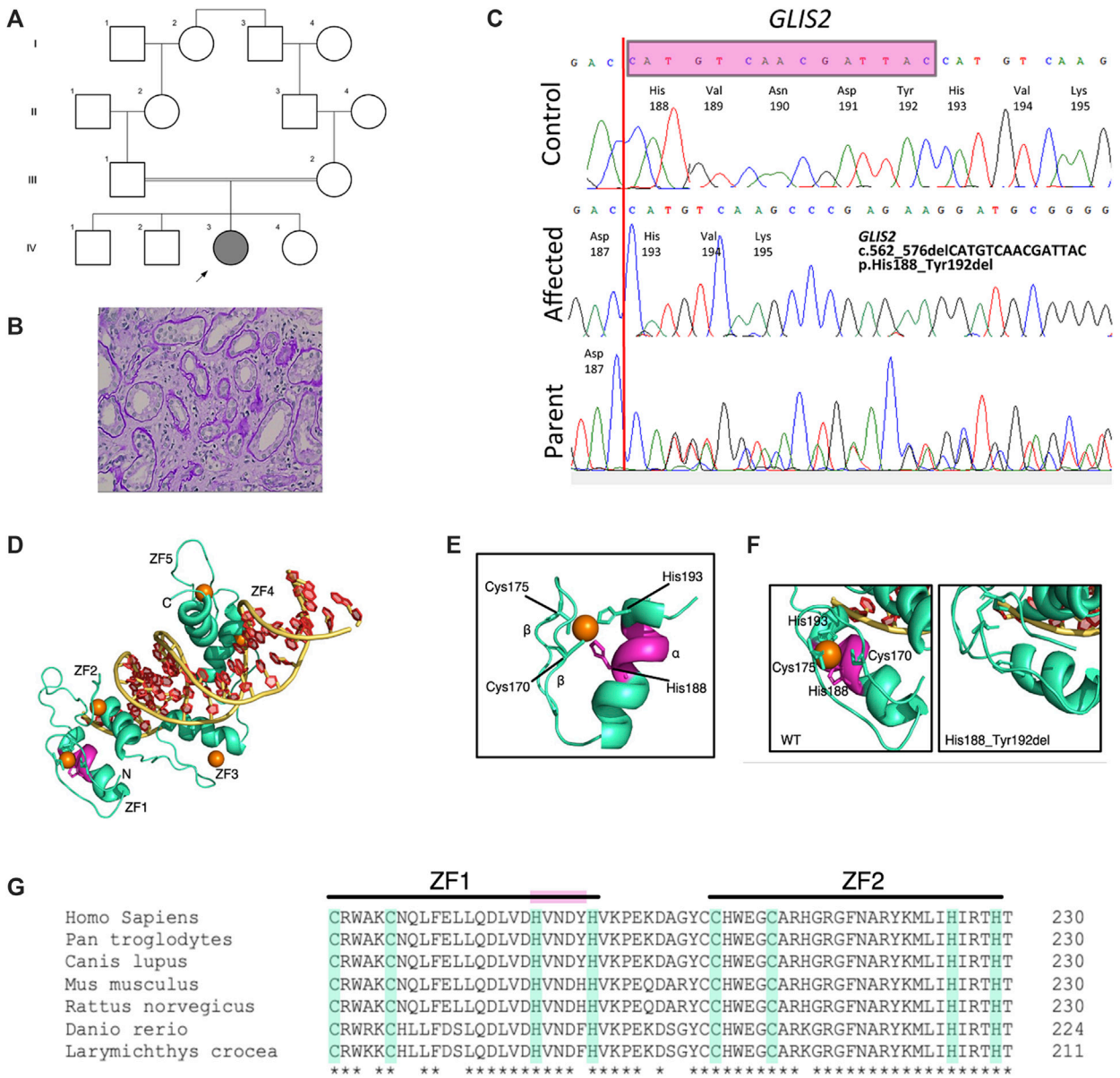

FIGURE 1 | Identification and in silico analysis of novel *GLIS2* variant leading to nephronophthisis. **(A)** Pedigree diagram showing proband (arrowed) and known family consanguinity. **(B)** Kidney biopsy histology from proband showing dilated tubules and thickening and duplication of tubular basement membranes (hematoxylin and eosin, x40). **(C)** Sequence chromatograms demonstrating homozygous in-frame deletion in *GLIS2* (NM 032575, c.562_576delCATGTCAACGATTAC; p.His188_Tyr192del) which was heterozygous in both parents. **(D–G)**. In-frame deletion of *GLIS2* is predicted to destroy the terminal motif sequence within the first zinc finger. **(D)** Protein model of human GLIS2 (green) bound to DNA (yellow and red) using structural homology to human GLI protein (PDB accession 2GLI). The predicted binding positions of Zn ions to each of the five zinc-finger (ZF) domains (labelled ZF1-5) are indicated by orange circles. **(E)** The predicted structure of GLIS2 ZF1 showing the classical ββα fold. The C_2H_2 residues Cys170, Cys175, His188, and His193 are labelled, and side chains are displayed. The five amino acid residues deleted in the His188_Tyr192 deletion are highlighted in magenta. **(F)** Zoomed in images from **(D)** of ZF1, showing the predicted wild-type structure **(left)** and predicted structure in the mutated protein **(right)**. Left, the C_2H_2 residues are labelled and side chains creating the zinc binding pocket are shown. The region deleted in the mutated protein is highlighted in magenta. Right, His193 replaces His188 in the zinc binding pocket, however, the classical ZF motif is lost in the His199_Tyr192del variant. **(G)** Multiple sequence alignment of GLIS2. The C_2H_2 motifs of ZF1 and ZF2 are highlighted in green. The deleted sequence in the mutated protein is highlighted in magenta. *, completely conserved residue.

(gnomAD) were excluded; (2) filtered SNVs and INDELs, predicted by in-silico algorithms to be damaging, were maintained; (3) variants classified as pathogenic and likely pathogenic according to American College of Medical Genetics (ACMG) guidelines remained (Richards, Aziz et al., 2015); and (4) co-segregation analysis was performed in the family using Sanger sequencing. Genetic variants were submitted to ClinVar (www.ncbi.nlm.nih.gov/clinvar).

RESULTS

Whole exome sequencing of the proband's genomic DNA was performed with 96.4% of the exome being covered at least 20-fold. Variants were filtered and analyzed as described, followed by Sanger sequencing validation. Within a large region of homozygosity on chromosome 16, a homozygous novel in-frame deletion variant (NM_032,575.3:c.560_574delACCATGTCAACGATT, p.H188_Y192del) in *GLIS2* was identified in the patient and was present in its heterozygous form in both parents but absent in the eldest unaffected sibling from whom DNA was available (**Figure 1C**). We did not find any other potential pathogenic variants associated with a ciliopathy-related phenotype. Variants in *GLIS2* have been previously identified in patients with NPHP (OMIM: 611498) who developed kidney failure in early childhood (Attanasio et al., 2007). This novel deletion variant that leads to a shortened protein missing 5 amino acids (H188, V189, N190, D191, Y192) located in exon 4 of the *GLIS2* gene was absent in the public database including 1000G and genomAD. Bioinformatics programs including PROVEAN (deleterious), SIFT (deleterious), and MutPredIndel (score: 0.45615) predicted that this variant (NM_032,575.3:c.560_574delACCATGTCAACGATT, p.H188_Y192del) is deleterious and located at evolutionarily conserved site of the GLIS2 protein close to the zinc-finger C2H2-type DNA-binding domain (**Figure 1D**). According to ACMG guidelines (Richards et al., 2015), this allele is classified as a variant of uncertain significance (VUS). The variant has been submitted to ClinVar (https://www.ncbi.nlm.nih.gov/clinvar/variation/1299703/).

Gli-similar 2 (GLIS2) is a member of the Krüppel-like family of transcription factors consisting of five contiguous zinc-finger motifs (**Figure 1D**) (Zhang et al., 2002). Classical zinc-finger domains (C_2H_2) are among the most common eukaryotic protein domains and often have the consensus sequence Cys-X_{2-4}-Cys-X_{12}-His-X_{2-6}-His (where X is any amino acid) (Pavletich and Pabo 1993). Metalloproteins, such as GLIS2 have been shown to co-assemble with Zn^{2+} ions during protein folding into the ββα zinc finger domains (**Figure 1E**). The His188_Tyr192 variant identified in this study removes 5 amino acids from the α helix of GLIS2 ZF1 (**Figure 1D**, magenta), removing the terminal sequence of the zinc-finger motif, even though His193 replaces His188 as H_1 (**Figures 1E–G**). The loss of this motif through an in-frame deletion could potentially result in misfolding of GLIS2. However, there is evidence to show that the individual zinc-finger domains fold independently of the bulk protein structure (Cox and McLendon 2000), and therefore an observed loss of function could be due to altered DNA-binding capacity of the *GLIS2* mutant. Downstream functional analyses are required to determine the loss-of-function mechanism.

DISCUSSION

Making a clinical diagnosis of NPHP is difficult given its non-specific features and therefore many patients with NPHP may be misdiagnosed with another nephropathy or diagnosed as CKD of unknown etiology (Srivastava and Sayer 2014; Snoek et al., 2018). Although clinical findings, kidney ultrasound examination, and kidney biopsy histology in our patient were suggestive of NPHP, a definitive diagnosis was only made following molecular genetic testing. In fact, as many causes of kidney failure may mimic the NPHP phenotype, molecular genetic testing is critical to distinguish NPHP from other inherited forms of kidney diseases.

NPHP is a rare disorder (Levy and Feingold 2000; Hildebrandt 2010) that illustrates genetic heterogeneity with at least 25 different recessive genes having been linked with the disease (Luo and Tao 2018). Almost all NPHP genes encode nephrocystins that localize to primary cilia, except for NPHP-like genes such as *XPNPEP3* and *SLC41A1* and *GLIS2* genes, with protein products located to mitochondria and nucleus, respectively (O'Toole et al., 2010; Srivastava and Sayer 2014; Luo and Tao 2018). Pathogenic variants in these genes can explain only up to one-third of cases and around 60% of cases remain genetically unsolved, suggesting additional genetic causes that have yet to be revealed (König et al., 2017; Luo and Tao 2018). The most common genetic cause of NPHP is variants in *NPHP1*, associated with 20% of cases (Hildebrandt et al., 2009), while variants in each of the remaining genes possibly contribute up to 1% of cases (Srivastava and Sayer 2014; Luo and Tao 2018).

The human *GLIS2*, encoding a member of the Kruppel-like zinc-finger protein family named GLIS family zinc-finger two or alternatively nephrocystin-7, is located on chromosome 16p13.3, and it contains 6 exons spanning ~3.7 kilobases. GLIS2 is located in the nucleus and cytoplasm and is mainly expressed in the kidney and weakly in the heart, lung, placenta, and colon (Zhang et al., 2002). Based on the cell context, GLIS2 can function as activator or repressor of gene transcription. For instance, it works as a repressor of the Hedgehog (Hh) signaling pathway by repressing Hh-dependent expression of Wnt4 as well as repressing transcriptional activation mediated by CTNNB1 in the Wnt signaling pathway. In addition, GLIS2 is required to retain the differentiated epithelial phenotype in kidney cells and in neuron differentiation (Zhang et al., 2002).

In 2007, a homozygous splice-site variant in *GLIS2* (c.755+1G > T) was identified in three affected Canadian Oji-Cree children with an autosomal recessive pattern of NPHP (Attanasio et al., 2007). Later, in 2013, a homozygous missense *GLIS2* variant (c.523T > C, p.C175R) was identified in a Turkish patient with isolated NPHP who reached kidney failure aged 15 years, as part of a worldwide cohort screen of patients with NPHP-RC (Halbritter et al., 2013). Variants in *GLIS2* have been classified

as NPHP7 (OMIM 611498) and within the variation database of ClinVar, there are 34 pathogenic variants, of which 31 are copy number variants (CNVs) while three are SNVs (two missense and one splicing) and there are 92 variants of uncertain significance (VUS). Here, we identified in *GLIS2* an in-frame deletion variant (NM_032,575.3: c.560_574delACCATGTCAACGATT, p.H188_Y192del) in Omani family with NPHP and early onset kidney failure. As far as we know, this variant is novel and expands the variant spectrum of *GLIS2* variants associated with NPHP.

The deletion affects the zinc-finger C2H2-type DNA-binding domain of GLIS2, which plays a role in the recognizing and binding to target DNA as well as mRNA and protein targets (Brayer and Segal 2008). This deletion leads to a change in protein length and feature as the position of the stop-codon in mutated protein will be 520 compared to 525 in the wild-type protein. Further functional studies may be performed in the future to examine the consequences of such deletion in *GLIS2* expression level.

In summary, by employing WES, we detected a novel in-frame deletion (NM_032,575.3: c.560_574delACCATGTCAACGATT, p.H188_Y192del) in *GLIS2* in an Omani family with NPHP and kidney failure. Therefore, this study has not only broadened the spectrum of variants within *GLIS2*, but also extended the molecular pathogenesis spectrum of kidney disease in Oman (Al Alawi et al., 2021) and allowed the confirmation of the clinical diagnosis of NPHP leading to kidney failure.

DATA AVAILABILITY STATEMENT

The original contributions presented in the study are publicly available. This data can be found here: GenBank accession number: BankIt2508176 GLIS2 OK482597.

ETHICS STATEMENT

The studies involving human participants were reviewed and approved by North-East Newcastle and North Tyneside 1 Research Ethics Committee (18/NE/350). Written informed consent to participate in this study was provided by the participants' legal guardian/next of kin. Written informed consent was obtained from the minor(s)' legal guardian/next of kin for the publication of any potentially identifiable images or data included in this article.

AUTHOR CONTRIBUTIONS

The study was conceived and designed by JS, IAA contributed to the acquisition, analysis of data, and writing the first draft. MA, MA-R, and IAS contributed to collecting the data and communicated with the patient's family. IAA, LP, and SR contributed to molecular genetic studies and in silico analysis. The final version was edited by JS. All authors edited and approved the final manuscript.

FUNDING

This study was supported by the Ministry of Health and The Research Council Grant for IAS (ORG/HSS/14/015), Oman. JS is funded by Kidney Research United Kingdom (Paed_RP_001_20180925) and the Northern Counties Kidney Research Fund.

ACKNOWLEDGMENTS

The authors thank the patients and family members who took part in this study as well as staff at the Royal Hospital, Oman.

REFERENCES

Al Alawi, I., Al Riyami, M., Barroso-Gil, M., Powell, L., Olinger, E., Al Salmi, I., et al. (2021). The Diagnostic Yield of Whole Exome Sequencing as a First Approach in Consanguineous Omani Renal Ciliopathy Syndrome Patients. *F1000Res* 10, 207. doi:10.12688/f1000research.40338.1

Attanasio, M., Uhlenhaut, N. H., Sousa, V. H., O'Toole, J. F., Otto, E., Anlag, K., et al. (2007). Loss of GLIS2 Causes Nephronophthisis in Humans and Mice by Increased Apoptosis and Fibrosis. *Nat. Genet.* 39 (8), 1018–1024. doi:10.1038/ng2072

Brayer, K. J., and Segal, D. J. (2008). Keep Your Fingers off My DNA: Protein-Protein Interactions Mediated by C2H2 Zinc finger Domains. *Cell Biochem Biophys* 50 (3), 111–131. doi:10.1007/s12013-008-9008-5

Chaki, M., Hoefele, J., Allen, S. J., Ramaswami, G., Janssen, S., Bergmann, C., et al. (2011). Genotype-phenotype Correlation in 440 Patients with NPHP-Related Ciliopathies. *Kidney Int.* 80 (11), 1239–1245. doi:10.1038/ki.2011.284

Cox, E., and McLendon, G. L. (2000). Zinc-dependent Protein Folding. *Curr. Opin. Chem. Biol.* 4 (2), 162–165. doi:10.1016/s1367-5931(99)00070-8

Halbritter, J., Porath, J. D., Porath, J. D., Diaz, K. A., Braun, D. A., Kohl, S., et al. (2013). Identification of 99 Novel Mutations in a Worldwide Cohort of 1,056 Patients with a Nephronophthisis-Related Ciliopathy. *Hum. Genet.* 132 (8), 865–884. doi:10.1007/s00439-013-1297-0

Hildebrandt, F., Attanasio, M., and Otto, E. (2009). Nephronophthisis: Disease Mechanisms of a Ciliopathy. *Jasn* 20 (1), 23–35. doi:10.1681/asn.2008050456

Hildebrandt, F. (2010). Genetic Kidney Diseases. *The Lancet* 375 (9722), 1287–1295. doi:10.1016/s0140-6736(10)60236-x

König, J., Kranz, B., König, S., Schlingmann, K. P., Titieni, A., Tönshoff, B., et al. (2017). Phenotypic Spectrum of Children with Nephronophthisis and Related Ciliopathies. *Cjasn* 12 (12), 1974–1983. doi:10.2215/cjn.01280217

Levy, M., and Feingold, J. (2000). Estimating Prevalence in Single-Gene Kidney Diseases Progressing to Renal Failure. *Kidney Int.* 58 (3), 925–943. doi:10.1046/j.1523-1755.2000.00250.x

Li, H., and Durbin, R. (2009). Fast and Accurate Short Read Alignment with Burrows-Wheeler Transform. *Bioinformatics* 25 (14), 1754–1760. doi:10.1093/bioinformatics/btp324

Luo, F., and Tao, Y. H. (2018). Nephronophthisis: A Review of Genotype-Phenotype Correlation. *Nephrology* 23 (10), 904–911. doi:10.1111/nep.13393

McConnachie, D. J., Stow, J. L., and Mallett, A. J. (2021). Ciliopathies and the Kidney: A Review. *Am. J. Kidney Dis.* 77 (3), 410–419. doi:10.1053/j.ajkd.2020.08.012

McKenna, A., Hanna, M., Banks, E., Sivachenko, A., Cibulskis, K., Kernytsky, A., et al. (2010). The Genome Analysis Toolkit: a MapReduce Framework for Analyzing Next-Generation DNA Sequencing Data. *Genome Res.* 20 (9), 1297–1303. doi:10.1101/gr.107524.110

O'Toole, J. F., Liu, Y., Davis, E. E., Westlake, C. J., Attanasio, M., Otto, E. A., et al. (2010). Individuals with Mutations in XPNPEP3, Which Encodes a Mitochondrial Protein, Develop a Nephronophthisis-like Nephropathy. *J. Clin. Invest.* 120 (3), 791–802. doi:10.1172/JCI40076

Pavletich, N. P., and Pabo, C. O. (1993). Crystal Structure of a Five-finger GLI-DNA Complex: New Perspectives on Zinc Fingers. *Science* 261 (5129), 1701–1707. doi:10.1126/science.8378770

Richards, S., Aziz, N., Aziz, N., Bale, S., Bick, D., Das, S., et al. (2015). Standards and Guidelines for the Interpretation of Sequence Variants: a Joint Consensus Recommendation of the American College of Medical Genetics and Genomics and the Association for Molecular Pathology. *Genet. Med.* 17 (5), 405–423. doi:10.1038/gim.2015.30

Simms, R. J., Eley, L., and Sayer, J. A. (2009). Nephronophthisis. *Eur. J. Hum. Genet.* 17 (4), 406–416. doi:10.1038/ejhg.2008.238

Snoek, R., van Setten, J., Keating, B. J., Israni, A. K., Jacobson, P. A., Oetting, W. S., et al. (2018). NPHP1 (Nephrocystin-1) Gene Deletions Cause Adult-Onset ESRD. *Jasn* 29 (6), 1772–1779. doi:10.1681/asn.2017111200

Srivastava, S., Molinari, E., Raman, S., and Sayer, J. A. (2017). Many Genes-One Disease? Genetics of Nephronophthisis (NPHP) and NPHP-Associated Disorders. *Front. Pediatr.* 5, 287. doi:10.3389/fped.2017.00287

Srivastava, S., and Sayer, J. A. (2014). Nephronophthisis. *J. Pediatr. Genet.* 3 (2), 103–114. doi:10.3233/PGE-14086

Tang, X., Liu, C., Liu, X., Chen, J., Fan, X., Liu, J., et al. (2020). Phenotype and Genotype Spectra of a Chinese Cohort with Nephronophthisis-Related Ciliopathy. *J. Med. Genet.* 0, 1–8. doi:10.1136/jmedgenet-2020-107184

Zhang, F., Nakanishi, G., Kurebayashi, S., Yoshino, K., Perantoni, A., Kim, Y.-S., et al. (2002). Characterization of Glis2, a Novel Gene Encoding a Gli-Related, Krüppel-like Transcription Factor with Transactivation and Repressor Functions. *J. Biol. Chem.* 277 (12), 10139–10149. doi:10.1074/jbc.m108062200

Conflict of Interest: The authors declare that the research was conducted in the absence of any commercial or financial relationships that could be construed as a potential conflict of interest.

Publisher's Note: All claims expressed in this article are solely those of the authors and do not necessarily represent those of their affiliated organizations, or those of the publisher, the editors, and the reviewers. Any product that may be evaluated in this article, or claim that may be made by its manufacturer, is not guaranteed or endorsed by the publisher.

frontiers | Frontiers in Genetics

ORIGINAL RESEARCH
published: 13 April 2022
doi: 10.3389/fgene.2022.861236

Spectrum of Genetic Variants in a Cohort of 37 Laterality Defect Cases

*Dinu Antony[1,2], Elif Gulec Yilmaz[3†], Alper Gezdirici[3†], Lennart Slagter[1], Zeineb Bakey[1,2], Helen Bornaun[4], Ibrahim Cansaran Tanidir[5], Tran Van Dinh[6], Han G. Brunner[1,7], Peter Walentek[8,9], Sebastian J. Arnold[9,10], Rolf Backofen[6,9] and Miriam Schmidts[1,2,9]**

[1]Genome Research Division, Human Genetics Department, Radboud University Medical Center and Radboud Institute for Molecular Life Sciences, Nijmegen, Netherlands, [2]Center for Pediatrics and Adolescent Medicine, University Hospital Freiburg, Faculty of Medicine, Freiburg, Germany, [3]Department of Medical Genetics, University of Health Sciences, Istanbul Kanuni Sultan Suleyman Training and Research Hospital, Istanbul, Turkey, [4]Department of Pediatric Cardiology, University of Health Sciences, Istanbul Kanuni Sultan Suleyman Training and Research Hospital, Istanbul, Turkey, [5]Department of Pediatric Cardiology, Basaksehir Cam and Sakura City Hospital, Istanbul, Turkey, [6]Bioinformatics Group, Department of Computer Science, University of Freiburg, Freiburg, Germany, [7]Maastricht University Medical Center and GROW School of Oncology and Development, Maastricht University, Maastricht, Netherlands, [8]Renal Division, Department of Medicine, University Hospital Freiburg, Faculty of Medicine, University of Freiburg, Freiburg, Germany, [9]CIBSS- Centre for Integrative Biological Signalling Studies, University of Freiburg, Freiburg, Germany, [10]Institute of Experimental and Clinical Pharmacology and Toxicology, Faculty of Medicine, University of Freiburg, Freiburg, Germany

Laterality defects are defined by the perturbed left–right arrangement of organs in the body, occurring in a syndromal or isolated fashion. In humans, primary ciliary dyskinesia (PCD) is a frequent underlying condition of defective left–right patterning, where ciliary motility defects also result in reduced airway clearance, frequent respiratory infections, and infertility. Non-motile cilia dysfunction and dysfunction of non-ciliary genes can also result in disturbances of the left–right body axis. Despite long-lasting genetic research, identification of gene mutations responsible for left–right patterning has remained surprisingly low. Here, we used whole-exome sequencing with Copy Number Variation (CNV) analysis to delineate the underlying molecular cause in 35 mainly consanguineous families with laterality defects. We identified causative gene variants in 14 families with a majority of mutations detected in genes previously associated with PCD, including two small homozygous CNVs. None of the patients were previously clinically diagnosed with PCD, underlining the importance of genetic diagnostics for PCD diagnosis and adequate clinical management. Identified variants in non-PCD-associated genes included variants in *PKD1L1* and *PIFO*, suggesting that dysfunction of these genes results in laterality defects in humans. Furthermore, we detected candidate variants in *GJA1* and *ACVR2B* possibly associated with situs inversus. The low mutation detection rate of this study, in line with other previously published studies, points toward the possibility of non-coding genetic variants, putative genetic mosaicism, epigenetic, or environmental effects promoting laterality defects.

Keywords: laterality defect, situs inversus, exome, cilium, primary ciliary dyskinesia, dynein, PIFO, PKD1L1

OPEN ACCESS

Edited by:
Steven LC Pei,
Yale University, United States

Reviewed by:
Naoto Keicho,
Japan Anti-tuberculosis Association, Japan
Richard Francis,
James Cook University, Australia

****Correspondence:***
Miriam Schmidts
miriam.schmidts@uniklinik-freiburg.de

†Present Address:
Elif Yilmaz Gulec,
Department of Medical Genetics, Istanbul Medeniyet University, School of Medicine, Istanbul Goztepe Prof Dr Suleyman Yalcin City Hospital, Istanbul, Turkey
Alper Gezdirici,
Department of Medical Genetics, Istanbul Cam and Sakura City Hospital, Istanbul, Turkey

Specialty section:
This article was submitted to Human and Medical Genomics, a section of the journal Frontiers in Genetics

Received: *24 January 2022*
Accepted: *03 March 2022*
Published: *13 April 2022*

Citation:
Antony D, Gulec Yilmaz E, Gezdirici A, Slagter L, Bakey Z, Bornaun H, Tanidir IC, Van Dinh T, Brunner HG, Walentek P, Arnold SJ, Backofen R and Schmidts M (2022) Spectrum of Genetic Variants in a Cohort of 37 Laterality Defect Cases. Front. Genet. 13:861236. doi: 10.3389/fgene.2022.861236

INTRODUCTION

Laterality defects in humans occur with a frequency of about 1: 10,000 (Lin et al., 2014). *Situs inversus totalis* presents with a complete mirror image of normal organ asymmetry throughout the body. In contrast, in *situs inversus thoracalis* or *abdominalis* (heterotaxy), only a subset of organs is affected. While *situs inversus* usually does not impair organ function, this is different in left or right isomerism or situs ambiguous, accounting for up to 5% of all laterality defect cases. Heterotaxy is commonly associated with complex heart defects such as transposition of the great arteries can significantly affect the quality of life and life expectancy (Lin et al., 2014). Furthermore, polysplenia can be observed with left isomerism, while right isomerism is associated with asplenia and increased risk for serious infections (Fliegauf et al., 2007) (**Figure 1**)

Left–right body asymmetry in vertebrates is determined very early in embryonic development, such as embryonic day 7.5 in mice (Marszalek et al., 1999) and 6–12 somite stage in zebrafish (Kawakami et al., 2005). In mammals, the so-called embryonic node is a transiently present structure which exhibits motile 9 + 0 monocilia and non-motile 9 + 0 monocilia (**Figures 2A,B**). Both types of cilia are considered essential for left–right patterning as functional defects of both motile and non-motile cilia can result in laterality defects in vertebrates (Pennekamp et al., 2015). Dysfunction of genes encoding for proteins essential for the ciliary motility apparatus such as dynein arm components results in left–right patterning defects in humans (Leigh et al., 2019) and mice (Tan et al., 2007), most often combined with recurrent respiratory tract infections due to impaired mucociliary clearance and often infertility (Fliegauf et al., 2007). This combination of laterality defects, bronchiectasis, and sinusitis is also referred to as Kartagener syndrome, observed in approximately 50% of all primary ciliary dyskinesia (PCD) cases (Knowles et al., 2016) (**Supplementary Table S1**). Of note, mutations in genes encoding for proteins associated with

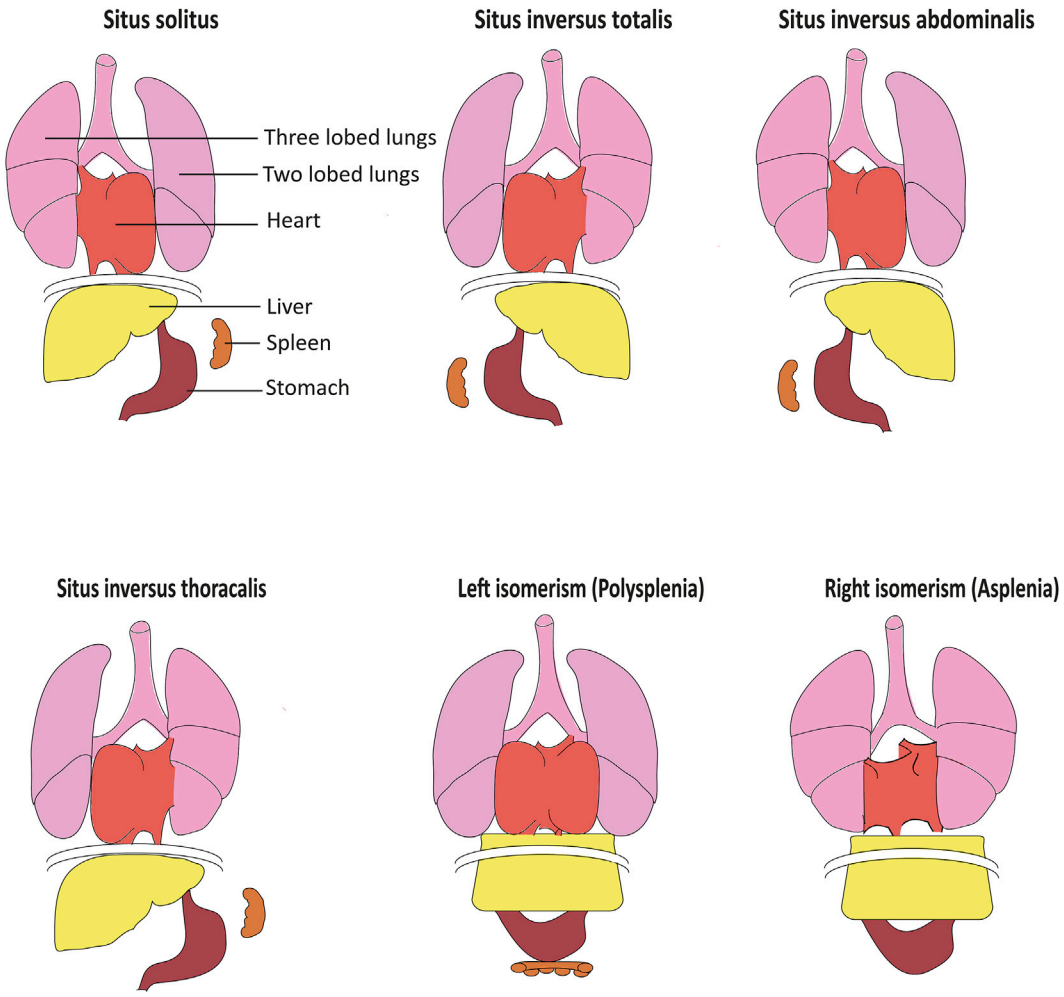

FIGURE 1 | Organ arrangement patterns in humans. While situs solitus represents the most frequent left–right organ arrangement, situs inversus represents the corresponding mirror image. In situs inversus thoracalis and situs inversus abdominalis, left–right patterning is inversed solely above or below the diaphragm. Left isomerism often results in polysplenia while accordingly, right isomerism can cause asplenia. Isomerism often also causes severe structural heart defects including defective arrangement of the great blood vessels, adapted from Fliegauf et al. (2007).

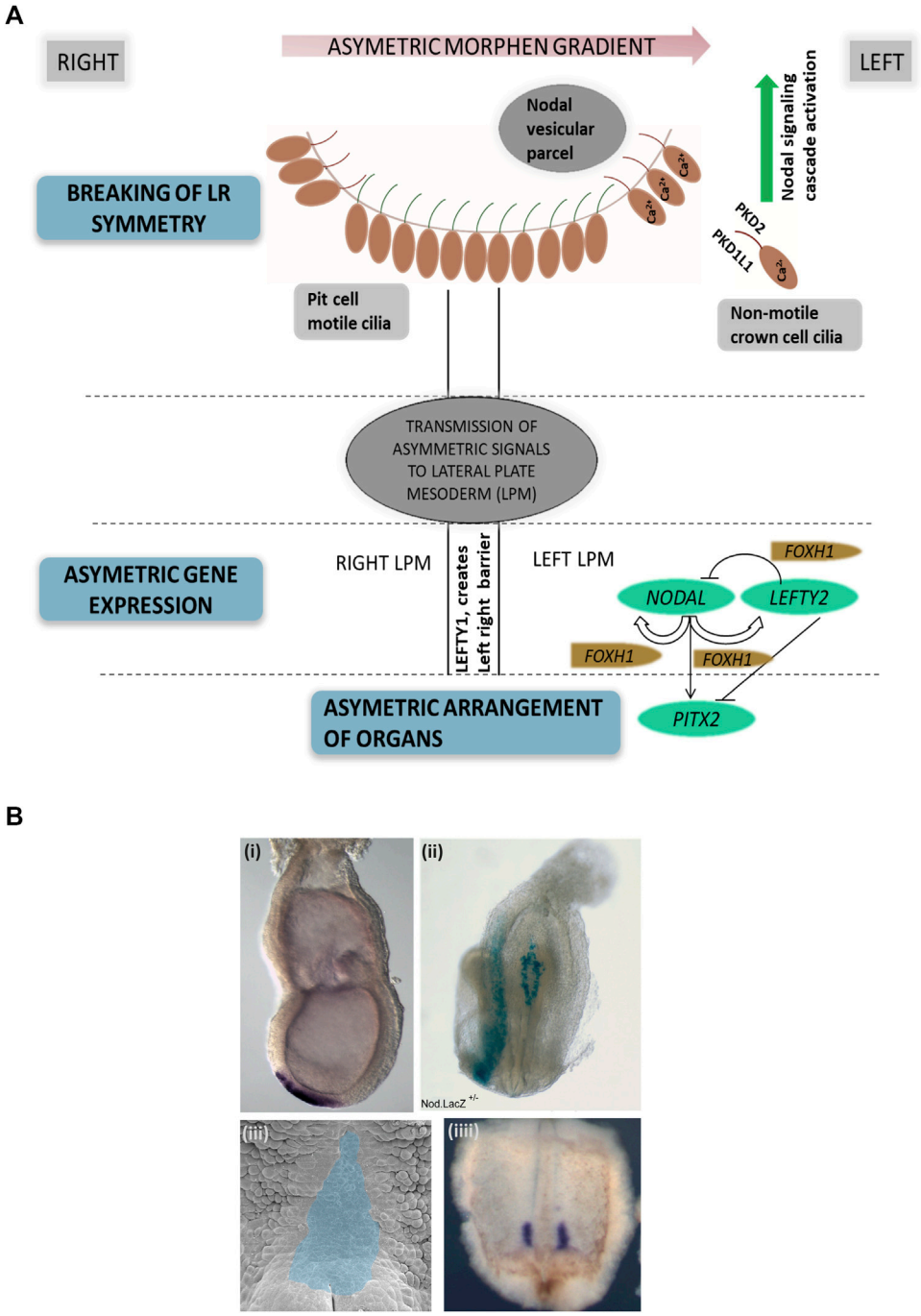

FIGURE 2 | Left–right asymmetry in mammals. **(A)** Simplified representation of left–right patterning initiation in mammals. Breaking of left–right asymmetry is initiated by motile cilia in the embryonic node generating a leftward fluid flow followed by signal propagation by non-motile cilia. Here, PKD2 and PKD1L1 channels at the ciliary membrane enable calcium currents, resulting in elevated Ca2+ concentrations on the left side of the node. Node asymmetry is then propgated to the lateral plate mesoderm, which in turn causes NODAL expression in the left lateral plate mesoderm, followed by PITX2 expression. LEFTY2 acts as a feedback inhibitor restricting the range of nodal signaling. LEFTY1 helps in maintaining the midline barrier. **(B)** Examples of left–right organizing centers in vertebrates. (i) *In situ* hybridization visualizing the embryonic node (Shh, purple), e7.5 mouse embryo; (ii) Nodal.LacZ reporter expression (blue) marking the embryonic node and the lateral left plate mesoderm in an E8.5 mouse embryo; (iii) *Xenopus* embryo stage 17 archenteron roof in ventral perspective (pseudocolored in blue) where cilia-mediated leftward flow initiates left–right asymmetry; (iiii) *Xenopus* embryo stage 17 with nodal expression marked in purple (*in situ* hybridization).

the central pair microtubules and radial spokes result in PCD but do not cause situs abnormalities due to the 9 + 0 ciliary ultrastructure in the node compared to a 9 + 2 ultrastructure of motile airway cilia (Knowles et al., 2016). This includes mutations in *RSPH4A*, *HYDIN*, *MCIDAS*, *RSPH9*, *RPGR*, *CCDC65*, *RSPH1*, *CCDC164*, and *STK36* (Edelbusch et al.,

TABLE 1 | Summary of previously published studies describing genetic screening in cohorts with laterality defects. Search terms included "laterality defect," "heterotaxy," "situs inversus," "primary ciliary dyskinesia," and "genetic" or "mutation." Success rates were stated as presented in the manuscripts or calculated from the results presented in the publications.

Cohort phenotype	Ethnicity	Variant identification methods used	Success rate	Publication
Congenital heart disease	European 2,063, African American 189, East Asian 36, South Asian 136, and Mexican 280, Other 167	Whole-exome sequencing of probands (2,871 cases)	10.1% of 2,871 cases.	Jin et al. (2017)
Fetuses with congenital heart defects and/or heterotaxy and no cytogenetic anomalies	Ethnicity information not available, two parents were consanguineous	Targeted NGS panel	10/80 fetuses (12.5%)	Liu et al. (2020)
Abnormal atrial situs (atrial isomerism or atrial situs inversus)	Arabic	Whole-exome sequencing	17/30 cases (56.6%)	Bolkier et al. (2021)
Transposition of the great arteries not associated with other situs anomalies	Italian	Coding sequence analysis of *ZIC3, ACVR2B, LEFTYA, CFC1, NODAL, NKX2.5, CRELD1, GATA4, GDF1*, and *FOXH1*	2/7 families (28.5%)	De Luca et al. (2010)
Heterotaxy patients with cardiac manifestations	Caucasian 21, Hispanic 11, African American 9, Asian and Southeast Asian 3, and other 3	Coding sequence analysis of *ZIC3, LEFTYA, ACVR2B*, and *CFC1*	4/47 cases (8.5%)	Ma et al. (2012)
Congenital heart disease and heterotaxy	Clinical Genetics, Maastricht University Medical Center, Maastricht, Netherlands Ethnicity not mentioned	Screened only for *ZIC3* variant	6/348 cases (1.7%)	Paulussen et al. (2016)
Sporadic heterotaxy patients with congenital heart defects	Chinese	Affymetrix CytoScan HD microarray and real-time polymerase chain reaction	19 rare CNVS in 63 cases (30.1%)	Liu et al. (2018)
Heterotaxy and heterotaxy-spectrum congenital heart disease	Arabic 2, Asian 2, Black or African American 13, Caucasian 90, mixed 8, unknown 42, and Hispanic/Latino 68	Array-based genotyping methods	CNVs identified in 20% of cases, total 225 patients were included in the study	Cowan et al. (2016)
Heterotaxy patients	European ancestry 120, Hispanic 104, African Americans 19, and all other ancestries 19	Genotyping using, Illumina 610Quad Bead chip platform	45 previously unrecorded CNVs in 39 different subjects, total 262 cases were included in the study (14.8%)	Fakhro et al. (2011)
Situs inversus totalis, heterotaxy, and congenital heart disease	Chinese	Whole-exome and genome sequencing of family trios	4/61 families (6.5%)	Chen et al. (2019)
Laterality defects	White non-Hispanic 158, Hispanic 109, African American 22, East Asian 10, Mediterranean 2, mixed 6, and unknown*16	Whole-exome sequencing	25/323 cases (7.7%)	Li et al. (2019)
15 situs inversus patients (6 with PCD and 9 without PCD)	Ethnicity information not available	Genome sequencing of 15 situs inversus cases and 15 controls to identify rare, highly penetrant variants in non-PCD situs inversus group	10/15 cases (66.6%)	Postema et al. (2020)
Primary ciliary dyskinesia	Dutch	Targeted-exome panel of 310 genes	50/74 cases (67.5%)	Paff et al. (2018)
Primary ciliary dyskinesia	Mixed (White, Sri Lankan, Portuguese, Hispanic, Pakistani, and Somali)	Sanger sequencing of 12 PCD-associated genes, followed by analysis of negative and single variant cases by targeted Copy Number Variation (CNV) and/or whole-exome sequencing	34/45 families (75.5%)	Marshall et al. (2015)
Suspected primary ciliary dyskinesia	Egyptian	Targeted-exome panel of 321 genes	23/33 families (69.6%)	Fassad et al. (2020b)
Primary ciliary dyskinesia	Chinese	Whole-exome sequencing	51/75 cases (68%)	Guan et al. (2021)

(Continued on following page)

TABLE 1 | (*Continued*) Summary of previously published studies describing genetic screening in cohorts with laterality defects. Search terms included "laterality defect," "heterotaxy," "situs inversus," "primary ciliary dyskinesia," and "genetic" or "mutation." Success rates were stated as presented in the manuscripts or calculated from the results presented in the publications.

Cohort phenotype	Ethnicity	Variant identification methods used	Success rate	Publication
36 cases primary ciliary dyskinesia, 8 cases without PCD (not diagnosed as PCD), and 4 cases with inconclusive diagnosis	Jewish 13, Arabic 35	Whole-exome sequencing	34/36 PCD cases (94.4%); 4/8 (50%) cases without PCD and none of the 4 cases with inconclusive diagnosis was solved	Gileles-Hillel et al. (2020)
Primary ciliary dyskinesia	European 74, South Asian 35, Arabic 29, and all other ancestries 23	Targeted NGS panel	132/161 families (82%)	Fassad et al. (2020a)
Primary ciliary dyskinesia	Turkish	Whole-exome sequencing	46/265 cases (17.3%)	Emiralioglu et al. (2020)
Primary ciliary dyskinesia	Unknown	Candidate gene screening or whole-exome sequencing	68/75 cases (90.6%)	Blanchon et al. (2020)
Suspected primary ciliary dyskinesia	Serbian	Clinical exome panel of 29 genes	9/21 cases (42.8%)	Andjelkovic et al. (2018)
Suspected primary ciliary dyskinesia	Arabic	Clinical exome sequencing	38/56 families (67.8%)	Shamseldin et al. (2020)
Suspected primary ciliary dyskinesia	Tunisian	Targeted NGS panel of 40 PCD genes	28/34 families (82.3%)	Mani et al. (2020)
Primary ciliary dyskinesia	Samples collected from the Czech Republic, ethnicity not mentioned	Targeted NGS panel and Sanger sequencing	22/33 families (66.6%)	Djakow et al. (2016)
Suspected primary ciliary dyskinesia	Japanese	Targeted NGS panel of 32 genes	10/46 cases (21.7%)	Takeuchi et al. (2018)

2017). Further, mutations in CCNO (Wallmeier et al., 2014) and MCIDAS (Boon et al., 2014) cause mucociliary clearance disorders without laterality disturbances. Likewise, mutations in genes encoding for ciliary proteins unrelated to motility in humans and mice can also result in a disturbed left–right body axis, including *PKD2* (Pennekamp et al., 2002; Bataille et al., 2011), *INVERSIN* (Simons et al., 2005), *NPHP3* (Olbrich et al., 2003), and *PKD1L1* (Field et al., 2011; Vetrini et al., 2016). These mutations are usually combined with additional developmental defects such as renal-hepatic dysplasia, polycystic kidney disease, nephronophthisis, chondrodysplasias, brain malformation, or retinal degeneration (Fliegauf et al., 2007; Deng et al., 2015) (**Supplementary Table S1**).

Normal motile cilia function is crucial for generating a leftward flow within the embryonic node in mammals (Nonaka et al., 1998), initiating cell signaling pathways driving the establishment of body laterality. The "two-cilia hypothesis" proposes that a leftward flow generated by motile node pit cell cilia is sensed by non-motile node crown cell cilia which causes calcium influx determining the left side of the embryonic node (McGrath et al., 2003). A second model proposes that the leftward nodal flow results in a morphogen gradient, including vesicular particles being transported toward the left side of the node where they release their content, creating a morphogen gradient (Tanaka et al., 2005) (**Figure 2A**). The definition of the left side of the embryonic node subsequently leads to the activation of the TGFβ-superfamily components, namely, *NODAL* and *LEFTY2*. The nodal antagonist *LEFTY2* prevents the activation of *NODAL* on the right side of the lateral plate mesoderm (Juan and Hamada, 2001; Shiratori and Hamada, 2006). On the left side, *NODAL* consecutively induces *PITX2* expression on the left side of the lateral plate mesoderm, enabling asymmetric heart, lung, and spleen development (Norris, 2012). Midline *LEFTY1* expression confines *NODAL*, *LEFTY2*, and *PITX2* expression to the left side as *LEFTY1* null mice display bilateral expression of *NODAL*, *LEFTY2*, and *PITX2* (Meno et al., 1998; Capdevila et al., 2000), (Grimes and Burdine, 2017) (**Figure 2A**). It is therefore not surprising that nodal dysfunction in mammals causes laterality defects (Mohapatra et al., 2009).

In addition to nodal signaling, Bmp, Notch, Hedgehog, and Fgf signaling also play important roles for left–right establishment (Sempou and Khokha, 2019). In humans, mutations in *ZIC3* (Gebbia et al., 1997), the TGF-beta signaling molecule *GDF1* (Karkera et al., 2007) or *ACVR2B* (Kosaki et al., 1999; Ma et al., 2012), and the metalloprotease *MMP21* (Guimier et al., 2015) have been associated with left–right patterning defects. However, past genetic studies investigating laterality defects in humans have had a surprisingly low yield of causative mutations, leaving up to 90% of cases genetically unexplained (**Table 1**). As progress has since been made with the identification of novel laterality defect genes and some of the previous studies did not use exome sequencing but targeted Sanger sequencing or gene panel sequencing, we performed an exome-based study in a cohort

of 37 Turkish individuals with laterality defects to determine the rate of mutations in known disease genes and to identify novel disease-causing alleles.

MATERIALS AND METHODS

DNA Samples

Inclusion criteria were the presence of situs inversus totalis, thoracalis or abdominalis, or left or right isomerism with or without the presence of structural heart defects. The majority of cases were children younger than 10 years, presenting to the local genetics clinic after a referral from local pediatricians or pediatric cardiologists, while the remaining cases were fetal cases diagnosed by prenatal ultrasound. None of the included children was reported by the parents to present with daily wet cough or chronic rhinitis. Informed consent was obtained from all the participants or their legal guardians. Ethical approval was obtained from the local ethics committee and samples were processed at Radboudumc in Nijmegen under the diagnostic innovation program to establish a genetic diagnosis (CMO-2006/048). Genomic DNA extraction was performed from EDTA blood samples using the standard salting out method (Miller et al., 1988) or commercially available kits such as Qiagen genomic DNA extraction kit (Germantown, MD, United States). The concentration of DNA was determined using the Nanodrop (Thermo Fisher Scientific, Waltham, MA, United States) or by Qubit 2.0 (Life Technologies, Carlsbad, CA, United States).

Whole-Exome Sequencing

Exome sequencing was performed as previously described (Loges et al., 2018). In brief, 2–5 micrograms of DNA from index cases were subjected to whole-exome sequencing (WES) at Novogene, Hong Kong. Exome capture was performed using the Agilent SureSelect Human All Exon V5 Kit; sequencing was performed using an Illumina HiSeq 2500 machine. Paired-end sequencing was performed resulting in sequences of 150 bases from each end of the fragments. UCSC hg19 was used as a reference genome. VarScan version 2.2.5 and MuTec and GATK Somatic Indel Detector were used to detect single-nucleotide variants (SNV) and InDels. Data were then filtered in-house using a minor allele frequency (MAF) < 1% in public control databases including dbSNP, ExAc, and gnomAD, and remaining variants were first filtered for known disease-causing genes with an emphasis on diseases compatible with the patient phenotype (laterality disorder) and genes causing laterality defects in animal models. We then filtered genes encoding for proteins present in the cilia proteome and subsequently used a list of genes expressed highly in the mouse embryonic node (*S. J. Arnold, unpublished data*) for further gene prioritization. A complete list of genes used for filtering is shown in **Supplementary Table S1**. Open exome analysis was subsequently performed for cases where no likely causative allele could be detected. We prioritized homozygous variants in known consanguineous families; however, compound heterozygosity or dominant inheritance was likewise considered. Additionally, visual BAM file inspection was performed for homozygous CNVs in genes previously associated with laterality defects, and exome data files were further analyzed for the presence of CNVs using ExomeDepth (Plagnol et al., 2012).

PCR and Sanger Sequencing

To confirm deletions identified by CNV analysis, respective exons (*DNAI2* exons 8–13 and *CCDC40* exons 1–3) were amplified using the one taq master mix following the manufacturer's instructions (New England Biolabs, Massachusetts, United States). Primers were designed using the primer blast tool, and sequences of the primers are available on request.

RESULTS

We performed genetic diagnostics using exome sequencing in 37 individuals, from 35 unrelated Turkish families, presenting with laterality defects to local genetics clinics. The included cases neither had a clinical history of PCD nor had an official diagnosis of PCD; however, airway ciliary motility assessment or nasal nitric oxide (NO) measurement was not performed prior to genetic investigations. Exome sequencing and CNV analysis identified likely causative variants in 14 families and candidate variants of unknown significance in 3 families, with the majority of mutations found in genes encoding for ciliary proteins of which in turn most encode for components of the ciliary motility apparatus such as dynein arms (DNAH5, DNAI1, DNAI2, DNAH9, and DNAH6), dynein arm-docking complex components (CCDC114), dynein assembly complex components (DNAAF3) or 96 nm ruler components (CCDC39 and CCDC40), and MNS1, a protein interacting with CCDC114 *in vitro* (**Table 2**). The vast majority of identified variants were found in a homozygous state which reflects the mainly autosomal recessive inheritance pattern seen in ciliopathies and the consanguineous nature of our subject population. In accordance with previous findings in mucociliary clearance disorders, we identified mainly nonsense, frameshift, or splice site variants (Fassad et al., 2020a). Of all causative variants identified, 8 variants have not been previously reported as disease-causing. In three additional families, we identified potential candidate disease variants in *GJA1* in SI-18, in *DNAH6* in SI-15, and in *CCDC39* and *ACVR2B* in SI-47 (**Table 2**).

Variants Identified in Genes Encoding for Ciliary Motility Component-Related Genes

In total, 12 out of 15 likely disease-causing variants were identified in genes encoding for ciliary motility related proteins associated with axonemal dynein motor, including two nonsense *DNAH5* variants in SI-17 and SI-45: p.Arg 2013* previously published by Hornef et al. (2006) and p.Arg3116* not previously reported as disease-causing. In SI-46, we identified a homozygous frameshift variant in *DNAH9*, p.Leu3376Phefs*57 (case and mutation meanwhile reported by Loges et al. (2018).

TABLE 2 | Genetic variants identified by exome sequencing in 35 laterality defect families.

Case	Phenotype	Consanguinity	Gene	cDNA position; dbSNP	Protein position	ClinVar/ published	gnomAD allele frequency	Protein function
SI-2	*Situs inversus totalis*	Yes	*MNS1* NM_018365.4	c.724C > T, rs185005213 Case previously published in Ta-Shma et al. (2018)	p.Arg242* Homozygous	Pathogenic (Ta-Shma et al., 2018)	0.0002366	Outer dynein arm docking complex
SI-3	Situs inversus totalis	Yes	*CCDC114* NM_001364171.2	c.1004-1005 del	p.Phe335Cysfs*2 Homozygous	Not reported	Not reported	Outer dynein arm docking complex
SI-7	Situs inversus totalis	Yes	*DNAAF3* NM_001256715.2	c. 1352T > C	p.Phe451Ser Homozygous	Not reported	Not reported	Dynein arm assembly factor
SI-8	Situs inversus totalis	No	*PKD1L1* NM_138295.5	c. 7663C > T rs200853469 c.7937C > G, rs752673990	p.Arg2555*, heterozygous p.Ser2646*, heterozygous (compound heterozygous)	Not reported Not reported (Berauer et al., 2019)	0.00005907 0.000003977	Ciliary calcium channel
SI-9	Situs inversus totalis	Yes	*DNAI2* NM_023036.6	c. 787C > T rs137852998	p.Arg263* Homozygous	Pathogenic (Loges et al., 2008)	0.00001774	Outer dynein arm intermediate chain
SI-16	Situs inversus totalis	Yes	*DNAI2* NM_023036.6	CNV, c.1212_1818del[#,+], Exon10-13 deletion	Homozygous	Not reported	Not reported	Outer dynein arm intermediate chain
SI-17	Situs inversus totalis	Yes	*DNAH5* NM_001369.3	c. 6037C > T, rs1273352530	p.Arg 2013* Homozygous	Pathogenic/ likely pathogenic (Hornef et al., 2006)	NA	Outer dynein arm heavy chain
SI-19	Situs inversus totalis	Yes	*CCDC40* NM_017950.4	CNV: c.1_93del[#,+] Exon1-2 deletion	Homozygous	Not reported	Not reported	Cilia 96-nm Axonemal ruler
SI-21	Situs inversus totalis	Yes	*CCDC114* NM_001364171.2	c.1502+5G > A, rs201133219	p.Ser469Argfs*7 homozygous	Pathogenic/ likely pathogenic (Knowles et al., 2013)	0.00007827	Outer dynein arm docking complex
SI-27	*Situs inversus totalis*		CCDC114 NM_001364171.2	c. 1244T > A, rs748335075	p.Ile415Asn Homozygous	Not reported	0.000003986	Outer dynein arm docking complex
SI-41	Situs inversus totalis	No	*PIFO* NM_181643.6	c. 239G > A[#], rs150508940	p.Arg80Lys, heterozygous	Not reported (Kinzel et al., 2010)	0.0002829	Regulates primary cilia disassembly, localized at basal body and ciliary necklace
SI-44	Situs inversus totalis	Yes	*DNAI1* NM_012144.4	c. 1333_1334insC [#]	p.Met445Thrfs*6 Homozygous	Not reported	Not reported	Outer dynein arm intermediate chain
SI_45	Situs inversus totalis	Yes	*DNAH5* NM_001369.3	c. 9346C > T[#] rs1264701182	p.Arg3116* Homozygous	Pathogenic	0.00001992	Outer dynein arm heavy chain
SI-46	Situs inversus totalis	Yes	*DNAH9* NM_001372.4	c.10127dupT rs867177356 Case previously published in Loges et al. (2018)	p.Leu3376Phefs*57 homozygous	Pathogenic (Loges et al., 2018)	Not reported	Outer dynein arm heavy chain

(Continued on following page)

TABLE 2 | (*Continued*) Genetic variants identified by exome sequencing in 35 laterality defect families.

Case	Phenotype	Consanguinity	Gene	cDNA position; dbSNP	Protein position	ClinVar/ published	gnomAD allele frequency	Protein function
SI-18	Situs inversus totalis	No	*GJA1* NM_000165.5	c. 1001C > T, rs1460872904,	p.Pro334Leu, heterozygous, *de novo*	Not reported	0.000007962	Gap junctions
SI-15	Situs inversus totalis	?	*DNAH6* NM_001370.2,	c. 1020C > A c.8829+208 C>T	p.Tyr340* heterozygous p.? heterozygous	Not reported Not reported	Not reported Not reported	Inner dynein arm heavy chain
SI-47	Situs inversus totalis	Yes	*CCDC39* NM_181426 rs1560092712 *ACVR2B* NM_001106	c. 350A > G # c. 925C > T #	p.Asp117Gly Homozygous p.Arg309Cys Heterozygous	Uncertain significance Uncertain significance	Not reported 0.00001770	Cilia 96-nm Axonemal ruler Gonadal polypeptide hormones

#no segregation analysis performed; + intronic breakpoints not defined.

We further found three families to carry variants in genes encoding for dynein intermediate chains: *DNAI1* c.1333_1334insC, p.Met445Thrfs*6 not previously reported as disease-causing or in gnomAD for SI-44 and *DNAI2* p.Arg263* previously identified by Loges et al. in SI-9 (Loges et al., 2008) and a homozygous CNV encompassing *DNAI2* exons 10–13 (c.1212_1818del) in SI-16 not previously reported and confirmed by PCR (**Supplementary Figures S1, S2**). Our analysis further revealed 3 homozygous variants in the outer dynein arm-docking complex (ODA-DC) component *CCDC114:* in SI-3, we identified c.1004-1005del, p.Phe335Cysfs*2 not previously reported, while in SI-21, we detected the previously reported splicing variant, c.1502+5G > A (Knowles et al., 2013) and a not previously reported homozygous missense, p.Ile415Asn in SI-27. Knowles et al. found that the splice site change in intron 12 results in a frameshift and introduces a stop codon (p.Ser469Argfs*7). The homozygous missense change p.Ile415Asn in SI-27 is not reported in ClinVar, predicted deleterious by SIFT, probably damaging (0.997) by PolyPhen and polymorphism by mutation taster. The mutant residue is bigger, and this will change the 3D structure and might lead to bumps. The different hydrophobicity of the wild-type and mutant residues could cause a loss of protein–protein interactions (mutation prediction program used: HOPE; https://www3.cmbi.umcn.nl/hope/). Segregation analysis revealed the mother to be a heterozygous carrier; however, the variant was not detected in the father. This could be due to a heterozygous not detected deletion on the other allele, non-paternity, *de novo* occurrence of the mutation in the child or maternal uniparental disomy. In SI-2, we identified a homozygous nonsense change (p.Arg242*) in *MNS1* (case and variant reported in Ta-Shma et al., 2018 (Ta-Shma et al., 2018). Interestingly, this variant was identified in several unrelated individuals with laterality defects and perturbed male fertility but no respiratory symptoms (Ta-Shma et al., 2018). MNS1 interacts with CCDC114, suggesting likewise a role for outer dynein arm docking (Ta-Shma et al., 2018). In SI-7, we identified a not previously reported homozygous missense variant, p.Phe451Ser in *DNAAF3.* The variant is probably damaged (0.998) by PolyPhen prediction and polymorphism using mutation taster analysis. The wild-type and mutant amino acids differ in size with the mutant residue being smaller, and this might influence the protein structure and protein–protein interactions. Furthermore, due to differences in hydrophobicity of the wild-type and mutant residue, hydrophobic interactions, either in the core of the protein or on the surface, could be lost (https://www3.cmbi.umcn.nl/hope/).

CNV analysis revealed a novel homozygous deletion encompassing c.1_93 of *CCDC40* in SI-19 conformed by PCR **Supplementary Figures S3, S4**. We could not identify the intronic breakpoints of the CNVs identified in this study.

Variants Identified in Other Ciliary Genes

We identified mutations in two genes encoding for ciliary proteins not related to ciliary motility, *PIFO* and *PKD1L1. PIFO* p.Arg80Lys was identified heterozygously in SI-41, previously reported by Kinzel et al. in two cases in a heterozygous state (Kinzel et al., 2010). One previously reported case represented a deceased neonate with thoracic–abdominal *situs inversus*, cystic kidneys, and liver fibrosis, and a second case suffered from isolated double-outlet right ventricle (Kinzel et al., 2010). *PIFO* has been previously identified as a gene expressed in the node by Tamplin et al. using microarray analysis in *Foxa2* mutant mouse embryos (Tamplin et al., 2008). Parental DNA was not available to confirm *de novo* occurrence of the variant in our case. *PKD1L1* p.Arg2555* and p.Ser2646* were identified as compound heterozygosity in SI-8, both not reported in ClinVar to date. Biallelic variants in *PKD1L1* have been previously reported in individuals with laterality defects and congenital heart malformations (Vetrini et al., 2016; Postema et al., 2020; Bolkier et al., 2021; Correa et al., 2021). The variant p.Ser2646* identified in our study was also reported by Berauer et al. in a case with polysplenia, biliary atresia, abdominal heterotaxy, congenital heart disease, and vascular anomalies (Berauer et al., 2019). PKD1L1 seems to form a ciliary protein complex with PKD2 in primary crown cell cilia in the node, and it thought to play a role in flow sensing (Field et al., 2011).

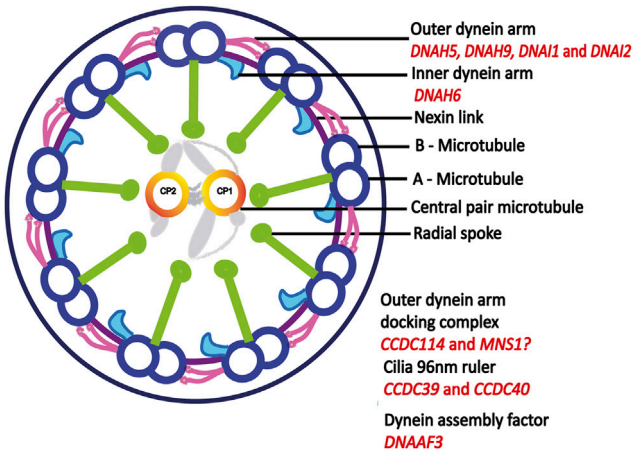

FIGURE 3 | Motile cilia ultrastructure. Motile cilia are microtubule based structures, dynein arms powers the sliding motion of microtubules which in turn generates ciliary movement. Outer dynein arm-docking complex helps in the attachment of dynein arms to A-microtubule. Dynein assembly factor is important for the assembly of both outer and inner dynein arms. Mutations in central pair and radial spoke genes does not cause laterality defect, adapted from (Antony et al., 2021). Proteins encoded by genes identified in this study are indicated in red.

Candidate Variants Identified

Candidate variants were identified in three families (SI-18, SI-15 and SI-47). SI-18 carries a heterozygous *de novo* missense variant in *GJA1* (p.Pro334Leu). The mutant residue is bigger, and this might lead to bumps. The mutation is located within a stretch of residues annotated in UniProt as a special protein–protein interaction region. The wild-type residue is a proline. Prolines are known to be very rigid and therefore induce a special backbone conformation which might be required at this position. The mutation can disturb this special conformation (https://www3.cmbi.umcn.nl/hope/). This variant is not reported in ClinVar and has a frequency of 0.000007962 in gnomad. The variant is predicted to be benign (0.020) by PolyPhen, disease-causing by mutation taster (score 98), and tolerated by SIFT prediction. The amino acid position is conserved in mammals including mice, chicken, and *Xenopus* while zebrafish carries an alanine instead here.

In SI-15, we identified a heterozygous stop variant, c.1020C > A, p.Tyr340* and a heterozygous deep-intronic substitution, c.8229+208C>T in *DNAH6*. While the Alamut program predicted only minimal splice site probabilities for the mutant allele compared to the wild-type sequence, ESE finder predicted a slightly changed pattern of ESE binding (**Supplementary Figures S5, S6**).

In SI-47, we identified variants in two genes, *CCDC39* and *ACVR2B*: a homozygous missense variant in *CCDC39* (p.Asp117Gly), not reported in gnomAD but in ClinVar as a variant of uncertain significance (VUS). The variant is predicted as polymorphism by mutation taster and PolyPhen benign with a score of 0.351. The variant is located at the first coiled–coil domain (16–122 amino acids; UniProt). Additionally, we identified a heterozygous variant in *ACVR2B,* p.Arg309Cys, predicted damaging by SIFT, probably damaging (1.000) by PolyPhen, and disease-causing by mutation taster, likewise reported as VUS in ClinVar. The variant is located in the protein kinase-binding domain (190–480 amino acids). Segregation analysis could not be performed to establish if the variant is *de novo*. Several previous studies have reported heterozygous *ACVR2B* variants in individuals with heterotaxy (Kosaki et al., 1999; Ma et al., 2012; Li et al., 2019). *ACVR2B* functions in the NODAL/TGF-beta signaling pathway (Li et al., 2019). A summary of all genetic findings is shown in **Table 2** and **Figures 3**, **4**.

DISCUSSION

Over the last 2 decades, genetic analyses of individuals with laterality defects have greatly advanced our understanding of establishment of left–right asymmetry. Eight variants reported here have not been previously reported as disease-causing, two of which are CNVs. This provides useful information for human genetic diagnostics and underlines the importance of CNV analysis.

Given the fact that none of the cases included in this study had a formal diagnosis of PCD nor was suspected with PCD clinically, we identified pathogenic or likely pathogenic variants in a rather large number of genes known to cause PCD when dysfunctional, including *DNAH5*, *DNAH9*, *CCDC114, DNAI1, DNAI2*, *CCDC39*, and *CCDC40*. *DNAH5* encodes an outer dynein arm γ—heavy chain distributed panaxonemally in respiratory cilia, and biallelic loss of function mutations are a frequent cause of PCD (Hornef et al., 2006). *DNAH9* encodes an outer dynein arm (ODA) heavy chain only present in one of 2 ODA subtypes, subtype 2. ODA2 localization is restricted to the distal half of the cilium and accordingly, and DNAH9 dysfunction results in a very subtle respiratory phenotype with perturbed distal ciliary movements (Loges et al., 2018). *CCDC114* mutation causes the absence of the outer dynein arm in affected individuals, and majority of the cilia are static with few showing some stiff movements (Knowles et al., 2013; Onoufriadis et al., 2013). *DNAAF3* encodes a cytoplasmic dynein preassembly factor. Dynein preassembly factors play a crucial role for the assembly of both outer and inner dynein arms and dysfunction results in cilia lacking dynein arms, causing ciliary immotility (Mitchison et al., 2012). *DNAI1* and *DNAI2* encode outer dynein arm intermediate chains and dysfunction of these genes results in the absence of outer dynein arms causing immotile cilia or cilia with minimum residual motility (Guichard et al., 2001; Loges et al., 2008). *CCDC40* encodes a 96-nm ruler protein, and CCDC40 loss of function results in a disorganized microtubule arrangement and radial spokes and nexin link defects and absence of inner dynein arms. The respiratory cilia of the individuals carrying biallelic *CCDC40* loss of function variants show defective ciliary beat regulation and ciliary movements with a reduced amplitude (Becker-Heck et al., 2011). *CCDC39* likewise encodes a 96-nm ruler protein in motile cilia and dysfunction results in disorganized microtubules, defects in radial spokes, inner dynein arms, and nexin links,

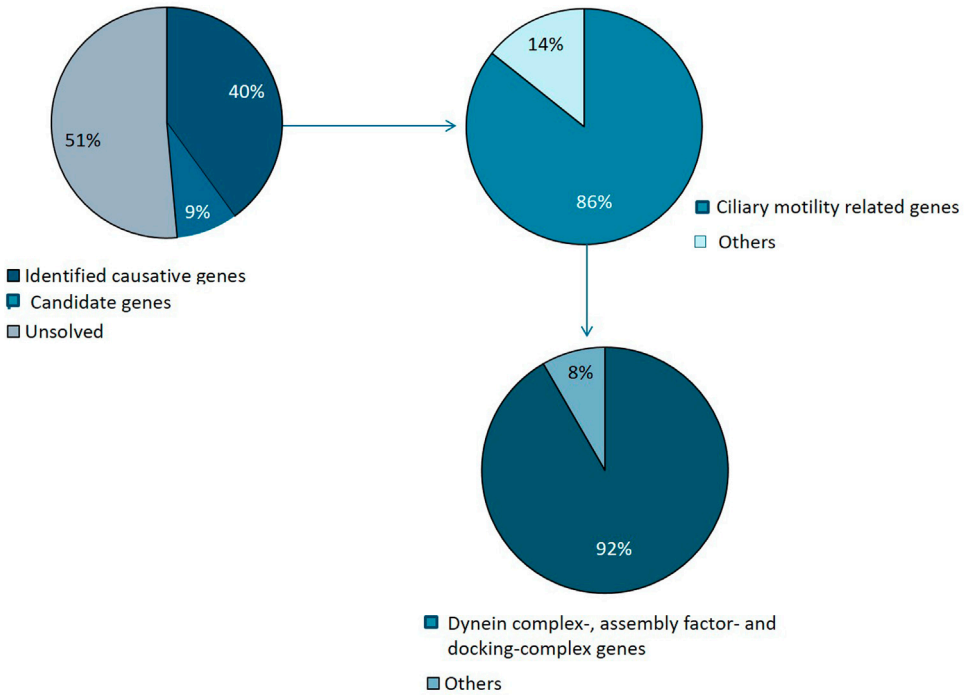

FIGURE 4 | Summary of genetic variants identified. Causative mutations were identified in 14 families and candidate variants in 3 families. The majority of identified variants were in ciliary genes, mainly encoding motility apparatus components, of which the majority represents dynein complex related factors.

similar to what is observed with dysfunction of CCDC40 (Merveille et al., 2011). Our findings confirm genetic PCD studies showing that *DNAH5* and *CCDC40* mutations represent common underlying causes (Fassad et al., 2020a).

We further identified candidate variants in *DNAH6* in *SI-15*. In humans, *DNAH6* encodes a heavy chain of the inner dynein arm (Hom et al., 2011). Li et al. suggested that *DNAH6* mutations play a role in laterality defects (Li et al., 2016) when they reported an individual with heterotaxy carrying a heterozygous *DNAH6* mutation and a heterozygous *DNAI1* mutation, suggesting digenic inheritance/genetic interaction. Moreover, 5/6 patients in their study with heterozygous *DNAH6* mutations also harbored heterozygous *DNAH5* mutations. The subthreshold double-morpholino knockdown of *DNAH6*/*DNAH5* and *DNAH6*/*DNAI1* in zebrafish resulted in likewise heterotaxy. Re-analyzing the exome data for potentially causative heterozygous mutations in *DNAI1* and *DNAH5* in SI-15 did not yield any new causative variants. Compound heterozygous mutations in *DNAH6* are also reported in patients with sperm flagella defects (Li et al., 2018; Tu et al., 2019).

The *PIFO* heterozygous variant we identified was previously reported to cause laterality defects in a single individual of Northern European descent (Kinzel et al., 2010). PIFO plays an important role in primary cilia disassembly through AuraA activation and it is localized at the basal body (Kinzel et al., 2010). The p.Arf80Lys variant seemed to inhibit AurA activation. Furthermore, overexpression caused cilia disassembly defects (Kinzel et al., 2010). In contrast to the previously described case, no liver or kidney cysts have been observed in our case to date; however, later development in life cannot be excluded and appropriate clinical monitoring has been initiated. Our study confirms that the identified *PIFO* variant is a rare cause of left–right pattern defects in humans, and it seems likely that future studies will reveal more disease-causing *PIFO* alleles.

PKD1L1 is a subunit of the heterodimeric TRP channel thought to regulate calcium currents (Delling et al., 2013) and is important for confining the NODAL expression to the left side during the left–right axis determination (Grimes et al., 2016). The PKD1L1 p.Arg2555* and p.Ser2646* variants we identified in this study are located at the extracellular domains before the trans-membrane domains 8 and 10 respectively (Rodriguez et al., 2019; Correa et al., 2021). These two compound heterozygous changes identified in this study could affect the function of trans-membrane domains 8–10, extracellular domains between them, and an intracellular coiled–coil domain, which interacts with PKD2. The PKD1L1 variants are similarly identified in other laterality defect cases at N-terminal extracellular domains preceding immunoglobulin-like PKD, REJ (receptor egg jelly), GPR (G-protein-coupled receptor proteolytic site), trans-membrane, and extracellular domains in the middle of the trans-membrane domains and intracellular C-terminal coiled–coil domain (Berauer et al., 2019; Rodriguez et al., 2019; Correa et al., 2021).

The association of *GJA1* with laterality defects or congenital heart disease remains unsure. *GJA1* encodes connexion 43 and is important for the formation of gap junction and inter cellular channels (Britz-Cunningham et al., 1995). Gap junctions could play an important role in the transfer of signals from the node to the lateral plate mesoderm in vertebrates (Saund et al., 2012). Britz-Cunningham et al. reported potentially disease-causing missense variants in *GJA1* in 6 patients with complex cardiac malformations and laterality defects (Britz-Cunningham et al., 1995). However, two later studies were not able to replicate these findings (Casey and Ballabio, 1995; Splitt et al., 1995). In 2001, Dasgupta et al. suggested that the inability to replicate the findings of the initial study could be caused by a PCR amplification bias toward the wild-type allele. Dasgupta et al. therefore used denaturing gradient gel electrophoresis (DGGE), followed by separate sequencing of two alleles and detected two heterozygous missense variants and 2 synonymous variants in eight individuals with hypoplastic left heart syndrome and one individual with atrioventricular canal defect. However, the four variants identified were identical to the pseudogene sequence at the nucleotide level (97% homology) (Dasgupta et al., 2001). Mutations in *GJA1* have further been identified in cases with autosomal recessive and dominant oculodentodigital dysplasia, where cardiac anomalies are rare (OMIM: 257850, 164200). Clinically, our cases did not exhibit features of oculodentodigital dysplasia, where about 50% of all cases represent *de novo* alleles.

Huang et al. could not confirm that *GJA1* dysfunction causes heart defects or left–right patterning defects in mice nor did they identify *GJA1* disease-causing variants in a cohort of 300 patients with congenital heart disease (Britz-Cunningham et al., 1995; Dasgupta et al., 2001; Huang et al., 2011). However, in a sudden infant death case, a *de novo* mutation in *GJA1* was detected and the patient tissue also demonstrated a mosaic expression of connexin43 (*GJA1*) (Van Norstrand et al., 2012). To our knowledge, no human cases with a laterality defect and a dominant *GJA1 de novo* variant have been described in the literature. The novel *GJA1* variant we identified (p.Pro334Leu) was located in the *UBQLN4* (ubiquilin 4)-binding region. The interaction of *GJA1* with this ubiquitin-like and ubiquitin-associated domain-containing protein is important for its homeostasis and function (Su et al., 2010). Putatively, the mutation could influence the *GJA1*–UBQLN4 interaction.

The variant of unknown significance in *ACVR2B* we identified in SI-47 represents the only variant we identified in a gene encoding for a nodal signaling pathway component. To date, less than ten cases with *ACVR2B* dominant variants have been reported (Kosaki et al., 1999; Ma et al., 2012; Li et al., 2019). Among those, the same variant (p.Arg40His) has been identified in four cases. Generally, mutations in *ACRV2B* seem to represent a rare cause of laterality defects (Ma et al., 2012). As we also identified a VUS in *CCDC39* in SI-47, the role of the *ACRV2B* variant we identified remains unclear.

To date, only few studies investigating cohorts of cases with laterality defects have been published and those have generally exhibited low mutation detection rates (**Table 1**), including a large study identifying pathogenic variants in just 25/323 cases (Li et al., 2019). Among non-PCD cases, mutations in *ZIC3* and *NODAL* appear to be the most common genetic causes (Li et al., 2019). In our cohort, the rate of detected likely disease-causing variants was somewhat higher (17 of 35 families (49%), potentially reflecting the large proportion of not previously clinically identified PCD cases and a high rate of consanguineous families in our series. The patients in our study were neither selected for the presence of additional symptoms indicating PCD nor tested for motile cilia dysfunction, but still we identified the majority of causative mutations in genes associated with the ciliary motility apparatus. This is in line with previous studies where 42% of congenital heart disease patients with heterotaxy defects that had a genetic cause were found to carry mutations in mucociliary clearance disorder genes (Nakhleh et al., 2012) as well as with a mouse recessive forward genetics screen for congenital heart defects (Li et al., 2015). Furthermore, mutation detection rates are higher among human PCD cases than isolated laterality defect cases (**Table 1**). Overall, dysfunction of proteins associated with ciliary motility seems to be responsible for the majority of human laterality defects where a monogenetic cause can be identified with the currently used genetic diagnostics methods (**Table 1**). Confirming previous studies, we find that mutations in genes encoding for dynein motor complex components make up a large proportion of identified genetic variants in genes associated with ciliary motility. None of the cases in our study carrying mutations in genes associated with PCD had previously been diagnosed with PCD underlines the importance of genetics for PCD diagnostics, especially when specialized PCD diagnostics are unavailable locally, as the diagnosis of PCD allows appropriate clinical management which can significantly alter the disease course (Storm van's Gravesande and Omran, 2005; Davis et al., 2019).

CONCLUSION

Our study provides a comprehensive list of laterality defect candidate genes based on human and animal studies. Future studies are needed to further validate candidate genes in regulating laterality patterning. In light of our findings, motile ciliary genes could be prioritized in laterality defect genetic screening studies. The overall low mutation detection rate in our laterality defect cohort (49%) and previous reports (**Table 1**) suggests the existence of non-coding monogenetic variants, genetic mosaicism within embryonic tissues or presence of epigenetic or environmental and non-genetic factors playing a significant role(s) in defective left-right patterning.

DATA AVAILABILITY STATEMENT

The datasets for this article are not publicly available due to concerns regarding participant/patient anonymity. Requests to access the datasets should be directed to the corresponding author.

ETHICS STATEMENT

The studies involving human participants were reviewed and approved by Innovative diagnostic program, Radboud UMC Nijmegen, Netherlands. Written informed consent to participate in this study was provided by the participants' legal guardian/next of kin.

AUTHOR CONTRIBUTIONS

DA, SJA, PW, RB, ZB, RB, LS, TVD, and MS performed experiments and analyzed data. EYG, AG, ICT and HB performed clinical evaluations. DA and MS wrote the manuscript. HGB critically revised the manuscript. All the authors read and approved the manuscript. MS supervised the study.

FUNDING

This study was funded by the European Research Council (ERC) (ERC starting grant to MS, grant No. 716344), the Deutsche Forschungsgemeinschaft (DFG, German Research Foundation)–Project-ID 431984000–SFB 1453) to MS, SJA, and PW and Radboud University Medical Center and Radboud University (Hypatia Research grant and Excellence Fellowship to MS). SJA acknowledges funding from the German Research Foundation (DFG) (AR 732/3-1, project grant AR 732/2-1). This study was supported by the Deutsche Forschungsgemeinschaft (DFG) under the Emmy Noether Programme (grant WA3365/2-1) to PW and under Germany's Excellence Strategy (CIBSS — EXC-2189 — project ID 390939984) to PW, SJA and MS.

ACKNOWLEDGMENTS

We thank all participating families and referring clinicians for their participation.

SUPPLEMENTARY MATERIAL

The Supplementary Material for this article can be found online at: https://www.frontiersin.org/articles/10.3389/fgene.2022.861236/full#supplementary-material

REFERENCES

Andjelkovic, M., Minic, P., Vreca, M., Stojiljkovic, M., Skakic, A., Sovtic, A., et al. (2018). Genomic Profiling Supports the Diagnosis of Primary Ciliary Dyskinesia and Reveals Novel Candidate Genes and Genetic Variants. *PLoS One* 13, e0205422. doi:10.1371/journal.pone.0205422

Antony, D., Brunner, H. G., and Schmidts, M. (2021). Ciliary Dyneins and Dynein Related Ciliopathies. *Cells* 10 (8), 1885. doi:10.3390/cells10081885

Bataille, S., Demoulin, N., Devuyst, O., Audrézet, M.-P., Dahan, K., Godin, M., et al. (2011). Association of PKD2 (Polycystin 2) Mutations with Left-Right Laterality Defects. *Am. J. Kidney Dis.* 58, 456–460. doi:10.1053/j.ajkd.2011.05.015

Becker-Heck, A., Zohn, I. E., Okabe, N., Pollock, A., Lenhart, K., B, Sullivan-Brown, J., et al. (2011). The Coiled-Coil Domain Containing Protein CCDC40 Is Essential For Motile Cilia Function And Left-Right Axis Formation. *Nature Genet.* 43, 79–84.

Berauer, J. P., Mezina, A. I., Okou, D. T., Sabo, A., Muzny, D. M., Gibbs, R. A., et al. (2019). Identification of Polycystic Kidney Disease 1 Like 1 Gene Variants in Children with Biliary Atresia Splenic Malformation Syndrome. *Hepatology* 70, 899–910. doi:10.1002/hep.30515

Blanchon, S., Legendre, M., Bottier, M., Tamalet, A., Montantin, G., Collot, N., et al. (2020). Deep Phenotyping, Including Quantitative Ciliary Beating Parameters, and Extensive Genotyping in Primary Ciliary Dyskinesia. *J. Med. Genet.* 57, 237–244. doi:10.1136/jmedgenet-2019-106424

Bolkier, Y., Barel, O., Marek-Yagel, D., Atias-Varon, D., Kagan, M., Vardi, A., et al. (2021). Whole-Exome Sequencing Reveals a Monogenic Cause in 56% of Individuals with Laterality Disorders and Associated Congenital Heart Defects. *J. Med. Genet.* doi:10.1136/jmedgenet-2021-107775

Boon, M., Wallmeier, J., Ma, L., Loges, N. T., Jaspers, M., Olbrich, H., et al. (2014). MCIDAS Mutations Result In A Mucociliary Clearance Disorder With Reduced Generation Of Multiple Motile Cilia. *Nat Commun.* 5, 4418. doi:10.1038/ncomms5418

Britz-Cunningham, S. H., Shah, M. M., Zuppan, C. W., and Fletcher, W. H. (1995). Mutations of the Connexin43 Gap-Junction Gene in Patients with Heart Malformations and Defects of Laterality. *N. Engl. J. Med.* 332, 1323–1330. doi:10.1056/nejm199505183322002

Capdevila, J., Vogan, K. J., Tabin, C. J., and Izpisúa Belmonte, J. C. (2000). Mechanisms of Left-Right Determination in Vertebrates. *Cell* 101, 9–21. doi:10.1016/s0092-8674(00)80619-4

Casey, B., and Ballabio, A. (1995). Connexin43 Mutations in Sporadic and Familial Defects of Laterality. *N. Engl. J. Med.* 333, 941–942. doi:10.1056/NEJM199510053331415

Chen, W., Zhang, Y., Yang, S., Shi, Z., Zeng, W., Lu, Z., et al. (2019). Bi-Allelic Mutations in NUP205 and NUP210 Are Associated with Abnormal Cardiac Left-Right Patterning. *Circ. Genom Precis Med.* 12, e002492. doi:10.1161/CIRCGEN.119.002492

Correa, A. R. E., Endrakanti, M., Naini, K., Kabra, M., and Gupta, N. (2021). Hydrops Fetalis in PKD1L1 -Related Heterotaxy: Report of Two Foetuses and Expanding the Phenotypic and Molecular Spectrum. *Ann. Hum. Genet.* 85, 138–145. doi:10.1111/ahg.12417

Cowan, J. R., Tariq, M., Shaw, C., Rao, M., Belmont, J. W., Lalani, S. R., et al. (2016). Copy Number Variation as a Genetic Basis for Heterotaxy and Heterotaxy-Spectrum Congenital Heart Defects. *Philos. Trans. R. Soc. Lond. B Biol. Sci.* 371 (1710), 20150406. doi:10.1098/rstb.2015.0406

Dasgupta, C., Martinez, A.-M., Zuppan, C. W., Shah, M. M., Bailey, L. L., and Fletcher, W. H. (2001). Identification of Connexin43 (α1) gap junction Gene Mutations in Patients with Hypoplastic Left Heart Syndrome by Denaturing Gradient Gel Electrophoresis (DGGE). *Mutat. Research/Fundamental Mol. Mech. Mutagenesis* 479, 173–186. doi:10.1016/s0027-5107(01)00160-9

Davis, S. D., Rosenfeld, M., Lee, H.-S., Ferkol, T. W., Sagel, S. D., Dell, S. D., et al. (2019). Primary Ciliary Dyskinesia: Longitudinal Study of Lung Disease by Ultrastructure Defect and Genotype. *Am. J. Respir. Crit. Care Med.* 199, 190–198. doi:10.1164/rccm.201803-0548oc

De Luca, A., Sarkozy, A., Consoli, F., Ferese, R., Guida, V., Dentici, M. L., et al. (2010). Familial Transposition of the Great Arteries Caused by Multiple Mutations in Laterality Genes. *Heart* 96, 673–677. doi:10.1136/hrt.2009.181685

Delling, M., Decaen, P. G., Doerner, J. F., Febvay, S., and Clapham, D. E. (2013). Primary Cilia Are Specialized Calcium Signalling Organelles. *Nature* 504, 311–314. doi:10.1038/nature12833

Deng, H., Xia, H., and Deng, S. (2015). Genetic Basis of Human Left-Right Asymmetry Disorders. *Expert Rev. Mol. Med.* 16, e19. doi:10.1017/erm.2014.22

Djakow, J., Kramná, L., Dušátková, L., Uhlík, J., Pursiheimo, J.-P., Svobodová, T., et al. (2016). An Effective Combination of Sanger and Next Generation

Sequencing in Diagnostics of Primary Ciliary Dyskinesia. *Pediatr. Pulmonol.* 51, 498–509. doi:10.1002/ppul.23261

Edelbusch, C., Cindrić, S., Dougherty, G. W., Loges, N. T., Olbrich, H., Rivlin, J., et al. (2017). Mutation of Serine/Threonine Protein Kinase 36 (STK36) Causes Primary Ciliary Dyskinesia with a Central Pair Defect. *Hum. Mutat.* 38, 964–969. doi:10.1002/humu.23261

Emiralioglu, N., Taskiran, E. Z., Kosukcu, C., Bilgic, E., Atilla, P., Kaya, B., et al. (2020). Genotype and Phenotype Evaluation of Patients with Primary Ciliary Dyskinesia: First Results from Turkey. *Pediatr. Pulmonol* 55, 383–393. doi:10.1002/ppul.24583

Fakhro, K. A., Choi, M., Ware, S. M., Belmont, J. W., Towbin, J. A., Lifton, R. P., et al. (2011). Rare Copy Number Variations In Congenital Heart Disease Patients Identify Unique Genes In Left-Right Patterning. *PNAS* 108, 2915–2920. doi:10.1073/pnas.1019645108

Fassad, M. R., Patel, M. P., Shoemark, A., Cullup, T., Hayward, J., Dixon, M., et al. (2020a). Clinical Utility of NGS Diagnosis and Disease Stratification in a Multiethnic Primary Ciliary Dyskinesia Cohort. *J. Med. Genet.* 57, 322–330. doi:10.1136/jmedgenet-2019-106501

Fassad, M. R., Shoman, W. I., Morsy, H., Patel, M. P., Radwan, N., Jenkins, L., et al. (2020b). Clinical and Genetic Spectrum in 33 Egyptian Families with Suspected Primary Ciliary Dyskinesia. *Clin. Genet.* 97, 509–515. doi:10.1111/cge.13661

Field, S., Riley, K.-L., Grimes, D. T., Hilton, H., Simon, M., Powles-Glover, N., et al. (2011). Pkd1l1 Establishes Left-Right Asymmetry and Physically Interacts with Pkd2. *Development* 138, 1131–1142. doi:10.1242/dev.058149

Fliegauf, M., Benzing, T., and Omran, H. (2007). When Cilia Go Bad: Cilia Defects and Ciliopathies. *Nat. Rev. Mol. Cel Biol* 8, 880–893. doi:10.1038/nrm2278

Gebbia, M., Ferrero, G. B., Pilia, G., Bassi, M. T., Aylsworth, A. S., Penman-Splitt, M., et al. (1997). X-Linked Situs Abnormalities Result from Mutations in ZIC3. *Nat. Genet.* 17, 305–308. doi:10.1038/ng1197-305

Gileles-Hillel, A., Mor-Shaked, H., Shoseyov, D., Reiter, J., Tsabari, R., Hevroni, A., et al. (2020). Whole-Exome Sequencing Accuracy in the Diagnosis of Primary Ciliary Dyskinesia. *ERJ Open Res.* 6 (4), 00213–02020. doi:10.1183/23120541.00213-2020

Grimes, D. T., and Burdine, R. D. (2017). Left-Right Patterning: Breaking Symmetry to Asymmetric Morphogenesis. *Trends Genet.* 33, 616–628. doi:10.1016/j.tig.2017.06.004

Grimes, D. T., Keynton, J. L., Buenavista, M. T., Jin, X., Patel, S. H., Kyosuke, S., et al. (2016). Genetic Analysis Reveals a Hierarchy of Interactions between Polycystin-Encoding Genes and Genes Controlling Cilia Function during Left-Right Determination. *Plos Genet.* 12, e1006070. doi:10.1371/journal.pgen.1006070

Guan, Y., Yang, H., Yao, X., Xu, H., Liu, H., Tang, X., et al. (2021). Clinical and Genetic Spectrum of Children with Primary Ciliary Dyskinesia in China. *Chest* 159, 1768–1781. doi:10.1016/j.chest.2021.02.006

Guichard, C., Harricane, M.-C., Lafitte, J.-J., Godard, P., Zaegel, M., Tack, V., et al. (2001). Axonemal Dynein Intermediate-Chain Gene (DNAI1) Mutations Result In Situs Inversus And Primary Ciliary Dyskinesia (Kartagener Syndrome). *Am. J. Hum. Genet.* 68, 1030–1035.

Guimier, A., Gabriel, G. C., Bajolle, F., Tsang, M., Liu, H., Noll, A., et al. (2015). MMP21 Is Mutated in Human Heterotaxy and Is Required for normal Left-Right Asymmetry in Vertebrates. *Nat. Genet.* 47, 1260–1263. doi:10.1038/ng.3376

Hom, E. F. Y., Witman, G. B., Harris, E. H., Dutcher, S. K., Kamiya, R., Mitchell, D. R., et al. (2011). A Unified Taxonomy for Ciliary Dyneins. *Cytoskeleton* 68, 555–565. doi:10.1002/cm.20533

Hornef, N., Olbrich, H., Horvath, J., Zariwala, M. A., Fliegauf, M., Loges, N. T., et al. (2006). DNAH5Mutations Are a Common Cause of Primary Ciliary Dyskinesia with Outer Dynein Arm Defects. *Am. J. Respir. Crit. Care Med.* 174, 120–126. doi:10.1164/rccm.200601-084oc

Huang, G.-Y., Xie, L.-J., Linask, K. L., Zhang, C., Zhao, X.-Q., Yang, Y. i., et al. (2011). Evaluating the Role of Connexin43 in Congenital Heart Disease: Screening for Mutations in Patients with Outflow Tract Anomalies and the Analysis of Knock-In Mouse Models. *J. Cardiovasc. Dis. Res.* 2, 206–212. doi:10.4103/0975-3583.89804

Jin, S. C., Homsy, J., Zaidi, S., Lu, Q., Morton, S., Depalma, S. R., et al. (2017). Contribution of Rare Inherited and De Novo Variants in 2,871 Congenital Heart Disease Probands. *Nat. Genet.* 49, 1593–1601. doi:10.1038/ng.3970

Juan, H., and Hamada, H. (2001). Roles of Nodal-Lefty Regulatory Loops in Embryonic Patterning of Vertebrates. *Genes Cells* 6, 923–930. doi:10.1046/j.1365-2443.2001.00481.x

Karkera, J. D., Lee, J. S., Roessler, E., Banerjee-Basu, S., Ouspenskaia, M. V., Mez, J., et al. (2007). Loss-of-Function Mutations in Growth Differentiation Factor-1 (GDF1) Are Associated with Congenital Heart Defects in Humans. *Am. J. Hum. Genet.* 81, 987–994. doi:10.1086/522890

Kawakami, Y., Raya, Á., Raya, R. M., Rodríguez-Esteban, C., and Belmonte, J. C. I. (2005). Retinoic Acid Signalling Links Left-Right Asymmetric Patterning and Bilaterally Symmetric Somitogenesis in the Zebrafish Embryo. *Nature* 435, 165–171. doi:10.1038/nature03512

Kinzel, D., Boldt, K., Davis, E. E., Burtscher, I., Trümbach, D., Diplas, B., et al. (2010). Pitchfork Regulates Primary Cilia Disassembly and Left-Right Asymmetry. *Develop. Cel* 19, 66–77. doi:10.1016/j.devcel.2010.06.005

Knowles, M. R., Leigh, M. W., Ostrowski, L. E., Huang, L., Carson, J. L., Hazucha, M. J., et al. (2013). Exome Sequencing Identifies Mutations in CCDC114 as a Cause of Primary Ciliary Dyskinesia. *Am. J. Hum. Genet.* 92, 99–106. doi:10.1016/j.ajhg.2012.11.003

Knowles, M. R., Zariwala, M., and Leigh, M. (2016). Primary Ciliary Dyskinesia. *Clin. Chest Med.* 37, 449–461. doi:10.1016/j.ccm.2016.04.008

Kosaki, R., Gebbia, M., Kosaki, K., Lewin, M., Bowers, P., Towbin, J. A., et al. (1999). Left-Right Axis Malformations Associated with Mutations inACVR2B, the Gene for Human Activin Receptor Type IIB. *Am. J. Med. Genet.* 82, 70–76. doi:10.1002/(sici)1096-8628(19990101)82:1<70::aid-ajmg14>3.0.co;2-y

Leigh, M. W., Horani, A., Kinghorn, B., O'Connor, M. G., Zariwala, M. A., and Knowles, M. R. (2019). Primary Ciliary Dyskinesia (PCD): A Genetic Disorder of Motile Cilia. *Transl Sci. Rare Dis.* 4, 51–75. doi:10.3233/trd-190036

Li, A. H., Hanchard, N. A., Azamian, M., D'Alessandro, L. C. A., Coban-Akdemir, Z., Lopez, K. N., et al. (2019). Genetic Architecture of Laterality Defects Revealed by Whole Exome Sequencing. *Eur. J. Hum. Genet.* 27, 563–573. doi:10.1038/s41431-018-0307-z

Li, L., Sha, Y. W., Xu, X., Mei, L. B., Qiu, P. P., Ji, Z. Y., et al. (2018). DNAH6 Is a Novel Candidate Gene Associated with Sperm Head Anomaly. *Andrologia* 50 (4), e12953. doi:10.1111/and.12953

Li, Y., Klena, N. T., Gabriel, G. C., Liu, X., Kim, A. J., Lemke, K., et al. (2015). Global Genetic Analysis in Mice Unveils central Role for Cilia in Congenital Heart Disease. *Nature* 521, 520–524. doi:10.1038/nature14269

Li, Y., Yagi, H., Onuoha, E. O., Damerla, R. R., Francis, R., Furutani, Y., et al. (2016). DNAH6 and its Interactions with PCD Genes in Heterotaxy and Primary Ciliary Dyskinesia. *Plos Genet.* 12, e1005821. doi:10.1371/journal.pgen.1005821

Lin, A. E., Krikov, S., Riehle-Colarusso, T., Frías, J. L., Belmont, J., Anderka, M., et al. (2014). Laterality Defects in the National Birth Defects Prevention Study (1998-2007): Birth Prevalence and Descriptive Epidemiology. *Am. J. Med. Genet.* 164, 2581–2591. doi:10.1002/ajmg.a.36695

Liu, C., Cao, R., Xu, Y., Li, T., Li, F., Chen, S., et al. (2018). Rare Copy Number Variants Analysis Identifies Novel Candidate Genes in Heterotaxy Syndrome Patients With Congenital Heart Defects. *Genome Med.* 10 (1), 40. doi:10.1186/s13073-018-0549-y

Liu, H., Giguet-Valard, A. G., Simonet, T., Szenker-Ravi, E., Lambert, L., Vincent-Delorme, C., et al. (2020). Next-Generation Sequencing in a Series of 80 Fetuses with Complex Cardiac Malformations And/or Heterotaxy. *Hum. Mutat.* 41, 2167–2178. doi:10.1002/humu.24132

Loges, N. T., Antony, D., Maver, A., Deardorff, M. A., Güleç, E. Y., Gezdirici, A., et al. (2018). Recessive DNAH9 Loss-Of-Function Mutations Cause Laterality Defects and Subtle Respiratory Ciliary-Beating Defects. *Am. J. Hum. Genet.* 103, 995–1008. doi:10.1016/j.ajhg.2018.10.020

Loges, N. T., Olbrich, H., Fenske, L., Mussaffi, H., Horvath, J., Fliegauf, M., et al. (2008). DNAI2 Mutations Cause Primary Ciliary Dyskinesia with Defects in the Outer Dynein Arm. *Am. J. Hum. Genet.* 83, 547–558. doi:10.1016/j.ajhg.2008.10.001

Ma, L., Selamet Tierney, E. S., Lee, T., Lanzano, P., and Chung, W. K. (2012). Mutations in ZIC3 and ACVR2B Are a Common Cause of Heterotaxy and Associated Cardiovascular Anomalies. *Cardiol. Young* 22, 194–201. doi:10.1017/s1047951111001181

Mani, R., Belkacem, S., Soua, Z., Chantot, S., Montantin, G., Tissier, S., et al. (2020). Primary Ciliary Dyskinesia Gene Contribution in Tunisia: Identification of a Major Mediterranean Allele. *Hum. Mutat.* 41, 115–121. doi:10.1002/humu.23905

Marshall, C. R., Scherer, S. W., Zariwala, M. A., Lau, L., Paton, T. A., Stockley, T., et al. (2015). Whole-Exome Sequencing and Targeted Copy Number Analysis

in Primary Ciliary Dyskinesia. *G3 (Bethesda)* 5, 1775–1781. doi:10.1534/g3.115.019851

Marszalek, J. R., Ruiz-Lozano, P., Roberts, E., Chien, K. R., and Goldstein, L. S. B. (1999). Situs Inversus and Embryonic Ciliary Morphogenesis Defects in Mouse Mutants Lacking the KIF3A Subunit of Kinesin-II. *Proc. Natl. Acad. Sci.* 96, 5043–5048. doi:10.1073/pnas.96.9.5043

McGrath, J., Somlo, S., Makova, S., Tian, X., and Brueckner, M. (2003). Two Populations of Node Monocilia Initiate Left-Right Asymmetry in the Mouse. *Cell* 114, 61–73. doi:10.1016/s0092-8674(03)00511-7

Meno, C., Shimono, A., Saijoh, Y., Yashiro, K., Mochida, K., Ohishi, S., et al. (1998). lefty-1 Is Required for Left-Right Determination as a Regulator of Lefty-2 and Nodal. *Cell* 94, 287–297. doi:10.1016/s0092-8674(00)81472-5

Merveille, A.-C., Davis, E. E., Becker-Heck, A., Legendre, M., Amirav, I., Bataille, G., et al. (2011). CCDC39 Is Required for Assembly of Inner Dynein Arms and the Dynein Regulatory Complex and for normal Ciliary Motility in Humans and Dogs. *Nat. Genet.* 43, 72–78. doi:10.1038/ng.726

Miller, S. A., Dykes, D. D., and Polesky, H. F. (1988). A Simple Salting Out Procedure for Extracting DNA from Human Nucleated Cells. *Nucl. Acids Res.* 16, 1215. doi:10.1093/nar/16.3.1215

Mitchison, H. M., Schmidts, M., Loges, N. T., Freshour, J., Dritsoula, A., Hirst, R. A., et al. (2012). Mutations In Axonemal Dynein Assembly Factor DNAAF3 Cause Primary Ciliary Dyskinesia. *Nature Genet.* 44, 381–389.

Mohapatra, B., Casey, B., Li, H., Ho-Dawson, T., Smith, L., Fernbach, S. D., et al. (2009). Identification and Functional Characterization of NODAL Rare Variants in Heterotaxy and Isolated Cardiovascular Malformations. *Hum. Mol. Genet.* 18, 861–871. doi:10.1093/hmg/ddn411

Nakhleh, N., Francis, R., Giese, R. A., Tian, X., Li, Y., Zariwala, M. A., et al. (2012). High Prevalence of Respiratory Ciliary Dysfunction in Congenital Heart Disease Patients with Heterotaxy. *Circulation* 125, 2232–2242. doi:10.1161/circulationaha.111.079780

Nonaka, S., Tanaka, Y., Okada, Y., Takeda, S., Harada, A., Kanai, Y., et al. (1998). Randomization of Left-Right Asymmetry Due to Loss of Nodal Cilia Generating Leftward Flow of Extraembryonic Fluid in Mice Lacking KIF3B Motor Protein. *Cell* 95, 829–837. doi:10.1016/s0092-8674(00)81705-5

Norris, D. P. (2012). Cilia, Calcium and the Basis of Left-Right Asymmetry. *BMC Biol.* 10, 102. doi:10.1186/1741-7007-10-102

Olbrich, H., Fliegauf, M., Hoefele, J., Kispert, A., Otto, E., Volz, A., et al. (2003). Mutations in a Novel Gene, NPHP3, Cause Adolescent Nephronophthisis, Tapeto-Retinal Degeneration and Hepatic Fibrosis. *Nat. Genet.* 34, 455–459. doi:10.1038/ng1216

Onoufriadis, A., Paff, T., Antony, D., Shoemark, A., Micha, D., Kuyt, B., et al. (2013). Splice-Site Mutations in the Axonemal Outer Dynein Arm Docking Complex Gene CCDC114 Cause Primary Ciliary Dyskinesia. *Am. J. Hum. Genet.* 92, 88–98. doi:10.1016/j.ajhg.2012.11.002

Paff, T., Kooi, I. E., Moutaouakil, Y., Riesebos, E., Sistermans, E. A., Daniels, H. J. M. A., et al. (2018). Diagnostic Yield of a Targeted Gene Panel in Primary Ciliary Dyskinesia Patients. *Hum. Mutat.* 39, 653–665. doi:10.1002/humu.23403

Paulussen, A. D. C., Steyls, A., Vanoevelen, J., Van Tienen, F. H., Krapels, I. P. C., Claes, G. R., et al. (2016). Rare Novel Variants in the ZIC3 Gene Cause X-Linked Heterotaxy. *Eur. J. Hum. Genet.* 24, 1783–1791. doi:10.1038/ejhg.2016.91

Pennekamp, P., Karcher, C., Fischer, A., Schweickert, A., Skryabin, B., Horst, J., et al. (2002). The Ion Channel Polycystin-2 Is Required for Left-Right axis Determination in Mice. *Curr. Biol.* 12, 938–943. doi:10.1016/s0960-9822(02)00869-2

Pennekamp, P., Menchen, T., Dworniczak, B., and Hamada, H. (2015). Situs Inversus and Ciliary Abnormalities: 20 Years Later, what Is the Connection? *Cilia* 4, 1. doi:10.1186/s13630-014-0010-9

Plagnol, V., Curtis, J., Epstein, M., Mok, K. Y., Stebbings, E., Grigoriadou, S., et al. (2012). A Robust Model for Read Count Data in Exome Sequencing Experiments and Implications for Copy Number Variant Calling. *Bioinformatics* 28, 2747–2754. doi:10.1093/bioinformatics/bts526

Postema, M. C., Carrion-Castillo, A., Fisher, S. E., Vingerhoets, G., and Francks, C. (2020). The Genetics of Situs Inversus without Primary Ciliary Dyskinesia. *Sci. Rep.* 10, 3677. doi:10.1038/s41598-020-60589-z

Rodriguez, S., Chaturvedi, R., Blanchette, V., Dell, S., Axford, M., Cada, M., et al. (2019). PKD1L1-Related Situs Inversus Associated with Sideroblastic Anemia. *Clin. Genet.* 95, 629–630. doi:10.1111/cge.13512

Saund, R. S., Kanai-Azuma, M., Kanai, Y., Kim, I., Lucero, M. T., and Saijoh, Y. (2012). Gut Endoderm Is Involved in the Transfer of Left-Right Asymmetry from the Node to the Lateral Plate Mesoderm in the Mouse Embryo. *Development* 139, 2426–2435. doi:10.1242/dev.079921

Sempou, E., and Khokha, M. K. (2019). Genes and Mechanisms of Heterotaxy: Patients Drive the Search. *Curr. Opin. Genet. Develop.* 56, 34–40. doi:10.1016/j.gde.2019.05.003

Shamseldin, H. E., Al Mogarri, I., Alqwaiee, M. M., Alharbi, A. S., Baqais, K., Alsaadi, M., et al. (2020). An Exome-First Approach to Aid in the Diagnosis of Primary Ciliary Dyskinesia. *Hum. Genet.* 139, 1273–1283. doi:10.1007/s00439-020-02170-2

Shiratori, H., and Hamada, H. (2006). The Left-Right Axis in the Mouse: from Origin to Morphology. *Development* 133, 2095–2104. doi:10.1242/dev.02384

Simons, M., Gloy, J., Ganner, A., Bullerkotte, A., Bashkurov, M., Krönig, C., et al. (2005). Inversin, the Gene Product Mutated in Nephronophthisis Type II, Functions as a Molecular Switch between Wnt Signaling Pathways. *Nat. Genet.* 37, 537–543. doi:10.1038/ng1552

Splitt, M. P., Burn, J., and Goodship, J. (1995). Connexin43 Mutations in Sporadic and Familial Defects of Laterality. *N. Engl. J. Med.* 333, 941–942. doi:10.1056/NEJM199510053331415

Storm Van's Gravesande, K., and Omran, H. (2005). Primary Ciliary Dyskinesia: Clinical Presentation, Diagnosis and Genetics. *Ann. Med.* 37, 439–449. doi:10.1080/07853890510011985

Su, V., Nakagawa, R., Koval, M., and Lau, A. F. (2010). Ubiquitin-Independent Proteasomal Degradation of Endoplasmic Reticulum-Localized Connexin43 Mediated by CIP75. *J. Biol. Chem.* 285, 40979–40990. doi:10.1074/jbc.m110.170753

Ta-Shma, A., Hjeij, R., Perles, Z., Dougherty, G. W., Abu Zahira, I., Letteboer, S. J. F., et al. (2018). Homozygous Loss-Of-Function Mutations in MNS1 Cause Laterality Defects and Likely Male Infertility. *Plos Genet.* 14, e1007602. doi:10.1371/journal.pgen.1007602

Takeuchi, K., Kitano, M., Kiyotoshi, H., Ikegami, K., Ogawa, S., Ikejiri, M., et al. (2018). A Targeted Next-Generation Sequencing Panel Reveals Novel Mutations in Japanese Patients with Primary Ciliary Dyskinesia. *Auris Nasus Larynx* 45, 585–591. doi:10.1016/j.anl.2017.09.007

Tamplin, O. J., Kinzel, D., Cox, B. J., Bell, C. E., Rossant, J., and Lickert, H. (2008). Microarray Analysis of Foxa2 Mutant Mouse Embryos Reveals Novel Gene Expression and Inductive Roles for the Gastrula Organizer and its Derivatives. *BMC Genomics* 9, 511. doi:10.1186/1471-2164-9-511

Tan, S. Y., Rosenthal, J., Zhao, X. Q., Francis, R. J., Chatterjee, B., Sabol, S. L., et al. (2007). Heterotaxy and Complex Structural Heart Defects in a Mutant Mouse Model of Primary Ciliary Dyskinesia. *J. Clin. Invest.* 117, 3742–3752. doi:10.1172/JCI33284

Tanaka, Y., Okada, Y., and Hirokawa, N. (2005). FGF-Induced Vesicular Release of Sonic Hedgehog and Retinoic Acid in Leftward Nodal Flow Is Critical for Left-Right Determination. *Nature* 435, 172–177. doi:10.1038/nature03494

Tu, C., Nie, H., Meng, L., Yuan, S., He, W., Luo, A., et al. (2019). Identification of DNAH6 Mutations in Infertile Men with Multiple Morphological Abnormalities of the Sperm Flagella. *Sci. Rep.* 9, 15864. doi:10.1038/s41598-019-52436-7

Van Norstrand, D. W., Asimaki, A., Rubinos, C., Dolmatova, E., Srinivas, M., Tester, D. J., et al. (2012). Connexin43 Mutation Causes Heterogeneous Gap Junction Loss and Sudden Infant Death. *Circulation* 125, 474–481. doi:10.1161/circulationaha.111.057224

Vetrini, F., D'Alessandro, L. C. A., Akdemir, Z. C., Braxton, A., Azamian, M. S., Eldomery, M. K., et al. (2016). Bi-Allelic Mutations in PKD1L1 Are Associated with Laterality Defects in Humans. *Am. J. Hum. Genet.* 99, 886–893. doi:10.1016/j.ajhg.2016.07.011

Wallmeier, J., Al-Mutairi, D. A., Chen, C.-T., Loges, N. T., Pennekamp, P., Menchen, T., et al. (2014). Mutations in CCNO Result in Congenital Mucociliary Clearance Disorder with Reduced Generation of Multiple Motile Cilia. *Nat. Genet.* 46, 646–651. doi:10.1038/ng.2961

Conflict of Interest: The authors declare that the research was conducted in the absence of any commercial or financial relationships that could be construed as a potential conflict of interest.

Publisher's Note: All claims expressed in this article are solely those of the authors and do not necessarily represent those of their affiliated organizations, or those of the publisher, the editors, and the reviewers. Any product that may be evaluated in this article, or claim that may be made by its manufacturer, is not guaranteed or endorsed by the publisher.

frontiers | Frontiers in Genetics

ORIGINAL RESEARCH
published: 22 June 2022
doi: 10.3389/fgene.2022.922287

Novel *RSPH4A* Variants Associated With Primary Ciliary Dyskinesia–Related Infertility in Three Chinese Families

Lin Wang[1,2,3†], *Rongchun Wang*[1,2,3†], *Danhui Yang*[1,2,3], *Chenyang Lu*[1,2,3], *Yingjie Xu*[1,2,3], *Ying Liu*[1,2,3], *Ting Guo*[1,2,3], *Cheng Lei*[1,2,3]* and *Hong Luo*[1,2,3]*

[1]*Department of Pulmonary and Critical Care Medicine, The Second Xiangya Hospital, Central South University, Changsha, China,* [2]*Research Unit of Respiratory Disease, Central South University, Changsha, China,* [3]*Hunan Diagnosis and Treatment Center of Respiratory Disease, Changsha, China*

OPEN ACCESS

Edited by:
Steven LC Pei,
Yale University, United States

Reviewed by:
Martin Breuss,
University of Colorado, United States
Lance Lee,
Sanford Research, United States

***Correspondence:**
Cheng Lei
leicheng@csu.edu.cn
Hong Luo
luohonghuxi@csu.edu.cn

[†]*These authors have contributed equally to this work*

Specialty section:
This article was submitted to Human and Medical Genomics, a section of the journal Frontiers in Genetics

Received: *17 April 2022*
Accepted: *02 May 2022*
Published: *22 June 2022*

Citation:
Wang L, Wang R, Yang D, Lu C, Xu Y, Liu Y, Guo T, Lei C and Luo H (2022) Novel RSPH4A Variants Associated With Primary Ciliary Dyskinesia–Related Infertility in Three Chinese Families. Front. Genet. 13:922287. doi: 10.3389/fgene.2022.922287

Background: The radial spoke head component 4A (*RSPH4A*) is involved in the assembly of radial spokes, which is essential for motile cilia function. Asthenoteratozoospermia in primary ciliary dyskinesia (PCD) related to *RSPH4A* variants has not been reported.

Materials and Methods: *RSPH4A* variants were identified and validated using whole-exome and Sanger sequencing in three unrelated Chinese families. High-speed video microscopy analysis (HSVA) was performed to measure the beating frequency and pattern of nasal cilia of the patients and healthy control. Papanicolaou staining and computer-aided sperm analysis were performed to analyze the morphology and motility of the sperm in patient 1. Immunofluorescence was adopted to confirm the structure deficiency of sperm and nasal cilia.

Results: Patient 1 from family 1 is a 22-year-old unmarried male presented with bronchiectasis. Semen analysis and sperm Papanicolaou staining confirmed asthenoteratozoospermia. Novel compound heterozygous *RSPH4A* variants c.2T>C, p.(Met1Thr) and c.1774_1775del, p.(Leu592Aspfs*5) were detected in this patient. Patients 2 and 3 are from two unrelated consanguineous families; they are both females and exhibited bronchiectasis and infertility. Two homozygous *RSPH4A* variants c.2T>C, p.(Met1Thr) and c.351dupT, p.(Pro118Serfs*2) were detected, respectively. HSVA showed that most of the cilia in patients 1 and 3 were with abnormal rotational movement. The absence of RSPH4A and RSPH1 in patient 1's sperm and patient 3's respiratory cilia was indicated by immunofluorescence. Patient 2 died of pulmonary infection and respiratory failure at the age of 35 during follow-up.

Conclusion: Dysfunctional sperm flagellum and motile cilia in the respiratory tract and the fallopian tube were found in patients with *RSPH4A* variants. Our study enriches the genetic spectrum and clinical phenotypes of *RSPH4A* variants in PCD, and c.2T>C, p.(Met1Thr) detected in our patients may be a hotspot *RSPH4A* variant in Chinese.

Keywords: primary ciliary dyskinesia, RSPH4A, infertility, asthenoteratozoospermia, MMAF, bronchiectasis

INTRODUCTION

Primary ciliary dyskinesia (PCD) is an autosomal recessive inherited disease, characterized by motile ciliary dysfunction (Mirra et al., 2017). The clinical manifestations of primary ciliary dyskinesia are varied including chronic upper and lower respiratory tract disease, left-right laterality defects, and infertility (Goutaki et al., 2016). Until now, more than 50 PCD-related pathogenic genes have been identified (Wallmeier et al., 2020).

Each radial spoke dimer contains at least 23 proteins and plays roles in controlling the activity of the dynein arm (Yang et al., 2006). As dynein serves as a molecular motor and the radial spoke complex functions as a mechanochemical senor underpinning the flagellar motility, the disruption of these axonemal components can therefore compromise the motility-related signal transmission and cause asthenospermia (Zhang et al., 2021). The radial spoke head component 4A (*RSPH4A*) is involved in the assembly of radial spokes, which is essential for motile cilia function. The genes belong to the radial spoke complex which is related to PCD including *DNAJB13*, *RSPH1, RSPH9, RSPH3,* and *RSPH4A* (Castleman et al., 2009; Wallmeier et al., 2020). Variants in *RSPH1, RSPH3,* and *RSPH9* genes have been reported to cause male infertility in humans (Reish et al., 2010; Knowles et al., 2014; Jeanson et al., 2015). However, the phenotype of the spermatozoa in patients with *RSPH4A* variants has not been reported.

In this study, we identified three novel *RSPH4A* variants in patients. We first demonstrated asthenoteratozoospermia was related to *RSPH4A* variants and reported two infertile female patients caused by *RSPH4A* variants.

CASE PRESENTATION

Three patients with *RSPH4A* variants were presented in our study. Patient 1 was a 22-year-old male from a non-consanguineous family I (**Figure 1A**). Patient 2 was a 34-year-old female from a consanguineous family II. Patient 3 was a 45-year-old female from a consanguineous family III. They all presented over 10 years of history of chronic cough, daily nasal congestion, and yellowish purulent (**Table 1**). High-resolution computed tomography (HRCT) showed bronchiectasis in all patients (**Figure 1B**). The nasal nitric oxide level was markedly reduced both in patient 1 (24.6 nl/

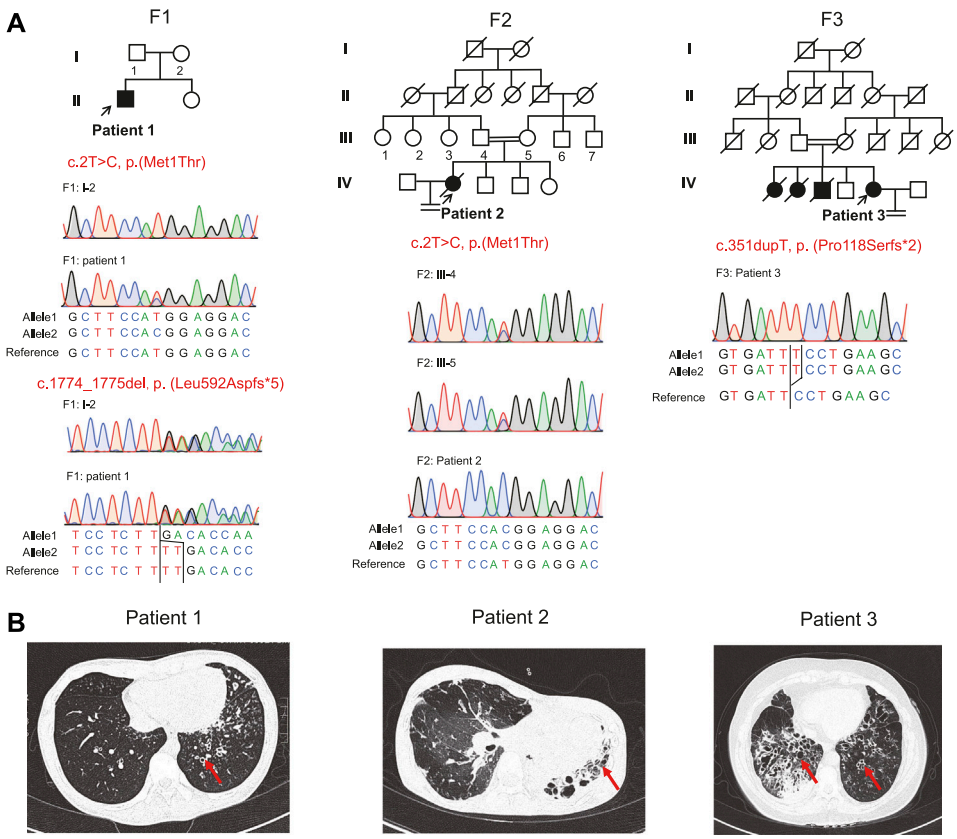

FIGURE 1 | Pedigrees, variants, and clinical features of these patients. **(A)** Pedigrees of three families (F1, F2, and F3) with *RSPH4A* variants and the segregation analysis by Sanger sequencing. The filled symbol represents the affected member, the empty symbol represents unaffected members, and the slashed symbols represent deceased members. Squares, males; circles, females. The patients (patient 1, patient 2, and patient 3) included in this study are indicated by a black arrow. **(B)** Chest high-resolution computed tomography showed bronchiectasis (red arrows) in these patients.

TABLE 1 | Summary of the clinical features of three patients with PCD.

Characteristic	Patient 1	Patient 2	Patient 3
Sex	Male	Female	Female
Age at diagnosis (years)	22	34	45
Onset	Childhood	Childhood	Childhood
Consanguinity	No	Yes	Yes
Inbreeding coefficient	NA	1/16	1/16
Lung high-resolution CT	Bronchiectasis	Bronchiectasis	Bronchiectasis
Fertility problems	Asthenoteratozoospermia	Yes	Yes
Sinuses CT	Sinusitis	NA	Sinusitis
Smell problem	No	No	Yes
Hearing problems	No	No	No
FEV1% prediction (%)	74.0	NA	45.0
FEV1/FVC (%)	75.0	NA	60.6
Nasal nitric oxide (nl/min)[a]	24.6	6.6	NA
Ciliary beat frequency (Hz)[b]	7.22 ± 1.93	NA	11.44 ± 1.21

NA, not available.

[a]*The nasal nitric oxide of the normal control is greater than 77 nl/min (Collins et al., 2014).*

[b]*The ciliary beat frequency of the normal control is 10.08 ± 1.60 Hz.*

min) and patient 2 (6.6 nl/min). Patient 1 was unmarried, but the semen analysis showed asthenoteratozoospermia. Both patients 2 and 3 exhibited infertility. Because of the failure to achieve pregnancy, their husbands had completed the fertility examination, and the semen test results were both reported to be normal. Patient 2 died of pulmonary infection and respiratory failure at 35 years of age during follow-up. Two sisters of patient 3 died when they were 1 year old due to repeated pulmonary infection and respiratory failure. One of the older brothers of patient 3 also presented over 10 years of history of chronic cough, daily nasal congestion, and yellowish purulent and died at 37 years of age for the same reason. All family members had no situs inversus reported.

MATERIALS AND METHODS

Ethical Compliance

This study was approved by the Review Board of the Second Xiangya Hospital of Central South University in China. Written informed consent was obtained from all participants.

DNA Extraction, Whole-Exome Sequencing, and Variant Calling

We collected blood samples from the patients and their family members, which were obtained with informed consent. According to the manufacturer's instructions, we used the QIAamp DNA Blood Mini Kit (250) (Cat #51106; QIAGEN, Valencia, CA, United States) to extract genomic DNA. As previously described, whole-exome capture and high-throughput sequencing were performed (Guo et al., 2017). Briefly, the genomic DNA of the patient was captured with the Agilent SureSelect Human All Exon V6 Kit (Agilent, CA, United States) and sequenced on Illumina Hiseq 4000 (Illumina Inc., San Diego, United States). After quality control, the sequencing reads were aligned to the NCBI human reference genome (GRCh37/hg19) by the bwa v7.1.0-r789 (RRID: SCR_010910) (Li and Durbin, 2010). GATK4.0.3.0 (RRID: SCR_001876) was used to call variants, and the variants were annotated with ANNOVAR (RRID: SCR_012821) (Wang et al., 2010; Van der Auwera et al., 2013).

Variant Filtering and *In Silico* Analysis

We filtered single-nucleotide variants (SNVs) and short insertions and deletions (InDels) as follows: *1*) we ruled out high-frequency variants (minor allele frequency >0.01) in the 1000 Genomes Project data set (RRID: SCR_008801), NHLBI Exome Sequencing Project Exome Variant Server (RRID: SCR_012761), Genome Aggregation Database (all datasets and East Asian population datasets of gnomAD v2.1.1 RRID: SCR_014964 genome database), and the inhouse database of Novogene. *2*) Noncoding and intronic variants were filtered. *3*) Synonymous missense variants were excluded. *4*) Homozygous or compound heterozygous variants were retained *5*) Disease-related variants were identified by a PCD or PCD-candidate gene list collected from the literature (Lei et al., 2022).

Sanger Sequencing

We adopted Sanger sequencing to validate the variants in the patients. An online tool (PrimerQuest, IDT, https://sg.idtdna.com/PrimerQuest) was used to design primers. The primer sequences used for Sanger sequencing are listed in **Supplementary Table S1**. PCR products were sequenced by using the ABI PRISM 3730 DNA Analyzer (RIDD: SCR_021899) using the BigDye Terminator v3.1 Cycle Sequencing Kit (Cat #4337454; Thermo Scientific).

Semen Analysis and Immunostaining of the Sperm and Cilia

Semen sample was collected *via* masturbation from patient 1 after 5 days of sexual abstinence. To obtain the sperm smears, we used a saline solution to wash, centrifuge, and smear spermatozoa from patient 1 and the fertile control individual and fixed in 4%

paraformaldehyde. We performed semen evaluation with semen parameters, according to the World Health Organization guideline (Cooper et al., 2010). On the basis of Papanicolaou staining, morphological abnormalities of the flagella were classified as absent, short, bent, coiled, or irregular width (Ben Khelifa et al., 2014). The percentages of morphologically normal and abnormal spermatozoa were assessed according to the WHO guidelines (Sánchez-Álvarez et al., 2010). Immunostaining of the slides was performed, as described previously (Dai et al., 2019). Sperm smears were incubated with primary antibodies: RSPH4A (Cat# HPA031196, RRID: AB_10601612; 1:25; Sigma-Aldrich), RSPH1 (Cat# HPA017382, RRID: AB_1858392; 1:25; Sigma-Aldrich), and anti-acetylated tubulin monoclonal antibody (Cat# T7451, RRID: AB_609894; 1:500; Sigma-Aldrich) for 2 h at 37°C. The binding of the antibodies was detected by incubating with Alexa Fluor 488 anti-mouse IgG (Cat# A-21121, RRID: AB_2535764; 1:400; Molecular Probes) and Alexa Fluor 555 anti-rabbit IgG (Cat# A-31572, RRID: AB_162543; 1:500; Molecular Probes) for 1 h at 37°C. Subsequently, the sperm smears were stained with 4',6-diamidino-2-phenylindole (DAPI) for 5 min. Finally, they were viewed using an Olympus BX53 microscope (Olympus, Tokyo, Japan) and a scientific complementary metal-oxide semiconductor (sCMOS) camera (Prime BSI; Teledyne Photometrics Inc., United States). Nasal brushing samples from patient 3 were suspended in Gibco Medium 199 (12350039; Gibco). We used an anti-acetylated tubulin monoclonal antibody (Cat# T7451, RRID: AB_609894; 1:500; Sigma-Aldrich) to mark the ciliary axoneme, RSPH4A (Cat# HPA031196, RRID: AB_10601612; 1:100; Sigma-Aldrich) and RSPH1 (Cat# HPA017382, RRID: AB_1858392; 1:100; Sigma-Aldrich) to label the radial spoke in the ciliary axoneme and DAPI to label the nuclei. Immunofluorescence was employed to profile the ciliary structure of patients with *RSPH4A* variants.

High-Speed Microscopy Analysis

Nasal brush biopsy samples from patients 1 and 3 were suspended in Gibco Medium 199 (12350039 Gibco). An Upright Olympus BX53 microscope (Olympus, Tokyo, Japan) with a ×40 objective lens was used to image strips of the ciliated epithelium. We recorded videos by using a scientific complementary metal-oxide semiconductor (sCMOS) camera (Prime BSI; Teledyne Photometrics Inc., United States) at a rate of 500 frames per second (fps) at room temperature and reviewed at 50 fps to perform an analysis of the ciliary beat pattern, as described previously (Lei et al., 2022). Six separate ciliated epithelium strips (five sideway edges and one from above) with mucus-free regions from the subject were analyzed. The ciliary beat frequency was calculated using the validated automated open-source software CiliarMove (Sampaio et al., 2021).

RESULTS

Identification of the *RSPH4A* Variants

Novel compound heterozygous variants c.2T>C, p.(Met1Thr) and c.1774_1775del, p.(Leu592Aspfs*5), a homozygous stat loss variant c.2T>C, p.(Met1Thr), and a novel frame-shift variant c.351dupT, p.(Pro118Serfs*2) in *RSPH4A* (NM_001010892.3) were identified in Proband 1, 2, and 3 through whole-exome sequencing. We did not identify these variants in the 1000 Genomes Project data set and NHLBI Exome Sequencing Project Exome Variant Server, gnomAD v2.1.1 database, and the Human Gene Mutation Database. Sanger sequencing validated the variants in this patient (**Figure 1A**). These variants were classified into pathogenic or likely pathogenic (**Table 2**), according to the ACMG guidelines.

Motile Cilia Analysis and Immunofluorescence of Nasal Epithelial Cilia

Rotational movement of the cilia was observed in patients 1 and 3 (**Figure 2A** and **Supplementary Videos S1 and S2**), while planar beating was observed in the healthy control (**Supplementary Video S3**). High-speed video microscopy analysis of nasal brush biopsy samples indicated that the nasal epithelial ciliary beat frequency of patients 1 and 3 with *RSPH4A* variants was not significantly different from the healthy control (**Table1**). Immunofluorescence of the nasal epithelial ciliary in patient 3 with *RSPH4A* variants showed both RSPH4A and RSPH1 were absent (**Figure 2B**).

Sperm Morphology and Immunofluorescence Analysis

The abnormalities of sperm morphology were revealed by Papanicolaou staining. Although there were also some spermatozoa with seemingly normal morphology, Papanicolaou staining showed morphological abnormalities in patient 1's sperm, including absent, bent, coiled, and short flagella, compared with the control individual (**Figure 3A**). The absent, bent, coiled, and short flagella, respectively, accounted for 11.5, 16.8, 49, and 9.5% in patient 1's sperm (n = 200; **Table 3**). We conducted semen analysis according to the WHO guidelines (**Table 3**) and concluded that the patient had asthenoteratospermia given the abnormal morphology of the sperm (Auger et al., 2016). To confirm abnormalities in the axonemal or peri-axonemal structures of the sperm flagella of patient 1, we performed immunostaining. In patient 1's spermatozoa, the staining signal of RSPH4A was undetectable compared with the normal control (**Figure 3B**). Moreover, we also could not detect the staining signal of RSPH1 in the sperm of patient 1 (**Figure 3B**).

Summary of Clinical and Functional Phenotypes of Patients With *RSPH4A* Variants

After a comprehensive literature search, 45 patients with *RSPH4A* biallelic pathogenic variants were identified (Ziętkiewicz et al., 2012; Daniels et al., 2013; Casey et al., 2015; Frommer et al., 2015; Emiralioğlu et al., 2020; De Jesús-Rojas et al., 2021) (**Figure 4**, **Supplementary Table S2**). About half of the 45 patients with *RSPH4A* variants are Hispanic (21/45), and 15 patients are from consanguineous families. There are 31 females (31/45) and 13

TABLE 2 | RSPH4A variants identified by exome sequencing for the three families.

Family	Gene	HGVS	Amino acid change	GnomAD frequency	MutationTaster	SIFT	PolyPhen-2	CADD	ACMG criterion	ACMG classification
1	*RSPH4A*	N M_001010892.3: c.1774_1775del	p.(Leu592Aspfs*5)	0	NA	NA	NA	NA	PVS1+PM2+PP5	Pathogenic
1	*RSPH4A*	NM_001010892.3: c.2T>C	p.(Met1Thr)	0	Disease-causing	Damaging	Probably damaging	24.0	PVS1+PM2+PM3	Pathogenic
2	*RSPH4A*	NM_001010892.3: c.2T>C	p.(Met1Thr)	0	Disease-causing	Damaging	Probably damaging	24.0	PVS1+PM2+PM3	Pathogenic
3	*RSPH4A*	NM_001010892.3: c.351dupT	p.(Pro118Serfs*2)	0	NA	NA	NA	NA	PVS1+PM2	Likely pathogenic

The variant c.2T>C was found both in patient 1 and patient 2. NA, not available; HGVS, human genome variation society; SIFT, Sorting Intolerant from Tolerant; CADD, Combined Annotation Dependent Depletion score; ACMG, American College of Medical Genetics.

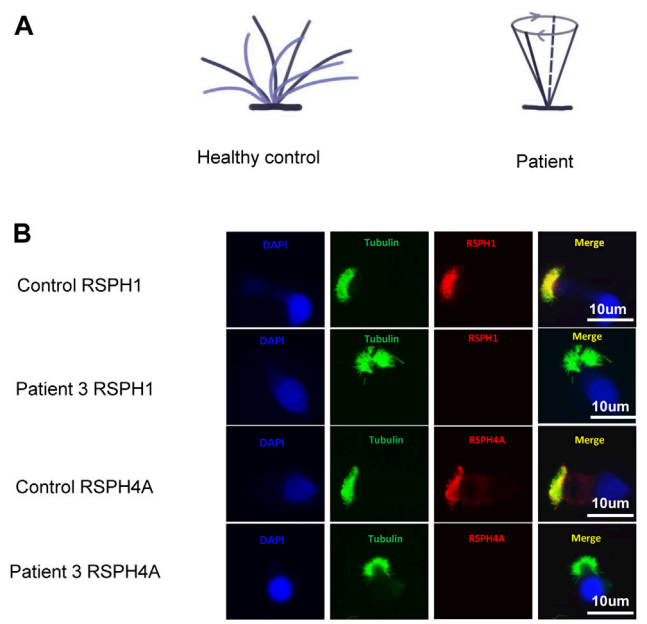

FIGURE 2 | (A) Ciliary beating patterns of healthy cilia and our patients with *RSPH4A* variants. **(B)** Immunofluorescence of nasal ciliated cells revealed the absence of RSPH4A and RSPH1 in patient 3 (red). An anti-acetylated tubulin monoclonal antibody was used to mark the ciliary axoneme (green), and DAPI was used to label the nuclei (blue).

adult patients (≥18 years old, 13/45). Situs inversus is not present in all patients. Only one female patient reported infertility. The nasal nitric oxide production rate was markedly reduced in all 15 patients. A stiff and rotatory beating pattern of HSVA was presented in 11 patients with *RSPH4A* deficiency. Central apparatus abnormalities or normal ciliary ultrastructure were shown in the TEM analysis of respiratory cilia.

DISCUSSION

This study describes one male and two females with PCD that carried biallelic disease-causing variants in the *RSPH4A* gene. Our cases enrich the variant spectrum and clinical phenotypes of *RSPH4A* variants in PCD.

According to our summary, no situs inversus was reported in patients with *RSPH4A* variants, and the nasal nitric oxide level was low. This is consistent with the clinical manifestations of the three patients in our study. In the *rsph4a* knock-out zebrafish model, there is no situs inversus, which may be related to the "9+0" structure of embryonic nodes without radial spokes, while other motile cilia are of the "9+2" structure (Han et al., 2018). Among the spoke head-related genes, variants of *RSPH4A* lead to the most severe phenotype on the cilia ultrastructure in the PCD patients (Daniels et al., 2013; Knowles et al., 2014). The absence of RSPH4A results in the deficient axonemal assembly of radial spoke head components RSPH1 and RSPH9 (Frommer et al., 2015). Therefore, it is probable that patients with *RSPH4A* variants presented the most serious clinical manifestations among the patients with radial spoke family deficiency. As previously reported, a male patient with the *RSPH4A* variant died at the age of 27 because of respiratory failure caused by pulmonary infection (Bian et al., 2021). In this study, patient 2 also died at the age of 35 because of respiratory failure.

The nasal cilia HSVA of patients with *RSPH4A* variants presented a reduced amplitude and rotatory beating pattern. The HSVA of motile cilia in the airway of the *Rsph4a* knock-out mouse presented rotational movement, which may be caused by the deficiency of radial spokes (Shinohara et al., 2015). The HSVA of our patients 1 and 3 showed rotational movement, and the nasal epithelial ciliary beat frequency was in the normal range. Among previously reported patients, the transmission electron microscope examination of respiratory cilia presented with central apparatus abnormalities and a normal structure. However, because of the COVID-19 epidemic situation, these patients are not able to finish the transmission electron microscope examination. According to European Respiratory Society guidelines (Lucas et al., 2017), we confirmed the diagnosis of PCD by the detection of biallelic variants or a low nasal nitric oxide level combined with the characteristic HSVA presentation of the nasal cilia.

One splicing variant, seven missense variants, two frame-shift variants, and two nonsense variants have been reported (**Supplementary Table S2**). The most reported variant was

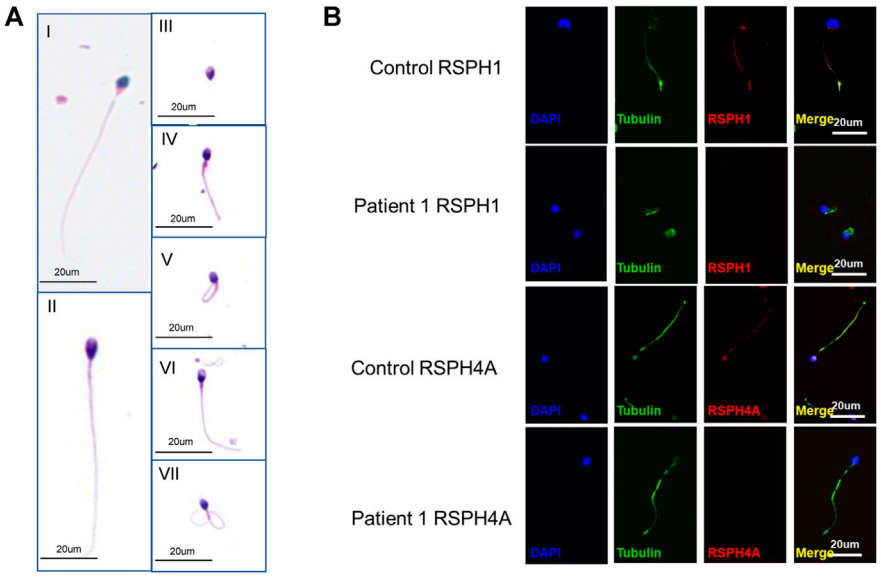

FIGURE 3 | Phenotypic features of the *RSPH4A* mutant sperm and RSPH4A immunostaining in human spermatozoa. **(A)** Papanicolaou staining of spermatozoa from patient 1 and a healthy control. **(A-I)** Normal morphology of spermatozoa from a healthy control male. **(A-II)** Observed normal length of the sperm from patient 1 with *RSPH4A* variants. In addition, multiple malformations can be observed, including **(A-III)** absent, **(A-IV)** short, **(A-V)** coiled, **(A-VI)** bent, and **(A-VII)** irregular caliber flagella. **(B)** RSPH4A and RSPH1 are expressed in the whole length of the sperm flagella in the normal control but absent in patient 1.

TABLE 3 | Semen parameters and sperm flagella morphology in patient 1 carrying *RSPH4A* variants.

	Patient	Normal control	Reference value
Semen parameters			
Sperm count (106/ml)	15.2	54.8	>15.0
Semen volume (ml)	3.0	3.4	>1.5
Motility (%)	49.1	70.1	>40.0
Progressive motility (%)	14.9	40.1	>32.0
Sperm morphology			
Normal flagella (%)	12	50	>23.0
Absent flagella (%)	11.5	7.5	<5.0
Short flagella (%)	9.5	10	<1.0
Coiled flagella (%)	49	15	<17.0
Bent flagella (%)	16.8	7.5	<13.0
Irregular caliber (%)	1.2	10	<2.0

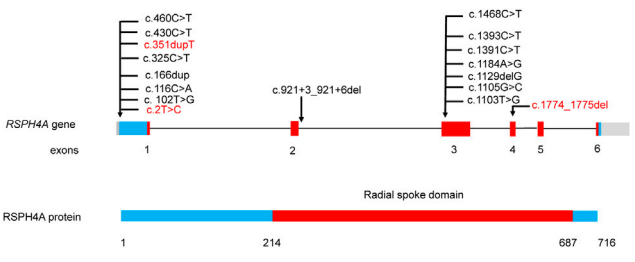

FIGURE 4 | *RSPH4A* gene and protein structure and the reported disease-causing variants of *RSPH4A*. Domains and their relative exons were filled using the same colors. Variants in our study were highlighted using red.

c.921+3_921+6del from the Hispanic family, which has been reported in 17 patients. There were two reported *RSPH4A* variants from the Chinese family including c.730+1G>A and c.1454C>G. In our study, three novel variants were identified. Two patients from two unrelated families carried the same variant c.2T>C, which may be the hotspot variant in Chinese patients with *RSPH4A* variants.

Infertility is defined as the failure to achieve pregnancy after 12 months of regular unprotected sexual intercourse (Carson and Kallen, 2021). PCD is a rare inherited disease in which genetic variants impair motile cilia function (Afzelius, 1976). Female and male infertility can be caused by defects in the cilia in the fallopian tubes or in sperm flagella, respectively (Wallmeier et al., 2020). The central apparatus and radial spokes play roles in mechano-chemical sensors to control motility in 9+2 cilia and flagella (Smith and Yang, 2004). The *RPSH4A* gene belongs to the radial spoke family. Therefore, it is persuasive to assume that male patients with *RSPH4A* variants present infertility such as *RSPH1*, *RSPH3*, and *RSPH9* (Castleman et al., 2009; Reish et al., 2010; Knowles et al., 2014).

According to a previous report, three male patients with *RSPH4A* variants were likely to be fertile (Vanaken, 2017). But there was no detailed clinical information, variant descriptions, and phenotype of motile cilia of those patients, and it is still unclear about the fertility status of the male patients with *RSPH4A* variants. Patient 1 in this study presented asthenozoospermia which is one of the main factors contributing to male infertility (Shahrokhi et al., 2020). Male infertility caused by the *RSPH1* or *RSPH9* variant has been clarified (Reish et al., 2010; Knowles et al., 2014). The absence of RSPH4A due to variants in *RSPH4A* results in deficient

axonemal assembly of radial spoke head components RSPH1 and RSPH9 (Frommer et al., 2015). Therefore, we have reason to assume that *RSPH4A* variants cause male infertility. Moreover, in a previous report, the sperm of a 21-year-old male with the *RSPH4A* variant was immotile (Bian et al., 2021). According to the semen analysis and sperm morphology, it is probable that the *RSPH4A* variants cause male infertility.

As previously reported, two female patients with *RSPH4A* variants presented infertility, which is consistent with the two female patients in our study. In a previous study, in the *Rsph4a* knock-out mice, the oviduct cilia showed two types of abnormal motion patterns: anti-clockwise rotation and beating with small amplitude, which may cause the failure of oocyte pickup (Yuan et al., 2021) and led to female mouse infertility (Yoke et al., 2020). The reason that female patients with *RSPH4A* variants presented infertility is probably because of the change in the beating pattern of the oviduct cilia. However, because of the difficulty to obtain the clinical sample, we cannot confirm the beating pattern of oviduct cilia in our patients.

In conclusion, our study reported three novel *RSPH4A* variants and first demonstrated asthenoteratozoospermia related to *RSPH4A* variants, which revealed the relationship between *RSPH4A* variants and male infertility. Moreover, we also described the detailed information of two infertile female patients with *RSPH4A* variants. Our study enriches the genetic spectrum and clinical phenotypes of *RSPH4A* variants in PCD and provides more evidence for future genetic counseling and gene-targeted therapy for this disease.

DATA AVAILABILITY STATEMENT

The original contributions presented in the study are included in the article/**Supplementary Materials**, further inquiries can be directed to the corresponding authors.

ETHICS STATEMENT

The studies involving human participants were reviewed and approved by the Review Board of the Second Xiangya Hospital of Central South University in China. Written informed consent to participate in this study was provided by the participants' legal guardian/next of kin. Written informed consent was obtained from the individual(s), and minor(s)' legal guardian/next of kin, for the publication of any potentially identifiable images or data included in this article.

AUTHOR CONTRIBUTIONS

LW: data collection, data analysis, basic experiments, and writing the manuscript; RW: data collection, data analysis, and writing the manuscript; DY: data collection and data analysis; CYL: basic experiments; YX: basic experiments; YL: basic experiments; TG: basic experiments; HL and CL: conceived and designed the experiments.

FUNDING

This study was supported by the National Natural Science Foundation of China (82070003 to HL), the Hunan Province Health Commission Scientific Research Project (B2019159 to HL), the Science and Technology Program of Changsha, China (kq1901120 to HL), the Xiangya Clinical Big Data System Construction Project in Pulmonary Inflammatory Disease of Central South University, and the National Key Clinical Specialty Construction Projects of China.

ACKNOWLEDGMENTS

We thank the patients and their families who participated in this study.

SUPPLEMENTARY MATERIAL

The Supplementary Material for this article can be found online at: https://www.frontiersin.org/articles/10.3389/fgene.2022.922287/full#supplementary-material

REFERENCES

Afzelius, B. A. (1976). A Human Syndrome Caused by Immotile Cilia. *Science* 193 (4250), 317–319. doi:10.1126/science.1084576

Auger, J., Jouannet, P., and Eustache, F. (2016). Another Look at Human Sperm Morphology. *Hum. Reprod.* 31 (1), 10–23. doi:10.1093/humrep/dev251

Ben Khelifa, M., Coutton, C., Zouari, R., Karaouzène, T., Rendu, J., Bidart, M., et al. (2014). Mutations in DNAH1, Which Encodes an Inner Arm Heavy Chain Dynein, Lead to Male Infertility from Multiple Morphological Abnormalities of the Sperm Flagella. *Am. J. Hum. Genet.* 94 (1), 95–104. doi:10.1016/j.ajhg.2013.11.017

Bian, C., Zhao, X., Liu, Y., Chen, M., Zheng, S., Tian, X., et al. (2021). Case Report of Neurofibromatosis Type 1 Combined with Primary Ciliary Dyskinesia. *Front. Med.* 15 (6), 933–937. doi:10.1007/s11684-021-0860-7

Carson, S. A., and Kallen, A. N. (2021). Diagnosis and Management of Infertility. *JAMA* 326 (1), 65–76. doi:10.1001/jama.2021.4788

Casey, J. P., McGettigan, P. A., Healy, F., Hogg, C., Reynolds, A., Kennedy, B. N., et al. (2015). Unexpected Genetic Heterogeneity for Primary Ciliary Dyskinesia in the Irish Traveller Population. *Eur. J. Hum. Genet.* 23 (2), 210–217. doi:10.1038/ejhg.2014.79

Castleman, V. H., Romio, L., Chodhari, R., Hirst, R. A., de Castro, S. C. P., Parker, K. A., et al. (2009). Mutations in Radial Spoke Head Protein Genes RSPH9 and RSPH4A Cause Primary Ciliary Dyskinesia with Central-Microtubular-Pair Abnormalities. *Am. J. Hum. Genet.* 84 (2), 197–209. doi:10.1016/j.ajhg.2009.01.011

Collins, S. A., Gove, K., Walker, W., and Lucas, J. S. A. (2014). Nasal Nitric Oxide Screening for Primary Ciliary Dyskinesia: Systematic Review and Meta-Analysis. *Eur. Respir. J.* 44 (6), 1589–1599. doi:10.1183/09031936.00088614

Cooper, T. G., Noonan, E., von Eckardstein, S., Auger, J., Baker, H. W. G., Behre, H. M., et al. (2010). World Health Organization Reference Values for Human Semen Characteristics*‡. *Hum. Reprod. update* 16 (3), 231–245. doi:10.1093/humupd/dmp048

Dai, C., Hu, L., Gong, F., Tan, Y., Cai, S., Zhang, S., et al. (2019). ZP2 Pathogenic Variants Cause In Vitro Fertilization Failure and Female Infertility. *Genet. Med.* 21 (2), 431–440. doi:10.1038/s41436-018-0064-y

Daniels, M. L. A., Leigh, M. W., Davis, S. D., Armstrong, M. C., Carson, J. L., Hazucha, M., et al. (2013). Founder Mutation inRSPH4AIdentified in Patients of Hispanic Descent with Primary Ciliary Dyskinesia. *Hum. Mutat.* 34 (10), 1352–1356. doi:10.1002/humu.22371

De Jesús-Rojas, W., Reyes-De Jesús, D., and Mosquera, R. A. (2021). Primary Ciliary Dyskinesia Diagnostic Challenges: Understanding the Clinical Phenotype of the Puerto Rican Founder Mutation. *Diagn. Base* 11 (2). 281. doi:10.3390/diagnostics11020281

Emiralioğlu, N., Taşkıran, E. Z., Koşukcu, C., Bilgiç, E., Atilla, P., Kaya, B., et al. (2020). Genotype and Phenotype Evaluation of Patients with Primary Ciliary Dyskinesia: First Results from Turkey. *Pediatr. Pulmonol.* 55 (2), 383–393. doi:10.1002/ppul.24583

Frommer, A., Hjeij, R., Loges, N. T., Edelbusch, C., Jahnke, C., Raidt, J., et al. (2015). Immunofluorescence Analysis and Diagnosis of Primary Ciliary Dyskinesia with Radial Spoke Defects. *Am. J. Respir. Cell Mol. Biol.* 53 (4), 563–573. doi:10.1165/rcmb.2014-0483oc

Goutaki, M., Meier, A. B., Halbeisen, F. S., Lucas, J. S., Dell, S. D., Maurer, E., et al. (2016). Clinical Manifestations in Primary Ciliary Dyskinesia: Systematic Review and Meta-Analysis. *Eur. Respir. J.* 48 (4), 1081–1095. doi:10.1183/13993003.00736-2016

Guo, T., Tan, Z.-P., Chen, H.-M., Zheng, D.-y., liu, L., Huang, X.-G., et al. (2017). An Effective Combination of Whole-Exome Sequencing and Runs of Homozygosity for the Diagnosis of Primary Ciliary Dyskinesia in Consanguineous Families. *Sci. Rep.* 7 (1), 7905. doi:10.1038/s41598-017-08510-z

Han, X., Xie, H., Wang, Y., and Zhao, C. (2018). Radial Spoke Proteins Regulate Otolith Formation during Early Zebrafish Development. *FASEB J.* 32 (7), 3984–3992. doi:10.1096/fj.201701359r

Jeanson, L., Copin, B., Papon, J.-F., Dastot-Le Moal, F., Duquesnoy, P., Montantin, G., et al. (2015). RSPH3 Mutations Cause Primary Ciliary Dyskinesia with Central-Complex Defects and a Near Absence of Radial Spokes. *Am. J. Hum. Genet.* 97 (1), 153–162. doi:10.1016/j.ajhg.2015.05.004

Knowles, M. R., Ostrowski, L. E., Leigh, M. W., Sears, P. R., Davis, S. D., Wolf, W. E., et al. (2014). Mutations inRSPH1Cause Primary Ciliary Dyskinesia with a Unique Clinical and Ciliary Phenotype. *Am. J. Respir. Crit. Care Med.* 189 (6), 707–717. doi:10.1164/rccm.201311-2047oc

Lei, C., Yang, D., Wang, R., Ding, S., Wang, L., Guo, T., et al. (2022). DRC1 Deficiency Caused Primary Ciliary Dyskinesia and MMAF in a Chinese Patient. *J. Hum. Genet.* 67 (4), 197–201. doi:10.1038/s10038-021-00985-z

Li, H., and Durbin, R. (2010). Fast and Accurate Long-Read Alignment with Burrows-Wheeler Transform. *Bioinforma. Oxf. Engl.* 26 (5), 589–595. doi:10.1093/bioinformatics/btp698

Lucas, J. S., Barbato, A., Collins, S. A., Goutaki, M., Behan, L., Caudri, D., et al. (2017). European Respiratory Society Guidelines for the Diagnosis of Primary Ciliary Dyskinesia. *Eur. Respir. J.* 49 (1). 1601090. doi:10.1183/13993003.01090-2016

Mirra, V., Werner, C., and Santamaria, F. (2017). Primary Ciliary Dyskinesia: An Update on Clinical Aspects, Genetics, Diagnosis, and Future Treatment Strategies. *Front. Pediatr.* 5, 135. doi:10.3389/fped.2017.00135

Reish, O., Slatkin, M., Chapman-Shimshoni, D., Elizur, A., Chioza, B., Castleman, V., et al. (2010). Founder Mutation(s) in theRSPH9Gene Leading to Primary Ciliary Dyskinesia in Two Inbred Bedouin Families. *Ann. Hum. Genet.* 74 (2), 117–125. doi:10.1111/j.1469-1809.2009.00559.x

Sampaio, P., da Silva, M. F., Vale, I., Roxo-Rosa, M., Pinto, A., Constant, C., et al. (2021). CiliarMove: New Software for Evaluating Ciliary Beat Frequency Helps Find Novel Mutations by a Portuguese Multidisciplinary Team on Primary Ciliary Dyskinesia. *ERJ Open Res.* 7 (1). 792. doi:10.1183/23120541.00792-2020

Sánchez-Álvarez, J., Cano-Corres, R., and Fuentes-Arderiu, X. (2010). A Complement for the WHO Laboratory Manual for the Examination and Processing of Human Semen (First Edition. *EJIFCC* 23 (3), 103–106.

Shahrokhi, S. Z., Salehi, P., Alyasin, A., Taghiyar, S., and Deemeh, M. R. (2020). Asthenozoospermia: Cellular and Molecular Contributing Factors and Treatment Strategies. *Andrologia* 52 (2), e13463. doi:10.1111/and.13463

Shinohara, K., Chen, D., Nishida, T., Misaki, K., Yonemura, S., and Hamada, H. (2015). Absence of Radial Spokes in Mouse Node Cilia Is Required for Rotational Movement but Confers Ultrastructural Instability as a Trade-Off. *Dev. Cell* 35 (2), 236–246. doi:10.1016/j.devcel.2015.10.001

Smith, E. F., and Yang, P. (2004). The Radial Spokes and Central Apparatus: Mechano-Chemical Transducers that Regulate Flagellar Motility. *Cell Motil. Cytoskelet.* 57 (1), 8–17. doi:10.1002/cm.10155

Van der Auwera, G. A., Carneiro, M. O., Hartl, C., Poplin, R., Del Angel, G., Levy-Moonshine, A., et al. (2013). From FastQ Data to High Confidence Variant Calls: the Genome Analysis Toolkit Best Practices Pipeline. *Curr. Protoc. Bioinforma.* 43, 11–33. doi:10.1002/0471250953.bi1110s43

Vanaken, G. J. (2017). "Infertility in an Adult Cohort with Primary Ciliary Dyskinesia: Phenotype-Gene association." Gert Jan Vanaken, Laurence Bassinet, Mieke Boon, Rahma Mani, Isabelle Honoré, Jean-Francois Papon, Harry Cuppens, Martine Jaspers, Natalie Lorent, André Coste, Estelle Escudier, Serge Amselem, Bernard Maitre, Marie Legendre and Sophie Christin-Maitre. Eur Respir J 2017; 50: 1700314. *Eur. Respir. J.* 50 (5). 1750314. doi:10.1183/13993003.50314-2017

Wallmeier, J., Nielsen, K. G., Kuehni, C. E., Lucas, J. S., Leigh, M. W., Zariwala, M. A., et al. (2020). Motile Ciliopathies. *Nat. Rev. Dis. Prim.* 6 (1), 77. doi:10.1038/s41572-020-0209-6

Wang, K., Li, M., and Hakonarson, H. (2010). ANNOVAR: Functional Annotation of Genetic Variants from High-Throughput Sequencing Data. *Nucleic Acids Res.* 38 (16), e164. doi:10.1093/nar/gkq603

Yang, P., Diener, D. R., Yang, C., Kohno, T., Pazour, G. J., Dienes, J. M., et al. (2006). Radial Spoke Proteins of Chlamydomonas Flagella. *J. Cell Sci.* 119 (Pt 6), 1165–1174. doi:10.1242/jcs.02811

Yoke, H., Ueno, H., Narita, A., Sakai, T., Horiuchi, K., Shingyoji, C., et al. (2020). Rsph4a Is Essential for the Triplet Radial Spoke Head Assembly of the Mouse Motile Cilia. *PLoS Genet.* 16 (3), e1008664. doi:10.1371/journal.pgen.1008664

Yuan, S., Wang, Z., Peng, H., Ward, S. M., Hennig, G. W., Zheng, H., et al. (2021). Oviductal Motile Cilia Are Essential for Oocyte Pickup but Dispensable for Sperm and Embryo Transport. *Proc. Natl. Acad. Sci. U. S. A.* 118 (22). e2102940118. doi:10.1073/pnas.2102940118

Zhang, X., Sun, J., Lu, Y., Zhang, J., Shimada, K., Noda, T., et al. (2021). LRRC23 Is a Conserved Component of the Radial Spoke that Is Necessary for Sperm Motility and Male Fertility in Mice. *J. Cell Sci.* 134 (20). jcs259381. doi:10.1242/jcs.259381

Ziętkiewicz, E., Bukowy-Bieryłło, Z., Voelkel, K., Klimek, B., Dmeńska, H., Pogorzelski, A., et al. (2012). Mutations in Radial Spoke Head Genes and Ultrastructural Cilia Defects in East-European Cohort of Primary Ciliary Dyskinesia Patients. *PloS One* 7 (3), e33667. doi:10.1371/journal.pone.0033667

Conflict of Interest: The authors declare that the research was conducted in the absence of any commercial or financial relationships that could be construed as a potential conflict of interest.

Publisher's Note: All claims expressed in this article are solely those of the authors and do not necessarily represent those of their affiliated organizations, or those of the publisher, the editors, and the reviewers. Any product that may be evaluated in this article, or claim that may be made by its manufacturer, is not guaranteed or endorsed by the publisher.

frontiers | Frontiers in Genetics

REVIEW
published: 30 June 2022
doi: 10.3389/fgene.2022.939527

Insights Gained From Zebrafish Models for the Ciliopathy Joubert Syndrome

Tamara D. S. Rusterholz[1,2], *Claudia Hofmann*[1,2] *and Ruxandra Bachmann-Gagescu*[1,2]*

[1]*Institute of Medical Genetics, University of Zurich, Schlieren, Switzerland,* [2]*Department of Molecular Life Sciences, University of Zurich, Zürich, Switzerland*

Cilia are quasi-ubiquitous microtubule-based sensory organelles, which play vital roles in signal transduction during development and cell homeostasis. Dysfunction of cilia leads to a group of Mendelian disorders called ciliopathies, divided into different diagnoses according to clinical phenotype constellation and genetic causes. Joubert syndrome (JBTS) is a prototypical ciliopathy defined by a diagnostic cerebellar and brain stem malformation termed the "Molar Tooth Sign" (MTS), in addition to which patients display variable combinations of typical ciliopathy phenotypes such as retinal dystrophy, fibrocystic renal disease, polydactyly or skeletal dystrophy. Like most ciliopathies, JBTS is genetically highly heterogeneous with ~40 associated genes. Zebrafish are widely used to model ciliopathies given the high conservation of ciliary genes and the variety of specialized cilia types similar to humans. In this review, we compare different existing JBTS zebrafish models with each other and describe their contributions to our understanding of JBTS pathomechanism. We find that retinal dystrophy, which is the most investigated ciliopathy phenotype in zebrafish ciliopathy models, is caused by distinct mechanisms according to the affected gene. Beyond this, differences in phenotypes in other organs observed between different JBTS-mutant models suggest tissue-specific roles for proteins implicated in JBTS. Unfortunately, the lack of systematic assessment of ciliopathy phenotypes in the mutants described in the literature currently limits the conclusions that can be drawn from these comparisons. In the future, the numerous existing JBTS zebrafish models represent a valuable resource that can be leveraged in order to gain further insights into ciliary function, pathomechanisms underlying ciliopathy phenotypes and to develop treatment strategies using small molecules.

Keywords: cilia, ciliopathies, Joubert syndrome, zebrafish, retina, CRISPR/Cas9, morpholino (MO)

OPEN ACCESS

Edited by:
Steven L. C. Pei,
Yale University, United States

Reviewed by:
Yang Sun,
Stanford University, United States
Naiara Akizu,
Children's Hospital of Philadelphia, United States

***Correspondence:**
Ruxandra Bachmann-Gagescu
ruxandra.bachmann@mls.uzh.ch

Specialty section:
This article was submitted to Human and Medical Genomics, a section of the journal Frontiers in Genetics

Received: *09 May 2022*
Accepted: *26 May 2022*
Published: *30 June 2022*

Citation:
Rusterholz TDS, Hofmann C and Bachmann-Gagescu R (2022) Insights Gained From Zebrafish Models for the Ciliopathy Joubert Syndrome. Front. Genet. 13:939527. doi: 10.3389/fgene.2022.939527

INTRODUCTION

Ciliopathies are a group of human Mendelian disorders caused by dysfunction of primary cilia. Cilia are evolutionarily conserved hair-like organelles that protrude from virtually every vertebrate cell. The basic structure of a primary cilium consists of nine microtubule doublets (A- and B-tubules) arranged in a circular array. This microtubule scaffold is ensheathed by a membrane harboring specific components important for signal transduction (Emmer et al., 2010; Rohatgi and Snell, 2010), which is the main function of this organelle. Primary cilia are structurally divided into three compartments: 1) The basal body (BB) is derived from the centriole apparatus and is the starting

point of cilium formation (Keeling et al., 2016). 2) The transition zone (TZ) is apical to the basal body and has a gatekeeper function for the cilium, controlling entry and exit of ciliary proteins (Szymanska and Johnson, 2012). 3) The axoneme protrudes from the basal body and defines the shape of the primary cilium (Singla and Reiter, 2006; Goetz and Anderson, 2010).

While the main role of primary cilia is signal transduction, these organelles have adopted diverse tissue-specific biological functions. Sensory signals for example are perceived in specialized cilia: In the retina, the outer segment of photoreceptors is a highly modified cilium which is required for light sensation (Kennedy and Malicki, 2009; Bachmann-Gagescu and Neuhauss, 2019), while olfaction is transduced by primary cilia on olfactory neurons (Singla and Reiter, 2006). Beyond such specialized sensory signals, primary cilia are equally important for sensing the environment and for transducing signals for crucial developmental pathways such as Hedgehog (Hh) signaling (Ishikawa and Marshall, 2011). Components of this pathway, which control key aspects of development such as patterning of the central nervous system (CNS) or limb buds, proliferation and differentiation of multiple cell types, localize to the cilium in a Hh-ligand dependent manner (Bangs and Anderson, 2017). Other developmental signaling pathways such as Wnt are also associated with primary cilia function, whereby the precise link is less well defined than for Hh signaling (Wheway et al., 2018).

To ensure their signaling function, primary cilia exert a tight control on the protein and lipid composition of their membrane, in order to concentrate receptors and channels required to perceive and regulate external stimuli. Since primary cilia lack protein translation machinery, all ciliary components need to be transported from the cytosol into the primary cilium, which is achieved through a combination of controlled vesicle trafficking and the conserved intraflagellar transport (IFT) system (Nachury et al., 2010).

In contrast to the single primary non-motile cilium present on most cells, motile cilia are usually present in multiple copies on one cell and beat in a synchronized manner to generate directed fluid flow. In humans, motile cilia are found only on a few specialized cell types such as the ependymal cells lining the ventricular surface in the brain, epithelial cells in the airways and in the reproductive tract (Goetz and Anderson, 2010). Different to primary cilia, motile cilia have an additional central microtubule pair, as well as dynein arms on the A-tubule to enable movement (Mitchell, 2007; Yamaguchi et al., 2018). Intermediates between primary and motile cilia are the motile cilia on cells of the embryonic node, important for left/right organization, which are single on a given cell and which lack the central microtubule pair (Babu and Roy, 2013).

Dysfunction of cilia leads to a group of disorders called ciliopathies. Dysfunction of cilium motility causes primary ciliary dyskinesia (PCD), which affects only organs where motile cilia are present, leading to recurrent respiratory infections, laterality defects and infertility. The larger group of "primary ciliopathies" includes disorders which can affect almost every organ system (Mitchison and Valente, 2017). Typical phenotypes include CNS malformations or dysfunction, retinal degeneration, liver fibrosis, fibrocystic kidney disease, hearing loss, anosmia, obesity, polydactyly and skeletal dysplasia. The precise clinical diagnosis, which depends on the constellation of phenotypes occurring in a given patient (Badano et al., 2006; Hildebrandt et al., 2011; Waters and Beales, 2011), can be challenging to establish given the important genetic and phenotypic overlap between individual disorders and the prominent phenotypic variability between individuals.

Ciliopathies are genetically heterogeneous disorders, typically inherited in a recessive manner, where bi-allelic mutations in one of many different genes can cause each disorder (Tobin and Beales, 2009). On the other hand, many ciliary genes can cause more than one ciliopathy disorder when mutated. Given this high genetic heterogeneity and the prominent phenotypic variability, it remains very challenging to predict the clinical outcome for a given individual and only very few genotype-phenotype correlations have been established in patients with ciliopathies (Mougou-Zerelli et al., 2009; Bachmann-Gagescu et al., 2015a), underscoring our still limited understanding of the mechanisms leading from mutations in ciliary genes to human disease phenotypes.

Joubert syndrome (JBTS) is a prototypical ciliopathy defined by a pathognomonic cerebellar and brainstem malformation called the "Molar Tooth Sign" (MTS), which is visible on axial brain magnetic resonance imaging (MRI). Clinically, the disorder is characterized by cerebellar ataxia, hypotonia, abnormal eye movements, and respiratory rhythm regulation disturbance (Romani et al., 2013). About 60% of JBTS patients display additional extra-CNS phenotypes such as retinal degeneration, kidney cysts, coloboma, polydactyly, liver fibrosis or encephalocele with high variability (Bachmann-Gagescu et al., 2015a). To date, 39 JBTS-associated genes, whose protein products localize to various compartments of the primary cilium, have been identified and are summarized in **Table 1** and **Figure 1** (Parisi, 2019; Bachmann-Gagescu et al., 2020). Mutations in several of these genes can also cause the more severe Meckel syndrome, which is characterized by encephalocele, polydactyly, cystic kidneys, hepatic fibrosis and other malformations, generally leading to fetal lethality (Hartill et al., 2017). In fact, based on the high degree of allelism, the two disorders are thought to represent extremes of the same disease spectrum.

Many JBTS proteins collaborate in multiprotein complexes at the ciliary transition zone (Garcia-Gonzalo et al., 2011; Sang et al., 2011; Williams et al., 2011), and JBTS has been proposed to be caused specifically by transition zone dysfunction (Shi et al., 2017). However many of the more recently identified JBTS-associated genes encode proteins that don't localize to the transition zone but to other ciliary subcompartments, with normal transition zone integrity (Kobayashi et al., 2014; Schwarz et al., 2017; Van De Weghe et al., 2017; Latour et al., 2020) (**Figure 1**). Thus, it remains elusive what distinguishes JBTS from other ciliopathies. Moreover, despite progress in understanding the function of primary cilia, the pathomechanism underlying ciliopathies remains partly unsolved. Given the well-established link between primary cilia

TABLE 1 | Phenotypes of JBTS zebrafish morphant (MO) and mutant models.

JBTS gene	Zebrafish orthologue	Conservation similarity/identity	Model(s)	Larval body curvature	Laterality defects	Hydrocephalus	Pronephric cysts	Otolith defects	Smaller eyes	Retinal dystrophy	CE defects	RNA rescue	Adult scoliosis	References
AHI1	*ahi1*[§]	67 /50	MO	+	+	+	+	+	+	+	+	+	NA	MO: Simms et al. (2012), Elsayed et al. (2015), Zhu et al. (2019) / mut: Lessieur et al. (2017), Zhu et al. (2019)
			TALEN *iri46*, CRISPR	+	NA	-	+	-	+/-	+	-	+	+	
ARL13B	*arl13b*[§]	75 / 60	MO	+	+	NA	+	NA	NA	NA	+	+	NA	MO: Sun et al. (2004), Duldulao et al. (2009), Zhu et al. (2020) / mut: Golling et al (2002), Cantagrel et al. (2008), Duldulao et al. (2009), Song et al. (2016), Zhu et al. (2020)
			ENU *hi459*	+	-	NA	+	NA	NA	+	NA	+	NA	
ARL3	*arl3a*	97 / 95												
	arl3b	98 / 95												
ARMC9	*armc9*[§]	72 / 58	CRISPR *zh502, zh503, zh504, zh505*	-	-	NA	+	NA	NA	NA	NA	NA	+	Latour et al. (2020)
B9D1	*b9d1*	94 / 83	MO	NA	NA	NA	NA	NA	NA	NA	NA	NA	NA	Zhao and Malicki (2011)
B9D2	*b9d2*	86 / 76	MO	+	NA	NA	-	NA	NA	+	NA	+	NA	Dowdle et al. (2011), Zhao and Malicki (2011)
C2CD3	*c2cd3*	58 / 43												
CC2D2A	*cc2d2a*[§]	74 / 58	ENU *w38* *	+	NA	NA	+	NA	-	+	NA	NA	+	Gorden et al. (2008), Owens et al. (2008), Bachmann-Gagescu et al. (2011), Stawicki et al. (2016)
CEP41	*cep41*	72 / 59	MO	+	+	+	NA	+	+	NA	NA	+	NA	MO: J. E. Lee et al. (2012), Patowary et al. (2019), Ki et al. (2020) / mut: Ki et al. (2020)
			CRISPR *skk1*	NA	NA	NA	NA	NA	NA	NA	NA	NA	NA	
CEP104	*cep104*	68 / 52	MO	+	+	NA	NA	NA	NA	NA	NA	+	NA	MO and mut: Frikstad et al. (2019)
			CRISPR F0	+	+	NA	NA	NA	NA	NA	NA	NA	NA	
CEP120	*cep120*	74 / 59	MO	+	NA	+	+	+	+	NA	NA	+	NA	Shaheen et al. (2015)
CEP290	*cep290*[§]	77 / 58	MO	+	+	+	+	+	+	+	NA	+	NA	MO: Sayer et al. (2006), Schäfer et al. (2008), Baye et al. (2011), Murga-Zamalloa et al. (2011), Cardenas-Rodriguez et al. (2021) / mut: Stawicki et al. (2016), Lessieur et al. (2019), Cardenas-Rodriguez et al. (2021)
			Tilling *fh297*, TALEN *fh378*, CRISPR *fb208**	+	-	NA	+/-	-	NA	+	NA	NA	+	
CPLANE1	-	-												
CSPP1	*cspp1a*	57 / 40	MO	+	NA	+	+	NA	NA	-	NA	NA	NA	Tuz et al. (2014)
	cspp1b	49 / 34	MO	+	NA	+	+	NA	NA	-	NA	NA	NA	Tuz et al. (2014)
FAM149B1	*fam149b1*	56 / 39												
HYLS1	-	-												
IFT172	*Ift172*[§]	88 / 75	MO	+	NA	+	+	+	NA	+	NA	+	NA	MO: Sun et al. (2004), Lunt et al. (2009), Halbritter et al. (2013), Bujakowska et al. (2015), Bergboer et al. (2018), Eisa-Beygi et al. (2018) / mut: Amsterdam et al. (1999), Sun et al. (2004), Gross et al. (2005), Lunt et al. (2009), Sukumaran and Perkins (2009), Eisa-Beygi et al. (2018)
			Retroviral insertion *hi2211*	+	NA	NA	+	NA	NA	+	NA	NA	NA	
INPP5E	*inpp5e*[§]	70 / 56	MO	+	NA	+	+	NA	+	+	NA	+	NA	MO: Luo et al. (2012), Xu et al. (2017) mut: Xu et al. (2017)
			CRISPR	+	NA	NA	+	NA	NA	NA	NA	NA	NA	
KIAA0556/ KATNIP	*katnip*	80 / 69	MO	+	NA	NA	NA	NA	NA	NA	NA	+	NA	Roosing et al. (2016)
KIAA0586/ TALPID3	*talpid3*[§]	50 / 33	ZFN *i262, i263, i264**	+	+	NA	+	NA	NA	+	NA	NA	NA	Ben et al. (2011), Ojeda Naharros et al. (2018)
KIAA0753/ OFIP	*ofip*	49 / 34	ENU *sa22657*	+	NA	NA	NA	NA	NA	NA	NA	NA	NA	Hammarsjö et al. (2017)

(Continued on following page)

TABLE 1 | (*Continued*) Phenotypes of JBTS zebrafish morphant (MO) and mutant models.

JBTS gene	Zebrafish orthologue	Conservation similarity/identity	Model(s)	Larval body curvature	Laterality defects	Hydrocephalus	Pronephric cysts	Otolith defects	Smaller eyes	Retinal dystrophy	CE defects	RNA rescue	Adult scoliosis	References
KIF7	*kif7*§	69 / 57	MO ZFN *i271, i272**, CRISPR *mw406*, CRISPR *co63*	NA +	+ +/-	NA -	NA NA	NA NA	NA NA	NA +	NA NA	+ +	NA +/-	MO: Tay et al. (2005), Wilson et al. (2009), Putoux et al. (2011) / mut: Maurya et al. (2013), Lewis et al. (2017), Terhune et al. (2021)
MKS1	*mks1*	40 / 26	MO CRISPR *w152*	NA NA	NA NA	NA NA	NA NA	NA NA	NA NA	NA NA	+ NA	+ NA	NA NA	MO: Leitch et al. (2008) mut: Stawicki et al. (2016)
NPHP1	*nphp1*	66 / 46	MO	+	-	NA	+	NA	NA	NA	+	+	NA	Slanchev et al. (2011), Lindstrand et al. (2014)
OFD1	*ofd1*	60 / 40	MO	+	+	+	NA	+	NA	NA	+	NA	NA	Ferrante et al. (2009), Lopes et al. (2011)
PDE6D	*pde6b*	98 / 91	MO	NA	NA	NA	NA	NA	+	-	NA	+	NA	Thomas et al. (2014)
PIBF1	*pibf1*	82 / 66												
RPGRIP1L	*rpgrip1l*§	72 / 54	MO CRISPR F2	+ -	+ -	+ -	NA -	NA NA	NA NA	NA -	+ NA	+ NA	NA +	MO: Khanna et al. (2009), Mahuzier et al. (2012) / mut: Vesque et al. (2019)
SUFU	*sufu*	90 / 83	MO	NA	NA	NA	NA	+	+	NA	NA	NA	NA	Koudijs et al. (2005), Maurya et al. (2013)
TCTN1	*tctn1*	57 / 39							-					
TCTN2	*tctn2*	53 / 38	MO	NA	+	NA	NA	NA	NA	NA	NA	NA	NA	Liu et al. (2018)
TCTN3	-	-												
TMEM67	*tmem67*§	75 / 59	MO TALEN *e3*	+ +	NA NA	+ -	+ +	+ NA	+ NA	NA NA	+ -	+ NA	NA +	MO: Adams et al. (2012), Leightner et al. (2013), Lee et al. (2017), Stayner et al. (2017) / mut: Zhu et al. (2021)
TMEM107	*tmem107*	76 / 61												
TMEM138	*tmem138*	80 / 68	MO	+	+	-	NA	NA	NA	NA	+	NA	NA	Lee J. H. et al. (2012)
TMEM216	*tmem216*§	77 / 58	MO CRISPR *snyΔ175*, *snyR8Δ60*	+ NA	+ NA	+ -	NA -	NA NA	NA NA	NA +	+ NA	+ NA	NA NA	MO: Valente et al. (2010), Lee J. H. et al. (2012) / mut: Liu et al. (2020)
TMEM231	*tmem231*	78 / 58												
TMEM237	*tmem237a* *tmem237b*	68 / 53 68 / 52	MO MO	NA NA	NA NA	NA NA	NA NA	NA NA	NA NA	NA NA	+ +	+ +	NA NA	Huang L. et al. (2011) Huang L. et al. (2011)
TOGARAM1	*togaram1*§	54 / 38	CRISPR *zh508*, *zh510*	+	-	NA	+	NA	NA	NA	NA	NA	+	Latour et al. (2020)

List of bona fide JBTS genes ordered alphabetically (genes with currently limited evidence are not included). Conservation between the zebrafish and the human gene is shown at the amino acid level (similarity / identity). To determine conservation, available sequence information from genome assemblies GRCz11 (zebrafish) and GRCh38.p13 (human) were used, apart for inpp5e, armc9 and togaram1, for which more complete sequence generated in our laboratory was available. §: Genes for which the zebrafish mutant model was described with sufficient information to allow inclusion for the comparisons shown in Figure 5. MO models are always listed first, mutant models second for genes where both are published. The references for each gene are separated according to model type (MO: morphant, mut: mutant).

CE: conversion-extension. The absence or presence of a defect in ciliary morphology in the different organs is shown in ***Supplementary Table S1.*** *+: phenotype present, -: phenotype absent, NA: not available/not described. *maternal-zygotic mutant available.*

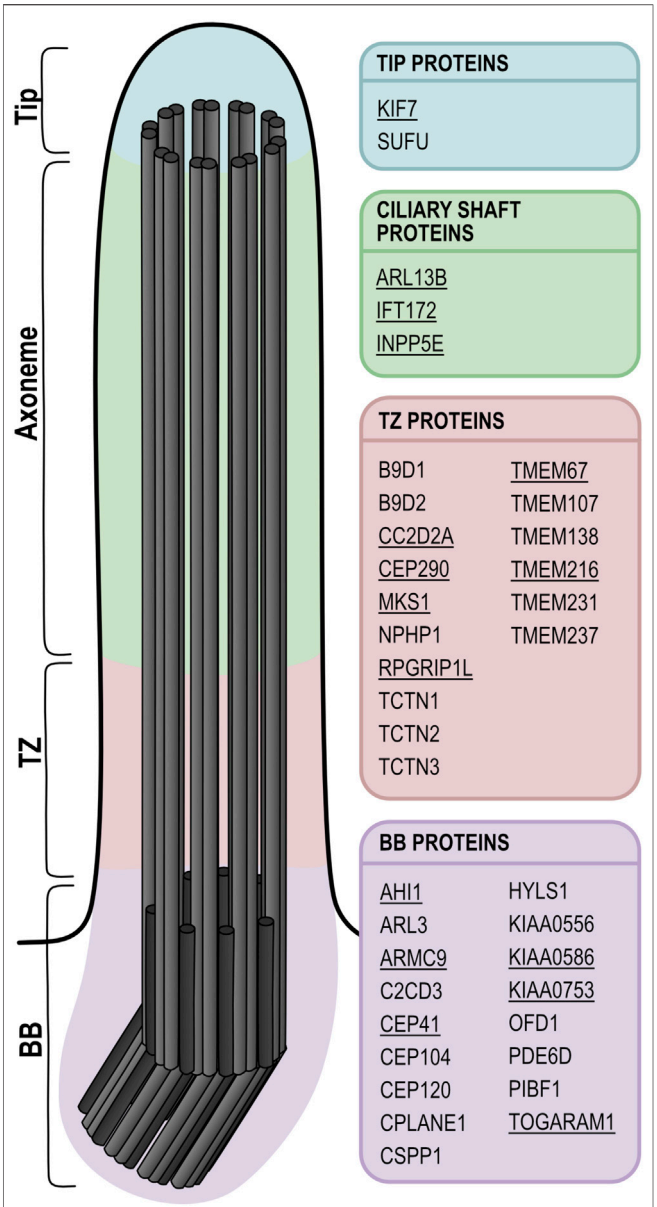

FIGURE 1 | Schematic of a primary cilium showing the localization of JBTS proteins. Underlined proteins have at least one zebrafish mutant model available. While in this schematic only the main localization for each protein is indicated, it has been shown that many of these proteins can localize to several distinct ciliary subcompartments, which could be explained by dynamic localization and/or tissue-specific functions. In the ciliary shaft, IFT172 is part of the IFT-B complex, whereas ARL13B and INPP5E associate with the ciliary membrane. The subciliary localization of FAM149B1 is not known. BB: basal body; TZ: transition zone.

and Hh signaling, aberrant regulation of this pathway is a likely mechanism explaining certain phenotypes such as polydactyly, skeletal abnormalities or craniofacial phenotypes. In contrast, the retinal phenotypes are unlikely to be explained by aberrant Hh signaling regulation and the cause for the CNS, kidney or liver phenotypes remains controversial, with multiple lines of evidence pointing towards a variety of pathomechanisms. Generating robust and well-characterized models for ciliopathies and JBTS therefore remains crucial, in order to elucidate the link leading from mutations in ciliary genes to the various ciliopathy-associated phenotypes.

ZEBRAFISH AS A MODEL ORGANISM FOR CILIOPATHIES AND JOUBERT SYNDROME

In the past two decades, the zebrafish (*Danio rerio*) has become a popular model to study human disease and gene function due to its practical advantages, including large numbers of externally developing transparent embryos. Rapid development leads to free swimming and behaving larvae with fully functioning organ systems within 5 days post fertilization (dpf). Transparency of embryos allows for unique imaging conditions, including in live animals, and the available genetic toolbox allows for efficient generation of transgenic and mutant lines (Kawakami, 2007; Santoriello and Zon, 2012; Howe et al., 2013). The zebrafish genome has a size of ~1,412 gigabases (Gb) distributed among 25 chromosomes with 26,206 protein-coding genes (Howe et al., 2013). About 71% of the ~20,500 human protein-coding genes have orthologues in the zebrafish genome, with 82% of human disease genes having a zebrafish orthologue (Howe et al., 2013). The higher number of genes in zebrafish compared to humans is explained by the teleost-specific whole genome duplication event that occurred about 320–350 million years ago (Glasauer and Neuhauss, 2014). While some of the resulting zebrafish paralogues were maintained, many duplicated genes were lost shortly after the duplication event (Sassen and Köster, 2015). Interestingly, genes that are involved in neuronal function often retained both paralogues (Glasauer and Neuhauss, 2014). In contrast, ciliary genes tend to not have more than one zebrafish orthologue. Specifically, of 39 JBTS-associated genes, only three (*TMEM237, CSPP1* and *ARL3*) have two paralogues in zebrafish (**Table 1**). All JBTS-genes apart from *CPLANE1*, *TCTN3*, *HYLS1* and *TOGARAM1* have an annotated zebrafish orthologue in the current genome assembly (GRCz11). However, this genome annotation remains incomplete to date and it is possible that zebrafish orthologues for these genes do exist. In fact, the zebrafish *togaram1* gene for instance was present in earlier annotations and has vanished in the most recent genome annotation. However, we have cloned this gene from zebrafish larvae and shown by synteny analysis that it is the true orthologue of human *TOGARAM1*. On average, JBTS zebrafish orthologues show a similarity of 71% and an identity of 57% (**Table 1**) with the human proteins, making the zebrafish an excellent model system to study Joubert syndrome (Howe et al., 2013).

One strength of the zebrafish as a model for human ciliopathies (including JBTS) is the variety of specialized cilia types present in this animal, similar to the human situation. Indeed, various types of cilia are found on virtually all zebrafish cells, including among others cells lining the Kupffer's vesicle (equivalent of the embryonic node), neuroephithelial cells in the

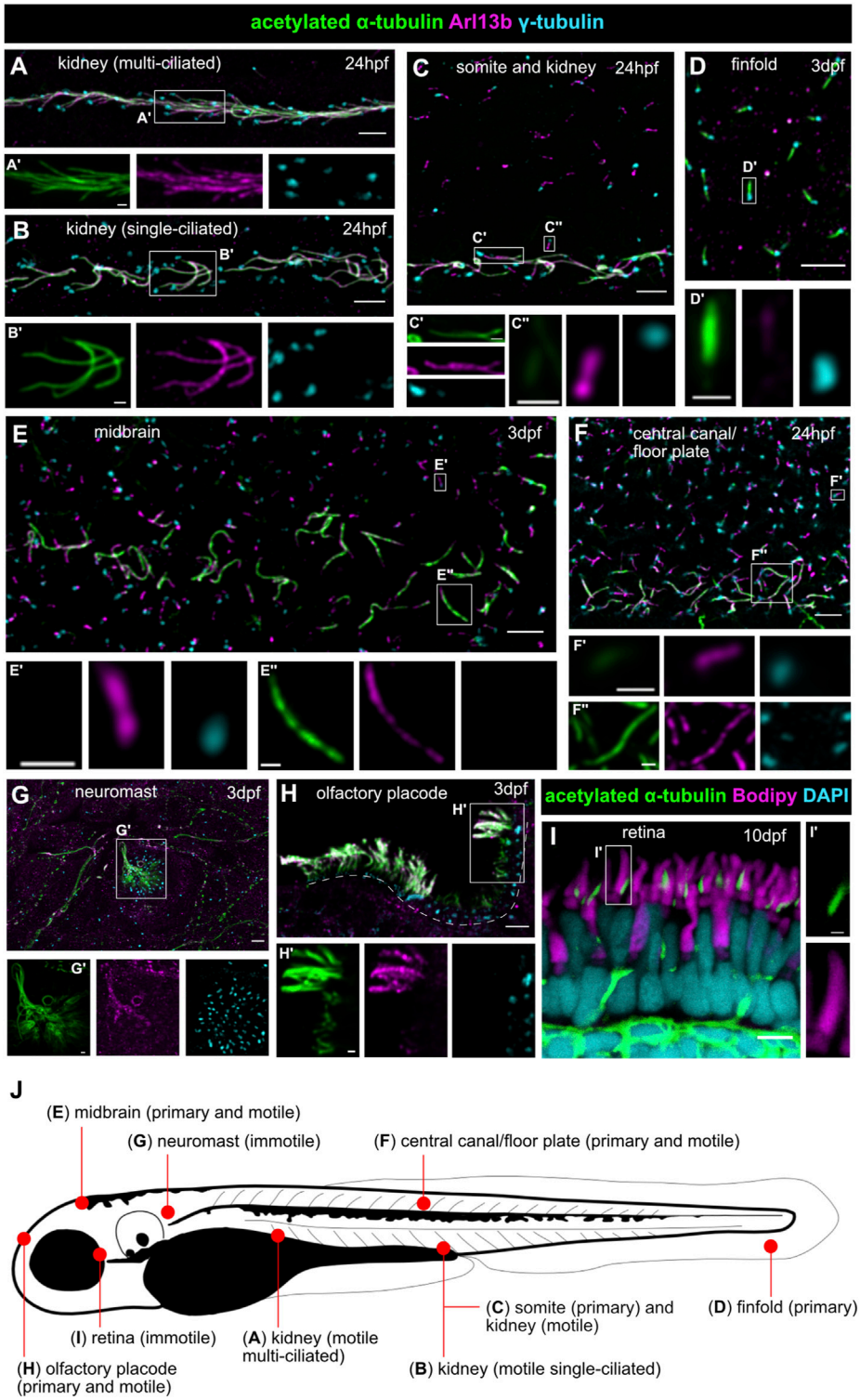

FIGURE 2 | Various types of motile and immotile cilia in zebrafish show distinct acetylated tubulin or Arl13b signal patterns. **(A,B)** Cilia in the pronephros are all motile, but multiple **(A)** or single **(B)** on tubular cells in the different portions of the nephron. **(C)** Long strongly acetylated α-tubulin positive motile kidney cilia **(C')** and shorter primary somite cilia **(C'')** with weaker acetylated α-tubulin signal. **(D)** Primary cilia on the finfold with very weak Arl13b signal. **(E)** Short primary neuronal cilia without visible acetylated α-tubulin signal (at least with these imaging settings) **(E')** and longer motile midbrain cilia strongly positive for acetylated α-tubulin at the same imaging conditions **(E'')**. **(F)** Short primary cilia in the central canal **(F')** with weak acetylated α-tubulin signal and longer acetylated α-tubulin positive motile floor plate cilia **(F'')**. **(G)** Immotile neuromast sensory cilia**. (H)** Long motile cilia at the border of the olfactory placode and shorter Arl13b-poor primary cilia in the center. Dotted

(*Continued*)

FIGURE 2 | lines mark the olfactory placode for orientation. **(I)** The outer segment of retinal photoreceptors (marked in magenta with bodipy) is a highly modified primary cilium; note the presence of the axoneme on the side of the outer segment, marked in green by acetylated α-tubulin. **(J)** Schematic overview of a zebrafish larva showing localization of the various cilia types. All images [except **(I)**] are whole mount immunofluorescence using anti-acetylated α-tubulin (green), anti-Arl13b (magenta) and anti-γ-tubulin (cyan), imaged using a spinning disk microscope at the following stages: 24 hpf **(A–C,F)** and 3 dpf **(D–H)**. Lateral views in **(A–D,F,G)**; dorsal view in **(E,H)**. **(I)** Immunofluorescence on a retinal cryosection at 10 dpf with anti-acetylated α-tubulin (green), bodipy (magenta) and DAPI (cyan) imaged by confocal microscopy. Scale bars are 5 µm in the overview pictures and 1 µm in the insets.

developing brain and those lining the brain ventricles and the central canal, cells of the olfactory placode, in the otic placode and later in the ear, neuromasts from the lateral line organ (sensing fluid flow), epithelial cells in kidney tubules or photoreceptors in the retina (**Figure 2**). In both human and zebrafish retinal photoreceptors, primary cilia have become highly specialized, forming what are called "outer segments" to perceive incoming light signals (Kennedy and Malicki, 2009; Bachmann-Gagescu and Neuhauss, 2019). These outer segments are composed of multiple stacks of membrane disks or folds, arranged around a typical microtubule-based axoneme. The transition zone is called connecting cilium in photoreceptors and links the large outer segment ciliary compartment to the inner segment, which is part of the cell body of the photoreceptor. This arrangement is perfectly conserved between zebrafish and humans. However, the distinction between primary immotile and motile cilia is somewhat blurred in the zebrafish compared to human in other organ systems, since some cilia which are immotile in humans (such as those present on renal tubular cells) are single but motile in the corresponding cell type in zebrafish larvae (Kramer-Zucker et al., 2005). The olfactory placode of zebrafish larvae contains both motile cilia on the periphery and immotile cilia in the center (Reiten et al., 2017). Likewise, the Kupffer's vesicle contains a mix of motile and immotile cilia. The cilia most frequently analyzed in currently existing ciliopathy models are those present on cells lining the brain ventricles, the olfactory placode, the kidney tubules, the central canal, the ear and the Kupffer's vesicle, which are single but mostly motile cilia. In fact, variation between cilia in different tissues has been little analyzed so far in the zebrafish. Typically used ciliary markers for which reliable antibodies exist in this model system are anti-Arl13b [zebrafish-specific antibody generated by Z. Sun (Duldulao et al., 2009)] and anti-acetylated tubulin (commercially available). When staining a range of primary and motile cilia in various zebrafish larval tissues, important variations of the relative intensities of these two signals are observed (**Figure 2**). A comprehensive analysis of tissue-specific differences in Arl13b, acetylated tubulin, polyglutamylated tubulin and other available ciliary markers remains to be performed.

Beyond the high conservation of ciliary genes between zebrafish and human and the variety of cilia types, the strong morphological conservation between tissues and/or functional conservation of various organs validate the use of this model system to study human ciliopathies. This conservation is particularly well illustrated in the retina, which has very similar tissular morphology and displays similar cell types, including rod and cone photoreceptors (Bibliowicz et al., 2011; Angueyra and Kindt, 2018), as in humans. The larval zebrafish pronephros represents a simplified version of the human nephron, the functional unit of a human kidney: the larval pronephros is formed by a single fused glomerulus with two symmetrical tubule systems converging in the cloaca and displays the same cell types in its glomerulus and the same specific segments in its tubular system as in human nephrons (Wingert and Davidson, 2008; Morales and Wingert, 2017). Being a vertebrate, the zebrafish is also an excellent model for scoliosis and other spinal anomalies (Boswell and Ciruna, 2017). Consequently, zebrafish harboring mutations in ciliopathy genes display typical ciliopathy phenotypes such as cystic kidneys or retinal dystrophy and degeneration, often accompanied by spinal curvature (**Figures 3**, **4**). A further advantage of the zebrafish system is the possibility to perform functional assays at the organismal level to quantify the function of various organs. For example, electroretinograms or the oculo-kinetic response (OKR) are well-established assays to evaluate the visual function of zebrafish (Fleisch and Neuhauss, 2006).

The genetic toolbox available in zebrafish to model human disorders, in this case ciliopathies, includes efficient mutagenesis and transgenesis (Kawakami, 2007; Sassen and Köster, 2015). Currently available zebrafish models for ciliopathies (including JBTS) were identified either in forward genetic screens (e.g., *cc2d2a*^{w38} and *arl13b*^{hi459}) or, more recently, were generated using reverse genetics approaches. The latter include TILLING (e.g., *cep290*^{fh297}), where a DNA library from ENU-mutagenized male zebrafish is screened for mutations in genes of interest (Moens et al., 2008), or directed mutagenesis of the gene of interest using Zinc-finger (*kif7*$^{i271/i272}$ and *talpid3*$^{i262/i263/i264}$), TALEN (*ahi1*^{iri46}, *cep290*^{fh378} and *tmem67*^{e3}) or most recently CRISPR-Cas mediated nucleases (e.g., *armc9*^{zh505}, *togaram1*^{zh510} and *kif7*^{mw406}) (Urnov et al., 2010; Huang P. et al., 2011; Zhang et al., 2014). The efficiency of CRISPR mutagenesis is such that phenotypes are often already observed in the F0 injected fish, which are mosaic for various induced mutations (and unmutated cells) (Shah et al., 2015). In parallel to knocking out genes of interest at the genomic level, a commonly used technique in the zebrafish is the transient oligonucleotide-based knockdown using morpholinos (MOs). The advantage of MOs lies in their rapid application as the phenotypes can be studied directly in the injected embryo (Nasevicius and Ekker, 2000). This represents an important advantage over generating stable mutants given the long (3-month) generation time for zebrafish. A further advantage of using MOs is that they avoid the potential problem of phenotypic rescue through maternally deposited mRNA in the egg (Abrams and Mullins, 2009). This can be circumvented in mutants by generating maternal zygotic mutants (offspring of a homozygous mutant mother) which is however a time-consuming endeavor. In addition, the level of gene knockdown can be titrated using morpholinos, which can

represent another advantage in case complete loss-of-function is lethal, for example. On the other hand, the limitation of using MOs lies in the frequent off-target effects, which need to be carefully controlled for, and in the limited duration of the knockdown effect, making it impossible to study adult phenotypes (Stainier et al., 2017). Transgenesis approaches, in which a fluorophore-tag is added to a protein of interest such as the ciliary protein Arl13b or the centrosomal protein Centrin, allow visualization of cilia or centrosomes (Borovina et al., 2010; Malicki et al., 2011).

The ubiquitous presence of specialized cilia on a variety of zebrafish cells, together with the strong conservation of organs and genes between human and zebrafish, and the technical toolbox available make the zebrafish a powerful model to study ciliopathies such as JBTS. Here, we review the various zebrafish models for JBTS published to date, comparing morphants with mutants for the same genes, as well as different mutants in various JBTS genes with each other, in an attempt to identify commonalities and discrepancies. By summarizing the insights gained from zebrafish models, we hope to reach a deeper understanding of the function of JBTS genes in ciliary biology and of the pathomechanism underlying this disorder.

COMPARISON BETWEEN ZEBRAFISH MODELS FOR JOUBERT SYNDROME

Currently, 39 genes have been identified to cause JBTS when mutated (**Table 1**), of which 29 (74%) have at least one zebrafish model available (morphant or mutant model). For 16 genes (41%), a stable mutant model has been published (**Figure 1**), with several alleles generated for eight of these: *ahi1, armc9, cc2d2a, cep290, kif7, kiaa0586/talpid3, tmem216* and *togaram1* (**Table 1**). Since identification of JBTS-causing genes and subsequent generation of zebrafish models occurred in parallel to the evolution of genome editing tools, this explains the broad variety of methods used to generate zebrafish models: ENU (n = 3), TILLING (n = 1), retroviral insertion (n = 1), ZFN (n = 2), TALEN (n = 3), CRISPR (n = 11), MO (n = 24) (**Table 1**). MOs have been used most commonly to generate JBTS zebrafish models given the advantages explained above (ease of use and short time to results). On the other hand, the CRISPR/Cas9 system has been used most frequently for permanent genome editing, despite the fact that it is the most recent technique, underscoring its efficiency to generate stable zebrafish mutant lines.

Phenotypes Observed in Zebrafish Morphant and/or Mutant Models of Joubert Syndrome

We first sought to compare MO models to the corresponding mutant models for the same genes, in order to investigate consistency and potential discrepancies of occurring phenotypes (Robu et al., 2007; Eisen and Smith, 2008). We found nine JBTS-causing genes that have both a MO and a mutant model with sufficient phenotypic characterization (**Table 1**; **Supplementary Table S1**). In general, MO models tend to exhibit more phenotypes than their corresponding mutant models (**Figure 5**). In particular, phenotypes such as laterality defects, hydrocephalus, otolith defects, small eyes, conversion-extension (CE) defects or Kupffer's vesicle (KV) cilia defects were described only in MO zebrafish models but not in mutant JBTS models (**Figures 5A,B**). Such phenotypes may represent off-target toxicity effects and may not be specific to downregulation of the targeted gene. Alternatively, the additional phenotypes seen only in morphants could be explained by compensation mechanisms occurring only in mutants (Rossi et al., 2015; El-Brolosy et al., 2019; Cardenas-Rodriguez et al., 2021) and/or by rescue of the phenotype in zygotic mutants through presence of maternally deposited mRNA and/or protein in the egg. However, for a small number of mutants, maternal zygotic mutants were generated and these still did not present with CE defects, laterality defects, smaller eyes or hydrocephalus (e.g., *cc2d2a*, *kif7*, *talpid3* and *cep290*). Unfortunately, control experiments are lacking for a number of morphants, such that non-specific off-target toxicity defects cannot be ruled out. On the other hand, some phenotypes including retinal defects, kidney cysts or body curvature are present in both MO and mutant models, supporting specificity of these phenotypes caused by ciliary dysfunction (**Figure 5**). However, a lack of systematic description of all possible phenotypic features in most models somewhat limits the comparison between MO and mutant models.

Comparison Between Zebrafish Mutants in Joubert Syndrome Genes

Focusing only on stable mutant lines described, we next compared the phenotypes present in the various JBTS mutants with each other. Since all these genes cause the same human disorder, we were expecting to find similar zebrafish phenotypes between the different mutants. Unfortunately, in most cases, a systematic analysis of all possible cilia-related phenotypes is lacking for the described JBTS zebrafish models (**Table 1**; **Supplementary Table S1**), which somewhat limits this analysis. Indeed, often only a specific phenotype of interest was investigated and described. Phenotypic characterization was mostly conducted on zygotic mutant zebrafish since adult zebrafish harboring mutations in JBTS-genes often exhibit reduced viability, scoliosis and reduced fertility (Mytlis et al., 2022), making the generation of maternal zygotic mutants *via* natural matings challenging (requires *in vitro* fertilization and/or generation of germline mosaic fish) (Ben et al., 2011).

We identified a total of 13 mutant zebrafish models with sufficient phenotypic characterization to be included in the following analysis (**Table 1**; **Figure 5**; **Supplementary Table S1**). For several genes, more than one stable mutant line has been generated using various genome editing tools. While in most cases the different alleles for a JBTS given gene were indistinguishable from each other, distinct phenotypes were occasionally described. For example, for *cep290*, the *fh297* allele exceptionally displays pronephric cysts while these are not observed in the *fh378* and *fb208* alleles, and for *kif7*, *i271/i272* mutants do not display scoliosis as adults, while *co63* mutants do.

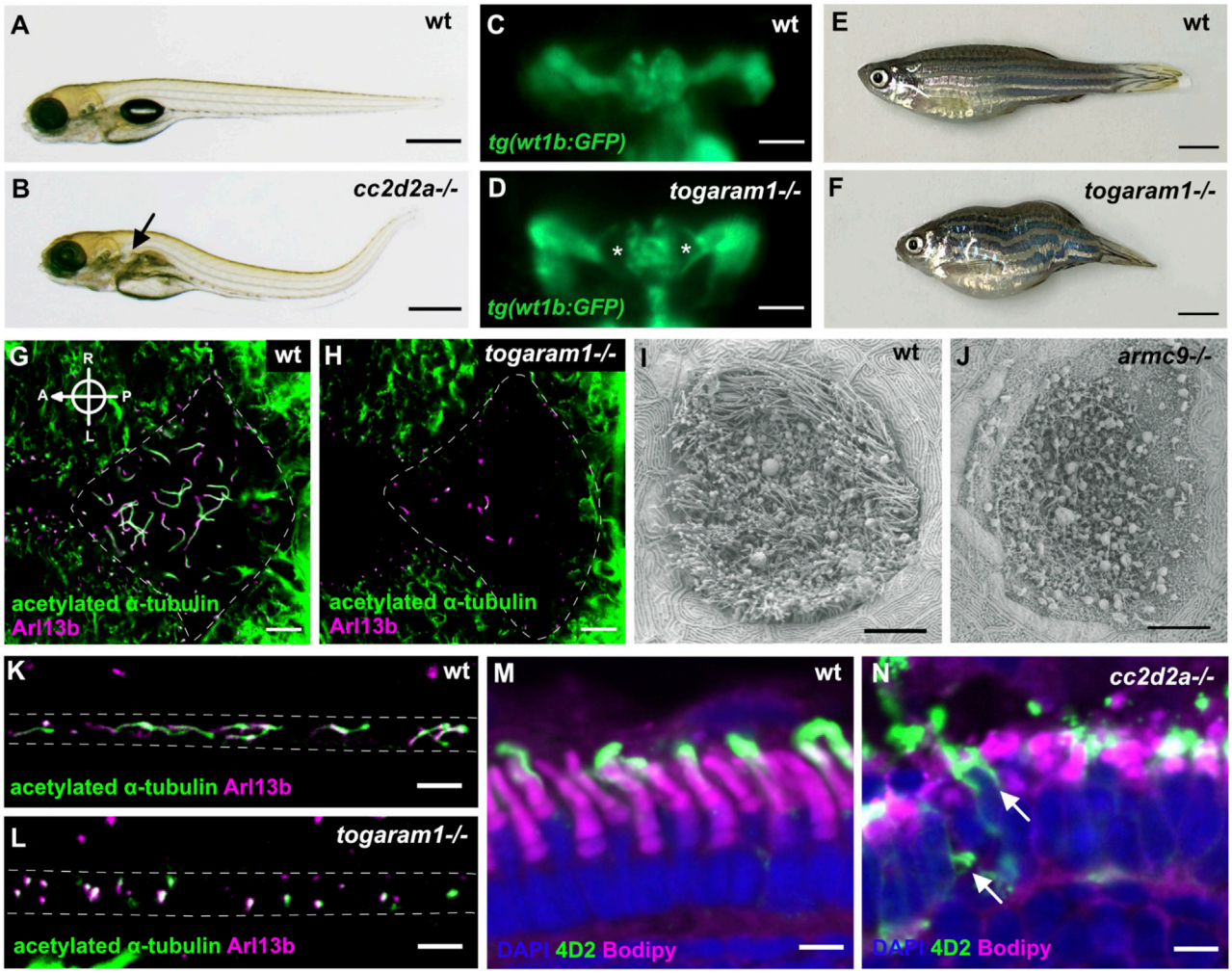

FIGURE 3 | Examples of typical ciliopathy phenotypes in various zebrafish JBTS mutants. **(A,B)** 5 dpf old wildtype larva with straight body **(A)**. Curved body shape and kidney cysts (black arrow) in *cc2d2a–/–* **(B)**. **(C,D)** Transgenic *tg(wt1b:GFP)* line highlighting the pronephros of 3 dpf wildtype **(C)** and *togaram1–/–* **(D)** larvae showing an enlargement of the proximal tubules close to the glomerular region (=kidney cysts) marked by asterisks in the mutant. Dorsal view, rostral to the top. **(E,F)** Adult wildtype zebrafish **(E)** with a straight body axis compared to scoliosis in *togaram1–/–* **(F)**. **(G,H)** Whole mount immunohistochemistry of forebrain ventricular cilia in 3 dpf old wildtype **(G)** and *togaram1–/–* **(H)** larvae showing shorter and fewer cilia in mutants with decreased acetylation (green, acetylated α-tubulin). Dotted lines mark the border of the ventricular space for orientation. Note that green signal outside of the ventricle stems from axons which are rich in acetylated α-tubulin. **(I,J)** Scanning electron microscopy (SEM) image of the olfactory placode cilia in 5 dpf old wildtype **(I)** and *armc9–/–* **(J)** larvae showing almost absent cilia in the olfactory placode of the mutant. **(K,L)** Immunohistochemistry of kidney cilia in 3 dpf old wildtype **(K)** and *togaram1–/–* **(L)** larvae showing shorter cilia in mutants. Dotted lines mark border of the pronephric tubule for orientation (lateral view with rostral to the left). **(M,N)** Immunohistochemistry on cryosections of 5 dpf wt **(M)** and *cc2d2a–/–* **(N)** larvae showing normal retinal lamination but shortened and dysmorphic outer segments (marked by bodipy in magenta) and mislocalization of opsins to the photoreceptor cell body (4D2 antibody in green, arrows) in mutants. Scale bars are 500 µm **(A,B)**, 50 µm **(C,D)**, 5 mm **(E,F)**, 10 µm **(G–J)** and 5 µm **(K–N)**.

Phenotypes seen most commonly in zebrafish JBTS mutants included larval body curvature, kidney cysts, retinal defects and scoliosis in adults (**Figure 5**). Notably, retinal and renal defects are also most common in individuals with JBTS in addition to the characteristic CNS malformation (Romani et al., 2013; Bachmann-Gagescu et al., 2015a). A cerebellar defect has been described in a single JBTS zebrafish model so far, namely for *arl13b* (Zhu et al., 2019). This work found that in *arl13b* morphant (and mutant) larvae, the number of cerebellar granule cells was reduced and the development of Purkinje cells was also affected, anomalies that were linked to defective WNT signaling. Of note, the described central nervous system phenotypes were relatively mild compared to the anomalies found in mouse models for *Arl13b* (Higginbotham et al., 2012; Suciu et al., 2021) or in human patients harboring *ARL13B* mutations (Cantagrel et al., 2008; Thomas et al., 2015). No other studies have described cerebellar anomalies in zebrafish JBTS models yet, whereby it remains unclear how thoroughly the central nervous system has been analyzed in the published zebrafish JBTS models to date. Morphological anomalies of cilia described most commonly in

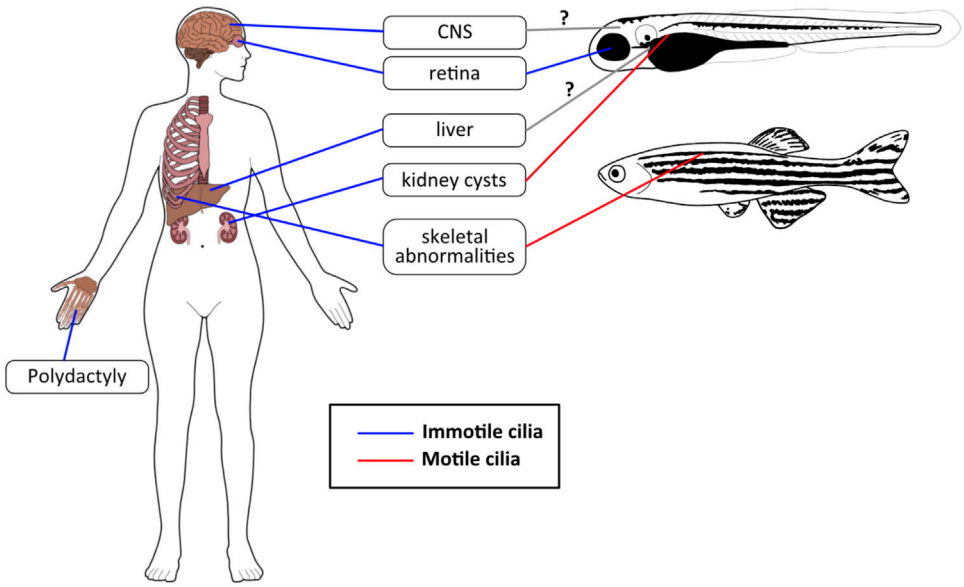

FIGURE 4 | JBTS phenotypes in humans and zebrafish. The most common JBTS phenotypes seen in humans have analogous phenotypes in zebrafish, although these are sometimes caused by motile cilia dysfunction rather than defects in primary cilia. Blue lines: immotile/primary cilia, red lines: motile cilia, gray lines with question mark (?): not clear yet whether zebrafish JBTS models display a phenotype in these organs (and which types of cilia would be involved).

JBTS zebrafish models included shortened/lack of renal cilia and defective outer segments (OSs) (**Supplementary Table S1**).

DISCUSSION: INSIGHTS INTO CILIARY FUNCTION AND JOUBERT SYNDROME PATHOMECHANISMS GAINED FROM ZEBRAFISH MODELS

One puzzling question in JBTS disease mechanism is how dysfunction of so many genes, whose protein products localize to different subcompartments of the primary cilium, results in the same disorder characterized by a pathognomonic hallmark, the distinctive "Molar Tooth Sign" (MTS). Given the large number of other non-JBTS associated ciliopathy genes, another way of putting this question is to ask what sets JBTS-associated genes apart from other ciliary genes. On the other hand, despite the unifying brain malformation of JBTS, the prominent phenotypic variability among individuals with JBTS, in particular with respect to associated non-CNS phenoytpes, suggests distinct roles in ciliary biology, possibly explained by the specific subciliary localization of the proteins, and/or by tissue-specific functions for different JBTS-genes. By comparing the phenotypes of the different zebrafish mutants for JBTS we aimed at identifying commonalities and differences between JBTS genes.

Given the strong conservation of the retina between human and zebrafish and the almost constant retinal involvement in zebrafish ciliopathy mutants, most data are available on this organ system, with thoroughly studied mutants for *cc2d2a, talpid3, ift172* and *ahi1*. Interestingly, even though these four mutants all display some degree of retinal dystrophy, which in patients would be considered as "the same phenotype," the underlying mechanism appears to be radically different. In the case of the *cc2d2a*^{w38} mutant, the retinal dystrophy is caused by deficient fusion of incoming opsin-carrier vesicles at the ciliary base, leading to massive accumulation of vesiculo-tubular structures in the inner segment of photoreceptors and dysmorphic outer segments. The proposed model suggests that Cc2d2a, localizing at the connecting cilium (the equivalent of the transition zone in photoreceptors), plays a dual role in the last steps of Rab8-controlled opsin carrier vesicle trafficking (Bachmann-Gagescu et al., 2011; Ojeda Naharros et al., 2017): On the one hand, the vesicle fusion machinery at the periciliary membrane, including SNAREs SNAP25 and Syntaxin3, is disorganized in the absence of Cc2d2a; on the other hand, Cc2d2a provides a docking point for incoming vesicles through a chain of interactions involving Cc2d2a-Ninl-Mical3-Rab8 (Bachmann-Gagescu et al., 2015b). The centrosomal protein Ninl also binds to the cytoplasmic dynein motors that move vesicles along microtubules towards the ciliary base. In contrast to Cc2d2a, Talpid3 deficiency causes retinal dystrophy through a radically different mechanism. *talpid3*$^{i262\text{-}264}$ zebrafish mutants demonstrate retinal degeneration with photoreceptors entirely lacking outer segments, which is secondary to defects in basal body positioning and docking at the apical cell surface (Ojeda Naharros et al., 2018). The very first step of ciliogenesis, which involves Rab8-dependent fusion of the ciliary vesicle onto the mother centriole, appears to be disrupted by loss of Talpid3. Interestingly, the deficient outer segment formation in *talpid3* mutant zebrafish could be rescued by overexpression of a constitutively active form of Rab8. While the ciliogenesis and loss of basal body docking had been previously described in other model systems (Davey et al., 2006; Bangs et al., 2011), and the link to Rab8 had already been identified in cell culture

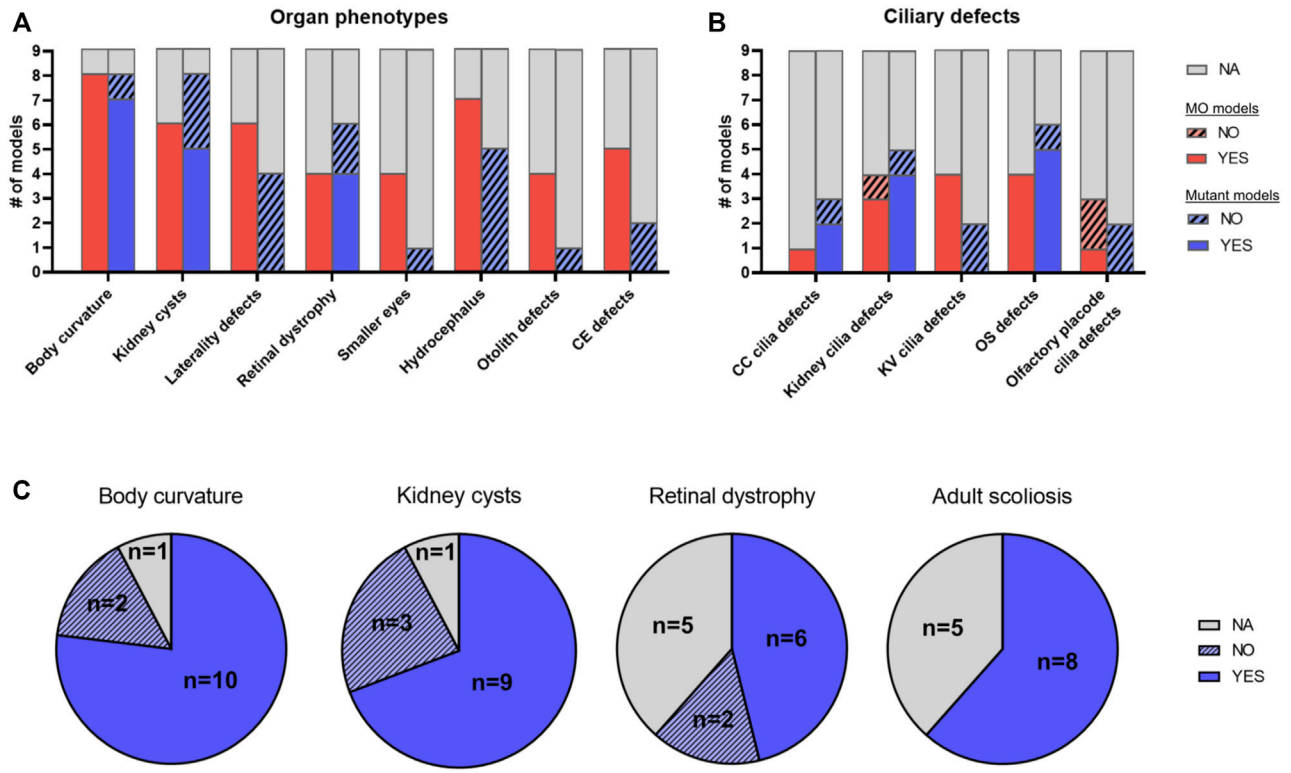

FIGURE 5 | Phenotypic comparison between JBTS zebrafish models. **(A,B)** Comparison of morphant and mutant models for nine different JBTS genes (*ahi1, arl13b, cep290, ift172, inpp5e, kif7, rpgrip1l, tmem67* and *tmem216*) where sufficient phenotypic information was available: Histogram plot illustrating the number of models displaying a given organ phenotype **(A)** or a given ciliary defect **(B).** Red: MO models, blue: mutant models. Note how some phenotypes such as laterality defects, hydrocephalus or convergence-extension defects are often described in morphant models but not in mutant models. **(C)** Comparison of mutant zebrafish models for 13 JBTS genes with sufficient phenotypic information [as indicated in **Table 1**; the 13 mutant lines analyzed here include the nine lines analyzed in **(A,B)** plus *armc9, cc2d2a, talpid3* and *togaram1*, for which no morphant phenotype has been described]. Pie chart plots showing the proportion of mutant models displaying each of the four most common ciliopathy phenotypes seen in zebrafish (body curvature, kidney cysts, retinal dystrophy and adult scoliosis). YES: model has the phenotype, NO: model does not have the phenotype, NA: not available/not described. Note that some mutants are included in both sets of comparisons in **(A)** and **(B)** (**Table 1**). CC: central canal; CE: conversion-extension; KV: Kupffer's vesicle; MO: morphant; OS: outer segment.

(Kobayashi et al., 2014), the zebrafish experiments allowed to place Talpid3 upstream of Rab8 activation. As a third mechanism underlying photoreceptor dysfunction, studies of an *ift172* zebrafish mutant revealed a distinct function in outer segment formation. Mutant photoreceptors failed to complete extension of the cilium, after successful basal body docking and formation of the connecting cilium. Additionally, large accumulation of membranous material was found within the inner segment, suggesting that photoreceptors try to assemble outer segment material, but fail to extend the ciliary structure (Sukumaran and Perkins, 2009). Finally, the mechanism underlying the retinal dystrophy in *ahi1* mutants is not definitely determined, but the described dysmorphic outer segments, aberrant disk stacking/orientation and accumulation of vesicular material with normal connecting cilium morphology could indicate a similar role in vesicular fusion as for Cc2d2a (Lessieur et al., 2017). These studies of zebrafish retina revealed different molecular mechanisms leading to the same ciliopathy phenotype, namely retinal dystrophy. Whereas Talpid3 and Ift172 play a role in ciliogenesis, either in proper BB docking at the onset of ciliogenesis or later in outer segment extension, the role of Cc2d2a lies downstream of ciliogenesis, in organizing the last steps of opsin vesicle trafficking and fusion. In fact, the distinct ciliary defects observed in the different mutants are consistent with the localization of the respective proteins: Talpid3 localizes to the BB, which can explain defects in early ciliogenesis steps, Ift172 is part of the IFT machinery, required to transport the building blocks for the extension of the ciliary axoneme and Cc2d2a at the ciliary transition zone organizes the periciliary membrane and provides a docking point for incoming vesicles. Whether these specific roles for each of the proteins are conserved in other cell types than photoreceptors remains open for investigation. Indeed, photoreceptors display such highly specialized cilia, that a cell-type specific role for JBTS proteins is plausible here.

To investigate another aspect of ciliary function, the *talpid3*$^{i262\text{-}264}$ mutants were initially generated to evaluate the role of this protein in Hh signaling (Ben et al., 2011). Indeed, despite the solid body of evidence linking primary cilia to Hh signaling in mammalian cells, this link appeared less clear in zebrafish, probably in part because major CNS anomalies which are typically present in mouse mutants for ciliary genes, appear to

be absent or too subtle to notice without in depth characterization in the corresponding zebrafish mutants, judging by the lack of such mentions in the literature (including for *talpid3* mutants). In contrast, the chick *talpid3* mutant was originally identified as a Hh-mutant, based on the characteristic phenotype including limb patterning defects and craniofacial anomalies (Davey et al., 2006). The *talpid3*$^{i262\text{-}264}$ zebrafish mutants lack cilia in all organs, consistent with the absent photoreceptor outer segments and with results from mouse and chick studies (Davey et al., 2006; Yin et al., 2009; Bangs et al., 2011). This absence of cilia was shown to result also in zebrafish in aberrant Hh signaling, as shown by expansion of the Hh-dependent muscle pioneer cells in the somites (Ben et al., 2011). Further confirming the involvement of cilia in zebrafish Hh signaling, the same group showed that zebrafish Kif7 directly interacts with Gli1 and Gli2a suggesting a function in sequestering Gli proteins in the cytoplasm (Maurya et al., 2013).

Interestingly, the *kif7* mutant generated in this study had no CNS patterning abnormality, which raises the possibility that this signaling pathway does not require cilia for CNS-patterning in zebrafish. Alternatively, functional redundancy between ciliary proteins may be more prominent in the zebrafish than in mammals, such that knock-out of more than one ciliary gene might be required to generate an obvious CNS phenotype, similar to what is observed in *C. elegans*, where double mutants are often required to observe strong ciliary anomalies (Williams et al., 2011). However, considering specifically the cerebellum, which is predominantly affected in individuals with JBTS, the importance of Hh signaling *per se* in zebrafish cerebellar development is still under debate (McFarland et al., 2008). Indeed, the Purkinje cells, which are an important source of SHH during mammalian and avian cerebellar development, appear not to secrete this morphogen in zebrafish. Since SHH is required for proliferation of cerebellar granule cells in mammals, this important difference may explain why no strong cerebellar phenotype has been published yet in zebrafish *kif7*, *talpid3* or other zebrafish JBTS-models. Nevertheless, a recent study did identify cerebellar eurydendroid cells as a source for SHH in the zebrafish cerebellum, such that a role for this pathway is still possible during cerebellar development in this organism (Biechl et al., 2016). Its link to primary cilia in development of the zebrafish cerebellum/CNS remains however an open question. An in-depth analysis of the CNS and specifically of the cerebellum in the available zebrafish mutants will be required to further tease apart the role of Hh signaling in cerebellar development in zebrafish and the role of primary cilia in regulating Hh signaling in the developing zebrafish cerebellum. To our knowledge, a single study has described some cerebellar anomalies in a zebrafish *arl13b* morphant (and mutant) model with a decrease in granule cells in the corpus cerebelli and alteration of expression levels of various cerebellar markers (Zhu et al., 2020). Interestingly, this phenotype was found to be linked to dysregulation of another key developmental signaling pathway, namely Wnt signaling, while Hh signaling was not investigated in this model. Further studies will be required to investigate the CNS phenotype of zebrafish JBTS mutants and to determine the role of primary cilia in developmental signaling in cerebellar/CNS development in this model system.

Such work would be of importance for understanding the pathomechanism underlying JBTS. Indeed, aberrant Hh signaling appears to be a possible common downstream consequence of dysfunction of many (if not all) JBTS-genes. Hh defects could explain many phenotypes associated with this disorder, whereby the retinal dystrophy may represent an exception. Indeed, retinal photoreceptors have such highly specialized cilia that cell-type specific roles of ciliary proteins are likely. Beyond that however, alterations in ciliary length, presence of cilia, or protein composition of the ciliary compartment may all result in aberrant Hh signaling, which in turn could explain patterning/differentiation/proliferation defects leading to signs such as polydactyly (patterning of the limb bud) or the MTS [for example, through deficient proliferation and premature differentiation of granule cell progenitors as shown in *talpid3* conditional knock-out mice (Bashford and Subramanian, 2019)]. Supporting the link between deficient Hh signaling and JBTS, is the fact that two of the more recently identified JBTS genes, namely *ARMC9* and *TOGARAM1*, were identified in a screen for Hh signaling. Zebrafish mutants in these genes display shortened cilia that have significantly decreased posttranslational tubulin modifications (acetylation and glutamylation), suggesting a stability defect for cilia lacking these proteins (Latour et al., 2020). This is associated with shorter cilia, which may affect signal transduction for morphological reasons. Moreover, tubulin posttranslational modifications are thought to alter protein interactions (e.g., motor proteins among others), which could also lead to defective Hh signaling component delivery (Breslow et al., 2018). While the ciliary localization of Armc9 and Togaram1 in zebrafish is still under investigation, work in other organisms has found these proteins, which function in a common module with JBTS proteins CSPP1 and CEP104, at the ciliary base and tip. Further work will be required to determine the role of JBTS-proteins in Hh signaling in zebrafish and the impact of their dysfunction in causing the observed phenotypes. The large number of zebrafish mutants now available in the community should allow to investigate this question conclusively.

One phenotype shared by virtually all zebrafish JBTS mutant models published to date is the body curvature in larvae and scoliosis in adults. The role of the Reissner fiber, a large aggregation of the glycoprotein SCO-spondin present in the central canal from head to tail tip, in maintaining a straight body axis has been clearly demonstrated (Vesque et al., 2019; Troutwine et al., 2020). Work on mutants in several ciliary genes has suggested a key role for motile ventricular cilia in the formation of this fiber (Cantaut-Belarif et al., 2018). Whether mutants in JBTS-genes display lack or immotility of these ventricular cilia, and whether the Reissner fiber is affected in these mutants remains open to investigation.

Another very consistent phenotype found in zebrafish JBTS models are the pronephric (kidney) cysts. Despite this frequently present feature, the pathomechanism leading from mutations in the respective JBTS gene to these cysts has been little investigated in JBTS zebrafish models. It may well be, that the motile cilia present in the zebrafish larval pronephric tubules play a different physiological role than the immotile primary cilia found on human renal tubular cells. In the zebrafish, it has been shown that lack of ciliary motility will cause kidney cysts (Kramer-Zucker et al., 2005; Sullivan-Brown et al., 2008; Zhao et al., 2013) (whereas cystic kidneys are not typically found in patients with

ciliary motility dysfunction in primary ciliary dyskinesia). Moreover, the renal phenotype in individuals with JBTS consists not only of cysts but also of fibrosis, while fibrosis is unlikely to be present in the larval zebrafish pronephros, where the cysts are really formed by a very proximal dilatation of the tubules right after the glomerulus. So while the presence of pronephric cysts in zebrafish harboring mutations in JBTS genes appears to be a good indicator of ciliary dysfunction, it remains to be proven if the pathomechanism leading to kidney cysts is comparable between human and zebrafish larvae.

Finally, one major open question in the field of JBTS research, is the prominent variability observed between patients, in particular with respect to the non-CNS phenotypes. Indeed, even intra-familial variability is very frequently observed, suggesting the presence of genetic modifiers (Phelps et al., 2018). Whether these modifiers are present among JBTS genes themselves can now be tested thanks to the available zebrafish mutants, where double mutants or various combinations of heterozygous/homozygous alleles can be easily generated and studied. Moreover, the comparison between morphant and mutant phenotypes for a given gene can allow the identification of transcriptional adaptations, which can rescue or ameliorate a phenotype. Recent work based on the very mild *cep290*^{fb208} mutant showed for example that *arl3*, *arl13b* and *unc119b*, which are important for cilia membrane transport, were upregulated in mutants but not in morphants to compensate for Cep290 loss (Cardenas-Rodriguez et al., 2021), thereby explaining the milder mutant than morphant phenotype. Another possible explanation for the observed phenotypic variability in individuals with JBTS is putative tissue-specific functions for JBTS proteins and/or cell-type specific protein isoforms. The variety of ciliated tissues in zebrafish allows to address the question of tissue-specificity by comparing ciliary phenotypes in different tissues of a given mutant. Indeed, among the JBTS mutants published to date, the severity of ciliary shortening appears to be variable in different tissues in the *togaram1* mutant for example (more severe in brain ventricles and less severe in olfactory placode cilia). Unfortunately, most studies so far have only focused on one given organ system such that a systematic analysis of all possible ciliopathy phenotypes is lacking (or has not been published) for most zebrafish JBTS mutant models, also limiting the conclusions that we can draw from the comparisons performed in this review. Future work based on comparisons of systematic analyses of the generated mutants could yield important insights, both into the question of tissue-specificity and to link dysfunction of the different subciliary compartments or protein modules to the distinct pathomechanisms.

FUTURE DIRECTIONS

The long-term goal of disease modeling in general, including of ciliary research, is to improve clinical management and to develop therapeutic strategies for patients. The existing zebrafish mutant models for JBTS have helped to gain more insights into ciliary biology and JBTS pathomechanism. Unfortunately, the published phenotypic characterization of these models is largely incomplete. In the future, a systematic analysis of the generated mutants will certainly yield more insights into tissue-specific ciliary functions underlying JBTS pathomechanism. This knowledge should generate models to test, for example, linking ciliary localization of an affected protein to a specific pathomechanism in a given tissue or identifying which combinations of gene alleles modify the phenotype. Such models should in turn improve our ability to predict the clinical outcome for affected individuals.

One powerful advantage of the zebrafish model is its transparency at larval stages and the external development of the embryos. This enables live imaging of developing larvae in an intact whole-tissue context using transgenic lines in which the ciliary membrane, axoneme and/or basal body are fluorescently labeled. To fully understand the dynamic life of a cilium, it is key to observe it in its natural environment. So far, the few studies performing live imaging on cilia were mostly conducted on *in vitro* cell systems, in which ciliogenesis or ciliary resorption are artificially induced by removal or addition of serum (Ott and Lippincott-Schwartz, 2012; Ijaz and Ikegami, 2019; Mirvis et al., 2019). Using the zebrafish, these key events in the life of a cilium can be studied in a physiological context. Given the ease of transgenesis in zebrafish and combined with modern techniques such as optogenetics or chemogenetics, the mechanisms underlying other aspects of ciliary function, including signaling, can now be elucidated. As an example, recent work showed how cAMP is interpreted in the cilia of whole zebrafish embryos (Truong et al., 2021).

Another strength of the zebrafish model is the possibility of conducting large-scale chemical screens. Larvae can be placed in 96-well plates and exposed to chemical compounds in the medium. Many such high-throughput chemical screens have been performed using zebrafish (Cassar et al., 2020; Zhang and Peterson, 2020), including drug screenings in kidney disease (Gehrig et al., 2018) and retinal degeneration (Ganzen et al., 2021), yielding interesting candidate molecules. Given the large number of JBTS zebrafish models available, these can now be used for identifying compounds that improve ciliopathy phenotypes as a first step for developing therapeutic strategies for JBTS patients.

In conclusion, zebrafish JBTS models have already played an important role in shaping our understanding of ciliary biology and disease pathomechanism. A systematic assessment of the large number of zebrafish models generated by the community will allow to gain further insights into the role of JBTS proteins, to advance our knowledge on disease mechanisms and to identify therapeutic approaches, harnessing the strengths of this model system.

AUTHOR CONTRIBUTIONS

TDSR and RB-G conceptualized and wrote the manuscript, TDSR and CH generated images for the figures.

FUNDING

TDSR, CH, and RB-G were supported by SNSF grant PP00P3_198895; TDSR was supported by a PhD student grant from the Zurich Neuroscience Center (ZNZ); RB-G is a member of the University Research Priority Program AdaBD of the University of Zurich.

ACKNOWLEDGMENTS

We thank members of the Bachmann lab for input on the manuscript and helpful discussions. We apologize for any work relevant for this review that we have not cited.

SUPPLEMENTARY MATERIAL

The Supplementary Material for this article can be found online at: https://www.frontiersin.org/articles/10.3389/fgene.2022.939527/full#supplementary-material

REFERENCES

Abrams, E. W., and Mullins, M. C. (2009). Early Zebrafish Development: It's in the Maternal Genes. *Curr. Opin. Genet. Dev.* 19, 396–403. doi:10.1016/j.gde.2009.06.002

Adams, M., Simms, R. J., Abdelhamed, Z., Dawe, H. R., Szymanska, K., Logan, C. V., et al. (2012). A Meckelin-Filamin A Interaction Mediates Ciliogenesis. *Hum. Mol. Genet.* 21, 1272–1286. doi:10.1093/hmg/ddr557

Amsterdam, A., Burgess, S., Golling, G., Chen, W., Sun, Z., Townsend, K., et al. (1999). A Large-Scale Insertional Mutagenesis Screen in Zebrafish. *Genes Dev.* 13, 2713–2724. doi:10.1101/gad.13.20.2713

Angueyra, J. M., and Kindt, K. S. (2018). Leveraging Zebrafish to Study Retinal Degenerations. *Front. Cell Dev. Biol.* 6, 110. doi:10.3389/fcell.2018.00110

Babu, D., and Roy, S. (2013). Left-Right Asymmetry: Cilia Stir Up New Surprises in the Node. *Open Biol.* 3, 130052. doi:10.1098/rsob.130052

Bachmann-Gagescu, R., and Neuhauss, S. C. (2019). The Photoreceptor Cilium and its Diseases. *Curr. Opin. Genet. Dev.* 56, 22–33. doi:10.1016/j.gde.2019.05.004

Bachmann-Gagescu, R., Phelps, I. G., Stearns, G., Link, B. A., Brockerhoff, S. E., Moens, C. B., et al. (2011). The Ciliopathy Gene Cc2d2a Controls Zebrafish Photoreceptor Outer Segment Development Through a Role in Rab8-Dependent Vesicle Trafficking. *Hum. Mol. Genet.* 20, 4041–4055. doi:10.1093/hmg/ddr332

Bachmann-Gagescu, R., Dempsey, J. C., Phelps, I. G., O'Roak, B. J., Knutzen, D. M., Rue, T. C., et al. (2015a). Joubert Syndrome: A Model for Untangling Recessive Disorders with Extreme Genetic Heterogeneity. *J. Med. Genet.* 52, 514–522. doi:10.1136/jmedgenet-2015-103087

Bachmann-Gagescu, R., Dona, M., Hetterschijt, L., Tonnaer, E., Peters, T., de Vrieze, E., et al. (2015b). The Ciliopathy Protein CC2D2A Associates with NINL and Functions in RAB8-MICAL3-Regulated Vesicle Trafficking. *PLoS Genet.* 11, e1005575. doi:10.1371/journal.pgen.1005575

Bachmann-Gagescu, R., Dempsey, J. C., Bulgheroni, S., Chen, M. L., D'Arrigo, S., Glass, I. A., et al. (2020). Healthcare Recommendations for Joubert Syndrome. *Am. J. Med. Genet.* 182, 229–249. doi:10.1002/ajmg.a.61399

Badano, J. L., Mitsuma, N., Beales, P. L., and Katsanis, N. (2006). The Ciliopathies: An Emerging Class of Human Genetic Disorders. *Annu. Rev. Genom. Hum. Genet.* 7, 125–148. doi:10.1146/annurev.genom.7.080505.115610

Bangs, F., and Anderson, K. V. (2017). Primary Cilia and Mammalian Hedgehog Signaling. *Cold Spring Harb. Perspect. Biol.* 9, a028175. doi:10.1101/cshperspect.a028175

Bangs, F., Antonio, N., Thongnuek, P., Welten, M., Davey, M. G., Briscoe, J., et al. (2011). Generation of Mice with Functional Inactivation of Talpid3, a Gene First Identified in Chicken. *Development* 138, 3261–3272. doi:10.1242/dev.063602

Bashford, A. L., and Subramanian, V. (2019). Mice with a Conditional Deletion of Talpid3 (KIAA0586) - a Model for Joubert Syndrome. *J. Pathol.* 248, 396–408. doi:10.1002/path.5271

Baye, L. M., Patrinostro, X., Swaminathan, S., Beck, J. S., Zhang, Y., Stone, E. M., et al. (2011). The N-Terminal Region of Centrosomal Protein 290 (CEP290) Restores Vision in a Zebrafish Model of Human Blindness. *Hum. Mol. Genet.* 20, 1467–1477. doi:10.1093/hmg/ddr025

Ben, J., Elworthy, S., Ng, A. S. M., van Eeden, F., and Ingham, P. W. (2011). Targeted Mutation of the Talpid3 Gene in Zebrafish Reveals its Conserved Requirement for Ciliogenesis and Hedgehog Signalling Across the Vertebrates. *Development* 138, 4969–4978. doi:10.1242/dev.070862

Bergboer, J. G. M., Wyatt, C., Austin-Tse, C., Yaksi, E., and Drummond, I. A. (2018). Assaying Sensory Ciliopathies Using Calcium Biosensor Expression in Zebrafish Ciliated Olfactory Neurons. *Cilia* 7, 2. doi:10.1186/s13630-018-0056-1

Bibliowicz, J., Tittle, R. K., and Gross, J. M. (2011). Toward a Better Understanding of Human Eye Disease Insights from the Zebrafish, *Danio rerio*. *Prog. Mol. Biol. Transl. Sci.* 100, 287–330. doi:10.1016/B978-0-12-384878-9.00007-8

Biechl, D., Dorigo, A., Köster, R. W., Grothe, B., and Wullimann, M. F. (2016). Eppur Si Muove: Evidence for an External Granular Layer and Possibly Transit Amplification in the Teleostean Cerebellum. *Front. Neuroanat.* 10, 49. doi:10.3389/fnana.2016.00049

Borovina, A., Superina, S., Voskas, D., and Ciruna, B. (2010). Vangl2 Directs the Posterior Tilting and Asymmetric Localization of Motile Primary Cilia. *Nat. Cell Biol.* 12, 407–412. doi:10.1038/ncb2042

Boswell, C. W., and Ciruna, B. (2017). Understanding Idiopathic Scoliosis: A New Zebrafish School of Thought. *Trends Genet.* 33, 183–196. doi:10.1016/j.tig.2017.01.001

Breslow, D. K., Hoogendoorn, S., Kopp, A. R., Morgens, D. W., Vu, B. K., Kennedy, M. C., et al. (2018). A CRISPR-Based Screen for Hedgehog Signaling Provides Insights into Ciliary Function and Ciliopathies. *Nat. Genet.* 50, 460–471. doi:10.1038/s41588-018-0054-7

Bujakowska, K. M., Zhang, Q., Siemiatkowska, A. M., Liu, Q., Place, E., Falk, M. J., et al. (2015). Mutations in IFT172 Cause Isolated Retinal Degeneration and Bardet-Biedl Syndrome. *Hum. Mol. Genet.* 24, 230–242. doi:10.1093/hmg/ddu441

Cantagrel, V., Silhavy, J. L., Bielas, S. L., Swistun, D., Marsh, S. E., Bertrand, J. Y., et al. (2008). Mutations in the Cilia Gene ARL13B Lead to the Classical Form of Joubert Syndrome. *Am. J. Hum. Genet.* 83, 170–179. doi:10.1016/j.ajhg.2008.06.023

Cantaut-Belarif, Y., Sternberg, J. R., Thouvenin, O., Wyart, C., and Bardet, P.-L. (2018). The Reissner Fiber in the Cerebrospinal Fluid Controls Morphogenesis of the Body Axis. *Curr. Biol.* 28, 2479–2486.e4. doi:10.1016/j.cub.2018.05.079

Cardenas-Rodriguez, M., Austin-Tse, C., Bergboer, J. G. M., Molinari, E., Sugano, Y., Bachmann-Gagescu, R., et al. (2021). Genetic Compensation for Cilia Defects in cep290/NPHP6 Mutants by Upregulation of Cilia-Associated Small GTPases. *J. Cell Sci.* 134, jcs258568. doi:10.1242/jcs.258568

Cassar, S., Adatto, I., Freeman, J. L., Gamse, J. T., Iturria, I., Lawrence, C., et al. (2020). Use of Zebrafish in Drug Discovery Toxicology. *Chem. Res. Toxicol.* 33, 95–118. doi:10.1021/acs.chemrestox.9b00335

Davey, M. G., Paton, I. R., Yin, Y., Schmidt, M., Bangs, F. K., Morrice, D. R., et al. (2006). The Chicken Talpid3 Gene Encodes a Novel Protein Essential for Hedgehog Signaling. *Genes Dev.* 20, 1365–1377. doi:10.1101/gad.369106

Dowdle, W. E., Robinson, J. F., Kneist, A., Sirerol-Piquer, M. S., Frints, S. G. M., Corbit, K. C., et al. (2011). Disruption of a Ciliary B9 Protein Complex Causes Meckel Syndrome. *Am. J. Hum. Genet.* 89, 94–110. doi:10.1016/j.ajhg.2011.06.003

Duldulao, N. A., Lee, S., and Sun, Z. (2009). Cilia Localization Is Essential for *In Vivo* Functions of the Joubert Syndrome Protein Arl13b/Scorpion. *Development* 136, 4033–4042. doi:10.1242/dev.036350

Eisa-Beygi, S., Benslimane, F. M., El-Rass, S., Prabhudesai, S., Abdelrasoul, M. K. A., Simpson, P. M., et al. (2018). Characterization of Endothelial Cilia Distribution During Cerebral-Vascular Development in Zebrafish (*Danio rerio*). *Arterioscler. Thromb. Vasc. Biol.* 38, 2806–2818. doi:10.1161/ATVBAHA.118.311231

Eisen, J. S., and Smith, J. C. (2008). Controlling Morpholino Experiments: Don't Stop Making Antisense. *Development* 135, 1735–1743. doi:10.1242/dev.001115

El-Brolosy, M. A., Kontarakis, Z., Rossi, A., Kuenne, C., Günther, S., Fukuda, N., et al. (2019). Genetic Compensation Triggered by Mutant mRNA Degradation. *Nature* 568, 193–197. doi:10.1038/s41586-019-1064-z

Elsayed, S. M., Phillips, J. B., Heller, R., Thoenes, M., Elsobky, E., Nürnberg, G., et al. (2015). Non-Manifesting AHI1 Truncations Indicate Localized Loss-Of-Function Tolerance in a Severe Mendelian Disease Gene. *Hum. Mol. Genet.* 24, 2594–2603. doi:10.1093/hmg/ddv022

Emmer, B. T., Maric, D., and Engman, D. M. (2010). Molecular Mechanisms of Protein and Lipid Targeting to Ciliary Membranes. *J. Cell Sci.* 123, 529–536. doi:10.1242/jcs.062968

Ferrante, M. I., Romio, L., Castro, S., Collins, J. E., Goulding, D. A., Stemple, D. L., et al. (2009). Convergent Extension Movements and Ciliary Function Are Mediated by Ofd1, a Zebrafish Orthologue of the Human Oral-Facial-Digital Type 1 Syndrome Gene. *Hum. Mol. Genet.* 18, 289–303. doi:10.1093/hmg/ddn356

Fleisch, V. C., and Neuhauss, S. C. F. (2006). Visual Behavior in Zebrafish. *Zebrafish* 3, 191–201. doi:10.1089/zeb.2006.3.191

Frikstad, K.-A. M., Molinari, E., Thoresen, M., Ramsbottom, S. A., Hughes, F., Letteboer, S. J. F., et al. (2019). A CEP104-CSPP1 Complex Is Required for Formation of Primary Cilia Competent in Hedgehog Signaling. *Cell Rep.* 28, 1907–1922.e6. doi:10.1016/j.celrep.2019.07.025

Ganzen, L., Ko, M. J., Zhang, M., Xie, R., Chen, Y., Zhang, L., et al. (2021). Drug Screening with Zebrafish Visual Behavior Identifies Carvedilol as a Potential Treatment for an Autosomal Dominant Form of Retinitis Pigmentosa. *Sci. Rep.* 11, 11432. doi:10.1038/s41598-021-89482-z

Garcia-Gonzalo, F. R., Corbit, K. C., Sirerol-Piquer, M. S., Ramaswami, G., Otto, E. A., Noriega, T. R., et al. (2011). A Transition Zone Complex Regulates Mammalian Ciliogenesis and Ciliary Membrane Composition. *Nat. Genet.* 43, 776–784. doi:10.1038/ng.891

Gehrig, J., Pandey, G., and Westhoff, J. H. (2018). Zebrafish as a Model for Drug Screening in Genetic Kidney Diseases. *Front. Pediatr.* 6, 183. doi:10.3389/fped.2018.00183

Glasauer, S. M. K., and Neuhauss, S. C. F. (2014). Whole-Genome Duplication in Teleost Fishes and its Evolutionary Consequences. *Mol. Genet. Genomics* 289, 1045–1060. doi:10.1007/s00438-014-0889-2

Goetz, S. C., and Anderson, K. V. (2010). The Primary Cilium: A Signalling Centre During Vertebrate Development. *Nat. Rev. Genet.* 11, 331–344. doi:10.1038/nrg2774

Golling, G., Amsterdam, A., Sun, Z., Antonelli, M., Maldonado, E., Chen, W., et al. (2002). Insertional Mutagenesis in Zebrafish Rapidly Identifies Genes Essential for Early Vertebrate Development. *Nat. Genet.* 31, 135–140. doi:10.1038/ng896

Gorden, N. T., Arts, H. H., Parisi, M. A., Coene, K. L. M., Letteboer, S. J. F., van Beersum, S. E. C., et al. (2008). CC2D2A Is Mutated in Joubert Syndrome and Interacts with the Ciliopathy-Associated Basal Body Protein CEP290. *Am. J. Hum. Genet.* 83, 559–571. doi:10.1016/j.ajhg.2008.10.002

Gross, J. M., Perkins, B. D., Amsterdam, A., Egaña, A., Darland, T., Matsui, J. I., et al. (2005). Identification of Zebrafish Insertional Mutants with Defects in Visual System Development and Function. *Genetics* 170, 245–261. doi:10.1534/genetics.104.039727

Halbritter, J., Bizet, A. A., Schmidts, M., Porath, J. D., Braun, D. A., Gee, H. Y., et al. (2013). Defects in the IFT-B Component IFT172 Cause Jeune and Mainzer-Saldino Syndromes in Humans. *Am. J. Hum. Genet.* 93, 915–925. doi:10.1016/j.ajhg.2013.09.012

Hammarsjö, A., Wang, Z., Vaz, R., Taylan, F., Sedghi, M., Girisha, K. M., et al. (2017). Novel KIAA0753 Mutations Extend the Phenotype of Skeletal Ciliopathies. *Sci. Rep.* 7, 15585. doi:10.1038/s41598-017-15442-1

Hartill, V., Szymanska, K., Sharif, S. M., Wheway, G., and Johnson, C. A. (2017). Meckel–Gruber Syndrome: An Update on Diagnosis, Clinical Management, and Research Advances. *Front. Pediatr.* 5, 244. doi:10.3389/fped.2017.00244

Higginbotham, H., Eom, T.-Y., Mariani, L. E., Bachleda, A., Hirt, J., Gukassyan, V., et al. (2012). Arl13b in Primary Cilia Regulates the Migration and Placement of Interneurons in the Developing Cerebral Cortex. *Dev. Cell* 23, 925–938. doi:10.1016/j.devcel.2012.09.019

Hildebrandt, F., Benzing, T., and Katsanis, N. (2011). Ciliopathies. *N. Engl. J. Med.* 364, 1533–1543. doi:10.1056/NEJMra1010172

Howe, K., Clark, M. D., Torroja, C. F., Torrance, J., Berthelot, C., Muffato, M., et al. (2013). The Zebrafish Reference Genome Sequence and its Relationship to the Human Genome. *Nature* 496, 498–503. doi:10.1038/nature12111

Huang, L., Szymanska, K., Jensen, V. L., Janecke, A. R., Innes, A. M., Davis, E. E., et al. (2011). TMEM237 Is Mutated in Individuals with a Joubert Syndrome Related Disorder and Expands the Role of the TMEM Family at the Ciliary Transition Zone. *Am. J. Hum. Genet.* 89, 713–730. doi:10.1016/j.ajhg.2011.11.005

Huang, P., Xiao, A., Zhou, M., ZhuLin, Z. S., and Zhang, S. B. (2011). Heritable Gene Targeting in Zebrafish Using Customized TALENs. *Nat. Biotechnol.* 29, 699–700. doi:10.1038/nbt.1939

Ijaz, F., and Ikegami, K. (2019). Live Cell Imaging of Dynamic Behaviors of Motile Cilia and Primary Cilium. *Microsc. (Oxf)* 68, 99–110. doi:10.1093/jmicro/dfy147

Ishikawa, H., and Marshall, W. F. (2011). Ciliogenesis: Building the Cell's Antenna. *Nat. Rev. Mol. Cell Biol.* 12, 222–234. doi:10.1038/nrm3085

Kawakami, K. (2007). Tol2: a Versatile Gene Transfer Vector in Vertebrates. *Genome Biol.* 8 (Suppl. 1), S7. doi:10.1186/gb-2007-8-s1-s7

Keeling, J., Tsiokas, L., and Maskey, D. (2016). Cellular Mechanisms of Ciliary Length Control. *Cells* 5, 6. doi:10.3390/cells5010006

Kennedy, B., and Malicki, J. (2009). What Drives Cell Morphogenesis: A Look Inside the Vertebrate Photoreceptor. *Dev. Dyn.* 238, 2115–2138. doi:10.1002/dvdy.22010

Khanna, H., Davis, E. E., Murga-Zamalloa, C. A., Estrada-Cuzcano, A., Lopez, I., den Hollander, A. I., et al. (2009). A Common Allele in RPGRIP1L Is a Modifier of Retinal Degeneration in Ciliopathies. *Nat. Genet.* 41, 739–745. doi:10.1038/ng.366

Ki, S. M., Kim, J. H., Won, S. Y., Oh, S. J., Lee, I. Y., Bae, Y. K., et al. (2020). CEP41-Mediated Ciliary Tubulin Glutamylation Drives Angiogenesis Through AURKA-Dependent Deciliation. *EMBO Rep.* 21, e48290. doi:10.15252/embr.201948290

Kobayashi, T., Kim, S., Lin, Y.-C., Inoue, T., and Dynlacht, B. D. (2014). The CP110-Interacting Proteins Talpid3 and Cep290 Play Overlapping and Distinct Roles in Cilia Assembly. *J. Cell Biol.* 204, 215–229. doi:10.1083/jcb.201304153

Koudijs, M. J., den Broeder, M. J., Keijser, A., Wienholds, E., Houwing, S., van Rooijen, E. M. H. C., et al. (2005). The Zebrafish Mutants Dre, Uki, and Lep Encode Negative Regulators of the Hedgehog Signaling Pathway. *PLoS Genet.* 1, e19. doi:10.1371/journal.pgen.0010019

Kramer-Zucker, A. G., Olale, F., Haycraft, C. J., Yoder, B. K., Schier, A. F., and Drummond, I. A. (2005). Cilia-Driven Fluid Flow in the Zebrafish Pronephros, Brain and Kupffer's Vesicle Is Required for Normal Organogenesis. *Development* 132, 1907–1921. doi:10.1242/dev.01772

Latour, B. L., Van De Weghe, J. C., Rusterholz, T. D. S., Letteboer, S. J. F., Gomez, A., Shaheen, R., et al. (2020). Dysfunction of the Ciliary ARMC9/TOGARAM1 Protein Module Causes Joubert Syndrome. *J. Clin. Invest.* 130, 4423–4439. doi:10.1172/JCI131656

Lee, S.-H., Nam, T.-S., Li, W., Kim, J. H., Yoon, W., Choi, Y.-D., et al. (2017). Functional Validation of Novel MKS3/TMEM67 Mutations in COACH Syndrome. *Sci. Rep.* 7, 10222. doi:10.1038/s41598-017-10652-z

Lee, J. E., Silhavy, J. L., Zaki, M. S., Schroth, J., Bielas, S. L., Marsh, S. E., et al. (2012). CEP41 Is Mutated in Joubert Syndrome and Is Required for Tubulin Glutamylation at the Cilium. *Nat. Genet.* 44, 193–199. doi:10.1038/ng.1078

Lee, J. H., Silhavy, J. L., Lee, J. E., Al-Gazali, L., Thomas, S., Davis, E. E., et al. (2012). Evolutionarily Assembled Cis-Regulatory Module at a Human Ciliopathy Locus. *Science* 335, 966–969. doi:10.1126/science.1213506

Leightner, A. C., Hommerding, C. J., Peng, Y., Salisbury, J. L., Gainullin, V. G., Czarnecki, P. G., et al. (2013). The Meckel Syndrome Protein Meckelin (TMEM67) Is a Key Regulator of Cilia Function but Is Not Required for Tissue Planar Polarity. *Hum. Mol. Genet.* 22, 2024–2040. doi:10.1093/hmg/ddt054

Leitch, C. C., Zaghloul, N. A., Davis, E. E., Stoetzel, C., Diaz-Font, A., Rix, S., et al. (2008). Hypomorphic Mutations in Syndromic Encephalocele Genes Are Associated with Bardet-Biedl Syndrome. *Nat. Genet.* 40, 443–448. doi:10.1038/ng.97

Lessieur, E. M., Fogerty, J., Gaivin, R. J., Song, P., and Perkins, B. D. (2017). The Ciliopathy Gene Ahi1 Is Required for Zebrafish Cone Photoreceptor Outer Segment Morphogenesis and Survival. *Invest. Ophthalmol. Vis. Sci.* 58, 448–460. doi:10.1167/iovs.16-20326

Lessieur, E. M., Song, P., Nivar, G. C., Piccillo, E. M., Fogerty, J., Rozic, R., et al. (2019). Ciliary Genes Arl13b, Ahi1 and Cc2d2a Differentially Modify Expression of Visual Acuity Phenotypes but Do Not Enhance Retinal Degeneration Due to Mutation of Cep290 in Zebrafish. *PLoS One* 14, e0213960. doi:10.1371/journal.pone.0213960

Lewis, T. R., Kundinger, S. R., Pavlovich, A. L., Bostrom, J. R., Link, B. A., and Besharse, J. C. (2017). Cos2/Kif7 and Osm-3/Kif17 Regulate Onset of Outer

Segment Development in Zebrafish Photoreceptors Through Distinct Mechanisms. *Dev. Biol.* 425, 176–190. doi:10.1016/j.ydbio.2017.03.019

Lindstrand, A., Davis, E. E., Carvalho, C. M. B., Pehlivan, D., Willer, J. R., Tsai, I.-C., et al. (2014). Recurrent CNVs and SNVs at the NPHP1 Locus Contribute Pathogenic Alleles to Bardet-Biedl Syndrome. *Am. J. Hum. Genet.* 94, 745–754. doi:10.1016/j.ajhg.2014.03.017

Liu, C., Cao, R., Xu, Y., Li, T., Li, F., Chen, S., et al. (2018). Rare Copy Number Variants Analysis Identifies Novel Candidate Genes in Heterotaxy Syndrome Patients with Congenital Heart Defects. *Genome Med.* 10, 40. doi:10.1186/s13073-018-0549-y

Liu, Y., Cao, S., Yu, M., and Hu, H. (2020). TMEM216 Deletion Causes Mislocalization of Cone Opsin and Rhodopsin and Photoreceptor Degeneration in Zebrafish. *Invest. Ophthalmol. Vis. Sci.* 61, 24. doi:10.1167/iovs.61.8.24

Lopes, C. A. M., Prosser, S. L., Romio, L., Hirst, R. A., O'Callaghan, C., Woolf, A. S., et al. (2011). Centriolar Satellites Are Assembly Points for Proteins Implicated in Human Ciliopathies, Including Oral-Facial-Digital Syndrome 1. *J. Cell Sci.* 124, 600–612. doi:10.1242/jcs.077156

Lunt, S. C., Haynes, T., and Perkins, B. D. (2009). Zebrafish Ift57, Ift88, and Ift172 Intraflagellar Transport Mutants Disrupt Cilia but Do Not Affect Hedgehog Signaling. *Dev. Dyn.* 238, 1744–1759. doi:10.1002/dvdy.21999

Luo, N., Lu, J., and Sun, Y. (2012). Evidence of a Role of Inositol Polyphosphate 5-Phosphatase INPP5E in Cilia Formation in Zebrafish. *Vis. Res.* 75, 98–107. doi:10.1016/j.visres.2012.09.011

Mahuzier, A., Gaudé, H.-M., Grampa, V., Anselme, I., Silbermann, F., Leroux-Berger, M., et al. (2012). Dishevelled Stabilization by the Ciliopathy Protein Rpgrip1l Is Essential for Planar Cell Polarity. *J. Cell Biol.* 198, 927–940. doi:10.1083/jcb.201111009

Malicki, J., Avanesov, A., Li, J., Yuan, S., and Sun, Z. (2011). Analysis of Cilia Structure and Function in Zebrafish. *Methods Cell Biol.* 101, 39–74. doi:10.1016/B978-0-12-387036-0.00003-7

Maurya, A. K., Ben, J., Zhao, Z., Lee, R. T. H., Niah, W., Ng, A. S. M., et al. (2013). Positive and Negative Regulation of Gli Activity by Kif7 in the Zebrafish Embryo. *PLoS Genet.* 9, e1003955. doi:10.1371/journal.pgen.1003955

McFarland, K. A., Topczewska, J. M., Weidinger, G., Dorsky, R. I., and Appel, B. (2008). Hh and Wnt Signaling Regulate Formation of Olig2+ Neurons in the Zebrafish Cerebellum. *Dev. Biol.* 318, 162–171. doi:10.1016/j.ydbio.2008.03.016

Mirvis, M., Siemers, K. A., Nelson, W. J., and Stearns, T. P. (2019). Primary Cilium Loss in Mammalian Cells Occurs Predominantly by Whole-Cilium Shedding. *PLoS Biol.* 17, e3000381–26. doi:10.1371/journal.pbio.3000381

Mitchell, D. R. (2007). The Evolution of Eukaryotic Cilia and Flagella as Motile and Sensory Organelles. *Adv. Exp. Med. Biol.* 607, 130–140. doi:10.1007/978-0-387-74021-8_11

Mitchison, H. M., and Valente, E. M. (2017). Motile and Non-Motile Cilia in Human Pathology: from Function to Phenotypes. *J. Pathol.* 241, 294–309. doi:10.1002/path.4843

Moens, C. B., Donn, T. M., Wolf-Saxon, E. R., and Ma, T. P. (2008). Reverse Genetics in Zebrafish by TILLING. *Briefings Funct. Genomics Proteomics* 7, 454–459. doi:10.1093/bfgp/eln046

Morales, E. E., and Wingert, R. A. (2017). Zebrafish as a Model of Kidney Disease. *Results Probl. Cell Differ.* 60, 55–75. doi:10.1007/978-3-319-51436-9_3

Mougou-Zerelli, S., Thomas, S., Szenker, E., Audollent, S., Elkhartoufi, N., Babarit, C., et al. (2009). CC2D2A Mutations in Meckel and Joubert Syndromes Indicate a Genotype-Phenotype Correlation. *Hum. Mutat.* 30, 1574–1582. doi:10.1002/humu.21116

Murga-Zamalloa, C. A., Ghosh, A. K., Patil, S. B., Reed, N. A., Chan, L. S., Davuluri, S., et al. (2011). Accumulation of the Raf-1 Kinase Inhibitory Protein (Rkip) Is Associated with Cep290-Mediated Photoreceptor Degeneration in Ciliopathies. *J. Biol. Chem.* 286, 28276–28286. doi:10.1074/jbc.M111.237560

Mytlis, A., Kumar, V., Qiu, T., Deis, R., Hart, N., Levy, K., et al. (2022). Control of Meiotic Chromosomal Bouquet and Germ Cell Morphogenesis by the Zygotene Cilium. *Science*, eabh3104. doi:10.1126/science.abh3104

Nachury, M. V., Seeley, E. S., and Jin, H. (2010). Trafficking to the Ciliary Membrane: How to Get Across the Periciliary Diffusion Barrier? *Annu. Rev. Cell Dev. Biol.* 26, 59–87. doi:10.1146/annurev.cellbio.042308.113337

Nasevicius, A., and Ekker, S. C. (2000). Effective Targeted Gene 'knockdown' in Zebrafish. *Nat. Genet.* 26, 216–220. doi:10.1038/79951

Ojeda Naharros, I., Gesemann, M., Mateos, J. M., Barmettler, G., Forbes, A., Ziegler, U., et al. (2017). Loss-of-Function of the Ciliopathy Protein Cc2d2a Disorganizes the Vesicle Fusion Machinery at the Periciliary Membrane and Indirectly Affects Rab8-Trafficking in Zebrafish Photoreceptors. *PLoS Genet.* 13, e1007150. doi:10.1371/journal.pgen.1007150

Ojeda Naharros, I., Cristian, F. B., Zang, J., Gesemann, M., Ingham, P. W., Neuhauss, S. C. F., et al. (2018). The Ciliopathy Protein TALPID3/KIAA0586 Acts Upstream of Rab8 Activation in Zebrafish Photoreceptor Outer Segment Formation and Maintenance. *Sci. Rep.* 8, 2211. doi:10.1038/s41598-018-20489-9

Ott, C., and Lippincott-Schwartz, J. (2012). Visualization of Live Primary Cilia Dynamics Using Fluorescence Microscopy. *Curr. Protoc. Cell Biol.* 57, 4.26.1–4.26.22. doi:10.1002/0471143030.cb0426s57

Owens, K. N., Santos, F., Roberts, B., Linbo, T., Coffin, A. B., Knisely, A. J., et al. (2008). Identification of Genetic and Chemical Modulators of Zebrafish Mechanosensory Hair Cell Death. *PLoS Genet.* 4, e1000020. doi:10.1371/journal.pgen.1000020

Parisi, M. A. (2019). The Molecular Genetics of Joubert Syndrome and Related Ciliopathies: The Challenges of Genetic and Phenotypic Heterogeneity. *Trd* 4, 25–49. doi:10.3233/TRD-190041

Patowary, A., Won, S. Y., Oh, S. J., Nesbitt, R. R., Archer, M., Nickerson, D., et al. (2019). Family-Based Exome Sequencing and Case-Control Analysis Implicate CEP41 as an ASD Gene. *Transl. Psychiatry* 9, 4. doi:10.1038/s41398-018-0343-z

Phelps, I. G., Dempsey, J. C., Grout, M. E., Isabella, C. R., Tully, H. M., Doherty, D., et al. (2018). Interpreting the Clinical Significance of Combined Variants in Multiple Recessive Disease Genes: Systematic Investigation of Joubert Syndrome Yields Little Support for Oligogenicity. *Genet. Med.* 20, 223–233. doi:10.1038/gim.2017.94

Putoux, A., Thomas, S., Coene, K. L. M., Davis, E. E., Alanay, Y., Ogur, G., et al. (2011). KIF7 Mutations Cause Fetal Hydrolethalus and Acrocallosal Syndromes. *Nat. Genet.* 43, 601–606. doi:10.1038/ng.826

Reiten, I., Uslu, F. E., Fore, S., Pelgrims, R., Ringers, C., Diaz Verdugo, C., et al. (2017). Motile-Cilia-Mediated Flow Improves Sensitivity and Temporal Resolution of Olfactory Computations. *Curr. Biol.* 27, 166–174. doi:10.1016/j.cub.2016.11.036

Robu, M. E., Larson, J. D., Nasevicius, A., Beiraghi, S., Brenner, C., Farber, S. A., et al. (2007). p53 Activation by Knockdown Technologies. *PLoS Genet.* 3, e78. doi:10.1371/journal.pgen.0030078

Rohatgi, R., and Snell, W. J. (2010). The Ciliary Membrane. *Curr. Opin. Cell Biol.* 22, 541–546. doi:10.1016/j.ceb.2010.03.010

Romani, M., Micalizzi, A., and Valente, E. M. (2013). Joubert Syndrome: Congenital Cerebellar Ataxia with the Molar Tooth. *Lancet Neurology* 12, 894–905. doi:10.1016/S1474-4422(13)70136-4

Roosing, S., Rosti, R. O., Rosti, B., de Vrieze, E., Silhavy, J. L., van Wijk, E., et al. (2016). Identification of a Homozygous Nonsense Mutation in KIAA0556 in a Consanguineous Family Displaying Joubert Syndrome. *Hum. Genet.* 135, 919–921. doi:10.1007/s00439-016-1689-z

Rossi, A., Kontarakis, Z., Gerri, C., Nolte, H., Hölper, S., Krüger, M., et al. (2015). Genetic Compensation Induced by Deleterious Mutations but Not Gene Knockdowns. *Nature* 524, 230–233. doi:10.1038/nature14580

Sang, L., Miller, J. J., Corbit, K. C., Giles, R. H., Brauer, M. J., Otto, E. A., et al. (2011). Mapping the NPHP-JBTS-MKS Protein Network Reveals Ciliopathy Disease Genes and Pathways. *Cell* 145, 513–528. doi:10.1016/j.cell.2011.04.019

Santoriello, C., and Zon, L. I. (2012). Hooked! Modeling Human Disease in Zebrafish. *J. Clin. Invest.* 122, 2337–2343. doi:10.1172/JCI60434

Sassen, W. A., and Köster, R. (2015). "A Molecular Toolbox for Genetic Manipulation of Zebrafish," in *Advances in Genomics and Genetics*.

Sayer, J. A., Otto, E. A., O'Toole, J. F., Nurnberg, G., Kennedy, M. A., Becker, C., et al. (2006). The Centrosomal Protein Nephrocystin-6 Is Mutated in Joubert Syndrome and Activates Transcription Factor ATF4. *Nat. Genet.* 38, 674–681. doi:10.1038/ng1786

Schäfer, T., Pütz, M., Lienkamp, S., Ganner, A., Bergbreiter, A., Ramachandran, H., et al. (2008). Genetic and Physical Interaction Between the NPHP5 and NPHP6 Gene Products. *Hum. Mol. Genet.* 17, 3655–3662. doi:10.1093/hmg/ddn260

Schwarz, N., Lane, A., Jovanovic, K., Parfitt, D. A., Aguila, M., Thompson, C. L., et al. (2017). Arl3 and RP2 Regulate the Trafficking of Ciliary Tip Kinesins. *Hum. Mol. Genet.* 26, 2480–2492. doi:10.1093/hmg/ddx143

Shah, A. N., Davey, C. F., Whitebirch, A. C., Miller, A. C., and Moens, C. B. (2015). Rapid Reverse Genetic Screening Using CRISPR in Zebrafish. *Nat. Methods* 12, 535–540. doi:10.1038/nmeth.3360

Shaheen, R., Schmidts, M., Faqeih, E., Hashem, A., Lausch, E., Holder, I., et al. (2015). A Founder CEP120 Mutation in Jeune Asphyxiating Thoracic Dystrophy Expands the Role of Centriolar Proteins in Skeletal Ciliopathies. *Hum. Mol. Genet.* 24, 1410–1419. doi:10.1093/hmg/ddu555

Shi, X., Garcia, G., Van De Weghe, J. C., McGorty, R., Pazour, G. J., Doherty, D., et al. (2017). Super-resolution Microscopy Reveals that Disruption of Ciliary Transition-Zone Architecture Causes Joubert Syndrome. *Nat. Cell Biol.* 19, 1178–1188. doi:10.1038/ncb3599

Simms, R. J., Hynes, A. M., Eley, L., Inglis, D., Chaudhry, B., Dawe, H. R., et al. (2012). Modelling a Ciliopathy: Ahi1 Knockdown in Model Systems Reveals an Essential Role in Brain, Retinal, and Renal Development. *Cell. Mol. Life Sci.* 69, 993–1009. doi:10.1007/s00018-011-0826-z

Singla, V., and Reiter, J. F. (2006). The Primary Cilium as the Cell's Antenna: Signaling at a Sensory Organelle. *Science* 313, 629–633. doi:10.1126/science.1124534

Slanchev, K., Pütz, M., Schmitt, A., Kramer-Zucker, A., and Walz, G. (2011). Nephrocystin-4 Is Required for Pronephric Duct-Dependent Cloaca Formation in Zebrafish. *Hum. Mol. Genet.* 20, 3119–3128. doi:10.1093/hmg/ddr214

Song, P., Dudinsky, L., Fogerty, J., Gaivin, R., and Perkins, B. D. (2016). Arl13b Interacts with Vangl2 to Regulate Cilia and Photoreceptor Outer Segment Length in Zebrafish. *Invest. Ophthalmol. Vis. Sci.* 57, 4517–4526. doi:10.1167/iovs.16-19898

Stainier, D. Y. R., Raz, E., Lawson, N. D., Ekker, S. C., Burdine, R. D., Eisen, J. S., et al. (2017). Guidelines for Morpholino Use in Zebrafish. *PLoS Genet.* 13, e1007000. doi:10.1371/journal.pgen.1007000

Stawicki, T. M., Hernandez, L., Esterberg, R., Linbo, T., Owens, K. N., Shah, A. N., et al. (2016). Cilia-Associated Genes Play Differing Roles in Aminoglycoside-Induced Hair Cell Death in Zebrafish. *G3 (Bethesda)* 6, 2225–2235. doi:10.1534/g3.116.030080

Stayner, C., Poole, C. A., McGlashan, S. R., Pilanthananond, M., Brauning, R., Markie, D., et al. (2017). An Ovine Hepatorenal Fibrocystic Model of a Meckel-Like Syndrome Associated with Dysmorphic Primary Cilia and TMEM67 Mutations. *Sci. Rep.* 7, 1601. doi:10.1038/s41598-017-01519-4

Suciu, S. K., Long, A. B., and Caspary, T. (2021). Smoothened and ARL13B Are Critical in Mouse for Superior Cerebellar Peduncle Targeting. *Genetics* 218. doi:10.1093/genetics/iyab084

Sukumaran, S., and Perkins, B. D. (2009). Early Defects in Photoreceptor Outer Segment Morphogenesis in Zebrafish Ift57, Ift88 and Ift172 Intraflagellar Transport Mutants. *Vis. Res.* 49, 479–489. doi:10.1016/j.visres.2008.12.009

Sullivan-Brown, J., Schottenfeld, J., Okabe, N., Hostetter, C. L., Serluca, F. C., Thiberge, S. Y., et al. (2008). Zebrafish Mutations Affecting Cilia Motility Share Similar Cystic Phenotypes and Suggest a Mechanism of Cyst Formation that Differs from Pkd2 Morphants. *Dev. Biol.* 314, 261–275. doi:10.1016/j.ydbio.2007.11.025

Sun, Z., Amsterdam, A., Pazour, G. J., Cole, D. G., Miller, M. S., and Hopkins, N. (2004). A Genetic Screen in Zebrafish Identifies Cilia Genes as a Principal Cause of Cystic Kidney. *Development* 131, 4085–4093. doi:10.1242/dev.01240

Szymanska, K., and Johnson, C. A. (2012). The Transition Zone: an Essential Functional Compartment of Cilia. *Cilia* 1, 10. doi:10.1186/2046-2530-1-10

Tay, S. Y., Ingham, P. W., and Roy, S. (2005). A Homologue of the Drosophila Kinesin-Like Protein Costal2 Regulates Hedgehog Signal Transduction in the Vertebrate Embryo. *Development* 132, 625–634. doi:10.1242/dev.01606

Terhune, E. A., Cuevas, M. T., Monley, A. M., Wethey, C. I., Chen, X., Cattell, M. V., et al. (2021). Mutations in KIF7 Implicated in Idiopathic Scoliosis in Humans and Axial Curvatures in Zebrafish. *Hum. Mutat.* 42, 392–407. doi:10.1002/humu.24162

Thomas, S., Wright, K. J., Corre, S. L., Micalizzi, A., Romani, M., Abhyankar, A., et al. (2014). A Homozygous PDE6D Mutation in Joubert Syndrome Impairs Targeting of Farnesylated INPP5E Protein to the Primary Cilium. *Hum. Mutat.* 35, 137–146. doi:10.1002/humu.22470

Thomas, S., Cantagrel, V., Mariani, L., Serre, V., Lee, J.-E., Elkhartoufi, N., et al. (2015). Identification of a Novel ARL13B Variant in a Joubert Syndrome-Affected Patient with Retinal Impairment and Obesity. *Eur. J. Hum. Genet.* 23, 621–627. doi:10.1038/ejhg.2014.156

Tobin, J. L., and Beales, P. L. (2009). The Nonmotile Ciliopathies. *Genet. Med.* 11, 386–402. doi:10.1097/GIM.0b013e3181a02882

Troutwine, B. R., Gontarz, P., Konjikusic, M. J., Minowa, R., Monstad-Rios, A., Sepich, D. S., et al. (2020). The Reissner Fiber Is Highly Dynamic *In Vivo* and Controls Morphogenesis of the Spine. *Curr. Biol.* 30, 2353–2362.e3. doi:10.1016/j.cub.2020.04.015

Truong, M. E., Bilekova, S., Choksi, S. P., Li, W., Bugaj, L. J., Xu, K., et al. (2021). Vertebrate Cells Differentially Interpret Ciliary and Extraciliary cAMP. *Cell* 184, 2911–2926.e18. doi:10.1016/j.cell.2021.04.002

Tuz, K., Bachmann-Gagescu, R., O'Day, D. R., Hua, K., Isabella, C. R., Phelps, I. G., et al. (2014). Mutations in CSPP1 Cause Primary Cilia Abnormalities and Joubert Syndrome With or Without Jeune Asphyxiating Thoracic Dystrophy. *Am. J. Hum. Genet.* 94, 62–72. doi:10.1016/j.ajhg.2013.11.019

Urnov, F. D., Rebar, E. J., Holmes, M. C., Zhang, H. S., and Gregory, P. D. (2010). Genome Editing with Engineered Zinc Finger Nucleases. *Nat. Rev. Genet.* 11, 636–646. doi:10.1038/nrg2842

Valente, E. M., Logan, C. V., Mougou-Zerelli, S., Lee, J. H., Silhavy, J. L., Brancati, F., et al. (2010). Mutations in TMEM216 Perturb Ciliogenesis and Cause Joubert, Meckel and Related Syndromes. *Nat. Genet.* 42, 619–625. doi:10.1038/ng.594

Van De Weghe, J. C., Rusterholz, T. D. S., Latour, B., Grout, M. E., Aldinger, K. A., Shaheen, R., et al. (2017). Mutations in ARMC9 , Which Encodes a Basal Body Protein, Cause Joubert Syndrome in Humans and Ciliopathy Phenotypes in Zebrafish. *Am. J. Hum. Genet.* 101, 23–36. doi:10.1016/j.ajhg.2017.05.010

Vesque, C., Anselme, I., Pezeron, G., Cantaut-Belarif, Y., Eschstruth, A., Djebar, M., et al. (2019). Loss of the Reissner Fiber and Increased URP Neuropeptide Signaling Underlie Scoliosis in a Zebrafish Ciliopathy Mutant. *BioRxiv*. doi:10.1101/2019.12.19.882258

Waters, A. M., and Beales, P. L. (2011). Ciliopathies: an Expanding Disease Spectrum. *Pediatr. Nephrol.* 26, 1039–1056. doi:10.1007/s00467-010-1731-7

Wheway, G., Nazlamova, L., and Hancock, J. T. (2018). Signaling Through the Primary Cilium. *Front. Cell Dev. Biol.* 6, 8. doi:10.3389/fcell.2018.00008

Williams, C. L., Li, C., Kida, K., Inglis, P. N., Mohan, S., Semenec, L., et al. (2011). MKS and NPHP Modules Cooperate to Establish Basal Body/Transition Zone Membrane Associations and Ciliary Gate Function during Ciliogenesis. *J. Cell Biol.* 192, 1023–1041. doi:10.1083/jcb.201012116

Wilson, C. W., Nguyen, C. T., Chen, M.-H., Yang, J.-H., Gacayan, R., Huang, J., et al. (2009). Fused Has Evolved Divergent Roles in Vertebrate Hedgehog Signalling and Motile Ciliogenesis. *Nature* 459, 98–102. doi:10.1038/nature07883

Wingert, R. A., and Davidson, A. J. (2008). The Zebrafish Pronephros: A Model to Study Nephron Segmentation. *Kidney Int.* 73, 1120–1127. doi:10.1038/ki.2008.37

Xu, W., Jin, M., Hu, R., Wang, H., Zhang, F., Yuan, S., et al. (2017). The Joubert Syndrome Protein Inpp5e Controls Ciliogenesis by Regulating Phosphoinositides at the Apical Membrane. *J. Am. Soc. Nephrol.* 28, 118–129. doi:10.1681/ASN.2015080906

T Yamaguchi, T Ishikawa, and Y. Imai (Editors) (2018). *5- Ciliary Motion* (Boston: Elsevier).

Yin, Y., Bangs, F., Paton, I. R., Prescott, A., James, J., Davey, M. G., et al. (2009). The Talpid3 Gene (KIAA0586) Encodes a Centrosomal Protein that Is Essential for Primary Cilia Formation. *Development* 136, 655–664. doi:10.1242/dev.028464

Zhang, T., and Peterson, R. T. (2020). "Chapter 51 - Zebrafish as a Platform for Drug Screening," in *The Zebrafish in Biomedical Research : American College of Laboratory Animal Medicine*. Editors S. C. Cartner, J. S. Eisen, S. C. Farmer, K. J. Guillemin, M. L. Kent, and G. E. Sanders (Academic Press), 659–675. doi:10.1016/b978-0-12-812431-4.00051-8

Zhang, F., Wen, Y., and Guo, X. (2014). CRISPR/Cas9 for Genome Editing: Progress, Implications and Challenges. *Hum. Mol. Genet.* 23, R40–R46. doi:10.1093/hmg/ddu125

Zhao, C., and Malicki, J. (2011). Nephrocystins and MKS Proteins Interact with IFT Particle and Facilitate Transport of Selected Ciliary Cargos. *EMBO J.* 30, 2532–2544. doi:10.1038/emboj.2011.165

Zhao, L., Yuan, S., Cao, Y., Kallakuri, S., Li, Y., Kishimoto, N., et al. (2013). Reptin/Ruvbl2 Is a Lrrc6/Seahorse Interactor Essential for Cilia Motility. *Proc. Natl. Acad. Sci. U.S.A.* 110, 12697–12702. doi:10.1073/pnas.1300968110

Zhu, L., Chen, L., Yan, L., Perkins, B. D., Li, S., Li, B., et al. (2019). Mutant Ahi1 Affects Retinal Axon Projection in Zebrafish via Toxic Gain of Function. *Front. Cell. Neurosci.* 13, 81. doi:10.3389/fncel.2019.00081

Zhu, J., Wang, H.-T., Chen, Y.-R., Yan, L.-Y., Han, Y.-Y., Liu, L.-Y., et al. (2020). The Joubert Syndrome Gene Arl13b Is Critical for Early Cerebellar Development in Zebrafish. *Neurosci. Bull.* 36, 1023–1034. doi:10.1007/s12264-020-00554-y

Zhu, P., Qiu, Q., Harris, P. C., Xu, X., and Lin, X. (2021). Mtor Haploinsufficiency Ameliorates Renal Cysts and Cilia Abnormality in Adult Zebrafish Tmem67 Mutants. *J. Am. Soc. Nephrol.* 32, 822–836. doi:10.1681/ASN.2020070991

Conflict of Interest: The authors declare that the research was conducted in the absence of any commercial or financial relationships that could be construed as a potential conflict of interest.

Publisher's Note: All claims expressed in this article are solely those of the authors and do not necessarily represent those of their affiliated organizations, or those of the publisher, the editors and the reviewers. Any product that may be evaluated in this article, or claim that may be made by its manufacturer, is not guaranteed or endorsed by the publisher.

frontiers | Frontiers in Genetics

ORIGINAL RESEARCH
published: 06 July 2022
doi: 10.3389/fgene.2022.943197

Strongly Truncated *Dnaaf4* Plays a Conserved Role in *Drosophila* Ciliary Dynein Assembly as Part of an R2TP-Like Co-Chaperone Complex With *Dnaaf6*

Jennifer Lennon[1†‡], *Petra zur Lage*[1†], *Alex von Kriegsheim*[2*] *and Andrew P. Jarman*[1*]

[1]Centre for Discovery Brain Sciences, Edinburgh Medical School, University of Edinburgh, Edinburgh, United Kingdom, [2]Edinburgh Cancer Research UK Centre, Institute of Genetics and Cancer, University of Edinburgh, Edinburgh, United Kingdom

OPEN ACCESS

Edited by:
Steven Lc Pei,
Yale University, United States

Reviewed by:
Paurav Desai,
University of Massachusetts Medical School, United States
Junmin Pan,
Tsinghua University, China
Walid A. Houry,
University of Toronto, Canada

***Correspondence:**
Andrew P. Jarman
andrew.jarman@ed.ac.uk

‡Present address:
Jennifer Lennon,
Department of Biology, New York University, New York, NY, United States

†These authors share first authorship

Specialty section:
This article was submitted to Human and Medical Genomics, a section of the journal Frontiers in Genetics

Received: 13 May 2022
Accepted: 16 June 2022
Published: 06 July 2022

Citation:
Lennon J, zur Lage P, von Kriegsheim A and Jarman AP (2022) Strongly Truncated Dnaaf4 Plays a Conserved Role in Drosophila Ciliary Dynein Assembly as Part of an R2TP-Like Co-Chaperone Complex With Dnaaf6. Front. Genet. 13:943197. doi: 10.3389/fgene.2022.943197

Axonemal dynein motors are large multi-subunit complexes that drive ciliary movement. Cytoplasmic assembly of these motor complexes involves several co-chaperones, some of which are related to the R2TP co-chaperone complex. Mutations of these genes in humans cause the motile ciliopathy, Primary Ciliary Dyskinesia (PCD), but their different roles are not completely known. Two such dynein (axonemal) assembly factors (DNAAFs) that are thought to function together in an R2TP-like complex are DNAAF4 (DYX1C1) and DNAAF6 (PIH1D3). Here we investigate the *Drosophila* homologues, *CG14921/Dnaaf4* and *CG5048/Dnaaf6.* Surprisingly, *Drosophila* Dnaaf4 is truncated such that it completely lacks a TPR domain, which in human DNAAF4 is likely required to recruit HSP90. Despite this, we provide evidence that *Drosophila* Dnaaf4 and Dnaaf6 proteins can associate in an R2TP-like complex that has a conserved role in dynein assembly. Both are specifically expressed and required during the development of the two *Drosophila* cell types with motile cilia: mechanosensory chordotonal neurons and sperm. Flies that lack *Dnaaf4* or *Dnaaf6* genes are viable but with impaired chordotonal neuron function and lack motile sperm. We provide molecular evidence that *Dnaaf4* and *Dnaaf6* are required for assembly of outer dynein arms (ODAs) and a subset of inner dynein arms (IDAs).

Keywords: cilium, flagellum, *Drosophila*, ciliopathies, chaperone, dynein

1 INTRODUCTION

Ciliary motility is driven by a highly conserved family of axonemal dynein motors, which are large multi-subunit complexes (King, 2016). Those that comprise the Outer Dynein Arms (ODA) are the main drivers of motility, whereas those of the Inner Dynein Arms (IDA) modulate ciliary movement. During ciliogenesis, the assembly of the motors into the cilium or flagellum is highly regulated. After subunit synthesis, complex assembly occurs within the cytoplasm (known as pre-assembly) prior to transport and docking within the cilium (Fok et al., 1994; Fowkes and Mitchell, 1998). This pre-assembly is facilitated by a series of regulators called dynein pre-assembly factors (DNAAFs) (King, 2016). Many of these factors were originally identified as causative genes of human Primary Ciliary Dyskinesia (PCD), but they are highly conserved among eukaryotes that have motile ciliated cells (Omran et al., 2008). This conservation was recently shown to be true for *Drosophila melanogaster*, which has an almost full complement of homologous genes for the axonemal dynein complexes and

TABLE 1 | Genes referred to in this study.

Drosophila	Flybase ID	Human*	*C. reinhardtii*	Danio rerio
pontin (pont)	FBgn0040078	*RUVBL1*	*CrRuvBL1*	*ruvbl1*
reptin (rept)	FBgn0040075	*RUVBL2*	*CrRuvBL2*	*ruvbl2*
spaghetti/Rpap3	FBgn0015544	*RPAP3*	*Cr02.g084900*	*rpap3*
Spag1	FBgn0039463	*SPAG1*	*Spag1*	*spag1a/b*
CG14921/Dnaaf4	FBgn0032345	*DNAAF4 (DYX1C1)*	*pf23/DYX1C1*	*dnaaf4*
Pih1D1	FBgn0032455	*PIH1D1*	*mot48?*	*pih1d1*
CG4022/Pih1D2	FBgn0035986	*PIH1D2*	*n/a*	*pih1d2*
CG5048/Dnaaf6	FBgn0036437	*DNAAF6 (PIH1D3)*	*twi(?)*	*twister*
Nop17l	FBgn0033224	*DNAAF2/KTU*	*pf13*	*ktu*
Heatr2/Dnaaf5	FBgn0051320	*DNAAF5/HEATR2*	*htr2*	*heatr2*

**Following nomenclature recommendations in Braschi et al. (2022).*

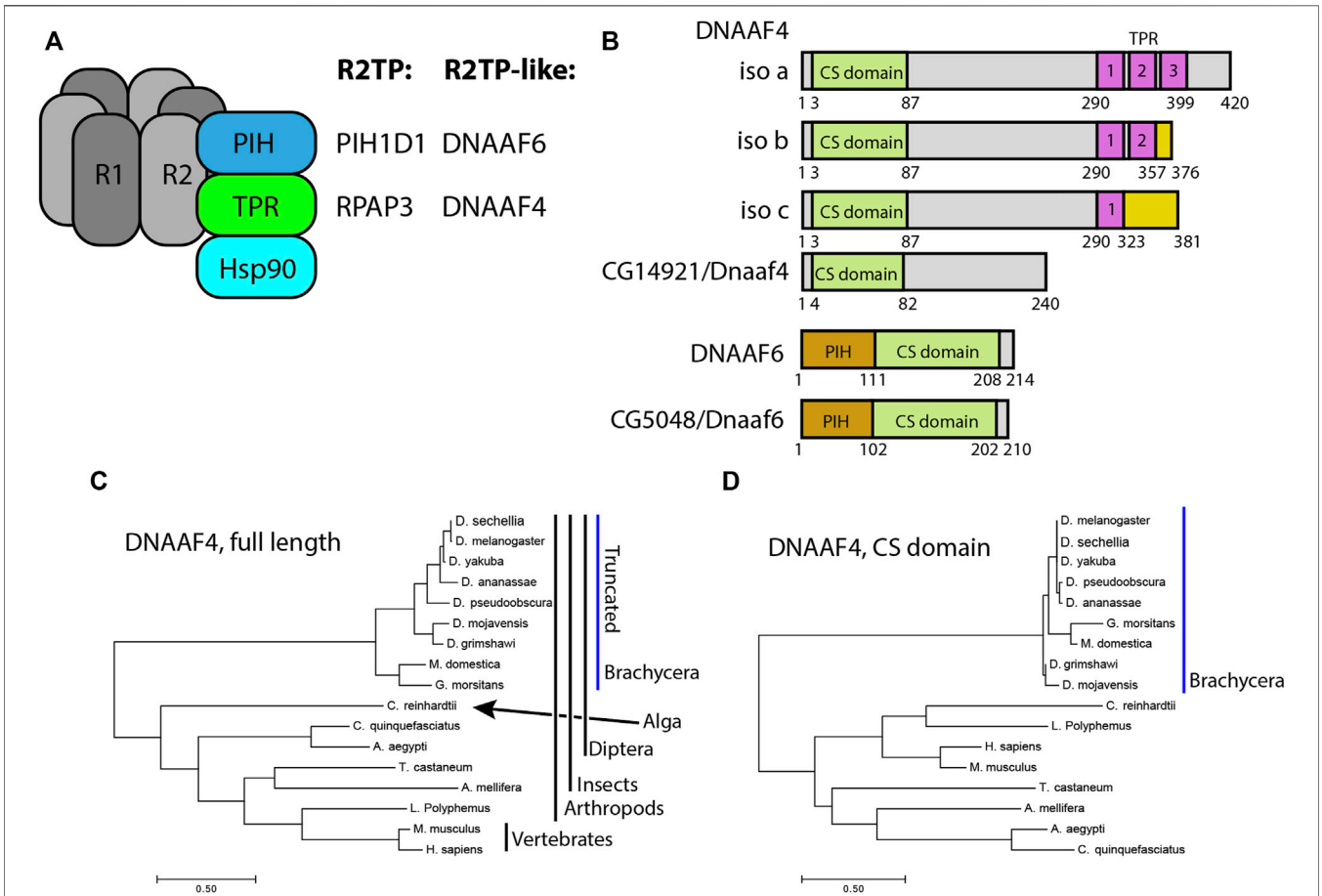

FIGURE 1 | *Drosophila* and mammalian Dnaaf4/Dnaaf6 proteins. **(A)** Schematic showing the composition of R2TP and putative DNAAF4/6-containing R2TP-like complexes. Note that association of DNAAF4/6 with RUVBL1 and RUVBL2 is speculative. **(B)** Schematic showing the protein domains of human DNAAF4, DNAAF6 and their *Drosophila* orthologues. Human isoforms and protein structures are based on Maurizy et al. (2018). **(C)** Phylogenetic tree of DNAAF4 sequences from selected species including vertebrates, arthropods and the unicellular green alga, *Chlamydomonas reinhardtii* (established ciliary motility model organism). Higher dipterans (Brachycera) form a distinct group that correlates with gene truncation (blue bar). **(D)** When comparing CS domains alone, the tree structure remains similar, with Brachycera distinct from other taxa. Organisms included in this tree: *Drosophila sechellia, D. melanogaster, D. yakuba, D. ananassae, D. pseudoobscura, D. mojavensis, D. grimshawi, Musca domestica, Glossina morsitans, Culex quinquefasciatus, Aedes aegypti, Tribolium castaneum, Apis mellifera, Chlamydomonas reinhardtii, Limulus polyphemus, Mus musculus* and *Homo sapiens*.

for dynein assembly factors (zur Lage et al., 2019). In the case of *Drosophila*, ciliary motility is confined to the sensory cilium of mechanosensory neurons (chordotonal neurons) and the sperm flagellum. Flies with dysfunctional dyneins are therefore deaf, uncoordinated and have immotile sperm, which makes the fly a convenient model for analysis of motile ciliogenesis (Diggle et al.,

2014; Moore et al., 2013; zur Lage et al., 2018; zur Lage et al., 2021).

The specific functions of DNAAFs are beginning to be unravelled, and in many cases they are thought to function as co-chaperones that regulate HSP70/90 to facilitate correct folding of the dynein heavy chains as well as subunit assembly (Fabczak and Osinka, 2019). Chaperones are important for many cellular functions including the assembly of large multi-subunit complexes like axonemal dynein motors. For several DNAAFs, such a function is strongly indicated by DNAAF sequence relationships with a known HSP90 co-chaperone, the R2TP complex (Maurizy et al., 2018). This co-chaperone was discovered in *S. cerevisiae* as facilitating RNA polymerase II assembly (Zhao et al., 2005). In humans, R2TP comprises the ATPases RUVBL1 and RUVBL2, a TPR (tetratricopeptide repeat) protein RPAP3, and a Pih domain protein PIH1D1 (**Table 1**). R2TP facilitates the assembly/stabilisation of several multi-subunit complexes, including RNA polymerase II and PIKKs (Kakihara and Houry, 2012; Houry et al., 2018). Much is known of the structural features of R2TP: for RPAP3, the TPR domains directly recruit HSP70 and HSP90 while the RPAP3_C domain binds to RUVBL2 (Martino et al., 2018). For PIH1D1, the PIH domain recruits client proteins, while the CS domain binds to a region of RPAP3 C-terminal to the TPR domain (Kakihara and Houry, 2012; Martino et al., 2018; Maurizy et al., 2018).

There is evidence that mutation of Ruvbl1/2 also causes ciliary dynein defects (Zhao et al., 2013; Li et al., 2017). While this may partly be due to involvement of R2TP in dynein pre-assembly as has been demonstrated in *Chlamydomonas*, zebrafish and *Drosophila* (Yamaguchi et al., 2018; zur Lage et al., 2018; Liu et al., 2019), it is thought that Ruvbl1/2 may also function with DNAAFs to form 'R2TP-like' complexes specifically required for dynein assembly (**Figure 1A**) (Pal et al., 2014; Vaughan, 2014; Olcese et al., 2017). Among the DNAAFs, SPAG1 has both TPR and RPAP3_C domains, while DNAAF4 (DYX1C1) has TPR and CS domains. Similarly, the CS and PIH domains of PIH1D1 are also present in several other PIH proteins: PIH1D2, DNAAF2 (KTU), and DNAAF6 (PIH1D3) (Dong et al., 2014). There is biochemical evidence that SPAG1 complexes with PIH1D2 and DNAAF2 (Maurizy et al., 2018; Smith et al., 2022). Different isoforms of DNAAF4 complex with DNAAF2 and DNAAF6 (Tarkar et al., 2013; Olcese et al., 2017; Paff et al., 2017; Maurizy et al., 2018). However, while these are also referred to as R2TP-like complexes (Olcese et al., 2017), it is not clear whether Ruvbl1/2 (i.e., R2) are involved, particularly as DNAAF4 lacks an RPAP3_C domain. Whether these putative complexes function *in vivo* and their precise role during dynein assembly are not fully established, but they may be required for different steps in the process or for the assembly of different dynein subtypes.

For the PIH proteins, the possibility of different roles during dynein assembly has been raised by experiments in zebrafish and *Chlamydomonas* (Yamamoto et al., 2010; Yamaguchi et al., 2018; Yamamoto et al., 2020). In zebrafish, *pih1d1*, *pih1d2* and *ktu* and *twister* (DNAAF6 homologue) have overlapping functions in the assembly of ODAs and IDA subsets based on analyses of mutant spermatozoa (Yamaguchi et al., 2018). Similarly, in a proteomic profiling of *Chlamydomonas* mutants, *mot48* (PIH1D1) *pf13* (DNAAF2) and *twi* (DNAAF6) have overlapping but distinct roles in assembly of dynein complex subsets (Yamamoto et al., 2010; Yamamoto et al., 2020).

Of the TPR-containing DNAAFs, *DNAAF4* is a cause of PCD in humans, with motile cilia showing reduction in subsets of ODAs and IDAs (Tarkar et al., 2013). In *Chlamydomonas* the DNAAF4 homologue also shows a partial reduction in ODAs and some IDAs (Yamamoto et al., 2017). In addition to this ciliary motility role, DNAAF4 was originally identified (as DYX1C1) as being affected by a chromosomal translocation associated with susceptibility to developmental dyslexia (Taipale et al., 2003), and subsequently a role for this gene in cortical neuron migration was proposed (Wang et al., 2006). Neither function has an obvious direct link to ciliary motility, suggesting that DNAAF4 may have wider roles beyond dynein pre-assembly. Similarly, SPAG1 may have roles in addition to dynein pre-assembly: R2SP complexes with PIH1D2 were characterised in cells that lack motile cilia (Maurizy et al., 2018; Chagot et al., 2019), and a constitutively expressed isoform exists (Horani et al., 2018). Interestingly, mice homozygous for a null allele of *Dnaaf2* do not progress beyond stage E9.5, and have multiple pathologies that are difficult to ascribe to failure of ciliary motility alone (Cheong et al., 2019).

Thus, the roles of TPR- and PIH-domain containing DNAAFs in assembling subsets of dynein complexes remain to be fully disentangled, as do the identities of the R2TP-like complexes that function *in vivo*. Moreover, the question of functions for TPR subunits (and by extension the complexes) beyond dynein assembly also remains open.

We have previously shown that *Drosophila* has homologues of *SPAG1* and *DNAAF4* (zur Lage et al., 2019) (**Table 1**), and that *Drosophila* Spag1 is required for dynein assembly and is able to form a complex with Ruvbl1/2 and Pih1d1 (zur Lage et al., 2018). However, the predicted Dnaaf4 protein is truncated such that it lacks any TPR domain, bringing into question its ability to function in a co-chaperone complex. *Drosophila* has homologues of all the PIH proteins (zur Lage et al., 2019). Most *Drosophila* PIH genes appear widely expressed, but *Dnaaf6* expression appears to be restricted to motile cilia cells. Here we characterise the function of *Drosophila Dnaaf4* and *Dnaaf6* as potential R2TP-like partners. Despite the truncation of Dnaaf4, we show that Dnaaf4 and Dnaaf6 proteins can form an R2TP-like complex, and that each is required for assembly of ODAs and a subset of IDAs. Moreover, there is no indication of functions other than dynein assembly.

2 MATERIALS AND METHODS

2.1 Fly Stocks

Fly stocks were maintained on standard media at 25°C. The following UAS RNAi stocks were obtained from the Vienna *Drosophila* Resource Center (Dietzl et al., 2007): KK60100 (genetic background stock used as negative control) KK111069 (*Dnaaf4*), KK108561 (*Dnaaf6*) and KK100470 (*Spag1*). The following were obtained from the Bloomington Drosophila Stock Centre: Or-R as wild-type control (#2376), UAS-*Dcr2* (#24644), w^{1118} y^{1} *M{vas-Cas9} ZH-2A/FM7c* (#51323), y^{1} w^{*} *P*

{y$^{t7.7}$ = nos-phiC31\int.NLS}X; P{y$^{t7.7}$ = CaryP}attP40 (#79604) and *w*; P{UASp-Venus.GAP43}7* (#30897). Dnali1-mVenus, Dnal1-mVenus are described in Xiang et al. (2022). Flies with UAS-int attp40 landing site were obtained from the Cambridge Microinjection facility. The *sca-Gal4* line used for sensory neuron knockdown was a gift from M. Mlodzik (Baker et al., 1996) and was used in conjunction with UAS-*Dcr2*. For male germline knockdown, *w; Tft/CyO; Bam-Gal4*-VP16 was a gift from Helen White-Cooper.

2.2 Sequence Analyses

For detecting orthology, DIOPT was used (Hu et al., 2011). For phylogenetic analysis, protein sequences were obtained from BLAST, Uniprot (Bateman et al., 2021) and Flybase (Larkin et al., 2021). Sequences were aligned using CLUSTALW/MUSCLE within MEGA7 (Kumar et al., 2016). Tree analysis was conducted using the Maximum Likelihood method within MEGA7.

2.3 *In situ* Hybridisation on Whole-Mount Embryos

Primers were designed to give a probe of around 420-bp with the reverse primer containing the T7 RNA polymerase promoter at its 5' end (all primers are in **Supplementary Table S1**). DNA was amplified from genomic DNA by PCR and then DIG-labelled RNA generated (DIG RNA Labelling Mix, Roche Cat. No.11277073910) using T7 RNA polymerase (Roche Cat. No. 10881767001). RNA *in situ* hybridisation was carried out according to zur Lage et al. (2019). In the case of RNA *in situ*/antibody staining double labelling, antibody staining was carried out after the ISH had been developed. Images were taken on an Olympus AX70 upright microscope with DIC optics.

2.4 Immunofluorescence

Immunohistochemistry on embryos and pupal antenna was described in zur Lage et al. (2018). *Drosophila* testis fixing and staining was carried out according to Sitaram et al. (2014). The following primary antibodies were used: goat anti-GFP antibody (1:500, ab6673), rabbit anti-GFP antibody (1:500, Life Technologies, A11122), mouse anti-Futsch antibody (1:200, Developmental Studies Hybridoma Bank, 22C10), mouse anti-pan polyglycylated tubulin (1:100, Merck, MABS276), rabbit anti-Sas-4 (1:350, gift from Jordan Raff) and rabbit anti-Dnah5 antibody [1:2000, (zur Lage et al., 2021)]. The following secondary antibodies were used: goat anti-Rabbit antibody (1:500, Alexa Fluor 488, Life Technologies, A11008) and goat anti-Mouse antibody (1:500, Alexa Fluor 568, Life Technologies, A11019), donkey anti-goat antibody (1:500, Alexa Fluor 488, Life Technologies, A11055), donkey anti-mouse antibody (1:500, Alexa Fluor 568, Life Technologies, A10037), and donkey anti-rabbit antibody (1:500, Alexa Fluor 647, Life Technologies, A31573). Phalloidin was used 1:2000 (Life Technologies, A12380). DNA in adult testes was stained with To-Pro-3 (1:1000, Life Technologies, T3605) or DAPI (14.3mM, Life Technologies) solution in the dark for 15 min. After several washes, the samples were mounted on slides with 85% glycerol and 2.5% propyl gallate (Sigma, P3130). Images were captured using a Zeiss LSM-5 PASCAL/Axioskop 2 and a Leica TCS SP8 confocal microscope and processed with Fiji.

2.5 mVenus Fusion Gene Construction

mVenus fusion genes were constructed for Dnaaf4 and Dnaaf6 by amplifying gene segments from genomic DNA and cloning into pDONR221 using the BP clonase II from Gateway technology (Thermo Fisher Scientific). The segment included introns, 5' UTR, TSS, and additional upstream flanking DNA of approximately 1 kb, but lacked the stop codon. The insert was subsequently transferred to the destination vector pBID-GV (modified from pBID-UASC-GV vector (Wang et al., 2012) where the UASC had been deleted) with the help of LR clonase II (Gateway technology, Thermo Fisher Scientific). This put the ORF in-frame with the mVenus coding sequence. Transformant fly lines were generated by microinjection into syncytial blastoderm embryos of the attP40 landing site line.

2.6 *Dnaaf4* and *Dnaaf6* CRISPR/Cas9 Mutant Construction

The CRISPR/Cas9 mutant lines were designed by substituting the coding regions of the gene with the mini-white gene. CRISPR primers were designed using the flyCRISPR OptimalTarget finder programme. The cloning was performed according to Vieillard et al. (2016) and injection into the Cas9 line was carried out by the *Drosophila* Microinjection Services (Department of Genetics, Cambridge, United Kingdom).

2.7 Fertility, Hearing and Climbing Assays

These assays were carried out as described in zur Lage et al. (2021). In the fertility assay, individual males were crossed to pairs of virgin OrR females and resulting progeny counted. For climbing assays, 2–5 day-old adult females were tested in batches of 15. For the larval hearing assay, batches of 5 third instar larvae on an agar plate placed on a speaker were tested for response to a 1000-Hz tone. *n* for each genotype = 5 batches of 5 larvae, each exposed to 3 tones 30 s apart. For visual analysis of spermatogenesis, testes were dissected, mounted in PBS, and then observed immediately by DIC optics.

2.8 Protein Expression Analysis of Testes by MS

Knockdown males were generated by crossing UAS-RNAi males from *Dnaaf4*, *Spag1*, and the KK control line to *Bam*-Gal4 at 25°C. 1–3 days post-eclosion male progeny were dissected in ice-cold PBS and 30 pairs of testes with four replicates per genotype were snap-frozen in liquid nitrogen before subsequently being processed and analysed for label-free mass-spectrometry as described in zur Lage et al. (2018). The mass spectrometry proteomics data have been deposited in the ProteomeXchange Consortium via the PRIDE (Perez-Riverol et al., 2019) partner repository with the dataset identifier PXD033608.

2.9 Transmission Electron Microscopy

Adult heads were cut off and the proboscis was removed to facilitate infiltration of the solution. The head were rinsed in 0.1 M phosphate buffer before fixing overnight at 4°C in freshly made 2.5% glutaraldehyde, 2% paraformaldehyde in 0.1 M phosphate buffer (pH 7.4) solution. Subsequently the samples were rinsed four times and then washed three times for 20min in 0.1 M phosphate buffer at room temperature. Further processing for TEM, post-fixing and imaging was carried by Tracey Davey at the Electron Microscopy Research Services, Newcastle University Medical School, using a Philips CM100 CompuStage (FEI) microscope and an AMT CCD camera.

2.10 Transfection and coIP of S2 Cells

RNA was prepared from *Drosophila* antennae or testes and mouse testes with the RNeasy Mini kit (Qiagen 74106). cDNA was synthesised, the open reading frames were PCR amplified and initially cloned into the pDONR221 plasmid using the BP clonase II of the Gateway system (Life Technology) before transferring the fragments using the LR clonase II to the C-terminal site of the destination plasmids pAWH (3xHA epitopes) and pAWF (3x FLAG epitopes) of the *Drosophila* Gateway Vector collection (Carnegie Institution for Science). Primers for synthesis are listed in **Supplementary Table S1**. The truncated mouse Dyx1c1DTPR protein contains the first 227 amino acids of the wildtype 420 amino acid protein, therefore omitting the whole of the C-terminal TPR domain and replacing it with a stop codon. Transfection into S2 cells was performed according to the X-TREME GENE HP DNA transfection reagent (Merck) protocol. After 48–72 h cells were harvested and coIP was carried out according to the FLAG Immunoprecipitation kit (Sigma-Aldrich). Samples were run on pre-cast gels (Bio-Rad) followed by Western blotting. The blots were then probed with mouse anti-FlagM2 (1:1,000; F1804; Sigma-Aldrich) and rabbit anti-HA (1:4,000; ab9110; Abcam) antibodies, followed by Li-COR secondary antibodies (IR Dye 680RD and IR Dye 800CW), before protein detection on a Li-COR Odyssey scanner using Image Studio v5.2 software.

2.11 GFP Trap Affinity Purification and Mass Spectrometry

150 pairs of testes in 3 replicates were dissected in ice-cold PBS for Dnaaf4-mVenus and control line UAS-GAP43-mVenus x Bam-Gal4). The samples were snap-frozen in liquid nitrogen. Lysis buffer (Tris-HCl pH7.5 50 mM, NaCl 100 mM, Glycerol 10%, EDTA 5mM, sodium deoxycholate 0.5%, Complete Mini protease inhibitor) was added to samples before they were homogenised on ice for 2 min. Samples were subsequently rotated, incubated in a lysis buffer for 30 min at 4°C, and then centrifuged, before being processed and analysed as described in zur Lage et al. (2018) with following alterations: the data was acquired using a Fusion Lumos mass spectrometer (Thermo Fisher) that was operated in an OT-IT configuration. 1-s cycle time, 120 k resolution in the orbitrap for MS and rapid scanning MS/MS in the ion-trap. Collision energy was set to 30.

3 RESULTS

3.1 *Drosophila* has Orthologues of DNAAF4 and DNAAF6, but the Former is Strongly Truncated Thereby Lacking a TPR Domain

Of the PIH genes in *Drosophila*, the orthology prediction tool DIOPT (Hu et al., 2011) identifies the orthologue of *DNAAF6* as *CG5048* (hereafter named *Dnaaf6*). Predicted *Drosophila* Dnaaf6 protein retains PIH and CS domains, and has 45% similarity and 30% identity with the human protein (**Figure 1B**). For *DNAAF4*, DIOPT identifies the gene *CG14921* as the *Drosophila* orthologue. However, the encoded protein of this gene (named *Dnaaf4*) is severely truncated relative to the human protein such that it lacks the C-terminal TPR domain (**Figure 1B**). Despite this, DIOPT predicts clear orthology with human DNAAF4 for the remaining protein, with 40% similarity and 25% identity. Moreover, the region of alignment is not limited to the CS domain (**Supplementary Figure S1**). Phylogenetic analysis indicates that this truncation occurred during dipteran evolution, as the truncation is shared by other higher dipterans (Brachycera) but not lower dipterans or other insects (**Figure 1C**). Interestingly, the DNAAF4 sequences of brachyceran flies form a distinct group in a phylogenetic tree, even if just the CS domains are compared (**Figure 1D**). This suggests significant sequence divergence occurred in these truncated *Dnaaf4* genes compared with the archetypal full-length genes present from single celled algae to vertebrates.

Human DNAAF4 binds to HSP90 (Tarkar et al., 2013) and this is predicted to occur via its TPR domain (Haslbeck et al., 2013). The loss of this domain in *Drosophila* Dnaaf4 may therefore be expected to have profound consequences for the conservation of *Drosophila Dnaaf4* function as an R2TP-like chaperone in dynein assembly. Below, this is explored by examining expression, protein interactions and gene function.

3.2 *Drosophila Dnaaf4* and *Dnaaf6* are Expressed Exclusively in Differentiating Motile Ciliated Cells

Transcription of both *Dnaaf4* and *Dnaaf6* is highly specific to tissues with motile ciliated cells. Examination of FlyAtlas 2 transcriptome data (Krause et al., 2022) indicates that *Dnaaf4* is expressed specifically in adult testis. In addition, *Dnaaf4* is 5.2-fold enriched in the transcriptome of developing embryonic chordotonal cells (zur Lage et al., 2019). *Dnaaf6* is also very highly expressed in testis, and found to be enriched in chordotonal cells (55.4-fold). RNA *in situ* hybridisation confirms that embryonic expression of each gene is confined to differentiating chordotonal neurons (**Figures 2A,C,E**). In *Dnaaf4* (but not *Dnaaf6*) this expression becomes restricted to a subset of lch5 neurons late in differentiation (**Figure 2B**). Expression of *Dnaaf6* was abolished in embryos homozygous for a mutation in *fd3F*, which encodes a transcription factor that regulates motile ciliary genes (Newton et al., 2012) (**Figure 2D**).

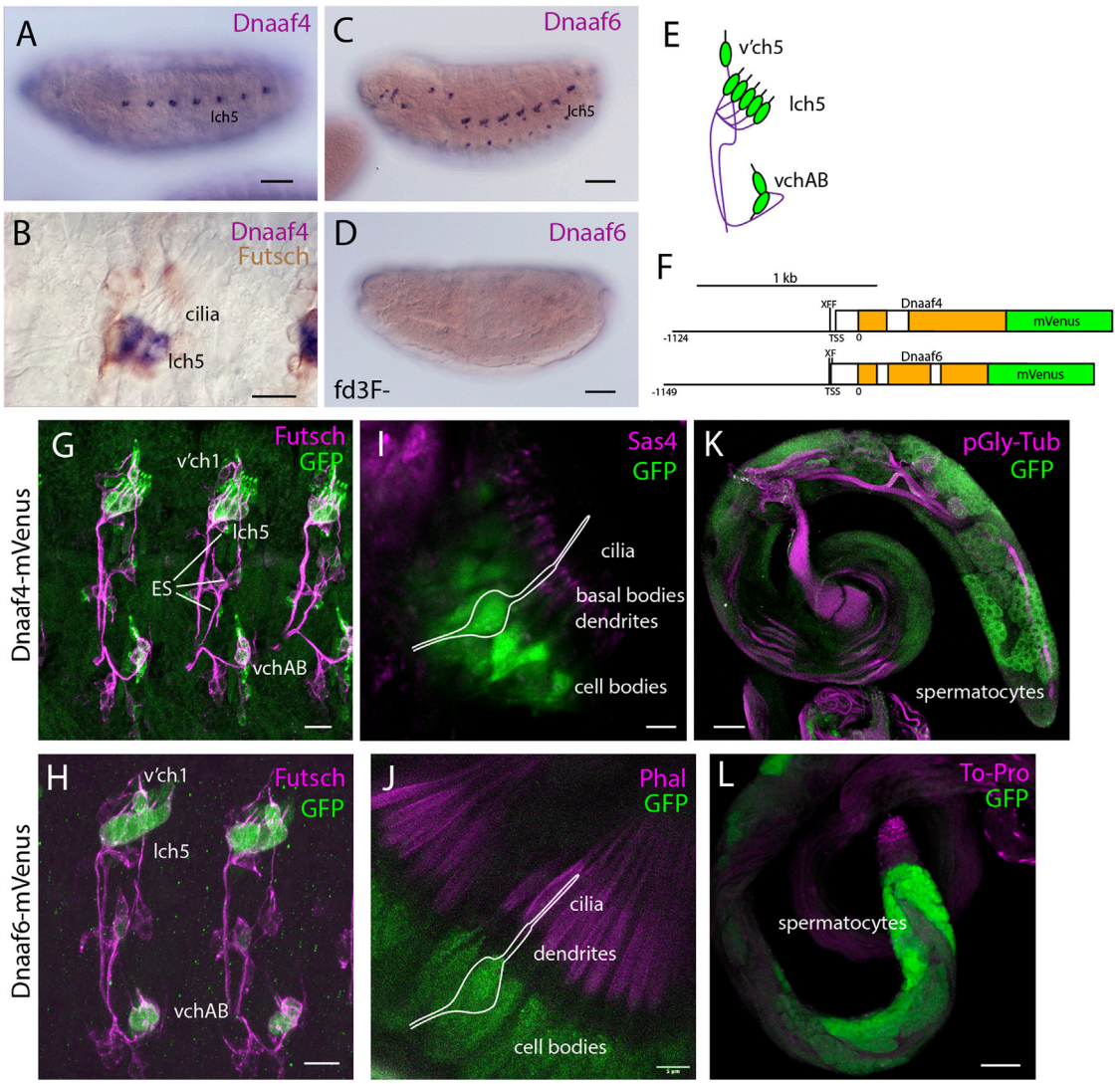

FIGURE 2 | Dnaaf4 and Dnaaf6 are both expressed in *Drosophila* motile cilia cells. **(A–D)** RNA *in situ* hybridisation (dark blue) conducted on late-stage whole-mount embryos. **(A)** *Dnaaf4* probe, *Dnaaf4* is expressed specifically in the chordotonal neurons. **(B)** Higher magnification indicates that this expression becomes restricted at a late stage to a subset of chordotonal neurons (lch5). Here the embryo has been counterstained with antibodies against Futsch (brown), which labels all sensory neurons. **(C)** *Dnaaf6* shows expression in developing chordotonal neurons. **(D)** In an embryo homozygous mutant for *fd3F*, expression of *Dnaaf6* is abolished. **(E)** Schematic of the arrangement of chordotonal neurons in embryonic abdominal segments. **(F)** Schematic illustrating mVenus fusion transgenes. Each includes 5' flanking DNA containing potential binding sites for the transcription factors fd3f (F) and Rfx (X) (Dnaaf4: CTGTTCACTTG, GTTCACTTGCAGC; Dnaaf6: ACTAAATAAACAA, GTTGCCAGGAAA). **(G–L)** Expression of Dnaaf4-mVenus detected by anti-GFP antibodies. **(G,H)** Late embryos counterstained with anti-Futsch (magenta) show expression of both fusion genes in chordotonal neurons. In the case of Dnaaf4-mVenus, some expression is observed in some external sensory (ES) neurons. As this is not observed for the mRNA, it is likely an artefact of the expression construct. **(I,J)** In pupal antennae, both fusion genes are expressed in the cell bodies of chordotonal neurons that form Johnston's Organ. A schematic of approximate neuronal location is shown. The counterstain (magenta) is the basal body marker Sas4. **(I)** or phalloidin **(J)**, which marks the actin basket (scolopale) that surrounds the cilia. **(K,L)** In adult testes, both fusion genes are expressed in differentiating germline cells (spermatocytes and spermatids). Counterstains (magenta) are polyglycylated tubulin **(K)** or To-Pro **(L)**. Scale bars are: (A,C,D,K,L) 50 μm **(B,G,H)** 10 μm **(I,J)** 5 μm. Number of samples imaged: **(G)** $n = 7$ **(I)** $n = 9$ **(K)** $n = 8$.

Expression was confirmed in flies with mVenus fusion transgenes, each including about 1-kb of upstream flanking sequence to drive expression under endogenous regulation (**Figure 2F**). In each reporter, there are predicted binding sites very close to the transcription start site for the cilia-associated transcription factors fd3F and Rfx (marked F and X in the schematic, **Figure 2F**), an arrangement that has been noted for many other motile cilia genes (Newton et al., 2012; Moore et al., 2013; Diggle et al., 2014; zur Lage et al., 2018). For both *Dnaaf4* and *Dnaaf6*, fusion protein was detected in embryonic chordotonal neurons (**Figures 2G,H**), the differentiating chordotonal neurons of Johnston's organ (JO) in the pupal antenna (**Figures 2I,J**), and also in developing spermatocytes (**Figure 2K,L**). The fusion

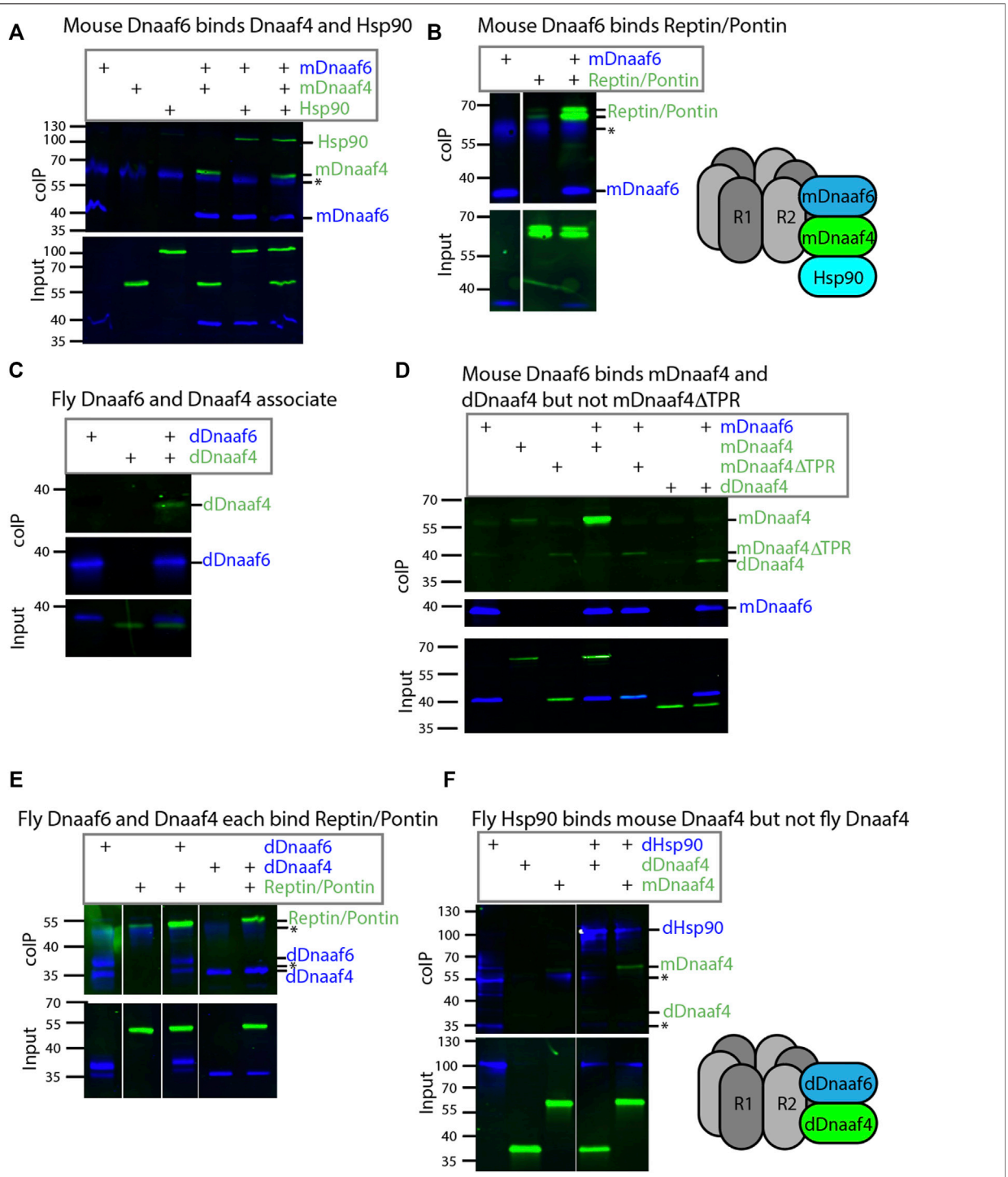

FIGURE 3 | *Drosophila* and mouse Dnaaf4/Dnaaf6 complexes. Coimmunoprecipitations of tagged proteins expressed in S2 cells. In each case, the bait protein is FLAG-tagged (blue) and the prey protein is HA-tagged (green). Proteins are from *Drosophila* unless indicated. "Input" represents Western blot of whole cell extracts with bait/prey simultaneously detected (anti-FLAG + anti-HA). "coIP" represents FLAG-mediated coIP followed by simultaneous detection of FLAG- and HA-tagged proteins on Western blot. *indicates non-specific bands. **(A)** Mouse FLAG-Dnaaf6 protein associates with mouse HA-Dnaaf4 and *Drosophila* HA-Hsp90. **(B)** Mouse FLAG-Dnaaf6 protein binds *Drosophila* HA-Reptin/HA-Pontin. **(C)** *Drosophila* FLAG-Dnaaf6 and HA-Dnaaf4 associate. **(D)** Mouse FLAG-Dnaaf6 binds both mouse HA-Dnaaf4 and *Drosophila* HA-Dnaaf4, but is unable to bind the mouse Dnaaf4 protein with TPR domain deleted (HA-Dnaaf4ΔTPR). **(E)** *Drosophila* FLAG-Dnaaf6 and FLAG-Dnaaf4 are each capable of binding HA-Reptin/HA-Pontin. **(F)** Drosophila FLAG-Hsp90 is able to bind mouse HA-Dnaaf4 but not Drosophila HA-Dnaaf4.

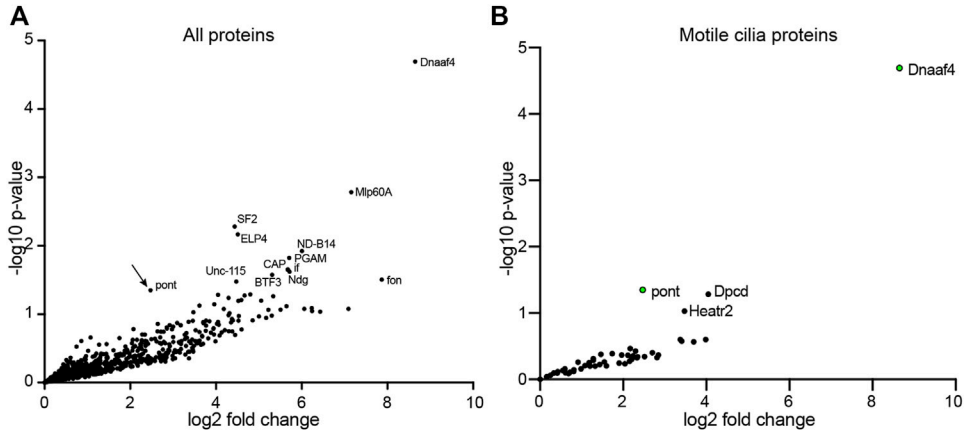

FIGURE 4 | Proteins preferentially associated with Dnaaf4 in *Drosophila* testes. Volcano plots of proteins detected by MS after affinity purification of Dnaaf4-mVenus, shown as relative abundance (fold change) compared with proteins associated with unrelated control protein (GAP43-mVenus). **(A)** All proteins, with those above threshold significance (-log10 (*p*-value)>1.3) labelled. Pontin of R2TP is significantly associated (arrow). **(B)** The same dataset filtered to extract proteins associated with motile cilia (zur Lage et al., 2021). Pontin is the only associated protein to reach statistical significance. However, two other proteins of interest are just below significance threshold: Dpcd and Heatr2 (Dnaaf5). Significance was determined using the Empirical Bayes method. *n* = 150 pairs of testes per replicate; 3 replicates per genotype.

protein was located in the cytoplasm of these cells, consistent with a dynein pre-assembly role.

In conclusion, despite the truncated nature of Dnaaf4, both proteins are expressed exclusively in motile ciliated cells, consistent with a conserved function in motile ciliogenesis.

3.3 *Drosophila* Dnaaf4 and Dnaaf6 can Associate in an R2TP-Like Complex

Protein interactions were explored by heterologous expression of tagged proteins in S2 cultured cells. Firstly, for comparison we investigated the interactions of mouse Dnaaf4 and Dnaaf6 with each other and with the *Drosophila* homologues of Hsp90, Ruvbl1, and Ruvbl2 (known as Pontin and Reptin in *Drosophila*). The mouse homologues have an almost identical length and domain structure to the human proteins shown in **Figure 1B**. Coimmunoprecipitation confirmed that full-length mouse Dnaaf4 and Dnaaf6 can participate in an R2TP-like complex that also includes Hsp90 (**Figures 3A,B**). Interestingly, these results suggest that Pontin and Reptin can form part of such Dnaaf4/6 complexes despite Dnaaf4's lack of RPAP3_C domain. We cannot exclude, however, that endogenous (untagged) proteins participate in the detected complexes, thereby facilitating or bridging these interactions.

We then investigated the *Drosophila* orthologues. *Drosophila* Dnaaf4 is able to complex with *Drosophila* Dnaaf6, although this interaction appears to be weaker than that between the equivalent mouse proteins (**Figure 3C**). Given this association, we asked whether a truncated version of mouse Dnaaf4 retains binding potential. However, this version (mDnaaf4ΔTPR) showed very poor ability to bind to mouse Dnaaf6 (**Figure 3D**). Interestingly each *Drosophila* protein is also able to complex with Reptin/Pontin (**Figure 3E**). As above, this could indicate a direct protein interaction, but it is also possible that endogenous proteins facilitate these interactions. Either way, *Drosophila* Dnaaf4 and Dnaaf6 can participate in complexes with Pontin and Reptin.

The lack of TPR domain in *Drosophila* Dnaaf4 implies that it is not able to recruit Hsp90. Indeed, we found that *Drosophila* Dnaaf4 could not complex with Hsp90, whereas mouse Dnaaf4 was able to do so (**Figure 3F**).

Given the lack of TPR domain in *Drosophila* Dnaaf4 and its consequent inability to recruit Hsp90, we searched for protein partners that may provide TPR functionality. A GFP-trap affinity purification was carried out on testes expressing the Dnaaf4-mVenus fusion protein. The associated proteins included Pontin (**Figure 4A**), which partially corroborates our findings in S2 cells above. However, of the other associated proteins identified, none appeared to have TPR domains or other features that would help clarify Dnaaf4 function. Filtering the data for proteins associated with motile cilia (zur Lage et al., 2021), we found two proteins of interest to be associated but at a *p* value that is below the threshold for significance (**Figure 4B**). Heatr2 (Dnaaf5) is a known dynein assembly factor (Diggle et al., 2014), while *CG13901* is the *Drosophila* orthologue of mouse *Dpcd*, a gene previously linked to ciliary motility and that associates with R2TP (Dafinger et al., 2018). Although these proteins lack TPR domains for direct Hsp90 association, we note that Heatr2/Dnaaf5 has been shown to interact with Dnaaf2 and is proposed to scaffold the formation of a multi-subunit early dynein pre-assembly complex, which could potentially include Hsp90 (Horani et al., 2018).

3.4 *Dnaaf4* and *Dnaaf6* are Required for Motile Ciliated Cell Function

To determine the functions of *Dnaaf4* and *Dnaaf6*, we initially examined the effects of knockdown using genetically supplied RNA interference. Knockdown of each gene in the male

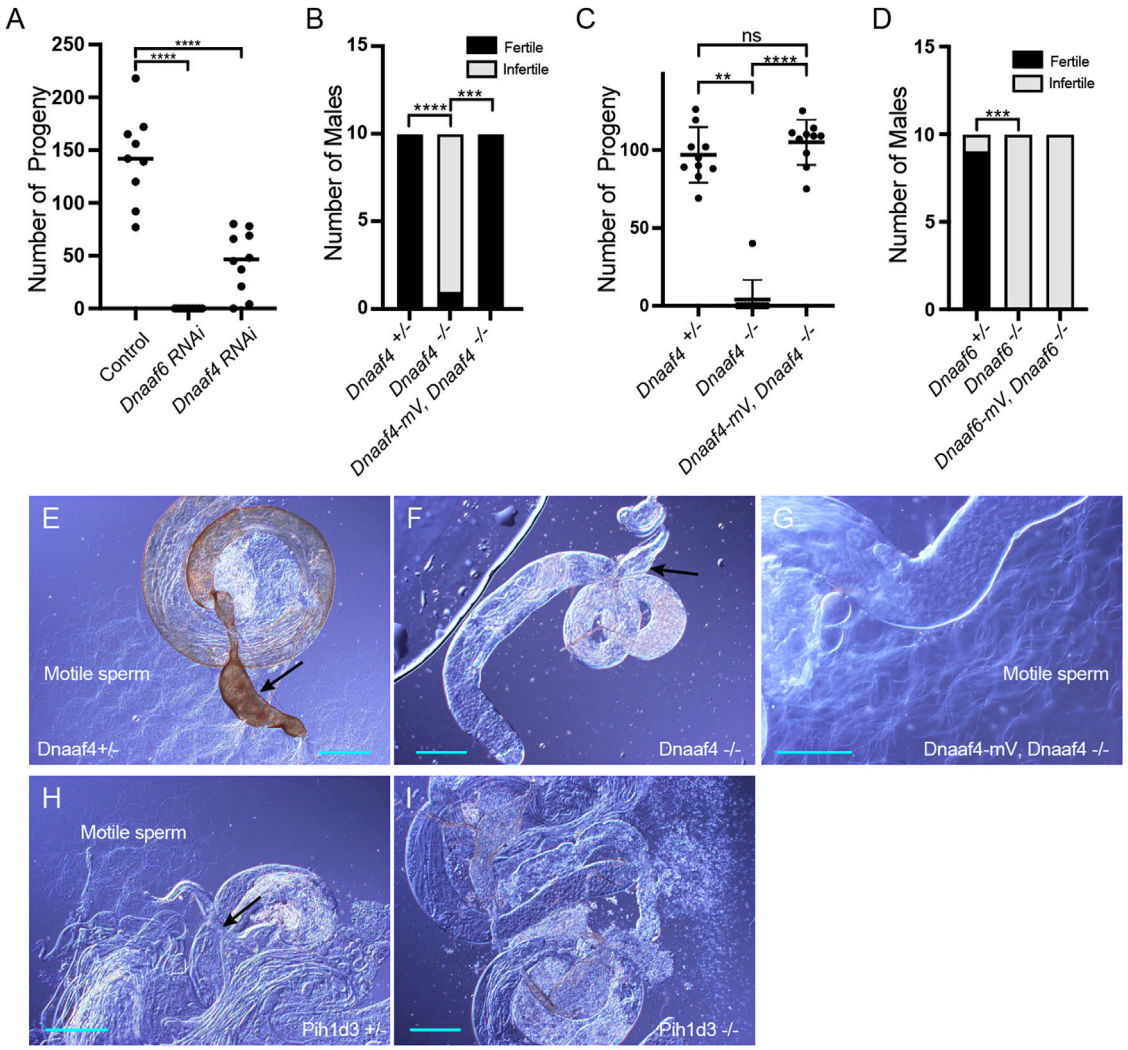

FIGURE 5 | Knockdown and Null mutants of *Dnaaf4* and *Dnaaf6* are male infertile. **(A)** *Dnaaf4* and *Dnaaf6* RNAi knockdown males (*BamGal4*) produce fewer progeny than control males. Progeny from individual males and median progeny value are shown. Knockdown of either gene significantly reduces progeny per male ($p < 0.0001$, One-way ANOVA followed by Sidak's Test for multiple comparisons). **(B,C)** Fertility of *Dnaaf4* null mutant males. **(B)** Proportion of males that are fully infertile. Most *Dnaaf4* mutant males are infertile but this is rescued by the Dnaaf4-mVenus transgene ($p = 0.001$, Fisher's exact test) **(C)** Number of progeny per male, showing that rescued homozygous males are fully fertile compared with heterozygotes ($p > 0.9999$, Kruskal–Wallis analysis followed by Dunn's test for multiple comparisons). $n = 10$ males for each genotype. **(C)** Data for males in **(B)** plotted as number of progeny per male. A single Dnaaf4 homozygote gave progeny, perhaps due to being non-virgin at collection—40 progeny compared with a mean of 96.9 for heterozygotes. **(D)** Fertility assay results showing a decrease in the number of fertile males in the *Dnaaf6* null mutant when compared to control groups (0.0001). *Dnaaf6* rescue did not produce progeny ($p < 0.0001$) like that of the homozygous null mutants. $n = 10$ males per genotype. **(E–I)** Testes and associated male reproductive structures dissected from adult males and observed by light microscopy. Scale bars, 50 μm. **(E)** *Dnaaf4* heterozygote testis showing S-shaped motile sperm emerging from large (sperm-filled) seminal vesicle (black arrow). **(F)** *Dnaaf4* homozygote testis showing small (empty) seminal vesicle (black arrow) and absence of motile sperm. **(G)** Testis from *Dnaaf4* homozygote with *Dnaaf4*-mVenus transgene showing rescue of motile sperm production. **(H)** *Dnaaf6* heterozygote showing S-shaped motile sperm emerging from large (sperm-filled) seminal vesicle (black arrow). **(I)** *Dnaaf6* homozygote testes homozygote testis showing absence of motile sperm.

germline (using *BamGal4* driver) resulted in males that produced significantly fewer progeny than controls (**Figure 5A**). A climbing assay was used to test the proprioceptive ability and coordination of adult flies. Knockdown of *Dnaaf4* in sensory neurons (UAS-*Dcr2*, *scaGal4*, UAS-*Dnaaf4* RNAi^{KK111069}) resulted in a significant reduction in climbing ability, consistent with defective chordotonal neuron function (**Figure 6A**). Similar reduction was seen for *Dnaaf6* (UAS-*Dcr2*, *scaGal4*, UAS-*Dnaaf6* RNAi^{KK108561}) (**Figure 6B**).

To confirm these phenotypes, CRISPR/Cas9 null mutants for *Dnaaf4* and *Dnaaf6* were generated, in which the open reading frame of each gene was replaced with the mini-*white* gene through homology-directed repair. For both *Dnaaf4* and *Dnaaf6,* homozygous null mutant flies are viable with no morphological defects, supporting the hypothesis that they are

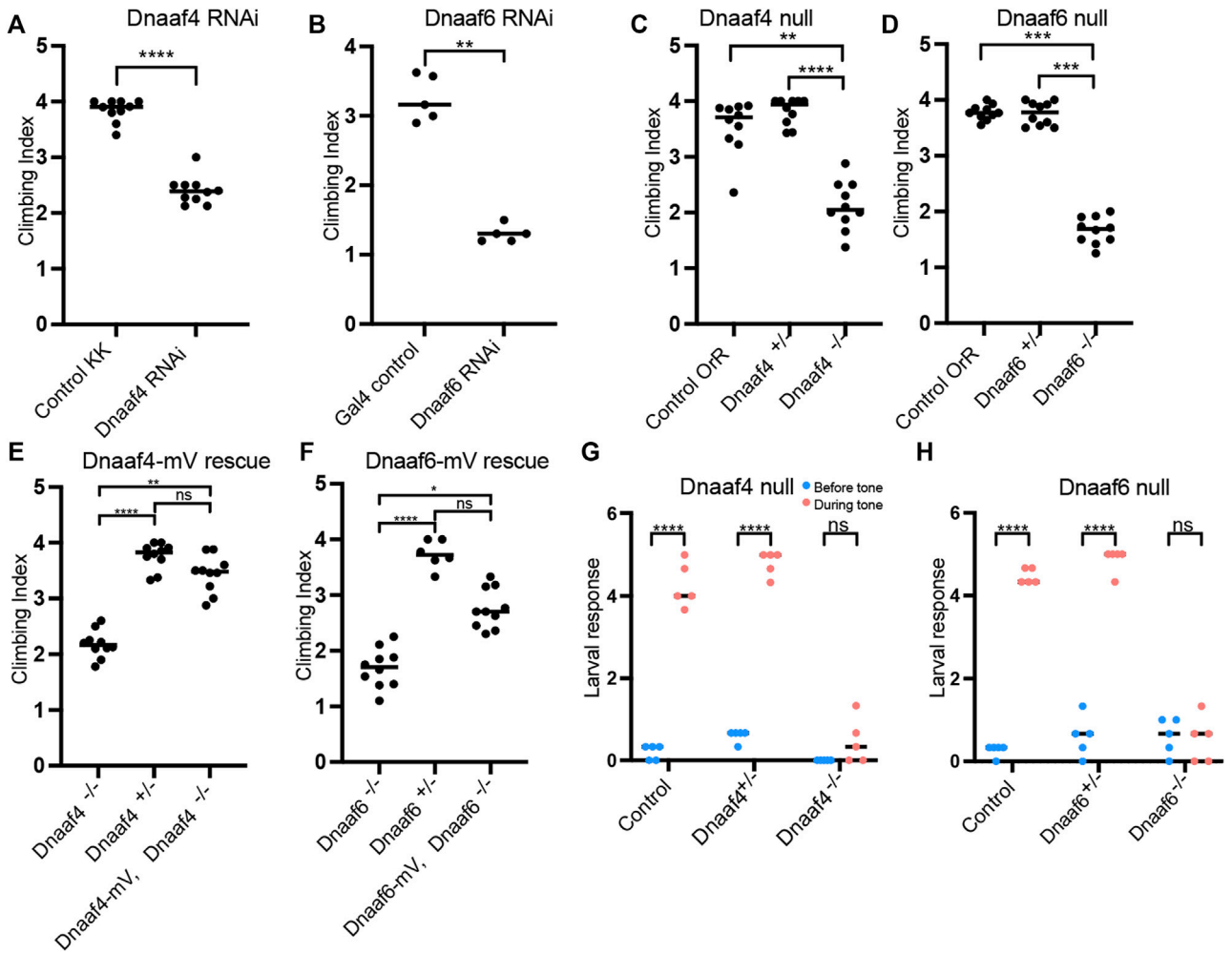

FIGURE 6 | Knockdown and Null mutants of *Dnaaf4* and *Dnaaf6* have defective chordotonal sensory function. **(A–F)** Adult climbing assays for proprioceptive ability. Plots (with median and individual values), each point is a batch of 8–12 females, $n = 10$ batches. **(A,B)** RNAi knockdown of *Dnaaf4* and *Dnaaf6* in sensory neurons (*scaGal4*) results in significant decrease in climbing ability. **(C,D)** Homozygote null adults for *Dnaaf4* and *Dnaaf6* have significantly decreased climbing ability compared with heterozygotes. **(E,F)** Rescue of null mutants. **(E)** *Dnaaf4*-mVenus transgene rescued the climbing ability of *Dnaaf4* null mutant flies, showing a significant increase in climbing performance when compared to null ($p = 0.0012$), restoring climbing ability to the same level as the heterozygotes ($p = 0.8130$). **(F)** *Dnaaf6*-mVenus transgene partial restores climbing ability of *Dnaaf6* null mutants ($p = 0.0103$), but not to levels seen in the heterozygote, although the latter difference does not reach significance ($p = 0.1282$). **(G,H)** Plots (with individual and median values) showing hearing assay performances for $Dnaaf4^{-/-}$ and $Dnaaf6^{-/-}$ larvae in comparison to heterozygote and wild-type (OrR) controls. Number of larvae contracting before and during a 1000-Hz tone was measured. Individual points are batches of 5 larvae, $n = 5$ batches. There is a significant difference between the number of larvae contracting before and during the tone ($p < 0.0001$) for control groups of both genotypes. There is no significant difference between the number of contractions occurring before and during the tone for *Dnaaf4* or *Dnaaf6* null mutants, indicating no behavioural response to stimulus. For climbing assays, significance was determined by Kruskal–Wallis followed by Dunn's test for multiple comparisons. For hearing assay, significance was determined by two-way RM ANOVA and Sidak's multiple comparisons test. Statistical significance on plots is indicated by asterisks: *, $p \leq 0.05$; **, $p \leq 0.01$; ***, $p \leq 0.001$; ****, $p \leq 0.0001$.

not required for general cellular functions. However, both *Dnaaf4* and *Dnaaf6* null males are infertile (**Figures 5B–D**). Dissection of testes showed normal anatomy but a complete lack of motile sperm (**Figures 5E–I**). In *Dnaaf4* null males, the development of motile sperm was rescued by the Dnaaf4-mVenus transgene (**Figures 5C,G**). However, the Dnaaf6-mVenus transgene did not rescue the fertility of *Dnaaf6* males (**Figure 5D**).

In a climbing assay, *Dnaaf4* and *Dnaaf6* homozygous null flies showed significant impairment compared to controls, consistent with defective chordotonal neuron function in proprioception (**Figures 6C,D**). Climbing ability of null flies was restored fully or partially by Dnaaf4-mVenus and Dnaaf6-mVenus transgenes respectively (**Figures 6E,F**).

To assess the auditory function of chordotonal neurons, a larval hearing assay was performed. Third-instar larvae normally respond to a 1000-Hz sine wave tone by momentarily contracting, a behaviour that requires functional dynein motors for mechanotransduction within chordotonal neuron cilia (zur Lage et al., 2021). Larvae homozygous for *Dnaaf4* or *Dnaaf6* mutations did not respond to a tone stimulus, consistent

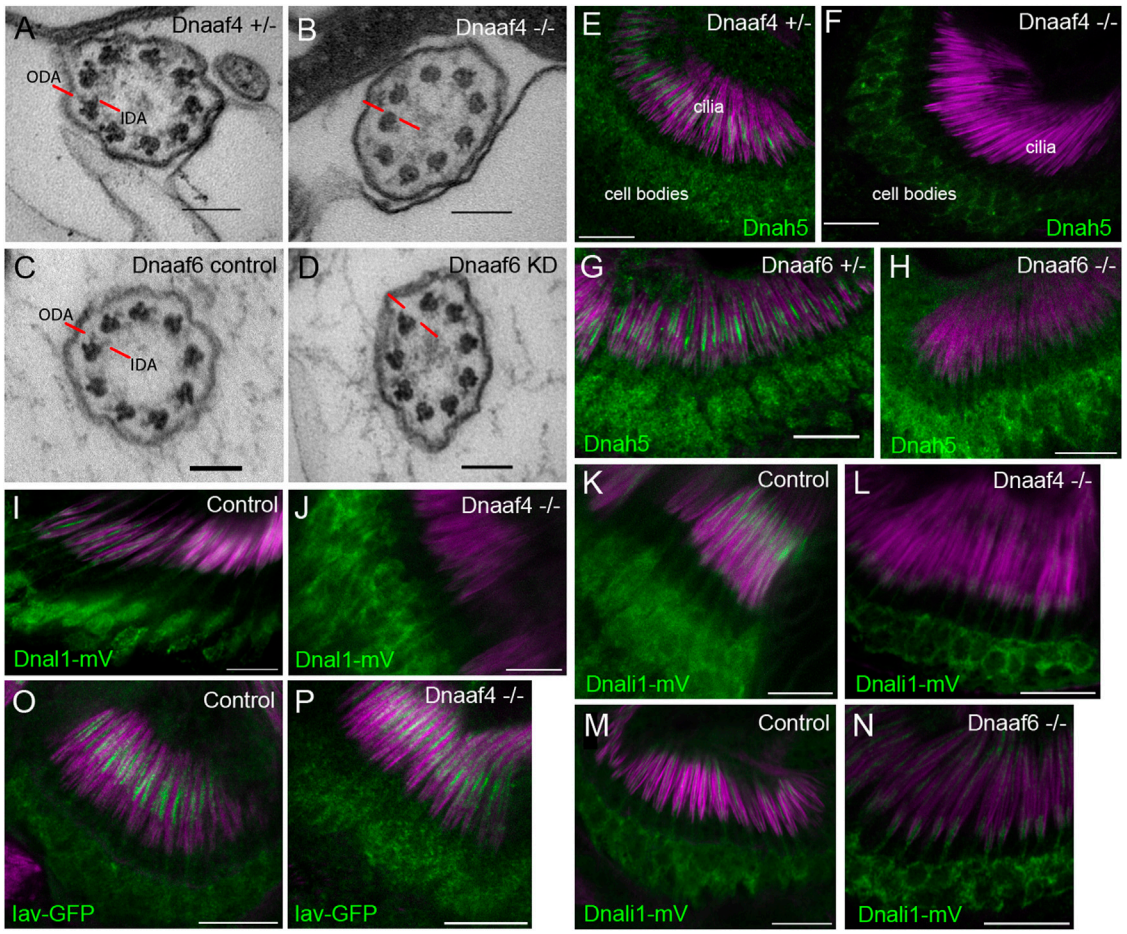

FIGURE 7 | Defective dynein motor localisation in mutants. **(A–D)** TEM of chordotonal neurons in adult antennae, transverse sections of cilia showing 9 + 0 axonemal arrangement. **(A)** Control (*Dnaaf4*$^{+/-}$ heterozygote) with ODAs and IDAs (red lines) on each microtubule doublet. **(B)** *Dnaaf4*$^{-/-}$ homozygote showing severe loss of ODA and IDA structures from the microtubule doublets. **(C)** RNAi control (*scaGal4*, UAS-*Dcr2*, KK line) and **(D)** *Dnaaf6* knockdown (*scaGal4*, UAS-*Dcr2*, UAS-*Dnaaf6*RNAi). The latter shows a reduction of ODA and IDA. **(E–P)** Immunofluorescence of ODA/IDA markers (green) in differentiating chordotonal neurons of pupal antennae. All are counterstained with phalloidin, detecting the scolopale structures surrounding the cilia (magenta). **(E–H)** ODA heavy chain Dnah5 localisation in cilia is lost from *Dnaaf4*$^{-/-}$ and *Dnaaf6*$^{-/-}$ homozygote mutants **(F,H)** compared to controls **(E,G)**, despite presence of protein in the cell bodies. **(I,J)** ODA marker, Dnal1-mVenus shows a similar loss of ciliary localisation in *Dnaaf4*$^{-/-}$ homozygote **(J)** relative to *w*$^{-}$ control **(I)**. **(K–N)** IDA marker, Dnali1-mVenus shows a partial loss of ciliary localisation in *Dnaaf4*$^{-/-}$ and *Dnaaf6*$^{-/-}$ homozygotes **(L,N)** relative to heterozygote controls **(K,M)**. **(O,P)** TRPV channel subunit Iav shows no difference in ciliary localisation between *Dnaaf4*$^{-/-}$ homozygote (P) and *w*$^{-}$ control (O). Scale bars: **(A–D)** 100 nm, **(E–P)** 10 mm. Number of antennae imaged for IF: **(E)** n = 7; **(F)** 7; **(G)** 6; **(H)** 5; **(I)** 5; **(J)** 10; **(K)** 5; **(L)** 9; **(M)** 8; **(N)** 9; **(O)** 6; **(P)** 7.

with functionally impaired chordotonal neurons in vibration sensing (**Figures 6G,H**).

3.5 Axonemal Dyneins are Defective in *Dnaaf4* and *Dnaaf6* Mutant Cilia

Overall, the phenotypes for *Dnaaf4* and *Dnaaf6* null flies are consistent with loss of dynein-driven motility in chordotonal neurons and sperm. To examine this further, TEM was performed on the chordotonal neuron array in the adult antenna (Johnston's Organ) of *Dnaaf4* null mutant flies. This revealed largely normal neuronal structures including well-formed cilia, suggesting that there is no disruption of neuronal differentiation or general ciliogenesis. However, ODA and IDA were strongly reduced or absent (**Figures 7A,B**). In antennae from *Dnaaf6* knockdown flies, TEM showed a strong reduction of IDAs and to a lesser extent ODAs (**Figures 7C,D**).

We extended these observations by examining the localisation of dynein markers in chordotonal neurons of pupal antennae. The ODA heavy chain, Dnah5, showed a complete loss of ciliary localisation in both *Dnaaf4* and *Dnaaf6* mutants (**Figures 7E–H**). For *Dnaaf4*, similar loss was observed for the ODA light chain marker, Dnal1-mVenus (**Figures 7I,J**). A marker of IDA subsets a,c,d, Dnali1-mVenus (light-intermediate chain 1), showed partial loss in ciliary localisation, which was more pronounced in *Dnaaf4* than *Dnaaf6* mutants (**Figure 7K–N**). In contrast, the cilium localised TRPV channel subunit, Iav, was not altered in *Dnaaf4* mutants (**Figure 7O,P**), suggesting that disruption of ciliary protein localisation is restricted to dynein complexes.

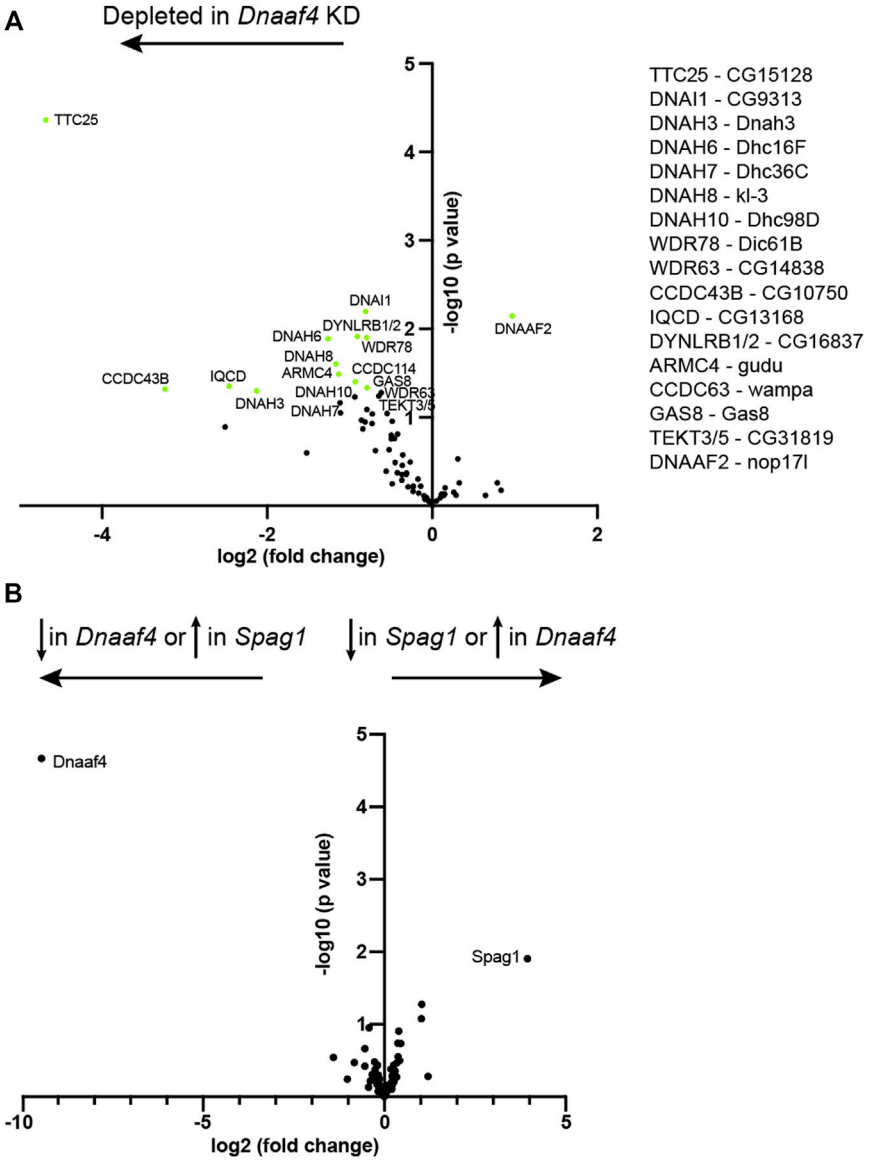

FIGURE 8 | Proteomic changes in *Dnaaf4* mutant testes. **(A)** Volcano plot of motile cilia-associated proteins detected by MS in testes. To the left of the Y axis are proteins that are more less abundant in *Dnaaf4RNAi* KD (*BamGal4,* UAS-*Dnaaf4RNAi*) testes compared with *BamGal4* control (depleted); to the right are proteins that are more abundant than in the control. Dnaaf4 protein itself is strongly depleted as expected (log2(FC) = −8.69, -log10 (*p* value) = 4.39) but for clarity it is not shown on plot. Proteins with -log10 (*p* value) > 1.3 (green points) are labelled with names of human homologues. The *Drosophila* gene names are shown to the right. *n* = 30 pairs of testes/replicate; 4 replicates per genotype. **(B)** Volcano plot comparing motile cilia-associated proteins detected in testes from *Dnaaf4* knockdown testes compared with *Spag1* knockdown testes (*BamGal4,* UAS-*Spag1RNAi*). The only proteins showing significant difference in abundance are Dnaaf4 and Spag1 themselves. Significance was determined using the Empirical Bayes method. *n* = 30 pairs of testes/replicate; 4 replicates per genotype.

Together, these observations suggest that both genes are required specifically for ciliary localisation of axonemal dyneins.

To investigate further, we assessed changes in protein abundance in *Dnaaf4* knock-down testes by label free quantitative mass spectrometry. In such experiments, a reduction in dynein chains has been considered consistent with instability resulting from defective cytoplasmic pre-assembly (zur Lage et al., 2018; zur Lage et al., 2021). Proteins detected in *Dnaaf4* knock-down testes were compared with control testes, and then filtered to concentrate on those associated with ciliary motility (dynein motors, nexin-dynein regulatory complex, radial spokes, etc., (zur Lage et al., 2019). As expected, Dnaaf4 protein is strongly depleted in knockdown testes [log2(FC) = −8.69] (**Figure 8A**). Of the other ciliary proteins detected, we found a small reduction in several ODA and IDA heavy chains, including kl-3 (orthologue: DNAH8, ODA), Dnah3 (DNAH3, IDA subsets a,b,c,e) and Dhc16 F (DNAH6, IDA subset g). Also reduced were CG15128 (paralogue of TTC25, ODA docking complex), CG10750

(CCDC43B, MIA complex) and CG13168 (IQCD, Nexin-DRC). This may reflect a reduction in axonemal stability that appears to be characteristic of dynein loss in spermiogenesis (zur Lage et al., 2021). Interestingly, there is a small increase in Dnaaf2, which is one of the potential partners of Dnaaf4. To compare with the phenotype of another DNAAF, we also determined protein changes upon knockdown of TPR-containing *Spag1* (zur Lage et al., 2018). After filtering for motile ciliary proteins, we found very little difference in protein abundances between *Dnaaf4* and *Spag1* knockdown testes, suggesting that the roles of these DNAAFs are similar, or at least not distinguishable by this technique (**Figure 8B**).

4 DISCUSSION

Drosophila Dnaaf4 and *Dnaaf6* are both required for axonemal dynein localisation within cilia, showing that despite the truncated nature of *Dnaaf4*, there is conservation of the roles assigned to homologues in other organisms. Physical evidence supports the possibility that they perform this role together in *Drosophila* as part of an R2TP-like complex that may include Pontin and Reptin (Ruvbl1 and 2). On the other hand, for neither gene do we find evidence of function beyond the differentiation of motile cilia, suggesting that in *Drosophila* at least, the role of these genes is specific to axonemal dynein assembly.

Vertebrate DNAAF4 is predicted to recruit HSP90 via its TPR domain, and we show that mouse Dnaaf4 is able to bind Hsp90. It is remarkable, therefore, that despite apparent conservation of function as an Hsp90 co-chaperone, *Drosophila* Dnaaf4 protein lacks the TPR domain and does not bind Hsp90. Perhaps an accessory TPR-containing protein works with *Drosophila* Dnaaf4. Interestingly, *Drosophila* Spag1 is also strongly truncated, but in this case the truncation retains the TPR domain and not much else (zur Lage et al., 2019). Does Spag1 work in partnership with Dnaaf4? Our proteomic analysis of knockdown testes suggests that Dnaaf4 and Spag1 have similar phenotypes. However, affinity purification analysis did not detect Spag1 as a Dnaaf4-interacting protein. On the other hand, this analysis also did not detect interaction with Dnaaf6, and so the conditions of the assay may not be conducive to identifying Dnaaf4 protein interactors efficiently.

There are questions regarding the role of the DNAAF4 TPR domain in humans too, since the protein exists in several isoforms with varying numbers of repeats in its TPR domain (**Figure 1B**). While isoform-a (which associates with DNAAF2) has a full 3-repeat TPR domain that is likely to be essential for HSP90 binding (Tarkar et al., 2013; Maurizy et al., 2018), isoform-c (which associates with DNAAF6) has only a single repeat (Paff et al., 2017; Maurizy et al., 2018). It seems unlikely that the limited TPR domain of isoform-c can bind HSP90 directly, and so it may not differ functionally from the *Drosophila* protein so strongly after all.

Interestingly, *Drosophila* truncated Dnaaf4 resembles the protein that would potentially be synthesised from the human gene bearing the pathogenic mutation detected in PCD: in the original report, 7 out of 9 *DNAAF4* variants in PCD patients were nonsense mutations predicted to encode a truncated protein lacking TPR domains (Tarkar et al., 2013). However, as nonsense-mediated decay (NMD) of the transcript is thought to occur, it is likely that no protein is produced. The finding that *Drosophila* truncated *Dnaaf4* is functional without a TPR domain raises the possibility that inhibition of NMD could restore some function to PCD patients with DNAAF truncating mutations, even if the protein produced lacks the TPR domain. On the other hand, we found in our heterologous expression system that the full TPR domain of mouse Dnaaf4 was required for strong interaction with Dnaaf6.

We find that *Drosophila* mutants of *Dnaaf4* and *Dnaaf6* show similar loss of dynein markers. While the markers available in *Drosophila* are limited, this finding supports them working in the same complex. There is a strong loss of ODA markers (Dnal1 and Dnah5 homologues) but a partial loss of IDA marker, Dnali1. This chain is predicted to be a subunit of single-headed IDA subsets a, c, and d, although it is not certain that d exists in *Drosophila* (zur Lage et al., 2019). In comparison, electron tomography analysis of human PIH1D3-mutant respiratory cilia showed a loss of subset g but no effect on subsets a or c (Olcese et al., 2017). Mutations of the Dnaaf4 homologue in *Chlamydomonas* resulted in strong reduction of most IDA subsets but a weak reduction of subset a (Yamamoto et al., 2017). In other organisms, homologues of these DNAAFs have also been proposed to have a role in the assembly of subset g. For further precision on the subsets affected in *Drosophila*, it would be desirable to generate heavy chain markers for IDA subsets such as antibodies raised against the IDA heavy chain DNAH6 homologue, *Dhc16*. Dnaaf4 is proposed to function with Dnaaf2 in addition to Dnaaf6, and it is not known whether this would be responsible for the assembly of other dynein complexes. Given that Dnali1 expression appears lower in the *Dnaaf4* mutant than the *Dnaaf6* mutant, this may also suggest a role for Dnaaf4 partners with proteins in addition to Dnaaf6.

Several DNAAFs are suspected of having additional non-ciliary functions. For example, mice *DNAAF2* homozygotes are reported to be embryonic lethal (Cheong et al., 2019) consistent with wider roles, and it may be significant that only a small number of PCD patients have been identified with mutations in *DNAAF2* (Omran et al., 2008). In *Drosophila*, *Dnaaf2* (*nop17l*) appears to be widely expressed in embryos (zur Lage et al., 2019), supporting the possibility of widespread roles for this *DNAAF*. In contrast, *Drosophila Dnaaf4* is specifically expressed in motile ciliated cells supporting the hypothesis that has no other roles than facilitating axonemal dynein assembly. In this light it is interesting to consider the roles proposed for vertebrate *DNAAF4*. Truncating mutations of *DNAAF4* were first identified as a candidate causative gene for dyslexia through a role in brain development and maturation (Taipale et al., 2003). Based on rodent models, it has been proposed that *DNAAF4* mutation affects neuronal migration in the developing neocortex (Wang et al., 2006) The link between *DNAAF4* and dyslexia requires further confirmation since this gene did not associate with dyslexia in follow-up studies on other populations (Scerri, 2004; Marino et al., 2005). It is not immediately clear how such a phenotype depends on ciliary

motility, raising the possibility that *DNAAF4* may have additional non-ciliary roles. Alternatively, a potential role in neuronal migration/dyslexia could also be an indirect effect of a motile cilia defect, since ciliary motility is required for CSF flow (Kumar et al., 2021). Another intriguing possibility arises from the observation that neuropsychiatric disorders such as schizophrenia, autism and dyslexia have been connected to left-right asymmetry (Valente et al., 2014; Trulioff et al., 2017), which is determined via motile cilia in the embryonic node. Indeed, a recent case report of mutations in the dynein heavy chain genes, *DNAH5* and *DNAH11* has raised the possibility of a link between situs inversus and developmental dyslexia (Bieder et al., 2020).

DATA AVAILABILITY STATEMENT

The datasets presented in this study can be found in online repositories. The names of the repository/repositories and accession number(s) can be found below: https://www.ebi.ac.uk/pride/archive/, PXD033608.

AUTHOR CONTRIBUTIONS

JL conducted many of the experiments and data analysis, contributed to experimental design, and contributed to writing the manuscript; PZL conducted S2 cell analysis and contributed to mVenus construction and analysis; AK provided the mass spectrometry analyses; AJ conducted data analysis, contributed to experimental design, and wrote the manuscript. All authors contributed to manuscript revision, read and approved the submitted manuscript.

FUNDING

This work was supported by funding from the Biotechnology and Biosciences Research Council (BBSRC, BB/S000801) to AJ, the Zhejiang-Edinburgh institute (Career development PhD program in Biomedical Sciences) to JL, and the Wellcome Trust (Multiuser Equipment Grant, 208402/Z/17/Z) to AK. Newcastle Electron Microscopy Research Services were supported by BBSRC grant BB/R013942. Bloomington *Drosophila* Stock Center was supported by NIH P40OD018537.

ACKNOWLEDGMENTS

We thank IfeOluwa Taiwo and Panagiota Stefannopoulou for preliminary contributions, and Jimi Wills for expert mass spectrometry and data processing. Tracy Davey of Electron Microscopy Research Services, Newcastle University Medical School carried out the TEM. Stocks obtained from the Bloomington *Drosophila* Stock Center were used in this study. A preprint version of this article is available on the preprint server BioRxiv, doi:10.1101/2022.05.12.491607. For the purpose of open access, the authors have applied a Creative Commons Attribution (CC BY) licence to any Author Accepted Manuscript version arising from this submission.

SUPPLEMENTARY MATERIAL

The Supplementary Material for this article can be found online at: https://www.frontiersin.org/articles/10.3389/fgene.2022.943197/full#supplementary-material

REFERENCES

Baker, N. E., Yu, S., and Han, D. (1996). Evolution of Proneural Atonal Expression during Distinct Regulatory Phases in the Developing Drosophila Eye. *Curr. Biol.* 6, 1290–1302. doi:10.1016/s0960-9822(02)70715-x

Bateman, A., Martin, M.-J., Orchard, S., Magrane, M., Agivetova, R., Ahmad, S., et al. (2021). UniProt: The Universal Protein Knowledgebase in 2021. *Nucleic Acids Res.* 49, D480–D489. doi:10.1093/nar/gkaa1100

Bieder, A., Einarsdottir, E., Matsson, H., Nilsson, H. E., Eisfeldt, J., Dragomir, A., et al. (2020). Rare Variants in Dynein Heavy Chain Genes in Two Individuals with Situs Inversus and Developmental Dyslexia: A Case Report. *BMC Med. Genet.* 21, 87. doi:10.1186/s12881-020-01020-2

Braschi, B., Omran, H., Witman, G. B., Pazour, G. J., Pfister, K. K., Bruford, E. A., et al. (2022). Consensus Nomenclature for Dyneins and Associated Assembly Factors. *J. Cell Biol.* 221, e202109014. doi:10.1083/jcb.202109014

Chagot, M.-E., Dos Santos Morais, R., Dermouche, S., Lefebvre, D., Manival, X., Chipot, C., et al. (2019). Binding Properties of the Quaternary Assembly Protein SPAG1. *Biochem. J.* 476, 1679–1694. doi:10.1042/bcj20190198

Cheong, A., Degani, R., Tremblay, K. D., and Mager, J. (2019). A Null Allele of Dnaaf2 Displays Embryonic Lethality and Mimics Human Ciliary Dyskinesia. *Hum. Mol. Genet.* 28, 2775–2784. doi:10.1093/hmg/ddz106

Dafinger, C., Rinschen, M. M., Borgal, L., Ehrenberg, C., Basten, S. G., Franke, M., et al. (2018). Targeted Deletion of the AAA-ATPase Ruvbl1 in Mice Disrupts Ciliary Integrity and Causes Renal Disease and Hydrocephalus. *Exp. Mol. Med.* 50, 1–17. doi:10.1038/s12276-018-0108-z

Dietzl, G., Chen, D., Schnorrer, F., Su, K.-C., Barinova, Y., Fellner, M., et al. (2007). A Genome-Wide Transgenic RNAi Library for Conditional Gene Inactivation in Drosophila. *Nature* 448, 151–156. doi:10.1038/nature05954

Diggle, C. P., Moore, D. J., Mali, G., zur Lage, P., Ait-Lounis, A., Schmidts, M., et al. (2014). HEATR2 Plays a Conserved Role in Assembly of the Ciliary Motile Apparatus. *PLoS Genet.* 10, e1004577. doi:10.1371/journal.pgen.1004577

Dong, F., Shinohara, K., Botilde, Y., Nabeshima, R., Asai, Y., Fukumoto, A., et al. (2014). Pih1d3 Is Required for Cytoplasmic Preassembly of Axonemal Dynein in Mouse Sperm. *J. Cell Biol.* 204, 203–213. doi:10.1083/jcb.201304076

Fabczak, H., and Osinka, A. (2019). Role of the Novel Hsp90 Co-Chaperones in Dynein Arms' Preassembly. *Int. J. Mol. Sci.* 20, 6174. doi:10.3390/ijms20246174

Fok, A. K., Wang, H., Katayama, A., Aihara, M. S., and Allen, R. D. (1994). 22S Axonemal Dynein Is Preassembled and Functional Prior to Being Transported to and Attached on the Axonemes. *Cell Motil. Cytoskelet.* 29, 215–224. doi:10.1002/cm.970290304

Fowkes, M. E., and Mitchell, D. R. (1998). The Role of Preassembled Cytoplasmic Complexes in Assembly of Flagellar Dynein Subunits. *Mol. Biol. Cell* 9, 2337–2347. doi:10.1091/mbc.9.9.2337

Haslbeck, V., Eckl, J. M., Kaiser, C. J. O., Papsdorf, K., Hessling, M., and Richter, K. (2013). Chaperone-Interacting TPR Proteins in *Caenorhabditis E. J. Mol. Biol.* 425, 2922–2939. doi:10.1016/j.jmb.2013.05.019

Horani, A., Ustione, A., Huang, T., Firth, A. L., Pan, J., Gunsten, S. P., et al. (2018). Establishment of the Early Cilia Preassembly Protein Complex during Motile Ciliogenesis. *Proc. Natl. Acad. Sci. U. S. A.* 115, E1221–E1228. doi:10.1073/pnas.1715915115

Houry, W. A., Bertrand, E., and Coulombe, B. (2018). The PAQosome, an R2TP-Based Chaperone for Quaternary Structure Formation. *Trends Biochem. Sci.* 43, 4–9. doi:10.1016/j.tibs.2017.11.001

Hu, Y., Flockhart, I., Vinayagam, A., Bergwitz, C., Berger, B., Perrimon, N., et al. (2011). An Integrative Approach to Ortholog Prediction for Disease-Focused

and Other Functional Studies. *BMC Bioinforma.* 12, 357. doi:10.1186/1471-2105-12-357

Kakihara, Y., and Houry, W. A. (2012). The R2TP Complex: Discovery and Functions. *Biochim. Biophys. Acta (BBA) - Mol. Cell Res.* 1823, 101–107. doi:10.1016/j.bbamcr.2011.08.016

King, S. M. (2016). Axonemal Dynein Arms. *Cold Spring Harb. Perspect. Biol.* 8, a028100. doi:10.1101/cshperspect.a028100

Krause, S. A., Overend, G., Dow, J. A. T., and Leader, D. P. (2022). FlyAtlas 2 in 2022: Enhancements to the *Drosophila M* Expression Atlas. *Nucleic Acids Res.* 50, D1010–D1015. doi:10.1093/nar/gkab971

Kumar, S., Stecher, G., and Tamura, K. (2016). MEGA7: Molecular Evolutionary Genetics Analysis Version 7.0 for Bigger Datasets. *Mol. Biol. Evol.* 33, 1870–1874. doi:10.1093/molbev/msw054

Kumar, V., Umair, Z., Kumar, S., Goutam, R. S., Park, S., and Kim, J. (2021). The Regulatory Roles of Motile Cilia in CSF Circulation and Hydrocephalus. *Fluids Barriers CNS* 18, 31. doi:10.1186/s12987-021-00265-0

Larkin, A., Marygold, S. J., Antonazzo, G., Attrill, H., dos Santos, G., Garapati, P. V., et al. (2021). FlyBase: Updates to the *Drosophila M* Knowledge Base. *Nucleic Acids Res.* 49, D899–D907. doi:10.1093/nar/gkaa1026

Li, Y., Zhao, L., Yuan, S., Zhang, J., and Sun, Z. (2017). Axonemal Dynein Assembly Requires the R2TP Complex Component Pontin. *Development* 144 (24), 4684–4693. doi:10.1242/dev.152314

Liu, G., Wang, L., and Pan, J. (2019). Chlamydomonas WDR92 in Association with R2TP-Like Complex and Multiple DNAAFs to Regulate Ciliary Dynein Preassembly. *J. Mol. Cell Biol.* 11, 770–780. doi:10.1093/jmcb/mjy067

Marino, C., Giorda, R., Luisa Lorusso, M., Vanzin, L., Salandi, N., Nobile, M., et al. (2005). A Family-Based Association Study Does Not Support DYX1C1 on 15q21.3 as a Candidate Gene in Developmental Dyslexia. *Eur. J. Hum. Genet.* 13, 491–499. doi:10.1038/sj.ejhg.5201356

Martino, F., Pal, M., Muñoz-Hernández, H., Rodríguez, C. F., Núñez-Ramírez, R., Gil-Carton, D., et al. (2018). RPAP3 Provides a Flexible Scaffold for Coupling HSP90 to the Human R2TP Co-Chaperone Complex. *Nat. Commun.* 9, 1501. doi:10.1038/s41467-018-03942-1

Maurizy, C., Quinternet, M., Abel, Y., Verheggen, C., Santo, P. E., Bourguet, M., et al. (2018). The RPAP3-Cterminal Domain Identifies R2TP-Like Quaternary Chaperones. *Nat. Commun.* 9, 2093. doi:10.1038/s41467-018-04431-1

Moore, D. J., Onoufriadis, A., Shoemark, A., Simpson, M. A., zur Lage, P. I., de Castro, S. C., et al. (2013). Mutations in ZMYND10, a Gene Essential for Proper Axonemal Assembly of Inner and Outer Dynein Arms in Humans and Flies, Cause Primary Ciliary Dyskinesia. *Am. J. Hum. Genet.* 93, 346–356. doi:10.1016/j.ajhg.2013.07.009

Newton, F. G., zur Lage, P. I., Karak, S., Moore, D. J., Göpfert, M. C., and Jarman, A. P. (2012). Forkhead Transcription Factor Fd3F Cooperates with Rfx to Regulate a Gene Expression Program for Mechanosensory Cilia Specialization. *Dev. Cell* 22, 1221–1233. doi:10.1016/j.devcel.2012.05.010

Olcese, C., Patel, M. P., Shoemark, A., Kiviluoto, S., Legendre, M., Williams, H. J., et al. (2017). X-Linked Primary Ciliary Dyskinesia Due to Mutations in the Cytoplasmic Axonemal Dynein Assembly Factor PIH1D3. *Nat. Commun.* 8, 14279. doi:10.1038/ncomms14279

Omran, H., Kobayashi, D., Olbrich, H., Tsukahara, T., Loges, N. T., Hagiwara, H., et al. (2008). Ktu/PF13 is Required for Cytoplasmic Pre-Assembly of Axonemal Dyneins. *Nature* 456, 611–616. doi:10.1038/nature07471

Paff, T., Loges, N. T., Aprea, I., Wu, K., Bakey, Z., Haarman, E. G., et al. (2017). Mutations in PIH1D3 Cause X-Linked Primary Ciliary Dyskinesia with Outer and Inner Dynein Arm Defects. *Am. J. Hum. Genet.* 100, 160–168. doi:10.1016/j.ajhg.2016.11.019

Pal, M., Morgan, M., Phelps, S. E. L., Roe, S. M., Parry-Morris, S., Downs, J. A., et al. (2014). Structural Basis for Phosphorylation-Dependent Recruitment of Tel2 to Hsp90 by Pih1. *Structure* 22, 805–818. doi:10.1016/j.str.2014.04.001

Perez-Riverol, Y., Csordas, A., Bai, J., Bernal-Llinares, M., Hewapathirana, S., Kundu, D. J., et al. (2019). The PRIDE Database and Related Tools and Resources in 2019: Improving Support for Quantification Data. *Nucleic Acids Res.* 47, D442–D450. doi:10.1093/nar/gky1106

Scerri, T. S. (2004). Putative Functional Alleles of DYX1C1 are not Associated with Dyslexia Susceptibility in a Large Sample of Sibling Pairs from the UK. *J. Med. Genet.* 41, 853–857. doi:10.1136/jmg.2004.018341

Sitaram, P., Hainline, S. G., and Lee, L. A. (2014). Cytological Analysis of Spermatogenesis: Live and Fixed Preparations of Drosophila Testes. *J. Vis. Exp.* 83, e51058. doi:10.3791/51058

Smith, A. J., Bustamante-Marin, X. M., Yin, W., Sears, P. R., Herring, L. E., Dicheva, N. N., et al. (2022). The Role of SPAG1 in the Assembly of Axonemal Dyneins in Human Airway Epithelia. *J. Cell Sci.* 135 (6), jcs259512. doi:10.1242/jcs.259512

Taipale, M., Kaminen, N., Nopola-Hemmi, J., Haltia, T., Myllyluoma, B., Lyytinen, H., et al. (2003). A Candidate Gene for Developmental Dyslexia Encodes a Nuclear Tetratricopeptide Repeat Domain Protein Dynamically Regulated in Brain. *Proc. Natl. Acad. Sci. U. S. A.* 100, 11553–11558. doi:10.1073/pnas.1833911100

Tarkar, A., Loges, N. T., Loges, N. T., Slagle, C. E., Francis, R., Dougherty, G. W., et al. (2013). DYX1C1 Is Required for Axonemal Dynein Assembly and Ciliary Motility. *Nat. Genet.* 45, 995–1003. doi:10.1038/ng.2707

Trulioff, A., Ermakov, A., and Malashichev, Y. (2017). Primary Cilia as a Possible Link between Left-Right Asymmetry and Neurodevelopmental Diseases. *Genes* 8, 48. doi:10.3390/genes8020048

Valente, E. M., Rosti, R. O., Gibbs, E., and Gleeson, J. G. (2014). Primary Cilia in Neurodevelopmental Disorders. *Nat. Rev. Neurol.* 10, 27–36. doi:10.1038/nrneurol.2013.247

Vaughan, C. K. (2014). Hsp90 Picks PIKKs via R2TP and Tel2. *Structure* 22, 799–800. doi:10.1016/j.str.2014.05.012

Vieillard, J., Paschaki, M., Duteyrat, J.-L., Augière, C., Cortier, E., Lapart, J.-A., et al. (2016). Transition Zone Assembly and its Contribution to Axoneme Formation in Drosophila Male Germ Cells. *J. Cell Biol.* 214, 875–889. doi:10.1083/jcb.201603086

Wang, Y., Paramasivam, M., Thomas, A., Bai, J., Kaminen-Ahola, N., Kere, J., et al. (2006). DYX1C1 Functions in Neuronal Migration in Developing Neocortex. *Neuroscience* 143, 515–522. doi:10.1016/j.neuroscience.2006.08.022

Wang, J.-W., Beck, E. S., and McCabe, B. D. (2012). A Modular Toolset for Recombination Transgenesis and Neurogenetic Analysis of Drosophila. *PLoS One* 7, e42102. doi:10.1371/journal.pone.0042102

Xiang, W., zur Lage, P., Newton, F. G., Qiu, G., and Jarman, A. P. (2022). The Dynamics of Protein Localisation to Restricted Zones within Drosophila Mechanosensory Cilia. bioRxiv 2022.03.02.482694. doi:10.1101/2022.03.02.482694

Yamaguchi, H., Oda, T., Kikkawa, M., and Takeda, H. (2018). Systematic Studies of All PIH Proteins in Zebrafish Reveal Their Distinct Roles in Axonemal Dynein Assembly. *Elife* 7, e36979. doi:10.7554/eLife.36979

Yamamoto, R., Obbineni, J. M., Alford, L. M., Ide, T., Owa, M., Hwang, J., et al. (2017). Chlamydomonas DYX1C1/PF23 is Essential for Axonemal Assembly and Proper Morphology of Inner Dynein Arms. *PLoS Genet.* 13, e1006996. doi:10.1371/journal.pgen.1006996

Yamamoto, R., Hirono, M., and Kamiya, R. (2010). Discrete PIH Proteins Function in the Cytoplasmic Preassembly of Different Subsets of Axonemal Dyneins. *J. Cell Biol.* 190, 65–71. doi:10.1083/jcb.201002081

Yamamoto, R., Yanagi, S., Nagao, M., Yamasaki, Y., Tanaka, Y., Sale, W. S., et al. (2020). Mutations in PIH Proteins MOT48, TWI1 and PF13 Define Common and Unique Steps for Preassembly of Each, Different Ciliary Dynein. *PLoS Genet.* 16, e1009126. doi:10.1371/journal.pgen.1009126

Zhao, L., Yuan, S., Cao, Y., Kallakuri, S., Li, Y., Kishimoto, N., et al. (2013). Reptin/Ruvbl2 is a Lrrc6/Seahorse Interactor Essential for Cilia Motility. *Proc. Natl. Acad. Sci. U.S.A.* 110, 12697–12702. doi:10.1073/pnas.1300968110

Zhao, R., Davey, M., Hsu, Y.-C., Kaplanek, P., Tong, A., Parsons, A. B., et al. (2005). Navigating the Chaperone Network: An Integrative Map of Physical and Genetic Interactions Mediated by the Hsp90 Chaperone. *Cell* 120, 715–727. doi:10.1016/j.cell.2004.12.024

zur Lage, P., Newton, F. G., and Jarman, A. P. (2019). Survey of the Ciliary Motility Machinery of Drosophila Sperm and Ciliated Mechanosensory Neurons Reveals Unexpected Cell-Type Specific Variations: A Model for Motile Ciliopathies. *Front. Genet.* 10, 24. doi:10.3389/fgene.2019.00024

zur Lage, P., Stefanopoulou, P., Styczynska-Soczka, K., Quinn, N., Mali, G., von Kriegsheim, A., et al. (2018). Ciliary Dynein Motor Preassembly is Regulated by Wdr92 in Association with HSP90 Co-Chaperone, R2TP. *J. Cell Biol.* 217, 2583–2598. doi:10.1083/jcb.201709026

zur Lage, P., Xi, Z., Lennon, J., Hunter, I., Chan, W. K., Bolado Carrancio, A., et al. (2021). The Drosophila Orthologue of the Primary Ciliary Dyskinesia-Associated Gene, DNAAF3, is Required for Axonemal Dynein Assembly. *Biol. Open* 10 (10), bio058812. doi:10.1242/bio.058812

Conflict of Interest: The authors declare that the research was conducted in the absence of any commercial or financial relationships that could be construed as a potential conflict of interest.

Publisher's Note: All claims expressed in this article are solely those of the authors and do not necessarily represent those of their affiliated organizations, or those of the publisher, the editors and the reviewers. Any product that may be evaluated in this article, or claim that may be made by its manufacturer, is not guaranteed or endorsed by the publisher.

frontiers | Frontiers in Genetics

ORIGINAL RESEARCH
published: 07 July 2022
doi: 10.3389/fgene.2022.931822

Identical *IFT140* Variants Cause Variable Skeletal Ciliopathy Phenotypes—Challenges for the Accurate Diagnosis

Joanna Walczak-Sztulpa[1†], Anna Wawrocka[1†], Cenna Doornbos[2], Ronald van Beek[2,3], Anna Sowińska-Seidler[1], Aleksander Jamsheer[1,4], Ewelina Bukowska-Olech[1], Anna Latos-Bieleńska[1], Ryszard Grenda[5], Ernie M. H. F. Bongers[2], Miriam Schmidts[6,7], Ewa Obersztyn[8], Maciej R. Krawczyński[1,4‡] and Machteld M. Oud[2,3‡]*

[1]Department of Medical Genetics, Poznan University of Medical Sciences, Poznan, Poland, [2]Department of Human Genetics, Radboud University Medical Center, Nijmegen, Netherlands, [3]Donders Institute for Brain, Cognition and Behaviour, Radboud University Medical Center, Nijmegen, Netherlands, [4]Centers for Medical Genetics, Poznan, Poland, [5]Department of Nephrology, Kidney Transplantation and Hypertension, The Children's Memorial Health Institute, Warsaw, Poland, [6]Center for Pediatrics and Adolescent Medicine, University Hospital Freiburg, Freiburg University Faculty of Medicine, Freiburg, Germany, [7]CIBSS—Centre for Integrative Biological Signalling Studies, Freiburg University, Freiburg, Germany, [8]Department of Medical Genetics, Institute of Mother and Child, Warsaw, Poland

OPEN ACCESS

Edited by:
Steven LC Pei,
Yale University, United States

Reviewed by:
Joshi Stephen,
Baylor College of Medicine, United States
Alanna Strong,
Children's Hospital of Philadelphia, United States
Peter Harris,
Mayo Clinic, United States

***Correspondence:**
Machteld M. Oud
Machteld.Oud@radboudumc.nl

[†]These authors have contributed equally and share first authorship

[‡]These authors have contributed equally and share last authorship

Specialty section:
This article was submitted to Human and Medical Genomics, a section of the journal Frontiers in Genetics

Received: 29 April 2022
Accepted: 15 June 2022
Published: 07 July 2022

Citation:
Walczak-Sztulpa J, Wawrocka A, Doornbos C, van Beek R, Sowińska-Seidler A, Jamsheer A, Bukowska-Olech E, Latos-Bieleńska A, Grenda R, Bongers EMHF, Schmidts M, Obersztyn E, Krawczyński MR and Oud MM (2022) Identical IFT140 Variants Cause Variable Skeletal Ciliopathy Phenotypes—Challenges for the Accurate Diagnosis. Front. Genet. 13:931822. doi: 10.3389/fgene.2022.931822

Ciliopathies are rare congenital disorders, caused by defects in the cilium, that cover a broad clinical spectrum. A subgroup of ciliopathies showing significant phenotypic overlap are known as skeletal ciliopathies and include Jeune asphyxiating thoracic dysplasia (JATD), Mainzer-Saldino syndrome (MZSDS), cranioectodermal dysplasia (CED), and short-rib polydactyly (SRP). Ciliopathies are heterogeneous disorders with >187 associated genes, of which some genes are described to cause more than one ciliopathy phenotype. Both the clinical and molecular overlap make accurate diagnosing of these disorders challenging. We describe two unrelated Polish patients presenting with a skeletal ciliopathy who share the same compound heterozygous variants in *IFT140* (NM_014,714.4) r.2765_2768del; p.(Tyr923Leufs*28) and exon 27–30 duplication; p.(Tyr1152_Thr1394dup). Apart from overlapping clinical symptoms the patients also show phenotypic differences; patient 1 showed more resemblance to a Mainzer-Saldino syndrome (MZSDS) phenotype, while patient 2 was more similar to the phenotype of cranioectodermal dysplasia (CED). In addition, functional testing in patient-derived fibroblasts revealed a distinct cilium phenotyps for each patient, and strikingly, the cilium phenotype of CED-like patient 2 resembled that of known CED patients. Besides two variants in *IFT140*, in depth exome analysis of ciliopathy associated genes revealed a likely-pathogenic heterozygous variant in *INTU* for patient 2 that possibly affects the same IFT-A complex to which IFT140 belongs and thereby could add to the phenotype of patient 2. Taken together, by combining genetic data, functional test results, and clinical findings we were able to accurately diagnose patient 1 with "IFT140-related ciliopathy with MZSDS-like features" and patient 2 with "IFT140-related ciliopathy with CED-like features". This study emphasizes that identical variants in one ciliopathy associated gene can lead to a

variable ciliopathy phenotype and that an in depth and integrated analysis of clinical, molecular and functional data is necessary to accurately diagnose ciliopathy patients.

Keywords: *IFT140*, skeletal ciliopathy, cilium phenotype, MZSDS-like features, CED-like features

1 INTRODUCTION

Ciliopathies are a group of rare disorders that show clinical and genetic heterogeneity. The majority of ciliopathies are recessively inherited, however, few autosomal dominant forms (e.g. polycystic kidney disease, ADPKD) and X-linked inheritance patterns (e.g. retinitis pigmentosa, RP) have been reported (Tsang and Sharma, 2018; Ma, 2021). To date 35 ciliopathies and >187 associated disease genes have been described in literature (Reiter and Leroux, 2017). Those ciliopathies presenting with significant skeletal abnormalities are collectively called skeletal ciliopathies, i.e. Jeune asphyxiating thoracic dystrophy (JATD), short-rib polydactyly syndrome (SRPS), Mainzer-Saldino syndrome (MZSDS) and cranioectodermal dysplasia (CED). The skeletal ciliopathy cluster of CED (also called Sensenbrenner syndrome, MIM#218330, MIM#613610, MIM#614099, MIM#614378), MZSDS (MIM#266920, MIM#615630) and JATD (MIM#611263, MIM#613091, MIM#613819, MIM#614376, MIM%208,500) share significant genetic and phenotypic overlap. All three syndromes are characterized by skeletal features; short stature, rhizomelic limb shortening, and narrowing of the thorax to a variable degree where JATD shows the most severe form. A defining feature of JATD and MZSDS is pelvic abnormalities, which distinguishes the two syndromes from CED. While ectodermal abnormalities (i.e. nail, teeth and hair abnormalities) and dysmorphic craniofacial features such as frontal bossing and craniosynostosis are typical for CED and moderately common for MZSDS. The combination of renal and retinal abnormalities is typical for MZSDS, but can also occur in CED and to a much lesser extent in JATD. The major cause of skeletal ciliopathies are defects in genes that encode components of the intraflagellar transport complex A (IFT-A) and complex B (IFT-B). IFT is an evolutionarily conserved bidirectional trafficking machinery that is driven by kinesin- and dynein motor complexes and is essential for proper cilia function and structure. The IFT-B complex is composed of 16 proteins and is responsible for the anterograde transport, while the much smaller IFT-A complex is associated with retrograde transport. The IFT-A complex can be divided into a three core proteins; IFT122, IFT140 and WDR19, and three peripheral proteins; IFT43, WDR35, TTC21B. Dysfunctional IFT140 results in an accumulation of IFT proteins at the ciliary tip and in cilium shortening (Piperno et al., 1998; Miller et al., 2013). Cilia play an important role in diverse signaling pathways including Hedgehog (Hh),Wingless (Wnt), platelet-derived growth factor receptors (PDGFR), mammalian target of rapamycin (mTOR), G-protein coupled receptors (GPCR), Hippo and Notch. These pathways are crucial for normal embryonic development and for tissue homeostasis after birth (Wheway et al., 2019).

Variants in *IFT140* are implicated in the pathogenesis of CED and MZSDS, but also in JATD, Bardet-Biedl syndrome (BBS), Optiz trigonocephaly C syndrome (OTCS), and isolated retinitis pigmentosa (RP) displaying the complexity of ciliopathies (Cole and Snell, 2009; Schmidts et al., 2013; Bifari et al., 2016; Schaefer et al., 2016; Pena-Padilla et al., 2017). Here, we present a clinical, molecular and functional study of two unrelated patients with identical compound heterozygous variants in *IFT140* and show that the observed clinical differences were supported by distinctive cilium phenotypes of the two patients. Moreover, we suggest an alternative description of MZSDS to better resemble the variability seen between patients within this cohort, i.e. "*IFT140*-related ciliopathy with MZSDS- or CED-like features".

2 MATERIALS AND METHODS

2.1 Ethical Considerations

The study was conducted to the ethical tenets of the Declaration of Helsinki and in agreement with the "Code of Conduct for responsible use of patient-derived material". This study was approved by the Bioethics Committee at Poznan University of Medical Sciences in compliance with The Good Clinical Practice (GCP) and Polish law. Written informed consent was obtained from the patients and their parents.

2.2 Collection of Samples

Genomic DNA from both patients and their parents was extracted from whole blood and used for exome sequencing (ES) using a standard method. Skin-derived fibroblasts from both patients were obtained and used for immunofluorescent imaging.

2.3 Exome Sequencing

Genomic DNA from the affected patients and the unaffected parents of patient 2 were used for ES . Prior to sequencing, samples were prepared with the Twist library preparation kit (TWIST Bioscience, San Francisco, CA, United States) followed by sequencing on an Illumina Novaseq sequencer (Illumina, San Diego, CA, United States). Reads were aligned to the human genome assembly GRCh37(HG19) using the Burrows-Wheeler aligner version 0.7.13. Variant calling was performed for SNV with GATK HaplotypeCaller version 3.4–46, and for CNV with ExomeDepth version 1.1.12.

2.4 *IFT140* Transcript Analysis

RNA was isolated from skin-derived cultured fibroblasts using a standard method. Samples were prepared using the Illumina Stranded mRNA Prep kit according to the manufacturer's instructions. A total of 18 samples were pooled, equimolar,

TABLE 1 | Clinical features of patients with compound heterozygous variants in *IFT140* described in this study and in literature.

Clinical Features	Patient 1	MZSDS[a]	Patient 2	CED[b]; CED[c]
Initial clinical diagnosis	Mainzer-Saldino syndrome (MZSDS)		Cranioectodermal dysplasia (CED)	
Variant protein IFT140 NM_014,714.3	p.(Tyr923Leufs*28) [Pat] + p.(Tyr1152_Thr1349dup) [Mat]		p.(Tyr923Leufs*28) [Pat] + p.(Tyr1152_Thr1349dup) [Mat]	
Family history	Patient born from the 1st pregnancy		Patient born from the 1st pregnancy. In the 2nd pregnancy the couple had a spontaneous miscarriage at 7th WG. A healthy female was born from the 3rd pregnancy	
Time of delivery	40 WG		39 WG	
Birth measurements				
- weight	- 3720 g (>50th percentile)		- 3410 g (50th percentile)	
- length	- 56 cm (>97th percentile)		- 56 cm (>97th percentile)	
- OFC	- 36 cm (<97th percentile)		- 37 cm (97th percentile)	
Age at examination/ current age	10 years/13.5 years		3 months - 13 years/16 years	
Sex	Male		Male	
Dolichocephaly	+	0/6	–	2/2; 7/8
Craniosynostosis	–	3/6	–	1/2; 4/5
Frontal bossing	+	3/3	+	3/3; 4/5
High forehead	+	4/4	+	1/1; NA
Full cheeks	+	3/6	–	3/3; 1/1
Telecanthus/epicanthus	–/+	NA	+/+	NA; 3/4
Broad nasal bridge	–	1/1	+	2/2; NA
Micrognathia	+	NA	–	NA; 2/4
Everted lower lip	–	1/1	+	1/2; 3/4
Low set/simple ears	+/+	2/2	+/+	3/3; 2/2
Narrow chest, pectus excavatum	+, –	7/12, NA	+, +	3/3, 1/2; 10/10, 4/6
Short stature	+	16/21	+	3/3; 4/4
Rhizomelic limb shortening	+	1/7	+	2/2; 8/8
Short ribs	+	2/2	+	2/2; 1/1
Joint laxity	–	NA	+	2/2; 5/5
Brachydactyly of fingers and toes	+	13/15	+	3/3; 11/11
Cone-shaped epiphyses of phalanges	+	17/18	+	3/3; NA
Abnormality of proximal femur	+	1/1	NA	NA; NA
Slender, thin bones	–	0/2	NA	NA; NA
Dental abnormalities	+	0/8	+	3/3; 11/11
- malformed	+		+	
- widely spaced	+		+	
- hypodontia	–		–	
Nail abnormalities	–	NA	+	2/2; 3/4
Thin and/or sparse hair	+/–	NA	–/–	3/3; 6/9
Skin laxity	–	NA	–	NA; 7/8
Inguinal hernias	–	NA	–	NA; 2/2
Kidney disease	+	17/23	+	3/3; 10/11
- chronic renal failure	+		+	
- nephronophthisis	#		–	
- renal cysts	+*		+*	
- sclerosing glomerulopathy	–		+	
Kidney transplantation	+/at 4.5 years of age	5/5	+/at 3 years of age	1/1; 3/3
Ophthalmological problems	+	21/22	+ progressive visual loss (at present time blindness)	3/3; 1/7
- nystagmus	+		+	
- retinal dystrophy	+		+	
- optic nerve atrophy	+ (partial)		+	
Liver disease	–	6/13	–	0/1; 4/10
- hepatic fibrosis	–		–	
- cirrhosis	–		–	
- hepatomegaly	–		–	
Heart defects/cardiac malformations	–/–	NA	–/–	0/3; 1/4
Recurrent respiratory infections	+	2/4	–	3/3; 2/5

(Continued on following page)

TABLE 1 | (*Continued*) Clinical features of patients with compound heterozygous variants in *IFT140* described in this study and in literature.

Clinical Features	Patient 1	MZSDS[a]	Patient 2	CED[b]; CED[c]
Developmental milestones		7/14 delayed		2/3 delayed; 0/4 delayed
- sitting	- 12 months (>99th percentile)		- 36 months (>99th percentile)	
- walking	- 16 months (97th percentile)		- 6 years (>99th percentile)	
- speech development	- 24 months		- absent speech	
Intelligence	Normal	NA	ID	1/3 ID; 0/2 ID
Cerebellar ataxia	+	NA	+	NA
Other findings (CT, MRI, X-rays, EEG etc.)	–		- Congenital CMV infection - Epilepsy (absence attacks) from the age of 13 years, treated with Valproate - MRI - normal	

[a]—*IFT140-related MZSDS, phenotype based on literature (Perrault et al., 2012; Schmidts et al., 2013; Geoffroy et al., 2018; Oud et al., 2018);* [b]—*IFT140-related CED, phenotype based on literature (Bayat et al., 2017; Walczak-Sztulpa et al., 2020);* [c]—*CED, phenotype based on literature, excluding IFT140 (Gilissen et al., 2010; Walczak-Sztulpa et al., 2010; Arts et al., 2011; Bredrup et al., 2011); CT, computed tomography; EEG, electroencephalography; ID, intellectual disability; Mat, maternally inherited variant; MRI, magnetic resonance imaging; NA, data not available; Pat, paternally inherited variant; WG, weeks of gestation. + feature present;—feature absent; *presence, number of renal cysts, revealed by repeated ultrasonography not seen at baseline, has increased over time of follow-up; # unclear.*

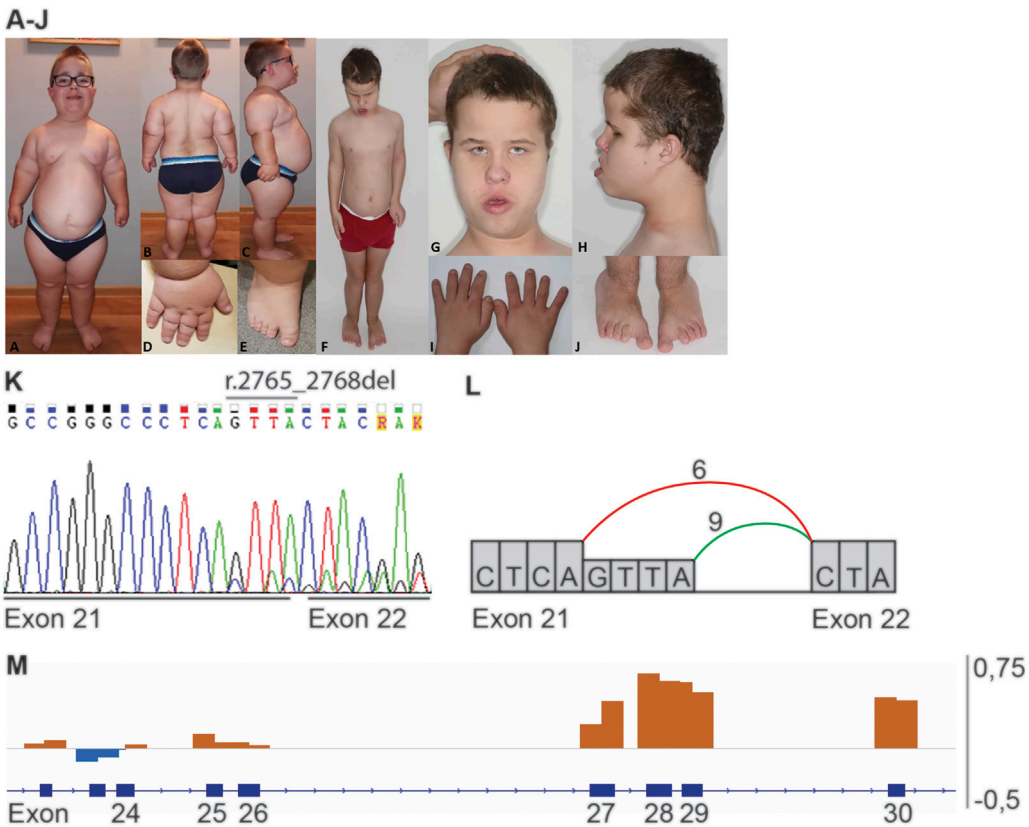

FIGURE 1 | Phenotype and genotype of patients 1 and 2. Proximal limb shortening, narrow thorax, frontal bossing, high forehead, low set and simple ears is present in both patients **(A,F,G,H)**. **(A–E)** Clinical features of patient 1: dolichocephalic head shape, full cheeks, micrognathia **(A)** obesity and hyperlordosis **(B,C)**, brachydactyly and sandal gap **(D,E)**. **(F–J)** Clinical features of patient 2: pectus excavatum **(F)**, epicanthal folds and telecanthus, broad nasal bridge, everted lower lip **(G)**, brachydactyly and sandal gap **(I,J)**. **(K)** Sanger sequence of heterozygous variant r.2765_2768del in *IFT140* (NM_014714.3: c.2767_2768+2del, p.(Tyr923Leufs*28)), representative for patient 1 and 2. **(L)** Schematic representation of the splicing effect caused by IFT140 r.2765_2768del. The coloured lines indicate the splicing between exons, in green the wildtype splicing between exon 21 and 22 and in red the aberrant splicing seen in patients 1 and 2. **(M)** Schematic overview of the heterozygous exon 27–30 duplication (p. (Tyr1152_Thr1394dup)) detected in patients 1 and 2. Orange bars indicate an increase in coverage and blue bars indicate a decrease in coverage.

and sequenced on a SP flowcell using the Illumina NovaSeq6000 (Illumina, San Diego, CA, United States). Demultiplexing and sample analysis with DRAGEN RNA Pipeline 3.7.5 was performed on the Illumina BaseSpace platform.

2.5 Cilium Phenotyping Using the Automated ALPACA Tool

The cilium phenotype for both patients was determined using a standardized immunofluorescent assay in skin-derived fibroblasts as described by Doornbos *et al.* (Doornbos et al., 2021). In brief, the fibroblasts were cultured under standard cell culture conditions on glass coverslips. Cilia formation was stimulated by replacement of the culture medium containing 20% fetal calf serum (FCS) to medium containing 0.2% FCS for 48 h prior to staining. Upon fixation, permeabilization and blocking, the cells were stained with antibodies to visualize different cilium parameters, *i.e.* ciliogenesis, cilium length, and retrograde IFT. The ciliogenesis parameter represents the percentage of ciliated cells and is visualized by acetylated-α-tubulin + ARL13B + PCNT. The cilium length was measured using the ALPACA tool, described in detail by Doornbos *et al.*, based on the length of the combined acetylated-α-tubulin and ARL13B signal. The ALPACA tool was also used to measure the surface area of IFT88 and an increased surface area of IFT88 indicates defective retrograde transport. The cilium length and the IFT88 measurement data were combined and plotted into a previously generated reference graph containing data from six control fibroblast lines and ten skeletal ciliopathy patient fibroblast lines (Doornbos et al., 2021).

3 CLINICAL REPORT

Detailed clinical characteristics of two unrelated male patients, showing clinical overlap but diagnosed with a different ciliopathy based on differences in the clinical phenotype, presented in **Table 1** and **Figures 1A–J**.

In summary, patient 1, a 10-year old boy was referred to a clinical geneticist due to severe retinal degradation, facial dysmorphisms, bone dysplasia, skeletal abnormalities and chronic renal failure (after kidney transplantation at 4.5 years of age). Patient 2, a 16-year old boy, presented with facial dysmorphisms, global developmental delay, epilepsy (from 14 years old), abnormal body proportions, skeletal abnormalities, ESRD and congenital CMV infection. The skeletal abnormalities in both patients include narrowing of the chest, short stature, rhizomelic limb shortening, brachydactyly, and cone-shaped epiphyses of phalanges. Besides the significant clinical overlap between patients 1 and 2 there are also typical phenotypic differences, including the presence of dolichocephaly, micrognathia and thin hair in patient 1 but not in patient 2, and, the presence of a broad nasal bridge, everted lower lip, nail abnormalities and joint laxity only in patient 2. In addition, there were striking differences in the development of both patients. Patient 1 showed normal psychomotor development and intelligence, while patient 2 showed developmental delay with intellectual disability and epilepsy. Even though both patients developed early-onset end-stage renal disease (ESRD) the development of the disease was different. Patient 1 developed ESRD at the age of 3 years, while patient 2 was diagnosed with rapid end-stage renal failure due to diffuse glomerulosclerosis and fibrosis at the age of 9 months. Moreover, patient 2 presented with a bilateral vesicoureteral reflux (VUR) grade II.

4 RESULTS

4.1 ES Revealed Identical Causative Variants in *IFT140*

A targeted analysis was performed selecting exonic and intronic position -20 to +8 variants in 170 ciliopathy associated genes (Radboudumc ciliopathy gene panel version DG3.00 (Radboudumc)) with a frequency <1% in dbSNP151, <5% in in-house db (containing data from >22.000 exomes), and <1% in gnomAD (version 2.1.1). This resulted in 16 variants for patient 1 and 19 variants for patient 2 (**Supplementary Tables S1 and S2**). CNV analysis was performed by selecting for segments containing any of the 170 ciliopathy associated genes and a frequency <1% in the in-house db. This resulted in two duplications for patient 1 and one duplication for patient 2 (**Supplementary Table S3**). Subsequently, the combined variants from SNV and CNV were filtered for a recessive inheritance model and a matching phenotype, resulting in a single gene, *IFT140*, in both patients. Both probands carry the same variants in *IFT140* Chr16 (GRCh37): g.1575886_1575889del; NM_014,714.4: r.2765_2768del; p.(Tyr923Leufs*28) and exon 27–30 duplication; p.(Tyr1152_Thr1349dup) (**Figure 1K-M**). Segregation analysis in both families fit with a recessive inheritance pattern. The deletion variant in *IFT140* r.2765_2768 has previously been reported as a likely pathogenic variant in ClinVar (VCV000863072.3) in a patient with retinal dystrophy, as well as, a patient with MZSDS. The duplication variant in *IFT140* NC_000016.9:g.1568118(NM_014714.4):c (4182 + 99)_(3558)dup is absent from ClinVar, but has been detected in two Polish skeletal ciliopathy patients and in eight families reported by Geoffroy (Geoffroy et al., 2018; Walczak-Sztulpa et al., 2020). These include six families (seven patients) diagnosed with MZSDS, one patient with JATD and one affected individual with features of CED.

A larger duplication, including the variant detected in patients 1 and 2, has been reported once in a patient with a skeletal ciliopathy (VCV000523177.1). In addition to the variants in *IFT140*, a heterozygous variant c.1354G > A; p.Ala452Thr in *INTU* (NM_015693.3) was detected in ES data from patient 2. The minor allele frequency of *INTU* variant c.1354G > A is 0.246% in GnomAD v2.1. 1 (accessed on 19 May 2022). The detected variant was previously described as likely pathogenic in a patient with nephronophthisis and growth retardation by Toriyama *et al.* (Toriyama et al., 2016). Furthermore, the molecular data from patient 2 was analyzed for rare variants (same filters

TABLE 2 | Cilium phenotypes. The cilium phenotypes of three clusters; control, Jeune asphyxiating thoracic dysplasia and cranioectodermal dysplasia published by Doornbos et al. (Doornbos et al., 2021). Followed by the measurements from this study, a control line, patient 1 and patient 2. The cilium phenotypes are represented by the ciliogenesis, cilium length and IFT-A (the IFT88 measurement along the ciliary axoneme).

Group	Ciliogenesis	Length	IFT-A
Controls (*n* = 6)	90 ± 8%	3.68 ± 0.04 μm	0.43 ± 0.01 μm^2
ATD (*n* = 5)	93 ± 6%	4.81 ± 0.06 μm	0.54 ± 0.03 μm^2
CED (*n* = 3)	80 ± 14%	2.44 ± 0.05 μm	0.82 ± 0.03 μm^2
Control 1	91 ± 1%	3.77 ± 0.23 μm	0.47 ± 0.05 μm^2
Patient 1	93 ± 3%	3.71 ± 0.07 μm	0.99 ± 0.08 μm^2
Patient 2	90 ± 3%	3.04 ± 0.15 μm	0.79 ± 0.08 μm^2

applied as described above) in genes associated with intellectual disability (ID) (Radboudumc ID gene panel version DG3.00 (Radboudumc, 2021)) and analyzed for ID-associated CNVs. The resulting variant list was filtered for both autosomal recessive and autosomal dominant inheritance models and subsequently checked for phenotypic overlap. This approach did not lead to candidate variants that could explain the ID phenotype seen in patient 2.

4.2 Aberrant Splicing of *IFT140* Transcript

RNA isolated from skin-derived fibroblasts from patients 1 and 2 was used for *IFT140* transcript analysis. Compared to the reference fibroblast sample both patient samples showed aberrant splicing at the splice donor site of exon 21 where ES revealed a 4bp deletion (**Figure 1L**). Approximately half of the reads originated from position r.2764 indicating a 4bp deletion r.2765_2768del and would result in a frameshift.

4.3 Different Cilium Phenotype Between Patients 1 and 2

Skin-derived fibroblasts from patients 1 and 2 were used to determine the cilium phenotype based on three parameters; ciliogenesis, cilium length, and retrograde IFT (**Supplementary Figure S1**). The results were compared to the "healthy cilium phenotype" and that of two distinct skeletal ciliopathy cohorts, ATD and CED, described by Doornbos *et al.* (**Table 2**) (Doornbos et al., 2021). Fibroblasts from both patients showed normal ciliogenesis >90% and a significantly increased IFT88 measurement of 0.99 ± 0.08μm^2 for patient 1 and 0.79 ± 0.08μm^2 for patient 2. While the cilium length for patient 1 was, although slightly increased, within normal range (3.71 ± 0.07 μm), the cilia of patient 2 were significantly shorter (3.04 ± 0.15 μm) (**Figure 2**). Based on these cilium length and IFT88 measurements, the cilium phenotype of patient 2 resembles that seen in CED patients whereas, the results of patient 1 are clearly abnormal, the cilium phenotype does not cluster with ATD nor CED.

5 DISCUSSION

The two patients described in this report share identical compound heterozygous variants in *IFT140*. Despite the large phenotypic overlap, the observed clinical differences between patients 1 and 2 led to the suspicion of two different diagnoses. Functional experiments were requested to further investigate the clinical variability, and indeed, the different cilium phenotypes of each patient emphasized the observed clinical variability. The cilium phenotyping data placed patient 2 (decreased cilium length and increased IFT88 measurement) on the border of the established CED cluster, whereas patient 1

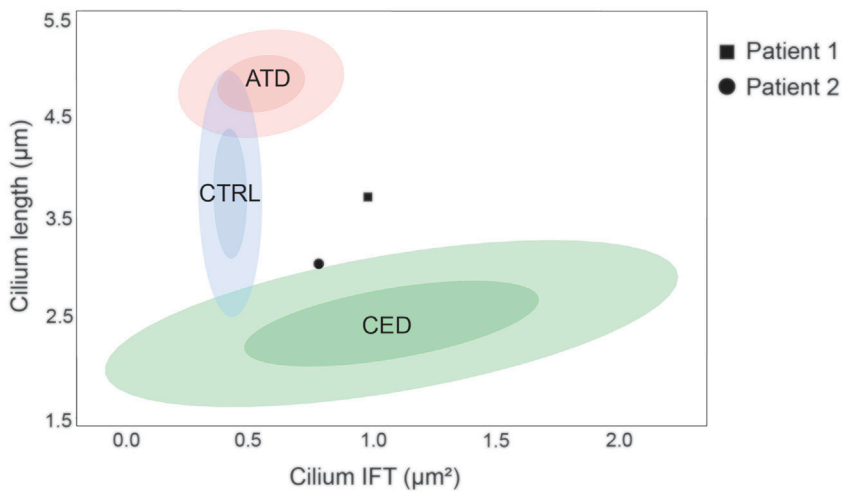

FIGURE 2 | Ciliopathy cilium phenotype clusters. The cilium phenotype clusters are based on two cilium parameters; cilium length (*Y*-axis) and IFT88 measurement (*X*-axis) published in Doornbos *et al.* (Doornbos et al., 2021). The confidence intervals (CI) of 0.5 and 0.9 are indicated per identifiable group, i.e. the control, ATD, and CED cohorts. The cilium phenotype of patient 1 showed a normal cilium length (3.71 ± 0.07 μm) and an increased IFT88 measurement (0.99 ± 0.08μm^2), therefore it does not fit in any cluster. Patient 2 showed a decreased cilium length (3.04 ± 0.15 μm) and an increased IFT88 measurement (0.79 ± 0.08μm^2), therefore it is positioned on the border of the CED cluster.

(normal cilium length and increased IFT88 measurement) did not fit in any previously defined cluster. Additional experiments are required to further elucidate the exact underlying mechanism that caused this difference in cilium phenotype.

One explanation for the cilium phenotypic difference could be the effect of the likely pathogenic variant found in *INTU* in the ES of patient 2, which was not present in patient 1. Interestingly, INTU has been described to interact with the IFT-A protein complex (Toriyama et al., 2016). Protein interaction studies showed that the ciliogenesis and planar polarity effector (CPLANE) complex proteins, consisting of INTU, FUZ, and WDPCP, interact with all six components of the retrograde IFT complex. The absence of CPLANE inhibits peripheral IFT proteins (IFT43, WDR35, and TTC21B) to localize to the basal body of the cilium and therefore do not assemble onto the IFT core proteins (IFT122, IFT140, WDR19). These data show that there is a connection between INTU and IFT-A components. Therefore, we can speculate that the detected *INTU* variant adds to the burden of the *IFT140* variants on proper functioning of the IFT-A complex. Recent literature has shown that mutations in *INTU* are causative for a short-rib polydactyly syndrome phenotype (Toriyama et al., 2016; Bruel et al., 2018). The *INTU* variant c.1354G > A that was detected in patient 2 has previously been described to be causative in a 13-year old female with nephronophthisis, ESRD at 10 years of age and growth retardation. The authors suggest that the variant may be hypomorphic since the affected residue is poorly conserved and the patient has a milder phenotype compared to other *INTU* patients. It is possible that the likely pathogenic *INTU* variant contributes to the more severe phenotype seen in patient 2 presented in this study, however, further functional studies are required to provide more evidence.

The heterogeneity of ciliopathies is well known. With over 187 associated genes and a pleiotropy of ciliopathy genes for which one gene can cause different phenotypes (Reiter and Leroux, 2017). One example is *WDR19* which is associated with JATD, CED, NPHP, RP, and Senior Løken syndrome (Bredrup et al., 2011; Coussa et al., 2013). In this report, we present two patients with identical compound heterozygous variants and a variable clinical phenotype. A similar case to what we found with the *INTU* variant, was presented by Maglic *et al.* who described two families with variants in *TMEM231* (Maglic et al., 2016). In these two families, of whom the fathers are identical twins, both had children affected with a ciliopathy caused by compound heterozygous variants in *TMEM231*. The mothers carried two different missense variants in *TMEM231* and the fathers carried the same variant. Family 1 had four children with Joubert syndrome (MIM#614970) of which three of the children had an identical phenotype whereas the fourth child was more severely affected. They suggest that an additional variant in the ciliopathy gene *BBS10,* only present in the fourth child, could explain the more severe phenotype. Moreover, the child in the second family presented with Meckel-Gruber syndrome (MIM#615397). Although the compound heterozygous variants between the two families are not identical, it is intriguing to find two different diagnoses in these two closely related families.

We cannot exclude that the developmental delay, ID and epilepsy are a result of the congenital CMV infection that patient 2 had. Recent literature showed that younger children (age 0–2) have an increased risk of developing epilepsy upon experiencing a congenital CMV infection (Lin et al., 2021).

While JATD and CED have cardinal features distinguishing one from the other, this is less clear for MZSDS as we showed in this study. Both presented patients, as well as, published patients with causative variants in *IFT140* display a variable phenotype sharing features with both JATD and CED. This may indicate that the classic description of the skeletal ciliopathy cluster, CED, MZSDS and JATD, does not adequately cover the observed variability within each cohort. Instead "IFT140-related ciliopathy with MZSDS- and/or CED-like features" could be considered to better represent the phenotype of the patient. In our study, the CED-like features such as the ectodermal- and craniofacial dysmorphisms were more prominent in patient 2 compared to patient 1, and together with the suggestive cilium phenotype results we would consider two different diagnoses for each patient. Patient 1 was diagnosed with "IFT140-related ciliopathy with MZSDS-like features" and patient 2 with "IFT140-related ciliopathy with CED-like features". The intra- and interfamilial clinical variability in patients with identical casual variants has been reported in ciliopathy patients. It is of note that the presence of modifying alleles, environmental factors, and other mechanisms such as epigenetics may play a role in the phenotypic variability. However, it is difficult to precisely define the impact of these factors on the clinical manifestation (Mitchison and Valente, 2017; Walczak-Sztulpa et al., 2021).

The definition of a diagnosis is not set in stone and calls for careful consideration of different facets of the disease. The initial clinical examination, often the guideline for ES analysis, will determine the course of the care path followed by the patient. In our experience the clinical symptoms are leading in defining the differential diagnosis for a patient, but we strongly believe that the addition and integration of molecular genetics data and functional work to the clinical phenotype is crucial to come to an accurate diagnosis for each patient. We showed that the observed clinical differences between two skeletal ciliopathy patients carrying identical causative variants were supported by different cilium phenotypes. Moreover, we suggest to describe the presented phenotypes as "IFT140-related ciliopathies with MZSDS- or CED-like features" to better represent a variable disease cohort. We advocate the necessity of combining clinical, molecular, and functional data to accurately diagnose ciliopathy patients.

DATA AVAILABILITY STATEMENT

The datasets for this article are not publicly available due to concerns regarding participant/patient anonymity. Requests to access the datasets should be directed to the corresponding author.

ETHICS STATEMENT

The studies involving human participants were reviewed and approved by Bioethics Committee at Poznan University of Medical Sciences, Poznan, Poland. Written informed consent to participate in this study was provided by the participants' legal guardian/next of kin. Written informed consent was obtained from the minor(s)' legal guardian/next of kin for the publication of any potentially identifiable images or data included in this article.

AUTHOR CONTRIBUTIONS

MO, JW-S, and AW designed the experiments. RvB, CD, and MS performed the functional experiments. EO, AS-S, AJ, and EB-O contributed to the molecular testing. EO, MRK, AL-B, MS, EB, and RG performed clinical examinations. JW-S, MO, and AW wrote the manuscript. All authors read and approved the manuscript.

FUNDING

MS acknowledges funding from the European Research Council (ERC) (ERC starting grant No. 716344), the Deutsche Forschungsgemeinschaft (DFG, German Research Foundation): Project-ID 431984000–SFB 1453 and under Germany's Excellence Strategy (CIBSS—EXC-2189—project ID 390939984).

ACKNOWLEDGMENTS

We thank the patients, parents, and family members for their participation in this study. We thank R. Derks for practical work and L.E.L.M Vissers and R. Roepman for their support of this study.

SUPPLEMENTARY MATERIAL

The Supplementary Material for this article can be found online at: https://www.frontiersin.org/articles/10.3389/fgene.2022.931822/full#supplementary-material

REFERENCES

Arts, H. H., Bongers, E. M. H. F., Mans, D. A., van Beersum, S. E. C., Oud, M. M., Bolat, E., et al. (2011). C14ORF179 Encoding IFT43 Is Mutated in Sensenbrenner Syndrome. *J. Med. Genet.* 48 (6), 390–395. doi:10.1136/jmg.2011.088864

Bayat, A., Kerr, B., Douzgou, S., and Study, D. D. D. (2017). The Evolving Craniofacial Phenotype of a Patient with Sensenbrenner Syndrome Caused by IFT140 Compound Heterozygous Mutations. *Clin. Dysmorphol.* 26 (4), 247–251. doi:10.1097/MCD.0000000000000169

Bifari, I. N., Elkhamary, S. M., Bolz, H. J., and Khan, A. O. (2016). The Ophthalmic Phenotype ofIFT140-Related Ciliopathy Ranges from Isolated to Syndromic Congenital Retinal Dystrophy. *Br. J. Ophthalmol.* 100 (6), 829–833. doi:10.1136/bjophthalmol-2015-307555

Bredrup, C., Saunier, S., Oud, M. M., Fiskerstrand, T., Hoischen, A., Brackman, D., et al. (2011). Ciliopathies with Skeletal Anomalies and Renal Insufficiency Due to Mutations in the IFT-A Gene WDR19. *Am. J. Hum. Genet.* 89 (5), 634–643. doi:10.1016/j.ajhg.2011.10.001

Bruel, A.-L., Levy, J., Elenga, N., Defo, A., Favre, A., Lucron, H., et al. (2018). INTU -related Oral-Facial-Digital Syndrome Type VI: A Confirmatory Report. *Clin. Genet.* 93 (6), 1205–1209. doi:10.1111/cge.13238

Cole, D. G., and Snell, W. J. (2009). SnapShot: Intraflagellar Transport. *Cell* 137 (4), 784. doi:10.1016/j.cell.2009.04.053

Coussa, R. G., Otto, E. A., Gee, H. Y., Arthurs, P., Ren, H., Lopez, I., et al. (2013). WDR19 : An Ancient, Retrograde, Intraflagellar Ciliary Protein Is Mutated in Autosomal Recessive Retinitis Pigmentosa and in Senior-Loken Syndrome. *Clin. Genet.* 84 (2), 150–159. doi:10.1111/cge.12196

Doornbos, C., van Beek, R., Bongers, E. M. H. F., Lugtenberg, D., Klaren, P. H. M., Vissers, L. E. L. M., et al. (2021). Cell-based Assay for Ciliopathy Patients to Improve Accurate Diagnosis Using ALPACA. *Eur. J. Hum. Genet.* 29 (11), 1677–1689. doi:10.1038/s41431-021-00907-9

Geoffroy, V., Stoetzel, C., Scheidecker, S., Schaefer, E., Perrault, I., Bär, S., et al. (2018). Whole-genome Sequencing in Patients with Ciliopathies Uncovers a Novel Recurrent Tandem Duplication in IFT140. *Hum. Mutat.* 39 (7), 983–992. doi:10.1002/humu.23539

Gilissen, C., Arts, H. H., Hoischen, A., Spruijt, L., Mans, D. A., Arts, P., et al. (2010). Exome Sequencing Identifies WDR35 Variants Involved in Sensenbrenner Syndrome. *Am. J. Hum. Genet.* 87 (3), 418–423. doi:10.1016/j.ajhg.2010.08.004

Lin, C.-H., Chou, I.-C., Lee, I.-C., and Hong, S.-Y. (2021). Cytomegalovirus Infection in Infancy May Increase the Risk of Subsequent Epilepsy and Autism Spectrum Disorder in Childhood. *Children* 8 (11), 1040. doi:10.3390/children8111040

Ma, M. (2021). Cilia and Polycystic Kidney Disease. *Seminars Cell & Dev. Biol.* 110, 139–148. doi:10.1016/j.semcdb.2020.05.003

Maglic, D., Stephen, J., Malicdan, M. C. V., Guo, J., Fischer, R., Konzman, D., et al. (2016). TMEM231Gene Conversion Associated with Joubert and Meckel-Gruber Syndromes in the Same Family. *Hum. Mutat.* 37 (11), 1144–1148. doi:10.1002/humu.23054

Miller, K. A., Ah-Cann, C. J., Welfare, M. F., Tan, T. Y., Pope, K., Caruana, G., et al. (2013). Cauli: A Mouse Strain with an Ift140 Mutation that Results in a Skeletal Ciliopathy Modelling Jeune Syndrome. *PLoS Genet.* 9 (8), e1003746. doi:10.1371/journal.pgen.1003746

Mitchison, H. M., and Valente, E. M. (2017). Motile and Non-motile Cilia in Human Pathology: from Function to Phenotypes. *J. Pathol.* 241 (2), 294–309. doi:10.1002/path.4843

Oud, M. M., Latour, B. L., Bakey, Z., Letteboer, S. J., Lugtenberg, D., Wu, K. M., et al. (2018). Cellular Ciliary Phenotyping Indicates Pathogenicity of Novel Variants in IFT140 and Confirms a Mainzer-Saldino Syndrome Diagnosis. *Cilia* 7, 1. doi:10.1186/s13630-018-0055-2

Peña-Padilla, C., Marshall, C. R., Walker, S., Scherer, S. W., Tavares-Macías, G., Razo-Jiménez, G., et al. (2017). Compound Heterozygous Mutations in theIFT140gene Cause Opitz Trigonocephaly C Syndrome in a Patient with Typical Features of a Ciliopathy. *Clin. Genet.* 91 (4), 640–646. doi:10.1111/cge.12924

Perrault, I., Saunier, S., Hanein, S., Filhol, E., Bizet, A. A., Collins, F., et al. (2012). Mainzer-Saldino Syndrome Is a Ciliopathy Caused by IFT140 Mutations. *Am. J. Hum. Genet.* 90 (5), 864–870. doi:10.1016/j.ajhg.2012.03.006

Piperno, G., Siuda, E., Henderson, S., Segil, M., Vaananen, H., and Sassaroli, M. (1998). Distinct Mutants of Retrograde Intraflagellar Transport (IFT) Share Similar Morphological and Molecular Defects. *J. Cell Biol.* 143 (6), 1591–1601. doi:10.1083/jcb.143.6.1591

Radboudumc. 2021. Radboudumc Gene Panels. [Online]. Available: https://www.radboudumc.nl/en/afdelingen/genetica/about-us/genomediagnostics/services/gene-panels [Accessed 2021].

Reiter, J. F., and Leroux, M. R. (2017). Genes and Molecular Pathways Underpinning Ciliopathies. *Nat. Rev. Mol. Cell Biol.* 18 (9), 533–547. doi:10.1038/nrm.2017.60

Schaefer, E., Stoetzel, C., Scheidecker, S., Geoffroy, V., Prasad, M. K., Redin, C., et al. (2016). Identification of a Novel Mutation Confirms the Implication of IFT172 (BBS20) in Bardet-Biedl Syndrome. *J. Hum. Genet.* 61 (5), 447–450. doi:10.1038/jhg.2015.162

Schmidts, M., Frank, V., Eisenberger, T., Al Turki, S., Bizet, A. A., Antony, D., et al. (2013). Combined NGS Approaches Identify Mutations in the Intraflagellar Transport Gene IFT140 in Skeletal Ciliopathies with Early Progressive Kidney Disease. *Hum. Mutat.* 34 (5), 714–724. doi:10.1002/humu.22294

Toriyama, M., Lee, C., Lee, C., Taylor, S. P., Duran, I., Cohn, D. H., et al. (2016). The Ciliopathy-Associated CPLANE Proteins Direct Basal Body Recruitment of Intraflagellar Transport Machinery. *Nat. Genet.* 48 (6), 648–656. doi:10.1038/ng.3558

Tsang, S. H., and Sharma, T. (2018). X-Linked Retinitis Pigmentosa. *Adv. Exp. Med. Biol.* 1085, 31–35. doi:10.1007/978-3-319-95046-4_8

Walczak-Sztulpa, J., Eggenschwiler, J., Osborn, D., Brown, D. A., Emma, F., Klingenberg, C., et al. (2010). Cranioectodermal Dysplasia, Sensenbrenner Syndrome, Is a Ciliopathy Caused by Mutations in the IFT122 Gene. *Am. J. Hum. Genet.* 86 (6), 949–956. doi:10.1016/j.ajhg.2010.04.012

Walczak-Sztulpa, J., Posmyk, R., Bukowska-Olech, E. M., Wawrocka, A., Jamsheer, A., Oud, M. M., et al. (2020). Compound Heterozygous IFT140 Variants in Two Polish Families with Sensenbrenner Syndrome and Early Onset End-Stage Renal Disease. *Orphanet J. Rare Dis.* 15 (1), 36. doi:10.1186/s13023-020-1303-2

Walczak-Sztulpa, J., Wawrocka, A., Stańczyk, M., Pesz, K., Dudarewicz, L., Chrul, S., et al. (2021). Interfamilial Clinical Variability in Four Polish Families with Cranioectodermal Dysplasia and Identical Compound Heterozygous Variants in WDR35. *Am. J. Med. Genet.* 185 (4), 1195–1203. doi:10.1002/ajmg.a.62067

Wheway, G., and Mitchison, H. M.Genomics England Research Consortium (2019). Opportunities and Challenges for Molecular Understanding of Ciliopathies-The 100,000 Genomes Project. *Front. Genet.* 10, 127. doi:10.3389/fgene.2019.00127

Conflict of Interest: The authors declare that the research was conducted in the absence of any commercial or financial relationships that could be construed as a potential conflict of interest.

Publisher's Note: All claims expressed in this article are solely those of the authors and do not necessarily represent those of their affiliated organizations, or those of the publisher, the editors and the reviewers. Any product that may be evaluated in this article, or claim that may be made by its manufacturer, is not guaranteed or endorsed by the publisher.

frontiers | Frontiers in Genetics

CASE REPORT
published: 12 July 2022
doi: 10.3389/fgene.2022.934920

Case Report: *DNAAF4* Variants Cause Primary Ciliary Dyskinesia and Infertility in Two Han Chinese Families

Ting Guo [1,2,3†], Chenyang Lu [1,2,3†], Danhui Yang [1,2,3], Cheng Lei [1,2,3], Ying Liu [1,2,3], Yingjie Xu [1,2,3], Binyi Yang [1,2,3], Rongchun Wang [1,2,3] and Hong Luo [1,2,3]**

[1]Department of Pulmonary and Critical Care Medicine, The Second Xiangya Hospital, Central South University, Changsha, China, [2]Research Unit of Respiratory Disease, Central South University, Changsha, China, [3]Hunan Diagnosis and Treatment Center of Respiratory Disease, Changsha, China

Background: Primary ciliary dyskinesia (PCD) is a rare genetic disorder, predominantly autosomal recessive. The dynein axonemal assembly factor 4 (*DNAAF4*) is mainly involved in the preassembly of multisubunit dynein protein, which is fundamental to the proper functioning of cilia and flagella. There are few reports of PCD-related pathogenic variants of *DNAAF4*, and almost no *DNAAF4*-related articles focused on sperm phenotype. Moreover, the association between *DNAAF4* and scoliosis has never been reported, to the best of our knowledge.

Materials and Methods: We recruited two patients with a clinical diagnosis of PCD. One came from a consanguineous and another from a non-consanguineous family. Clinical data, laboratory test results, and imaging data were analyzed. Through whole exome sequencing, immunofluorescence, electron microscopy, high-speed video microscopy analysis, and hematoxylin–eosin (HE) staining, we identified the disease-associated variants and validated the pathogenicity.

Results: Proband 1 (P1, F1: II-1), a 19-year-old man, comes from a non-consanguineous family-I, and proband 2 (P2, F2: II-1), a 37-year-old woman, comes from a consanguineous family-II. Both had sinusitis, bronchiectasis, situs inversus, and scoliosis. P1 also had asthenoteratozoospermia, and P2 had an immature uterus. Two homozygous pathogenic variants in *DNAAF4* (NM_130810.4), c.988C > T, p.(Arg330Trp), and *DNAAF4* (NM_130810.4), c.733 C > T, p.(Arg245*), were identified through whole exome sequencing. High-speed microscopy analysis showed that most of the cilia were static in P1, with complete static of the respiratory cilia in P2. Immunofluorescence showed that the outer dynein arms (ODA) and inner dynein arms (IDA) were absent in the respiratory cilia of both probands, as well as in the sperm flagellum of P1. Transmission electron microscopy revealed the absence of ODA and IDA of respiratory cilia of P2, and HE staining showed irregular, short, absent, coiled, and bent flagella.

Conclusion: Our study identified a novel variant c.733C > T, which expanded the spectrum of *DNAAF4* variants. Furthermore, we linked *DNAAF4* to asthenoteratozoospermia and likely scoliosis in patients with PCD. This study will contribute to a better understanding of PCD.

Keywords: primary ciliary dyskinesia, scoliosis, *DNAAF4*, bronchiectasis, situs inversus, asthenoteratozoospermia

OPEN ACCESS

Edited by:
Steven L. C. Pei,
Yale University, United States

Reviewed by:
Raymond H. Kim,
University of Toronto, Canada
Kuokuo Li,
Anhui Medical University, China

****Correspondence:***
Hong Luo
luohonghuxi@csu.edu.cn
Rongchun Wang
198202060@csu.edu.cn

[†]These authors have contributed equally to this work

Specialty section:
This article was submitted to Human and Medical Genomics, a section of the journal Frontiers in Genetics.

Received: *03 May 2022*
Accepted: *01 June 2022*
Published: *12 July 2022*

Citation:
Guo T, Lu C, Yang D, Lei C, Liu Y, Xu Y, Yang B, Wang R and Luo H (2022) Case Report: DNAAF4 Variants Cause Primary Ciliary Dyskinesia and Infertility in Two Han Chinese Families. Front. Genet. 13:934920. doi: 10.3389/fgene.2022.934920

INTRODUCTION

Primary ciliary dyskinesia (PCD, MIM:244400) is a rare genetic disorder caused by motile cilia dysfunction (Mirra et al., 2017). It has diverse clinical manifestations involving multiple systems, such as recurrent respiratory infections, sinusitis, situs inversus, and infertility (Knowles et al., 2016). To date, there have been no diagnostic tests that could be completely relied upon to confirm this disease (Shapiro et al., 2016). About 50 genes have been reported as causative for PCD, of which those reported to be associated with asthenoteratozoospermia (reduced sperm motility and abnormal sperm morphology) and scoliosis are even rarer (Coutton et al., 2015; Aprea et al., 2021; Lu et al., 2021). Asthenoteratozoospermia is an important cause of male infertility, which affects approximately 7% of the male population. In addition, genetic factors account for at least 15% of the causes of male infertility (Krausz and Riera-Escamilla, 2018). Hence, finding novel genetic factors for idiopathic infertility is crucial for PCD and male infertility. In addition, scoliosis is another PCD-related phenotype reported in this article, which was defined as a spinal malformation in a patient who has skeletal maturation with a Cobb angle in the coronal plane >10° (Aebi, 2005). Scoliosis can be observed in mice with some PCD causative gene variants, but it requires more attention in patients with PCD (Baschal et al., 2015; Gao et al., 2015; Zhou et al., 2015; Lu et al., 2021).

Dynein axonemal assembly factor 4 (*DNAAF4*, OMIM: 608706), also called *DYX1C1*, encodes a 420-aa protein with a tetratricopeptide repeat domains (Taipale et al., 2003). Previous studies of *DNAAF4* focused on neuroscience and showed that it was involved in the migration of nerve cells (Taipale et al., 2003; Tapia-Páez et al., 2008). In recent years, with the in-depth research of the DNAAF family, the correlation between *DNAAF4* and motile cilia gradually emerged. DNAAF4 is localized in the cytoplasm and it was mainly involved in the preassembly of cilia multi-subunit dynein protein (Aprea et al., 2021). Variants in *DNAAF4* have been reported to be associated with bronchiectasis, situs inversus, female infertility, and abnormal ultrastructure of sperm (Guo et al., 2017; Aprea et al., 2021).

This study analyzed clinical data and whole exome sequencing data from two PCD patients, and two pathogenic variants of *DNAAF4* were identified. Thereafter, we validated the pathogenicity of the variants by high-speed microscopy, immunofluorescence, hematoxylin-eosin (HE) staining, and transmission electron microscopy (TEM). We provide the detailed report of the association of *DNAAF4* with asthenoteratozoospermia and scoliosis.

MATERIALS AND METHODS

Patients and Clinical Materials

The study protocol was approved by the review board of the Second Xiangya Hospital of Central South University in China. Informed consent was obtained from all subjects. All experiments were performed in accordance with the relevant guidelines and regulations. Two patients diagnosed with PCD and their families were recruited, in which one patient was from a consanguineous family and the other from a non-consanguineous family. The medical records of the subjects, including pulmonary, paranasal sinuses, abdominal computed tomography (CT) (**Figure 1**), X-ray of the spine, and nasal nitric oxide (nNO) levels results (**Supplementary Table S1**) were documented and reviewed.

Whole Exome Sequencing, Sanger Sequencing, and Bioinformatic Analysis

Blood samples from the patients and their family members were obtained with informed consent. Genomic DNA was extracted using the QIAamp DNA Blood MiniKit (250) (Qiagen, Valencia, CA) according to the manufacturer's instructions. Whole exome capture and high-throughput sequencing were performed as previously described. In brief, genomic DNA of the patient was captured using the Agilent SureSelect Human All Exon V6 Kit (Agilent, California, United States) and sequenced on Illumina Hiseq 4000 (Illumina Inc., San Diego, United States). Following quality control, the sequencing reads were aligned to the NCBI human reference genome (GRCh37/hg19) by the Burrows Wheeler Aligner. ANNOVAR was employed to annotate the variant call format file.

Single-nucleotide variants (SNVs) and short insertions and deletions (indels) were filtered as follows: 1) Retain rare variants (minor allele frequency <0.01) in 1,000 Genomes Project (1,000G), NHLBI-ESP project, Exome Aggregation Consortium (ExAC4), and in-house database of Novogene. 2) Noncoding and intronic variants were filtered. 3) Synonymous missense variants were excluded. 4) Bioinformatics analyses (SIFT, Polyphen-2, MutationTaster, MutationAssessor, and CADD) were used for the remaining variants. 5) A PCD or PCD-candidate gene list derived from literatures was used to identify the disease-associated variant, as described in our previous study (Lei et al., 2022).

Sanger sequencing was used to validate the variant in the individuals. Primers were designed using an online tool (PrimerQuest, IDT, https://sg.idtdna.com/PrimerQuest). The primer sequences were as follows: proband 1, forward 5′-GCCCATCCCTGAGTCAATTA -3′, reverse 5′-GAGACCTGC CTGTGCAATA-3'; proband 2, forward 5′-GTGACTTGTTTG CTACCATTGTT-3′, reverse 5′-AGTCGGTATTCTCTTATC ACTATTCTG-3′. PCR products were sequenced by the ABI PRISM 3730 DNA Analyzer using the BigDye Terminator v3.1 Cycle Sequencing Kit.

Evolutionary conservation analysis was performed by aligning the amino acid sequences of DNAAF4 proteins from different vertebrate species obtained from the GenBank database (https://www.ncbi.nlm.nih.gov/homologene/).

Transmission Electron Microscopy

To understand the abnormalities in the ultrastructure of the respiratory cilia, cilia were examined by means of electron microscopy. Samples of nasal mucosa (F2: II-1 and control) were fixed in 2.5% glutaraldehyde in 0.1 M sodium cacodylate buffer at 4°C, washed overnight, and postfixed in 1% osmium

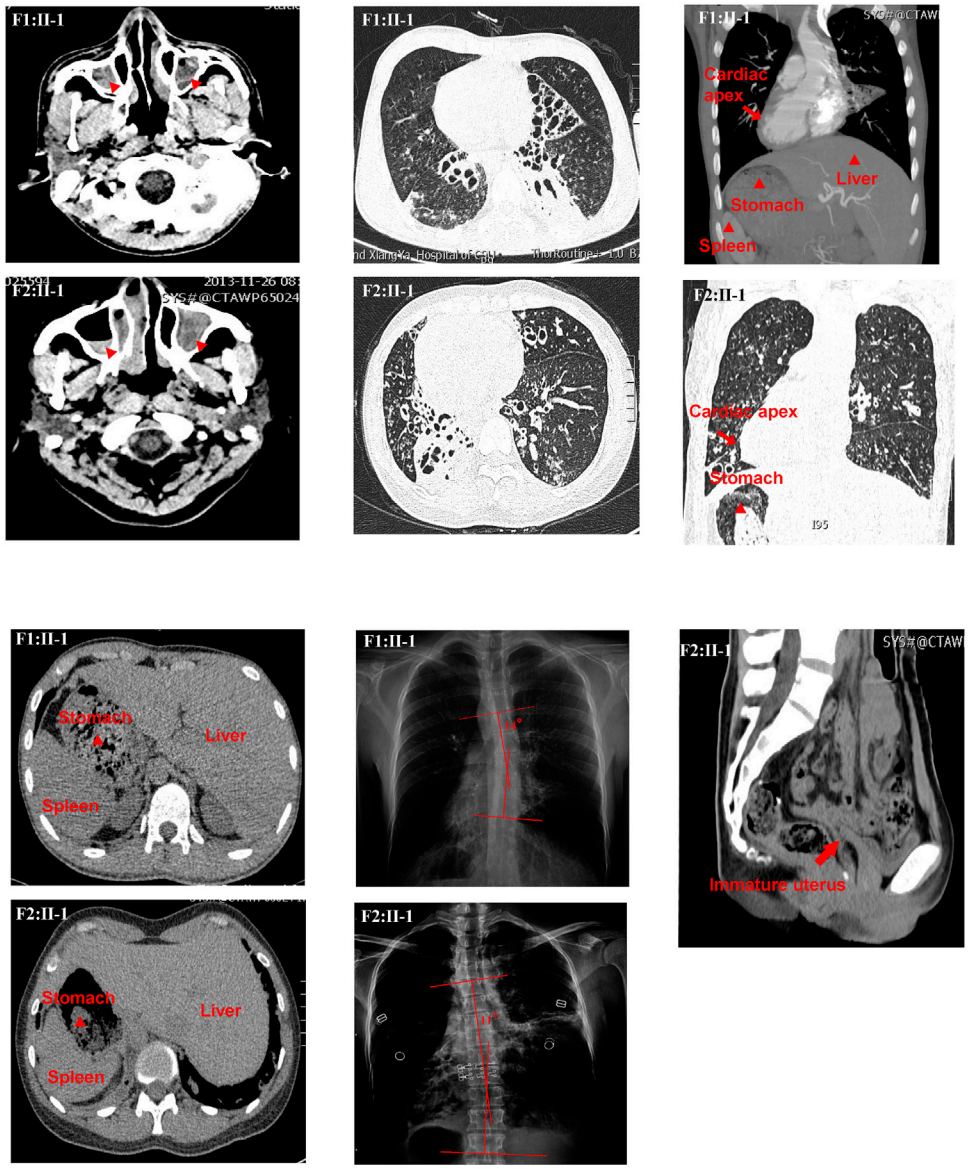

FIGURE 1 | Clinical features of the two patients. The chest high-resolution computed tomography (HRCT) scan of P1 (F1:II-1) showed bronchiectasis, rhinosinusitis, and situs inversus. Radiographic image of P1 (F1:II-1) showed scoliosis with a Cobb's angle of 14°. The HRCT scan of P2 (F2:II-1) showed bronchiectasis, rhinosinusitis, situs inversus, and immature uterus. Radiographic image of P2 (F2:II-1) showed scoliosis with a Cobb's angle of 11°.

tetroxide. Following dehydration, the samples were embedded in epoxy resin. Following polymerization, several sections were picked out onto copper grids. The sections were stained with aqueous 1% uranyl acetate and Reynold's lead citrate. An AHT7700 Hitachi electron microscope (Hitachi, Tokyo, Japan) and a MegaView Iii digital camera (Olympus Soft Imaging Solutions GmbH, Münster, Germany) were used to capture images.

Immunofluorescence Analysis

Nasal brushing biopsy samples (F1: II-1, F2: II-1, and control) and sperm specimens (F1: II-1 and control) were collected. For immunofluorescence analysis, the slides were incubated with primary antibodies (DNAH5, DNALI1, DNAI1, and anti-acetylated tubulin monoclonal antibody, respectively) for 2.5 h at 37°C. The slides were then incubated with secondary antibodies [Alexa Fluor® 488 antimouse IgG (A-21121) and Alexa Fluor® 555 anti-rabbit IgG (A31572)] for 1.5 h at 37°C. We used anti-acetylated tubulin monoclonal antibody (T7451, 1:500, Sigma-Aldrich, Missouri, United States) to mark the ciliary axonemal, DNAH5 (HPA037470, 1:25, Sigma-Aldrich, Missouri, United States) to label the outer dynein arm (ODA), DNALI1 (HPA028305, 1:25, Sigma-Aldrich, Missouri, United States) to label the inner dynein arm (IDA) of respiratory mucosa, DNAI1 (ab171964,1:25, Abcam, Cambridgeshire, United Kingdom) to outer dynein arm (ODA) of sperm, and DAPI to label the nuclei.

An upright Olympus BX53 microscope (Olympus, Tokyo, Japan) and cellSens Dimension software (Olympus, Tokyo, Japan) were utilized to photograph fluorescence signals.

High-Speed Video Microscopy Analysis

Nasal brush biopsy samples (F1: II-1, F2: II-1, and control) were suspended in Gibco Medium 199 (12350039 Gibco). Strips of ciliated epithelium were imaged using an upright Olympus BX53 microscope (Olympus, Tokyo, Japan) with a 40x objective lens. Videos were recorded using a scientific complementary metal oxide semiconductor camera (Prime BSI, Teledyne Photometrics Inc., United States) at a rate of 500 frames per second (fps) at room temperature. Intact ciliated edge >50 μm was used for functional analysis only.

RESULTS

Clinical Summary

Proband 1 (P1, F1: II-1), a 19-year-old man, comes from a nonconsanguineous family-1. He had typical PCD symptoms, such as chronic cough and sputum production, dyspnea, hemoptysis, sinusitis, etc. In addition, he complained of abnormalities in his sense of smell and hearing. However, his fertility was unknown because he was not married. He denied any history of asthma, tuberculosis, measles pneumonia, or drowning. No relevant family history was reported. High-resolution CT (HRCT) showed sinusitis, bronchiectasis, and situs inversus. Upright radiograph revealed scoliosis with a Cobb's angle of 14° (**Figure 1**). Furthermore, the semen routine test showed that the percentage of motile sperm was 0. Proband 2 (P2, F2: II-1), a 37-year-old woman, comes from a consanguineous family-2. She had chronic cough and sputum, dyspnea, and sinusitis. She also had abnormalities in the sense of smell and hearing. In addition, she suffered from infertility. HRCT findings were similar to P1, and upright radiograph revealed scoliosis with a Cobb's angle of 11° (**Figure1**). The HRCT also indicated an immature uterus. Her forced expiratory volume in 1 second (FEV1)%prediction, forced vital capacity (FVC)%prediction, FEV1/FVC, and nasal NO were 36%, 50%, 60%, and 8.4 nL/min, respectively (**Supplementary Tables S1–S3**; **Figure1**).

Whole Exome Sequencing Identified the *DNAAF4* Variants

We used the patient's peripheral blood to extract DNA for Whole exome sequencing (WES). After WES, 12.02 and 6.8 GB data were used for subsequent analysis. The percentages of bases with a coverage depth of more than 10× were 99.6% and 98.1%, respectively. Two variants, *DNAAF4* (NM_130810.4): c.988C > T (p.Arg330Trp) in P1 and a novel variant *DNAAF4* (NM_130810.4): c.733C > T (p.Arg245Ter) in P2, were identified. We classified the pathogenicity of the two variants according to ACMG (Richards et al., 2015). The results showed the variant in P1 was consistent with PM2+PM3+PP3+PP5 (likely pathogenic), and the variant in P2 met the criteria PVS1+PM2+PP5 (pathogenic). These two disease-causing variants were validated by Sanger sequencing (**Supplementary Table S2**; **Figure2**).

Experimental Validation of the Pathogenicity of Variants

High-speed microscopy showed complete static of sperm flagella and a few residual beating of respiratory cilia in P1 and complete static of the respiratory cilia in P2 compared with normal control (**Supplementary Videos S1–S3**). Immunofluorescence showed the deficiency of DNAH5 and DNALI1, which labelled ODA and IDA, respectively, in the respiratory cilia of both probands. In addition, the DNALI1 and DNAI1 which respectively labelled the ODA and IDA in the sperm flagellum of P1 were also absent. TEM revealed the absence of ODA and IDA of P2 respiratory cilia. HE staining showed irregular flagella, short, absent, coiled, and bent, indicating asthenoteratozoospermia (**Figure3**).

DISCUSSION

In this study, whole exome sequencing and Sanger sequencing were used to identify and confirm homozygous variants in *DNAAF4*. The pathogenicity of the variants was validated by high-speed microscopy, immunofluorescence, HE staining, and TEM. Both patients were infertile, one of whom was diagnosed with asthenoteratozoospermia. In addition, the upright radiograph suggested scoliosis in both cases.

PCD is a genetic disorder caused by motile cilia dysfunction (Lucas et al., 2020). Motile cilia are hair-like structures. The ultrastructure of most motile cilia shows that they are composed of nine peripheral duplex microtubules, two central single microtubules and corresponding spokes (9 + 2 structure) (Fliegauf et al., 2007). Flagella have a similar structure. In addition, there are many multisubunit motor protein complexes within the cilia and flagella, such as outer dynein arms (ODA) and inner dynein arms (IDA) that attach to the peripheral microtubules. They are essential for the generation, and the regulation of cilia and flagella beating (Fliegauf et al., 2007; Aprea et al., 2021).

DNAAF4 is located on Chromosome 15 with 10 exons encoding a 420 aa protein. It is associated with the preassembly of axonemal arms and is involved in the integration and stabilization of the intermediate chain, which is an integral component of both the ODA and IDA (Tarkar et al., 2013; Aprea et al., 2021). Here, we have reviewed the literature and summarized the 15 PCD-associated variants in *DNAAF4* (**Figure 2E**; **Supplementary Table S4**) (Tarkar et al., 2013; Marshall et al., 2015; Guo et al., 2017; Ceyhan-Birsoy et al., 2019; Olm et al., 2019; Blanchon et al., 2020; Aprea et al., 2021). Most studies focused on the respiratory phenotype of patients, and a small number of studies reported situs inversus. Moreover, few DNAAF4-related studies reported the details of the sperm phenotype (Tarkar et al., 2013; Guo et al., 2017; Aprea et al., 2021). Both our patients with *DNAAF4* variants had situs inversus, and the male patient had asthenoteratozoospermia. In these two cases, two homozygous *DNAAF4* variants were

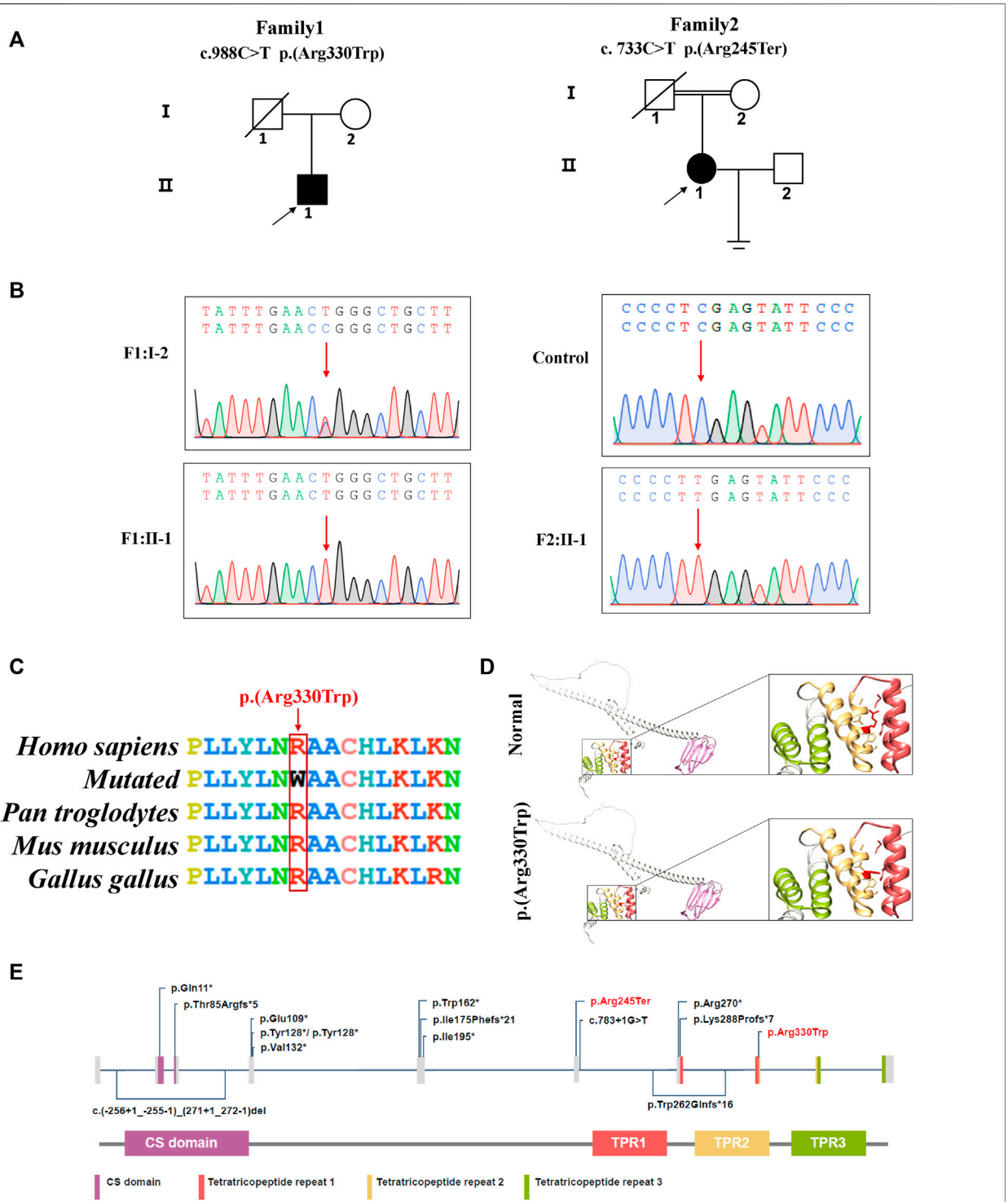

FIGURE 2 | *DNAAF4* variants were identified in two patients with PCD. **(A)** pedigree analysis of the two patients from two Han Chinese families, where family 2 is a consanguineous family. Circles indicate women. Squares indicate men. Solid symbols indicate patients. Crossed-out symbols mean that subjects had passed away. The arrows indicate the probands. **(B)** the two variants were validated by Sanger sequencing. Red arrows indicate the variant sites; **(C)** conservative analysis of the missense variant **(C)** 988C > T (p.Arg330Trp). Red box indicates mutant amino acid sites. **(D)** 3D mock structure of DNAAF4. The purple region is the CS domain, while green, yellow, and brick red indicate the three tetratricopeptide repeats, respectively. The variant p.(Arg330Trp) is indicated by red color. **(E)** DNAAF4 protein structure and the reported disease-causing variants of DNAAF4. Variants reported in this study are highlighted in red.

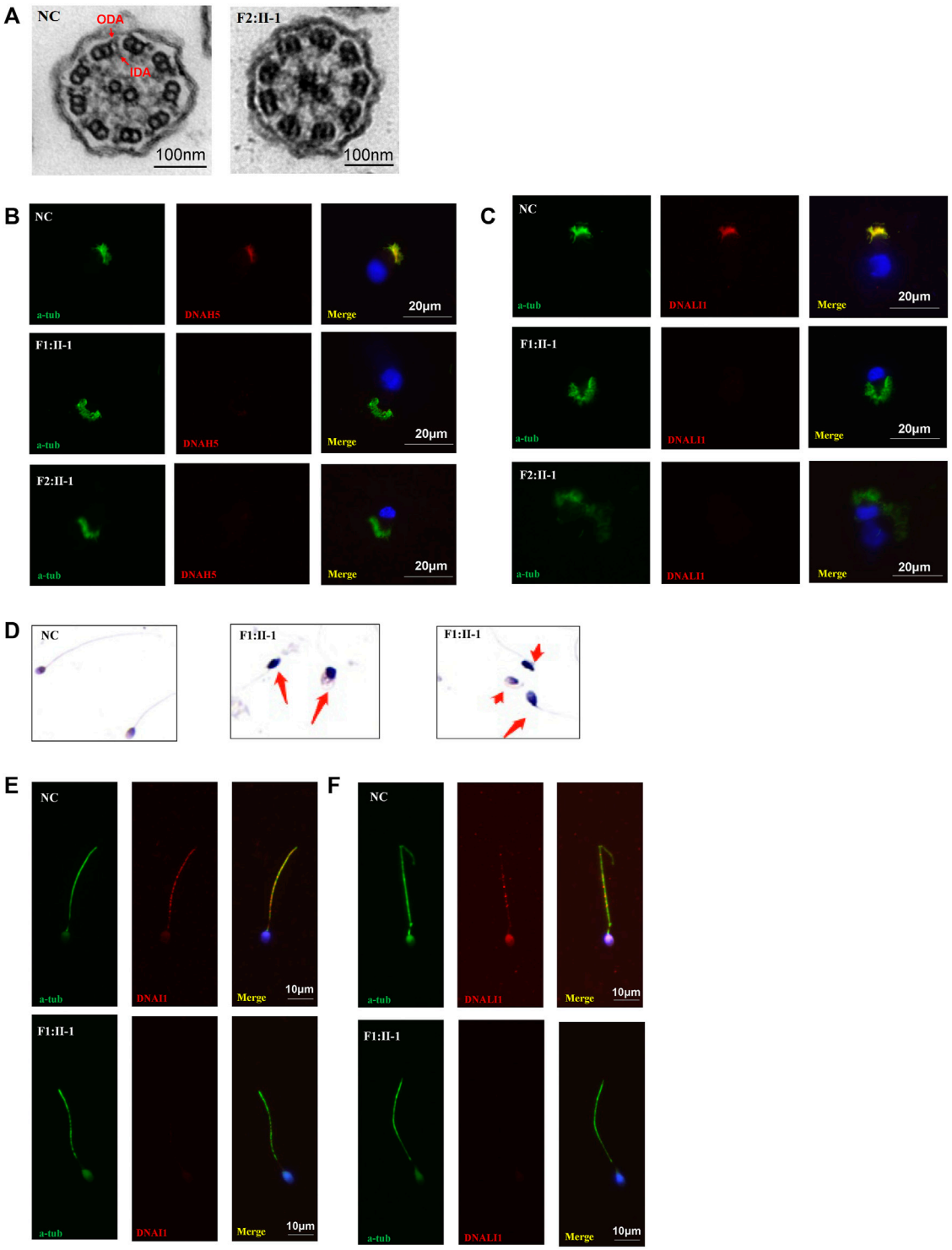

FIGURE 3 | TEM, HE staining, and immunofluorescence analysis of the nasal ciliated cells and sperm. **(A)** TEM analysis indicated loss of IDAs and ODAs of P2 (F1: II-1) compared with the normal control. Scale bars, 100 nm; **(B,C)** immunofluorescence of nasal ciliated cells revealed the absence of DNAH5 and DNALI1 (red) of the two patients compared with normal control. Anti-acetylated tubulin monoclonal antibody was used to mark the ciliary axoneme. DNAH5 was used to label the outer dynein arm (ODA), DNALI1 was used to label the inner dynein arm (IDA), and DAPI was used to label the nuclei. Scale bars, 20 μm; **(D)** HE staining of sperm. Compared to normal controls, the patient's sperm had significant short, coiled, and irregular tails. **(E)** immunofluorescence analysis showed the absence of DNALI1 and DNAI1 (red) in the mutant sperm from P1 (F1: II-1) compared with the normal control. Scale bars, 10 μm.

reported in this study, and the pathogenicity of the variants was validated by high-speed microscopy, immunofluorescence, HE staining, and TEM. *DNAAF4* c.988C > T leads to immotility of most respiratory cilia and complete static of sperm flagella. HE staining indicated typical teratozoospermic. Although this variant has been reported before, only electron microscopic findings of respiratory cilia have been described. No observations were made on sperm phenotype. Furthermore, previously reported patient did not have situs inversus (Marshall et al., 2015). *DNAAF4* c.733 C > T results in completely respiratory cilia static. In both cases, the respiratory cilia showed the absence of ODA and IDA. Furthermore, in the male patient, both ODA and IDA of the sperm flagellum were absent.

Although asthenoteratozoospermia has been proposed for a long time, it is only recently that the research has focused on the contribution of abnormal sperm ultrastructure to pathogenesis (Sandler, 1952). Abnormalities in the development of the axoneme and its accessory structures are thought to be the main cause of asthenoteratozoospermia (Jiao et al., 2021). Asthenoteratozoospermia was previously described separately as asthenozoospermia and teratozoospermia. When the percentage of motile sperm in the semen is <40%, it is called asthenozoospermia. Teratozoospermia means that the spermatozoa of patients with deformed spermatozoa including defects in the head, midpiece, and/or tail (tend to be short, coiled, absent, or irregular flagella) (Ben Khelifa et al., 2014). Teratozoospermia is currently diagnosed by light microscopic staining or scanning electron microscopy of sperm morphology and asthenozoospermia by high-speed microscope (WHO, 2021). They can severely reduce male fertility, but have received less attention in previous PCD studies (Dávila Garza and Patrizio, 2013; Sironen et al., 2020). Although >50 PCD-associated pathogenic genes have been reported, a few have been reported to be associated with asthenoteratozoospermia, such as *DNAH9*, *DNAH1*, *ARMC4*, *BRWD1*, *CCDC39*, *CCDC40*, *DRC1*, *CFAP74*, and *SPEF2* (Neesen et al., 2001; Sha et al., 2020; Tu et al., 2020; Chen et al., 2021; Gao et al., 2021; Guo et al., 2021; Lei et al., 2022; Xu et al., 2022). In most other cases, researchers have not analyzed the semen of male patients. Despite advances in male infertility testing, in 40% of patients, it was not possible to identify the cause. Given that the sperm flagellum has a similar structure to the respiratory cilia, semen analysis in men with PCD can help identify the cause of male infertility and thus provide a reference for assisted reproduction (Krausz and Riera-Escamilla, 2018).

In addition, both patients had the classic PCD phenotype as well as the more commonly overlooked scoliosis. Although scoliosis is currently reported less commonly in patients with PCD, this phenotype is more frequently observed in model organisms carrying the causative gene for PCD, including *CCDC40*, *DNAAF4*, *ODAD3*, and *ZMYND10* (Grimes et al., 2016; Kobayashi et al., 2017; Lu et al., 2021). A previous study evaluated chest radiographs in 198 patients with PCD and found a Cobb angle >10° in 8% of patients, but that study did not perform genetic analysis (Schlösser et al., 2017). The etiology of idiopathic scoliosis is not well understood, and different hypotheses have been proposed (Aebi, 2005; Cheng et al., 2015; Oliazadeh et al., 2017). Of these, abnormal cilia function has been suggested as a possible cause. Researchers believed that "sensory organs," including motor cilia, neurons in contact with the cerebrospinal fluid, Reissner fibers, and Urotensin neuropeptide signals, were essential for the proper development of the perceptual axis (Bearce and Grimes, 2021). An alternative hypothesis is that scoliosis in patients with PCD is because of situs inversus (Schlösser et al., 2017). However, scoliosis is often overlooked in patients with PCD as anteroposterior and lateral radiographs of the spine are not a routine examination. Although there are few reports linking scoliosis to PCD, some genes have been reported to be associated with abnormal cilia beating and scoliosis in previous research (Fei et al., 2010; Makrythanasis et al., 2014; Baschal et al., 2015; Zhou et al., 2015; Lu et al., 2021; Nita et al., 2021). As an increasing number of PCD model organisms are observed with scoliosis, the spinal examination of the patient needs to be taken seriously.

It should be noted that the female patient reported here also had an infantile uterus. Therefore, the effect of the variant on female fertility caused by dysfunctional cilia in fallopian tubes cannot be determined. Furthermore, as scoliosis is currently less commonly reported in PCD-related human genetic studies, the effect of *DNAAF4* variants on the human spine needs further validation (Muñoz-Montecinos et al., 2021).

Overall, we identified two homozygous variants in the PCD-associated gene *DNAAF4*, c.988C > T and c.733 C > T, which expand the genetic spectrum of PCD. In particular, we provide additional references for asthenoteratozoospermia and scoliosis in patients with PCD, which has previously received less attention.

DATA AVAILABILITY STATEMENT

The datasets for this article are not publicly available due to concerns regarding participant/patient anonymity. Requests to access the datasets should be directed to the corresponding author.

ETHICS STATEMENT

The studies involving human participants were reviewed and approved by the Review Board of the Second Xiangya Hospital of Central South University in China. Written informed consent was obtained from the individual(s), and minor(s)' legal guardian/next of kin, for the publication of any potentially identifiable images or data included in this article.

AUTHOR CONTRIBUTIONS

All the authors meet the authorship criteria. The following are the main aspects implemented by each author. TG: data collection, data analysis, basic experiment, writing paper; CYL: data

collection, data analysis, basic experiment, writing paper; DY and CL: designed the experiments, data collection, data analysis; YL, YX, and BY: basic experiment; RW and HL conceived and designed the experiments.

FUNDING

This study was supported by the National Natural Science Foundation of China (81900002 to TG, 82070003 to HL), Natural Science Foundation of Hunan Province, China (2020JJ5805 to TG, 2021JJ30943 to HL), the Hunan Province Health Commission Scientific Research Project (B2019159 to HL), the Science and Technology Program of Changsha, China (kq1901120 to HL), the Fundamental Research Funds for the Central Universities of Central South University (2022ZZTS0859 to CYL), Xiangya Medical Big Data of Central South University (Pulmonary Inflammatory Disease), and the National Key Clinical Specialty Construction Projects of China [(2012) No. 650].

ACKNOWLEDGMENTS

We thank the patients and their families who participated in this study.

SUPPLEMENTARY MATERIAL

The Supplementary Material for this article can be found online at: https://www.frontiersin.org/articles/10.3389/fgene.2022.934920/full#supplementary-material

REFERENCES

Aebi, M. (2005). The Adult Scoliosis. *Eur. Spine J.* 14, 925–948. doi:10.1007/s00586-005-1053-9

Aprea, I., Raidt, J., Höben, I. M., Loges, N. T., Nöthe-Menchen, T., Pennekamp, P., et al. (2021). Defects in the Cytoplasmic Assembly of Axonemal Dynein Arms Cause Morphological Abnormalities and Dysmotility in Sperm Cells Leading to Male Infertility. *PLoS Genet.* 17, e1009306. doi:10.1371/journal.pgen.1009306

Baschal, E. E., Swindle, K., Justice, C. M., Baschal, R. M., Perera, A., Wethey, C. I., et al. (2015). Sequencing of the TBX6 Gene in Families with Familial Idiopathic Scoliosis. *Spine Deform.* 3, 288–296. doi:10.1016/j.jspd.2015.01.005

Bearce, E. A., and Grimes, D. T. (2021). On Being the Right Shape: Roles for Motile Cilia and Cerebrospinal Fluid Flow in Body and Spine Morphology. *Seminars Cell Dev. Biol.* 110, 104–112. doi:10.1016/j.semcdb.2020.07.005

Ben Khelifa, M., Coutton, C., Zouari, R., Karaouzène, T., Rendu, J., Bidart, M., et al. (2014). Mutations in DNAH1, Which Encodes an Inner Arm Heavy Chain Dynein, Lead to Male Infertility from Multiple Morphological Abnormalities of the Sperm Flagella. *Am. J. Hum. Genet.* 94, 95–104. doi:10.1016/j.ajhg.2013.11.017

Blanchon, S., Legendre, M., Bottier, M., Tamalet, A., Montantin, G., Collot, N., et al. (2020). Deep Phenotyping, Including Quantitative Ciliary Beating Parameters, and Extensive Genotyping in Primary Ciliary Dyskinesia. *J. Med. Genet.* 57, 237–244. doi:10.1136/jmedgenet-2019-106424

Ceyhan-Birsoy, O., Murry, J. B., Machini, K., Lebo, M. S., Yu, T. W., Fayer, S., et al. (2019). Interpretation of Genomic Sequencing Results in Healthy and Ill Newborns: Results from the BabySeq Project. *Am. J. Hum. Genet.* 104, 76–93. doi:10.1016/j.ajhg.2018.11.016

Chen, D., Liang, Y., Li, J., Zhang, X., Zheng, R., Wang, X., et al. (2021). A Novel CCDC39 Mutation Causes Multiple Morphological Abnormalities of the Flagella in a Primary Ciliary Dyskinesia Patient. *Reprod. Biomed. Online* 43, 920–930. doi:10.1016/j.rbmo.2021.07.005

Cheng, J. C., Castelein, R. M., Chu, W. C., Danielsson, A. J., Dobbs, M. B., Grivas, T. B., et al. (2015). Adolescent Idiopathic Scoliosis. *Nat. Rev. Dis. Prim.* 1, 15030. doi:10.1038/nrdp.2015.30

Coutton, C., Escoffier, J., Martinez, G., Arnoult, C., and Ray, P. F. (2015). Teratozoospermia: Spotlight on the Main Genetic Actors in the Human. *Hum. Reprod. Update* 21, 455–485. doi:10.1093/humupd/dmv020

Dávila Garza, S. A., and Patrizio, P. (2013). Reproductive Outcomes in Patients with Male Infertility Because of Klinefelter's Syndrome, Kartagener's Syndrome, Round-Head Sperm, Dysplasia Fibrous Sheath, and 'stump' Tail Sperm. *Curr. Opin. Obstet. Gynecol.* 25, 229–246. doi:10.1097/gco.0b013e32835faae5

Fei, Q., Wu, Z., Wang, H., Zhou, X., Wang, N., Ding, Y., et al. (2010). The Association Analysis of TBX6 Polymorphism with Susceptibility to Congenital Scoliosis in a Chinese Han Population. *Spine* 35, 983–988. doi:10.1097/brs.0b013e3181bc963c

Fliegauf, M., Benzing, T., and Omran, H. (2007). When Cilia Go Bad: Cilia Defects and Ciliopathies. *Nat. Rev. Mol. Cell Biol.* 8, 880–893. doi:10.1038/nrm2278

Gao, C., Chen, B. P., Sullivan, M. B., Hui, J., Ouellet, J. A., Henderson, J. E., et al. (2015). Micro CT Analysis of Spine Architecture in a Mouse Model of Scoliosis. *Front. Endocrinol.* 6, 38. doi:10.3389/fendo.2015.00038

Gao, Y., Xu, C., Tan, Q., Shen, Q., Wu, H., Lv, M., et al. (2021). Case Report: Novel Biallelic Mutations in ARMC4 Cause Primary Ciliary Dyskinesia and Male Infertility in a Chinese Family. *Front. Genet.* 12, 715339. doi:10.3389/fgene.2021.715339

Grimes, D. T., Boswell, C. W., Morante, N. F. C., Henkelman, R. M., Burdine, R. D., and Ciruna, B. (2016). Zebrafish Models of Idiopathic Scoliosis Link Cerebrospinal Fluid Flow Defects to Spine Curvature. *Science* 352, 1341–1344. doi:10.1126/science.aaf6419

Guo, T., Tan, Z.-P., Chen, H.-M., Zheng, D.-y., Liu, L., Huang, X.-G., et al. (2017). An Effective Combination of Whole-Exome Sequencing and Runs of Homozygosity for the Diagnosis of Primary Ciliary Dyskinesia in Consanguineous Families. *Sci. Rep.* 7, 7905. doi:10.1038/s41598-017-08510-z

Guo, T., Tu, C.-F., Yang, D.-H., Ding, S.-Z., Lei, C., Wang, R.-C., et al. (2021). Biallelic BRWD1 Variants Cause Male Infertility with Asthenoteratozoospermia and Likely Primary Ciliary Dyskinesia. *Hum. Genet.* 140, 761–773. doi:10.1007/s00439-020-02241-4

Jiao, S.-Y., Yang, Y.-H., and Chen, S.-R. (2021). Molecular Genetics of Infertility: Loss-Of-Function Mutations in Humans and Corresponding Knockout/mutated Mice. *Hum. Reprod. Update* 27, 154–189. doi:10.1093/humupd/dmaa034

Knowles, M. R., Zariwala, M., and Leigh, M. (2016). Primary Ciliary Dyskinesia. *Clin. Chest Med.* 37, 449–461. doi:10.1016/j.ccm.2016.04.008

Kobayashi, D., Asano-Hoshino, A., Nakakura, T., Nishimaki, T., Ansai, S., Kinoshita, M., et al. (2017). Loss of Zinc Finger MYND-type Containing 10 (Zmynd10) Affects Cilia Integrity and Axonemal Localization of Dynein Arms, Resulting in Ciliary Dysmotility, Polycystic Kidney and Scoliosis in Medaka (*Oryzias latipes*). *Dev. Biol.* 430, 69–79. doi:10.1016/j.ydbio.2017.08.016

Krausz, C., and Riera-Escamilla, A. (2018). Genetics of Male Infertility. *Nat. Rev. Urol.* 15, 369–384. doi:10.1038/s41585-018-0003-3

Lei, C., Yang, D., Wang, R., Ding, S., Wang, L., Guo, T., et al. (2022). DRC1 Deficiency Caused Primary Ciliary Dyskinesia and MMAF in a Chinese Patient. *J. Hum. Genet.* 67, 197–201. doi:10.1038/s10038-021-00985-z

Lu, C., Yang, D., Lei, C., Wang, R., Guo, T., and Luo, H. (2021). Identification of Two Novel DNAAF2 Variants in Two Consanguineous Families with Primary Ciliary Dyskinesia. *Pharmgenomics Pers. Med.* 14, 1415–1423. doi:10.2147/pgpm.s338981

Lucas, J. S., Davis, S. D., Omran, H., and Shoemark, A. (2020). Primary Ciliary Dyskinesia in the Genomics Age. *Lancet Respir. Med.* 8, 202–216. doi:10.1016/s2213-2600(19)30374-1

Makrythanasis, P., Temtamy, S., Aglan, M. S., Otaify, G. A., Hamamy, H., and Antonarakis, S. E. (2014). A Novel Homozygous Mutation in FGFR3 Causes Tall Stature, Severe Lateral Tibial Deviation, Scoliosis, Hearing Impairment, Camptodactyly, and Arachnodactyly. *Hum. Mutat.* 35, 959–963. doi:10.1002/humu.22597

Marshall, C. R., Scherer, S. W., Zariwala, M. A., Lau, L., Paton, T. A., Stockley, T., et al. (2015). Whole-Exome Sequencing and Targeted Copy Number Analysis in Primary Ciliary Dyskinesia. *G3 (Bethesda)* 5, 1775–1781. doi:10.1534/g3.115.019851

Mirra, V., Werner, C., and Santamaria, F. (2017). Primary Ciliary Dyskinesia: An Update on Clinical Aspects, Genetics, Diagnosis, and Future Treatment Strategies. *Front. Pediatr.* 5, 135. doi:10.3389/fped.2017.00135

Muñoz-Montecinos, C., Romero, A., Sepúlveda, V., Vira, M., Fehrmann-Cartes, K., Marcellini, S., et al. (2021). Turning the Curve into Straight: Phenogenetics of the Spine Morphology and Coordinate Maintenance in the Zebrafish. *Front. Cell Dev. Biol.* 9, 801652. doi:10.3389/fcell.2021.801652

Neesen, J., Kirschner, R., Ochs, M., Schmiedl, A., Habermann, B., Mueller, C., et al. (2001). Disruption of an Inner Arm Dynein Heavy Chain Gene Results in Asthenozoospermia and Reduced Ciliary Beat Frequency. *Hum. Mol. Genet.* 10, 1117–1128. doi:10.1093/hmg/10.11.1117

Nita, A., Abraham, S. P., Krejci, P., and Bosakova, M. (2021). Oncogenic FGFR Fusions Produce Centrosome and Cilia Defects by Ectopic Signaling. *Cells* 10, 1445. doi:10.3390/cells10061445

Oliazadeh, N., Gorman, K. F., Eveleigh, R., Bourque, G., and Moreau, A. (2017). Identification of Elongated Primary Cilia with Impaired Mechanotransduction in Idiopathic Scoliosis Patients. *Sci. Rep.* 7, 44260. doi:10.1038/srep44260

Olm, M. A. K., Marson, F. A. L., Athanazio, R. A., Nakagawa, N. K., Macchione, M., Loges, N. T., et al. (2019). Severe Pulmonary Disease in an Adult Primary Ciliary Dyskinesia Population in Brazil. *Sci. Rep.* 9, 8693. doi:10.1038/s41598-019-45017-1

Richards, S., Aziz, N., Bale, S., Bick, D., Das, S., Gastier-Foster, J., et al. (2015). Standards and Guidelines for the Interpretation of Sequence Variants: A Joint Consensus Recommendation of the American College of Medical Genetics and Genomics and the Association for Molecular Pathology. *Genet. Med.* 17, 405–424. doi:10.1038/gim.2015.30

Sandler, B. (1952). The Relation of Cervical Mucus and Asthenospermia in Sterility. *J. Obstet. Gynaecol. Br. Emp.* 59, 202–207. doi:10.1111/j.1471-0528.1952.tb04115.x

Schlösser, T. P. C., Semple, T., Carr, S. B., Padley, S., Loebinger, M. R., Hogg, C., et al. (2017). Scoliosis Convexity and Organ Anatomy Are Related. *Eur. Spine J.* 26, 1595–1599. doi:10.1007/s00586-017-4970-5

Sha, Y., Wei, X., Ding, L., Ji, Z., Mei, L., Huang, X., et al. (2020). Biallelic Mutations of CFAP74 May Cause Human Primary Ciliary Dyskinesia and MMAF Phenotype. *J. Hum. Genet.* 65, 961–969. doi:10.1038/s10038-020-0790-2

Shapiro, A. J., Zariwala, M. A., Ferkol, T., Davis, S. D., Sagel, S. D., Dell, S. D., et al. (2016). Diagnosis, Monitoring, and Treatment of Primary Ciliary Dyskinesia: PCD Foundation Consensus Recommendations Based on State of the Art Review. *Pediatr. Pulmonol.* 51, 115–132. doi:10.1002/ppul.23304

Sironen, A., Shoemark, A., Patel, M., Loebinger, M. R., and Mitchison, H. M. (2020). Sperm Defects in Primary Ciliary Dyskinesia and Related Causes of Male Infertility. *Cell. Mol. Life Sci.* 77, 2029–2048. doi:10.1007/s00018-019-03389-7

Taipale, M., Kaminen, N., Nopola-Hemmi, J., Haltia, T., Myllyluoma, B., Lyytinen, H., et al. (2003). A Candidate Gene for Developmental Dyslexia Encodes a Nuclear Tetratricopeptide Repeat Domain Protein Dynamically Regulated in Brain. *Proc. Natl. Acad. Sci. U.S.A.* 100, 11553–11558. doi:10.1073/pnas.1833911100

Tapia-Páez, I., Tammimies, K., Massinen, S., Roy, A. L., and Kere, J. (2008). The Complex of TFII-I, PARP1, and SFPQ Proteins Regulates the DYX1C1 Gene Implicated in Neuronal Migration and Dyslexia. *FASEB J.* 22, 3001–3009. doi:10.1096/fj.07-104455

Tarkar, A., Loges, N. T., Loges, N. T., Slagle, C. E., Francis, R., Dougherty, G. W., et al. (2013). DYX1C1 is Required for Axonemal Dynein Assembly and Ciliary Motility. *Nat. Genet.* 45, 995–1003. doi:10.1038/ng.2707

Tu, C., Nie, H., Meng, L., Wang, W., Li, H., Yuan, S., et al. (2020). Novel Mutations in SPEF2 Causing Different Defects between Flagella and Cilia Bridge: The Phenotypic Link between MMAF and PCD. *Hum. Genet.* 139, 257–271. doi:10.1007/s00439-020-02110-0

WHO (2021). *WHO Laboratory Manual for the Examination and Processing of Human Semen*. sixth edition. Geneva: World Health Organization.

Xu, Y., Yang, B., Lei, C., Yang, D.-h., Ding, S., Lu, C., et al. (2022). Novel Compound Heterozygous Variants in CCDC40 Associated with Primary Ciliary Dyskinesia and Multiple Morphological Abnormalities of the Sperm Flagella. *Pharmgenomics Pers. Med.* 15, 341–350. doi:10.2147/pgpm.s359821

Zhou, S., Xie, Y., Tang, J., Huang, J., Huang, Q., Xu, W., et al. (2015). FGFR3 Deficiency Causes Multiple Chondroma-like Lesions by Upregulating Hedgehog Signaling. *PLoS Genet.* 11, e1005214. doi:10.1371/journal.pgen.1005214

Conflict of Interest: The authors declare that the research was conducted in the absence of any commercial or financial relationships that could be construed as a potential conflict of interest.

Publisher's Note: All claims expressed in this article are solely those of the authors and do not necessarily represent those of their affiliated organizations, or those of the publisher, the editors and the reviewers. Any product that may be evaluated in this article, or claim that may be made by its manufacturer, is not guaranteed or endorsed by the publisher.

frontiers | Frontiers in Genetics

ORIGINAL RESEARCH
published: 08 August 2022
doi: 10.3389/fgene.2022.933381

Functional Evaluation and Genetic Landscape of Children and Young Adults Referred for Assessment of Bronchiectasis

Jeffrey Fong Ting Chau[1], Mianne Lee[1], Martin Man Chun Chui[1], Mullin Ho Chung Yu[1], Jasmine Lee Fong Fung[1], Christopher Chun Yu Mak[1], Christy Shuk-Kuen Chau[2], Ka Ka Siu[2], Jacqueline Hung[2], Kit San Yeung[1], Anna Ka Yee Kwong[1], Christopher O'Callaghan[3], Yu Lung Lau[1,2], Chun-Wai Davy Lee[1,4], Brian Hon-Yin Chung[1,2,4] and So-Lun Lee[2]**

[1]Department of Paediatrics and Adolescent Medicine, School of Clinical Medicine, LKS Faculty of Medicine, The University of Hong Kong, Pok Fu Lam, Hong Kong SAR, China, [2]Department of Paediatrics and Adolescent Medicine, Queen Mary Hospital, Pok Fu Lam, Hong Kong SAR, China, [3]UCL Great Ormond Street Institute of Child Health, UCL and GOSH NIHR BRC, London, United Kingdom, [4]Department of Paediatrics and Adolescent Medicine, Duchess of Kent Children's Hospital, Pok Fu Lam, Hong Kong SAR, China

OPEN ACCESS

Edited by:
Stephen J Bush,
University of Oxford, United Kingdom

Reviewed by:
Amjad Horani,
Washington University in St. Louis, United States
Yaping Liu,
Chinese Academy of Medical Sciences, China

***Correspondence:**
Brian Hon-Yin Chung
bhychung@hku.hk
So-Lun Lee
slleem@hku.hk

Specialty section:
This article was submitted to Human and Medical Genomics, a section of the journal Frontiers in Genetics

Received: 30 April 2022
Accepted: 23 June 2022
Published: 08 August 2022

Citation:
Chau JFT, Lee M, Chui MMC, Yu MHC, Fung JLF, Mak CCY, Chau CS-K, Siu KK, Hung J, Yeung KS, Kwong AKY, O'Callaghan C, Lau YL, Lee C-WD, Chung BH-Y and Lee S-L (2022) Functional Evaluation and Genetic Landscape of Children and Young Adults Referred for Assessment of Bronchiectasis. Front. Genet. 13:933381. doi: 10.3389/fgene.2022.933381

Bronchiectasis is the abnormal dilation of the airway which may be caused by various etiologies in children. Beyond the more recognized cause of bacterial and viral infections and primary immunodeficiencies, other genetic conditions such as cystic fibrosis and primary ciliary dyskinesia (PCD) can also contribute to the disease. Currently, there is still debate on whether genome sequencing (GS) or exome sequencing reanalysis (rES) would be beneficial if the initial targeted testing results returned negative. This study aims to provide a back-to-back comparison between rES and GS to explore the best integrated approach for the functional and genetics evaluation for patients referred for assessment of bronchiectasis. In phase 1, an initial 60 patients were analyzed by exome sequencing (ES) with one additional individual recruited later as an affected sibling for ES. Functional evaluation of the nasal nitric oxide test, transmission electron microscopy, and high-speed video microscopy were also conducted when possible. In phase 2, GS was performed on 30 selected cases with trio samples available. To provide a back-to-back comparison, two teams of genome analysts were alternatively allocated to GS or rES and were blinded to each other's analysis. The time for bioinformatics, analysis, and diagnostic utility was recorded for evaluation. ES revealed five positive diagnoses (5/60, 8.3%) in phase 1, and four additional diagnoses were made by rES and GS (4/30, 13%) during phase 2. Subsequently, one additional positive diagnosis was identified in a sibling by ES and an overall diagnostic yield of 10/61 (16.4%) was reached. Among those patients with a clinical suspicion of PCD (n = 31/61), the diagnostic yield was 26% (*n* = 8/31). While GS did not increase the diagnostic yield, we showed that a variant of uncertain significance could only be detected by GS due to improved coverage over ES and hence is a potential benefit for GS in the future. We show that genetic testing is an essential component for the diagnosis of early-onset bronchiectasis and is most effective when used in combination with functional tools such as TEM or HSVM.

Our comparison of rES vs. GS suggests that rES and GS are comparable in clinical diagnosis.

Keywords: exome sequencing, genome sequencing, early-onset bronchiectasis, transmission electron microscopy, high-speed video microscopy, primary ciliary dyskinesia

INTRODUCTION

Bronchiectasis is the abnormal dilation of the airway causing clinical symptoms such as persistent or recurrent bronchial infection, inflamed airways, and airway obstruction. It is responsible for the significant loss of lung function, significant morbidity, and early mortality if not treated correctly (Metersky et al., 2022). Bronchiectasis is a common phenotype for various diseases and has the potential to be the starting point for functional and genetic investigation for the underlying pathological diseases. Beyond bacterial and viral infections or primary immunodeficiencies, bronchiectasis could also be caused by genetic conditions such as cystic fibrosis (CF) and primary ciliary dyskinesia (PCD). CF is an inherited disorder that causes sticky mucus to build up in the respiratory airway and digestive system caused by mutations in the *CFTR* gene (Southern et al., 2007), and PCD is a rare genetic condition characterized by ciliary defects, causing ineffective ciliary movement that causes impaired mucociliary clearance. The prevalence of PCD is currently estimated to be approximately 1 in 10,000 to 1 in 15,000 in European ethnicity with an increased prevalence of approximately 1 in 2,200 births for a highly consanguineous population (Afzelius and Stenram, 2006; O'Callaghan et al., 2010). Persistent symptoms typically arise during early infancy for PCD, but it is often diagnosed in late childhood or adulthood (Kuehni et al., 2010). A major contributing factor to the missed or late diagnosis is the lack of a "one-size-fit-all" diagnostic test.

Current approaches to the clinical diagnosis of PCD involve multiple diagnostic investigations. International diagnostic guidelines published by the European Respiratory Society (ERS) in 2017 and American Thoracic Society (ATS) in 2018 recognize a combination of several examinations required for diagnosis including nasal nitric oxide concentration (nNO), transmission electron microscopy (TEM), high-speed video microscopy analysis (HSVM), and genetic testing (Lucas et al., 2017; Shapiro et al., 2018). The genetic etiology of PCD follows a monogenic rare Mendelian disease pattern typically inherited in an autosomal recessive manner. Between 1999 and 2010, PCD-causing mutations were only described in 11 genes (Knowles et al., 2013). Currently, over 50 genes have been reported as disease-causing for PCD (Wheway et al., 2021). Approximately 85% of disease-causing mutations identified are loss-of-function mutations including nonsense, frameshift insertion or deletions, canonical splice-site variants, and copy number variants (CNV). Multiple studies have identified CNV in PCD-related genes which contribute to a genetic diagnosis. Furthermore, a 27,748-bp large CNV deletion in *DRC1* and a 3,549-bp large deletion in *DNAAF4* were reported as founder mutations in East Asian and Irish populations, respectively (Zariwala et al., 1993; Keicho et al., 2020). At this time, there is no consensus by the ERS and ATS guidelines on which genes should be evaluated for PCD, and current commercial panels are not inclusive of all genes associated with PCD (Shoemark et al., 2019). Each diagnostic test is predicted to miss a proportion of cases; for example, standard electron microscopy may miss up to 30%, hence the importance of utilizing multiple diagnostic tests during investigations (Fassad et al., 2020). This is mainly due to the high genetic heterogeneity nature and the varying presentation of PCD.

Exome sequencing (ES) is more widely used than genome sequencing (GS) in the current genetic practice of Hong Kong due to the lower cost while covering the majority of pathogenic variants in the exonic regions (Tsang et al., 2019; Chung et al., 2020). Even though ES is a strong diagnostic tool, a large proportion of individuals persist as genetically undiagnosed. Negative ES results can be explained by several reasons including mosaicism, poor coverage of the exonic region, poor understanding of the genetic heterogeneity of the rare disease, lack of pathogenic evidence for detected variants, and variants that remain undetectable via ES such as CNVs, SVs, and deep intronic mutations (Frésard and Montgomery, 2018). Multiple strategies have been suggested to tackle situations where exome-negative results arise including exome sequencing reanalysis (rES), GS, long-read sequencing, transcriptome, metabolome, RNA sequencing, or investigate other cell types.

Among the several strategies suggested, rES is the most accessible and inexpensive method to use because there is no additional sequencing cost required. Studies have shown that rES is an effective measure of increasing diagnostic yield ranging from 6 to 47% (Stark et al., 2019; Fung et al., 2020). An intrinsic limitation to rES as a strategy is that rES can only analyze the variants already detected within the protein-coding region. Moreover, owing to the performance variations in the library capturing kit and sequencing instrument, there will be regions with poor uniform coverage. GS provides the capability to detect variants in regions poorly captured by ES. Approximately 30,000 rare variants can be observed in each individual with possible important impacts on gene expressions or altering conventional splicing patterns (Li et al., 2017). However, while in theory, GS is the complete sequencing strategy with the ability to detect deep non-coding variants, utilizing GS as a second-tier test for a negative ES is not as well-studied.

Since a comprehensive assessment of suspected early-onset bronchiectasis is not available in Hong Kong, we examined and evaluated the functional investigations and genetic results of 61 patients referred for assessment of bronchiectasis. Additionally, a back-to-back utility comparison between GS and rES was explored to determine the optimal strategy following an initial exome-negative result.

MATERIALS AND METHODS

Patient Recruitment

From 2015 to 2020, a total of 61 individuals with suspected bronchiectasis evaluated according to the pediatrics respirology

team in Queen Mary Hospital (QMH) were recruited into the study, which included one additional patient recruited during phase 2 as a potentially affected sibling. Participants were selected based on one of the following symptoms: 1) early-onset bronchiectasis confirmed by high-resolution computed tomography (HRCT) thorax with suggestive clinical features; 2) chronic suppurative lung disease, defined by a prolonged (>6 weeks) moist or productive cough, features of reactive airway disease, growth failure, recurrent chest infections, adventitious sound, or lung hyperinflation; and 3) "difficult to control" asthma as it has been shown that symptoms attributed to childhood asthma that are atypical or which respond poorly to conventional treatment. Specifically, school-aged children requiring step 4 or above management and step 3 or above management in pre-school age children according to the British Guideline on Management of Asthma, after excluding causes such as faulty inhaler technique, poor compliance, and environmental factors. Written informed consent was obtained from the patient's parent or guardian to participate in the study. All eligible families were invited for next-generation sequencing. Functional investigations were offered when possible. Ethics approvals were granted by the Institutional Review Board, the University of Hong Kong (HKU)/Hospital Authority Hong Kong West Cluster (UW12-211; UW18-520).

Functional Investigation

Functional investigation of nNO, TEM, and HSVM was performed at the Department of Paediatrics and Adolescent Medicine, at HKU and QMH as previously published (Lam et al., 2021). Sweat test and immune function workup including immunoglobulin levels were performed for all cases, and other appropriate investigations were performed if indicated. Nasal NO concentrations were measured utilizing the non-velum closure techniques in parts per billion (ppb). The nNO results were compared against the ranges previously published for healthy and PCD patients (Marthin and Nielsen, 2013). Two measurements of TEM and HSVM of the intact ciliary axoneme were targeted for this study. TEM and HSVM results were compared against the normal age-related reference range established in healthy children and adults in Hong Kong (Lee et al., 2020). Measurements and data analysis for both TEM and HSVM were performed by a trained laboratory technician.

Next-Generation Sequencing

Exome sequencing was performed either in-house at the Department of Paediatrics and Adolescent Medicine, HKU, or performed at the Centre of PanorOmic Sciences (CPOS), HKU. In-house library preparation was prepared using either Illumina's TruSeq™ Exome Library Prep Kit or Nextera™ Exome Kit Illumina according to manufacturer instructions. DNA libraries were then sequenced by the in-house NextSeq500 with a targeted ES depth coverage of 100×. Library preparation for ES samples sent to CPOS was prepared based on xGen Exome Research Panel v1.0 and sequenced using the Illumina NovaSeq 6000. Family-based ES was performed whenever possible. An average of 90 × depth coverage was targeted for ES sequenced at CPOS. Library preparation and sequencing for GS were performed at the Centre of PanorOmics Service, HKU. All of the libraries were prepared based on the KAPA Hyper Prep Kit (KR0961-V1.14) according to manufacturer instructions. An average of 30× coverage was targeted for GS.

Back-to-Back Utility Comparison Between Exome Reanalysis and Genome Sequencing

After the phase 1 study, which included an initial round of 60 exome analyses, 30 exome-negative samples were recruited for genome sequencing in phase 2, to perform a back-to-back comparison investigating the diagnostic utility between rES and GS. The back-to-back comparison methodology was modified from Tan et al. (2019). NGS data were analyzed separately by two teams comprising a pair of genome analysts. Each team was blinded to each other's analyses. The genome analysts discussed within their teams and provided a consensus result for the analysis. Consensus results were then used to calculate the diagnostic utility. Alternating rES and GS were given to each team to remove potential bias arising from different exome sequencing library kits and differing levels of variant pathogenicity assessment experience. Results including coverage comparison, number of variants detected, bioinformatics pipeline time taken, genomic analysis time taken, and overall diagnostic yield change were evaluated.

Bioinformatics Pipeline

An in-house developed bioinformatics pipeline was used for the processing of raw ES and GS FASTQ files following the Genome Analysis ToolKit's (GATK) best practices for germline single nucleotide polymorphisms and insertions/deletions in whole genome and exomes as previously reported (McKenna et al., 2010; Tsang et al., 2020). Raw reads were mapped to the hg19 reference human genome using the Burrows–Wheeler Aligner (BWA v.0.7.15) (Li and Durbin, 2009). Variant calling was performed using the GATK v.3.4-46 HaplotypeCaller. The same variant calling pipeline was used for the initial ES, GS, and rES cases. The analysis-ready variants for the initial ES with raw SNPs and Indels VCF file were annotated using Annotation Variation (ANNOVAR Build 20180708) (Wang et al., 2010). The variants from rES and GS were annotated using ANNOVAR Build 20200223. Variant annotation included allelic frequency from 1000 genome project, Exome Aggregation Consortium (ExAC), and Genome Aggregate Database (gnomAD v.2.1.1); in-silico prediction scores Sorting Intolerant from Tolerant (SIFT), PolyPhen2, Combined Annotation Dependent Depletion (CADD), and Rare Exome Variant Ensemble Learner (REVEL). Peddy were performed for quality control validating family inheritance and removal of duplicated samples (Pedersen and Quinlan, 2017). A virtual gene panel was used for the evaluation of genetic mutations in PCD patients from Genomics England PanelApp Primary Ciliary Dyskinesia v1.29 containing 139 genes (Martin et al., 2019).

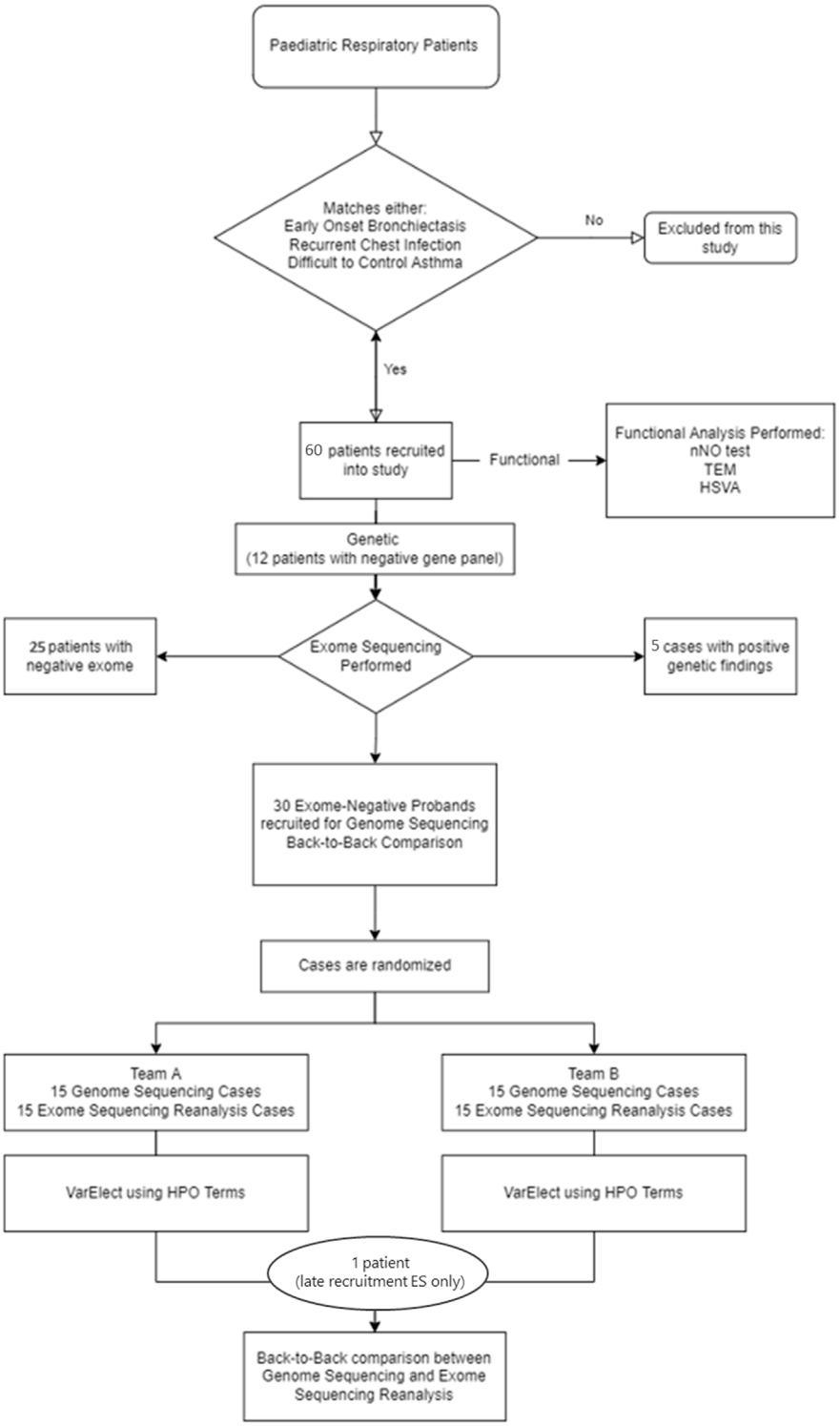

FIGURE 1 | Diagnostic workflow. The diagram shows this study design and workflow. In phase 1, 61 patients were recruited into the study for genetic and functional analysis. In phase 2, 30 exome-negative probands were recruited for GS and rES back-to-back comparison analysis. HSVM = high-speed video microscopy; HPO = human phenotype ontology; nNO test = nasal NO test; TEM = transmission electron microscopy.

TABLE 1 | Comprehensive functional and genetic landscape of early-onset bronchiectasis patients in Hong Kong.

Case	Clinical history	Gene	Allele 1 (ACMG classification)	Allele 2 (ACMG classification)	Phase	Family type	nNO (ppb)	TEM	HSVM
6	Bronchiectasis, situs inversus, dextrocardia, sinusitis, and bilateral otitis media	*CCDC40*	NM_017950.4(*CCDC40*) c.626_627del p. (Gly209GlufsTer59) [likely pathogenic]	Homozygous	1	Duos (Father)	12	Disarranged cilia	Slow-moving and dyskinetic
12	History of *pseudomonas aeruginosa* infection, recurrent bronchiolitis, bilateral bronchiectasis	*CFTR*	NM_000492.4(*CFTR*) c.274-1G>C [pathogenic]	Homozygous	1	Singleton[a]	91	Normal	Normal
36	Bronchiectasis, allergic rhinitis, history of pneumonia, sinopulmonary infection	*RSPH4A*	NM_001010892.3 (*RSPH4A*) c.1774_1775delTT p. (Leu592AspfsTer5) [likely pathogenic]	Homozygous	1	Trios	19	Central microtubules defect	Circular beat pattern
61	Bronchiectasis, history of *Pseudomonas aeruginosa* infection, history of *Staphylococcus aureus* infection, mixed restrictive and obstructive disease	*CFTR*	NM_000492.4(*CFTR*) c.2912_2948del p. (Ile972MetfsTer16) Paternal [pathogenic]	NM_000492.4(*CFTR*) c.1766+5G>T Unknown [pathogenic]	1	Duos (Father)	N/A	N/A	N/A
63	Dextrocardia, situs inversus, congenital pneumonia, persistent nasal discharge	*DNAH11*	NM_001277115.2 (*DNAH11*) c.11749_11752delGTTA p. (Val3917LysfsTer20) [likely pathogenic]	Homozygous	1	Trios	N/A	Normal	Static beat pattern
2	Chronic suppurative lung disease, bronchiectasis, rhinitis, recurrent chronic bilateral otitis media	*DNAI1*	NM_012144.4 (*DNAI1*) c.634C>T p. (Gln212Ter) Maternal [likely pathogenic]	NM_012144.4 (*DNAI1*) c.1355_1357del p. (Phe452del) Paternal [likely pathogenic]	2	Trios	25	Outer dynein arm defect	Slow-moving and dyskinetic
5	Biliary atresia, dextrocardia, situs inversus with normal heart structure, chronic lung disease	*DNAAF3*	NM_178837.4 (*DNAAF3*) c.493G>C p. (Gly165Arg) [VUS]	Homozygous	2	Trios [a]	N/A	Outer dynein arm and inner dynein arm defect	Immotile cilia
25	Bilateral bronchiectasis, severe necrotizing pneumonia, mixed obstructive and restrictive lung disease with insignificant bronchodilator response, pneumothorax, recurrent chest infection, previous tracheostomy performed	*DNAH9*	NM_001372.4 (*DNAH9*) c.3648delG p. Ala1217GlnfsTer4 Paternal [likely pathogenic]	NM_001372.4 (*DNAH9*) c.5093G>A p. (Gly1698Asp) Maternal [VUS]	2	Trios	N/A	Normal	Slow-moving
54	Bronchiectasis-suspected small airway disease, bronchiolitis, complicated with cystic bronchiectasis, right upper lobes, and right lower lobes medial segment collapse, pneumothorax, recurrent wet cough	*CCNO*	NM_021147.5(*CCNO*) c.788G>C p.Arg263Pro [VUS]	Homozygous	2	Trios	N/A	Only non-ciliated epithelia seen	Few cilia seen

(Continued on following page)

TABLE 1 | (*Continued*) Comprehensive functional and genetic landscape of early-onset bronchiectasis patients in Hong Kong.

Case	Clinical history	Gene	Allele 1 (ACMG classification)	Allele 2 (ACMG classification)	Phase	Family type	nNO (ppb)	TEM	HSVM
59	Recurrent sinopulmonary infections, recurrent right middle lobes consolidation and collapse, persistent *Haemophilus influenzae* infection, bronchiectasis	*DNAH11*	NM_001277115.2 (*DNAH11*) c.3426-1G>A Maternal [pathogenic]	NM_001277115.2 (*DNAH11*) c.10264G>A p. (Gly3422Arg) Paternal [likely pathogenic]	2	Quadruple	N/A	Normal	Static
62	Bronchiectasis in bilateral lower lobes, complete collapse of right middle lobe, right bronchomalacia with *Haemophilus influenzae*, right middle lobe pneumonia	*DNAH5*	NM_001369.3 (*DNAH5*) c.10438G>T p. (Glu3480Ter) Maternal [pathogenic]	NM_001369.3 (*DNAH5*) c.4355+5G>A Paternal [likely pathogenic]	2	Quadruple	N/A	Inconsistent results	N/A
64	Daily wet cough, perinatal pneumonia, and right middle lobe pneumonia, active bilateral airway inflammation, severe bronchomalacia with complete collapse right middle lobe, lower left lobe bronchi, bronchiectasis with sputum retention, tonsil and adenoid hypertrophy, bronchial wall thickening of central airways of bilateral lower lobes	*DNAH5*	NM_001369.3 (*DNAH5*) c.10438G>T p. (Glu3480Ter) Maternal [pathogenic]	NM_001369.3 (*DNAH5*) c.4355+5G>A Paternal [likely pathogenic]	2	Quadruple	N/A	Outer Dynein Arm defect	N/A
69	Sinusitis, mile bronchiectasis, suspected diffuse pan bronchiolitis, suggestive of mucus impaction and endobronchial spread of infection	*DNAH11*	NM_001277115.2 (*DNAH11*) c.3426-1G>A Maternal [pathogenic]	NM_001277115.2 (*DNAH11*) c.10264G>A p. (Gly3422Arg) Paternal [likely pathogenic]	2	Quadruple	N/A	N/A	N/A

[a]*Consanguineous parent.*

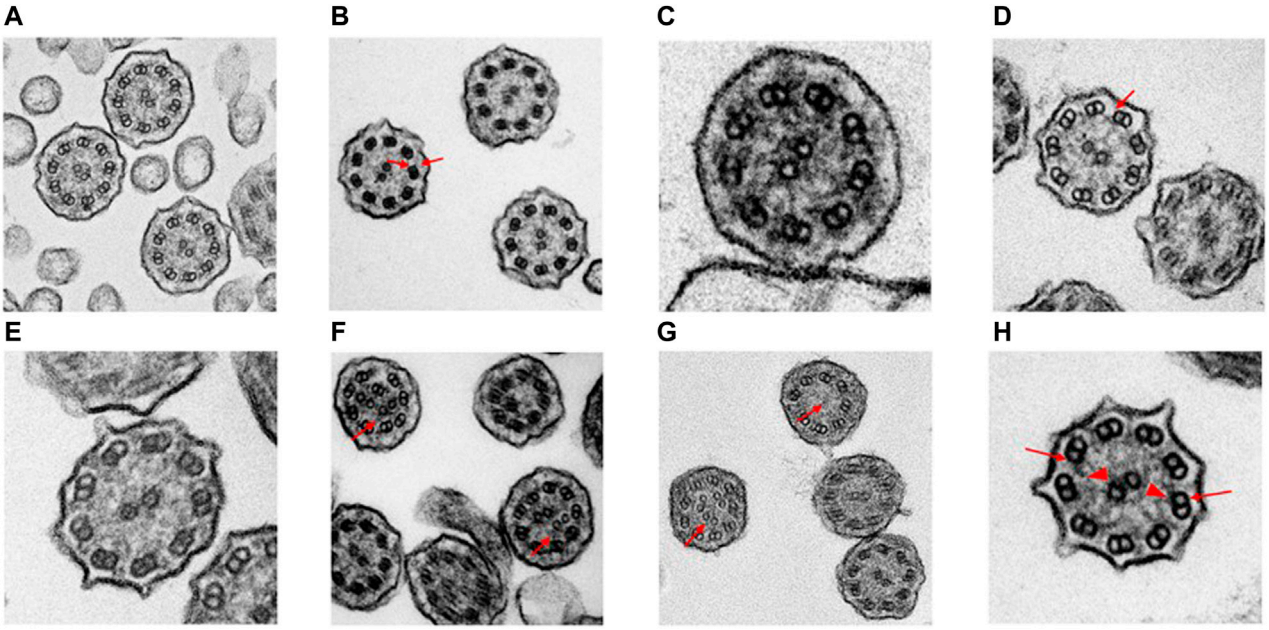

FIGURE 2 | Transmission electron microscopy results of suspected early-onset bronchiectasis patients in Hong Kong. **(A)** Case 12—Confirmed CF case showed a normal ciliary ultrastructure. **(B)** Case 5—A homozygous recessive *DNAAF3* c 493G>C variant was identified. TEM results showed an outer and inner dynein arm (arrows) defect which is similar to previously reported cases **(C)**. Case 25 cilia proximal arm—A compound heterozygous variants could be seen in *DNAH9*. The literature has shown that subtle outer dynein arm defect can be seen in TEM. The ciliary ultrastructure analysis in the proximal arm shows a normal ultrastructure **(D)**. Case 25 cilia distal arm shows a subtle outer dynein arm (arrow) defect. (E) Case 63—TEM results showed a normal ciliary ultrastructure. A pathogenic homozygous recessive *DNAH11* c.11749_11752delGTTA was identified and confirmed the clinical diagnosis despite the normal ultrastructure. HSVM showed a static beat pattern in 50% of cilia samples **(F)**. Case 6—TEM results showed that 47% of cilia were in a disarranged pattern (arrows). This matches the literature of loss-of-function mutations in the *CCDC40* gene. The frameshift deletion detected was *CCDC40* c.626_627del. **(G)**. Case 36—A trio-based ES revealed a frameshift deletion mutation on the *RSPH4A* gene, c.1774_1775del. Two separate TEM results showed 43 and 35% of ciliary samples with missing/extra-central microtubules (arrows). Previously reported literature has shown that patients with *RSPH4A* mutations are also presented with circular beating patterns and cilia without central microtubules **(H)**. Case 2—A compound heterozygous of two variants detected in trans within the *DNAI1* gene was seen in both trio-based rES and GS. ODA (arrows) defect was also detected in the TEM investigation which showed an average of 3.4 outer dynein arms detected per cilia (arrowheads, inner dynein arm). (bar = 100 nm).

For genome sequencing data, an additional bioinformatics pipeline was used to call CNV or SV variants. Variant calling of CNV followed the recommendations from Trost et al. (2018). The generation of CNV variants was performed using ERDS v.1.1 and CNVnator v.0.4.1 (Abyzov et al., 2011; Zhu et al., 2012). A concordant CNV VCF file was generated by merging the ERDS VCF file with the CNVnator VCF file using BEDTools v.2.27.1 set at 50% reciprocal overlap (Quinlan and Hall, 2010). Variant calling of SV was performed as previously described, if only one pathogenic/likely pathogenic variant or variant of uncertain significance (VUS) was identified (Yu et al., 2020). SV variants were called using MANTA v.1.6.0 and LUMPY v.0.2.13 (Layer et al., 2014; Chen et al., 2016). Anomalous read-pairs defined as paired ends reads that map to two different chromosomes with an abnormal insert-size or unexpected strand orientation were selected for breakpoint analysis. SpliceAI, a neural network machine learning–based algorithm to predict splicing variants, was performed on samples when one pathogenic/likely pathogenic variant or VUS was identified in a gene (Jaganathan et al., 2019). CNV and SV variant annotation was performed using Annotation and Ranking of Human Structural Variations (AnnotSV v.2.2). Manual inspection of the CNV and SV identified by the bioinformatics pipeline was performed on Integrative Genomics Viewer (IGV).

The pathogenicity interpretation of rare SNP and Indel genetic variants was performed following the American College of Medical Genetics (ACMG) Variant Interpretation guidelines (Richards et al., 2015). In addition, loss-of-function variants were classified utilizing the modified recommendations from the ClinGen Sequence Variant Interpretation Working Group (Abou Tayoun et al., 2018). The ACMG guideline modifications utilizing a Bayesian framework were also used in this study to evaluate the likelihood of pathogenicity in VUS cases (Tavtigian et al., 2018). Pathogenicity interpretation of CNVs was classified according to the ACMG/ClinGen guidelines (Riggs et al., 2020). The full study workflow can be seen in **Figure 1**.

RESULTS

Cohort Characteristics: A total of 61 participants were recruited into the study for exome sequencing, which constituted 33 males and 28 females. Twelve participants previously had gene panel genetic testing (*CCDC103*,

CCDC114, *CCDC39*, *CCDC40*, *CFTR*, *DNAAF1*, *DNAAF2*, *DNAAF3*, *DNAH11*, *DNAH5*, *DNAI1*, *DNAI2*, *DNAL1*, *HEATR2*, *INVS*, *LRRC6*, *NME8*, *OFD1*, *RPGR*, *RSPH4A*, and *RSPH9*) with negative results. Age at recruitment ranged from 1 to 32 years old (median: 11 years old). Fifty-two patients (85.2%) were below 18 years at the recruitment. Cases were recruited as trios (50.8%) if available. The remaining families were sequenced as singleton (13.1%), duos (27.9%), and quadruple (8.2%). Three cases were recruited into the study with a possible affected sibling due to the similar clinical features and positive familial genetic results. Two families recruited in this study were consanguineous (Case 5 and 12). All samples passed sample-level quality control, that is, with correct familial inheritance pattern and sexes within each family and no duplicated samples were found in the cohort. Thirty cases from phase 1 were recruited for GS in phase 2. Participants with trio-based sequencing data available and relevant functional results including low nNO, TEM defects, low ciliary beat frequency, or abnormal ciliary beat pattern by HSVM, were prioritized for GS. The majority of patients (n = 28; 93.3%) recruited were below 18 years at the initial age of recruitment with 13 males and 17 females. Two duos (6.7%) cases were recruited into GS due a clinical history strongly suggestive of PCD. **Supplementary Table S1** lists all the PCD participant characteristics for both initial ES and GS. **Supplementary Table S2** lists the clinical features and molecular diagnosis for all 61 patients. **Supplementary Table S3** lists the number of SNP and indels variants generated by rES and GS annotated and grouped by ANNOVAR.

Phase 1 and Phase 2 Analyses

Phase 1 Exome Sequencing

Sixty participants underwent ES as the first-tier diagnostic test in phase 1 of this study. ES analysis was performed from 2019 to 2020. A total of five individuals received a positive genetic diagnosis which corresponds to an exome sequencing diagnostic yield of 5/60 (8.3%), and none of them have been diagnosed by other tests.

Phase 2 Back-to-Back rES and GS Analysis

Phase 2 which included the back-to-back rES and GS analysis was performed from January to June 2021. Four individuals received a positive genetic diagnosis during phase 2 of the study (*DNAI1*, *DNAH11*, and *DNAH5* x2). These four positive genetic diagnoses could only be made during phase 2 by both rES and GS due to updated literature. While the back-to-back analysis comparison was taking place, case 69 (sibling of the case 59) was recruited into the ES study. An additional positive diagnosis was made for case 69 (*DNAH11*) by ES, which at the same time led to an additional diagnosis for case 59.

Diagnostic Yield

Diagnostic yield for phase 1 was 8.3% (n = 5/60) and diagnostic yield for phase 2 was 13.3% (n = 4/30). Combining all diagnoses, a diagnostic yield of 10/61 (16.4%) was obtained. The ten participants with a positive genetic diagnosis had a total of 12 unique mutations in seven genes that met the pathogenic or likely pathogenic criteria according to the ACMG classification. No clinically relevant CNVs/SVs were detected in this study. **Table 1** lists the full details with patient's clinical history, genetic mutation, pathogenic classification, and functional results.

In addition, we retrospectively classified 31/61 patients in our cohort of suspected bronchiectasis into those with clinically suspicious of PCD, based on the ERS guidelines (Lucas et al.). Limited by the lack of nNO for majority of patients, only clinical features were being investigated. Patients with two or more of the recommended six clinical features from the ERS guidelines were classified as those clinically suspicious of PCD. The six clinical features included 1) persistent wet cough, 2) situs anomalies, 3) congenital cardiac defects, 4) persistent rhinitis, 5) chronic middle ear disease with or without hearing loss, and 6) a history in term infants of neonatal upper and lower respiratory symptoms or neonatal intensive care admittance. We also included any patients with a confirmed PCD diagnosis in a sibling prior to the study. Among the 31 patients with clinical suspicion of PCD, the diagnostic yield was 26% (n = 8/31). In contrast, for patients who did not fulfill the clinical criteria of PCD, no PCD-related molecular diagnosis was obtained, and CF was diagnosed in two patients by the presence of biallelic CFTR mutations.

Integrated Approach in a Cohort of Suspected Bronchiectasis

In addition to the main findings, we report cases that illustrate the need for an integrated approach to a cohort of suspected bronchiectasis, which is demonstrated by 1) a case of CF bronchiectasis, 2) a case of normal ciliary ultrastructure that would have been missed if genetic testing was not done, as well as 3) two cases where VUS may highlight the genotype-phenotype correlation between the genetic and functional results, and 4) one case to illustrate the advantage of increased coverage in GS.

CF Bronchiectasis

Case 12: A 4-year-old South Asian male from a consanguineous family presented with clinical symptoms of bronchiolitis, bilateral bronchiectasis, and history of *Pseudomonas aeruginosa* infection. Singleton-ES showed a homozygous splice-site mutation, NM_000492.4(*CFTR*):c.274-1G>C. Subsequent Sanger sequencing showed both parents were heterozygous for the variant. The *CFTR* gene is a well-known gene with a strong genotype–phenotype correlation with cystic fibrosis (OMIM #219700). This splice mutation was previously reported as pathogenic on ClinVar (accession: VCV000048680.12) and the following two positive sweat tests of 91.2 and 107.1 mmol/L confirmed the cystic fibrosis diagnosis. Functional examination confirms our understanding of the diagnosis as cystic fibrosis patients are not presented with any changes in ciliary ultrastructure or beat pattern and frequency. **Figure 2A** shows normal ciliary ultrastructure from the TEM examination. The reduced nNO test of 91 ppb is concurrent with the current understanding of nitric oxide levels in cystic fibrosis patients (Michl et al., 2013).

PCD with Normal Ciliary Ultrastructure

Case 59: A 17-year-old East Asian female presented with recurrent sinopulmonary infections, recurrent right middle lobes consolidation and collapse, persistent *Haemophilus influenzae* infection, and bronchiectasis. This case was recruited into phase 2 because phase 1 was inconclusive. A compound heterozygous of maternally inherited pathogenic canonical splice-site variant NM_001277115.2 (*DNAH11*): c.3426-1G>A and paternally inherited likely pathogenic missense variant NM_001277115.2 (*DNAH11*):c.10264G>A: p. (Gly3422Arg) was detected using both rES and GS. *DNAH11* is also a heavy-chain protein that encodes the outer dynein arm (ODA) in the anemone and is typically associated with PCD with an autosomal recessive inheritance pattern. Case 63 also had compound heterozygous pathogenic mutations in *DNAH11*. The nNO test was not performed due to COVID-19 restrictions, and TEM investigations showed a normal ciliary ultrastructure. Functional investigations for HSVM results returned confirming a functional diagnosis of PCD. The HSVM investigations further supports the diagnosis of PCD and showed a static ciliary beat pattern in 50% of cilia samples. For the remaining cilia, 46% showed normal beating and 4% showed stiff beating. Overall beat frequency is at 10.77 Hz.

To further strengthen the pathogenicity of the *DNAH11* variants, case 69, a 12-year-old younger sister of case 59, who presented with clinical symptoms of sinusitis, mild bronchiectasis, suspected diffuse pan bronchiolitis, suggestive of mucus impaction, and endobronchial spread of infection, was recruited during phase 2 of our study. Although no functional assessments were performed due to the emergence of COVID-19, genetic results showed that the same segregation of c.3426-1G>A and p.(Gly3422Arg) variants were detected in case 69. This further increases the pathogenicity classification of the mutations due to the familial segregation of the disease-causing variants.

Functionally Relevant PCD Cases in Cases with Variant of Unknown Significance

Case 25: A 21-year-old East Asian female with clinical symptoms of bilateral bronchiectasis, severe necrotizing pneumonia, mixed obstructive and restrictive lung disease with insignificant bronchodilator response, pneumothorax, and recurrent chest infection was recruited into the study. Initial ES detected a compound heterozygous mutation in the *DNAH9* gene including a paternally inherited frameshift NM_001372.4 (*DNAH9*):c.3649del: p. (Ala1217GlnfsTer4) and a maternally inherited missense NM_001372.4 (*DNAH9*): c.5093G>A: p. (Gly1698Asp) variant. Both rES and GS were able to detect the two variants. *DNAH9* is a gene recently discovered in 2018 with a genotype–phenotype correlation with PCD, and is inherited in an autosomal recessive manner. The frameshift p.(Ala1217GlnfsTer4) and missense p.(Gly1698Asp) variants were classified as likely pathogenic and VUS, respectively, according to the ACMG guidelines. There were no changes in ACMG classification since the initial ES analysis.

Functional investigations were performed for this case and showed a strong genotype–phenotype correlation. TEM results showed an average of 7.7 outer and 7.8 inner dynein arm count which suggests a normal ciliary ultrastructure (**Figure 2C**). However, TEM photos of the distal axoneme showed ciliary ultrastructure lacking in the outer dynein arm (**Figure 2D**). The HSVM investigations showed slow-moving cilia beat frequency at 6.5 Hz. A total of 98% of the cilia showed normal beating, while 2% were immotile cilia. There was no obvious stiffness at the base of the cilia. Despite the functional investigations matching the genetic findings, the variant was not upgraded to likely pathogenic due to the stringent nature of ACMG criteria.

Case 54: An 18-year-old East Asian female presented with bronchiectasis, suspected small airway disease, bronchiolitis, complicated with cystic bronchiectasis, right upper lobes and right lower lobes medial segment collapse, pneumothorax, and recurrent wet cough was recruited into the study. Initial ES results were negative, and this case was subsequently recruited into the back-to-back comparison. A homozygous missense mutation was detected in both rES and GS, NM_021147.5(*CCNO*):c.788G>C: p.(Arg263Pro). This variant was inherited from both parents. Cyclin O, also known as *CCNO*, plays an important role in the function of deuterostome-dependent amplification of basal bodies and their docking mechanism (Wallmeier et al., 2014). *CCNO* is known to have a genotype–phenotype correlation with PCD and is inherited in an autosomal recessive manner. The missense variant is considered rare with an allelic frequency of 0.00001423 in the gnomAD v2.1.1 database but was not predicted pathogenic by most bioinformatics prediction tools. Based on the current evidence, the p.(Arg263Pro) variant was classified as a VUS.

This variant was reported due to the strong genotype–phenotype correlation with the TEM and HSVM functional results. Both functional investigations showed there were a limited number of epithelial cilia that can be observed in the patient's live ciliary sample. Current understanding of the reduced generation of motile cilia can only be seen in two genes, *MCIDAS* and *CCNO* (Boon et al., 2014). Further investigation into *MCIDAS* yielded no relevant mutations in both rES and GS. Despite the genetic result matching with the functional findings, the mutation lacked further evidence to be upgraded according to the ACMG guidelines. Further experimental methodologies would be required to upgrade the pathogenicity of this variant.

Benefit of GS over ES Demonstrated by Differences in Coverage of a VUS Variant

Case 5: A 5-year-old South Asian male from a consanguineous family who was recruited into the study presented with clinical symptoms of biliary atresia, dextrocardia, situs inversus with normal heart structure, and chronic lung disease. Initial ES did not detect any genetic findings in any clinically relevant genes. GS was pursued for this case, and a homozygous missense variant NM_178837.4 (*DNAAF3*):c.493G>C p. (Gly165Arg) was discovered. This variant was not detected during the initial exome sequencing due to the low coverage of the region. Mutations in *DNAAF3* cause defects in the cytoplasmic preassembly of the dynein arms and are associated with the phenotype primary

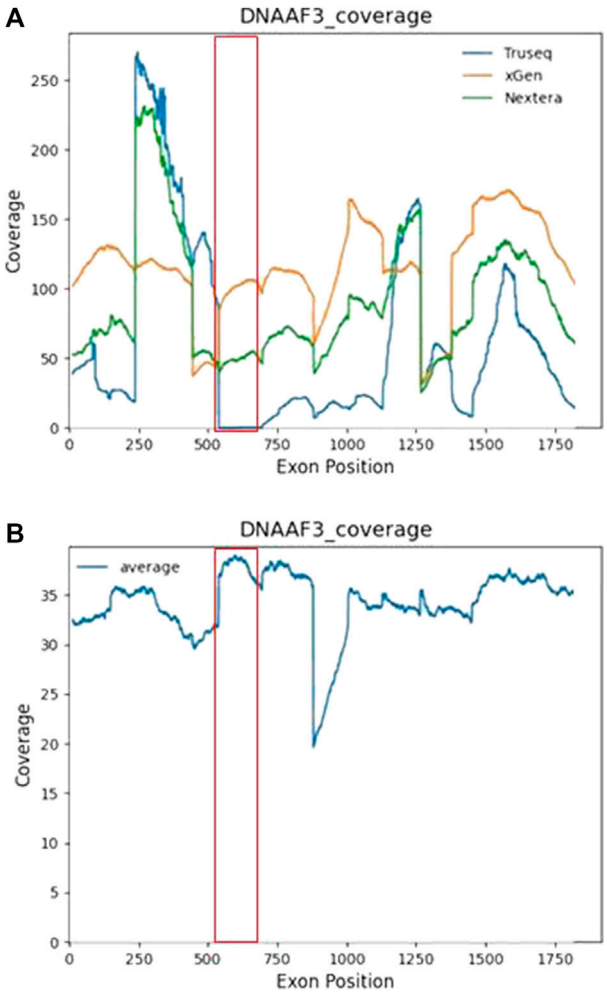

FIGURE 3 | Nucleotide by nucleotide coverage of *DNAAF3* in ES and GS. The line plot shows the average coverage of each nucleotide in the *DNAAF3* gene. **(A)** Coverage of ES split across library preparation kits. Across 30 ES samples that used Truseq, an average of 0× read depth was seen for exon 5 of *DNAAF3*. **(B)** Coverage of GS across the *DNAAF3* gene.

ciliary dyskinesia with an autosomal recessive inheritance pattern. The variant was classified as VUS according to the ACMG guidelines as there is limited information about the effects of this mutation.

Functional investigations were performed for this case and showed a strong genotype–phenotype correlation. The TEM results for case 5 showed an ODA + inner dynein arm (IDA) defect (**Figure 2B**). The HSVM investigations showed completely immotile cilia beat frequency that was confirmed on retesting. Literature has shown that PCD patients with *DNAAF3* mutations present with similar phenotypes (Mitchison et al., 2012). Despite the functional investigations matching the genetic findings, the variant was not upgraded to likely pathogenic due to the stringent ACMG criteria and the scarcity of medical literature on the gene and the functional investigations.

DISCUSSION

In this study, we performed ES on 61 patients referred for assessment of bronchiectasis, which included patients with suspected early-onset bronchiectasis, recurrent chest infections, and difficult-to-control asthma in Hong Kong. Cases with trio samples available, strong clinical phenotypes, or functionally relevant investigations were recruited for GS. A back-to-back comparison between rES and GS was performed on 30 initially negative exome cases. There is an increase in diagnostic yield with rES but with minimal additional increase over rES with GS.

The virtual gene panel used for the evaluation of genetic mutations in PCD patients was obtained from Genomics England PanelApp Primary Ciliary Dyskinesia v1.29 containing 139 genes. Within the 139–virtual-gene panel

screened, 135 genes screened had at least 10 × read depth across the exonic region in over 90% of the PCD rES results (**Supplementary Figure S1**). Notable exceptions included *BBS5*, *CLRN1*, *CRX*, and *GDF1*. With the exception of the *RPGR* gene, 138 genes met 10 × read depth across the exonic region in over 90% of the GS samples requirement. *RPGR* is notably a gene that is listed as a diagnostic-grade green (strong confidence) genotype–phenotype correlation with PCD.

An overall diagnostic yield of 10/61 (16.4%) was made by ES or rES and GS combined. The additional yield of rES and GS beyond the initial ES analysis was 4/30 (13.3%). The diagnostic yield of this study is not comparable to other PCD cohorts due to the different nature of the recruitment process. In our study, patients with either bronchiectasis, chronic suppurative lung disease, or "difficult to control" asthma were recruited into the study. Functional investigations were performed parallel to genetic investigations. This differs from other studies highlighted by ERS and ATS, which performs genetic investigations only on patients with strong clinical phenotypes of PCD or functionally confirmed to be PCD (Lucas et al., 2017; Shapiro et al., 2018). By performing functional investigations prior to the genetic testing, this would exclude samples with weak phenotypes. Another reason for the lower yield in ES is that 12 cases were negative from a previous gene panel analysis which included 20 PCD genes and *CFTR*. Moreover, the genetic basis of PCD is still unknown in 20–30% of confirmed cases. As a result, a lower diagnostic yield compared to other reported PCD studies is expected.

In this study, a back-to-back clinical utility comparison between rES and GS was performed. Other analysis points were also analyzed including bioinformatics pipeline time taken, HPO terms used for analysis, and genomic analysis time taken (**Supplementary Tables S4, S5, S6**). Both rES and GS were able to find the same genetic variants identified in phase 2; however, only GS was able to detect the VUS *DNAAF3* c.493G>C variant due to non-uniform coverage of the exons in ES. Changes in pathogenicity classification in rES cases were mainly due to updated literature, correlation with functional investigations, and improvements in in-silico bioinformatics predictions for splicing variants. Despite the added benefits of detecting deep intronic variants, intergenic variants, and CNV by GS, no functionally relevant CNV mutations were detected in this study. As CNV mutations were detected in PCD patients from other studies, the lack of detection could be attributed to the small sample size or differences in genetic etiology (Morimoto et al., 2019; Keicho et al., 2020; Wheway et al., 2021). This reduced the added benefits of GS in comparison to rES. This also demonstrated a limited benefit in proceeding to GS instead of performing rES.

Further examination into the ES coverage data showed uneven coverage across exons in different ES library preparation kits which explained the detection of *DNAAF3* c.493G>C exclusively in GS (**Figure 3**). Case 5 used the TruSeq Exome Library Prep Kit, which showed poor coverage over exon 5 in the *DNAAF3* gene. Across 30 exome samples that used TruSeq, a 0× average read depth was seen across exon 5 of *DNAAF3*. The low coverage of exon 5 of *DNAAF3* is not limited to TruSeq. In gnomAD exome coverage with 141,456 samples, the average coverage over this nucleotide is 1.7×. Newer exome library preparation kits such as xGen and Nextera have fixed the issue of low coverage in this exon and have sufficient coverage of exon 5. This case shows that despite the great utility of rES, resequencing samples should be considered if the initial sequencing was performed a few years ago, preferably with a new exome capture kit. Improvements in ES library preparation can reduce concerns such as uneven coverage.

One of the major advantages of utilizing genetic testing as a diagnostic tool in suspected early-onset bronchiectasis is the lack of a "one-size-fit-all" diagnostic test. Genetic testing was able to identify pathogenic mutations in the *DNAH11* gene in cases 59, 63, and 69. As previously mentioned, pathogenic mutations within the *DNAH11* gene do not cause structural defects identifiable from TEM investigations. For case 59, a compound heterozygous variant including a maternally inherited splicing variant c.3426-1G>A and paternally inherited missense variant p.(Gly3422Arg) were detected. The variants were both previously detected during the initial round of exome sequencing, but a genetic diagnosis was not completed due to insufficient evidence as the p.(Gly3422Arg) missense variant was classified as a VUS. The previous combination of ACMG criteria used included absent from controls (PM2), detected in trans with a pathogenic variant (PM3), and multiple lines of computational evidence support a deleterious effect on the gene or gene product (PP3). In phase 2, functional TEM and HSVM results confirmed a functional diagnosis of PCD. Similar to case 63, the TEM results returned a normal ciliary ultrastructure consistent with *DNAH11* findings and HSVM results showed a static ciliary beat pattern. The added combination of TEM and HSVM results allowed the usage of PP4 criteria, the patient's phenotype or family history is highly specific for a disease with a single genetic etiology. The new combination of PM2, PM3, PP3, and PP4 satisfies the ACMG combination criteria of a likely pathogenic variant, thereby reaching a genetic diagnosis. The usage of combining functional and genetic results could also be seen in other cases too. Both TEM and HSVM were also useful tools to confirm the genetic diagnosis in case 63, 6, 36, and 2 (**Figures 2E–H**). This shows that the combination of functional examination and genetic testing is useful in the diagnosis of early-onset bronchiectasis due to the complex functional presentation of PCD.

With the rate of growth in discovering new genes for a genetically heterogeneous condition such as PCD, reanalysis is expected to be useful in helping patients reach a genetic diagnosis for their condition. Initial ES detected a compound heterozygous mutation in the *DNAH9* gene including a paternally inherited loss-of-function p.(Ala1217GlnfsTer4) and a maternally inherited missense p.(Gly1698Asp) variant. Both rES and GS were able to detect the two variants. *DNAH9* is a gene recently discovered in 2018 with an autosomal recessive inheritance pattern (Fassad et al., 2018; Shoemark et al., 2018). Due to the recent discovery of *DNAH9*, there is currently limited evidence for functional investigations and genotype–phenotype correlation. The gene is currently listed in the PanelApp gene panel under the category of "No List," suggesting curation for this gene is yet to be completed. Patients with *DNAH9* mutations have been reported to have relatively mild or no respiratory phenotypes which contradicts the severe clinical phenotype identified in case 25 (Loges et al., 2018; Lucas et al., 2020). Furthermore, TEM results showed no

ciliary ultrastructure defect which is possibly compatible with the subtle ODA defect observed in *DNAH9* cases. The lack of cases and understanding of missense variants within the *DNAH9* gene greatly restricts the pathogenicity classification. Without an abundance of cases or experimental evidence of the p.(Gly1698Asp) variant, it remains a VUS variant under the ACMG recommendations. This highlights the importance of performing genetic analysis in combination with functional tests for better genotype–phenotype correlation. In order for genes to be rated green on PanelApp, pathogenic variants need to be identified in ≥3 independent families. This emphasizes the importance of identifying and investigating early-onset bronchiectasis to increase evidence level for amber/red/no list genes. Further investigations will need to be performed and ensure the genetic diagnosis.

Limitations

The study design focuses on suspected early-onset bronchiectasis cases which has potential non-genetic causes. While this study has effectively shown the mutational spectrum and genetic landscape of early-onset bronchiectasis patients in Hong Kong, more patients will need to be recruited to effectively show the genetic diagnosis. Genetic analysis will also need to be frequently reanalyzed due to the growing list of genes associated with PCD.

The back-to-back comparison of rES and GS in this study was limited by resources. Ideally, all exome-negative samples would have also undergone GS for a larger cohort and thus better comparison. The remaining 25 cases with negative ES result would be subject to GS when resources become available to see if there is any confounding effect. Additionally, the patient's phenotype was not evaluated by a standardized HPO terms approach which would have utilized clinical geneticists and clinicians in standardizing the patient's phenotype and cohort phenotype characteristics. Furthermore, a better comparison between rES and GS would ideally include patients with a wider spectrum of disease conditions. Different inheritance patterns and disease mechanism could potentially show the added benefits of detecting intronic variants, repeat expansion, CNV, and SV variants in GS over rES.

Lastly, this study was also affected by the COVID-19 pandemic. As suspected, bronchiectasis and PCD is a respiratory disease, so further patient recruitment and functional investigations were halted for safety concerns. Some samples did not undergo typical functional investigations despite reaching a genetic diagnosis. This limited the ability to correlate genetic findings with functional results.

CONCLUSION

In this cohort of early-onset bronchiectasis, recurrent chest infections, and difficult-to-control asthma patients suspected of primary ciliary dyskinesia, an overall diagnostic yield of 16.4% was achieved. This study has shown that utilizing genetic testing in combination with functional investigations has increased diagnostic yield for patients with pathogenic mutations in PCD genes due to the lack of a "one-size-fit-all" diagnostic test. A back-to-back comparison between rES and GS has shown that rES and GS are comparable in clinical diagnosis. It may appear there was a little added benefit that could be seen from proceeding to GS in this study; this is due to the lack of effective means to evaluate intronic mutations and the lack of clinically relevant CNV detected in this study. While resequencing samples is recommended if the initial sequencing was performed more than a few years ago, the issue of uneven gene coverage in ES may not be completely resolved by either resequencing or reanalysis of ES. This study has shown that further investigation is required to evaluate other complementary approaches after an exome-negative result.

DATA AVAILABILITY STATEMENT

The datasets for this article are not publicly available due to concerns regarding minor participant/patient anonymity. Requests to access the datasets should be directed to the corresponding authors. Data available from the corresponding authors will be de-identified before the data is handed over to qualified researchers.

ETHICS STATEMENT

The studies involving human participants were reviewed and approved by Institutional Review Board, the University of Hong Kong Institutional Review Board, Hospital Authority Hong Kong West Cluster. Written informed consent to participate in this study was provided by the participants' legal guardian/next of kin.

AUTHOR CONTRIBUTIONS

JC was responsible for manuscript writing and data analysis as well as project coordination. ML and MC helped with manuscript writing and revision. JC, MY, JF, and CM performed genomic analysis. ML helped with the lab work. CS-KC, KK, and JH helped with functional investigation and clinical details. KY and AK helped with the data analysis and supervision. CO and YL gave advice and provided intellectual input to the manuscript. C-WD performed functional evaluation. BH-YC and S-LL supported the case recruitment, provided the clinical details, supervision, and financial support. All authors contributed to the article and approved the submitted version.

FUNDING

This work was supported by funds from The Society for the Relief of Disabled Children and The Edward and Yolanda Wong Fund. CO'C is supported by the Great Ormond Street Children's Hospital BRC.

SUPPLEMENTARY MATERIAL

The Supplementary Material for this article can be found online at: https://www.frontiersin.org/articles/10.3389/fgene.2022.933381/full#supplementary-material

REFERENCES

Abou Tayoun, A. N., Pesaran, T., Distefano, M. T., Oza, A., Rehm, H. L., Biesecker, L. G., et al. (2018). Recommendations for Interpreting the Loss of Function PVS1 ACMG/AMP Variant Criterion. *Hum. Mutat.* 39, 1517–1524. doi:10.1002/humu.23626

Abyzov, A., Urban, A. E., Snyder, M., and Gerstein, M. (2011). CNVnator: an Approach to Discover, Genotype, and Characterize Typical and Atypical CNVs from Family and Population Genome Sequencing. *Genome Res.* 21, 974–984. doi:10.1101/gr.114876.110

Afzelius, B. A., and Stenram, U. (2006). Prevalence and Genetics of Immotile-Cilia Syndrome and Left-Handedness. *Int. J. Dev. Biol.* 50, 571–573. doi:10.1387/ijdb.052132ba

Boon, M., Wallmeier, J., Ma, L., Loges, N. T., Jaspers, M., Olbrich, H., et al. (2014). MCIDAS Mutations Result in a Mucociliary Clearance Disorder with Reduced Generation of Multiple Motile Cilia. *Nat. Commun.* 5, 4418. doi:10.1038/ncomms5418

Chen, X., Schulz-Trieglaff, O., Shaw, R., Barnes, B., Schlesinger, F., Källberg, M., et al. (2016). Manta: Rapid Detection of Structural Variants and Indels for Germline and Cancer Sequencing Applications. *Bioinformatics* 32, 1220–1222. doi:10.1093/bioinformatics/btv710

Chung, C. C. Y., Leung, G. K. C., Mak, C. C. Y., Fung, J. L. F., Lee, M., Pei, S. L. C., et al. (2020). Rapid Whole-Exome Sequencing Facilitates Precision Medicine in Paediatric Rare Disease Patients and Reduces Healthcare Costs. *Lancet Reg. Health - West. Pac.* 1, 100001. doi:10.1016/j.lanwpc.2020.100001

Fassad, M. R., Shoemark, A., Legendre, M., Hirst, R. A., Koll, F., Le Borgne, P., et al. (2018). Mutations in Outer Dynein Arm Heavy Chain DNAH9 Cause Motile Cilia Defects and Situs Inversus. *Am. J. Hum. Genet.* 103, 984–994. doi:10.1016/j.ajhg.2018.10.016

Fassad, M. R., Patel, M. P., Shoemark, A., Cullup, T., Hayward, J., Dixon, M., et al. (2020). Clinical Utility of NGS Diagnosis and Disease Stratification in a Multiethnic Primary Ciliary Dyskinesia Cohort. *J. Med. Genet.* 57, 322–330. doi:10.1136/jmedgenet-2019-106501

Frésard, L., and Montgomery, S. B. (2018). Diagnosing Rare Diseases after the Exome. *Cold Spring Harb. Mol. Case Stud.* 4, a003392. doi:10.1101/mcs.a003392

Fung, J. L. F., Yu, M. H. C., Huang, S., Chung, C. C. Y., Chan, M. C. Y., Pajusalu, S., et al. (2020). A Three-Year Follow-Up Study Evaluating Clinical Utility of Exome Sequencing and Diagnostic Potential of Reanalysis. *Npj Genom. Med.* 5, 37. doi:10.1038/s41525-020-00144-x

Jaganathan, K., Kyriazopoulou Panagiotopoulou, S., Mcrae, J. F., Darbandi, S. F., Knowles, D., Li, Y. I., et al. (2019). Predicting Splicing from Primary Sequence with Deep Learning. *Cell* 176, 535–548.24. doi:10.1016/j.cell.2018.12.015

Keicho, N., Hijikata, M., Morimoto, K., Homma, S., Taguchi, Y., Azuma, A., et al. (2020). Primary Ciliary Dyskinesia Caused by a Large Homozygous Deletion Including Exons 1-4 of DRC1 in Japanese Patients with Recurrent Sinopulmonary Infection. *Mol. Genet. Genomic Med.* 8, e1033. doi:10.1002/mgg3.1033

Knowles, M. R., Daniels, L. A., Davis, S. D., Zariwala, M. A., and Leigh, M. W. (2013). Primary Ciliary Dyskinesia. Recent Advances in Diagnostics, Genetics, and Characterization of Clinical Disease. *Am. J. Respir. Crit. Care Med.* 188, 913–922. doi:10.1164/rccm.201301-0059ci

Kuehni, C. E., Frischer, T., Strippoli, M.-P. F., Maurer, E., Bush, A., Nielsen, K. G., et al. (2010). Factors Influencing Age at Diagnosis of Primary Ciliary Dyskinesia in European Children. *Eur. Respir. J.* 36, 1248–1258. doi:10.1183/09031936.00001010

Lam, W.-Y., Tang, C. S.-M., So, M.-T., Yue, H., Hsu, J. S., Chung, P. H.-Y., et al. (2021). Identification of a Wide Spectrum of Ciliary Gene Mutations in Nonsyndromic Biliary Atresia Patients Implicates Ciliary Dysfunction as a Novel Disease Mechanism. *EBioMedicine* 71, 103530. doi:10.1016/j.ebiom.2021.103530

Layer, R. M., Chiang, C., Quinlan, A. R., and Hall, I. M. (2014). LUMPY: a Probabilistic Framework for Structural Variant Discovery. *Genome Biol.* 15, R84. doi:10.1186/gb-2014-15-6-r84

Lee, S.-L., O'Callaghan, C., Lau, Y.-L., and Lee, C.-W. D. (2020). Functional Analysis and Evaluation of Respiratory Cilia in Healthy Chinese Children. *Respir. Res.* 21, 259. doi:10.1186/s12931-020-01506-w

Li, H., and Durbin, R. (2009). Fast and Accurate Short Read Alignment with Burrows-Wheeler Transform. *Bioinformatics* 25, 1754–1760. doi:10.1093/bioinformatics/btp324

Li, X., Kim, Y., Kim, Y., Tsang, E. K., Davis, J. R., Damani, F. N., et al. (2017). The Impact of Rare Variation on Gene Expression across Tissues. *Nature* 550, 239–243. doi:10.1038/nature24267

Loges, N. T., Antony, D., Maver, A., Deardorff, M. A., Güleç, E. Y., Gezdirici, A., et al. (2018). Recessive DNAH9 Loss-Of-Function Mutations Cause Laterality Defects and Subtle Respiratory Ciliary-Beating Defects. *Am. J. Hum. Genet.* 103, 995–1008. doi:10.1016/j.ajhg.2018.10.020

Lucas, J. S., Barbato, A., Collins, S. A., Goutaki, M., Behan, L., Caudri, D., et al. (2017). European Respiratory Society Guidelines for the Diagnosis of Primary Ciliary Dyskinesia. *Eur. Respir. J.* 49, 1601090. doi:10.1183/13993003.01090-2016

Lucas, J. S., Davis, S. D., Omran, H., and Shoemark, A. (2020). Primary Ciliary Dyskinesia in the Genomics Age. *Lancet Respir. Med.* 8, 202–216. doi:10.1016/s2213-2600(19)30374-1

Marthin, J. K., and Nielsen, K. G. (2013). Hand-Held Tidal Breathing Nasal Nitric Oxide Measurement - A Promising Targeted Case-Finding Tool for the Diagnosis of Primary Ciliary Dyskinesia. *PLoS One* 8, e57262. doi:10.1371/journal.pone.0057262

Martin, A. R., Williams, E., Foulger, R. E., Leigh, S., Daugherty, L. C., Niblock, O., et al. (2019). PanelApp Crowdsources Expert Knowledge to Establish Consensus Diagnostic Gene Panels. *Nat. Genet.* 51, 1560–1565. doi:10.1038/s41588-019-0528-2

McKenna, A., Hanna, M., Banks, E., Sivachenko, A., Cibulskis, K., Kernytsky, A., et al. (2010). The Genome Analysis Toolkit: a MapReduce Framework for Analyzing Next-Generation DNA Sequencing Data. *Genome Res.* 20, 1297–1303. doi:10.1101/gr.107524.110

Metersky, M. L., Choate, R., Aksamit, T. R., Conrad, D., Lapinel, N. C., Maselli, D. J., et al. (2022). Stenotrophomonas Maltophilia in Patients with Bronchiectasis: An Analysis of the US Bronchiectasis and NTM Research Registry. *Respir. Med.* 193, 106746. doi:10.1016/j.rmed.2022.106746

Michl, R. K., Hentschel, J., Fischer, C., Beck, J. F., and Mainz, J. G. (2013). Reduced Nasal Nitric Oxide Production in Cystic Fibrosis Patients with Elevated Systemic Inflammation Markers. *PLoS One* 8, e79141. doi:10.1371/journal.pone.0079141

Mitchison, H. M., Schmidts, M., Loges, N. T., Freshour, J., Dritsoula, A., Hirst, R. A., et al. (2012). Mutations in Axonemal Dynein Assembly Factor DNAAF3 Cause Primary Ciliary Dyskinesia. *Nat. Genet.* 44, 381s381–389382. doi:10.1038/ng.1106

Morimoto, K., Hijikata, M., Zariwala, M. A., Nykamp, K., Inaba, A., Guo, T. C., et al. (2019). Recurring Large Deletion in DRC1 (CCDC164) Identified as Causing Primary Ciliary Dyskinesia in Two Asian Patients. *Mol. Genet. Genomic Med.* 7, e838. doi:10.1002/mgg3.838

O'Callaghan, C., Chetcuti, P., and Moya, E. (2010). High Prevalence of Primary Ciliary Dyskinesia in a British Asian Population. *Archives Dis. Child.* 95, 51–52. doi:10.1136/adc.2009.158493

Pedersen, B. S., and Quinlan, A. R. (2017). Who's Who? Detecting and Resolving Sample Anomalies in Human DNA Sequencing Studies with Peddy. *Am. J. Hum. Genet.* 100, 406–413. doi:10.1016/j.ajhg.2017.01.017

Quinlan, A. R., and Hall, I. M. (2010). BEDTools: a Flexible Suite of Utilities for Comparing Genomic Features. *Bioinformatics* 26, 841–842. doi:10.1093/bioinformatics/btq033

Richards, S., Aziz, N., Bale, S., Bick, D., Das, S., Gastier-Foster, J., et al. (2015). Standards and Guidelines for the Interpretation of Sequence Variants: a Joint Consensus Recommendation of the American College of Medical Genetics and Genomics and the Association for Molecular Pathology. *Genet. Med.* 17, 405–424. doi:10.1038/gim.2015.30

Riggs, E. R., Andersen, E. F., Cherry, A. M., Kantarci, S., Kearney, H., Patel, A., et al. (2020). Technical Standards for the Interpretation and Reporting of Constitutional Copy-Number Variants: a Joint Consensus Recommendation of the American College of Medical Genetics and Genomics (ACMG) and the Clinical Genome Resource (ClinGen). *Genet. Med.* 22, 245–257. doi:10.1038/s41436-019-0686-8

Shapiro, A. J., Davis, S. D., Polineni, D., Manion, M., Rosenfeld, M., Dell, S. D., et al. (2018). Diagnosis of Primary Ciliary Dyskinesia. An Official American Thoracic Society Clinical Practice Guideline. *Am. J. Respir. Crit. Care Med.* 197, e24–e39. doi:10.1164/rccm.201805-0819st

Shoemark, A., Moya, E., Hirst, R. A., Patel, M. P., Robson, E. A., Hayward, J., et al. (2018). High Prevalence of CCDC103 p.His154Pro Mutation Causing Primary Ciliary Dyskinesia Disrupts Protein Oligomerisation and Is Associated with Normal Diagnostic Investigations. *Thorax* 73, 157–166. doi:10.1136/thoraxjnl-2017-209999

Shoemark, A., Dell, S., Shapiro, A., and Lucas, J. S. (2019). ERS and ATS Diagnostic Guidelines for Primary Ciliary Dyskinesia: Similarities and Differences in Approach to Diagnosis. *Eur. Respir. J.* 54, 1901066. doi:10.1183/13993003.01066-2019

Southern, K. W., Munck, A., Pollitt, R., Travert, G., Zanolla, L., Dankert-Roelse, J., et al. (2007). A Survey of Newborn Screening for Cystic Fibrosis in Europe. *J. Cyst. Fibros.* 6, 57–65. doi:10.1016/j.jcf.2006.05.008

Stark, Z., Schofield, D., Martyn, M., Rynehart, L., Shrestha, R., Alam, K., et al. (2019). Does Genomic Sequencing Early in the Diagnostic Trajectory Make a Difference? A Follow-Up Study of Clinical Outcomes and Cost-Effectiveness. *Genet. Med.* 21, 173–180. doi:10.1038/s41436-018-0006-8

Tan, T. Y., Lunke, S., Chong, B., Phelan, D., Fanjul-Fernandez, M., Marum, J. E., et al. (2019). A Head-To-Head Evaluation of the Diagnostic Efficacy and Costs of Trio versus Singleton Exome Sequencing Analysis. *Eur. J. Hum. Genet.* 27, 1791–1799. doi:10.1038/s41431-019-0471-9

Tavtigian, S. V., Greenblatt, M. S., Harrison, S. M., Nussbaum, R. L., Prabhu, S. A., Boucher, K. M., et al. (2018). Modeling the ACMG/AMP Variant Classification Guidelines as a Bayesian Classification Framework. *Genet. Med.* 20, 1054–1060. doi:10.1038/gim.2017.210

Trost, B., Walker, S., Wang, Z., Thiruvahindrapuram, B., Macdonald, J. R., Sung, W. W. L., et al. (2018). A Comprehensive Workflow for Read Depth-Based Identification of Copy-Number Variation from Whole-Genome Sequence Data. *Am. J. Hum. Genet.* 102, 142–155. doi:10.1016/j.ajhg.2017.12.007

Tsang, M. H.-Y., Leung, G. K.-C., Ho, A. C.-C., Yeung, K.-S., Mak, C. C.-Y., Pei, S. L.-C., et al. (2019). Exome Sequencing Identifies Molecular Diagnosis in Children with Drug-Resistant Epilepsy. *Epilepsia Open* 4, 63–72. doi:10.1002/epi4.12282

Tsang, M. H. Y., Kwong, A. K. Y., Chan, K. L. S., Fung, J. L. F., Yu, M. H. C., Mak, C. C. Y., et al. (2020). Delineation of Molecular Findings by Whole-Exome Sequencing for Suspected Cases of Paediatric-Onset Mitochondrial Diseases in the Southern Chinese Population. *Hum. Genomics* 14, 28. doi:10.1186/s40246-020-00278-0

Wallmeier, J., Al-Mutairi, D. A., Chen, C.-T., Loges, N. T., Pennekamp, P., Menchen, T., et al. (2014). Mutations in CCNO Result in Congenital Mucociliary Clearance Disorder with Reduced Generation of Multiple Motile Cilia. *Nat. Genet.* 46, 646–651. doi:10.1038/ng.2961

Wang, K., Li, M., and Hakonarson, H. (2010). ANNOVAR: Functional Annotation of Genetic Variants from High-Throughput Sequencing Data. *Nucleic Acids Res.* 38, e164. doi:10.1093/nar/gkq603

Wheway, G., Thomas, N. S., Carroll, M., Coles, J., Doherty, R., Goggin, P., et al. (2021). Whole Genome Sequencing in the Diagnosis of Primary Ciliary Dyskinesia. *BMC Med. Genomics* 14, 234. doi:10.1186/s12920-021-01084-w

Yu, M. H. C., Chau, J. F. T., Au, S. L. K., Lo, H. M., Yeung, K. S., Fung, J. L. F., et al. (2020). Evaluating the Clinical Utility of Genome Sequencing for Cytogenetically Balanced Chromosomal Abnormalities in Prenatal Diagnosis. *Front. Genet.* 11, 620162. doi:10.3389/fgene.2020.620162

Zariwala, M. A., Knowles, M. R., and Leigh, M. W. (1993). "Primary Ciliary Dyskinesia," in *GeneReviews(®)*. Editors M. P. Adam, H. H. Ardinger, R. A. Pagon, S. E. Wallace, L. J. H. Bean, K. W. Gripp, et al. (Seattle (WA): University of Washington). Seattle Copyright © 1993-2021, University of Washington, Seattle. GeneReviews is a registered trademark of the University of Washington, Seattle. All rights reserved.

Zhu, M., Need, A. C., Han, Y., Ge, D., Maia, J. M., Zhu, Q., et al. (2012). Using ERDS to Infer Copy-Number Variants in High-Coverage Genomes. *Am. J. Hum. Genet.* 91, 408–421. doi:10.1016/j.ajhg.2012.07.004

Conflict of Interest: The authors declare that the research was conducted in the absence of any commercial or financial relationships that could be construed as a potential conflict of interest.

Publisher's Note: All claims expressed in this article are solely those of the authors and do not necessarily represent those of their affiliated organizations, or those of the publisher, the editors, and the reviewers. Any product that may be evaluated in this article, or claim that may be made by its manufacturer, is not guaranteed or endorsed by the publisher.

frontiers | Frontiers in Genetics

TYPE Original Research
PUBLISHED 19 August 2022
DOI 10.3389/fgene.2022.982127

OPEN ACCESS

EDITED BY
Steven LC Pei,
Yale University, United States

REVIEWED BY
Christian Hanna,
Mayo Clinic, United States
Wolfgang Baehr,
The University of Utah, United States

*CORRESPONDENCE
Hemant Khanna,
hemant.khanna@umassmed.edu,
hemant.khanna@ivericbio.com

†PRESENT ADDRESS
Laura Moreno-Leon,
Iveric Bio, Parsippany, NJ, United States
Hemant Khanna,
Iveric Bio, Parsippany, NJ, United States

SPECIALTY SECTION
This article was submitted to Human and Medical Genomics, a section of the journal Frontiers in Genetics

RECEIVED 30 June 2022
ACCEPTED 25 July 2022
PUBLISHED 19 August 2022

CITATION
Moreno-Leon L, Quezada-Ramirez MA, Bilsbury E, Kiss C, Guerin A and Khanna H (2022), Prenatal phenotype analysis and mutation identification of a fetus with meckel gruber syndrome. *Front. Genet.* 13:982127. doi: 10.3389/fgene.2022.982127

Prenatal phenotype analysis and mutation identification of a fetus with meckel gruber syndrome

Laura Moreno-Leon[1†], Marco A. Quezada-Ramirez[1], Evan Bilsbury[1], Courtney Kiss[2], Andrea Guerin[2] and Hemant Khanna[1*†]

[1]Department of Ophthalmology and Visual Sciences, UMass Chan Medical School, Worcester, MA, United States, [2]Kingston Health Sciences Centre, Queen's Medical School, Kingston, ON, Canada

Ciliopathies are a class of inherited severe human disorders that occur due to defective formation or function of cilia. The *RPGRIP1L* (retinitis pigmentosa GTPase regulator-interacting protein1-like) gene encodes for a ciliary protein involved in regulating cilia formation and function. Mutations in *RPGRIP1L* cause ciliopathies associated with severe embryonic defects, such as Meckel-Gruber Syndrome (MKS). Here we report *RPGRIP1L* mutation analysis in a family diagnosed with MKS. The clinical manifestations of the fetus included thoraco-lumbar open neural tube defect with associated Chiari type II malformation and hydrocephalus, bilateral club feet, and single right kidney/ureter. Analysis of the parental DNA samples revealed that the father carried a previously reported mutation R1236C/+ whereas the mother had a novel splice site mutation IVS6+1 G > A/+ in *RPGRIP1L*. The splice site mutation resulted in the exclusion of in-frame exon 6 of *RPGRIP1L* (RPGRIP1L-ΔEx6) but expressed a stable protein in fibroblasts derived from the parents' skin biopsies. The GFP-RPGRIP1L-ΔEx6 mutant protein exhibited relatively reduced ciliary localization in transiently-transfected cultured RPE-1 cells. Taken together, this study identifies a novel RPGRIP1L variant RPGRIP1L-ΔEx6, which in combination with RPGRIP1L-R1236C is associated with MKS. We also suggest that the deletion of exon 6 of RPGRIP1L leads to reduced ciliary localization of RPGRIP1L, indicating a plausible mechanism of associated disease.

KEYWORDS

cilia, ciliopathies, *RPGRIP1L*, meckel-gruber syndrome, ciliary defects

Introduction

Cilia are extracellular membrane extensions, which function primarily as sensors to mediate communication between the cell and the extracellular environment (Satir and Christensen, 2007). Disruptions to cilia or cilia anchoring structures leads to a group of pleiotropic genetic disorders called ciliopathies (Hildebrandt et al., 2011). These disorders are characterized by extreme genetic heterogeneity and phenotypic variety. Many of the phenotypic characteristics of these disorders are caused by the disruption of normal cilia function in the process of embryonic development (Eggenschwiler and Anderson, 2007).

Despite the identification of numerous genes involved in ciliopathies the role of these genes in disease is still being delineated.

Meckel syndrome (MKS) and Joubert syndrome (JBTS) are severe, recessive neurodevelopmental disorders caused by mutations in a variety of genes leading to defective primary cilia which disrupts the process of embryonic development (Brancati et al., 2010; Parelkar et al., 2013). Although they are clinically distinct syndromes, there is large genetic/allelic overlap between MKS and JBTS, as well as between these disorders and other ciliopathies such as Bardet-Biedl syndrome (BBS) (Baker and Beales, 2009; Szymanska et al., 2014). The most common clinical features of these disorders are rod-cone dystrophy, post axial polydactyly, neural tube defects (NTD) and renal/genitourinary malformations. The most severe, MKS, is the most common form of syndromic NTD and is neonatally lethal (Logan et al., 2011).

Mutations in 13 genes can account for 75% of all cases of MKS. Among these genes, the most strongly associated with MKS include *CEP290*, *MKS1* and *RPGRIP1L*. Retinitis pigmentosa GTPase regulator-interacting protein-1 like (*RPGRIP1L*), also known as *MKS-5* and *NPHP8*, is a ciliary protein that localizes to the base of the cilium and interacts with retinitis pigmentosa GTPase regulator (*RPGR*) (Arts et al., 2007; Khanna et al., 2009). Essential to the function of *RPGRIP1L* is its ability to localize to the base of the cilium where it controls ciliary gating by maintaining the amount of *CEP290* at the transition zone (TZ) (Wiegering et al., 2021). Disruption of these properties can lead to phenotypes encompassed by MKS and JBTS (Delous et al., 2007; Chen et al., 2011).

Here, we characterize a Canadian family of U.K (paternal) and presumed European descent (maternal) with a history of MKS carrying compound heterozygous variants in *RPGRIP1L*. Identification and characterization of these variations allows for an increased understanding of the pathophysiological processes leading to ciliary dysfunction in MKS and retinal degeneration.

Results

Clinical examination

Routine fetal anatomy ultrasound at 19 weeks revealed a large neural tube defect involving the thoracic spine, ventriculomegaly (measuring 11–15 mm), Chiari malformation, bilateral club feet and two vessel cord/single umbilical artery. Fetal kidneys, cavum septi pellcuidi and cisterna magna were unable to be visualized. Amniocentesis was pursued for genetic testing by way of QF-PCR for chromosomes 13, 18, 21 (normal) and sex chromosomes (consistent with a male fetus). Fetal chromosomal microarray analysis did not reveal any clinically significant copy number changes. Fetal whole exome sequencing (including submission of parental samples to perform trio analysis) revealed a paternally inherited *RPGRIP1L* variant c.706C > T/p.R1236C and a maternally inherited *RPGRIP1L* variant c.776 + 1G > A/IVS6 + 1G > A. No additional variants were reported including no American College of Medical Genetics and Genomics secondary findings. The pregnancy was terminated at 20 weeks 3 days gestation due to the presence of multiple fetal anomalies.

External physical examination of the fetus by geneticist was consistent with an open neural tube defect; mild 5th finger clinodactyly was also present. Fetal autopsy showed thoracolumbar region open neural tube defect, cerebellar tonsillar herniation/Chiari type II malformation, bilateral club feet, imperforate anus, single right kidney/ureter, single or fused midline adrenal gland and two umbilical vessels. Radiologial skeletal survey showed multiple formation/segmentation defects evident throughout the spine with widening/dysraphic change apparent within the lower thoracic lumbar and sacral regions. Neuropathological examination showed extensive thoraco-lumbar open neural tube defect with associated Chiari type II malformation and hydrocephalus. We specifically asked about the possibility of molar tooth sign given that this is often a finding in Joubert syndrome and related disorders; neuropathology was unable to confirm or rule out molar tooth sign upon further examination.

Genomic analysis of the *RPGRIP1L* gene in the family

Whole genome sequence analysis of the miscarried fetus identified two potentially disease-associated variants in *RPGRIP1L* (Supplementary Figure S1). The asymptomatic mother carried a heterozygous variant *RPGRIP1L* (NM_015272.2):IVS6+1G > A and the asymptomatic father was heterozygous for *RPGRIP1L* (NM_015272.2):c.3706C > T (R1236C). The fetus, on the other hand had compound heterozygous mutations possessing both variants (Figure 1A). While IVS6+1G > A is located at the donor splice-site between exon 6 (encoding a coiled-coil domain) and intron 6, c.3706C > T (R1236C) is located within the RPGR-interacting domain-like region of *RPGRIP1L* (Figure 1B).

RPGRIP1L expression analysis in fibroblasts

Point mutations in the 5′ donor (GT) or 3′ acceptor (AG) splice-sites can lead to either exon skipping or intron retention (Baralle, 2005). IVS6+1G > A is located at the exon-intron boundary between exon 6 and intron 6. Splice site prediction analysis revealed that the IVS6+1G > A mutation leads to the loss of the donor splice-site sequence motif by replacing the Guanine residue in the GT consensus sequence with an Adenosine residue (Supplementary Figure S2A). We hypothesized that loss of the 5′ donor splice-site at the 5′-end of intron 6 would lead to skipping of exon 6 (Figure 2A). To test this hypothesis, we

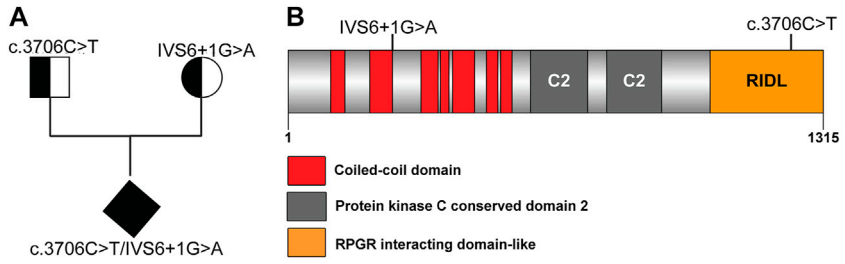

FIGURE 1
Novel *RPGRIP1L* mutation identified in an unborn fetus. **(A)** Pedigree of the family carrying *RPGRIP1L* mutations. **(B)** Schematic representation or the *RPGRIP1L* mutations reported in *RPGRIP1L* patients.

generated fibroblasts from skin biopsy specimens of the IVS6+1G > A/+ (mother) as well as control fibroblasts and examined the expression of *RPGRIP1L* mRNA using primer combinations encompassing the splice-site region (Supplementary Table S1 and Figure 2A). RT-PCR analysis using primer pair P1-P3 showed the expression of a shorter PCR product (160 bp) in addition to the expected WT–RPGRIP1L (wild type; ~304 bp) product. Sequence analysis of the shorter product revealed a deletion of exon 6 (RPGRIP1L-ΔEx 6) (Figure 2B). No change in the PCR profile of *RPGRIP1L* was observed in the R1236C/+ parent fibroblasts.

We next performed quantitative RT—PCR (qRT-PCR) analysis to ask whether the identified variants affect the mRNA levels of *RPGRIP1L* in parents' fibroblasts (Figure 2C). As predicted, mRNA was undetectable for the P5-P3 primer combination (encompassing the mutant transcript without exon 6) in the control and R1236C/+ fibroblasts. The wild-type and the mutant transcripts with primer pairs P5-P3 (mutant transcript) and P4-P3 (wild-type) were detected at 50% levels in the IVS6+1G > A/+ fibroblasts ($p \leq 0.0001$).

We then performed immunoblotting of protein extracts of parents' fibroblasts using an anti-*RPGRIP1L* antibody (Figure 2D). Bands corresponding to *RPGRIP1L*-ΔEx6 and *RPGRIP1L* were observed in the IVS6+1G > A/+ fibroblasts indicating the production of an aberrant shorter polypeptide. A single band, corresponding to the full-length *RPGRIP1L* protein was observed in the R1236C/+ fibroblasts. The specificity of the *RPGRIP1L* antibody was validated by immunoblotting using the HEK293 cells transiently transfected with plasmids encoding the GFP-fused *RPGRIP1L* WT and mutant proteins (Supplementary Figures S2B,C).

Ciliary localization of *RPGRIP1L*

RPGRIP1L has previously been shown to localize to the BB of cilia and function as a ciliary gatekeeper allowing only certain proteins to cross the TZ (Lin et al., 2018; Wiegering et al., 2021). To test if the observed variations in *RPGRIP1L* alter its ability to localize to the BB, we transiently transfected hTERT-RPE1 cells with plasmid DNA encoding GFP-fused *RPGRIP1L*-WT, RPGRIP1L-ΔEx6 or RPGRIP1L-R1236C followed by cilia growth and immunofluorescent staining using acetylated tubulin (AcTub; cilia marker), γ-tubulin (γ-Tub; BB marker), and GFP antibodies (Figure 3A). Consistent with previous reports (Arts et al., 2007), RPGRIP1L-WT and RPGRIP1L-R1236C co-localized with γ-Tub to the BB of the cilia in ~70% of the cells (arrows in Figure 3A). In contrast, BB localization of RPGRIP1L-ΔEx6 was detectable only in ~40% of the cells (Figure 3B; $p \leq 0.001$). Quantification of the BB/cytoplasm intensity ratio of *RPGRIP1L* showed ~80% reduction in the localization of RPGRIP1L-ΔEx6 at the BB ($p \leq 0.0001$) (Figure 3C). A statistically significant reduction ($p \leq 0.01$) in relative intensity ratio was also observed for RPGRIP1L-R1236C compared to RPGRIP1L-WT (Figure 3C).

Discussion

Several of the known ciliopathy-causing genes either contribute to a recessive form of the disease (such as in MKS) or modulate the penetrance and expressivity of other causative genes. The significant pleiotropy of *RPGRIP1L* is reflected by the multiple names (*MKS5*, *NPHP8*, *JBTS7*) by which it is referred to when involved in distinct disease processes of varying severity (Andreu-Cervera et al., 2021). Even within the spectrum of MKS, pleiotropy exists between different types of mutations; for example, while homozygous truncating mutations of *RPGRIP1L* typically produce MKS it has been shown that the presence of at least one missense mutation can modify the disease severity and lead to less severe and later onset disease (Reiter and Leroux, 2017). Homozygous missense mutations, frameshift, and splice-site mutations in *RPGRIP1L* have been reported in individuals with JBTS, another severe ciliopathy (Devuyst and Arnould, 2008). Additionally, polymorphic variation in *RPGRIP1L* has been shown to be a modifier of retinal

10.3389/fgene.2022.982127

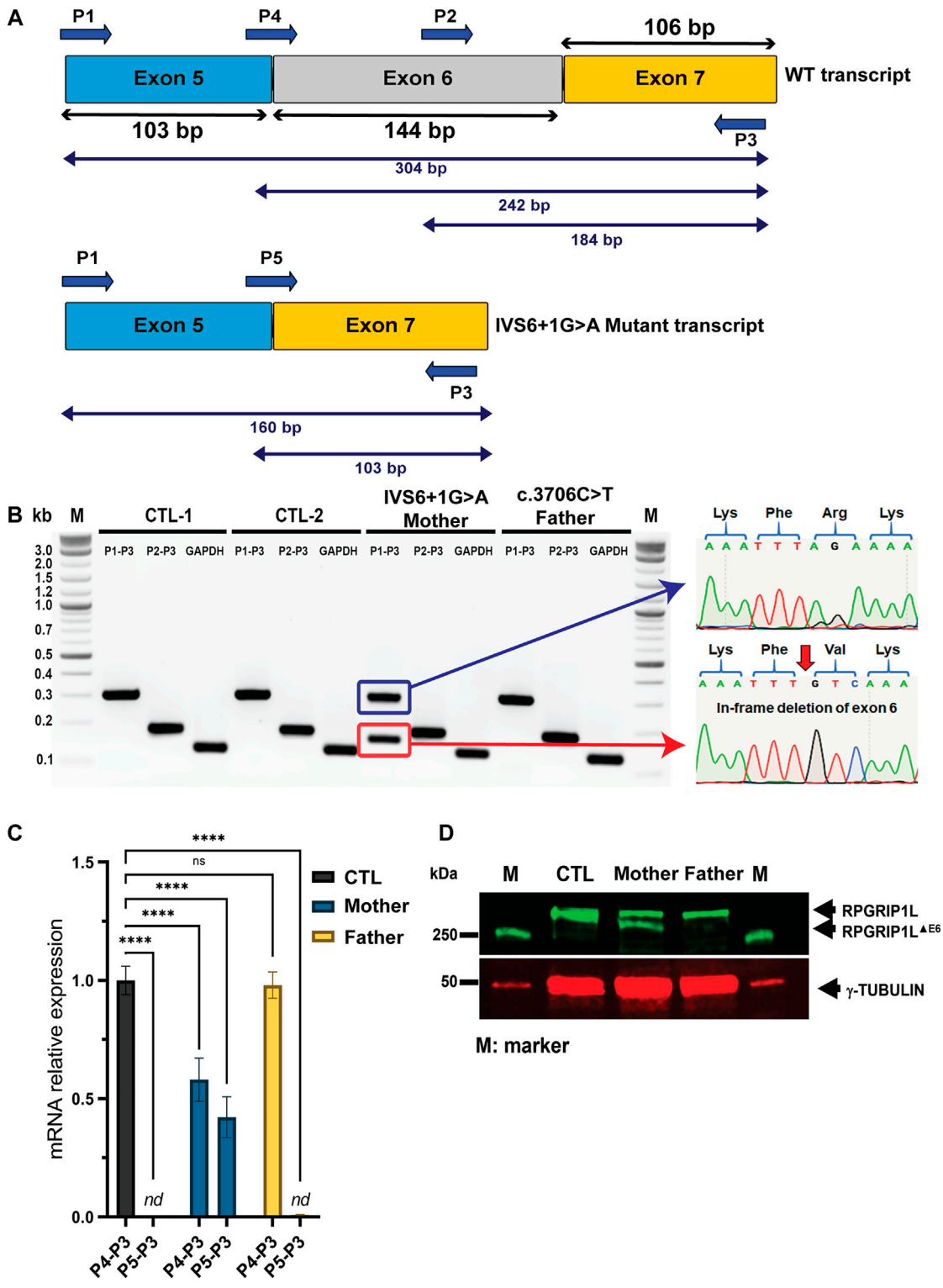

FIGURE 2
Molecular characterization of the novel *RPGRIP1L* IVG6+1G > A mutation in a Canadian family with frequent birth miscarriage. **(A)** Structure of the *RPGRIP1L* gene flanking the IVG6+1G > A mutation with exons size drawn to scale and predicted alternative splicing. Lower panel illustrates the anticipated exon 6 skipping. **(B)** RT-PCR analysis using the indicated primer combinations was performed using fibroblasts derived from the mother and father samples as well as two unrelated controls (CTL-1 and CTL-2) A shorter transcript (~160 bp; red box) was detected in the mother carrying the splice site variant. Sanger sequencing of the aberrant product confirmed the exclusion of exon 6. **(C)** Quantification of the exon 6-skipped *RPGRIP1L* isoform was performed by qRT-PCR analysis. The results are analyzed from three independent experiments. *nd*, *non detectable*. **(D)** Immunoblotting using *RPGRIP1L* antibody (green) and γ-tubulin (red) showing skipping of exon 6 (RPGRIP1L-ΔEx6) leads to the expression of an aberrant shorter polypeptide in the fibroblasts derived from the mother.

10.3389/fgene.2022.982127

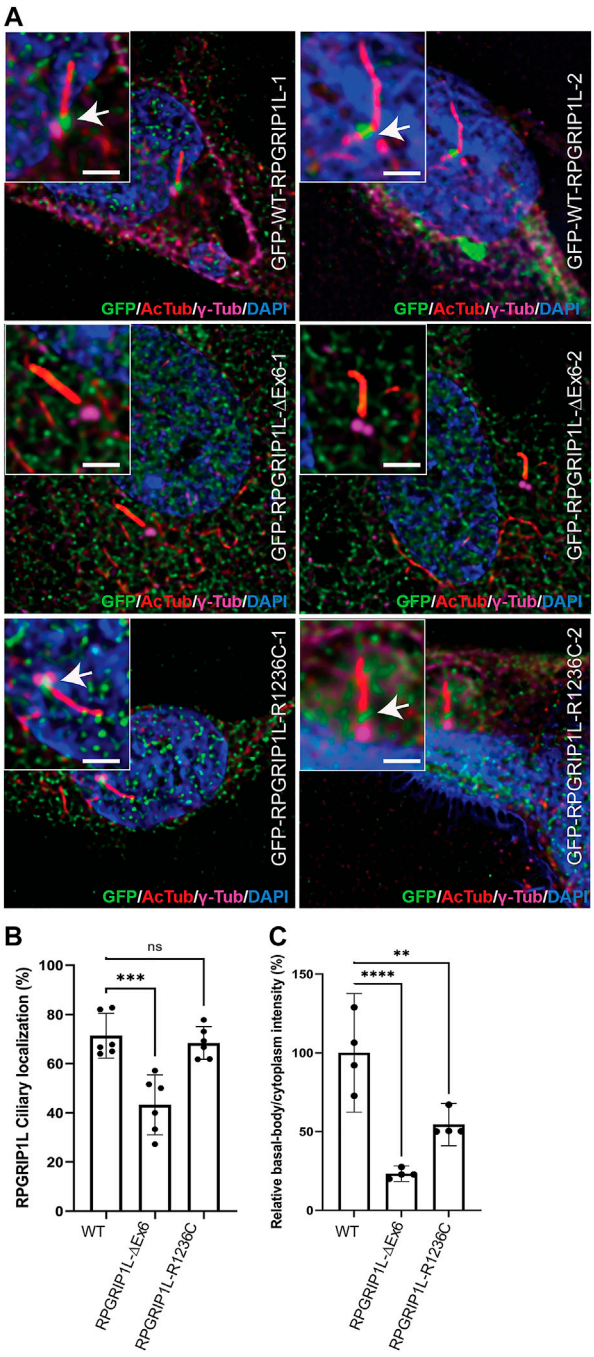

FIGURE 3
Ciliary distribution of the RPGRIP1L-WT-GFP, RPGRIP1L-ΔEx6-GFP and RPGRIP1L-R1236C-GFP in hTERT-RPE1 cells. **(A)** Immunostaining of the ciliary markers acetylated-tubulin (red) and γ-tubulin (magenta) showing the absence (RPGRIP1L-ΔEx6-GFP, green) or reduction (RPGRIP1L-R1236C-GFP, green) of the mutant *RPGRIP1L* localization at the cilia. Insets show the localization of *RPGRIP1L* to the proximal transition zone region of the cilium. Scale: 2 μm **(B)** Quantification of the ciliated cells with RPGRIP1 localization either to the basal body or to the transition zone showed significant reduction of RPGRIP1L-ΔEx6 at the cilia. **(C)** Quantification of *RPGRIP1L* intensity at the basal body compared to the cytoplasm showing a reduction of *RPGRIP1L* ciliary localization of both RPGRIP1L-ΔEx6 and RPGRIP1L-R1236C mutants.

degeneration in ciliopathies (Khanna et al., 2009). Understanding the molecular basis for the varying severity of these mutations is essential for the accurate prediction of phenotypes *via* genetic screenings in the future.

Exon 6 of *RPGRIP1L* encodes a coiled-coil domain. Coiled-coil domains have previously been shown to act as "tags" for oligomerization, notably, of the BBS2 and BBS7 subunits of the BBSome, which is an octameric protein complex involved in regulating protein trafficking at the basal body (BB) of primary cilia (Chou et al., 2019). The BBSome is thusly named because 7 of the eight proteins involved are known causes of Bardet-Biedl syndrome (BBS), another ciliopathy characterized by rod-cone dystrophy, polydactyly, and kidney dysfunction. In addition to this, the coiled-coil domain of exon 6 in *RPGRIP1L* has been shown to be necessary for the proper localization of CEP290 to the transition zone (Li et al., 2016).

Our results show that exon 6 is necessary for proper localization of *RPGRIP1L* to the TZ. There are 7 coiled-coil domains in the protein all of which may engage in oligomerization at the TZ. In *C. elegans*, it has been shown that MKS-5 (mammalian RPGRIP1L/RPGRIP1 orthologue) is crucial for the assembly of a ciliary transition zone and is required for the correct localization of all known *C. elegans* transition zone proteins (Jensen et al., 2015). Jensen et al. were able to demonstrate that the coiled-coil domains of *C. elegans* MKS-5 were, in fact, sufficient for transition zone localization of the protein through truncation studies. This suggests a similar role of the coiled-coil domain of exon 6 in human *RPGRIP1L*.

MKS displays an autosomal recessive (AR) inheritance pattern and parents are usually not aware that they are carriers until after they have an affected child. Once pathogenic variants have been identified in a family, it is possible to prenatally diagnose the disorder using chorionic villus sampling or amniocentesis (Watson et al., 2016). Alternatively, some families may proceed with assisted reproductive technologies such as *in vitro* fertilization with pre-implantation genetic testing for monogenic disease (IVF with PGT-M) to avoid having an affected pregnancy. However, the identification of pathogenic variants is often hindered by an incomplete understanding of the role of different alleles within previously identified causative MKS genes. Currently, the genetic and molecular mechanisms which lead to MKS are known in only ~60% of cases (Szymanska et al., 2012). It has been documented that in some cases, multiple allelism at a single locus or within a single gene can account for some of this phenotypic variability (Chang et al., 2006; Chen, 2007). Recently novel compound variants have been reported in CEP290 (Peng et al., 1935), and aggregating results regarding mutations in *MKS1* have resulted in a proposed genotype-phenotype correlation linking the severity of mutations and the domains affected to diagnoses of either MKS, JBTS or BBS (Leitch et al., 2008; Luo et al., 2020;

Lin et al., 2022). Further studies are needed to not only understand the genotype-phenotype correlation in ciliopathies but also formulate efficient genetic testing so that counseling can be provided to families predisposed to developing debilitating ciliopathies. Based on these results, the family was offered assisted reproductive technologies for future pregnancies. They are currently pursuing *in vitro* fertilization with egg donor. The family was counselled regarding all options, including PGT-M.

Methods

Study approval

The skin biopsies were obtained from *RPGRIP1L* patients and previously published unaffected individuals after written informed consent. Written consent was obtained from the family for publication. All procedures followed the Declaration of Helsinki and approved by the Institutional Review Board of the University of Toronto and UMass Chan Medical School.

Plasmid DNA constructs

Plasmids encoding human WT or mutated *RPGRIP1Ls* were obtained with cDNA synthesized from parental skin biopsies using SuperScript™ First-Strand Synthesis System for RT-PCR (Life Technologies). The *RPGRIP1L* coding region was amplified with PrimerSTAR GXL polymerase (Takara) and directly cloned into pMiniT vector (New England Biolabs). The thermal cycle setting was: 98°C for 2 min (activation), 98°C for 10 s and 68°C for 6 min (annealing/extension), for a total 40 cycles. Subsequenlty, *RPGRIP1L* was subcloned into pEGFP-C1 to express N-terminal GFP-tagged proteins under the control of CMV promoter. Primer details are provided in Supplementary Table S1.

Fibroblast isolation, cell culture and transient transfection

The skin biopsies were dissociated as previously described to obtain primary fibroblasts (Shimada et al., 2017; Moreno-Leon et al., 2020). Briefly, biopsies were washed in iodine followed by three washes in phosphate-buffered saline (Invitrogen). The sample was minced with a sharp scalpel in a culture plate and incubated with Dulbecco's-modified Eagle's medium (DMEM)/F12 (Gibco) supplemented with 20% fetal bovine serum (FBS) (Sigma-Aldrich, Saint-Louis, MO, United States), penicillin and streptomycin at 37°C in a humidified 5% CO2 incubator. Ten days after harvesting, the skin was removed, and fibroblasts were passaged for storage and analysis.

Dissociated primary fibroblasts and hTERT-RPE1 cells (ATCC, CRL-4000) were grown in DMEM/F12 media (Gibco) while HEK293 cells were grown in DMEM media (Gibco), 1% Sodium Pyruvate. All cells were supplemented with 10% FBS (Sigma-Aldrich, Saint-Louis, MO, United States) and grown at 37°C and 5% CO_2 incubator. All analyses were done in the fibroblasts at the same passage stages.

Plasmid DNA transfections were performed using Lipofectamine 2000 (Invitrogen) in HEK293 cells and FuGENE 6 (Promega) in hTERT-RPE1 cells at a 3:1 Transfection Reagent: DNA ratio according to the manufacturer's protocol.

RNA extraction and quantitative reverse transcriptase-polymerase chain reaction analysis

Total RNAs were isolated from primary fibroblasts with QIAzol Lysis Reagent (Qiagen) and precipitated according to the manufacturer's instructions. Reverse transcription was performed with 1 µg of total RNAs using the SuperScript™ First-Strand Synthesis System for RT-PCR (Invitrogen). The resulting cDNA was used to perform DNA amplification using PrimeStar GXL DNA polymerase (Takara) according to manufacturer's instruction. Alternative splicing defects were analyzed by agarose gel electrophoresis. Gene expression analysis was performed using the BioRad CFX96 qPCR instrument and Power SYBR Green PCR Master Mix (Thermo Fisher Scientific). All RT-PCR and RT-qPCR primers are described in Supplementary Table S1.

Immunoblotting

The cells were lyzed on ice in Pierce RIPA Buffer (Thermo Scientific) containing Halt™ Protease Inhibitor Cocktail (100X, Thermo Fisher). Lysates were sonicated and centrifugated at 12 000 g for 15 min. Supernatants were quantified and 20 µg of total protein lysate was incubated for 5 min at 95°C with Laemmli sample buffer. Proteins were separated on a 4–20% Mini-PROTEAN® TGX™ Precast Protein Gel (BioRad) and transferred to a nitrocellulose membrane (BioRad). The blots were processed using LI-COR western blotting instructions and blocking, and primary and secondary antibodies solutions were prepared in Intercept Blocking buffer (LI-COR). Primary antibodies were incubated overnight at 4°C and secondary antibodies were incubated at room temperature for 2 h (Supplementary Table S2 for antibodies details and dilution information). Protein expression was detected using LI-COR Odyssey Fc detection system.

Immunofluorescence, microscopy and co-localization analysis

The primary fibroblasts and hTERT-RPE1 cells were plated at 90% confluency on coverslips (AmScope CS-R18-100). Primary fibroblasts were serum-starved for 48 h, 24 h after plating. hTERT-RPE1 cells were serum-starved 24 h post-transfection for 24 h. Cells were fixed in 4% paraformaldehyde/1X Dulbecco's phosphate-buffered saline (DPBS; potassium chloride 0.2 g/L, potassium dihydrogen phosphate 0.2 g/L, sodium chloride 8 g/L and disodium hydrogen phosphate 1.15 g/L) for 10 min, washed three times in DPBS and blocked in DPBS containing 5% normal goat serum and 0.5% Triton X-100 for 1 h. Primary antibody solution was prepared in blocking solution and incubated overnight at 4°C. After washing in DPBS, cells were incubated in blocking solution containing Alexa-488-conjugated and Alexa-546-conjugated (Invitrogen) for 1 h. Finally, cells were washed in DPBS and incubated for 5 min with DAPI for nuclear staining. Coverslips were mounted with Antifade Mounting Media (Vectashield) and all images were visualized over ×63 objective using a Leica DM6 Thunder microscope with a 16-bit monochrome camera.

The IMARIS platform was used to process the two channel intensities simultaneously and to measure the degree of overlap of the two channels. After setting intensity threshold, the basal body marker γ-tubulin was used to define a region of interest and a co-localization channel was built on different z-stacks to obtain the percentage of co-localized signal and intensity. When needed, adjacent optical sections were merged in the *z*-axis to form a projected image (ImageJ). Signal intensity and Co-localization values were plotted using the GraphPad Prism software.

Statistics

All data are presented as means ± standard derivation from the mean. Two groups comparison was analyzed by Student's t-tests using the Prism GraphPad software. Multiple groups comparison was performed with one-way analysis of variance. Differences between groups were considered statistically significant if $p < 0.05$. The statistical significance is denoted with asterisks ($*p < 0.05$; $**p < 0.01$; $***p < 0.005$; $****p < 0.001$).

Data availability statement

The original contributions presented in the study are included in the article/Supplementary Material, further inquiries can be directed to the corresponding author.

Ethics statement

The studies involving human participants were reviewed and approved by Kingston Health Science Center. The patients/participants provided their written informed consent to participate in this study.

Author contributions

CK, AG, and HK conceived the study; LM-L, MQ-R, and EB performed the experiments; CK and AG collected patient data; LM-L, MQ-R, EB, CK, AG, and HK wrote the paper.

Funding

This work was supported by a grant from the NIH EY022372 to HK.

Acknowledgments

The authors thank the patients for their generosity and willingness to participate in the study. We also thank the members of the Khanna lab for their support and critique.

Conflict of interest

The authors declare that the research was conducted in the absence of any commercial or financial relationships that could be construed as a potential conflict of interest.

Publisher's note

Supplementary material

The Supplementary Material for this article can be found online at: https://www.frontiersin.org/articles/10.3389/fgene.2022.982127/full#supplementary-material

References

Andreu-Cervera, A., Catala, M., and Schneider-Maunoury, S. (2021). Cilia, ciliopathies and hedgehog-related forebrain developmental disorders. *Neurobiol. Dis.* 150, 105236. doi:10.1016/j.nbd.2020.105236

Arts, H. H., Doherty, D., van Beersum, S. E., Parisi, M. A., Letteboer, S. J., Gorden, N. T., et al. (2007). Mutations in the gene encoding the basal body protein RPGRIP1L, a nephrocystin-4 interactor, cause Joubert syndrome. *Nat. Genet.* 39, 882–888. doi:10.1038/ng2069

Baker, K., and Beales, P. L. (2009). Making sense of cilia in disease: the human ciliopathies. *Am. J. Med. Genet. C Semin. Med. Genet.* 151C, 281–295. doi:10.1002/ajmg.c.30231

Baralle, M. B. D. (2005). Splicing in action: assessing disease causing sequence changes. *J. Med. Genet.* 42, 737–748. doi:10.1136/jmg.2004.029538

Brancati, F., Dallapiccola, B., and Valente, E. M. (2010). Joubert Syndrome and related disorders. *Orphanet J. Rare Dis.* 5, 20. doi:10.1186/1750-1172-5-20

Chang, B., Khanna, H., Hawes, N., Jimeno, D., He, S., Lillo, C., et al. (2006). In-frame deletion in a novel centrosomal/ciliary protein CEP290/NPHP6 perturbs its interaction with RPGR and results in early-onset retinal degeneration in the rd16 mouse. *Hum. Mol. Genet.* 15, 1847–1857. doi:10.1093/hmg/ddl107

Chen, J., Smaoui, N., Hammer, M. B. H., Jiao, X., Riazuddin, S. A., Harper, S., et al. (2011). Molecular analysis of bardet-biedl syndrome families: report of 21 novel mutations in 10 genes. *Invest. Ophthalmol. Vis. Sci.* 52, 5317–5324. doi:10.1167/iovs.11-7554

Chen, C.-P. (2007). Meckel syndrome: genetics, perinatal findings, and differential diagnosis. *Taiwan. J. Obstet. Gynecol.* 46, 9–14. doi:10.1016/S1028-4559(08)60100-X

Chou, H.-T., Apelt, L., Farrell, D. P., White, S. R., Woodsmith, J., Svetlov, V., et al. (2019). The molecular architecture of native BBSome obtained by an integrated structural approach. *Structure* 27, 1384–1394.e4. doi:10.1016/j.str.2019.06.006

Delous, B. L. M., Salomon, R., Laclef, C., Vierkotten, J., Tory, K., Golzio, C., et al. (2007). The ciliary gene RPGRIP1L is mutated in cerebello-oculo-renal syndrome (Joubert syndrome type B) and Meckel syndrome. *Nat. Genet.* 39, 875–881. doi:10.1038/ng2039

Devuyst, O., and Arnould, V. J. (2008). Mutations in RPGRIP1L : extending the clinical spectrum of ciliopathies. *Nephrol. Dial. Transpl.* 23, 1500–1503. doi:10.1093/ndt/gfn033

Eggenschwiler, J. T., and Anderson, K. V. (2007). Cilia and developmental signaling. *Annu. Rev. Cell Dev. Biol.* 23, 345–373. doi:10.1146/annurev.cellbio.23.090506.123249

Hildebrandt, F., Benzing, T., and Katsanis, N. (2011). Ciliopathies. *N. Engl. J. Med.* 364, 1533–1543. doi:10.1056/nejmra1010172

Jensen, V. L., Li, C., Bowie, R. V., Clarke, L., Mohan, S., Blacque, O. E., et al. (2015). Formation of the transition zone by Mks5/Rpgrip1L establishes a ciliary zone of exclusion (CIZE) that compartmentalises ciliary signalling proteins and controls PIP2 ciliary abundance. *EMBO J.* 34, 2537–2556. doi:10.15252/embj.201488044

Khanna, H., Davis, E., Murga-Zamalloa, C., Estrada-Cuzcano, A., Lopez, I., den Hollander, A. I., et al. (2009). A common allele in RPGRIP1L is a modifier of retinal degeneration in ciliopathies. *Nat. Genet.* 41, 739–745. doi:10.1038/ng.366

Leitch, C. C., Davis, E. E., Stoetzel, C., Diaz-Font, A., Rix, S., Alfadhel, M., et al. (2008). Hypomorphic mutations in syndromic encephalocele genes are associated with Bardet-Biedl syndrome. *Nat. Genet.* 40, 443–448. doi:10.1038/ng.97

Li, C., Jensen, V. L., Park, K., Kennedy, J., Garcia-Gonzalo, F. R., Romani, M., et al. (2016). MKS5 and CEP290 dependent assembly pathway of the ciliary transition zone. *PLoS Biol.* 14, e1002416. doi:10.1371/journal.pbio.1002416

Lin, H., Guo, S., and Dutcher, S. K. (2018). RPGRIP1L helps to establish the ciliary gate for entry of proteins. *J. Cell Sci.* 131, jcs220905. doi:10.1242/jcs.220905

Lin, T., Ma, Y., Zhou, D., Sun, L., Chen, K., Xiang, Y., et al. (2022). Case report: preimplantation genetic testing for Meckel syndrome induced by novel compound heterozygous mutations of MKS1. *Front. Genet.* 13, 843931. doi:10.3389/fgene.2022.843931

Logan, C. V., Abdel-Hamed, Z., and Johnson, C. A. (2011). Molecular genetics and pathogenic mechanisms for the severe ciliopathies: insights into neurodevelopment and pathogenesis of neural tube defects. *Mol. Neurobiol.* 43, 12–26. doi:10.1007/s12035-010-8154-0

Luo, M., He, R., Lin, Z., Shen, Y., Zhang, G., Cao, Z., et al. (2020). Novel compound heterozygous variants in MKS1 leading to Joubert Syndrome. *Front. Genet.* 11, 576235. doi:10.3389/fgene.2020.576235

Moreno-Leon, L., West, E. L., O'Hara-Wright, M., Li, L., Nair, R., He, J., et al. (2020). RPGR isoform imbalance causes ciliary defects due to exon ORF15 mutations in X-linked retinitis pigmentosa (XLRP). *Hum. Mol. Genet.* 29, 3706–3716. doi:10.1093/hmg/ddaa269

Parelkar, K. S. S. V., Sanghvi, B. V., Joshi, P. B., Mundada, D., and Oak, S. N. (2013). Meckel-gruber syndrome: a rare and lethal anomaly with review of literature. *J. Pediatr. Neurosci.* 8, 154–157. doi:10.4103/1817-1745.117855

Peng, M., Han, S., Sun, J., He, X., Lv, Y., and Yang, L. (1935). Evaluation of novel compound variants of CEP290 in prenatally suspected case of Meckel syndrome through whole exome sequencing. *Mol. Genet. Genomic Med.* 10, e1935. doi:10.1002/mgg3.1935

Reiter, J. F., and Leroux, M. R. (2017). Genes and molecular pathways underpinning ciliopathies. *Nat. Rev. Mol. Cell Biol.* 18, 533–547. doi:10.1038/nrm.2017.60

Satir, P., and Christensen, S. T. (2007). Overview of structure and function of mammalian cilia. *Annu. Rev. Physiol.* 69, 377–400. doi:10.1146/annurev.physiol.69.040705.141236

Shimada, H., Lu, Q., Insinna-Kettenhofen, C., Nagashima, K., English, M. A., Semler, E. M., et al. (2017). *In vitro* modeling using ciliopathy-patient-derived cells reveals distinct cilia dysfunctions caused by CEP290 mutations. *Cell Rep.* 20, 384–396. doi:10.1016/j.celrep.2017.06.045

Szymanska, K., Berry, I., Logan, C. V., Cousins, S. R., Lindsay, H., Jafri, H., et al. (2012). Founder mutations and genotype-phenotype correlations in Meckel-Gruber syndrome and associated ciliopathies. *Cilia* 1, 18–8. doi:10.1186/2046-2530-1-18

Szymanska, K., Hartill, V. L., and Johnson, C. A. (2014). Unraveling the genetics of Joubert and meckel-gruber syndromes. *J. Pediatr. Genet.* 3, 65–78. doi:10.3233/PGE-14090

Watson, C. M., Crinnion, L. A., Berry, I. R., Harrison, S. M., Lascelles, C., Antanaviciute, A., et al. (2016). Enhanced diagnostic yield in Meckel-Gruber and Joubert syndrome through exome sequencing supplemented with split-read mapping. *BMC Med. Genet.* 17, 1–9. doi:10.1186/s12881-015-0265-z

Wiegering, A., Dildrop, R., Vesque, C., Khanna, H., Schneider-Maunoury, S., and Gerhardt, C. (2021). Rpgrip1l controls ciliary gating by ensuring the proper amount of Cep290 at the vertebrate transition zone. *Mol. Biol. Cell* 32, 675–689. doi:10.1091/mbc.E20-03-0190

frontiers | Frontiers in Genetics

TYPE Original Research
PUBLISHED 13 September 2022
DOI 10.3389/fgene.2022.1009430

OPEN ACCESS

EDITED BY
Steven L. C. Pei,
School of Medicine, Yale University,
United States

REVIEWED BY
Naoyuki Tanimoto,
University of Kiel, Germany
Brian Perkins,
Cole Eye Institute, Cleveland Clinic,
United States

*CORRESPONDENCE
Gabrielle Wheway,
G.wheway@soton.ac.uk

SPECIALTY SECTION
This article was submitted to Human and Medical Genomics, a section of the journal Frontiers in Genetics

RECEIVED 01 August 2022
ACCEPTED 19 August 2022
PUBLISHED 13 September 2022

CITATION
Nazlamova L, Villa Vasquez SS, Lord J, Karthik V, Cheung M-K, Lakowski J and Wheway G (2022), Microtubule modification defects underlie cilium degeneration in cell models of retinitis pigmentosa associated with pre-mRNA splicing factor mutations. *Front. Genet.* 13:1009430. doi: 10.3389/fgene.2022.1009430

Microtubule modification defects underlie cilium degeneration in cell models of retinitis pigmentosa associated with pre-mRNA splicing factor mutations

Liliya Nazlamova[1], Suly Saray Villa Vasquez[1], Jenny Lord[1], Varshini Karthik[1], Man-Kim Cheung[2], Jörn Lakowski[3] and Gabrielle Wheway[1]*

[1]Human Development and Health, Faculty of Medicine, University of Southampton, Southampton, United Kingdom, [2]Centre for Research in Biosciences, University of the West of England, Bristol, United Kingdom, [3]Clinical and Experimental Sciences, Faculty of Medicine, University of Southampton, Southampton, United Kingdom

Retinitis pigmentosa (RP) is the most common cause of hereditary blindness, and may occur in isolation as a non-syndromic condition or alongside other features in a syndromic presentation. Biallelic or monoallelic mutations in one of eight genes encoding pre-mRNA splicing factors are associated with non-syndromic RP. The molecular mechanism of disease remains incompletely understood, limiting opportunities for targeted treatment. Here we use CRISPR and base edited *PRPF6* and *PRPF31* mutant cell lines, and publicly-available data from human *PRPF31*$^{+/-}$ patient derived retinal organoids and *PRPF31* siRNA-treated organotypic retinal cultures to confirm an enrichment of differential splicing of microtubule, centrosomal, cilium and DNA damage response pathway genes in these cells. We show that genes with microtubule/centrosome/centriole/cilium gene ontology terms are enriched for weak 3′ and 5′ splice sites, and that subtle defects in spliceosome activity predominantly affect efficiency of splicing of these exons. We suggest that the primary defect in *PRPF6* or *PRPF31* mutant cells is microtubule and centrosomal defects, leading to defects in cilium and mitotic spindle stability, with the latter leading to DNA damage, triggering differential splicing of DNA damage response genes to activate this pathway. Finally, we expand understanding of "splicing factor RP" by investigating the function of *TTLL3*, one of the most statistically differentially expressed genes in *PRPF6* and *PRPF31* mutant cells. We identify that *TTLL3* is the only tubulin glycylase expressed in the human retina, essential for monoglycylation of microtubules of the cilium, including the retinal photoreceptor cilium, to prevent cilium degeneration and retinal degeneration. Our preliminary data suggest that rescue of tubulin glycylation through overexpression of *TTLL3* is sufficient to rescue cilium number in *PRPF6* and *PRPF31* mutant cells, suggesting that this defect underlies the cellular defect

and may represent a potential target for therapeutic intervention in this group of disorders.

KEYWORDS

cilia, ciliopathies, retinitis pigmentosa, pre-mRNA splicing, photoreceptor

1 Introduction

Retinitis pigmentosa (RP) (OMIM#268000) is the most common cause of hereditary blindness, affecting 1:2000 to 1: 5000 people worldwide (Sharon and Banin, 2015; Verbakel et al., 2018). It is a progressive retinal dystrophy which is characterised by night blindness with restriction of peripheral vision developing into tunnel vision due to dysfunction of the rod photoreceptors of the retina. Later in the disease cones are also affected leading to loss of central and colour vision. Symptoms generally begin to develop in early adulthood, although age and rate of onset is variable, linked to some extent to the genetic lesion associated with the disease. It is inherited in a recessive, dominant and X-linked pattern, depending on the gene mutated in the affected individual.

RP occurs in isolation as a non-syndromic condition, or in combination with other clinical features as part of syndromes such as Usher's syndrome (USH), Bardet-Biedl syndrome (BBS) and Joubert syndrome (JS). More than 70 genes are known to cause non-syndromic RP and around 200 genes have been associated with the syndromic and non-syndromic forms of the disease collectively. Around one third of genetic subtypes of RP are associated with defects in primary cilia, the cells' signalling organelle (Estrada-Cuzcano et al., 2012; Bujakowska et al., 2017), and retinal dystrophies are a common feature of syndromic ciliopathies, diseases associated with defects in cilia. This is due to the presence of highly specialised ciliated cells in the retina; the photoreceptors. The outer segment of the rod and cone photoreceptor is considered to be a highly modified primary cilium (Oud et al., 2017). This structure is anchored at the base by a gamma tubulin basal body, from which extends the backbone of the cilium, the alpha- and beta-tubulin axoneme. Unlike the microtubules of the dynamic cytoskeleton, the axonemal microtubules are stable, and this stability is achieved through multiple post-translational modifications including acetylation, tyrosination, glutamylation and glycylation.

Non syndromic RP can also be caused by biallelic or monoallelic mutations in one of eight pre-mRNA splicing factors; *PRPF3* (Chakarova et al., 2002), *PRPF4* (Chen et al., 2014; Linder et al., 2014), *PRPF6* (Tanackovic et al., 2011), *PRPF8* (McKie et al., 2001), *PRPF31* (Vithana et al., 2001), *SNRNP200* (Zhao et al., 2009), *RP9* (*PAP1*) (Keen et al., 2002), *DHX38* (*PRPF16*) (Ajmal et al., 2014). Mutations in *PRPF8* and *PRPF31* each account for roughly 2% of cases of RP, *PRPF3* mutations account for around 1% of cases (Sullivan et al., 2006), and *SNRNP200* mutations are found in 1.6% of autosomal dominant RP patients (Bowne et al., 2013). *PRPF4*, *PRPF6*, *RP9* and *DHX38* mutations are rarer causes of RP. Collectively mutations in pre-mRNA splicing factor proteins are the second most common cause of autosomal dominant RP (Wheway et al., 2020). These proteins are all components of, or associated with, the U4/U6.U5 small nuclear ribonucleoprotein (tri-snRNP), a core component of the spliceosome, the huge molecular machine which catalyses splicing (Will and Luhrmann, 2011). Nearly all eukaryotic genes are spliced, and this process occurs in all cells which transcribe and express proteins. As a result it was a very unexpected discovery that mutations in these genes should cause a phenotype restricted to the retina, and for many years the molecular disease mechanism has remained poorly understood. Early work suggested that mutations in splicing factors cause spliceosome assembly or activity defects (Wilkie et al., 2006; Frio et al., 2008; Wilkie et al., 2008; Huranova et al., 2009; Yin et al., 2011), and higher demand for splicing, with concomitant higher expression of splicing factors, in the retina explains why only this tissue manifests disease in patients (Cao et al., 2011). However, studies of cells from human patients with PRPF mutations showed variable effects on splicing (Ivings et al., 2008; Wilkie et al., 2008). An alternative theory proposed was that transcripts of retinal-specific genes are more severely affected by splicing factor mutations than other groups of genes (Yuan et al., 2005; Mordes et al., 2007; Linder et al., 2011; Yin et al., 2011; Liu et al., 2015). This was supported by findings that different gene-specific splicing defects result from mutation of different core spliceosomal proteins (Pleiss et al., 2007; Papasaikas et al., 2015; Wickramasinghe et al., 2015). Another alternative model proposed that there are no splicing-related defects in this form of RP, and that the disease manifests due to the protein-folding response as mutant proteins aggregate in cells, which is more pronounced in retina due to UV-induced photooxidative damage (Comitato et al., 2007; Shinde et al., 2016). Oxidative stress has been shown in photoreceptor cultures derived from induced pluripotent stem cells (iPSCs) from RP patients with mutations in RP9 (Jin et al., 2011) and other work links the ischaemia-hypoxia response proteins to splicing factors (Schmidt-Kastner et al., 2008). Modelling retinal disease has advanced with the ability to culture retinal organoids from human patient-derived iPSCs. Prior to this the lack of clarity of disease mechanism in splicing factor RP was complicated by a lack of good mammalian models.

Some Prpf knock-in and knock-out mice show no RP phenotype (Graziotto et al., 2008; Bujakowska et al., 2009; Graziotto et al., 2011), others show very late onset RPE defects, which could be confused with general age-related retinal defects (Graziotto et al., 2011; Farkas et al., 2014).

In 2015 a hypothesis-neutral high-throughput high-content siRNA knockdown screen designed to identify all proteins required for normal primary cilium structure and function revealed a major unexpected insight into pre-mRNA splicing factors and primary cilia. This work showed that a significant number of proteins involved in splicing including pre-mRNA splicing factors PRPF6, 8 and 31, are required for normal cilium growth and function, and that when these proteins are lost, there are profound effects on ciliogenesis (Wheway et al., 2015). Immunofluorescence imaging showed that PRPF6, PRPF8 and PRPF31 localise to the base of the cilium in mouse- and human-derived ciliated cell lines, consistent with earlier findings that a range of splicing factors, including PRPF8, interact with 32 known centrosomal proteins in a large-scale centrosomal proteomics study (Jakobsen et al., 2011). Immunoelectron microscopy showed that PRPF6 and PRPF8 localize to the apical inner segment, basal body complex, apical connecting cilium of photoreceptor cells and postsynapse of secondary retinal neurons. Fibroblasts from human patients with frame-shift deletion mutation in *PRPF31* exhibited cilia defects, with shorter and/or fewer cilia than controls. A *C. elegans prpf8* null mutant had a partial ciliogenesis defect, with truncated or fewer microtubules in the amphid channel sensory cilia. Collectively, these data suggest that these forms of RP associated with PRPF6, 8 and 31 mutations are retinal ciliopathies (Wheway et al., 2015). The observation of pre-mRNA splicing factor at the base of the cilium led some investigators to speculate whether these proteins have specific roles in RNA metabolism at this subcellular localisation, independent of their role in splicing, and that defects in these specific cilia functions underlie disease (Johnson and Malicki, 2019). This hypothesis has been strengthened by the recent findings that mRNAs are localised to the base of the cilium for localised translation of ciliary mRNAs into protein (Iaconis et al., 2017; Hao et al., 2021). Nucleo-cytoplasmic shuttling of an accessory splicing factor is required for development and cilia function, further suggesting that core pre-mRNA splicing factors may be involved in a similar process, moving between the nucleus and base of the cilium to control which mRNAs are expressed in the cilium in a highly time-dependent manner (Haward et al., 2021). In a further publication, protein interaction data showed that PRPF6, 8 and 31 interact with many proteins involved in processes beyond splicing, including translation, mRNA stability, mRNA export and DNA damage response (Boldt et al., 2016), further suggestion that these proteins have roles in addition to splicing and that it may be dysregulation of these functions which underlie RP. Indeed, PRPF31 has subsequently been shown to play a direct role in mitotic chromosome segregation, through binding to kinetochore and centromere components (Pellacani et al., 2018), which has impacts on mitotic progression and differentiation of retinal progenitor cells in zebrafish (Li et al., 2021). This stall in mitotic progression leads to accumulation of DNA damage in Prpf31 crispant zebrafish retinal progenitors, exacerbated by enrichment of mis-splicing of DNA damage repair pathway transcripts (particularly those with weak 5′ splice sites) in these mutants, leading to apoptosis (Li et al., 2021). Depletion of PRPF8 has similarly been shown to lead to defects in mitotic progression, with specific defects in splicing of transcripts involved in mitotic progression, especially those with weak 5′ splice sites (Wickramasinghe et al., 2015).

Further study in human iPSC-derived retinal organoids and retinal pigment epithelium (RPE) from patients with *PRPF31* mutations showed decreased efficiency of splicing in an E1A minigene reporter assay (Buskin et al., 2018). RPE from patient iPSCs also showed a substantial downregulation of SART1, a U5 snRNP protein important for the formation of the pre-catalytic spliceosomal B complex, but no changes in the expression of PRPF8 or PRPF4. Retinal organoids from patients showed differential expression of actin cytoskeleton, ciliary membrane, primary cilium, photoreceptor inner and outer segment, axon terminal and phototransduction proteins. Retinal organoids from patients with *PRPF31* mutations showed an enrichment of mis-spliced centriole and microtubule organisation genes, with skipped exons, retained introns, alternative 5′ and 3′ splice sites, and mutually exclusive exons. In both RPE and retinal organoids derived from $PRPF31^{-/-}$ patients, the most significantly mis-spliced genes were genes involved in pre-mRNA and alternative mRNA splicing via the spliceosome. This suggests that ciliogenesis, cilium function, and pre-mRNA splicing are all regulated by alternative splicing in the retina, and this is defective in patients carrying *PRPF31* mutations (Buskin et al., 2018).

To further resolve the function of pre-mRNA splicing factors in regulating ciliogenesis and cilium stability in the retina we generated clonal CRISPR and base edited cell lines for study of cilia, protein and splicing in these cell models of human disease.

2 Materials and methods

2.1 Cell culture

Wild-type and $PRPF31^{+/-}$ (heterozygous NC_000019.10: g.54123455_54123456insA (NM_015629.4:c.422_423insA) (p.Glu141fs)) (Nazlamova et al., 2020) hTERT-RPE1 cells (ATCC CRL-4000) were cultured in DMEM/F12 (50:50 mix) + 10% FCS at 37°C, 5% CO_2, and split at a ratio of 1:8 once per week. Wild-type and $PRPF6^{+/c.2185C>T}$ (described below) HEK293 cells (ATCC CRL-1573) were cultured in high glucose DMEM) + 10% FCS at 37°C, 5% CO_2, and split at a

ratio of 1:8 once per week. Cells were routinely tested for mycoplasma infection using a PCR-based method.

2.2 Base editing

We removed cas9/GFP from PX461 (Addgene #48140) (Ran et al., 2013) and replaced with GFP/Zeocin from pTRACER-EF/V5-His A (Life Technologies). GFP/Zeocin expression was controlled by the CMV promoter on PX461.s gRNA GGC GCGGGAAGCCTATAACC (PAM AGG) to target *PRPF6* c.2185C > T p.Arg729Trp was cloned into the BbsI sites, for expression from the U6 promoter. This was co-transfected with pCMV-BE3 (Addgene #73021) (Komor et al., 2016) which contains the BE3 gene (Base Editor; cytidine deaminase) under the control of a CMV promoter, into HEK293 cells using PEI. Cells were selected with zeocin.

2.3 Analysis of on-target changes

A proportion of bulk edited cells were harvested for DNA extraction and PCR amplification of the relevant targeted region of *PRPF6* using OneTaq polymerase (NEB). PCR products were cleaned using ExoSAP-IT (Thermo Fisher) and Sanger sequencing was performed by Source Biosciences. Traces from base edited cell lines were analysed visually to identify C > T changes at the predicted mutation site. Base editing efficiency of *PRPF6* c.2185C > T in HEK293 cells was around 50%. Although we tried multiple times to replicate this in hTERT-RPE1 cells and 661W cells we were unsuccessful. We took the edited HEK293 cells forward for single cell isolation.

2.4 Single cell cloning

Cells were dissociated using Accutase at room temperature, counted and transferred to a conical tube. Cells were collected by centrifugation at 200 g and washed with sterile sort buffer (Ca & Mg free PBS, 25 mM HEPES pH 7.0, 1–2.5 mM EDTA and 0.5% BSA or 1%–2% FCS). Cells were collected again and resuspended at a concentration of 5–8×10^6 cells/ml. Untransfected cells were used for gating cell size on the FACS Aria cell sorter (BD) and edited cells then sorted into 150 µL DMEM/F12 + 20% FCS + 10% antibiotic and antimycotic + 10 µM Y-27632 ROCK inhibitor (STEMCELL Technologies) into each well of a 96 well plate.

2.5 Cell fractionation

Cells were fractionated into nuclear and cytoplasmic fractions. Cells were collected by scraping into fractionation buffer (20 mM HEPES pH7.4, 10 mM KCl, 2 mM $MgCl_2$, 1 mM EDTA, 1 mM EGTA) on ice, lysed through a 27 gauge needle, on ice. The nuclear pellet was collected by centrifugation at 720 × g, washed and dispersed through a 25 gauge needle. The supernatant containing cytoplasm was centrifuged at 10,000 g to remove mitochondria and any cell debris. The dispersed nuclear pellet was collected again by centrifugation at 720 × g, resuspended in TBS with 0.1% SDS and sonicated to shear genomic DNA and homogenize the lysate.

2.6 RNA extraction

RNA was extracted from fractionated samples using TRIzol Reagent (Thermo Fisher). RNA quality and concentration was measured using an RNA Nano chip on the Agilent Bioanalyser 2100. Samples with total RNA concentration ≥20 ng/µl, RIN ≥ 6.8 and OD 260/280 were taken forward for cDNA library preparation and sequencing.

2.7 cDNA library preparation and sequencing

cDNA libraries were prepared using Ribo-Zero Magnetic Kit for rRNA depletion and NEBNext Ultra Directional RNA Library Prep Kit library prep kit by Novogene Inc. Library quality was assessed using a broad range DNA chip on the Agilent Bioanalyser 2100. Library concentration was assessed using Qubit and q-PCR. Libraries were pooled, and paired-end 150 bp sequencing to a depth of 20 M reads per fraction (40M reads per sample) was performed on an Illumina HiSeq2500 by Novogene Inc.

2.8 Data processing

2.8.1 Raw data quality control

Raw FASTQ reads were subjected to adapter trimming and quality filtering (reads containing N > 10%, reads where >50% of read has Qscore ≤ 5) by Novogene Inc.

Quality of sequence was assessed using FastQC v0.11.5 (https://www.bioinformatics.babraham.ac.uk/projects/fastqc/). No further data filtering or trimming was applied.

2.9 Data deposition

Raw FASTQ reads after adapter trimming and quality filtering (reads containing N > 10%, reads where > 50% of read has Qscore ≤ 5) were deposited on the Sequence Read Archive, SRA accession PRJNA622794.

2.10 Alignment to reference genome

Paired FASTQ files were aligned to GRCh38 human genome reference using GENCODE v29 gene annotations (Frankish et al., 2019) and STAR v2.6.0a splice aware aligner (Dobin et al., 2013), using ENCODE recommend options (3.2.2 in the STAR manual (https://github.com/alexdobin/STAR/blob/master/doc/STARmanual.pdf). The two-pass alignment method was used, with soft clipping activated.

2.11 Alignment quality control

BAM files sorted by chromosomal coordinates were assessed for saturation of known splice junctions were using RSeqQC v3.0.1 (Wang et al., 2012).

2.12 Differential gene expression analysis

Reads were counted using HTSeq (Anders et al., 2015) and differential gene expression analysis was performed with edgeR v3.24.1 (Robinson et al., 2010; McCarthy et al., 2012) with statistical significance expressed as a p value adjusted for a false discovery rate of 0.05 using Benjamini-Hochberg correction.

2.13 Alignment to reference transcriptome and transcript level abundance estimates

The tool Salmon was used to perform transcript abundance estimates from raw FASTQ files using selective alignment with a decoy-aware transcriptome built from GRCh38 (Patro et al., 2017).

2.14 Differential splicing analysis

rMATs v4.0.2 (rMATS turbo) (Shen et al., 2014) was used to statistically measure differences in splicing between replicates of wild-type and mutant sequence. BAM files aligned with STAR v2.6.0a two-pass method with soft clipping suppressed were used as input.

Pathway enrichment was carried out using Enrichr (Chen et al., 2013; Kuleshov et al., 2016).

2.15 Differental exon usage analysis

DEXSeq-Count v1.28.1.0 was used to count exons in sorted bam files, using GENCODE v29 gene annotations. The differential exon usage was then determined between the control sample and the PRPF31 siRNA samples, using the DEXSeq (R version 3.5.1), again using GENCODE v29 gene annotations.

2.16 Splice site strength measurement

Using splice site coordinates from STAR splice junction output files and rMATS output files, splice site sequences were extracted from GRCh38 using bedtools, and splice strength calculated using MaxEntScan (Yeo and Burge, 2004).

2.17 Protein extraction

Total protein was extracted from cells using 1% NP40 lysis buffer and scraping. Insoluble material was pelleted by centrifugation at 10,000 × g. Cell fractionation was carried out by scraping cells into fractionation buffer containing 1 mM DTT and passed through a syringe 10 times. Nuclei were pelleted at 720 × g for 5 min and separated from the cytoplasmic supernatant. Insoluble cytoplasmic material was pelleted using centrifugation at 10,000 × g for 5 min. Nuclei were washed, and lysed with 0.1% SDS and sonication. Insoluble nuclear material was pelleted using centrifugation at 10,000 × g for 5 min.

2.18 SDS-PAGE and western blotting

20 µg of total protein per sample with 2 × SDS loading buffer was loaded onto pre-cast 4%–12% Bis-Tris gels (Life Technologies) alongside Spectra Multicolor Broad range Protein ladder (Thermo Fisher). Samples were separated by electrophoresis. Protein was transferred to PVDF membrane. Membranes were incubated with blocking solution (5% (w/v) non-fat milk/PBS), and incubated with primary antibody overnight at 4°C. After washing, membranes were incubated with secondary antibody for 1 h at room temperature and exposed using 680 nm and/or 780 nm laser (LiCor Odyssey, Ferrante, Giorgio et al.), or incubated with SuperSignal West Femto reagent (Pierce) and exposed using Chemiluminescence settings on ChemiDoc MP imaging system (Bio-Rad)

2.19 Primary antibodies for WB

Mouse anti ß actin clone AC-15 (Sigma-Aldrich A1978) 1:4000

Rabbit anti-PRPF6 primary antibody (Proteintech) 1:1000

Mouse anti-PCNA-HRP (BioRad MCA1558P) 1:1000

Mouse anti-monoglycylated tubulin (TAP952) (Sigma Aldrich MABS277) 1:100

2.20 Secondary antibodies for WB

Donkey anti mouse 680 (LiCor) 1:20,000

Donkey anti rabbit 800 (LiCor) (Ferrante et al., 2001) 1: 20,000

Donkey anti mouse HRP (Dako) 1:10,000

Donkey anti rabbit HRP (Dako) 1:10,000

2.21 Immunocytochemistry of cells grown on cover slips for regular confocal imaging

HEK293s were plated on Poly-D-Lysine and laminin double-coated glass cover slips then serum starved for 6 days to induce ciliogenesis. hTERT RPE1 cells were grown on glass coverslips and serum starved for 48 h to induce ciliogenesis. Cells were rinsed in warm DPBS and fixed in ice-cold methanol at −20°C for 5 min. Cells were then immediately washed with PBS, and incubated with blocking solution (1% w/v non-fat milk powder/PBS) for 15 min at room temperature. Coverslips were inverted onto primary antibodies in blocking solution in a humidity chamber and incubated at 4°C overnight. After 3 washes with PBS, cells were incubated with secondary antibodies and DAPI for 1 h at room temperature in the dark. After 3 PBS washes and 1 dH2O wash, cells were mounted onto slides with Mowiol.

When staining with anti acetylated alpha tubulin, cells were incubated on ice for 15 min prior to fixation to reduce background staining of cell body microtubules.

2.22 Immunocytochemistry of cells grown on cover slips for STED confocal imaging

HEK293s were plated on Poly-D-Lysine and laminin double-coated high performance (high tolerance) #1.5 glass cover slips (Zeiss) then serum starved for 6 days to induce ciliogenesis. Cells were rinsed in warm DPBS and fixed in ice-cold methanol at −20°C for 5 min. Cells were then immediately washed with PBS, and incubated with blocking solution (1% w/v non-fat milk powder/PBS) for 15 min at room temperature. Coverslips were inverted onto primary antibodies at 5x higher concentration than the normal concentration optimsed for regular confocal imaging, in blocking solution in a humidity chamber and incubated at 4°C overnight. After 3 washes with PBS, cells were incubated with secondary antibodies at 10x higher concentration than the normal concentration optimsed for regular confocal imaging without DAPI for 1 h at room temperature in the dark. After 3 PBS washes and 1 dH2O wash, cells were mounted onto slides with Prolong Gold.

2.23 Manual confocal image capture and analysis

Confocal images were obtained at the Centre for Research in Biosciences Imaging Facility at UWE Bristol, using a HC PL APO 63x/1.40 oil objective CS2 lens on a Leica DMi8 inverted epifluorescence microscope, attached to a Leica SP8 AOBS laser scanning confocal microscope. Images were captured using LASX software and deconvolution of selected images was carried out using Hyvolution (Leica/Huygens). Images were assembled in Image J, Adobe Photoshop and Illustrator. Percentage of ciliated cells was measured by counting cilia and counting nuclei in 5 fields of view. 50 random cilia from 5 fields of view were measured manually using the scale bar as reference.

2.24 STED confocal image capture

STED images were obtained at Wolfson Bioimaging Facility at the University of Bristol Image using a 592 nm STED laser and 660 nm STED laser sequentially using a 100x APO oil immersion lens on a Leica DMi8 inverted epifluorescence microscope, attached to a Leica SP8 AOBS laser scanning confocal microscope with STED module. Images were captured using LASX software, and assembled in Image J, Adobe Photoshop and Illustrator.

2.25 Imaging plate setup

Cells were plated at a density of 1×10^5 cells ml^{-1} into 100 µl complete media per well in 96 well optical bottom Perkin Elmer ViewPlates. The outer wells were filled with media without cells to reduce edge effects. Cells were cultured for 48 h before media was changed to serum-free media. Cells were fixed 24 h later.

2.26 UV treatment

Media was removed from each well and replaced with 10 µl DPBS to ensure the cells did not dry out, but not so much that the UV wasn't able to penetrate. The plate lid was removed, mock-treated wells covered with foil, and a total dose of 25 J/m^2 UV delivered to exposed wells in a UVP CL-1000 Ultraviolet crosslinker. Media was immediately replaced and plates returned to the incubator.

2.27 Nucleofection of PRPF31 and TTLL3 constructs

1 µg PRPF31 construct or TTLL3 construct was nucleofected into 200,000 hTERT-RPE1 cells using 20 µl P3 + supplement and

programme EA104 in strip cuvettes on the Lonza Nucleofector 4D. 80 µl complete pre-warmed media was immediately added to each cuvette in the strip and cell suspension was returned to the incubator to recover for 15 min before adding 25 µl from each cuvette to 4 wells of a 96 well optical bottom Perkin Elmer ViewPlate containing 100 µl pre-warmed complete media per well.

2.28 Immunocytochemistry and imaging of 96 well plates

Wells were emptied by inversion of plates, and washed with warm Dulbecco's PBS (Sigma). DPBS was removed by plate inversion and cells were fixed with ice cold methanol for 5 min at −80°C. Methanol was removed by plate inversion and cells were washed twice with PBS and non-specific antibody binding sites blocked with 1% non-fat milk powder/PBS (w/v) for 15 min at room temperature. Cells were incubated with primary antibodies in blocking solution for 1 h at room temperature and secondary antibodies + DAPI for 1 h at room temperature in the dark. Mowiol was added to wells, and plates stored until imaging. Imaging was carried out on a Perkin Elmer Opera LX with 20x and 60x water immersion lenses at Wolfson Bioimaging Centre, University of Bristol.

2.29 Automated image analysis

Image analysis was performed using custom scripts optimized on CellProfiler (Carpenter et al., 2006). Analysis included nuclear recognition and counting, cell recognition, exclusion of border objects and counting of whole cells, cilia recognition and counting, and quantification of the percentage of whole cells with a single cilium. Median and median absolute deviation of untransfected cells were used to calculate robust z scores (Zhang, 2007; Chung et al., 2008; Birmingham et al., 2009) of cell number and percentage of whole cells with a single cilium in transfected cells.

2.30 Retinal organoid culture

The Mastershef7 hESC line was differentiated into retinal organoids using a previously published protocol. Cells were seeded on LN521 in Nutristem hESC XF media (Biological Industries, #05-100-1A) and allowed to reach near confluence. Once confluent differentiation was initiated by culture in embryoid body media [EB media; DMEM/F12 (Gibco), Knockout serum replacement (Gibco), 1x MEM non-essential amino acids (Gibco), 1x Glutamax (Gibco)] for 72 h in the presence of WNT inhibitor 3 µM IWR1e (Merck). On day 4, the media was changed to Neural Induction Medium [NIM; DMEM/F12 (Gibco), 1x MEM non-essential amino acids (Gibco), N2 supplement (Gibco), Heparin (Sigma), 1x Glutamax (Gibco)] and feeding continued three times a week to stimulate forebrain development. On day 12 cultures were transitioned to Retinal Differentiation Medium (RDM; DMEM (Gibco), F12 (Gibco), B27 supplement (Gibco), 1x Glutamax (Gibco) and 10% Fetal Bovine Serum (LifeTech) and cultures fed on alternating days. After 18 days of differentiation, RDM was supplemented with Taurine (100 µM, Sigma), T3 (20 nM, Sigma), IGF-1 (5 ng/ml, Sigma). Cultures were supplemented with Retinoic Acid (0.5 µM, Sigma) after 100 days. After 3 weeks, Optic Vesicles (OVs) begin to form which appeared as rounded neuroepithelial structures growing adjacent to a patch of cells that form retinal pigment epithelium (RPE). The OVs were manually excised between day 25–35 and cultured in RDM in low attachment 10 cm plates until analysis.

2.31 Retinal organoid immunocytochemistry and imaging

Samples comprised of 10–20 OVs were fixed in 4% PFA/PBS for 10 min at room temperature and subsequently washed three times in PBS for 10 min each. The OVs were then cryopreserved by soaking in a PBS/30% sucrose solution overnight at 4°C. Embedding was carried out using OCT compound and frozen samples stored at −80°C. Frozen blocks were sliced into 18 µm cryosections and transferred on glass slides. OCT compound was removed by a 15 min incubation in PBS at 37°C. Sections were then blocked for 1 h (PBS/0.1% Triton-x, 10% FBS, 1% BSA) and then incubated with the primary antibodies overnight at 4°C. The next day, primary antibodies were washed off and the samples were incubated with secondary antibodies for 1 h at room temperature. Slides were then mounted and sealed with nail polish. Images were produced, from independent samples with a Leica SP8 Confocal microscope and processed using ImageJ software.

2.32 Primary antibodies for immunocytochemistry

Rabbit anti-PRPF6 (Proteintech 23929-1-AP) 1:100

Mouse anti-PRPF6 (Santa Cruz sc-166889) 1:100/1:50 for STED imaging

Rabbit anti-ARL13B (Proteintech 17711-1-AP) 1:200

Rabbit anti-gamma tubulin (Abcam ab11317) 1:50 (for STED imaging)

Mouse anti-polyglutamylated tubulin (GT335) (Adipogen Life Sciences AG-20B-0020) 1:1000

Rabbit anti-XPA (Abcam ab85914) 1:200

Mouse anti-monoglycylated tubulin (TAP952) (Sigma Aldrich MABS277) 1:100

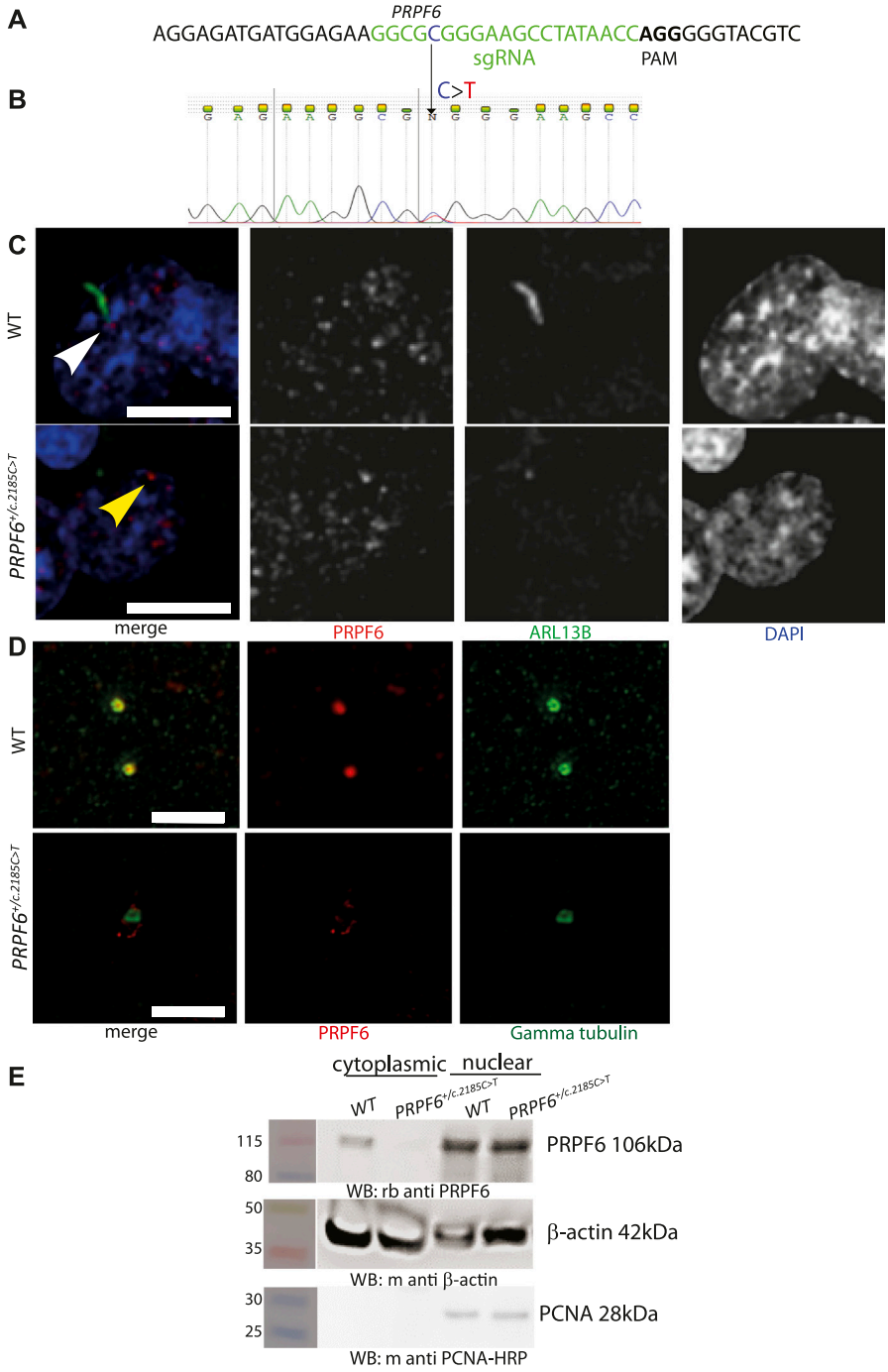

FIGURE 1
Generation and characterisation of *PRPF6*$^{+/c.2185C>T}$ base edited HEK293 cells. **(A)** Illustration of location and sequence of *PRPF6* guide RNA in green, with PAM sequencing in bold. **(B)** Electropherogram of PRPF6 sequence from of *PRPF6*$^{+/c.2185C>T}$ base edited HEK293 cells to confirm the heterozygous change. **(C)** Confocal microscopy images of WT and *PRPF6*$^{+/c.2185C>T}$ base edited HEK293 cells immunostained with anti PRPF6 (red) and ARL13B (green) antibodies, showing the ARL13B-stained cilium in wild-type (WT) cells (white arrowhead), lost in *PRPF6*$^{+/c.2185C>T}$ cells, and the loss of PRPF6 from the base of the cilium (yellow arrowhead). Scale bar 10 μm. **(D)** Stimulated emission depletion (STED) microscopy images of wild-type (WT) and *PRPF6*$^{+/c.2185C>T}$ base edited HEK293 cells immunostained with anti PRPF6 (red) and gamma tubulin (green) antibodies, showing colocalization of PRPF6 with the gamma tubulin-stained basal body in WT cells and loss of this colocalisation in *PRPF6*$^{+/c.2185C>T}$ cells. Scale bar 2 μm. **(E)** Western blot image showing presence of PRPF6 protein in the nucleus of WT and *PRPF6*$^{+/c.2185C>T}$ cells, but absence of PRPF6 protein from the cytoplasm of *PRPF6*$^{+/c.2185C>T}$ cells, beta actin is shown as a cytoplasmic loading control, and PCNA is shown as a nuclear loading control.

Rabbit anti-recoverin (Millipore AB5585) 1:1000

Mouse anti-CRX (M02) clone 4G11 (Sigma H00001406-M02)

2.33 Secondary antibodies for immunocytochemistry

Donkey anti mouse IgG AlexaFluor 488 (ThermoFisher) 1:500

Donkey anti rabbit IgG AlexaFluor 568 (ThermoFisher) 1:500

Goat anti rabbit IgG AlexaFluor 488 (ThermoFisher) 1:1000/ 1:100 for STED imaging

Goat anti mouse IgG AlexaFluor 568 (ThermoFisher) 1:1000

Goat anti mouse IgG Highly cross-absorbed AlexaFluor 555 (ThermoFisher) 1:100 (for STED imaging)

2.34 Statistical analysis

Data were tabulated, graphs were produced and statistical analyses were performed in GraphPad Prism v9.0.1 (GraphPad Software Inc., San Diego, CA, United States) unless otherwise indicated. Normality of data was assessed using Shapiro-Wilk test to inform whether to apply parametric or non-parametric statistical tests. Statistical analyses of single comparisons of two groups utilized Student's t-test or Mann-Whitney U test for parametric and non-parametric data respectively. Results were considered significant if $p \leq 0.05$, where $^{*}p \leq 0.05$, $^{**}p \leq 0.005$, $^{***}p \leq 0.001$, $^{****}p \leq 0.0001$.

3 Results

Using third generation base editing (BE3) (Komor et al., 2016) vectors and a specific sgRNA (Figure 1A) we produced multiple clones of HEK293 cells with heterozygous knock-in point mutations in *PRPF6* [NC_000020.11:g.64027138C > T NM_012469.4(PRPF6):c.2185C > T (p.Arg729Trp)] previously reported in human autosomal dominant RP patients (Tanackovic et al., 2011), which we confirmed by Sanger sequencing (Figure 1B). We analysed the phenotype of 4 different mutant clones compared to 4 different wild-type clones which had undergone the same transfection and cloning process but not been edited. Immunofluorescence confocal imaging showed that, as has been shown in PRPF6 siRNA knockdown-treated cells (Wheway et al., 2015), $PRPF6^{+/c.2185C>T}$ mutant clones tended to lack cilia and PRPF6 staining could not be seen at the base of the cilium, whereas it could be seen in the wild-type sister clones (Figure 1C). PRPF6 staining in the nucleus appeared the same in mutants and wild-type cells (Figure 1C). To gain higher resolution images of the base of the cilium we immunostained cells with PRPF6 antibody and an antibody to gamma tubulin to label the basal body. This more clearly showed colocalization of PRPF6 with the basal body in the WT cells, and loss of this colocalization in the $PRPF6^{+/c.2185C>T}$ mutant clones (Figure 1D). Some faint PRPF6 staining could be seen to be loosely associated with the basal body in the mutant clones (Figure 1D) but when we fractionated cell lysates into cytoplasmic and nuclear fractions and analysed these by western blotting we could not detect PRPF6 in the cytoplasm in $PRPF6^{+/c.2185C>T}$ mutant clones (Figure 1E). We proceeded to quantify the cell defect seen in the $PRPF6^{+/c.2185C>T}$ mutant clones using deconvolution confocal imaging and manual counting of cilia and measurement of cilium length. This showed that $PRPF6^{+/c.2185C>T}$ mutant clones had statistically significantly lower percentage of cells with a single cilium (Figure 2A) and statistically significantly shorter cilia (Figure 2B), although with a small population of cells with long cilia (Figures 2B,C).

We extracted RNA from 3 independent $PRPF6^{+/c.2185C>T}$ mutant clones and 3 wild-type sister clones, prepared stranded cDNA libraries and performed paired-end RNA sequencing. We first carried out differential gene expression analysis, and defined a statistically significantly differentially expressed gene as one with a false discovery rate (FDR) adjusted p-value of <0.05 and a $\log_2$ fold change of greater than 1 or less than -1. This showed that 8 genes were statistically significantly differentially expressed in $PRPF6^{+/c.2185C>T}$ mutant clones compared to wild-type sister clones; 5 downregulated and 3 upregulated (Supplementary Table S1). Gene ontology (GO) term enrichment analysis using Enrichr (Chen et al., 2013; Kuleshov et al., 2016) showed statistically significant (adjusted p-value >0.05) enrichment of GO molecular function terms microtubule binding (GO:0008017; $p = 0.003$), tubulin binding (GO: 0015631; $p = 0.004$), dynein complex binding (GO:0070840) and GO cellular component terms axon (GO:0030424; $p = 0.001$) and cytoskeleton (GO:0005856; 0.017) and GO biological process terms intermediate filament bundle assembly (GO:0045110; $p = 2.098 \times 10^{-6}$) and axon development (GO:0061564; $p = 6.008 \times 10^{-4}$).

To investigate differential splicing in our RNAseq dataset we used rMATS programme (Shen et al., 2014) to perform differential splicing analysis in our 3 independent $PRPF6^{+/c.2185C>T}$ mutant clones and 3 wild-type sister clones. We supplemented this analysis with differential splicing analysis of RNAseq data from 3 independent mutant $PRPF31^{+/-}$ hTERT-RPE1 clones and 3 independent wild-type sister hTERT-RPE1 clones, which we previously described (Nazlamova et al., 2020), and publicly available RNAseq data from day 150 retinal organoids derived from induced pluripotent stem cells (iPSCs) from 7 *PRPF31* patients severely affected with RP, compared to 6 unaffected controls (Buskin et al., 2018).

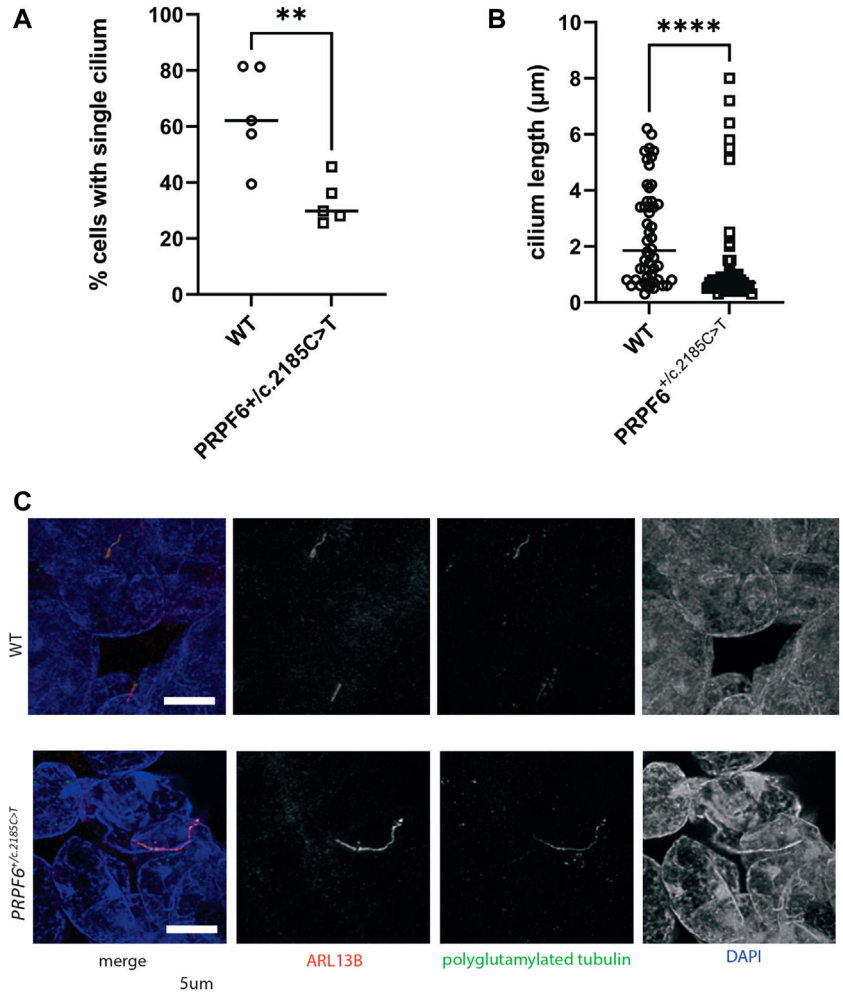

FIGURE 2
Quantification of ciliary phenotype in *PRPF6*$^{+/c.2185C>T}$ base edited HEK293 cells. **(A)** Dot plot of the percentage of cells with a single cilium in WT and *PRPF6*$^{+/c.2185C>T}$ cells, showing a statistically significant reduction in the percentage of cells with a single cilium in *PRPF6*$^{+/c.2185C>T}$ cells. Two-tailed unpaired *t* test, *p* value 0.0070, ** = $p < 0.005$, t, df t = 3.596, df = 8. One data point represents data from one cover slip (average from 6 fields of view per coverslip, 5 coverslips, each coverslip is one independent experiment). **(B)** Dot plot of single cilium length in WT and *PRPF6*$^{+/c.2185C>T}$ cells, showing a statistically significant reduction in cilium length in *PRPF6*$^{+/c.2185C>T}$ cells. Two-tailed Mann Whitney test, *p* value <0.0001 (exact), **** = $p <$ 0.0001, Sum of ranks in column A, B 3095, 1955, Mann-Whitney U 680. One data point represents measurement of one cilium (measurements taken from individual cilia across 6 fields of view per coverslip, each coverslip is one independent experiment). **(C)** Confocal image of *PRPF6*$^{+/c.2185C>T}$ base edited HEK293 cells immunostained with anti ARL13B (red) and anti polyglutamylated tubulin (green) antibodies, showing the an example of a lengthened cilium in *PRPF6*$^{+/c.2185C>T}$ cells. Scale bar 5 µm.

Analysis included differential alternative 3′ splice site usage (A3′SS), alternative 5′ splice site usage (A5′SS), retention of introns (RI) and skipping of exons (SE). We accepted any event with FDR $p < 0.05$ as a significantly different splicing event. In *PRPF6* and *PRPF31* mutant cell lines and organoids the predominant differential splicing event was exon skipping (Figure 3A). To further investigate exon skipping we used DEXSeq to study differential exon usage in publicly available RNAseq data from 3 human organotypic retinal cultures treated with *PRPF31* siRNA compared to 1 non-targeting siRNA control (PRJNA509001) (Azizzadeh Pormehr et al., 2019). In these samples rMATS could not be used as only 1 control sample was available and rMATS requires replicate data.

Pathway and ontology enrichment analysis using Enrichr (Chen et al., 2013; Kuleshov et al., 2016) of differentially spliced genes in *PRPF6* and *PRPF31* mutant cell lines and organoids and *PRPF31* siRNA-treated organotypic retinal cultures showed an enrichment of gene ontology cellular component terms “centrosome”, “microtubule organising center”, “centriole” (Table 1) and an enrichment of pathways related to primary cilium development and DNA damage response (Table 2) across

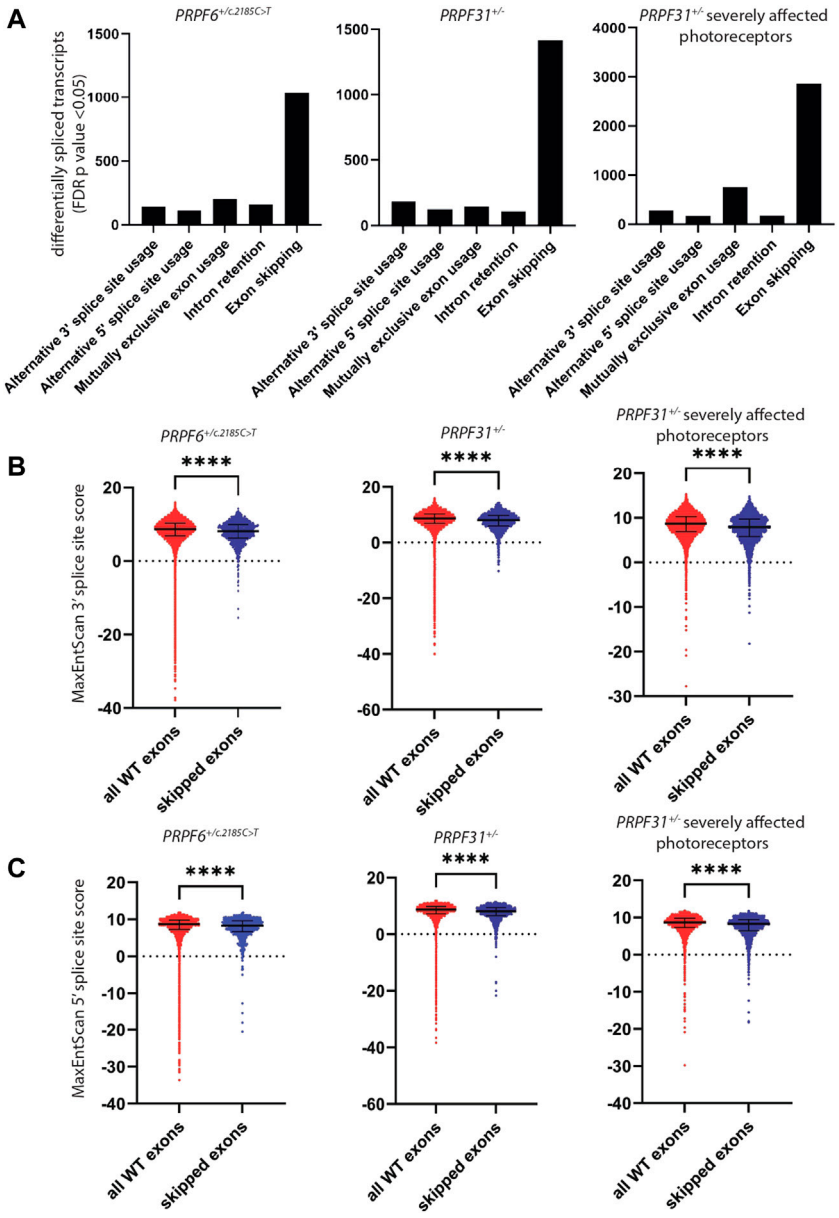

FIGURE 3
Analysis of differentially spliced transcripts and splice sites in *PRPF6*$^{+/c.2185C>T}$ cells, *PRPF31*$^{+/-}$ cells and retinal organoids derived from *PRPF31*$^{+/-}$ patients severely affected with RP. **(A)** Bar chart showing the number of cases of statistically significant (FDR $p < 0.05$) alternative 3′ splice site usage, alternative 5′ splice site usage, mutually exclusive exon usage, intron retention and exon skipping in *PRPF6*$^{+/c.2185C>T}$ cells, *PRPF31*$^{+/-}$ cells and retinal organoids derived from *PRPF31*$^{+/-}$ patients severely affected with RP compared to relevant controls, showing the abundance of exon skipping in all 3 cell/organoid types. **(B)** Dot plots showing MaxEntScan 3′ splice site score for every wild-type exon and every skipped exon identified in **(A)**, showing that skipped exons have lower 3′ splice site scores, i.e., weaker 3′ splice sites are skipped in *PRPF6* and *PRPF31* mutant cells. Individual data points plus median and interquartile range are shown ****$p < 0.0001$ Mann-Whitney in all cases. PRPF6 3′ WT median 8.680, SE media 8.150 n = 1039, PRPF31 3′ WT median 8.670, SE media 8.110 n = 1419, PRPF31 retinal organoids 3′ WT median 8.680, SE media 7.900 n = 2866. **(C)** Dot plots showing MaxEntScan 5′ splice site score for every wild-type exon (red) and every skipped exon (blue) identified in **(A)**, showing that skipped exons have lower 5′ splice site scores, ie weaker 5′ splice sites are skipped in *PRPF6* and *PRPF31* mutant cells. Individual data points plus median and interquartile range are shown ****$p < 0.0001$ Mann-Whitney in all cases. PRPF6 5′ WT median 8.700, SE median 8.345 n = 2866, PRPF31 5′ WT median 8.680, SE median 8.100 n = 1419, PRPF31 retinal organoids 5′ WT median 8.690, SE median 8.310 n = 2866.

TABLE 1 FDR adjusted *p* values from gene ontology enrichment analysis of differentially spliced exons in PRPF6 base edited cells, PRPF31 edited cells, PRPF31$^{+/-}$patient-derived retinal organoids and PRPF31 siRNA-treated retinal cultures. Statistically significantly enriched GO terms and their FDR-adjusted *p* values are highlighted in bold.

	PRPF6$^{+/c.2185C>T}$ cells	*PRPF31*$^{+/-}$ cells	*PRPF31*$^{+/-}$ retinal organoids	*PRPF31* siRNA retinal cultures
Centrosome (GO:0005813)	**0.0031675420683829124**	**0.013562462**	**2.06E-04**	**1.81E-12**
Microtubule organizing center (GO:0005815)	**0.0031675420683829124**	**0.013309689**	**7.72E-04**	**5.66E-13**
Microtubule cytoskeleton (GO:0015630)	**0.021273276446275965**	0.82041854	0.388079555	**5.12E-06**
Microtubule organizing center part (GO:0044450)	0.3085426153586124	**0.01370083**	**0.010723266**	**0.002760253**
Centriole (GO:0005814)	0.6358832467779791	**0.028962917**	**0.011200905**	**0.043848651**
Mitochondrion (GO:0005739)	0.4365736275258775	**0.014404009**	0.131502434	0.264241865
PML body (GO:0016605)	0.7420592042778611	**0.025598309**	0.603125898	**1.00E-03**
Cytoskeleton (GO:0005856)	0.3199658477886017	0.932445377	**0.002457416**	**4.41E-05**
Spindle (GO:0005819)	0.5088351587057507	0.82041854	**0.006151164**	**0.008996979**
Vesicle coat (GO:0030120)	0.42128440695526675	0.82041854	**0.010723266**	**0.031007285**
Golgi membrane (GO:0000139)	0.8513466009078202	0.82041854	**0.037578067**	**0.002760253**
Spindle pole (GO:0000922)	0.5088351587057507	0.82041854	**0.049142179**	**0.003143342**

TABLE 2 FDR-adjusted *p* values from Wikipathway pathway enrichment analysis of differentially spliced exons in PRPF6 base edited cells, PRPF31 edited cells, PRPF31$^{+/-}$patient-derived retinal organoids and PRPF31 siRNA-treated retinal cultures. Statistically significantly enriched pathways and their FDR-adjusted *p* values are highlighted in bold.

	PRPF6$^{+/c.2185C>T}$ cells	*PRPF31*$^{+/-}$ cells	*PRPF31*$^{+/-}$ retinal organoids	*PRPF31* siRNA retinal cultures
Genes related to primary cilium development (based on CRISPR) WP4536	0.3367102392058503	**2.33E-04**	**0.018904**	**4.98E-07**
DNA IR-damage and cellular response via ATR WP4016	0.7281307063162956	**0.01784**	0.999995	**0.036337**
Glycosylation and related congenital defects. WP4521	0.4937868948330625	0.787006	**0.018904**	0.82024
Nucleotide Metabolism WP404	-	0.777887	**0.041867**	0.877967

all *PRPF6* and *PRPF31* cells or retina. This is consistent with previous reports that centrosome and cilium transcript are differentially spliced in *PRPF31* mutants (Buskin et al., 2018; Azizzadeh Pormehr et al., 2020; Li et al., 2021).

Analysis of Sashimi plots showed that this differential exon usage included skipping of single and multiple constitutive exons, skipping of novel unannotated exons which are included in wild-type cells, and skipping of constitutive exons alongside differential 3′ and 5’ splice site usage (Supplementary Figure S1).

It has been reported that regulation of splicing by PRPF8 is determined by 5′ splice site strength (Wickramasinghe et al., 2015), and that exons which are differentially spliced in the developing retina of *prpf31* mutant zebrafish have weaker 5′ splice sites (Li et al., 2021). To investigate the strength of 3′ and 5′ splice sites of exons skipped we extracted sequences of all splice sites used in control cells (>5 uniquely mapped reads per sample) and the splice sites of the exons skipped in mutant samples, and calculated splice site scores using MaxEntScan (Yeo and Burge, 2004). This showed a small but highly statistically significant difference in both 3′ and 5′ splice site strength of skipped exons in mutant samples compared to controls (Figures 3B,C). This suggests that subtle defects in spliceosome activity due to mutations in *PRPF6* or *PRPF31* predominantly affect efficiency of splicing of exons with weak splice sites. To investigate this further we performed enrichment analysis of genes with skipped exons with the weakest splice site scores (MaxEntScan < 1). Although there were no statistically significant (FDR $p > 0.05$) enrichments of pathways or ontologies we did observe consistent enrichment of genes with cellular component gene ontology term microtubule/centrosome/centriole/cilium. This suggests that exons in

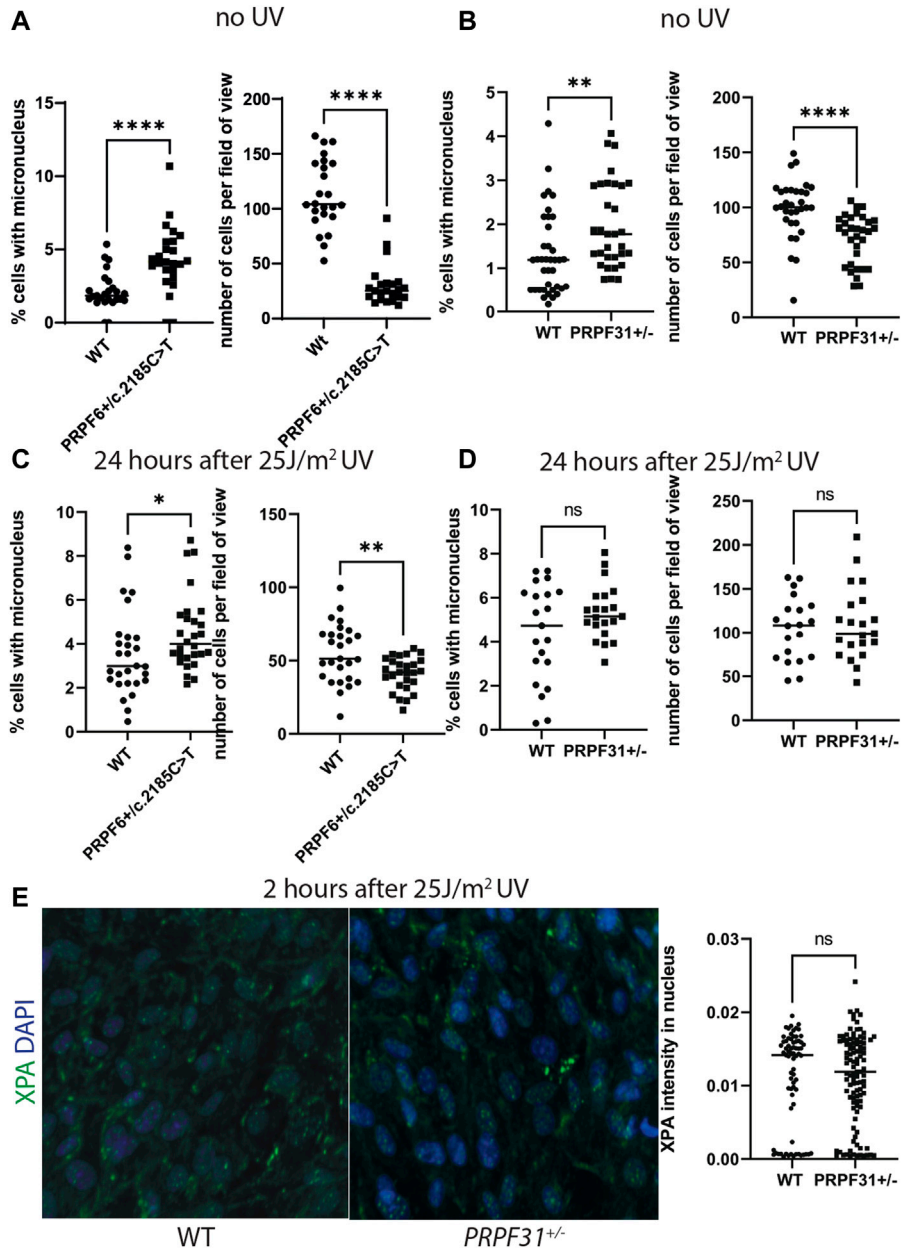

FIGURE 4
Analysis of micronucleus and cell number in *PRPF6*$^{+/c.2185C>T}$ cells and *PRPF31*$^{+/-}$ cells before and after UV exposure, and analysis of XPA nuclear staining in *PRPF31*$^{+/-}$ cells after UV exposure. **(A)** Dot plots showing percentage of cells with a micronucleus (left) and number of cells per field of view (right) in untreated WT cells and *PRPF6*$^{+/c.2185C>T}$ cells. *PRPF6*$^{+/c.2185C>T}$ cells have statistically significantly more micronuclei and statistically significantly fewer cells. **(B)** Dot plots showing percentage of cells with a micronucleus (left) and number of cells per field of view (right) in WT cells and *PRPF31*$^{+/-}$ cells. *PRPF31*$^{+/-}$ cells have statistically significantly more micronuclei and statistically significantly fewer cells. **(C)** Dot plots showing percentage of cells with a micronucleus (left) and number of cells per field of view (right) in WT cells and *PRPF6*$^{+/c.2185C>T}$ cells 24 h after 25 J/m^2 UV. *PRPF6*$^{+/c.2185C>T}$ cells have statistically significantly more micronuclei and statistically significantly fewer cells, but these differences are less statistically significant than in untreated cells. **(D)** Dot plots showing percentage of cells with a micronucleus (left) and number of cells per field of view (right) in WT cells and *PRPF31*$^{+/-}$ cells 24 h after 25 J/m^2 UV. *PRPF31*$^{+/-}$ cells do not have statistically significantly more or fewer micronuclei, nor statistically significantly more or fewer cells. **(E)** Confocal image (left) of WT and *PRPF31*$^{+/-}$ cells immunostained with XPA (green) and DAPI nuclear stain (blue) and dot plot (right) of XPA staining intensity in nucleus 2 h after 25 J/m^2 UV exposure. No statistical difference is seen in mutants compared to WT cells.

particular genes encoding microtubule/centrosome/centriole/cilium proteins may be particularly weak and susceptible to mis-splicing in cells with defects in pre-mRNA splicing. We hypothesised that the primary defect in cells was defective microtubule and centrosomal defects, and that this leads to defects in cilium stability and mitotic spindle stability, and the latter leads to DNA damage, triggering a secondary differential splicing of DNA damage response proteins. It has been well documented that differential splicing of DNA damage proteins is a central cellular response to DNA damage (Paulsen et al., 2009; Dutertre et al., 2010; Adamson et al., 2012; Shkreta and Chabot, 2015; Tresini et al., 2015).

To test this hypothesis we used our cell models to investigate DNA damage using high-content imaging. We assayed micronuclei number 24 h after treating cells with with 25J/m^2 UV or giving a mock treatment. We found statistically significantly higher percentage of cells with micronuclei and lower cell number in mock treated *PRPF6*$^{+/c.2185C>T}$ mutants (Figure 4A) and *PRPF31*$^{+/-}$ cells (Figure 4B) than their respective wild-type sister clones, but the size and significance of this difference was reduced after UV exposure (Figures 4C,D). We also assayed intensity of XPA nuclear staining in *PRPF31*$^{+/-}$ cells and wild-type sister clones and found no statistical difference in mutants compared to wild type cells (Figure 4E). We conclude that mutant cells are more prone to genomic instability, but the DNA damage response is intact.

To further investigate the effect of differential splicing of microtubule regulating proteins on *PRPF6* and *PRPF31* mutant cells we focussed on one particular gene of interest, *TTLL3*, which was one of the most statistically differentially spliced genes in all mutants, and has some of the weakest splice sites of any gene identified. rMATS analysis identified multiple significant splicing defects in *TTLL3*, including intron retention, exon skipping and alternative 3′ and 5′ splice site usage. Most of these affected exons 5–7. The most significant intron retention in *PRPF6*$^{+/c.2185C>T}$ mutant cells was in *TTLL3*. Exon skipping in multiple transcripts of *TTLL3 was* highly significant in *PRPF6*$^{+/c.2185C>T}$ mutants. Exon skipping and A5′SS usage in *TTLL3* was also highly significant. *TTLL3* undergoes complex alternative splicing to produce 33 transcripts, including 18 protein coding transcripts which encode tubulin glycylase type 3, TTLL3. Glycylation is one of several post-translational modifications of tubulin in cilium axonemal tubulins which stabilise these structures. Whilst cell body microtubules undergo a range of post-translational modifications, glycylation is a modification unique to axonemal microtubules of both motile and primary cilia (Bosch Grau et al., 2013; Gadadhar et al., 2017). TTLL3 catalyses monoglycylation of the cilium microtubules and is required for ciliogenesis (Wloga et al., 2009; Rocha et al., 2014). Both mono- and polyglycylation coexist on axonemal MTs in most mammals, with three TTLL glycylases working together to generate polyglycylation of tubulins; TTLL3 and TTLL8 are initiating glycylases, TTLL10 elongates the polyglycylated chain (Rogowski et al., 2009). However, in humans polyglycylation is absent (Rogowski et al., 2009). GTEx expression data (GTEx Consortium, 2013; GTEx Consortium, 2015) suggests that TTLL3 is the only glycylase which is expressed in humans. *Ttll3*$^{-/-}$ mice lack glycylation in photoreceptors, which results in shortening of connecting cilia and slow retinal degeneration (Bosch Grau et al., 2017). Alterations in the balance of tubulin glycylation and glutamylation in photoreceptors has been shown to lead to retinal degeneration (Bosch Grau et al., 2017); absence of glycylation results in increased levels of tubulin glutamylation in photoreceptor cilia which leads to cilium degeneration. Furthermore, human mutations in *CCP5* (also known as *AGBL5*), a tubulin deglutamylase are associated with RP, presumably due to an increase in polyglutamylation (Kastner et al., 2015; Astuti et al., 2016; Branham et al., 2016; Patel et al., 2016). Another tubulin-modifying enzyme, *TTLL5*, a tubulin polyglutamylase, is also associated with cone-rod dystrophy type 9 (CORD9) and RP (Sergouniotis et al., 2014; Astuti et al., 2016; Bedoni et al., 2016) although it is thought that this is due to defective glutamylation of RPGR (Sun et al., 2016).

With the emerging role of enzymes involved in tubulin glycylation and glutamylation in retinal degeneration, the clinical and cellular phenotype associated with *PRPF6* and *PRPF31* mutations, TTLL3 is an extremely interesting candidate for further investigation.

We analysed publicly available RNAseq datasets from human retina to study expression of all tubulin tyrosine ligases (TTLLs) in different stages of human retinal development. Single cell sequence data from retinal organoids at day 60, 90 and 200 of differentiation (Collin et al., 2019) showed that *TTLL7* is the tubulin tyrosine ligase expressed by the largest proportion of cells across all time points (around half of all cells), with *TTLL4* and *TTLL5* also expressed by more than 20% of cells (Figure 5A). *TTLL3*, *12* and *1* are expressed by around 10% of cells, TTLL6, 9, 11 and 13P by a small number of cells and, consistent with GTex data, *TTLL8* and *TTLL10* not expressed at all (Figure 5A). There is an increase in level of expression of most TTLL genes at day 200 (except *TTLL9*, *TTLL6*, *TTLL13P*) which correlates with development of mature outer segments at day 200 (Figure 5A). There was no obvious pattern of co-expression of any TTLL genes at any time point. Similar findings were observed in single cell RNAseq data from foetal human retina from week 5–week 24 (day 29–day 168) of development (Hu et al., 2019). The TTLL gene most commonly expressed in cells across all time points is *TTLL7* (expressed in around half of the cells of the retina) (Figure 5B). *TTLL4, 5, 3, 12* and *1* are expressed by one fifth to one third of cells of the retina (Figure 5B). *TTLL8* and *10* are not expressed at all. It is difficult to assess relative levels of expression across timepoints without normalisation but they would seem to be

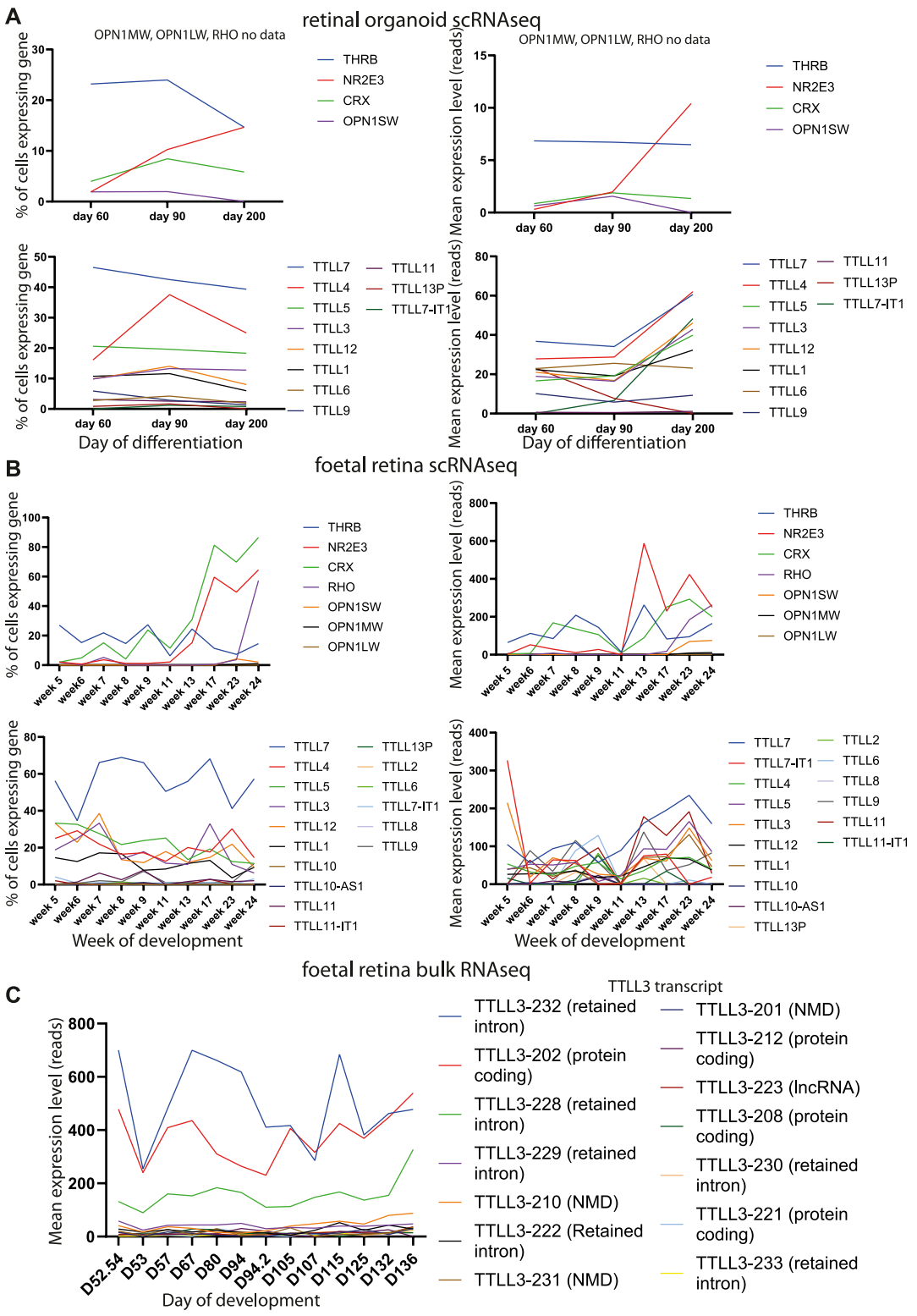

FIGURE 5
Analysis of retinal gene and TTLL gene expression in developing retinal organoids and foetal retina. **(A)** Line graphs plotting % of cells expressing genes (left) and mean expression level in raw reads of genes (right) in single cell expression datasets from retinal organoids. Data are shown from genes related to specific functions of different retinal cells (top) and TTLL genes (bottom) at different stages of retinal organoid differentiation. **(B)** Line graphs plotting % of cells expressing genes (left) and mean expression level in raw reads of genes (right) in single cell expression datasets from human foetal retinal. Data are shown from genes related to specific functions of different retinal cells (top) and TTLL genes (bottom) at different stages of retinal development. **(C)** Line graphs plotting mean expression level in raw reads of genes in bulk expression datasets from human foetal retinal. Data are shown for TTLL genes at different stages of retinal development.

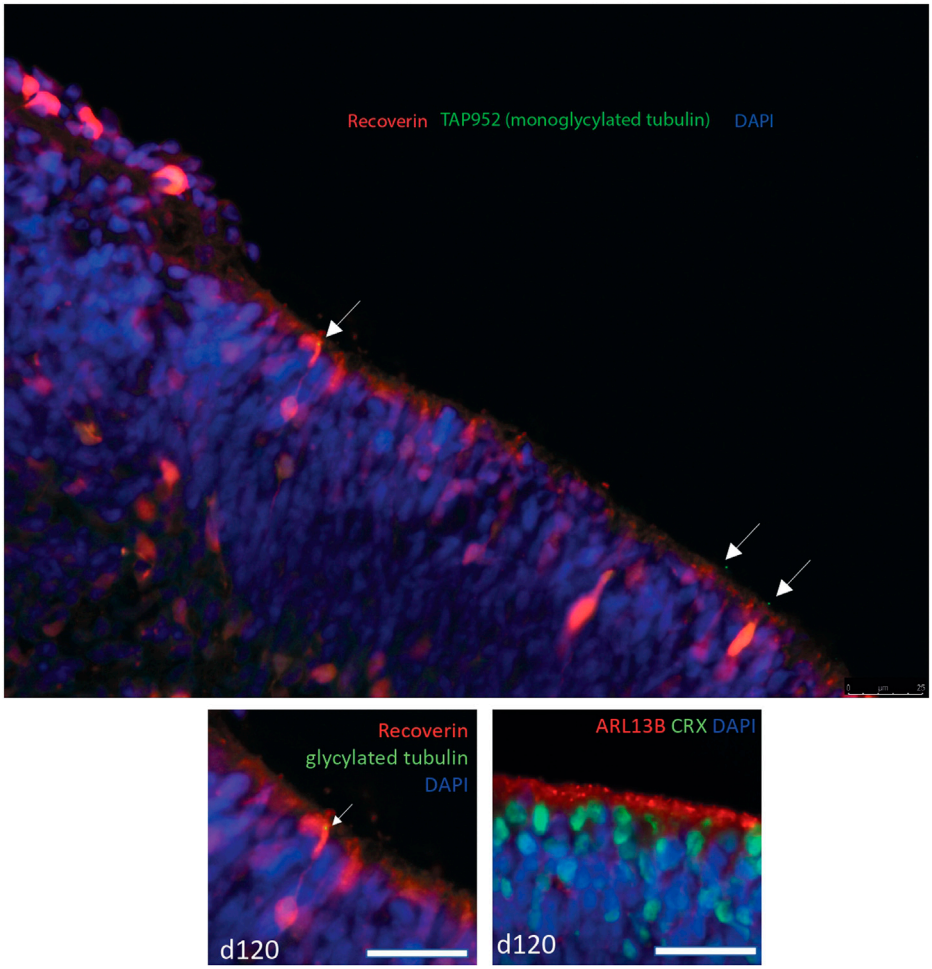

FIGURE 6
Confocal microscopy image of immunostaining of day 120 human embryonic stem cell derived retinal organoids. Recoverin is stained in red, monoglycylated tubulin is stained with TAP952 antibody in green, nuclei are stained with DAPI in blue. Monoglycylated tubulin staining is seen in recoverin positive cells in puncta reminiscent of basal bodies of connecting cilia (white arrows). The lower panel shows a magnified insert of the top panel (left) and a panel at the same magnification of the same D120 organoid stained with ARL13B (red) as a marker for cilia and CRX (green) photoreceptor cell marker.

fairly consistent across TTLLs and timepoints, although expression of *TTLL7* and *TTLL3* was high in week 5, suggesting these genes may have a role in early retinal development (Figure 5B). Transcript-level analysis of *TTLL3* in publicly available bulk RNAseq data from 13 whole human fetal retina samples spanning 12 time points (D52/54, D53, D57, D67, D80, D94 (2 samples), D105, D107, D115, D125, D132 and D136) (Hoshino et al., 2017), showed that 4 main protein coding transcripts of *TTLL3* (Ensembl transcript TTLL3-202, TTLL3-212, TTLL3-208 and TTLL3-221) are expressed across all timepoints of differentiation, with TTLL3-202 being the main protein coding transcript expressed. However, the highest level of expression of any transcript is of TTLL3-232, a retained intron transcript (Figure 5C). Together, the expression pattern of *TTLL3* and other TTLLs suggests that TTLL3 is the only tubulin glycylase expressed in the human retina, it is expressed by around 10%–25% of retinal cells throughout week 5 to week 24 of differentiation, and that the predominant expressed transcripts are 4834 bp TTLL-202 which encodes a 352 amino acid protein (the consensus coding sequence encodes a 915 amino acid protein) and a 5282bp transcript with a retained intron. RNAseq data does not give insight into when TTLL3 may play a functional role in tubulin monoglycylation in the retina, so we carried out immunostaining of monoglycylated tubulins in day 120 human embryonic stem cell derived retinal organoids; monoglycylation was seen specifically seen in RECOVERIN positive cells in D120 organoids in puncta reminiscent of basal bodies of connecting cilia (Figure 6).

With data suggesting that TTLL3 is required for monoglycylation in the retina photoreceptor cells, and

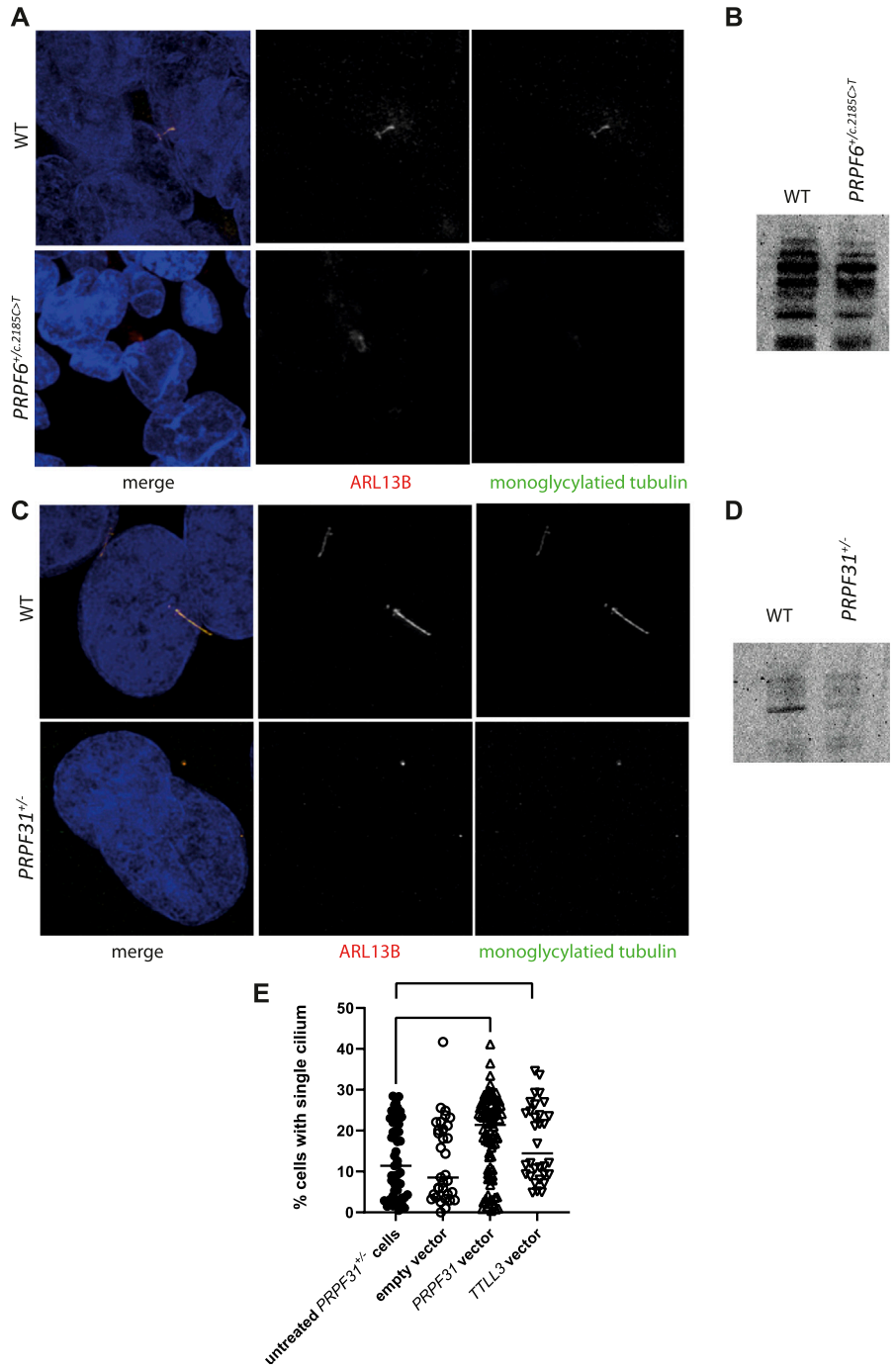

FIGURE 7
Analysis of monoglycylation in *PRPF6*$^{+/c.2185C>T}$ cells and *PRPF31*$^{+/-}$ cells, and rescue of ciliation in *PRPF31*$^{+/-}$ cells. **(A)** Confocal image of WT cells and *PRPF6*$^{+/c.2185C>T}$ cells immunostained with cilia marker anti ARL13B (red) and anti monoglycylated tubulin (green) antibody showing loss of monoglycylated tubulin from the cilium of mutant cells. **(B)** Western blot image showing reduction in levels of total monoglycylated tubulin in *PRPF6*$^{+/c.2185C>T}$ cells compared to WT sister clones. **(C)** Confocal image of WT cells and *PRPF31*$^{+/-}$ cells immunostained with cilia marker anti ARL13B (red) and anti monoglycylated tubulin (green) antibody showing loss of cilia from *PRPF31*$^{+/-}$ cells, but retention of monoglycylated tubulin at the basal body. **(D)** Western blot image showing reduction in levels of total monoglycylated tubulin in *PRPF31*$^{+/-}$ cells compared to WT sister clones. **(E)** Dot plot showing percentage of cells with a single cilium in untreated *PRPF31*$^{+/-}$ cells, and in *PRPF31*$^{+/-}$ transfected with an empty vector, a positive control rescue vector (*PRPF31*) or a *TTLL3* expression vector, showing statistically significant increase in percentage of cells with a single cilium in mutant cells transfected with either *PRPF31* or *TTLL3* construct.

evidence that differential splicing of this transcript is associated with *PRPF6* and *PRPF31* mutations and cilium defects, we investigated whether tubulin glycylation underlies cilium instability in PRPF6 and PRPF31 mutant cells. We immunostained cilia in our mutant cells and carried out western blotting with an antibody to monoglycylated tubulin. This showed lower levels of tubulin monoglycylation in *PRPF6*$^{+/c.2185C>T}$ and *PRPF31*$^{+/-}$ mutant cells compared to wild-type sister clones (Figures 7A–D). We next attempted rescue experiments in our *PRPF31*$^{+/-}$ mutant cells in which we transfected and expressed either an empty vector, a positive control rescue vector (*PRPF31*) or a *TTLL3* expression vector and assayed the effect on cilia using high content imaging and automated image analysis. This showed a rescue of cilium number in mutant cells transfected with either *PRPF31* and *TTLL3* (Figure 5C) suggesting that replacement of TTLL3 is sufficient to rescue cilium stability in PRPF31 mutant cells.

4 Discussion

It has been more than twenty years since mutations in pre-mRNA splicing factor genes were first identified as a cause of RP. Since then, considerable efforts have been made to understand why defects in proteins with constitutive functions in splicing in all cells only cause disease in the retina. In this study we used data from four complementary culture models; *PRPF6* and *PRPF31* mutant cell lines (Figures 1, 2), *PRPF31* patient-derived retinal organoids and *PRPF31* siRNA treated organotypic retinal cultures to corroborate a number of previous research findings, and provide new data to offer new insights into "splicing factor RP". Consistent with previous studies, we show an enrichment of differentially spliced cilium and centrosomal genes in *PRPF6* and *PRPF31* mutant cells, organoids and organotypic cultures (Tables 1, 2; Supplementary Figure S1), and that these splicing differences are associated with weaker 5′ splice sites but for the first time we also show that these splicing changes are associated with weaker 3′ splice sites (Figure 3). No explanation for the specific mis-splicing of cilium and centrosomal genes in *PRPF6* and *PRPF31* mutant cells has ever been posited; our data provides a possible explanation, as it suggests that cilium and centrosomal genes are particularly enriched for weak splice sites, and are thus more prone to mis-splicing in cells carrying mutant pre-mRNA splicing factors. We hypothesise that this leads to cilium and centrosomal defects which are more pronounced in the retina due to the highly specialised structure and function of the retinal photoreceptor cilium. Our data is also consistent with previously published studies in identifying significant differential splicing of DNA damage response genes in *PRPF6* and *PRPF31* mutant cells and tissues (Figure 4, Tables 1, 2). Again, little explanation for this observation has been offered in the past. Our data suggests that, as is widely reported, differential splicing of DNA damage response genes is simply a marker of activation of the DNA damage response pathway in these cells, rather than symptomatic of a defect in the DNA damage response pathway. Our data suggests that the DNA damage response pathway is more highly activated in *PRPF6* and *PRPF31* mutant cells because of underlying microtubule and microtubule organising centre (centrosome) defects in these cells (Figure 4; Tables 1, 2). However, UV exposure is unlikely to play a role in RP disease progression *in vivo*, as little UV penetrates through the vitreous humor in the eye to reach the retina. In this study UV exposure is used as a research tool to investigate the effect of DNA damage on *PRPF6* and *PRPF31* mutant cells, but oxidative stress, from the high level of reactive oxygen species in the RPE cells, plays more of a role in retinal degeneration *in vivo* (Perdices et al., 2018; Murakami et al., 2020; Vingolo et al., 2022). It will be important to study the effects of reactive oxygen species on the rates of DNA damage response pathway in these model cell lines to further understand the likely disease mechanism of *PRPF6* and *PRPF31*-associated RP.

We further add to the existing literature by investigating the expression of one gene which is particularly significantly differentially spliced gene in *PRPF6* and *PRPF31* mutant cells; *TTLL3*, a tubulin glycylase. *TTLL3* contains a number of very weak splice sites, and undergoes complex splicing to produce a diverse array of transcripts, many of which were differentially expressed in *PRPF6* and *PRPF31* mutant cells. TTLL3 catalyses monoglycylation of the cilium microtubules and is required for ciliogenesis; alterations in the balance of tubulin glycylation and glutamylation in photoreceptors has been shown to lead to retinal degeneration; absence of glycylation results in increased levels of tubulin glutamylation in photoreceptor cilia which leads to cilium degeneration. *Ttll3*$^{-/-}$ mice develop retinal degeneration. Thus, the mis-splicing of *TTLL3* is highly interesting in the context of RP associated with *PRPF6* and *PRPF31* mutations. *TTLL3* RNA expression data in the human retina suggests that *TTLL3* is the only tubulin glycylase expressed in the human retina, expressed by around 10%–25% of retinal cells from week 5 to week 24 of differentiation (Figure 5). We also note that this timing of *TTLL3* RNA expression correlates with when we observe monoglycylated tubulins in RECOVERIN positive cells in human embryonic stem cell derived retinal organoids (day 120), further suggesting that this *TTLL3* RNA is translated into protein and plays a role in tubulin monoglycylation in the retina (Figure 6). However, RNA expression does not always correlate with protein expression, and the absence of TTLL3 protein expression data, in the form of western blot or immunofluorescence, is a notable gap in our paper, in the *Ttll3*$^{-/-}$ mouse study (Bosch Grau et al., 2017) and in the literature in general. It will be important to follow up this paper with studies of

TTLL3 protein expression, if specific antibodies are available. We observe a reduction in monoglycylation in *PRPF6* and *PRPF31* mutant cells accompanied by a general loss of cilia (Figures 7A–D), although *PRPF6* mutant cells do retain some long cilia which exhibit glutamylation (Figure 2C), consistent with previously published literature showing an inverse relationship between glycylation and glutamylation levels in the *Ttll3*$^{-/-}$ mouse and *pcd* mouse (Bosch Grau et al., 2017). Our experiments with expression of exogenous *TTLL3* from a plasmid expression construct further suggest a functional role for *TTLL3* in ciliated retinal cells *in vitro* as this expression was able to rescue tubulin glycylation and ciliogenesis in PRPF mutant cells (Figure 7). This preliminary data demonstrating the rescue of tubulin glycylation and cilium number through exogenous *TTLL3* expression suggests that changes in *TTLL3* splicing and expression underlies the cilium defect in these cell models and may represent a potential target for therapeutic intervention in this group of disorders. It will be important to continue this work in human derived retinal organoids to investigate whether this is the disease mechanism *in vivo* and whether targeting of TTLL3 will be a useful therapeutic intervention for patients with this form of RP.

Data availability statement

The datasets presented in this study can be found in online repositories. The names of the repository/repositories and accession number(s) can be found below: https://www.ncbi.nlm.nih.gov/, PRJNA622794.

Author contributions

GW conceived of and obtained funding for the study, designed experiments, conducted experiments, analysed data, prepared figures and wrote the paper. LN and JLa conducted experiments, analysed data and prepared figures. JLo, VK, M-KC conducted experiments, and analysed data. All authors approved the final submission of the manuscript.

Funding

This work was funded by National Eye Research Council Small Award SAC019, Wellcome Trust Seed Award in Science 204378/Z/16/Z, UWE Bristol Quality Research funds and University of Southampton RMC Award. Suly Saray Villa Vasquez is supported by a University of Southampton Presidential Scholarship. Jenny Lord is funded by an NIHR Research Professorship awarded to Diana Baralle (RP-2016-07-011).

Acknowledgments

The authors acknowledge the use of the IRIDIS High Performance Computing Facility, and associated support services at the University of Southampton, in the completion of this work. We thank Stephen Cross, who is supported by the Elizabeth Blackwell Institute, through its Wellcome Trust ISSF Award, for high-throughput imaging support, and Dominic Alibhai for STED imaging support.

Conflict of interest

The authors declare that the research was conducted in the absence of any commercial or financial relationships that could be construed as a potential conflict of interest.

Publisher's note

Supplementary material

The Supplementary Material for this article can be found online at: https://www.frontiersin.org/articles/10.3389/fgene.2022.1009430/full#supplementary-material

SUPPLEMENTARY FIGURE S1
Sashimi plots showing differential splicing of exons in genes with gene ontology terms "centrosome", "microtubule organising center", "centriole" and in pathways related to primary cilium development and DNA damage response in PRPF31$^{+/-}$ cells and PRPF6$^{+/c.2185C>T}$ cells.

References

Adamson, B., Smogorzewska, A., Sigoillot, F. D., King, R. W., and Elledge, S. J. (2012). A genome-wide homologous recombination screen identifies the RNA-binding protein RBMX as a component of the DNA-damage response. *Nat. Cell Biol.* 14, 318–328. doi:10.1038/ncb2426

Ajmal, M., Khan, M. I., Neveling, K., Khan, Y. M., Azam, M., Waheed, N. K., et al. (2014). A missense mutation in the splicing factor gene DHX38 is associated with early-onset retinitis pigmentosa with macular coloboma. *J. Med. Genet.* 51, 444–448. doi:10.1136/jmedgenet-2014-102316

Anders, S., Pyl, P. T., and Huber, W. (2015). HTSeq--a Python framework to work with high-throughput sequencing data. *Bioinformatics* 31, 166–169. doi:10.1093/bioinformatics/btu638

Astuti, G. D., Arno, G., Hull, S., Pierrache, L., Venselaar, H., Carss, K., et al. (2016). Mutations in AGBL5, encoding α-tubulin deglutamylase, are associated with autosomal recessive retinitis pigmentosa. *Invest. Ophthalmol. Vis. Sci.* 57, 6180–6187. doi:10.1167/iovs.16-20148

Azizzadeh Pormehr, L., Ahmadian, S., Daftarian, N., Mousavi, S. A., and Shafiezadeh, M. (2019). PRPF31 reduction causes mis-splicing of the phototransduction genes in human organotypic retinal culture. *Eur. J. Hum. Genet.* 28, 491–498. doi:10.1038/s41431-019-0531-1

Azizzadeh Pormehr, L., Ahmadian, S., Daftarian, N., Mousavi, S. A., and Shafiezadeh, M. (2020). PRPF31 reduction causes mis-splicing of the phototransduction genes in human organotypic retinal culture. *Eur. J. Hum. Genet.* 28, 491–498. doi:10.1038/s41431-019-0531-1

Bedoni, N., Haer-Wigman, L., Vaclavik, V., Tran, V. H., Farinelli, P., Balzano, S., et al. (2016). Mutations in the polyglutamylase gene TTLL5, expressed in photoreceptor cells and spermatozoa, are associated with cone-rod degeneration and reduced male fertility. *Hum. Mol. Genet.* 25, 4546–4555. doi:10.1093/hmg/ddw282

Birmingham, A., Selfors, L. M., Forster, T., Wrobel, D., Kennedy, C. J., Shanks, E., et al. (2009). Statistical methods for analysis of high-throughput RNA interference screens. *Nat. Methods* 6, 569–575. doi:10.1038/nmeth.1351

Boldt, K., van Reeuwijk, J., Lu, Q., Koutroumpas, K., Nguyen, T. M. T., Texier, Y., et al. (2016). An organelle-specific protein landscape identifies novel diseases and molecular mechanisms. *Nat. Commun.* 7, 11491. doi:10.1038/ncomms11491

Bosch Grau, M., Gonzalez Curto, G., Rocha, C., Magiera, M. M., Marques Sousa, P., Giordano, T., et al. (2013). Tubulin glycylases and glutamylases have distinct functions in stabilization and motility of ependymal cilia. *J. Cell Biol.* 202, 441–451. doi:10.1083/jcb.201305041

Bosch Grau, M., Masson, C., Gadadhar, S., Rocha, C., Tort, O., Marques Sousa, P., et al. (2017). Alterations in the balance of tubulin glycylation and glutamylation in photoreceptors leads to retinal degeneration. *J. Cell Sci.* 130, 938–949. doi:10.1242/jcs.199091

Bowne, S. J., Sullivan, L. S., Avery, C. E., Sasser, E. M., Roorda, A., Duncan, J. L., et al. (2013). Mutations in the small nuclear riboprotein 200 kDa gene (SNRNP200) cause 1.6% of autosomal dominant retinitis pigmentosa. *Mol. Vis.* 19, 2407–2417.

Branham, K., Matsui, H., Biswas, P., Guru, A. A., Hicks, M., Suk, J. J., et al. (2016). Establishing the involvement of the novel gene AGBL5 in retinitis pigmentosa by whole genome sequencing. *Physiol. Genomics* 48, 922–927. doi:10.1152/physiolgenomics.00101.2016

Bujakowska, K., Maubaret, C., Chakarova, C. F., Tanimoto, N., Beck, S. C., Fahl, E., et al. (2009). Study of gene-targeted mouse models of splicing factor gene Prpf31 implicated in human autosomal dominant retinitis pigmentosa (RP). *Invest. Ophthalmol. Vis. Sci.* 50, 5927–5933. doi:10.1167/iovs.08-3275

Bujakowska, K. M., Liu, Q., and Pierce, E. A. (2017). Photoreceptor cilia and retinal ciliopathies. *Cold Spring Harb. Perspect. Biol.* 9, a028274. doi:10.1101/cshperspect.a028274

Buskin, A., Zhu, L., Chichagova, V., Basu, B., Mozaffari-Jovin, S., Dolan, D., et al. (2018). Disrupted alternative splicing for genes implicated in splicing and ciliogenesis causes PRPF31 retinitis pigmentosa. *Nat. Commun.* 9, 4234. doi:10.1038/s41467-018-06448-y

Cao, H., Wu, J., Lam, S., Duan, R., Newnham, C., Molday, R. S., et al. (2011). Temporal and tissue specific regulation of RP-associated splicing factor genes PRPF3, PRPF31 and PRPC8--implications in the pathogenesis of RP. *PloS one* 6, e15860. doi:10.1371/journal.pone.0015860

Carpenter, A. E., Jones, T. R., Lamprecht, M. R., Clarke, C., Kang, I. H., Friman, O., et al. (2006). CellProfiler: Image analysis software for identifying and quantifying cell phenotypes. *Genome Biol.* 7, R100–R2006. doi:10.1186/gb-2006-7-10-r100

Chakarova, C. F., Hims, M. M., Bolz, H., Abu-Safieh, L., Patel, R. J., Papaioannou, M. G., et al. (2002). Mutations in HPRP3, a third member of pre-mRNA splicing factor genes, implicated in autosomal dominant retinitis pigmentosa. *Hum. Mol. Genet.* 11, 87–92. doi:10.1093/hmg/11.1.87

Chen, E. Y., Tan, C. M., Kou, Y., Duan, Q., Wang, Z., Meirelles, G. V., et al. (2013). Enrichr: Interactive and collaborative HTML5 gene list enrichment analysis tool. *BMC Bioinforma.* 14, 128. doi:10.1186/1471-2105-14-128

Chen, X., Liu, Y., Sheng, X., Tam, P. O. S., Zhao, K., Chen, X., et al. (2014). PRPF4 mutations cause autosomal dominant retinitis pigmentosa. *Hum. Mol. Genet.* 23, 2926–2939. doi:10.1093/hmg/ddu005

Chung, N., Zhang, X. D., Kreamer, A., Locco, L., Kuan, P. F., Bartz, S., et al. (2008). Median absolute deviation to improve hit selection for genome-scale RNAi screens. *J. Biomol. Screen.* 13, 149–158. doi:10.1177/1087057107312035

Collin, J., Queen, R., Zerti, D., Dorgau, B., Hussain, R., Coxhead, J., et al. (2019). Deconstructing retinal organoids: Single cell RNA-seq reveals the cellular components of human pluripotent stem cell-derived retina. *Stem Cells* 37, 593–598. doi:10.1002/stem.2963

Comitato, A., Spampanato, C., Chakarova, C., Sanges, D., Bhattacharya, S. S., and Marigo, V. (2007). Mutations in splicing factor PRPF3, causing retinal degeneration, form detrimental aggregates in photoreceptor cells. *Hum. Mol. Genet.* 16, 1699–1707. doi:10.1093/hmg/ddm118

Dobin, A., Davis, C. A., Schlesinger, F., Drenkow, J., Zaleski, C., Jha, S., et al. (2013). Star: Ultrafast universal RNA-seq aligner. *Bioinformatics* 29, 15–21. doi:10.1093/bioinformatics/bts635

Dutertre, M., Sanchez, G., De Cian, M. C., Barbier, J., Dardenne, E., Gratadou, L., et al. (2010). Cotranscriptional exon skipping in the genotoxic stress response. *Nat. Struct. Mol. Biol.* 17, 1358–1366. doi:10.1038/nsmb.1912

Estrada-Cuzcano, A., Roepman, R., Cremers, F. P., den Hollander, A. I., and Mans, D. A. (2012). Non-syndromic retinal ciliopathies: Translating gene discovery into therapy. *Hum. Mol. Genet.* 21, R111–R124. doi:10.1093/hmg/dds298

Farkas, M. H., Lew, D. S., Sousa, M. E., Bujakowska, K., Chatagnon, J., Bhattacharya, S. S., et al. (2014). Mutations in pre-mRNA processing factors 3, 8, and 31 cause dysfunction of the retinal pigment epithelium. *Am. J. Pathol.* 184, 2641–2652. doi:10.1016/j.ajpath.2014.06.026

Ferrante, M. I., GiorGio, G., Feather, S. A., Bulfone, A., Wright, V., GhianiM., et al. (2001). Identification of the gene for oral-facial-digital type I syndrome. *Am. J. Hum. Genet.* 68, 569–576. doi:10.1086/318802

Frankish, A., Diekhans, M., Ferreira, A. M., Johnson, R., Jungreis, I., Loveland, J., et al. (2019). GENCODE reference annotation for the human and mouse genomes. *Nucleic Acids Res.* 47, D766–D773. doi:10.1093/nar/gky955

Frio, R., Ransijn, A., Berson, E. L., Beckmann, J. S., and Rivolta, C. (2008). Premature termination codons in PRPF31 cause retinitis pigmentosa via haploinsufficiency due to nonsense-mediated mRNA decay. *J. Clin. Invest.* 118, 1519–1531. doi:10.1172/JCI34211

Gadadhar, S., Dadi, H., Bodakuntla, S., Schnitzler, A., Bieche, I., Rusconi, F., et al. (2017). Tubulin glycylation controls primary cilia length. *J. Cell Biol.* 216, 2701–2713. doi:10.1083/jcb.201612050

Graziotto, J. J., Farkas, M. H., Bujakowska, K., Deramaudt, B. M., Zhang, Q., Nandrot, E. F., et al. (2011). Three gene-targeted mouse models of RNA splicing factor RP show late-onset RPE and retinal degeneration. *Invest. Ophthalmol. Vis. Sci.* 52, 190–198. doi:10.1167/iovs.10-5194

Graziotto, J. J., Inglehearn, C. F., Pack, M. A., and Pierce, E. A. (2008). Decreased levels of the RNA splicing factor Prpf3 in mice and zebrafish do not cause photoreceptor degeneration. *Invest. Ophthalmol. Vis. Sci.* 49, 3830–3838. doi:10.1167/iovs.07-1483

GTEx Consortium. (2015). Human genomics. The genotype-tissue expression (GTEx) pilot analysis: Multitissue gene regulation in humans. *Science* 348, 648–660. doi:10.1126/science.1262110

GTEx Consortium. (2013). The genotype-tissue expression (GTEx) project. *Nat. Genet.* 45, 580–585. doi:10.1038/ng.2653

Hao, K., Chen, Y., Yan, X., and Zhu, X. (2021). Cilia locally synthesize proteins to sustain their ultrastructure and functions. *Nat. Commun.* 12, 6971. doi:10.1038/s41467-021-27298-1

Haward, F., Maslon, M. M., Yeyati, P. L., Bellora, N., Hansen, J. N., Aitken, S., et al. (2021). Nucleo-cytoplasmic shuttling of splicing factor SRSF1 is required for development and cilia function. *eLife* 10, e65104. doi:10.7554/eLife.65104

Hoshino, A., Ratnapriya, R., Brooks, M. J., Chaitankar, V., Wilken, M. S., Zhang, C., et al. (2017). Molecular anatomy of the developing human retina. *Dev. Cell* 43, 763e764–779. doi:10.1016/j.devcel.2017.10.029

Hu, Y., Wang, X., Hu, B., Mao, Y., Chen, Y., Yan, L., et al. (2019). Dissecting the transcriptome landscape of the human fetal neural retina and retinal pigment epithelium by single-cell RNA-seq analysis. *PLoS Biol.* 17, e3000365. doi:10.1371/journal.pbio.3000365

Huranova, M., Hnilicova, J., Fleischer, B., Cvackova, Z., and Stanek, D. (2009). A mutation linked to retinitis pigmentosa in HPRP31 causes protein instability and impairs its interactions with spliceosomal snRNPs. *Hum. Mol. Genet.* 18, 2014–2023. doi:10.1093/hmg/ddp125

Iaconis, D., Monti, M., Renda, M., van Koppen, A., Tammaro, R., Chiaravalli, M., et al. (2017). The centrosomal OFD1 protein interacts with the translation machinery and regulates the synthesis of specific targets. *Sci. Rep.* 7, 1224. doi:10.1038/s41598-017-01156-x

Ivings, L., Towns, K. V., Matin, M. A., Taylor, C., Ponchel, F., Grainger, R. J., et al. (2008). Evaluation of splicing efficiency in lymphoblastoid cell lines from patients with splicing-factor retinitis pigmentosa. *Mol. Vis.* 14, 2357–2366.

Jakobsen, L., Vanselow, K., Skogs, M., Toyoda, Y., Lundberg, E., Poser, I., et al. (2011). Novel asymmetrically localizing components of human centrosomes

identified by complementary proteomics methods. *EMBO J.* 30, 1520–1535. doi:10.1038/emboj.2011.63

Jin, Z. B., Okamoto, S., Osakada, F., Homma, K., Assawachananont, J., Hirami, Y., et al. (2011). Modeling retinal degeneration using patient-specific induced pluripotent stem cells. *PloS one* 6, e17084. doi:10.1371/journal.pone.0017084

Johnson, C. A., and Malicki, J. J. (2019). The nuclear arsenal of cilia. *Dev. Cell* 49, 161–170. doi:10.1016/j.devcel.2019.03.009

Kastner, S., Thiemann, I. J., Dekomien, G., Petrasch-Parwez, E., Schreiber, S., Akkad, D. A., et al. (2015). Exome sequencing reveals AGBL5 as novel candidate gene and additional variants for retinitis pigmentosa in five Turkish families. *Invest. Ophthalmol. Vis. Sci.* 56, 8045–8053. doi:10.1167/iovs.15-17473

Keen, T. J., Hims, M. M., McKie, A. B., Moore, A. T., Doran, R. M., Mackey, D. A., et al. (2002). Mutations in a protein target of the Pim-1 kinase associated with the RP9 form of autosomal dominant retinitis pigmentosa. *Eur. J. Hum. Genet.* 10, 245–249. doi:10.1038/sj.ejhg.5200797

Komor, A. C., Kim, Y. B., Packer, M. S., Zuris, J. A., and Liu, D. R. (2016). Programmable editing of a target base in genomic DNA without double-stranded DNA cleavage. *Nature* 533, 420–424. doi:10.1038/nature17946

Kuleshov, M. V., Jones, M. R., Rouillard, A. D., Fernandez, N. F., Duan, Q., Wang, Z., et al. (2016). Enrichr: A comprehensive gene set enrichment analysis web server 2016 update. *Nucleic Acids Res.* 44, W90–W97. doi:10.1093/nar/gkw377

Li, J., Liu, F., Lv, Y., Sun, K., Zhao, Y., Reilly, J., et al. (2021). Prpf31 is essential for the survival and differentiation of retinal progenitor cells by modulating alternative splicing. *Nucleic Acids Res.* 49, 2027–2043. doi:10.1093/nar/gkab003

Linder, B., Dill, H., Hirmer, A., Brocher, J., Lee, G. P., Mathavan, S., et al. (2011). Systemic splicing factor deficiency causes tissue-specific defects: A zebrafish model for retinitis pigmentosa. *Hum. Mol. Genet.* 20, 368–377. doi:10.1093/hmg/ddq473

Linder, B., Hirmer, A., Gal, A., Ruther, K., Bolz, H. J., Winkler, C., et al. (2014). Identification of a PRPF4 loss-of-function variant that abrogates U4/U6.U5 tri-snRNP integration and is associated with retinitis pigmentosa. *PloS one* 9, e111754. doi:10.1371/journal.pone.0111754

Liu, Y., Chen, X., Qin, B., Zhao, K., Zhao, Q., Staley, J. P., et al. (2015). Knocking down Snrnp200 initiates demorphogenesis of rod photoreceptors in zebrafish. *J. Ophthalmol.* 2015, 816329. doi:10.1155/2015/816329

McCarthy, D. J., Chen, Y., and Smyth, G. K. (2012). Differential expression analysis of multifactor RNA-Seq experiments with respect to biological variation. *Nucleic Acids Res.* 40, 4288–4297. doi:10.1093/nar/gks042

McKie, A. B., McHale, J. C., Keen, T. J., Tarttelin, E. E., Goliath, R., van Lith-Verhoeven, J. J., et al. (2001). Mutations in the pre-mRNA splicing factor gene PRPC8 in autosomal dominant retinitis pigmentosa (RP13). *Hum. Mol. Genet.* 10, 1555–1562. doi:10.1093/hmg/10.15.1555

Mordes, D., Yuan, L., Xu, L., Kawada, M., Molday, R. S., and Wu, J. Y. (2007). Identification of photoreceptor genes affected by PRPF31 mutations associated with autosomal dominant retinitis pigmentosa. *Neurobiol. Dis.* 26, 291–300. doi:10.1016/j.nbd.2006.08.026

Murakami, Y., Nakabeppu, Y., and Sonoda, K. H. (2020). Oxidative stress and microglial response in retinitis pigmentosa. *Int. J. Mol. Sci.* 21, E7170. doi:10.3390/ijms21197170

Nazlamova, L., Thomas, N. S., Cheung, M. K., Legebeke, J., Lord, J., Pengelly, R. J., et al. (2020). A CRISPR and high-content imaging assay compliant with ACMG/AMP guidelines for clinical variant interpretation in ciliopathies. *Hum. Genet.* 140, 593–607. doi:10.1007/s00439-020-02228-1

Oud, M. M., Lamers, I. J., and ArtsCiliopathies, H. H. (2017). Ciliopathies: Genetics in pediatric medicine. *J. Pediatr. Genet.* 6, 18–29. doi:10.1055/s-0036-1593841

Papasaikas, P., Tejedor, J. R., Vigevani, L., and Valcarcel, J. (2015). Functional splicing network reveals extensive regulatory potential of the core spliceosomal machinery. *Mol. Cell* 57, 7–22. doi:10.1016/j.molcel.2014.10.030

Patel, N., Aldahmesh, M. A., Alkuraya, H., Anazi, S., Alsharif, H., Khan, A. O., et al. (2016). Expanding the clinical, allelic, and locus heterogeneity of retinal dystrophies. *Genet. Med.* 18, 554–562. doi:10.1038/gim.2015.127

Patro, R., Duggal, G., Love, M. I., Irizarry, R. A., and Kingsford, C. (2017). Salmon provides fast and bias-aware quantification of transcript expression. *Nat. Methods* 14, 417–419. doi:10.1038/nmeth.4197

Paulsen, R. D., Soni, D. V., Wollman, R., Hahn, A. T., Yee, M. C., Guan, A., et al. (2009). A genome-wide siRNA screen reveals diverse cellular processes and pathways that mediate genome stability. *Mol. Cell* 35, 228–239. doi:10.1016/j.molcel.2009.06.021

Pellacani, C., Bucciarelli, E., Renda, F., Hayward, D., Palena, A., Chen, J., et al. (2018). Splicing factors Sf3A2 and Prp31 have direct roles in mitotic chromosome segregation. *Elife* 7, e40325. doi:10.7554/eLife.40325

Perdices, L., Fuentes-Broto, L., Segura, F., Ben Gdara, N., Sanchez-Cano, A. I., Insa, G., et al. (2018). Hepatic oxidative stress in pigmented P23H rhodopsin transgenic rats with progressive retinal degeneration. *Free Radic. Biol. Med.* 124, 550–557. doi:10.1016/j.freeradbiomed.2018.07.005

Pleiss, J. A., Whitworth, G. B., Bergkessel, M., and Guthrie, C. (2007). Transcript specificity in yeast pre-mRNA splicing revealed by mutations in core spliceosomal components. *PLoS Biol.* 5, e90. doi:10.1371/journal.pbio.0050090

Ran, F. A., Hsu, P. D., Lin, C. Y., Gootenberg, J. S., Konermann, S., Trevino, A. E., et al. (2013). Double nicking by RNA-guided CRISPR Cas9 for enhanced genome editing specificity. *Cell* 154, 1380–1389. doi:10.1016/j.cell.2013.08.021

Robinson, M. D., McCarthy, D. J., and Smyth, G. K. edgeR. (2010). edgeR: a Bioconductor package for differential expression analysis of digital gene expression data. *Bioinformatics* 26, 139–140. doi:10.1093/bioinformatics/btp616

Rocha, C., Papon, L., Cacheux, W., Marques Sousa, P., Lascano, V., Tort, O., et al. (2014). Tubulin glycylases are required for primary cilia, control of cell proliferation and tumor development in colon. *Embo J.* 33, 2247–2260. doi:10.15252/embj.201488466

Rogowski, K., Juge, F., van Dijk, J., Wloga, D., Strub, J. M., Levilliers, N., et al. (2009). Evolutionary divergence of enzymatic mechanisms for posttranslational polyglycylation. *Cell* 137, 1076–1087. doi:10.1016/j.cell.2009.05.020

Schmidt-Kastner, R., Yamamoto, H., Hamasaki, D., Yamamoto, H., Parel, J. M., Schmitz, C., et al. (2008). Hypoxia-regulated components of the U4/U6.U5 tri-small nuclear riboprotein complex: Possible role in autosomal dominant retinitis pigmentosa. *Mol. Vis.* 14, 125–135.

Sergouniotis, P. I., Chakarova, C., Murphy, C., Becker, M., Lenassi, E., Arno, G., et al. (2014). Biallelic variants in TTLL5, encoding a tubulin glutamylase, cause retinal dystrophy. *Am. J. Hum. Genet.* 94, 760–769. doi:10.1016/j.ajhg.2014.04.003

Sharon, D., and Banin, E. (2015). Nonsyndromic retinitis pigmentosa is highly prevalent in the Jerusalem region with a high frequency of founder mutations. *Mol. Vis.* 21, 783–792.

Shen, S., Park, J. W., Lu, Z. x., Lin, L., Henry, M. D., Wu, Y. N., et al. (2014). rMATS: robust and flexible detection of differential alternative splicing from replicate RNA-Seq data. *Proc. Natl. Acad. Sci. U. S. A.* 111, E5593–E5601. doi:10.1073/pnas.1419161111

Shinde, V., Kotla, P., Strang, C., and Gorbatyuk, M. (2016). Unfolded protein response-induced dysregulation of calcium homeostasis promotes retinal degeneration in rat models of autosomal dominant retinitis pigmentosa. *Cell Death Dis.* 7, e2085. doi:10.1038/cddis.2015.325

Shkreta, L., and Chabot, B. (2015). The RNA splicing response to DNA damage. *Biomolecules* 5, 2935–2977. doi:10.3390/biom5042935

Sullivan, L. S., Bowne, S. J., Birch, D. G., Hughbanks-Wheaton, D., Heckenlively, J. R., Lewis, R. A., et al. (2006). Prevalence of disease-causing mutations in families with autosomal dominant retinitis pigmentosa: A screen of known genes in 200 families. *Invest. Ophthalmol. Vis. Sci.* 47, 3052–3064. doi:10.1167/iovs.05-1443

Sun, X., Park, J. H., Gumerson, J., Wu, Z., Swaroop, A., Qian, H., et al. (2016). Loss of RPGR glutamylation underlies the pathogenic mechanism of retinal dystrophy caused by TTLL5 mutations. *Proc. Natl. Acad. Sci. U. S. A.* 113, E2925–E2934. doi:10.1073/pnas.1523201113

Tanackovic, G., Ransijn, A., Ayuso, C., Harper, S., Berson, E. L., and Rivolta, C. (2011). A missense mutation in PRPF6 causes impairment of pre-mRNA splicing and autosomal-dominant retinitis pigmentosa. *Am. J. Hum. Genet.* 88, 643–649. doi:10.1016/j.ajhg.2011.04.008

Tresini, M., Warmerdam, D. O., Kolovos, P., Snijder, L., Vrouwe, M. G., Demmers, J. A. A., et al. (2015). The core spliceosome as target and effector of non-canonical ATM signalling. *Nature* 523, 53–58. doi:10.1038/nature14512

Verbakel, S. K., Van Huet, R. A. C., Boon, C. J. F., Den Hollander, A. I., Collin, R. W. J., Klaver, C. C. W., et al. (2018). Non-syndromic retinitis pigmentosa. *Prog. Retin. eye Res.* 66, 157–186. doi:10.1016/j.preteyeres.2018.03.005

Vingolo, E. M., Casillo, L., Contento, L., Toja, F., and Florido, A. (2022). Retinitis pigmentosa (RP): The role of oxidative stress in the degenerative process progression. *Biomedicines* 10, 582. doi:10.3390/biomedicines10030582

Vithana, E. N., Abu-Safieh, L., Allen, M. J., CArey, A., PapaioannouM.Chakarova, C., et al. (2001). A human homolog of yeast pre-mRNA splicing gene, PRP31, underlies autosomal dominant retinitis pigmentosa on chromosome 19q13.4 (RP11). *Mol. Cell* 8, 375–381. doi:10.1016/s1097-2765(01)00305-7

Wang, L., Wang, S., and Li, W. (2012). RSeQC: Quality control of RNA-seq experiments. *Bioinformatics* 28, 2184–2185. doi:10.1093/bioinformatics/bts356

Wheway, G., Douglas, A., Baralle, D., and Guillot, E. (2020). Mutation spectrum of PRPF31, genotype-phenotype correlation in retinitis pigmentosa, and opportunities for therapy. *Exp. Eye Res.* 192, 107950. doi:10.1016/j.exer.2020.107950

Wheway, G., Schmidts, M., Mans, D. A., Szymanska, K., Nguyen, T. M. T., Racher, H., et al. (2015). An siRNA-based functional genomics screen for the identification of regulators of ciliogenesis and ciliopathy genes. *Nat. Cell Biol.* 17, 1074–1087. doi:10.1038/ncb3201

Wickramasinghe, V. O., Gonzalez-Porta, M., Perera, D., Bartolozzi, A. R., Sibley, C. R., Hallegger, M., et al. (2015). Regulation of constitutive and alternative mRNA splicing across the human transcriptome by PRPF8 is determined by 5' splice site strength. *Genome Biol.* 16, 201. doi:10.1186/s13059-015-0749-3

Wilkie, S. E., Morris, K. J., Bhattacharya, S. S., Warren, M. J., and Hunt, D. M. (2006). A study of the nuclear trafficking of the splicing factor protein PRPF31 linked to autosomal dominant retinitis pigmentosa (ADRP). *Biochim. Biophys. Acta* 1762, 304–311. doi:10.1016/j.bbadis.2005.12.004

Wilkie, S. E., Vaclavik, V., Wu, H., Bujakowska, K., Chakarova, C. F., Bhattacharya, S. S., et al. (2008). Disease mechanism for retinitis pigmentosa (RP11) caused by missense mutations in the splicing factor gene PRPF31. *Mol. Vis.* 14, 683–690.

Will, C. L., and Luhrmann, R. (2011). Spliceosome structure and function. *Cold Spring Harb. Perspect. Biol.* 3, a003707. doi:10.1101/cshperspect.a003707

Wloga, D., Webster, D. M., Rogowski, K., Bre, M. H., Levilliers, N., Jerka-Dziadosz, M., et al. (2009). TTLL3 Is a tubulin glycine ligase that regulates the assembly of cilia. *Dev. Cell* 16, 867–876. doi:10.1016/j.devcel.2009.04.008

Yeo, G., and Burge, C. B. (2004). Maximum entropy modeling of short sequence motifs with applications to RNA splicing signals. *J. Comput. Biol.* 11, 377–394. doi:10.1089/1066527041410418

Yin, J., Brocher, J., Fischer, U., and Winkler, C. (2011). Mutant Prpf31 causes pre-mRNA splicing defects and rod photoreceptor cell degeneration in a zebrafish model for Retinitis pigmentosa. *Mol. Neurodegener.* 6, 56. doi:10.1186/1750-1326-6-56

Yuan, L., Kawada, M., Havlioglu, N., Tang, H., and Wu, J. Y. (2005). Mutations in PRPF31 inhibit pre-mRNA splicing of rhodopsin gene and cause apoptosis of retinal cells. *J. Neurosci.* 25, 748–757. doi:10.1523/JNEUROSCI.2399-04.2005

Zhang, X. D. (2007). A pair of new statistical parameters for quality control in RNA interference high-throughput screening assays. *Genomics* 89, 552–561. doi:10.1016/j.ygeno.2006.12.014

Zhao, C., Bellur, D. L., Lu, S., Zhao, F., Grassi, M. A., Bowne, S. J., et al. (2009). Autosomal-dominant retinitis pigmentosa caused by a mutation in SNRNP200, a gene required for unwinding of U4/U6 snRNAs. *Am. J. Hum. Genet.* 85, 617–627. doi:10.1016/j.ajhg.2009.09.020

frontiers | Frontiers in Genetics

TYPE Original Research
PUBLISHED 30 September 2022
DOI 10.3389/fgene.2022.985227

OPEN ACCESS

EDITED BY
Steven L. C. Pei,
Yale University, United States

REVIEWED BY
Shiaulou Yuan,
Massachusetts General Hospital and Harvard Medical School, United States
Raymond H. Kim,
University of Toronto, Canada
Naoyuki Sone,
Kyoto University, Japan

*CORRESPONDENCE
Anu I. Sironen,
a.sironen@ucl.ac.uk

SPECIALTY SECTION
This article was submitted to Human and Medical Genomics, a section of the journal Frontiers in Genetics

RECEIVED 03 July 2022
ACCEPTED 24 August 2022
PUBLISHED 30 September 2022

CITATION
Schultz R, Elenius V, Fassad MR, Freke G, Rogers A, Shoemark A, Koistinen T, Mohamed MA, Lim JSY, Mitchison HM and Sironen AI (2022), CFAP300 mutation causing primary ciliary dyskinesia in Finland.
Front. Genet. 13:985227.
doi: 10.3389/fgene.2022.985227

CFAP300 mutation causing primary ciliary dyskinesia in Finland

Rüdiger Schultz[1], Varpu Elenius[2], Mahmoud R. Fassad[3,4], Grace Freke[3], Andrew Rogers[5], Amelia Shoemark[5,6], Tiina Koistinen[7], Mai A. Mohamed[3,8], Jacqueline S. Y. Lim[3], Hannah M. Mitchison[3] and Anu I. Sironen[3,9]*

[1]Allergy Centre, Tampere University Hospital, Tampere, Finland, [2]Department of Pediatrics, Turku University Hospital, University of Turku, Turku, Finland, [3]Great Ormond Street Institute of Child Health, University College London, London, United Kingdom, [4]Human Genetics Department, Medical Research Institute, Alexandria University, Alexandria, Egypt, [5]PCD Diagnostic Team and Department of Paediatric Respiratory Medicine, Royal Brompton Hospita, London, United Kingdom, [6]School of Medicine, University of Dundee, Dundee, United Kingdom, [7]Department of Otorhinolaryngology, Head and Neck Surgery, Kuopio University Hospital and University of Eastern Finland, Kuopio, Finland, [8]Biochemistry Division, Chemistry Department, Faculty of Science, Zagazig University, Zagazig, Egypt, [9]Natural Resources Institute Finland (Luke), Helsinki, Finland

Primary ciliary dyskinesia (PCD) is a rare genetic condition characterized by chronic respiratory tract infections and in some cases laterality defects and infertility. The symptoms of PCD are caused by malfunction of motile cilia, hair-like organelles protruding out of the cell that are responsible for removal of mucus from the airways and organizing internal organ positioning during embryonic development. PCD is caused by mutations in genes coding for structural or assembly proteins in motile cilia. Thus far mutations in over 50 genes have been identified and these variants explain around 70% of all known cases. Population specific genetics underlying PCD has been reported, thus highlighting the importance of characterizing gene variants in different populations for development of gene-based diagnostics. In this study, we identified a recurrent loss-of-function mutation c.198_200delinsCC in *CFAP300* causing lack of the protein product. PCD patients homozygous for the identified *CFAP300* mutation have immotile airway epithelial cilia associated with missing dynein arms in their ciliary axonemes. Furthermore, using super resolution microscopy we demonstrate that CFAP300 is transported along cilia in normal human airway epithelial cells suggesting a role for CFAP300 in dynein complex transport in addition to preassembly in the cytoplasm. Our results highlight the importance of CFAP300 in dynein arm assembly and improve diagnostics of PCD in Finland.

KEYWORDS

motile cilia, primary ciliary dyskinesia, CFAP300, dynein arm preassembly, diagnostics

Introduction

Primary ciliary dyskinesia (PCD) is an inherited, genetically and clinically heterogenous disorder caused by mutations in genes encoding proteins crucial for cilia motility. Motile cilia line the respiratory tract and are required for efficient mucus removal from the airways. Children with PCD suffer from early onset chronic airway infections and congestion leading to a distinctive, chronic wet cough (Lucas et al., 2020; Shoemark and Harman, 2021). If untreated, the condition may progress towards bronchiectasis in later life. During embryonic development, motile cilia determine the left-right positioning of body organs and nearly half of PCD patients have laterality problems. The brain ventricles are also lined with motile ependymal cilia, which are required for the flow of cerebrospinal fluid. However, hydrocephalus caused by defective ependymal cilia is rare in PCD patients. Motile cilia of the airways have a 9 + 2 axonemal core structure with a central pair of microtubules surrounded by nine peripheral doublet microtubules, which have outer and inner dynein arms (ODA and IDA, respectively) attached along their length. These ODA and IDA are motors that power cilia motility and are preassembled in the cytoplasm then transported via intraflagellar transport (IFT) to the cilium (Horani et al., 2018). Mutations in many preassembly factors have been identified as a cause for PCD in addition to mutations in structural genes of cilia components. Dynein arm preassembly factors DNAAF1 (Duquesnoy et al., 2009; Loges et al., 2009), DNAAF2 (Omran et al., 2008), DNAAF3 (Mitchison et al., 2012), DNAAF4 (Tarkar et al., 2013), DNAAF5 (Horani et al., 2012; Diggle et al., 2014), DNAAF11 (Kott et al., 2012; Horani et al., 2013; Inaba et al., 2016) and DNAAF6 (Olcese et al., 2017; Paff et al., 2017) are strictly localized in the cytoplasm, but interestingly ZMYND10 (Moore et al., 2013; Zariwala et al., 2013), CFAP298 (Austin-Tse et al., 2013; Jaffe et al., 2016) and CFAP300 (Fassad et al., 2018) are also found in the ciliary compartment, suggesting a combined role in assembly and transport. The core structure of the sperm flagellum is very similar to that of motile cilia, although some differences exist. Furthermore, male specific motile cilia are present in the efferent duct of the male reproductive tract and female specific motile cilia in the oviduct. Therefore, PCD is also associated with infertility, especially in men (Sironen et al., 2019), However, genotype/phenotype correlation between PCD and fertility is poorly understood and requires further studies.

PCD is inherited as an autosomal-recessive or rarely as X-linked disease. Thus far mutations in over 50 genes have been identified to cause PCD, explaining approximately 70% of cases. Over 300 genes encode essential components of the motile ciliary machinery and a large number of patients are still without a genetic diagnosis (Lucas et al., 2020). The aim of this study was to identify disease causing variants in the Finnish PCD population, where until now only two variants in *DNAH11* have been previously reported (Schultz et al., 2020). It is important to increase the understanding of genetic causes for PCD, which can be most effectively traced in a genetically isolated population such as the Finns. This study contributes to the understanding of genetic causes of PCD by identification of a causative loss of function (LoF) mutation in *CFAP300* in Finnish PCD patients. Population specific mutations play an important role in PCD and thus it is important to investigate the genetic variability in different populations (Fassad et al., 2020; Mitchison and Smedley, 2022). We also show that additional to a role in the cytoplasmic preassembly of dynein arms, human CFAP300 is involved in protein transport to motile cilia, which was previously only suggested in model organisms.

Methods

Subject

Blood samples were collected from thirteen PCD patients, recruited at the University Hospitals of Turku, Kuopio and Tampere after written informed consent was given. For variant segregation analysis saliva samples were collected from families (healthy parents and siblings when possible). Patients were interviewed and scored using the PICADAR questionnaire (Behan et al., 2016). The study was ethically approved by the University of Turku Ethics Committee (ETMK 69–2017), London Bloomsbury Research Ethics Committee approved by the Health Research Authority (08/H0713/82), and the referring hospitals.

Nasal nitric oxide analysis

For nasal nitric oxide (nNO) analysis a CLD 88sp analyser equipped with a Denox 88 module for flow control was used (Eco Physics, Dürnten, Switzerland). If cooperativity was established, three consecutive trials were taken, from which the highest value was recorded. Nasal nitric oxide analysis was repeated on two different occasions.

High-speed video microscopy analysis

Nasal epithelial cells were suspended in DMEM medium and evaluated under a differential-interference microscope (Zeiss, Oberkochen, Germany) at ×1,000 magnification and cilia beat was recorded with a digital high-speed video (DHSV) camera (Hamamatsu Orca Flash 4.0, Hamamatsu Japan) with a frame rate of 256 Hz. The detailed protocol for HSVM can be found in Schultz et al., 2022. DHSV video sequences were played back frame by frame and cilia beat frequency (CBF) was determined by calculating the mean of all recorded cilia beat cycles and the

cilia beating pattern (CBP) was determined by two independent expert operators. HSVM was repeated on two different occasions.

Whole exome sequencing

The Nonacus Cell3 Exome panel was used for whole exome sequencing of patient samples (https://nonacus.com/cell3tm-target). Unmapped reads were aligned to the current Human reference genome (GRCh38 build) by Burrows-Wheeler Aligner tool (Bwa-mem2 version) (Li and Durbin, 2010), SAM files were produced and indexed and converted to BAM format previous to marking and removing duplicates using Picard (https://broadinstitute.github.io/picard/). Subsequent analysis was executed following best practices guidelines for GATK from the Broad Institute (https://gatk.broadinstitute.org/hc/en-us). Firstly, base quality score recalibration (BQSR) was done to numerically correct individual base calls. Variant discovery was carried out in a two-step pipeline: variant calling with HaplotypeCaller followed by joint genotyping with GenotypeGVCFs. Once obtained a multi-sample VCF file containing all definitive variant records, VariantRecalibrator was operated to fulfil Variant Quality Score Recalibration (VQSR) and refinement of the obtained variant callset.

Variants were individually selected for each sample. The called variants, including both single nucleotide variants (SNVs) and indels, were then annotated using ANNOVAR (http://www.openbioinformatics.org/annovar/). Such tool enables functional annotation, and thus obtaining final VCF files that contain detailed information for each variant site in the sample, such as their impact within a gene, predicted pathogenicity scores, minor allele frequency (MAF), zygosity status or reporting whether they have been recorded in large-scale databases like dbSNP.

Variant prioritization

Variants were filtered for MAF <1%, their predicted functional impact on the encoded protein (missense, splicing, frameshift or nonsense) and frequency (<0.001) in the Genome Aggregation Database (gnomAD, broadinstitute.org). A list of genes with high expression during motile cilia development (n = 652, reanalyzed gene list based on data in Marcet et al., 2011) was used to further filter variants in genes with potential roles in motile cilia. Finally, the pathogenicity of the identified variants was estimated with Combined Annotation Dependent Depletion tool (CADD, https://cadd.gs.washington.edu/snv) and a CADD score >20 was considered significant pathogenicity score. Due to the known inheritance pattern of PCD homozygous variants were prioritized, but output files were also analyzed for the presence of compound heterozygous variants.

Sanger sequencing

The identified NM_032930.3 *CFAP300* variant was confirmed in the probands and segregation within family members by Sanger sequencing. Primers flanking the mutation were designed using the NCBI Primer-BLAST tool, forward GTATGTCAGTTGTTACGAAGGCAAT, reverse TGC TCTTATGTGTTAAGCCAGC. The genomic sequence was amplified using standard PCR conditions and predicted primer annealing temperature. The specificity of the PCR product was confirmed on agarose gel and purified using Exosap for Sanger sequencing.

Electron microscopy

Samples were fixed in 2.5% glutaraldehyde in cacodylate buffer and processed for electron microscopy. Defects were quantified using the method described by Shoemark et al. (2012). Briefly, cells were washed in sodium cacodylate buffer, post-fixed with 1% osmium tetroxide and centrifuged in agar or agarose to generate a pellet. Using a series of increasing concentrations of methanol followed by propylene oxide, cells were dehydrated before embedding in resin then 70–90 nm sections were cut using an ultramicrotome, mounted onto copper grids. Heavy metal staining was performed with uranyl acetate and lead citrate. Assessment of the respiratory epithelium and ciliary ultrastructure was made on a Jeol 1500 transmission electron microscope (TEM). Quantification of cells, microtubular arrangement in the axoneme and the presence of dynein arms was performed by a clinical electron microscopist blinded to the case information. Care was taken to assess cilia from a number of healthy cells from locations proximal and distal to the epithelial cell surface. Transverse sections of cilia were methodically quantified until either the entire section or >200 cilia had been counted.

Immunofluoresence

Nasal ciliated cells from nasal brushing of a PCD patient with *CFAP300* mutations and a control sample were stained after blocking (10% BSA, in PBS) using DNAH5 (HPA037470, Cambridge Bioscience), DNAH7 (HPA037724, Atlas Antibodies), DNAI1 (HPA021649, Atlas Antibodies), RSPH4A (HPA031196, Sigma-Aldrich) and CFAP300 (c11orf70, HPA038585, Sigma-Aldrich) antibodies and colocalized with cilia marker alpha-tubulin (322588, Invitrogen). After washes with PBST the slides were incubated with secondary antibodies Alexa Fluor 488 anti-mouse and Alexa Fluor 594 anti-rabbit (1: 500). Slides were imaged using Zeiss Axio Observer seven and deconvoluted using Huygens Deconvolution software (https://svi.nl/Huygens-Deconvolution). High resolution images were

TABLE 1 PCD patient characteristics for patients with LoF mutations in *CFAP300*.

Patient ID	Year of birth	Sex	Cilia beating frequency (Hz)	Beating pattern in HSVM	Nasal NO	Situs inversus	Picadar score	Clinical symptoms	TEM
I-1	2014	F	0	static with weak residual movement	8	Yes	na	Chronic wet cough, otitis media	na
II-1	2016	M	0	stiff, nearly static	na	Yes	10/12	Chronic wet cough, otitis media	lack of ODA and IDA
III-1	1998	F	12.2	stiff, unsynchronized	21	No	4/12	Cronic wet cough, recurrent otitis media and pneumonia	na

na: not available.

taken using a Zeiss LSM 880 upright confocal multiphoton microscope with AiryscanFast using ×63 objective and excitation lasers for 488 and 594. Images were processed using Zen software.

Statistical analysis

Unpaired *t*-test was used for statistical analysis between patient and control samples. p-value < 0.05 was considered statistically significant.

Results

Clinical identification of PCD patients

Patients were diagnosed based on low nasal NO, altered ciliary beating pattern in HSVM and clinical patient data (Table 1). Cystic fibrosis was excluded for all patients using a sweat test. All patients showed classic PCD symptoms early in life including chronic wet cough and otitis media, but to date no bronchiectasis has been observed (Table 1). Pneumonia was detected in one patient later in life, who had a low Picadar score (4/12, patient III-1). The low Picadar score was probably due to lack of situs defects in this patient. Defective beating of airway cilia was observed by HSVM showing stiff or static cilia in all patients. Some residual unsyncronized movement was detected in patient III-1. This variation in ciliary beating might be due to variable levels of dynein arms, however no samples for electron microscopy or immunofluorescence were available from patient III-1 preventing more detailed examination.

Whole exome sequencing identified patients carrying variants in *CFAP300*

We conducted whole exome sequencing of 13 Finnish PCD patients, which identified a homozygous LoF mutation in exon 3 of the *CFAP300* gene. The variant was present in homozygous state in three unrelated Finnish patients with typical symptoms of PCD including chronic respiratory infections and static/stiff cilia in HSVM and two of the patients had *situs inversus* (Table 1). No other candidate homozygous or compound heterozygous variants were detected in these patients. The presence of the mutations was confirmed by Sanger sequencing and it also segregated consistently in two of the families where familial samples were available (Figure 1, samples unavailable for the third family). Sanger sequencing confirmed a 3bp deletion and insertion of CC at chr11:102058886-102058888, causing a frameshift c.198_200delinsCC predicted to cause a premature stop codon at position 76 in the protein sequence, p. Phe67fs (Figure 2A). The variant is not present in gnomAD and it seems to be specific to PCD patients as it has previously been reported in German, Israeli and Slavic populations (Höben et al., 2018; Zietkiewicz et al., 2019), providing strong evidence that the variant is disease causing based on American College of Medical Genetics and Genomics (ACMG) guidelines (Richards et al., 2015). Protein alignment showed the premature stop codon position after 75 aa (Figure 2B). The effect of the frameshift on protein structure was predicted by Phyre2 (PHYRE2 Protein Fold Recognition Server (ic.ac.uk)), which showed lack of helical structures in the patient protein prediction (Figure 2C). Based on the *in silico* analysis, it can be predicted that the identified frameshift mutation in *CFAP300* is disease causing.

CFAP300 is missing in the PCD patient with a frameshift mutation resulting in a lack of dynein arms

To confirm the functional effect of the identified frameshift variant in *CFAP300*, we investigated the localization of the protein product in control and patient ciliated airway epithelial cells. In control ciliated airway epithelial cells CFAP300 localized in the cytoplasm, which is consistent with its predicted function as a dynein arm preassembly factor

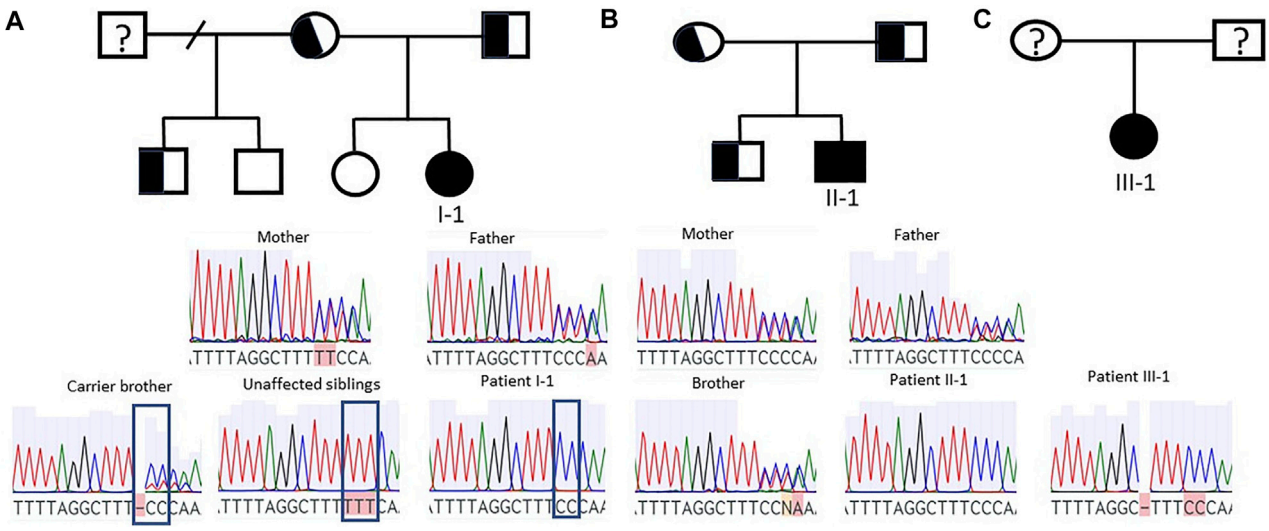

FIGURE 1
Segregation of *CFAP300* mutations. Patients I-1 and II-1 were homozygous for the mutation while parents were heterozygous. **(A)**. Patient I-1 family with carrier parents and one carrier brother and two unaffected siblings. The mutation site is indicated in carrier and unaffected siblings and in patient I-1. **(B)**. Patient II-1 family with carrier parents and brother. **(C)**. Sanger sequencing result for patient III-1.

(Figure 2D). CFAP300 staining was not detected or extremely weak in cells from patients homozygous for the c.198_200delinsCC variant compared to the control, consistent with likely nonsense mediated decay of the defective mRNA transcripts (Figure 2D). The peptide sequence for CFAP300 antibody corresponds to 113-188 aa in the CFAP300 protein sequence (ENSP00000414390), which is expected to be affected by the predicted premature stop codon at position 75 aa. The weak staining detected in patient cells could potentially originate from a short protein isoform of CFAP300 containing 109-262 aa (ENST00000529204). TEM analysis showed a high number of ciliated cells and normal arrangement of microtubules in the PCD patient with *CFAP300* LoF mutations. However, the orientations of the basal feet were disorganized (Figure 3A). For a synchronized beating pattern the basal feet at the motile cilia base all have to be organized to the same directions in all cilia (Nguyen et al., 2020). This defect may be secondary, due to the lack of cilia motility in the patient and additional studies are needed to confirm the order of events of basal foot orientation in the presence of the *CFAP300* frameshift variant. The main structural change in cilia cross sections was the lack of dynein arms (Figure 3B). The cross-sectional morphology of cilia appeared abnormal with a partial to total absence of ODA and IDA. Both dynein arms were occasionally present as complete structures or truncated 'horns' in the case of ODA. Ciliary cross sections with majority of arms absent were counted as both arms absent. In the patient with *CFAP300* mutation no cross sections with normal dynein arms were detected, which was statistically significant compared to control (>97% cross sections with normal dynein arms). No significant microtubular disorganization was detected in TEM. The lack of dynein arms was confirmed by immunofluorescence using antibodies against IDA protein DNAH7 and ODA proteins DNAI1 and DNAH5. These proteins appeared completely missing in patient cilia with strong staining retained in the cytoplasm (Figure 3C). In the control sample, DNAH7, DNAH5 and DNAI1 were specifically localized along the cilia. Furthermore, radial spoke protein RSPH4A was present in the patient cilia, although staining was also detected in the cytoplasm (Figure 3C). This may be due to inhibited transport of proteins to the cilium in patients with the *CFAP300* mutation, but the mutational mechanism requires additional studies.

CFAP300 is transported to cilia in airway epithelial cells

Using Airyscan super resolution imaging we characterized the strong cytoplasmic staining of CFAP300 across the cytoplasm, which was present as granular spots in control ciliated airway epithelial cells. Previously, it has been shown in model species (*Paramecium* and *Chlamydomonas*) that a small amount of CFAP300 is also transported to the cilium (Fassad et al., 2018). To investigate the potential localization of CFAP300 in human cilia in addition to its strong staining

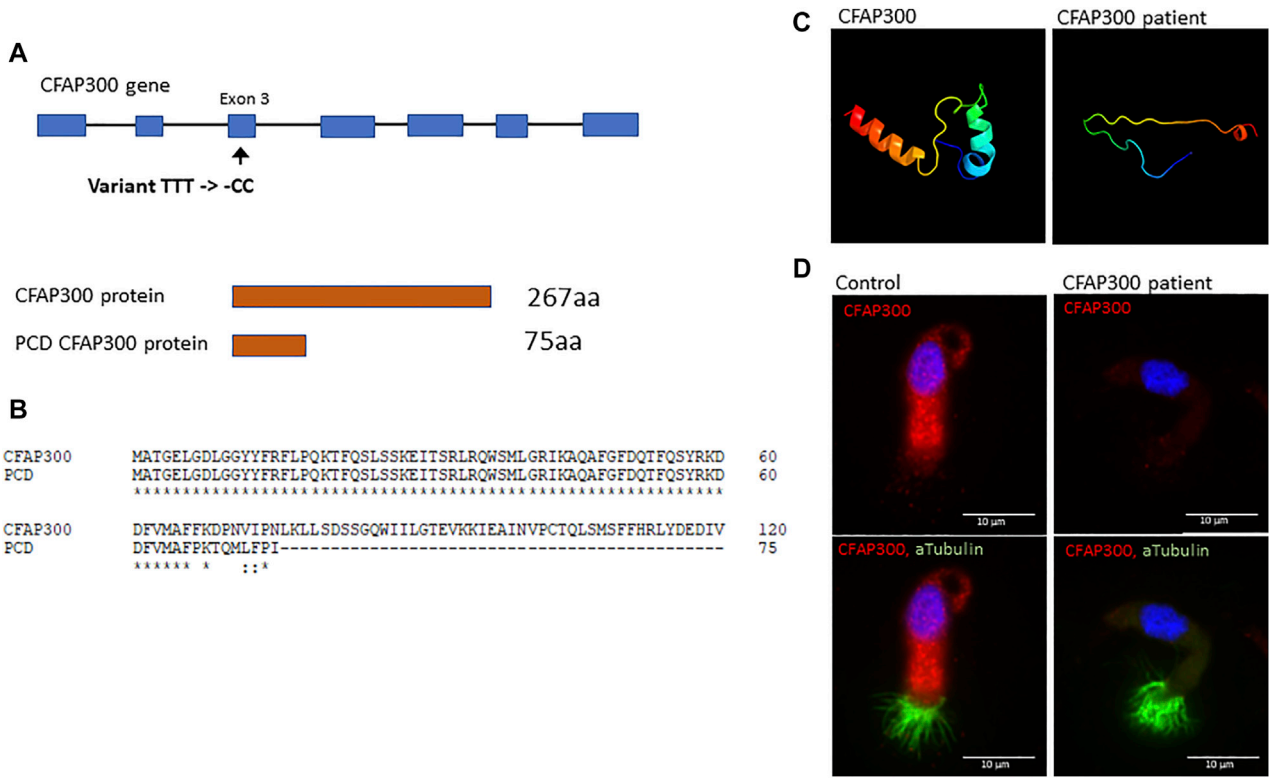

FIGURE 2
The effect of the *CFAP300* variant on protein function. **(A)**. The *CFAP300* variant **(C)**.198_200delinsCC results in premature stop codon at 76 aa and protein product. **(B)**. Clustal Omega alignment of the control and PCD patient CFAP300 protein sequence. **(C)**. Structural changes in the CFAP300 protein folding based on Phyre2. **(D)**. Cytoplasmic localization of the CFAP300 protein product appears missing in the PCD patient (patient II-1). αTubulin was used as a marker for cilia and Dapi as a nuclear stain. Scale bar is 10 µm.

in the cytoplasm (Figure 2D), we focused on imaging of CFAP300 along the cilium. We found that CFAP300 was present along the ciliary axoneme indicating that it is also transported to the cilium (Figure 4). Both cytoplasmic and cilia CFAP300 staining was depleted in the PCD patient sample with LoF mutations in *CFAP300* (Figure 2D).

Discussion

In this study we have identified a mutation in *CFAP300* causative for PCD in Finland and analysed the effect of the mutation on motile cilia formation and function. The main defect in axonemal cross-sections was the lack of dynein arms as described in previous studies (Fassad et al., 2018; Höben et al., 2018; Zietkiewicz et al., 2019; Aprea et al., 2021; Bolkier et al., 2021; Yiallouros et al., 2021). Furthermore, we detected misorientation of the basal feet of the airway cilia, which we believe is most likely to be a secondary defect due to the lack of cilia motility and is also seen in PCD cases due to mutations in other genes. Previously it has been shown that cilia motility is required for correct polarization of basal bodies (Mitchell et al., 2007). However, it cannot be ruled out that CFAP300 has a more direct role in basal body polarization, as has been suggested for another dynein arm preassembly factor CFAP298 (Jaffe et al., 2016). We have demonstrated the main localization of CFAP300 to be in the cytoplasm of normal ciliated airway epithelial cells, but we find in addition the presence of small amount of CFAP300 along the ciliary length (Figure 4) suggesting that CFAP300 has a potential role in transport of dynein complexes into the cilium. These results are consistent with previous studies in model organisms Paramecium and *Chlamydomonas*, where CFAP300 orthologs have been shown to be mainly present in the cytoplasm with small amount along the cilia (Fassad et al., 2018). Gene silencing experiments indicated that localization of CFAP300 along the axoneme is IFT dependent (Fassad et al., 2018). These studies suggest that CFAP300 is involved in chaperone-mediated preassembly of dynein arms and transporting these complexes to motile cilia, which is supported by our results in human cells.

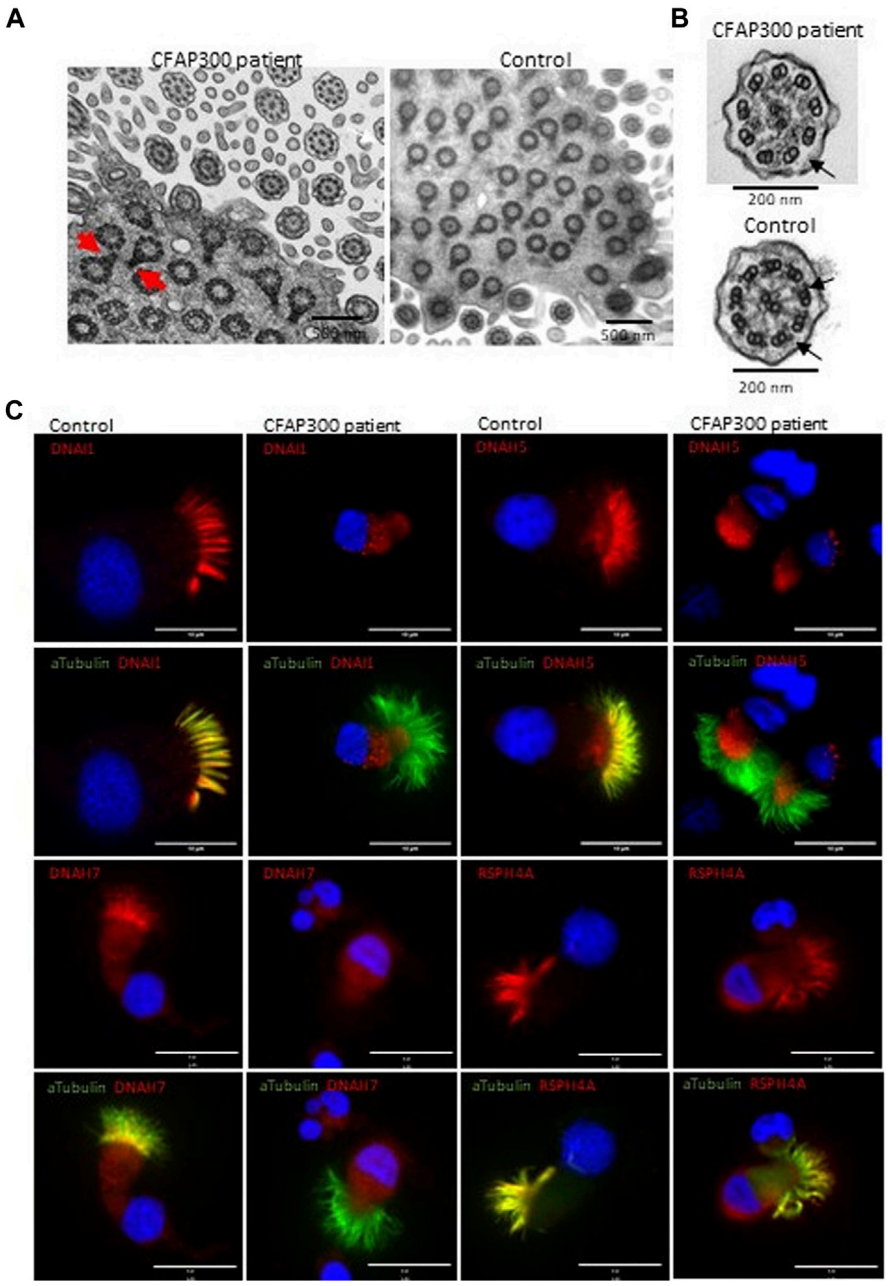

FIGURE 3
Localization of axonemal proteins in airway cilia of a control and PCD patient (patient II-1) with *CFAP300* mutations. **(A)**. High number of cilia cross sections were present in the nasal brushing sample of a PCD patient with *CFAP300* c.198_200delinsCC mutations, but the orientation of the basal foot (red arrows) was disorganized compared to control. **(B)**. The main finding in TEM of cilia cross sections in a patient with the *CFAP300* variant was lack of dynein arms (black arrows). **(C)**. ODA (DNAH5 and DNAI1) and IDA (DNAH7) proteins were missing from cilia in the patient airway epithelial cilia, while strong staining is present in the control sample. Radial spoke protein RSPH4A is present in the patient cilia. αTubulin was used as a marker for cilia and Dapi as a nuclear stain. Scale bar is 10 μm.

Previously children with *CFAP300* mutations have been shown to share a consistent PCD phenotype from early life with laterality defects and immotile respiratory cilia displaying combined loss of IDA and ODA (Fassad et al., 2018). Finnish PCD patients with *CFAP300* LoF mutations showed a similar phenotype with laterality defects in two of

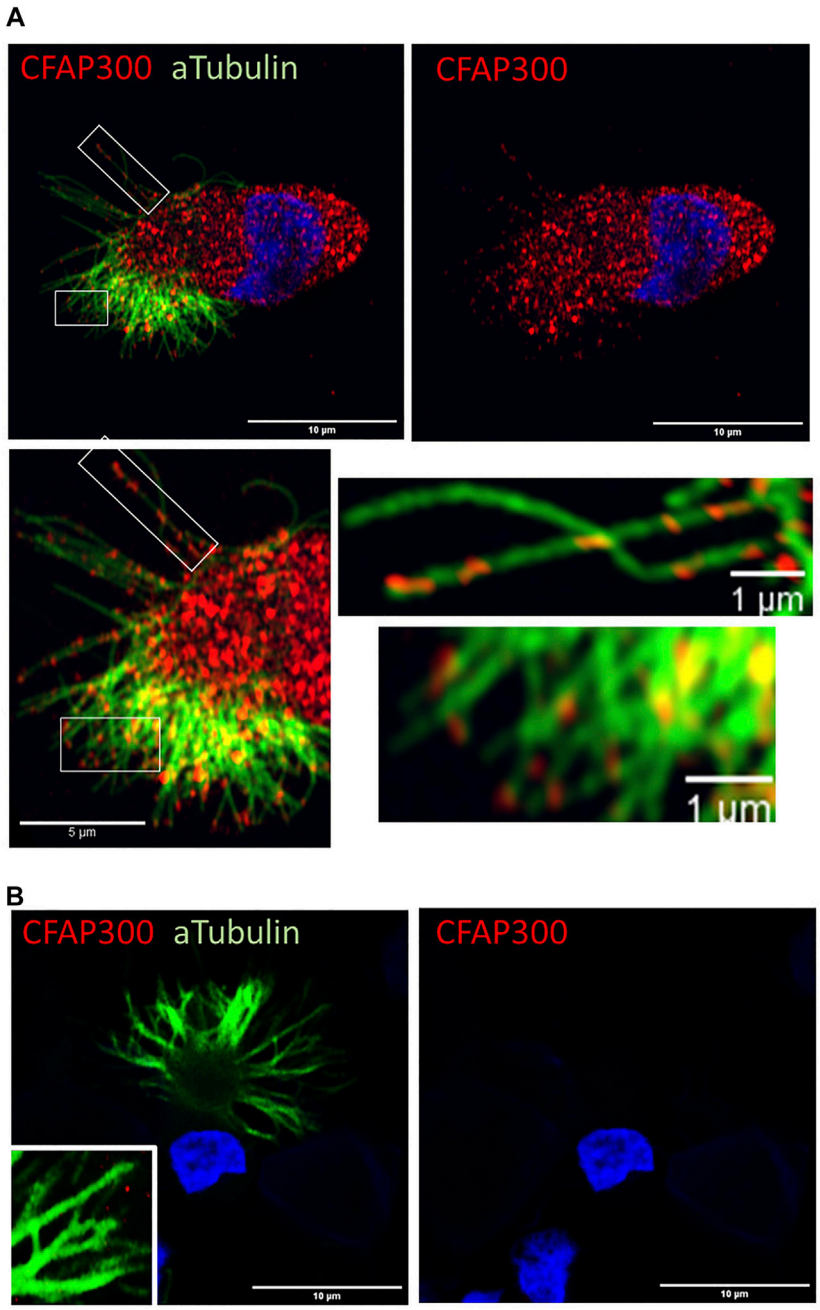

FIGURE 4
CFAP300 is transported along the motile airway epithelial cilium. **(A)**. In normal airway epithelial cells most of the CFAP300 protein is localized in the cytoplasm, but some of the protein appears to be transported into the cilium. **(B)**. No CFAP300 staining was detected in the patient airway epithelial cells.

the patients and consistent chronic wet cough. The respiratory distress was already evident in the neonatal care unit and HSVM showed static or stiff cilia with loss of dynein arms as described previously. The variant identified in this study has also been previously reported in one German and Israeli case (Höben et al., 2018) and 14 PCD patients in the Slavic population (Zietkiewicz et al., 2019), which along with this study indicates that it is a reasonably common cause of CFAP300 PCD that could arise from an ancient European founder mutation. ODA loss was reported in 67–95% and IDA

TABLE 2 *CFAP300* mutations identified in PCD patients.

Population	Variant	Protein	Zygosity	Number of patients	Cilia motility	Functionality	References
Israel	c.198_200 delinsCC	p.Phe67Profs*10	Homozygous	1	na	Frameshift > stop gain	Höben et al. (2018)
Germany	c.198_200 delinsCC, c.433A>T	p.Phe67Profs*10, p.Arg145*	Homozygous	2	immotile/na	Stop gain	Höben et al. (2018)
Turkey	c.361C>T	p.Arg121*	Homozygous	1	immotile	Stop gain	Höben et al. (2018)
Italy	c.361C>T	p.Arg121*	Homozygous	1	immotile	Stop gain	Höben et al. (2018)
Pakistan	c.776A>G	p.His259Arg	Homozygous	2	immotile	Missense	Fassad et al. (2018)
India	c.154C>T, c.361C>T	p.Gln52*, p.Arg121*	Compound heterozygous	1	immotile	Stop gain	Fassad et al. (2018)
not known	c.361C>T	p.Arg121*	Homozygous	1	immotile	Stop gain	Aprea et al. (2021)
Poland	c.198_200 delinsCC	p.Phe67Profs*10	Homozygous	14	na	Frameshift > stop gain	Zietkiewicz et al. (2019)
Poland	c.198_200 delinsCC, c.353A > G	p.Phe67Profs*10, p.Asp118Gly	Compound heterozygous	1	na	Frameshift > stop gain, exonic splice site	Zietkiewicz et al. (2019)
Poland	c.198_200 delinsCC, c.675 + 3_6 delAAGT	p.Phe67Profs*10, na	Compound heterozygous	1	na	Frameshift > stop gain, intronic splice site	Zietkiewicz et al. (2019)
Greece-Cyprus	c.95_103delGCCGGCTCC	p.Arg33_Arg35del	Homozygous	6	immotile, stiff	Inframe deletion	Yiallouros et al. (2021)
Arab–Muslim	c.693_694insGA	p.Cys231fs	Homozygous	2	na	Frameshift	Bolkier et al. (2021)
Finland	c.198_200 delinsCC	p.Phe67Profs*10	Homozygous	3	immotile, stiff	Frameshift > stop gain	This study

loss in 75–95% of axonemal cross sections in patients with homozygous missense mutations at c.776A>G (p.His259Arg) and compound heterozygous stop gain mutations at c.154C>T and c.361C>T (p.Gln52*, p. Arg121*), respectively (Fassad et al., 2018). DNAH5 and DNALI1 staining was missing in patient cilia, but RSPH4A and GAS8 staining was comparable to controls (Fassad et al., 2018). In a patient with a homozygous stop gain mutation c.361C>T (p.Arg121*) in *CFAP300*, DNAI1, DNAI2 and DNALI1 were reported to be missing in cilia and TEM reported only ODA defect (Aprea et al., 2021). In frame deletion c.98_106del (p.Arg33_Arg35del) in six patients of Greek-Cypriot population was associated with IDA and ODA loss in most cilia cross-sections based on TEM and there was an extremely stiff CBP (Yiallouros et al., 2021). The c.198_200delinsCC frameshift variant identified in this study caused lack or truncation of IDA or ODA in all axonemal cross sections based on TEM of patient II-1 and lack of DNAH5, DNAI1 and DNAH7 suggesting a severe defect in dynein arm assembly. Patient III-1 showed stiff cilia movement with a beat frequency of 12 Hz. Although we were unable to confirm the axonemal defects in this patient, the residual movement could be due to different levels of dynein arm formation as has been shown in previous studies (Fassad et al., 2018; Aprea et al., 2021; Yiallouros et al., 2021). Variable cilia beat frequency has also been reported for variant c.98_106del (0–9.1 Hz, Yiallouros et al., 2021). All the *CFAP300* mutations reported to date are listed in Table 2.

In the Finnish population two novel mutations in *DNAH11* have been previously reported, suggesting a distinct genetic pool for PCD in Finland. The *CFAP300* mutation reported here in contrast appears to be common with Slavic, German and Israeli populations, suggesting a common genetic origin. It is important to establish the genetic causes of PCD in different populations including Finland to improve the genetic diagnosis of PCD. This can lead to development of a population specific gene panel for the diagnostic pipeline and the opportunity for targeted specific personalised medicines in future.

Our results and previously reported studies in model organisms and PCD patients underline the crucial role of CFAP300 in dynein arm preassembly and transport to motile cilia. The exact role of CFAP300 requires additional studies in mammalian species to establish the molecular mechanisms behind the preassembly and transport of dynein arm complexes. Interestingly, CFAP300 seems to be involved in transporting the complexes along the cilia possibly acting as a linker between the IFT machinery and dynein motor complexes.

Data availability statement

The data presented in the study are deposited in the UCL Research Data Repository DOI 10.5522/04/20793235.

Ethics statement

The studies involving human participants were reviewed and approved by University of Turku Ethics Committee (ETMK 69–2017) and London Bloomsbury Research Ethics Committee approved by the Health Research Authority (08/H0713/82). Written informed consent to participate in this study was provided by the participants' legal guardian/next of kin.

Author contributions

RS, VE, and TK diagnosed the patients and collected patient samples, MF analysed the exome data, GF and MM conducted the Sanger sequencing of patients and family members, AS and AR conducted cilia motility and ultrastructure assessment, JL did the immunofluorescence staining, HM supervised the study, AS analyzed the data, conducted microscopy imaging and wrote the manuscript.

Funding

Part of this research was funded by BBSRC grant BB/V011251/1. AS was funded by Marie Sklodowska-Curie individual fellowship No. 800556 from the European Union's Horizon 2020 Research and Innovation Programme. MF was supported by a Wellcome Trust Collaborative Award in Science (210585/Z/18/Z).

Acknowledgments

We thank the patients and their families for participating in the study and Melissa Dixon (Royal Brompton Hospital) for her contributions to data used in this manuscript. Several study authors and data contributors participate in the BEAT-PCD clinical research collaboration, supported by the European Respiratory Society.

Conflict of interest

The authors declare that the research was conducted in the absence of any commercial or financial relationships that could be construed as a potential conflict of interest.

Publisher's note

References

Aprea, I., Raidt, J., Höben, I. M., Loges, N. T., Nöthe-Menchen, T., and Pennekamp, P., (2021). Defects in the cytoplasmic assembly of axonemal dynein arms cause morphological abnormalities and dysmotility in sperm cells leading to male infertility. *PLoS Genet.* 17, e1009306. doi:10.1371/journal.pgen.1009306

Austin-Tse, C., Halbritter, J., Zariwala, M. A., Gilberti, R. M., Gee, H. Y., and Hellman, N., (2013). Zebrafish ciliopathy screen plus human mutational analysis identifies C21orf59 and CCDC65 defects as causing primary ciliary dyskinesia. *Am. J. Hum. Genet.* 93, 672–686. doi:10.1016/j.ajhg.2013.08.015

Behan, L., Dimitrov, B. D., Kuehni, C. E., Hogg, C., Carroll, M., and Evans, H. J., (2016). Picadar: A diagnostic predictive tool for primary ciliary dyskinesia. *Eur. Respir. J.* 47, 1103–1112. doi:10.1183/13993003.01551-2015

Bolkier, Y., Barel, O., Marek-Yagel, D., Atias-Varon, D., Kagan, M., and Vardi, A., (2021). Whole-exome sequencing reveals a monogenic cause in 56% of individuals with laterality disorders and associated congenital heart defects. *J. Med. Genet.* 59, 691–696. doi:10.1136/jmedgenet-2021-107775

Diggle, C. P., Moore, D. J., Mali, G., zur Lage, P., Ait-Lounis, A., and Schmidts, M., (2014). HEATR2 plays a conserved role in assembly of the ciliary motile apparatus. *PLoS Genet.* 10, e1004577. doi:10.1371/journal.pgen.1004577

Duquesnoy, P., Escudier, E., Vincensini, L., Freshour, J., Bridoux, A. M., and Coste, A., (2009). Loss-of-function mutations in the human ortholog of chlamydomonas reinhardtii ODA7 disrupt dynein arm assembly and cause primary ciliary dyskinesia. *Am. J. Hum. Genet.* 85, 890–89. doi:10.1016/j.ajhg.2009.11.008

Fassad, M. R., Patel, M. P., Shoemark, A., Cullup, T., Hayward, J., and Dixon, M., (2020). Clinical utility of NGS diagnosis and disease stratification in a multiethnic primary ciliary dyskinesia cohort. *J. Med. Genet.* 57 (5), 322–330. doi:10.1136/jmedgenet-2019-106501

Fassad, M. R., Shoemark, A., le Borgne, P., Koll, F., Patel, M., and Dixon, M., (2018). C11orf70 mutations disrupting the intraflagellar transport-dependent assembly of multiple axonemal dyneins cause primary ciliary dyskinesia. *Am. J. Hum. Genet.* 102, 956–972. doi:10.1016/j.ajhg.2018.03.024

Höben, I. M., Hjeij, R., Olbrich, H., Dougherty, G. W., Nöthe-Menchen, T., and Aprea, I., (2018). Mutations in C11orf70 cause primary ciliary dyskinesia with randomization of left/right body asymmetry due to defects of outer and inner dynein arms. *Am. J. Hum. Genet.* 102 (5), 973–984. doi:10.1016/j.ajhg.2018.03.025

Horani, A., Druley, T. E., Zariwala, M. A., Patel, A. C., Levinson, B. T., and Van Arendonk, L. G., (2012). Whole-exome capture and sequencing identifies HEATR2 mutation as a cause of primary ciliary dyskinesia. *Am. J. Hum. Genet.* 91, 685–693. doi:10.1016/j.ajhg.2012.08.022

Horani, A., Ferkol, T. W., Shoseyov, D., Wasserman, M. G., Oren, Y. S., and Kerem, B., (2013). LRRC6 mutation causes primary ciliary dyskinesia with dynein arm defects. *PLoS One* 8, e59436. doi:10.1371/journal.pone.0059436

Horani, A., Ustione, A., Huang, T., Firth, A. L., Pan, J., and Gunsten, S. P., (2018). Establishment of the early cilia preassembly protein complex during motile ciliogenesis. *Proc. Natl. Acad. Sci. U. S. A.* 115, E1221–E1228. doi:10.1073/pnas.1715915115

Inaba, Y., Shinohara, K., Botilde, Y., Nabeshima, R., Takaoka, K., and Ajima, R., (2016). Transport of the outer dynein arm complex to cilia

requires a cytoplasmic protein Lrrc6. *Genes cells.* 21, 728–739. doi:10.1111/gtc.12380

Jaffe, K. M., Grimes, D. T., Schottenfeld-Roames, J., Werner, M. E., Ku, T. S., and Kim, S. K., (2016). c21orf59/kurly controls both cilia motility and polarization. *Cell Rep.* 14, 1841–1849. doi:10.1016/j.celrep.2016.01.069

Kott, E., Duquesnoy, P., Copin, B., Legendre, M., Dastot-Le Moal, F., and Montantin, G., (2012). Loss-of-function mutations in LRRC6, a gene essential for proper axonemal assembly of inner and outer dynein arms, cause primary ciliary dyskinesia. *Am. J. Hum. Genet.* 91, 958–964. doi:10.1016/j.ajhg.2012.10.003

Li, H., and Durbin, R. (2010). Fast and accurate long-read alignment with Burrows-Wheeler transform. *Bioinformatics* 26, 589–595. doi:10.1093/bioinformatics/btp698

Loges, N. T., Olbrich, H., Becker-Heck, A., Häffner, K., Heer, A., and Reinhard, C., (2009). Deletions and point mutations of LRRC50 cause primary ciliary dyskinesia due to dynein arm defects. *Am. J. Hum. Genet.* 85, 883–889. doi:10.1016/j.ajhg.2009.10.018

Lucas, J. S., Davis, S. D., Omran, H., and Shoemark, A. (2020). Primary ciliary dyskinesia in the genomics age. *Lancet. Respir. Med.* 8, 202–216. doi:10.1016/S2213-2600(19)30374-1

Marcet, B., Chevalier, B., Luxardi, G., Coraux, C., Zaragosi, L. E., and Cibois, M., (2011). Control of vertebrate multiciliogenesis by miR-449 through direct repression of the Delta/Notch pathway. *Nat. Cell Biol.* 13 (6), 693–699. doi:10.1038/ncb2241

Mitchell, B., Jacobs, R., Li, J., Chien, S., and Kintner, C. (2007). A positive feedback mechanism governs the polarity and motion of motile cilia. *Nature* 447, 97–101. doi:10.1038/nature05771

Mitchison, H. M., and Smedley, D. (2022). Primary ciliary dyskinesia: A big data genomics approach. *Lancet. Respir. Med.* 10 (5), 423–425. doi:10.1016/S2213-2600(22)00009-1

Mitchison, H. M., Schmidts, M., Loges, N. T., Freshour, J., Dritsoula, A., and Hirst, R. A., (2012). Mutations in axonemal dynein assembly factor DNAAF3 cause primary ciliary dyskinesia. *Nat. Genet.* 44 (381-9), 381–389. doi:10.1038/ng.1106

Moore, D. J., Onoufriadis, A., Shoemark, A., Simpson, M. A., zur Lage, P. I., and de Castro, S. C., (2013). Mutations in ZMYND10, a gene essential for proper axonemal assembly of inner and outer dynein arms in humans and flies, cause primary ciliary dyskinesia. *Am. J. Hum. Genet.* 93, 346–356. doi:10.1016/j.ajhg.2013.07.009

Nguyen, Q. P. H., Liu, Z., Albulescu, A., Ouyang, H., Zlock, L., and Coyaud, E., (2020). Comparative super-resolution mapping of basal feet reveals a modular but distinct architecture in primary and motile cilia. *Dev. Cell* 55, 209–223. doi:10.1016/j.devcel.2020.09.015

Olcese, C., Patel, M. P., Shoemark, A., Kiviluoto, S., Legendre, M., and Williams, H. J., (2017). X-linked primary ciliary dyskinesia due to mutations in the cytoplasmic axonemal dynein assembly factor PIH1D3. *Nat. Commun.* 8, 14279. doi:10.1038/ncomms14279

Omran, H., Kobayashi, D., Olbrich, H., Tsukahara, T., Loges, N. T., and Hagiwara, H., (2008). Ktu/PF13 is required for cytoplasmic pre-assembly of axonemal dyneins. *Nature* 456, 611–616. doi:10.1038/nature07471

Paff, T., Loges, N. T., Aprea, I., Wu, K., Bakey, Z., and Haarman, E. G., (2017). Mutations in PIH1D3 cause X-linked primary ciliary dyskinesia with outer and inner dynein arm defects. *Am. J. Hum. Genet.* 100, 160–168. doi:10.1016/j.ajhg.2016.11.019

Richards, S., Aziz, N., Bale, S., Bick, D., Das, S., and Gastier-Foster, J., (2015). Laboratory quality assurance committee. Standards and guidelines for the interpretation of sequence variants: A joint consensus recommendation of the American College of medical genetics and genomics and the association for molecular PathologyTwo novel mutations in the DNAH11 gene in primary ciliary dyskinesia (CILD7) with considerable variety in the clinical and beating cilia phenotype. *Genet. Med. MayBMC Med. Genet.* 1721 (5), 405237–24020011712. doi:10.1038/gim.2015.3010.1186/s12881-020-01171-2

Schultz, R., Peromaa, T., Lukkarinen, H., and Elenius, V. (2022). High-speed video microscopy analysis for first-line diagnosis of primary ciliary dyskinesia. *J. Vis. Exp.* 19. doi:10.3791/63292

Shoemark, A., Dixon, M., Corrin, B., and Dewar, A. (2012). Twenty-year review of quantitative transmission electron microscopy for the diagnosis of primary ciliary dyskinesia. *J. Clin. Pathol.* 65, 267–271. doi:10.1136/jclinpath-2011-200415

Shoemark, A., and Harman, K. (2021). Primary ciliary dyskinesia. *Semin. Respir. Crit. Care Med.* 42, 537–548. doi:10.1055/s-0041-1730919

Sironen, A., Shoemark, A., Patel, M., Loebinger, M. R., and Mitchison, H. M. (2019). Sperm defects in primary ciliary dyskinesia and related causes of male infertility. *Cell. Mol. Life Sci.* 77, 2029–2048. doi:10.1007/s00018-019-03389-7

Tarkar, A., Loges, N. T., Slagle, C. E., Francis, R., Dougherty, G. W., and Tamayo, J. V., (2013). DYX1C1 is required for axonemal dynein assembly and ciliary motility. *Nat. Genet.* 45, 995–1003. doi:10.1038/ng.2707

Yiallouros, P. K., Kouis, P., Kyriacou, K., Evriviadou, A., Anagnostopoulou, P., and Matthaiou, A., (2021). Implementation of multigene panel NGS diagnosis in the national primary ciliary dyskinesia cohort of cyprus: An island with a high disease prevalence. *Hum. Mutat.* 42, e62–e77. doi:10.1002/humu.24196

Zariwala, M. A., Gee, H. Y., Kurkowiak, M., Al-Mutairi, D. A., Leigh, M. W., and Hurd, T. W., (2013). ZMYND10 is mutated in primary ciliary dyskinesia and interacts with LRRC6. *Am. J. Hum. Genet.* 93, 336–345. doi:10.1016/j.ajhg.2013.06.007

Zietkiewicz, E., Bukowy-Bieryllo, Z., Rabiasz, A., Daca-Roszak, P., Wojda, A., and Voelkel, K., (2019). CFAP300: Mutations in slavic patients with primary ciliary dyskinesia and a role in ciliary dynein arms trafficking. *Am. J. Respir. Cell Mol. Biol.* 61, 440–449. doi:10.1165/rcmb.2018-0260OC

frontiers | Frontiers in Genetics

TYPE Brief Research Report
PUBLISHED 07 October 2022
DOI 10.3389/fgene.2022.1021037

OPEN ACCESS

EDITED BY
Steven LC Pei,
Yale University, United States

REVIEWED BY
Kazuhisa Nakayama,
Kyoto University, Japan
John Andrew Sayer,
Newcastle University, United Kingdom

*CORRESPONDENCE
Karel F. Liem,
Karel.Liem@yale.edu

†These authors have contributed equally to this work

SPECIALTY SECTION
This article was submitted to Human and Medical Genomics, a section of the journal Frontiers in Genetics

RECEIVED 16 August 2022
ACCEPTED 22 September 2022
PUBLISHED 07 October 2022

CITATION
Jafari Khamirani H, Palicharla VR, Dastgheib SA, Dianatpour M, Imanieh MH, Tabei SS, Besse W, Mukhopadhyay S and Liem KF (2022), A pathogenic variant of TULP3 causes renal and hepatic fibrocystic disease. *Front. Genet.* 13:1021037. doi: 10.3389/fgene.2022.1021037

A pathogenic variant of TULP3 causes renal and hepatic fibrocystic disease

Hossein Jafari Khamirani[1†], Vivek Reddy Palicharla[2†], Seyed Alireza Dastgheib[1], Mehdi Dianatpour[1,3], Mohammad Hadi Imanieh[4], Seyed Sajjad Tabei[5], Whitney Besse[6], Saikat Mukhopadhyay[2] and Karel F. Liem Jr.[7*]

[1]Department of Medical Genetics, Shiraz University of Medical Sciences, Shiraz, Iran, [2]Department of Cell Biology, University of Texas Southwestern Medical Center, Dallas, TX, United States, [3]Stem Cells Technology Research Center, Shiraz University of Medical Sciences, Shiraz, Iran, [4]Gastroenterohepatology Research Center, Shiraz University of Medical Sciences, Shiraz, Iran, [5]Shiraz Nephro-Urology Research Center, Shiraz University of Medical Sciences, Shiraz, Iran, [6]Department of Internal Medicine, Section of Nephrology, Yale School of Medicine, New Haven, CT, United States, [7]Vertebrate Developmental Biology Program, Department of Pediatrics, Yale University School of Medicine, New Haven, CT, United States

Patient variants in *Tubby Like Protein-3 (TULP3)* have recently been associated with progressive fibrocystic disease in tissues and organs. TULP3 is a ciliary trafficking protein that links membrane-associated proteins to the intraflagellar transport complex A. In mice, mutations in Tulp3 drive phenotypes consistent with ciliary dysfunction which include renal cystic disease, as part of a ciliopathic spectrum. Here we report two sisters from consanguineous parents with fibrocystic renal and hepatic disease harboring a homozygous missense mutation in *TULP3* (NM_003324.5: c.1144C>T, p.Arg382Trp). The R382W patient mutation resides within the C-terminal Tubby domain, a conserved domain required for TULP3 to associate with phosphoinositides. We show that inner medullary collecting duct-3 cells expressing the TULP3 R382W patient variant have a severely reduced ability to localize the membrane-associated proteins ARL13b, INPP5E, and GPR161 to the cilium, consistent with a loss of TULP3 function. These studies establish Arginine 382 as a critical residue in the Tubby domain, which is essential for TULP3-mediated protein trafficking within the cilium, and expand the phenotypic spectrum known to result from recessive deleterious mutations in *TULP3*.

KEYWORDS

cilia, tubby domain, cyst, fibrosis, PKD, liver, ciliopathy, kidney

Introduction

Primary cilia are small signaling organelles that project from the surface of nearly all cells of the human body. Mutations in genes that affect cilia are at the origin of a group of human genetic diseases referred to as "ciliopathies." Disease phenotypes caused by mutations in cilia-related genes are characterized by an overlapping spectrum of

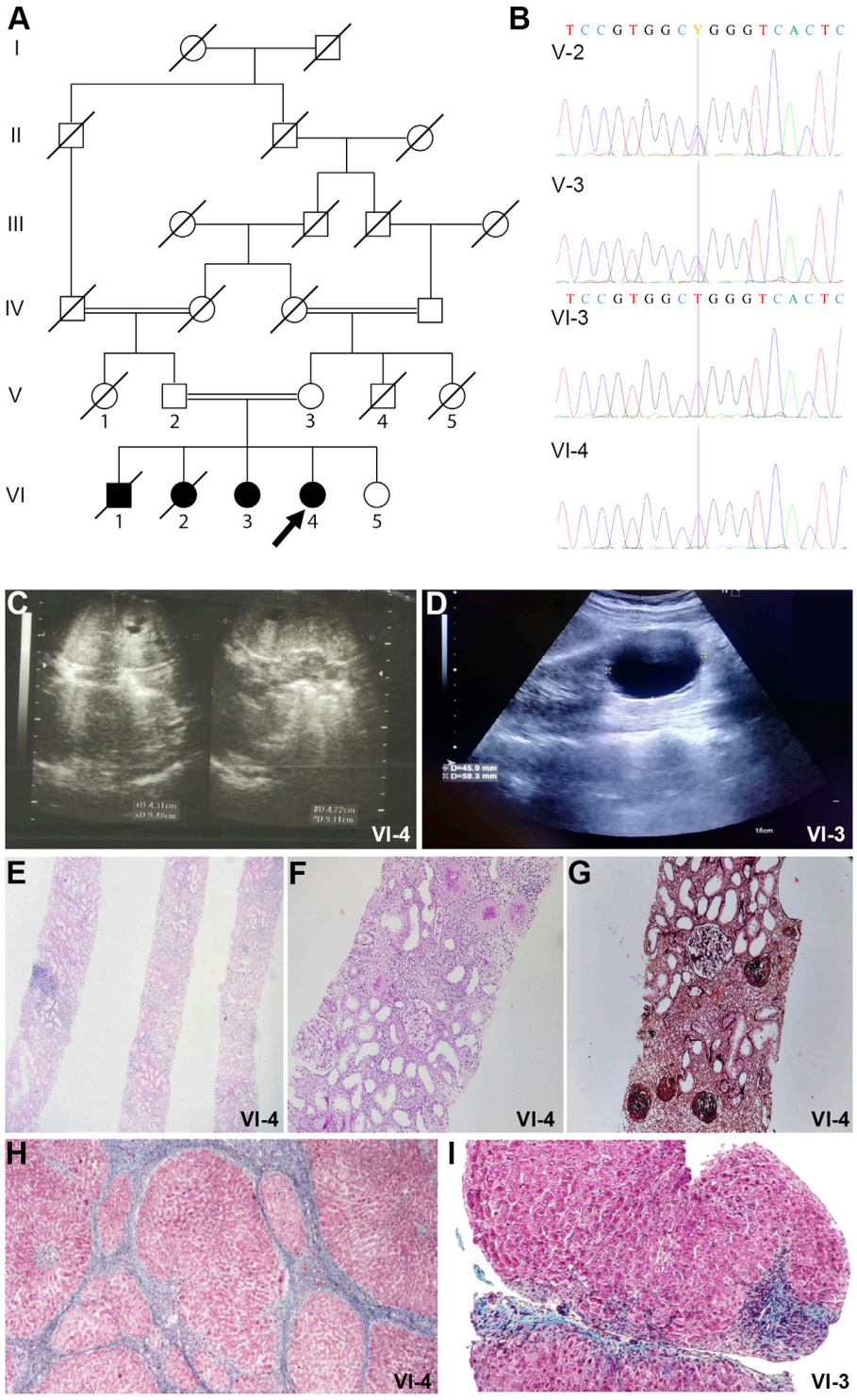

FIGURE 1
Pedigrees and imaging studies of *TULP3* patients. **(A)**. Pedigree of the family. The pedigree of the family illustrates the recessive inheritance of the pathogenic variant in the family. Double lines in pedigrees indicate consanguinity. Filled and unfilled circles/squares represent affected and unaffected individuals respectively, while circle/squares with diagonal lines indicate deceased individuals. Proband is VI-4 (arrow). **(B)** Electropherogram of the family. The homozygous variant in the proband (individual VI-4) and her sister (individual VI-3). The heterozygous variant in their parents (individual V-3 and V-4). Missense variant c.1144C>T results in alteration of Arginine to Tryptophan in position 382 of the TULP3 protein. **(C)** Abdominopelvic Sonography of patient VI-4. Kidney ultrasonography of the patient shows enlarged kidneys and several small cysts. **(D)** Abdominopelvic Sonography of patient VI-3. There is a simple cortical cyst measuring 45 × 59 mm in the mid pole of the left kidney. **(E)**
(*Continued*)

FIGURE 1 (Continued)
Kidney core needle biopsy of patient VI-4. Histology shows diffuse global glomerulosclerosis, tubular atrophy and moderate interstitial infiltration of mononuclear inflammatory cells (H&E stain, magnification ×40). **(F)** Kidney core needle biopsy of patient VI-4. PAS stain, magnification ×100. **(G)** Kidney core needle biopsy of patient VI-4. Jones silver stain, magnification ×100. **(H)** Section from liver needle biopsy of patient VI-4. Masson-Trichrome stain shows bridging fibrosis and nodule formation and distorted lobular and vascular architecture with micronodule formation. Individual hepatocytes show ballooning degeneration. **(I)** Section from liver needle biopsy of patient VI-3. Masson-Trichrome stain shows distorted lobular and vascular architecture with micronodule formation. Individual hepatocytes show ballooning degeneration. Marked bridging fibrosis is present with occasional nodules portal spaces.

multisystem disorders which include renal cystic disease, skeletal malformations, neural developmental defects and retinal degeneration, among others (Goetz and Anderson, 2010; Reiter and Leroux, 2017). Many genes are involved with building a functional cilium and the severity and nature of the disease resulting from their mutations depend on the individual gene affected and the nature of the mutation.

Recently, variants in the *Tubby like protein-3 (TULP3)* have been associated with multisystem fibrotic disease in patients (Devane et al., 2022). TULP3 (Tubby like protein-3; MIM: 604730) encodes a member of the Tubby domain family of proteins (Mukhopadhyay and Jackson, 2011) which contain a signature carboxy-terminal Tubby domain that functions to bind selectively to membrane phosphoinositides (Santagata et al., 2001; Mukhopadhyay et al., 2010). In addition, the TULP3 amino terminus contains a short, conserved domain that strongly binds proteins of the Intraflagellar transport complex A (IFT-A) (Mukhopadhyay et al., 2010), an essential protein complex required for the trafficking proteins in and out of the cilium (Liem et al., 2012). In the mouse, deletion or strong loss of function alleles of *Tulp3* are associated with embryonic lethality, neural tube defects, and limb patterning defects (Ikeda et al., 2002; Cameron et al., 2009; Norman et al., 2009; Patterson et al., 2009). Unlike most ciliary mutations, *Tulp3* mutations do not cause major structural defects in cilia (Norman et al., 2009; Hwang et al., 2019; Legue and Liem, 2019; Legue and Liem, 2020). *Tulp3* phenotypes have been shown to cause a gain of function in the Sonic Hedgehog (Shh) pathway in mutant mice, which has been shown to be Gli dependent (Norman et al., 2009; Legue and Liem, 2020). Changes in Shh signaling pathways affect multiple developmental pathways and underlie a subset of the phenotypes of the ciliopathic spectrum.

Here we present two sibling patients from a consanguineous Iranian family presenting with fibrocystic renal and hepatic disease and harboring a homozygous *R382W TULP3* mutation. We have modeled the effect of the mutation on TULP3 function *in vitro* and show that the amino acid substitution acts to disrupt protein trafficking to the primary cilium. Our results show that the mutation causes a loss of function consistent with a disruption of the conserved Tubby domain. These results identify R382 as a critical residue for TULP3 function and expand our knowledge of recessive fibrosis-associated disease mutations in patients.

Materials and methods

Patient identification

The proband (VI-4) is a 12-year-old female with a suspected inherited hepatic renal syndrome. The proband is from an Iranian family with four affected children born to first-degree consanguineous parents (Figure 1A). Following clinical and genetic investigation, the family consented to written informed approval for participation in this study and publication of the results.

Genetic studies

DNA from peripheral blood samples were collected from the subjects for Whole Exome Sequencing (WES) and Sanger Sequencing using QIAamp DNA Blood Mini Kit (Qiagen). WES identified a homozygous variant (NM_003324.5:c.1144C>T, p.Arg382Trp) of *TULP3* in the proband. The missense variant (NM_003324.5: c.1144C>T, p. Arg382Trp) detected by WES in *TULP3* is classified as " Likely Pathogenic" based on the PM2, PP3, and PS3 criteria of the ACMG/AMP guidelines (Richards et al., 2015). It has a minor allele frequency of 1.6 × 10-5 in gnomAD (Karczewski et al., 2020). The variant was classified as a "disease-causing," "pathogenic," or "damaging" based on pathogenicity prediction tools including MetaLR, MetaSVM, MetaRNN, REVEL, BayesDel addAF, BayesDel noAF, CADD, DEOGEN2, EIGEN, FATHMM, LIST-S2, LRT, M-CAP, MutPred, MVP, Mutation Assessor, MutationTaster, PROVEAN, Polyphen, PrimateAI and SIFT.

PCR amplification and Sanger Sequencing

The primers were designed using Oligo Primer Designer (Rychlik, 2007). Forward primer (5′- CTTCTGGTTTACCCT TTCTG), reverse primer (5′- ATGATTATCTGCTGACTGTC). The presence of the variant in the tenth exon of the TULP3 gene was confirmed by Sanger sequencing.

Protein structure

Using AlphaFold Protein Structure Database, the predicted three-dimensional structure of TULP3 protein based on amino

acid sequence and the position of the pathogenic variant in this study was modeled. Domains of Tubby-Like Protein 3 in the two-dimensional structure were collected from InterPro. The two-dimensional and three-dimensional structures of TULP3 protein illustrate the position of the variant identified in this study.

Expression constructs

pENTR221-INPP5E construct was from Life technologies (IOH40212). Retroviral constructs of HA-INPP5E were generated by cloning into pQXIN-HA vector. pG-LAP1 (pCDNA5/FRT/TO-EGFP-TEV-Stag-X) was from Addgene (Torres et al., 2009). N-terminal LAP-tagged retroviral constructs of full length and mutant TULP3 were generated by Gateway cloning into a gateway LAP1 version of pBABE. Retroviral constructs of HA-INPP5E were generated by cloning into pQXIN vector. TULP3 R382W was generated by Q5 site-directed mutagenesis (New England Biolabs).

Cell culture and generation of *Tulp3* knock out and stable cell lines

CRISPR/Cas9 knockout lines for *Tulp3* were generated in IMCD3 Flp-In (Invitrogen) cells by cloning targeting sequences in exon 3 of mouse *Tulp3* (ACGTCGCTGCGAGGCATCTG and TGGCTTTAACCTTCGCAGCC) into pLentiCRISPR backbone. Single clones were isolated using serial dilution method. Clonal lines were tested for knockout by Sanger sequencing and immunoblotting for Tulp3 (Palicharla et al., 2021). Stable lines expressing N-terminal LAP-tagged full length or mutant TULP3 and HA-INPP5E were generated by retroviral infection and antibiotic selection. IMCD3 cells were cultured in DMEM high glucose (Sigma-Aldrich; supplemented with 10% cosmic serum, 0.05 mg/ml penicillin, 0.05 mg/ml streptomycin, and 4.5 mM glutamine).

Immunofluorescence of cultured cells and microscopy

Cells were cultured on coverslips until confluent and starved for indicated periods. Cells were fixed with 4% PFA. After blocking with 5% normal donkey serum, application of primary antibody was for 1 h, and secondary antibodies for 30 min with Hoechst 33,342 (Invitrogen). Primary antibodies used were Acetylated tubulin (T6793); ARL13B (Caspary et al., 2007), HA-tag (3F10, Roche), and GPR161 (Pal et al., 2016). Secondary antibodies were from the Jackson Immuno. Coverslips were mounted using Fluoromount G (SouthernBiotech). Images were acquired on a microscope (AxioImager.Z1; ZEISS), sCMOS camera (PCO Edge; BioVision Technologies), and Plan Apochromat objectives (×40/1.3 NA oil; and 63×/1.4 NA oil) controlled using Micro-Manager software (UCSF). Between 8 and 20 z sections at 0.5–0.8-μm intervals were acquired. For quantitative analysis of ciliary localization, stacks of images were acquired from three to eight consecutive fields and percentages of protein-positive ciliated cells were counted. Maximal projections from stacks were exported from ImageJ/Fiji (NIH) using a custom-written macro (M. Mettlen, UT Southwestern) using similar parameters for image files from the same experiment. For measuring ciliary pixel intensities, image stacks were acquired with z sections at 0.8-μm intervals. An image interval with maximal intensity was chosen, and cilia were demarcated with a region of interest using the fluorescence signal for acetylated α-tubulin. The mean pixel intensities for the corresponding protein were exported from ImageJ/Fiji.

Statistical analyses

Statistical analyses were performed using ANOVA and Tukey's post hoc multiple comparisons between all possible pairs using GraphPad Prism.

Results

The proband in this study is a twelve-year old female, the fourth child from a healthy consanguineous Iranian couple (Figures 1A,B, individual VI-4, arrow). The couple reported that their first two children died at the age of 2 years (VI-1) and at 3 months (VI-2) and they were told that the cause of death was kidney failure, but they knew no further information, and no specimen was available for subsequent genetic investigation. She (VI-4) was born following full-term pregnancy, however given her sibling history, she had an abdominal ultrasound within days after her birth. This revealed enlarged kidneys with many small cysts. Subsequent ultrasounds over the first 4 years of her life showed more prominent size of cystic kidneys and increased corticomedullary echogenicity, with reference to grade 1 hydronephrosis in some studies (Figure 1C). Polyuria was reported. Serum Creatinine was 1.8 mg/dl by age 4. A kidney core needle biopsy at age 5 showed diffuse global glomerulosclerosis and tubular atrophy with tubular dilations (Figures 1E–G). The patient underwent a kidney transplantation at age 5, which continues to function well.

Ultrasonography initially described a normal appearing liver, however concern was raised about the liver at age 4 based on elevated SGOT and SGPT, low ferritin, and abnormal coagulation parameters. Subsequent liver ultrasounds from age 5 to age 11 showed initially a mildly enlarged liver with heterogeneous echogenicity, but subsequently smaller in size with lobulated border suggestive of cirrhosis, and with persistent splenomegaly (19.9 cm). A needle biopsy of the liver

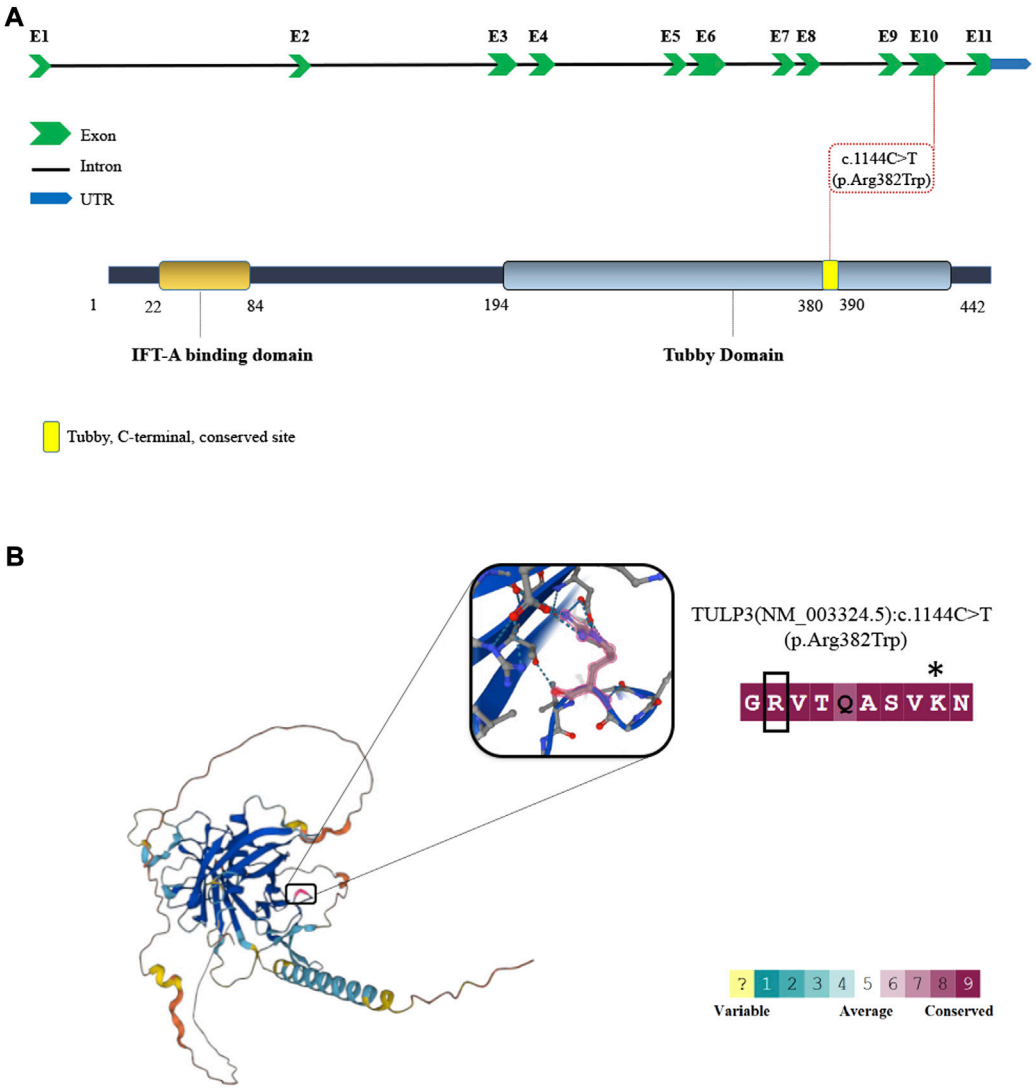

FIGURE 2
The schematic depiction of *TULP3* mutation. **(A)** Schematic depiction of the human *TULP3* locus with 11 exons (top) and Tubby-like protein 3 (bottom). The red dash line represents the variant in the present study. **(B)** Three-dimensional structure of TULP3 protein and illustration of the conservation scores. The position of the pathogenic variant in this study (pink) are shown on the Protein Structure and illustration of the conservation scores (consurf). * represents the site of lysine to isoleucine missense mutation in the mouse *Tulp3* associated with cystic kidneys (Legue and Liem, 2019).

showed distorted lobular and vascular architecture with micronodule formation with individual hepatocytes showing ballooning degeneration. Masson-Trichrome showed bridging fibrosis and nodule formation (Figure 1H).

The proband's older sister was also evaluated for fibrocystic kidney and liver disease (Figure 1A, individual VI-3). Ultrasonography revealed a simple kidney cyst that has grown to 4.5 cm × 5.9 cm (Figure 1D). She has urine volumes in the range of 2 L per day. Her liver function and appearance have been abnormal similar to that of the proband. At age ten years, a liver needle biopsy revealed distorted lobular and vascular architecture with micronodule formation with individual hepatocytes showing ballooning degeneration (Figure 1I).

Whole exome sequencing of the proband's genomic DNA was performed and a novel homozygous variant in *TULP3* was identified and verified by Sanger sequencing. The identified homozygous missense mutation (NM_003324.5: c.1144C>T, p. Arg382Trp) in *TULP3* was present as a heterozygous variant in both unaffected parents (Figures 1A,B). Both the proband and her affected sibling harbored this homozygous mutation while their unaffected sibling did not carry the mutation. Two additional deceased siblings who had

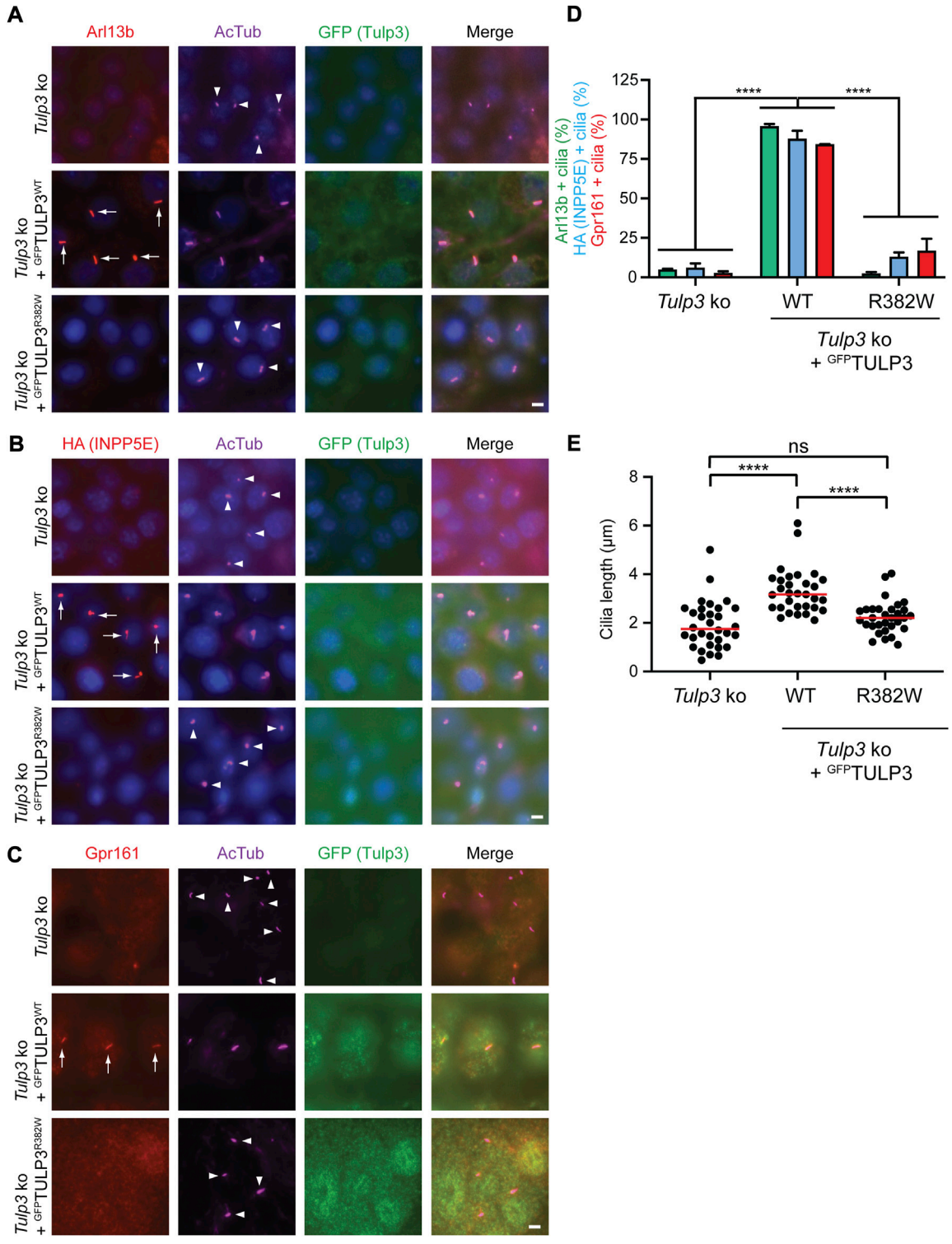

FIGURE 3
Analysis of the TULP3 R382W variant in ciliary trafficking. **(A)**-C. *Tulp3* ko IMCD3 parental line or lines stably expressing HA-INPP5E and LAP-tagged wild type TULP3 or R382W mutant were grown to confluence, serum starved for 36 h before fixation and immune-stained for Arl13B **(A)**, HA **(B)** or Gpr161 **(C)** and GFP, acetylated tubulin (AcTub) and counterstained for DNA. Arrows and arrowheads indicate cilia positive or negative for the indicated proteins, respectively. Scale = 5 µm. **(D)**. Cilia in GFP(TULP3) expressing cells counted from at least 2 experiments, $n > 200$/condition. Data represents mean ± SD. ****$p < 0.0001$, two-way ANOVA followed by Tukey multiple comparison test. **(E)**. Cilia lengths (n = 30 cilia/condition). ****$p < 0.0001$; ns, not significant by using one-way ANOVA followed by Tukey multiple comparison test.

hepatorenal disease were not analyzed in this study (Figure 1A). See Supplementary Material S1 for a homozygosity plot of the proband and Supplementary Material S2 for additional variant information.

Variants in *TULP3* have recently been identified in patients with variable and progressive organ fibrosis (Devane et al., 2022). The *TULP3* locus contains 11 exons and encodes a 442 amino acid protein with a N-terminal IFT-A binding domain and a C-terminal Tubby domain (Figure 2A). The mutation affects a highly conserved residue within the Tubby domain substituting the invariant basic arginine to a polar neutral tryptophan, resulting in a change of charge (Figure 2B). This mutation was predicted damaging as assessed by multiple bioinformatics programs. The R382W mutation lies within the Tubby domain which has been shown to be required for the binding of TULP3 to phosphoinositides as well as for the proper trafficking of a subset of membrane-associated proteins into the primary cilium (Santagata et al., 2001; Mukhopadhyay et al., 2010; Badgandi et al., 2017).

In mice, *Tulp3* mutations disrupt ciliary trafficking leading to abnormal ciliary protein composition, defects in cellular signaling and renal cystic disease (Hwang et al., 2019; Legue and Liem, 2019). To determine how the patient variant R382W affected TULP3 protein function, we analyzed its effect on ciliary trafficking *in vitro*. We generated *Tulp3* knock out (ko) inner medullary collecting duct-3 (IMCD3) cells using CRISPR/Cas9 gene editing methods. We transfected *Tulp3* ko IMCD3 cells with constructs encoding either GFP-tagged TULP3 WT or TULP3 R382W mutant proteins. TULP3 has been shown to facilitate the transport of specific membrane associated proteins into the cilia and IMCD3 cells are routinely used to analyze ciliary trafficking phenotypes. Arl13b, Gpr161, or Inpp5e proteins have all been previously shown to localize to the cilium in a TULP3-dependent manner (Badgandi et al., 2017; Hwang et al., 2019; Legue and Liem, 2019). We first tested the ability of R382W TULP3 to facilitate the ciliary transport of *Arl13b*, a small G-protein associated with Joubert's Syndrome that requires *Tulp3* for transport into the cilium in kidney cells (Hwang et al., 2019; Legue and Liem, 2019). As expected, Arl13b did not localize to the cilium in *Tulp3* ko IMCD3 cells (Figure 3A). However, transfection of *Tulp3* ko IMCD3 cells with a WT TULP3 construct rescued ciliary transport, as endogenous Arl13b was robustly detected in cilia by immunofluorescence staining (Figure 3A). In contrast, transfection of *Tulp3* ko IMCD3 cells with a R382W TULP3 construct failed to rescue ciliary transport of Arl13b, which was not detected in cilia (Figures 3A,D). This result indicated that the mutant R382W form of TULP3 lacked the ability to facilitate the transport of Arl13b to the cilium.

We next tested the ability of R382W TULP3 to facilitate the transport of Inpp5e into the cilium using *Tulp3* ko IMCD3 cells expressing HA-INPP5E. INPP5E is a ciliary phosphoinositide phosphatase that localizes to cilia where it regulates PI(4)P levels (Kisseleva et al., 2000; Chavez et al., 2015; Garcia-Gonzalo et al., 2015; Jacoby et al., 2009; Bielas et al., 2009) and INPP5E localization into cilia has been shown to be dependent on TULP3 function (Badgandi et al., 2017). *Tulp3* ko IMCD3 cells did not transport HA-tagged INPP5E into the cilium (Figure 3B). However, *Tulp3* ko IMCD3 cells expressing the WT TULP3-GFP rescued transport of HA-tagged INPP5E into cilia as detected by immunofluorescence staining with an antibody to HA (Figure 3B). In contrast, *Tulp3* ko IMCD3 cells expressing R382W mutant TULP3 failed to restore ciliary transport of HA-INPP5E as ciliary levels of HA-INPP5E were significantly reduced compared to WT TULP3 (Figures 3B,D), indicating the mutant form had diminished function.

In addition, we tested the ability of R382W TULP3 to transport the receptor Gpr161 into the cilium. Tulp3 has been previously shown to be required for the transport of numerous G-protein coupled receptors into the cilium, including Gpr161 (Mukhopadhyay et al., 2010; Mukhopadhyay et al., 2013). *Tulp3* ko IMCD3 cells did not transport Gpr161 into the cilium (Figure 3C), however cells expressing WT TULP3 rescued ciliary transport with endogenous Gpr161 localized to cilia as detected by immunofluorescence (Figure 3C). In contrast, *Tulp3* ko IMCD3 cells expressing R382W TULP3 had diminished levels of Gpr161 into the cilium, as cilia contained significantly less Gpr161 (Figures 3C,D). These results again indicated that R382W is a loss of functional allele with a compromised ability to facilitate the transport of membrane-associated proteins into the cilium (Figure 3D).

Finally, we tested the effect of expressing the patient variant R382W form of TULP3 on cilia formation. Cilia in *Tulp3* ko IMCD3 cilia expressing either WT TULP3 or R382W TULP3 were examined by immunofluorescence staining using an anti-acetylated alpha tubulin antibody, which labels the ciliary axonemes. *Tulp3* ko IMCD3 cells expressing the R382W variant form of TULP3 did not affect ciliogenesis but showed a mild reduction in cilia length compared with the same cells expressing WT TULP3, similar to the cilia length reduction in the un-transfected *Tulp3* ko IMCD3 cells (Figure 3E). Taken together, these results indicated that the R382W TULP3 variant identified in patients with fibrocystic renal and hepatic disease caused a loss of function of TULP3 by disrupting protein transport to the primary cilium.

Discussion

Hepatorenal fibrocystic diseases are inherited disorders that involve developmental and degenerative abnormalities of the liver and kidneys (Gunay-Aygun, 2009). Many of the identified genes that are associated with renal or hepatic cystic and fibrotic diseases encode proteins that are localized to the primary cilium,

strongly implicating these signaling organelles in regulating fibrocystic and cystic pathways (Tobin and Beales, 2009; Hildebrandt et al., 2011; Walker et al., 2022). Here we present two sisters with inherited fibrocystic kidney and liver disease attributable to a rare homozygous mutation in the ciliary protein TULP3. The spectrum of phenotypes is consistent with that reported by (Devane et al., 2022), however, our proband had earlier kidney failure than any previously reported case. It is also possible that her deceased siblings had the same genotype and kidney failure even sooner, however insufficient data is available to draw conclusions. Variants in *TULP3* have a variable disease presentation (Devane et al., 2022) and R382W appears to cause relatively severe disease within this spectrum based on the early disease phenotype observed in the proband, although clear phenotypic variability exists among the siblings. Hypertrophic cardiomyopathy in the 6th and 7th decade of life has also been associated with *TULP3* patient variants (Devane et al., 2022). However, the younger patients presented here have an unremarkable clinical cardiac exam and have yet to undergo echocardiography. The recessive inheritance of *TULP3* mutations is also consistent with our genetic studies in the mouse where the conditional knockout of both copies of *Tulp3* in renal epithelial cells drive kidney cysts, while deletion of a single copy of *Tulp3* failed to show phenotypes (Hwang et al., 2019; Legue and Liem, 2019). The results did not support the association of a heterozygous R382W variant in TULP3 with anencephaly (Kuang et al., 2022). Taken together, these findings strongly support the idea the R382W disrupts a key region required for Tubby domain function.

The R382W mutation resides in the Tubby domain of TULP3, a protein motif that binds to phosphoinositides. The Tubby domain has been shown to be required for Tulp3 function to facilitate the trafficking of proteins to the ciliary membrane (Badgandi et al., 2017). The human Tubby domain proteins include TUB, TULP1, TULP2, and TULP3, and are characterized by a conserved C-terminal Tubby domain structurally characterized by a *ß*-barrel surrounding a central alpha helix (Boggon et al., 1999). The Arginine at position 382 is highly conserved in the family of Tubby domain-containing proteins and is present in human as well as *S. cerevisiae* and Arabidopsis (Boggon et al., 1999). The expression of R382W mutant form of TULP3 was unable to rescue ciliary trafficking of Arl13b, INPP5E and Gpr161 in *Tulp3* knockout IMCD3 cells, indicating that the mutation disrupts TULP3 function. This phenotype is reminiscent of earlier studies showing that mutations or deletions of the Tubby domain strongly affected the trafficking of proteins into the cilium (Mukhopadhyay et al., 2010). The R382W amino acid substitution disrupts a similar region of the Tubby domain as the N-ethyl-N-nitrosourea (ENU)-induced missense mutation K407I in the mouse Tulp3 (position 389 in the human protein, Figure 2) (Legue and Liem, 2019). This recessive hypomorphic allele was identified in a forward genetic screen in the mouse that caused rapid cystic renal disease (Legue and Liem, 2019) and the analogous mutation in human TULP3, K389I, disrupted ciliary trafficking of ARL13B, GPR161, and INPP5E (Palicharla et al., 2021).

Patient sequencing studies have also helped to identify critical residues within the Tubby domain that are essential for protein function. Amino acid substitutions within the beta strands have been linked to TULP3-associated disease, including variants C204W and R408H (Devane et al., 2022). Homozygous mutant R408H urine-derived epithelial cells (UREC) also showed ciliary trafficking defects in ARL13B, GPR161 and INPP5E (Devane et al., 2022). In our study, we identified the R382W variant in TULP3 that changes a highly conserved positively charged amino acid with a neutral residue (Figure 2). Interestingly, amino acid substitutions of this conserved arginine within the Tubby domain in the related gene TULP1 have also been identified in retinitis pigmentosa patients (den Hollander et al., 2007; Ajmal et al., 2012). The substitution of this key arginine with a residue that results in a change of charge could alter putative interactions of the Tubby domain or disrupt the 3-dimensional protein structure in this critical region, causing loss of Tubby domain function and disease.

The mechanisms by which mutations in TULP3 drive hepatorenal fibrocystic disease are not understood. However, there is clear evidence that TULP3 facilitates the transport of a critical subset of membrane associated proteins into the primary cilium and that the proper localization of these proteins are thought to be essential for their function (Badgandi et al., 2017). Multiple integral membrane and lipidated proteins are preferentially localized to the cilium (Hilgendorf et al., 2016). These proteins include Arl13b, a Joubert syndrome associated protein which causes cystic renal disease when conditionally deleted in renal epithelial cells in the mouse (Seixas et al., 2016; Li et al., 2016). Deletion of *Inpp5e* in renal epithelial cells also results in strong cystic phenotypes while changing the composition of the ciliary membrane (Bielas et al., 2009). Moreover, Tulp3 has also been shown to regulate the trafficking of other critical disease-associated proteins to cilia such as Polycystins 1 and 2 (mutated in ADPKD) and fibrocystin (mutated in ARPKD) (Badgandi et al., 2017). Therefore, a mutation in the Tubby domain of TULP3 may result in fibrocystic disease in patients by disrupting the transport of multiple signaling proteins regulated by the cilium. A missense mutation in the Tubby domain also results in Sonic Hedgehog dependent phenotypes, a cilia dependent pathway that could also contribute to the disease (Legue and Liem, 2020). However other mechanisms not involving ciliary trafficking, such as TULP3 functions in the nucleus have also been proposed and could regulate fibrocystic pathways (Devane et al., 2022).

In sum, we identified a missense mutation in the gene *TULP3* by WES in two Iranian sisters from a consanguineous family presenting with fibrocystic renal and hepatic disease. The identification of the *TULP3* variant (NM_003324.5: c.1144C>T,

p. Arg382Trp) broadens our knowledge of pathogenic mutations in patients and identifies a critical residue within the C-terminal Tubby domain of TULP3 required for proper trafficking of membrane associated proteins to cilia.

Data availability statement

The datasets presented in this study can be found in online repositories. The names of the repository/repositories and accession number(s) can be found in the article/ Supplementary Material.

Ethics statement

The studies involving human participants were reviewed and approved by Ethics Committee of Shiraz University of Medical Sciences. Written informed consent to participate in this study was provided by the participants' legal guardian/next of kin.

Author contributions

HJK conceptualization, data collection, methodology, writing VP experimentation, methodology, writing SD physical examination clinical characterization MI physical examination and clinical characterization SST physical examination and clinical characterization MD physical examination and clinical characterization WB writing, editing SM experimentation, methodology, data, writing KL conceptualization, writing, methodology.

Funding

This project was funded by the National Institutes of Health (R01DK128089 to SM and R01NS097928 and R56DK132266 to KL), a PKD Foundation postdoctoral fellowship to VP (214F19a), and a PKD Foundation grant to KL (232G18). The content is solely the responsibility of the authors and does not necessarily represent the official views of the National Institutes of Health.

Acknowledgments

The authors thank the patients and family members who took part in this study. We thank Emilie Legué for comments on the manuscript and help with figures. We thank Tamara Caspary for the Arl13b antibody. We thank Sun-hee Hwang for help with mutagenesis.

Conflict of interest

The authors declare that the research was conducted in the absence of any commercial or financial relationships that could be construed as a potential conflict of interest.

Publisher's note

Supplementary material

The Supplementary Material for this article can be found online at: https://www.frontiersin.org/articles/10.3389/fgene.2022.1021037/full#supplementary-material

References

Ajmal, M., Khan, M. I., Micheal, S., Ahmed, W., Shah, A., Venselaar, H., et al. (2012). Identification of recurrent and novel mutations in Tulp1 in Pakistani families with early-onset retinitis pigmentosa. *Mol. Vis.* 18, 1226–1237.

Badgandi, H. B., Hwang, S. H., Shimada, I. S., Loriot, E., and Mukhopadhyay, S. (2017). Tubby family proteins are adapters for ciliary trafficking of integral membrane proteins. *J. Cell Biol.* 216, 743–760. doi:10.1083/jcb.201607095

Bielas, S. L., Silhavy, J. L., Brancati, F., Kisseleva, M. V., Al-Gazali, L., Sztriha, L., et al. (2009). Mutations In Inpp5e, Encoding Inositol Polyphosphate-5-Phosphatase E, Link Phosphatidyl Inositol Signaling To The Ciliopathies. *Nat. Genet.* 41, 1032–1036. doi:10.1038/ng.423

Boggon, T. J., Shan, W. S., Santagata, S., Myers, S. C., and Shapiro, L. (1999). Implication of Tubby proteins as transcription factors by structure-based functional analysis. *Science* 286, 2119–2125. doi:10.1126/science.286.5447.2119

Cameron, D. A., Pennimpede, T., and Petkovich, M. (2009). Tulp3 is A critical repressor of mouse Hedgehog signaling. *Dev. Dyn.* 238, 1140–1149. doi:10.1002/dvdy.21926

Caspary, T., Larkins, C. E., and Anderson, K. V. (2007). The graded response to sonic Hedgehog depends on cilia architecture. *Dev. Cell* 12, 767–778. doi:10.1016/j.devcel.2007.03.004

Chavez, M., Ena, S., Van Sande, J., De Kerchove d'Exaerde, A., Schurmans, S., and Schiffmann, S. N. (2015). Modulation of ciliary phosphoinositide content regulates trafficking and sonic hedgehog signaling output. *Dev. Cell* 34, 338–350.

Den Hollander, A. I., Van Lith-Verhoeven, J. J., Arends, M. L., Strom, T. M., Cremers, F. P., and Hoyng, C. B. (2007). Novel compound heterozygous Tulp1 mutations in A family with severe early-onset retinitis pigmentosa. *Arch. Ophthalmol.* 125, 932–935. doi:10.1001/archopht.125.7.932

Devane, J., Ott, E., Olinger, E. G., Epting, D., Decker, E., Friedrich, A., et al. (2022). Progressive liver, kidney, and heart degeneration in children and adults affected by Tulp3 mutations. *Am. J. Hum. Genet.* 109, 928–943. doi:10.1016/j.ajhg.2022.03.015

Garcia-gonzalo, F. R., Phua, S. C., Roberson, E. C., Garcia, G., Abedin, M., Schurmans, S., et al. (2015). Phosphoinositides regulate ciliary protein trafficking to modulate hedgehog signaling. *Dev. Cell* 34, 400–409.

Goetz, S. C., and Anderson, K. V. (2010). The primary cilium: A signalling centre during vertebrate development. *Nat. Rev. Genet.* 11, 331–344. doi:10.1038/nrg2774

Gunay-Aygun, M. (2009). Liver and kidney disease in ciliopathies. *Am. J. Med. Genet. C Semin. Med. Genet.* 151c, 296–306. doi:10.1002/ajmg.c.30225

Hildebrandt, F., Benzing, T., and Katsanis, N. (2011). Ciliopathies. *N. Engl. J. Med.* 364, 1533–1543. doi:10.1056/NEJMra1010172

Hilgendorf, K. I., Johnson, C. T., and Jackson, P. K. (2016). The primary cilium as A cellular receiver: Organizing ciliary gpcr signaling. *Curr. Opin. Cell Biol.* 39, 84–92. doi:10.1016/j.ceb.2016.02.008

Hwang, S. H., Somatilaka, B. N., Badgandi, H., Palicharla, V. R., Walker, R., Shelton, J. M., et al. (2019). Tulp3 regulates renal cystogenesis by trafficking of cystoproteins to cilia. *Curr. Biol.* 29, 790–802. doi:10.1016/j.cub.2019.01.047

Ikeda, A., Nishina, P. M., and Naggert, J. K. (2002). The tubby-like proteins, A family with roles in neuronal development and function. *J. Cell Sci.* 115, 9–14. doi:10.1242/jcs.115.1.9

Jacoby, M., Cox, J. J., Gayral, S., Hampshire, D. J., Ayub, M., Blockmans, M., et al. (2015). INPP5E mutations cause primary cilium signaling defects, ciliary instability and ciliopathies in human and mouse. *Nat. Genet.* 41, 1027–1031.

Karczewski, K. J., Francioli, L. C., Tiao, G., Cummings, B. B., Alfoldi, J., Wang, Q., et al. (2020). The mutational constraint spectrum quantified from variation in 141, 456 humans. *Nature* 581, 434–443. doi:10.1038/s41586-020-2308-7

Kisseleva, M. V., Wilson, M. P., and Majerus, P. W. (2000). The isolation and characterization of a cDNA encoding phospholipid-specific inositol polyphosphate 5-phosphatase. *J. Biol. Chem.* 275, 20110–20116.

Kuang, L., Jiang, Y., Chen, S., Su, K., Peng, R., Yang, X., et al. (2022). Rare variants in Tulp3 abolish the suppressive effect on sonic Hedgehog signaling and contribute to human neural tube defects. *Genes Dis.* 9, 1174–1177. doi:10.1016/j.gendis.2021.11.010

Legue, E., and Liem, K. F., Jr. (2020). Mutations in ciliary trafficking genes affect sonic hedgehog-dependent neural tube patterning differentially along the anterior-posterior Axis. *Neuroscience* 450, 3–14. doi:10.1016/j.neuroscience.2020.07.015

Legue, E., and Liem, K. F., Jr. (2019). Tulp3 is A ciliary trafficking gene that regulates polycystic kidney disease. *Curr. Biol.* 29, 803–812. doi:10.1016/j.cub.2019.01.054

Li, Y., Tian, X., Ma, M., Jerman, S., Kong, S., Somlo, S., et al. (2016). Deletion of adp ribosylation factor-like gtpase 13b leads to kidney cysts. *J. Am. Soc. Nephrol.* 27, 3628–3638. doi:10.1681/ASN.2015091004

Liem, K. F., Jr., Ashe, A., He, M., Satir, P., Moran, J., Beier, D., et al. (2012). The ift-A complex regulates Shh signaling through cilia structure and membrane protein trafficking. *J. Cell Biol.* 197, 789–800. doi:10.1083/jcb.201110049

Mukhopadhyay, S., and Jackson, P. K. (2011). The Tubby family proteins. *Genome Biol.* 12, 225. doi:10.1186/gb-2011-12-6-225

Mukhopadhyay, S., Wen, X., Chih, B., Nelson, C. D., Lane, W. S., Scales, S. J., et al. (2010). Tulp3 bridges the ift-A complex and membrane phosphoinositides to promote trafficking of G protein-coupled receptors into primary cilia. *Genes Dev.* 24, 2180–2193. doi:10.1101/gad.1966210

Mukhopadhyay, S., Wen, X., Ratti, N., Loktev, A., Rangell, L., Scales, S. J., et al. (2013). The ciliary G-protein-coupled receptor Gpr161 negatively regulates the sonic Hedgehog pathway via camp signaling. *Cell* 152, 210–223. doi:10.1016/j.cell.2012.12.026

Norman, R. X., Ko, H. W., Huang, V., Eun, C. M., Abler, L. L., Zhang, Z., et al. (2009). Tubby-like protein 3 (Tulp3) regulates patterning in the mouse embryo through inhibition of Hedgehog signaling. *Hum. Mol. Genet.* 18, 1740–1754. doi:10.1093/hmg/ddp113

Pal, K., Hwang, S. H., Somatilaka, B., Badgandi, H., Jackson, P. K., Defea, K., et al. (2016). Smoothened determines beta-arrestin-mediated removal of the G protein-coupled receptor Gpr161 from the primary cilium. *J. Cell Biol.* 212, 861–875. doi:10.1083/jcb.201506132

Palicharla, V. R., Hwang, S.-H., Somatilaka, B. N., Badgandi, H. B., Legué, E., Tran, V. M., et al. (2021). Interactions between Tulp3 Tubby domain cargo site and Arl13b amphipathic helix promote lipidated protein transport to cilia. *Biorxiv* 05.25, 445488. doi:10.1101/2021.05.25.445488

Patterson, V. L., Damrau, C., Paudyal, A., Reeve, B., Grimes, D. T., Stewart, M. E., et al. (2009). Mouse hitchhiker mutants have spina bifida, dorso-ventral patterning defects and polydactyly: Identification of Tulp3 as A novel negative regulator of the sonic Hedgehog pathway. *Hum. Mol. Genet.* 18, 1719–1739. doi:10.1093/hmg/ddp075

Reiter, J. F., and Leroux, M. R. (2017). Genes and molecular pathways underpinning ciliopathies. *Nat. Rev. Mol. Cell Biol.* 18, 533–547. doi:10.1038/nrm.2017.60

Richards, S., Aziz, N., Bale, S., Bick, D., Das, S., Gastier-Foster, J., et al. (2015). Standards and guidelines for the interpretation of sequence variants: A joint consensus recommendation of the American college of medical genetics and genomics and the association for molecular pathology. *Genet. Med.* 17, 405–424. doi:10.1038/gim.2015.30

Rychlik, W. (2007). Oligo 7 primer analysis software. *Methods Mol. Biol.* 402, 35–60. doi:10.1007/978-1-59745-528-2_2

Santagata, S., Boggon, T. J., Baird, C. L., Gomez, C. A., Zhao, J., Shan, W. S., et al. (2001). G-protein signaling through Tubby proteins. *Science* 292, 2041–2050. doi:10.1126/science.1061233

Seixas, C., Choi, S. Y., Polgar, N., Umberger, N. L., East, M. P., Zuo, X., et al. (2016). Arl13b and the exocyst interact synergistically in ciliogenesis. *Mol. Biol. Cell* 27, 308–320. doi:10.1091/mbc.E15-02-0061

Tobin, J. L., and Beales, P. L. (2009). The nonmotile ciliopathies. *Genet. Med.* 11, 386–402. doi:10.1097/GIM.0b013e3181a02882

Torres, J. Z., Miller, J. J., and Jackson, P. K. (2009). High-throughput generation of tagged stable cell lines for proteomic analysis. *Proteomics* 9, 2888–2891. doi:10.1002/pmic.200800873

Walker, R. V., Maranto, A., Palicharla, V. R., Hwang, S. H., Mukhopadhyay, S., and Qian, F. (2022). Cilia-localized counterregulatory signals as drivers of renal cystogenesis. *Front. Mol. Biosci.* 9, 936070.doi:10.3389/fmolb.2022.936070

frontiers | Frontiers in Genetics

TYPE Original Research
PUBLISHED 10 October 2022
DOI 10.3389/fgene.2022.1017280

OPEN ACCESS

EDITED BY
Steven L. C. Pei,
Yale University, United States

REVIEWED BY
Steven L. Brody,
Washington University in St. Louis, United States
Andrew Paul Jarman,
University of Edinburgh, United Kingdom
Susan Dutcher,
Washington University in St. Louis, United States

*CORRESPONDENCE
Dalal A. Al-Mutairi,
dalal.almutairi@ku.edu.kw

SPECIALTY SECTION
This article was submitted to Human and Medical Genomics, a section of the journal Frontiers in Genetics

RECEIVED 11 August 2022
ACCEPTED 23 September 2022
PUBLISHED 10 October 2022

CITATION
Al-Mutairi DA, Alsabah BH, Alkhaledi BA, Pennekamp P and Omran H (2022), Identification of a novel founder variant in DNAI2 cause primary ciliary dyskinesia in five consanguineous families derived from a single tribe descendant of Arabian Peninsula. *Front. Genet.* 13:1017280. doi: 10.3389/fgene.2022.1017280

Identification of a novel founder variant in *DNAI2* cause primary ciliary dyskinesia in five consanguineous families derived from a single tribe descendant of Arabian Peninsula

Dalal A. Al-Mutairi[1]*, Basel H. Alsabah[2], Bashar A. Alkhaledi[3], Petra Pennekamp[4] and Heymut Omran[4]

[1]Department of Pathology, Faculty of Medicine, Health Sciences Center, Kuwait University, Kuwait City, Kuwait, [2]Zain Hospital for Ear, Nose and Throat, Kuwait, Kuwait, [3]Pediatric Pulmonary Unit, Al-Sabah Hospital, Kuwait, Kuwait, [4]Department of General Pediatrics, University Hospital Muenster, Muenster, Germany

Introduction: Primary ciliary dyskinesia (PCD) is caused by dysfunction of motile cilia resulting in insufficient mucociliary clearance of the lungs. The overall aim of this study is to identify disease causing genetic variants for PCD patients in the Kuwaiti population.

Methods: A cohort of multiple consanguineous PCD families was identified from Kuwaiti patients and genomic DNA from the family members was analysed for variant screening. Transmission electron microscopy (TEM) and immunofluorescent (IF) analyses were performed on nasal brushings to detect specific structural abnormalities within ciliated cells.

Results: All the patients inherited the same founder variant in *DNAI2* and exhibited PCD symptoms. TEM analysis demonstrated lack of outer dynein arms (ODA) in all analysed samples. IF analysis confirmed absence of DNAI1, DNAI2, and DNAH5 from the ciliary axoneme. Whole exome sequencing, autozygosity mapping and segregation analysis confirmed that seven patients carry the same homozygous missense variant (*DNAI2*:c.740G>A; p.Arg247Gln; rs755060592).

Conclusion: *DNAI2*:c.740G>A is the founder variant causing PCD in patients belonging to a particular Arabian tribe which practices consanguineous marriages.

KEYWORDS

primary ciliary dyskinesia, genetics of ciliopathy, *DNAI2* gene, consanguinity, pulmonary disease

Introduction

Primary ciliary dyskinesia (PCD; OMIM: 244400) is a genetically and clinically heterogeneous group of disorders affecting motile cilia. PCD individuals usually have a history of neonatal respiratory distress and suffer from lifelong symptoms of wet cough, rhinosinusitis and otitis media. Recurrent chest infections eventually lead to bronchiectasis and a progressive decline in pulmonary function (Ratjen et al., 2016; Davis et al., 2019). Nearly one-half of PCD patients display laterality defects, mainly *situs inversus totalis* and other *situs abnormalities*, due to dysmotility of the embryonic motile node monocilia. Male infertility and female subfertility are also associated with PCD (Zariwala et al., 2007; Leigh et al., 2009; Zariwala et al., 2011). The estimated prevalence of PCD worldwide is around 1:16,000, nevertheless it increases to 1:2,265 in the United Kingdom South Asian inbred population (Lucas et al., 2014; O'Callaghan et al., 2010). A similar high incidence is also seen in a highly inbred Kuwaiti population due to practising consanguinity over multiple generations. Early diagnosis is essential for reducing the morbidity of PCD (Shah et al., 2016). The best diagnostic approach includes genetic testing along with determining the ultrastructural defects of the cilia (Shapiro et al., 2018; Dalrymple and Kenia, 2019). Radiological findings of the chest for PCD individuals mainly show atelectasis in the lingua or right middle lobe (Magnin et al., 2012).

PCD is characterized by dysfunction of multiple motile cilia resulting in abnormal mucociliary clearance. Currently, more than 50 PCD genes are identified, mainly encoding for components of the complex structures of axonemes of motile cilia and sperm flagella. The most common PCD gene that is defective in most of PCD individuals of mainly European origin is Dynein Axonemal Heavy Chain 5 (DNAH5) (MIM: 603335), associated with the absence of outer dynein arms (ODA) (Failly et al., 2009). The second most frequent PCD gene associated with the absence of ODA is Dynein Axonemal Intermediate Chain 1 (DNAI1) (Zariwala et al., 2006; Lucas et al., 2014). In general, there are six dynein structural genes associated with PCD and ODA defects. Three genes encode for axonemal ODA heavy chains *DNAH5* (Olbrich et al., 2002; Hornef et al., 2006; Failly et al., 2009), *DNAH9* (Loges et al., 2018), and *DNAH11* (Schwabe et al., 2008; Pifferi et al., 2010; Knowles et al., 2012). Two genes encode for axonemal ODA intermediate chains *DNAI1* (Zariwala et al., 2006) and *DNAI2* (Loges et al., 2008). One gene encodes for axonemal ODA light chains *DNAL1* (Mazor et al., 2011).

The evolutionarily conserved role for *DNAI2* in the assembly of ODA was previously studied in *Chlamydomonas oda6* mutant strain; pathogenic variants in *IC2* (*IC69*) orthologous to *DNAI2* lead to disrupted ODA complexes (Fowkes and Mitchell, 1998). Another study shown pathogenic variants in the *Chlamydomonas* ortholog (*IC69*) caused reduction in motility of mutant strain (*oda6*) compared to the wild type parent and loss of ODA (Pennarun et al., 2000). The same phenotype was also seen in the *pf28* (*oda2*) mutant strain harbouring pathogenic variants in the γ-dynein heavy chain orthologous to *DNAH5*, indicating the role of the DNAI2 and *DNAH5* orthologs in the assembly of ODA in both human and *Chlamydomonas reinhardtii* (Mitchell and Rosenbaum, 1985).

Dynein Axonemal Intermediate Chain 2 (DNAI2) located in human on chromosome 17q25 (MIM no. 605483) is a component of the ODA complex and is essential for the assembly of this multimeric complex. *DNAI2* was initially cloned and characterized as a PCD gene using the candidate gene approach (Loges et al., 2008). Pathogenic variants in *DNAI2* are a rare cause of PCD. Early studies did not show disease-causing variants of this gene in 16 PCD families, analysed with microsatellite marker alleles concordant for loci on chromosome 17q25 (*DNAI2* locus) (Pennarun et al., 2000; Loges et al., 2008). Homozygosity mapping performed in other studies identified linkage to the *DNAI2* locus and a homozygous splice variant (*DNAI2*:IVS11+1G<A) in all affected individuals of a Jewish Iranian family (Loges et al., 2008). Moreover, in the same study sequence analysis of additional 105 unrelated patients (48 presenting with ODA defects) identified a homozygous nonsense variant (*DNAI2*: c.787C>T; R263X) in a German PCD individual and a homozygous splice variant (*DNAI2*:IVS3-3T<G) in a Hungarian PCD family (Pennarun et al., 2000). Overall, *DNAI2* variants were found in ~2% of all PCD families and 4% of PCD families with documented ODA defects (Loges et al., 2008). In this study, a founder variant in *DNAI2* was identified in seven patients belonging to the same Arabian tribe.

Methods

Human subjects

Ethical approval for this project was obtained from Ministry of Health Research Ethics Committee (Ethics ID: 62/2013). This study was carried out with the permission of all participating family members; informed written consent was obtained from adult participants and from the parents of children for collection of blood samples from the patients and non-affected parents as well as the nasal biopsy. Pedigrees for the families were constructed using Cyrillic version 2.1 (http://www.cyrillicsoftware.com/) according to the Supplier's guidelines. Radiological data were collected for most of the patients under study to correlate the genotype with the clinical phenotype.

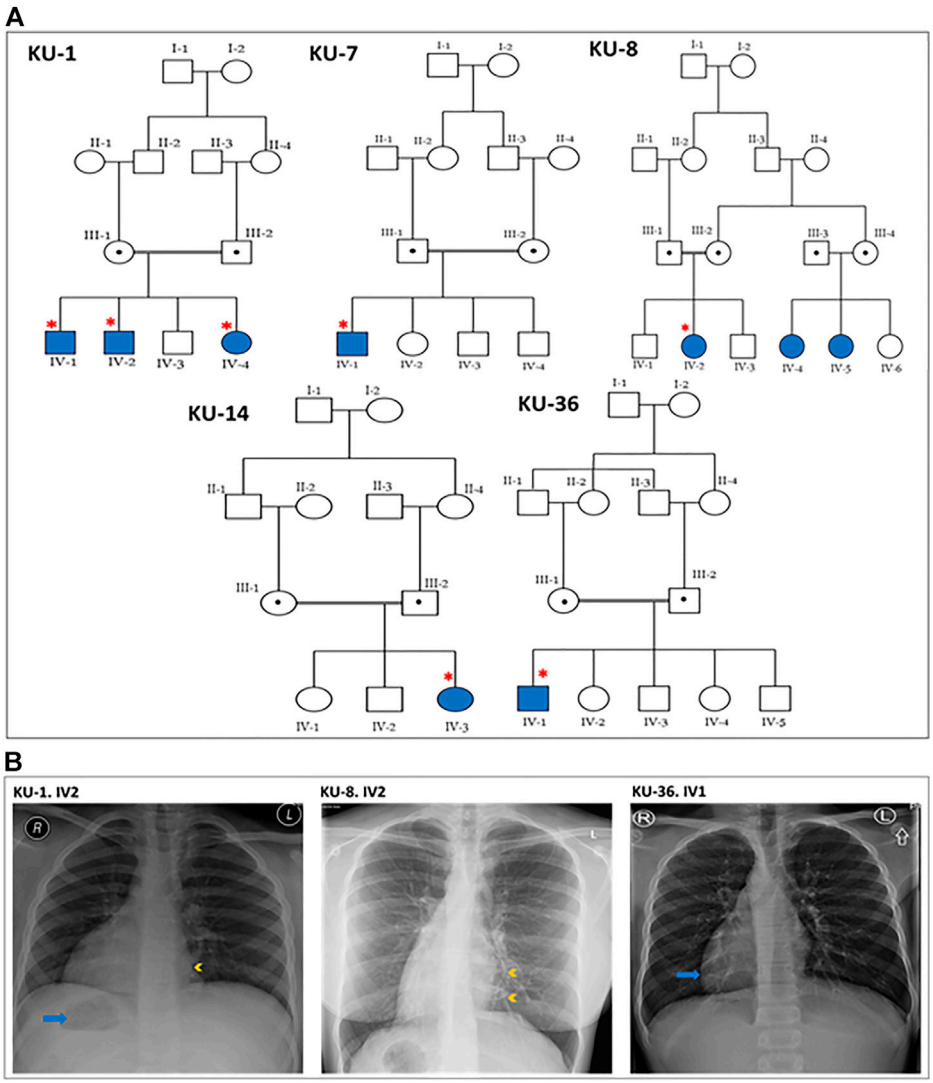

FIGURE 1
Pedigrees and the chest X-rays for the PCD individuals. **(A)** shows the five pedigrees of families under study. The DNA samples and nasal biopsies were taken from the affected individuals (highlighted with asterisks). For KU-1.IV2 patient, only DNA samples were taken later for Sanger sequencing. **(B)** shows selected chest X-rays for three of the patients. The three patients have *dextrocardia* and a right-sided gastric shadow (arrow), in keeping with *situs inversus*. Patient KU-1.IV2 has a small patch of consolidation seen in the paracardiac region of the left lung (arrowhead). Patient KU-8.IV2 has diffuse bronchiectasis as seen in the medial left lower zone (arrowheads). Patient KU-36.IV1 shows dextrocardia (arrow) consistent with *situs inversus*.

Genomic DNA and exome sequencing

Genomic DNA was extracted from whole blood using the QIAamp mini-isolation kit (Qiagen); concentrations were determined by UV spectrophotometry using a Nanodrop N1000 (Nanodrop Technologies Inc.). Exome sequencing of genomic DNA was performed for six individuals highlighted with asterisks (Figure 1) by the Cologne Centre for Genomics, Germany. Target enrichment was performed, following manufacturer's protocols, using SureSelect hybridization capture reagents with V6 (Agilent Technologies). Enriched library preparations were sequenced on HiSeq 2500 platform (Illumina). Linkage analysis using exome data was performed using pipeline-produced variant call format (VCF) files.

Autozygosity mapping and variant screening

Genetic screening using autozygosity mapping was performed using software written at the University of Leeds, United Kingdom (Carr et al., 2009; Carr et al., 2011a; Carr et al.,

2011b; Carr et al., 2013; Watson et al., 2015). Initially, AgileMultiIdeogram software was used to visualize the homozygous intervals using exome data for linkage in which all the homozygous intervals are displayed against a circular ideogram for the 22-autosomal chromosomes for the relative patients (Carr et al., 2013). The reference of genome annotation used was Human Genome Build hg19 (UCSC genome browser).

Primers for variant confirmation and segregation analyses were designed using Primer3 software (http://frodo.wi.mit.edu/primer3/). The exon sequences were obtained from the University of California, Santa Cruz Genome Browser (http://genome.ucsc.edu/) for exon 7 of *DNAI2* gene. For the founder variant rs755060592, the sequence of the forward primer used was "GATTTGAACCAAGCCCTGAT" and the sequence of the reverse primer used "GCCAACATAGTGAAGCACCA".

All targets were amplified using a commercial PCR master mix (Promega, Southampton, United Kingdom). PCR was performed in a total reaction volume of 20 µl. The master mix contained 4 µl of 5x Flexi buffer, 1.2 µl of 25 mM $MgCl_2$, 0.4 µl of 10 mM dNTP that contained a mixture of dATP, dCTP, dGTP, and dTTP nucleotides and 1.2 units of TaqFlexi DNA polymerase. The amount of DNA amplified using that master mix was 40 ng of genomic DNA. For all amplicons initial denaturation was at 95°C for 30 s, followed by 30 cycles of 95°C for 15 s, 58°C for 15 s, 72°C for 30 s and a final 300 s extension at 72°C. Amplicons were purified by using ExoSAP-IT exonuclease (USB Corporation, Cleveland, United States) according to the manufacturer's instructions. PCR products were stained by ethidium bromide and analysed by separation on a 1.5% agarose gel. Sequencing was performed using the BigDye 3.1 kit (Applied Biosystems, Foster City, United States). Sequencing reactions were ethanol-precipitated and re-suspended in HiDi formamide (Applied Biosystems) before analysis on a 3130xl genetic analyzer with a 36 cm capillary array. The Sanger sequencing results were analysed using a GeneScreen software (Carr et al., 2011b).

Immunofluorescent analyses of nasal biopsies

Respiratory epithelial cells were obtained by nasal brush biopsy and suspended in cell culture medium. Samples were spread onto glass slides, air dried and stored at −80°C until use. The respiratory epithelial cells from healthy control and six PCD-affected individuals highlighted with asterisks (Figure 1) were dual labelled for IF analysis with antibodies against axonemal components (visualized with red fluorescent secondary antibody) and antibodies to acetylated anti-Tubulin (visualized with green fluorescent secondary antibody) as ciliary marker. Nuclei were stained with Hoechst 33342 (blue fluorescent) (Wallmeier et al., 2014). Immunofluorescence images were taken with a Zeiss LSM 800 confocal microscope and processed with ZEN and ImageJ software.

The panel of primary antibodies used for initial screening included mouse monoclonal anti-tubulin (acetylated) antibody (Sigma Aldrich, T6793) to stain ciliary microtubules and rabbit polyclonal antibodies as follows: anti-DNAI2 (1:300) (HPA050565, Atlas Antibodies), anti-DNAH5 (1:300) (HPA037470, Atlas Antibodies), anti-DNAI1 (1:300) (HPA021649, Atlas Antibodies). The secondary antibodies used were highly cross absorbed secondary antibodies, including Alexa Fluor 488-conjugated goat antibodies to mouse (1:1000) (A11029, Molecular Probes, Invitrogen) and Alexa Fluor 546-conjugated goat antibodies to rabbit (1:1000) (A11035, Molecular Probes, Invitrogen).

Transmission electron microscopy analysis of nasal biopsies

For transmission electron microscopy (TEM), nasal biopsies were taken from the middle turbinate. The ciliated cells were fixed with glutaraldehyde (2.5%) in Sorensen's phosphate buffered (pH 7.4). After post-fixation, the samples were treated with osmium tetroxide (1.3%), dehydrated through graded ethanol series and immersed in hexamethyldisilazane, a chemical drying reagent. The samples were embedded in 1,2-Epoxypropan-Epon- mixture (1:1) at 4°C overnight. After polymerisation, several sections were picked out onto copper grids. The sections were stained with Reynold's lead citrate. TEM was performed with the Philips CM10 (Wallmeier et al., 2014).

Validating the *DNAI2* founder variant in Arab population

The allele frequency of the identified variant was validated using real time PCR by performing the allelic discrimination test using the same primers designed for Sanger sequencing as described above (Applied Biosystems). Briefly, PCR reactions were carried out using 25 µl reaction mixture containing 25 ng DNA, 1X Taqman primer/probe mix (Applied Biosystems), 1X genotyping Taqman master mix (Applied Biosystems) and sterile DNA/RNA free water. In each experiment, positive (cases for which genotype was confirmed by Sanger sequencing) and negative (water) controls were included. A batch of an ethnically matched Arab control DNA panel collected from 100 normal subjects that belong to different Arabian tribes was run in parallel. Genotyping steps were performed in a 7500 Fast Real-Time PCR System according to the manufacturer's instruction (Applied Biosystems).

Results

Autozygosity mapping reveals a founder homozygous variant in *DNAI2*

Patients were referred for genetic assessment to clinics run by the Ministry of Health in Kuwait. Most patients were suspected to carry disease causing hereditary variants as more than one individual in their families exhibited the same phenotype. Five unrelated families were independently ascertained with PCD diagnosis in a cohort of 50 multiplex families recruited from different hospitals in Kuwait; affected family members showed clinical features typical of the hallmark disease of PCD (MIM: PS244400), mainly neonatal respiratory distress, chronic respiratory disease with symptoms of chronic airway infections, rhinosinusitis, otitis media, bronchiectasis, and *situs inversus totalis*. The ethnic background of all the patients under this study are Asian Arabs belonging to the same tribe from Arabian Peninsula.

This report summarizes the overall genetic analyses for these five families KU-1, KU-7, KU-8, KU-14, and KU-36 with a total number of seven PCD individuals, all members of the same tribe, which is the largest tribe in Kuwait. As seen in pedigrees (Figure 1A), there are two multiplex families that have more than one affected individual. In addition, the informed consent and the questionnaire indicated that there are many other potential PCD individuals belonging to the same tribe that could not be included on the pedigrees as we faced difficulty in reaching them since they live in isolated areas in the more remote regions of Kuwait.

All seven patients were diagnosed with PCD *via* both genetic studies and structural analysis of the respiratory cilia. The paediatric pulmonologist performed a differential diagnosis for six of the patients and excluded other conditions including cystic fibrosis, asthma, anatomic anomalies and immunodeficiencies. The median age at diagnoses was 2 years, with range 1–12 years. All patients included in this study started showing symptoms during early infancy. The patients were hospitalized during infancy for mild respiratory distress and required oxygen administration. All of the patients reported the following symptoms: wheeze, dyspnea, recurrent pneumonias, a chronic productive cough, and constant nasal mucopurulent secretions. These symptoms gradually became more progressive with age. All individuals participating in our study were asked to undergo serial spirometries in the period following up. Three individuals showed only an obstructive pattern; the other four individuals showed a decline in the respiratory function with both an obstructive and restrictive (mixed) pattern. Infertility was reported in the adult PCD male KU-36. IV-1, but no sperm analysis was available. The most commonly reported specific presentations of PCD was *situs inversus totalis*, which was found in all patients in this study. Previous studies have shown truncated variants in *DNAI2* result in randomization of left/right body asymmetry and develop *situs inversus totalis* due to altered motility of nodal cilia (Nonaka et al., 1998; Loges et al., 2008).

It is important when managing these patients to have a considerate approach. This includes administrating intermittent antibiotic therapy for patients presenting with acute chest exacerbations, and preventive antibiotic therapy (macrolides) for the patients who presented with recurrent chest exacerbations. Chest physiotherapy is also strongly advised, and annual vaccinations against influenza and pneumococcus. None of the patients required surgical intervention for bronchiectasis. According to their radiographic images, three cases underwent high-resolution computed tomography (HRCT). They showed clear evidence of bronchiectasis, including thickened bronchial wall with mucoid impaction (data not shown). The chest X-ray images for three PCD individuals confirm a clinical diagnosis of PCD including *situs inversus totalis,* consolidation and bronchiectasis (Figure 1B).

Linkage analysis using autozygosity mapping approach has been performed for all the available affected individuals belonging to the same family, such as family KU-1 in one setting together. This was also performed for the two patients belonging to families KU-7 and KU-8 since the mothers of the affected children are distant relatives. Linkage analysis was performed for families KU-14 and KU-36 separately. The linkage analysis was performed for all the subjects using the lowest level of allele read frequency 10% instead of 25%, which is the default setting for obtaining VCF format for linkage using the exome data. Decreasing the allele frequency was done for the purpose of increasing the resolution of linkage especially for the cases that had a minimal shared interval of Identical by Descent (IBD) across the disease gene locus, as typically seen in families KU-7, KU-8, and KU-36 (Figure 2A). In addition, the resolution of linkage analysis using exome data was further increased by using higher capture-V6 that covers bigger regions of non-coding sequence (61 Mb) compared with the standard capture V7 (37 Mb).

The IBD intervals were determined for each patient at the beginning of the study to estimate the shared IBD intervals, especially for either closely or distantly affected relatives. Mapping the shared IBD intervals is the key for disease-gene identification in patients belonging to multiplex families, or in a group of patients belonging to singleton families derived from the same tribe, as presented in this study. The thickness of the IBD interval represents the extent of the autozygous regions (Carr et al., 2012; Carr et al., 2013). The estimated homozygous intervals in each chromosome were precisely determined using AgileVCFMapper software (Watson et al., 2015).

After that, multiple linkage analysis was performed for six PCD individuals using AgileVCFMapper software, which is an Autozygous Variant Viewer application that analyse each chromosome separately (Watson et al., 2015). This analysis

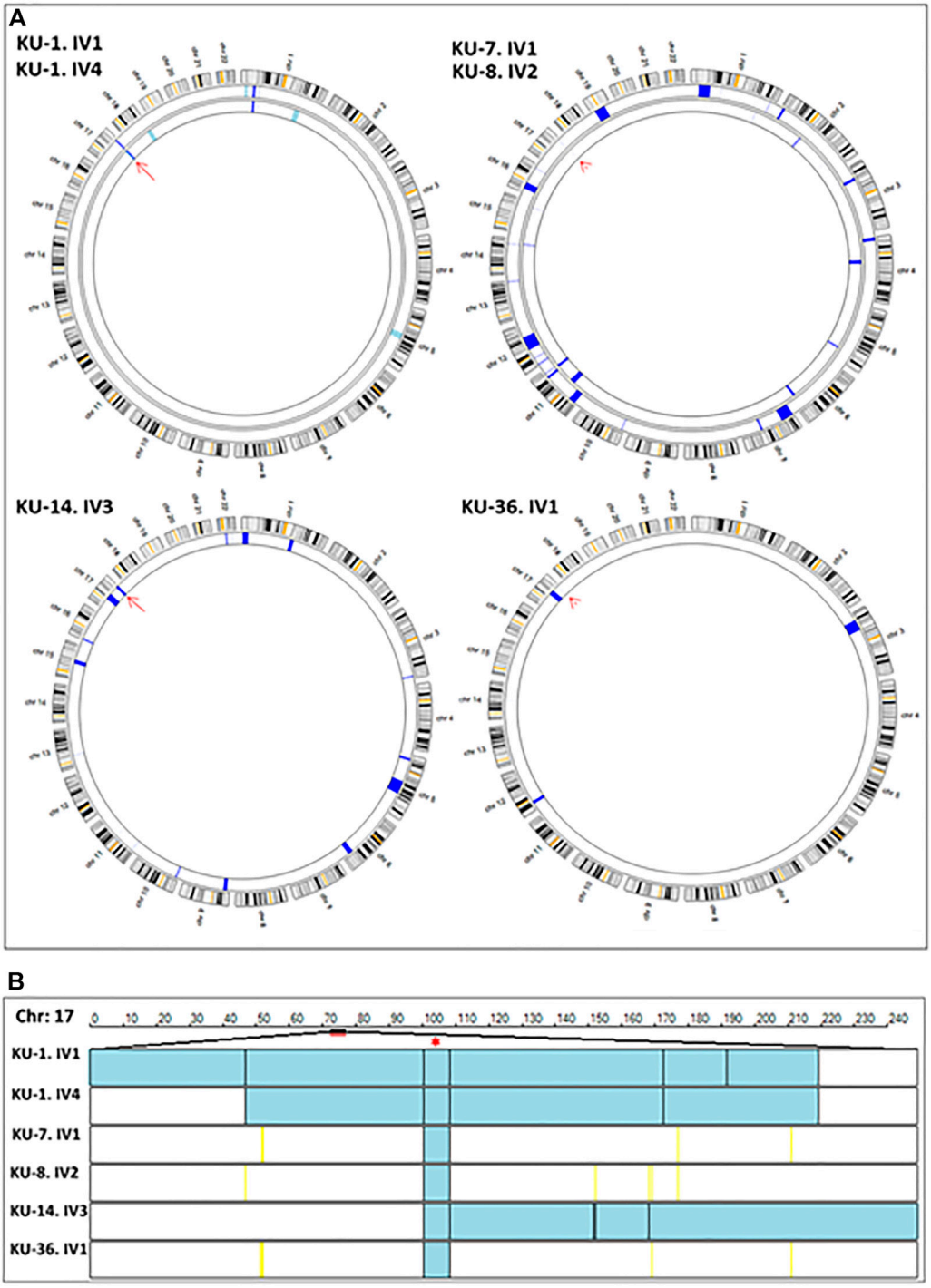

FIGURE 2
Linkage analyses using exome data. **(A)** summarizes the linkage analysis using AgileMultiIdeogram software and presented in such a way that each ideogram shows the overall linkage for the patients belonging to the same family and each lane accounts for one patient. The density of IBD is represented by the bulk of navy-blue bars for the shared regions of homozygosity (autozygous intervals). The light blue bars specify the unshared ROH regions in multiplex families. In singleton families, having one affected individual, all the detected ROH are displayed as navy blue bars, since there is no shared ROH to be prioritized by the software as seen for families KU-14 and KU-36. Linkage results show the two affected siblings belonging to the KU-1 family have an exclusive autozygous interval across the *DNAI2* locus highlighted by a red arrow. Linkage analysis was performed for the two patients from families KU-7 and KU-8 together since they are distantly relatives and the results show a minute IBD interval across the gene locus that indicated by the red arrowhead. The same results were seen for KU-36, although this patient has another significant ROH interval upstream of the *DNAI2* locus suggesting that the founder variant in *DNAI2* has a very high penetrance. **(B)** shows the linkage scan for the six

(*Continued*)

FIGURE 2 (Continued)
patients inheriting a founder variant in *DNAI2* using AgileVCFMapper software. Linkage scan highlighted a unique autozygous interval indicated by two black lines at chromosome 17 across the *DNAI2* locus that emphasised by red asterisk. In this figure, each row represents the genotypes for chromosome 17 for one patient as illustrated in the figure. In mapped autozygous regions, the blue bars indicate the extent of autozygous regions. The black vertical lines represent concordant "common homozygous variants" that are shared among patients with the same founder variant. The yellow vertical lines indicate the positions of nonconcordant "rare homozygous variants". White bars indicate the "no-calls" and that predominantly seen in autozygosity mapping using exome data.

enables mapping of the haplotype for shared regions of autozygosity. This was used successfully to determine the autozygous intervals that harbour founder variants shared across several families by estimating the overlapping homozygous and concordant variants shared among unrelated affected individuals, as seen in Figure 2B.

Screening for deleterious variants in the known PCD genes, in a total of 50 PCD genes to date, was performed in parallel with filtering of the variants at the IBD segments that were determined for all affected individuals in the cohort by estimating all regions of homozygosity (ROH); shared ROH was also estimated between the affected siblings for each family (data not shown).

Initial linkage analyses showed that patients belonging to families KU-1, KU-14 and KU-36 have a detectable ROH segment across the *DNAI2* locus at Chr:17 (Figure 2A). Multiple linkage analysis results showed a unique autozygous interval (blue bar) at chromosome 17 across the *DNAI2* locus shared among the six PCD individuals (Figure 2B). Interestingly, this unique autozygous interval can only be detected using a high resolution of linkage SNP-genotyping. As seen in our data, a shared IBD interval that cannot be clearly visualized with AgileMultiIdeogram software in three patients in Figure 2A (KU-7, KU-8, and KU-36) was detected using AgileVCFMapper software (Figure 2B). Multiple linkage results suggested that a pathogenic variant in *DNAI2* is likely disease causing in these families under study. After that, analysis of exome data at the shared IBD interval revealed a homozygous variant (c.740G>A; p.Arg247Gln) at *DNAI2* locus inherited in the six PCD individuals. Sequencing chromatograms for all seven PCD individuals confirm that all the patients are harbouring the same homozygous missense variant detected in *DNAI2*.

The variant was checked using different algorithms and statistical measurements that predict the pathogenicity of the variants. We used VarSome in initial *in silico* analysis to predict pathogenicity of the *DNAI2*:c.740G>A variant. Here, six metatools that each determine a pathogenicity based on the combined evidence from multiple other *in silico* predictors predict this variant to be damaging (MetaLR, MetaSVM, MetaRNN, BayesDel noAF, BayesDel addAF) or pathogenic (REVEL), 16 out of 18 individual prediction programs that largely use dbNSFP version 4.2 database developed for functional prediction and annotation of all potential non-synonymous single-nucleotide variants (nsSNVs) in the human genome predict the *DNAI2*:c.740G>A variant as pathogenic/damaging/deleterious and/or disease causing, including widely used prediction programs such as: DANN, MutPred, Mutation assessor, MutationTaster, Provean or Polyphen-2 (Loges et al., 2008; Mazor et al., 2011; Knowles et al., 2012).

The results of other algorithms are described in more detail: Firstly, Rejected Substitutions (RS), defined as the number of substitutions expected under a neutral model minus the number "observed" (estimated) for a particular alignment (Pazour et al., 2006). Secondly, Polymorphism Phenotyping (PolyPhen), a tool that predicts possible impact of an amino acid substitution on the structure and function of a human protein (Adzhubei et al., 2013). Thirdly, Residual Variation Intolerance Score (RVIS), a gene score based module intended to help in the interpretation of human sequence data (Petrovski et al., 2013). The missense variant in *DNAI2* (c.740G>A) resulting in an amino acid exchange (p.Arg247Gln) has RS = 5.2, PPH = 3 and RVIS = 0.01, all of which indicate that the variant is highly damaging.

Additional *in silico* analyses on protein level showed that this variant is located between WD40 domains 2 (aa208-246) and 3 (aa253-294), essentially right at the end of WD40 2 (UniProt). However, no specific motifs were found in that area by using EMBL-ELM (eukaryotic linear motif) that could help to explain the impact of this variant on DNAI2 protein function.

In the initial stage of the investigation this variant was mapped in Families KU-1, KU-7 and KU-8 and was not validated on Ensembl database. Recently, it has been given a RefSNPs (rs) number (rs755060592). Remarkably, the allele frequency of the normal allele (G) is 100% in all ethnic backgrounds according to the Ensembl genome browser. In this study, it has very high penetrance as it was found to be inherited in patients with low ROH score that belong to families KU-7, KU-8, and KU-36.

This indicates that the missense variant in *DNAI2* is likely a founder variant causing PCD this tribe (Figure 3). Following the linkage and sequencing analyses, segregation analysis was performed to confirm that the identified variant in seven patients segregates with the disease phenotype. The results of segregation analysis confirmed that all the parents are heterozygous carriers for the founder variant, which indicates that the variant segregates with the disease phenotype and is the pathogenic PCD variant, as seen in Figure 4.

After that, allelic discrimination assay for the *DNAI2* founder variant was performed using RT-PCR. It was

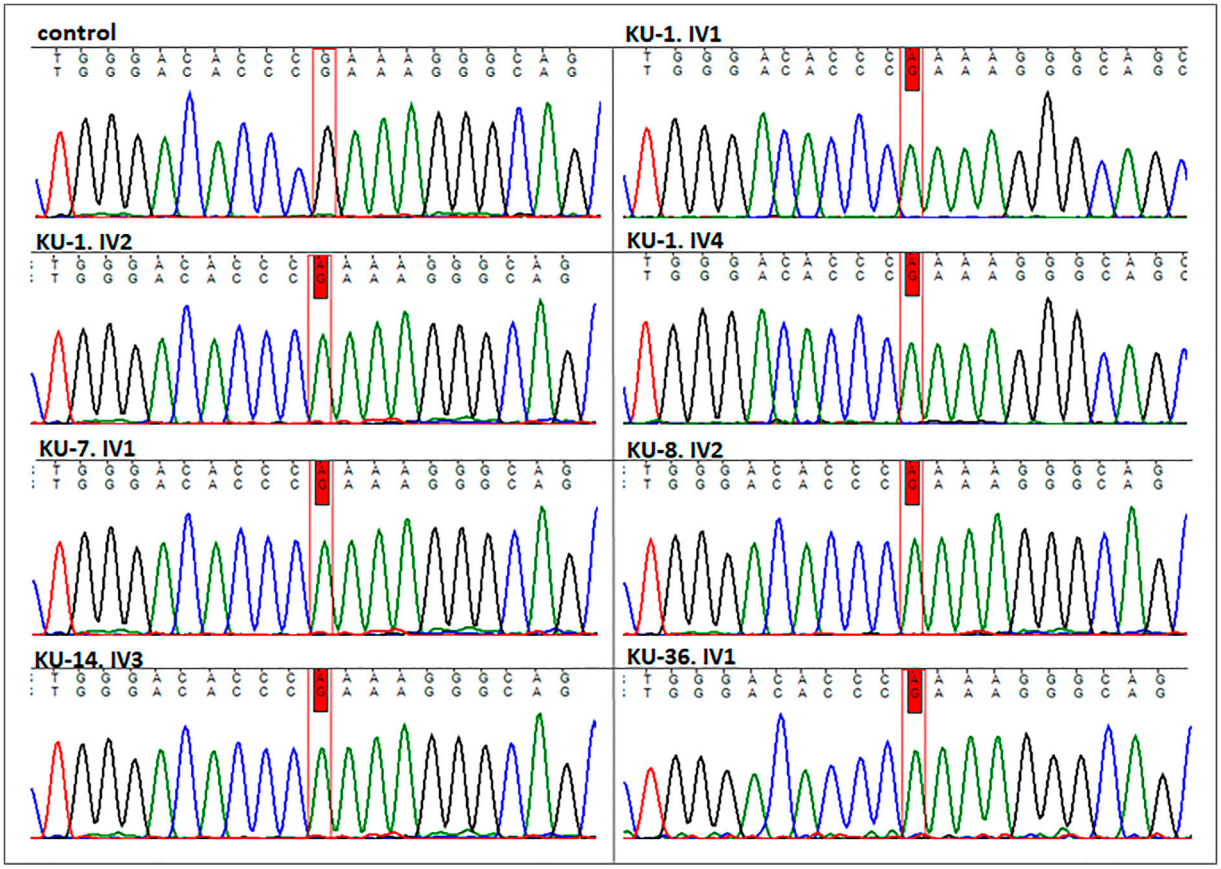

FIGURE 3
Sequencing chromatographs for the seven PCD individuals. All the patients having homozygous missense variant (*DNAI2*:c.740 G>A; p.Arg247Gln) rs755060592 in exon 7 as illustrated *vs.* heathy individual as control.

performed in order to estimate the carrier rate frequency of the founder variant (*DNAI2*:c.740G>A) using an Arab control panel composed of 100 DNA samples for normal individuals belonging to different Arabian tribes. As shown in Supplementary Figure S3, the genotype for the six PCD individuals is homozygous for the missense variant (A), and all their parents are heterozygous carriers for the wild type allele (G) and the defective allele (A) which is consistent with Sanger sequencing data. Interestingly, the genotypes for the Arab control DNA panel show that all the healthy individuals have the two wild type allele (G). This indicates that the variant is very rare and the carriers are rarely existing in Arab populations.

Detection of ultrastructural defects of the cilia

TEM and IF analyses were performed on nasal biopsies derived from five PCD individuals that carry the homozygous missense variant *DNAI2*:c.740G>A to identify any structural abnormalities of the ciliary axoneme of respiratory epithelia. IF results showed negative staining for DNAI2, DNAI1 and DNAH5 proteins in the cilia indicating the absence of outer dynein arm components in all PCD individuals, as seen in Figure 5, Supplementary Figures S1, S2. However, results of IF staining showed a normal localization of GAS8 and RSPH9 that are routinely checked in PCD individuals with dynein arm genes defect (data not shown). This indicates that these proteins are localized normally in the cilia of the affected individuals, as in control cells. TEM analysis also demonstrated lack of ODAs (Figure 6), consistent with previously published report (Loges et al., 2008).

Discussion

Autozygosity mapping is a powerful technique for determining the disease-causing founder variants in related patients. Practically, it is more successfully used for investigating the pathogenic variants in distantly related

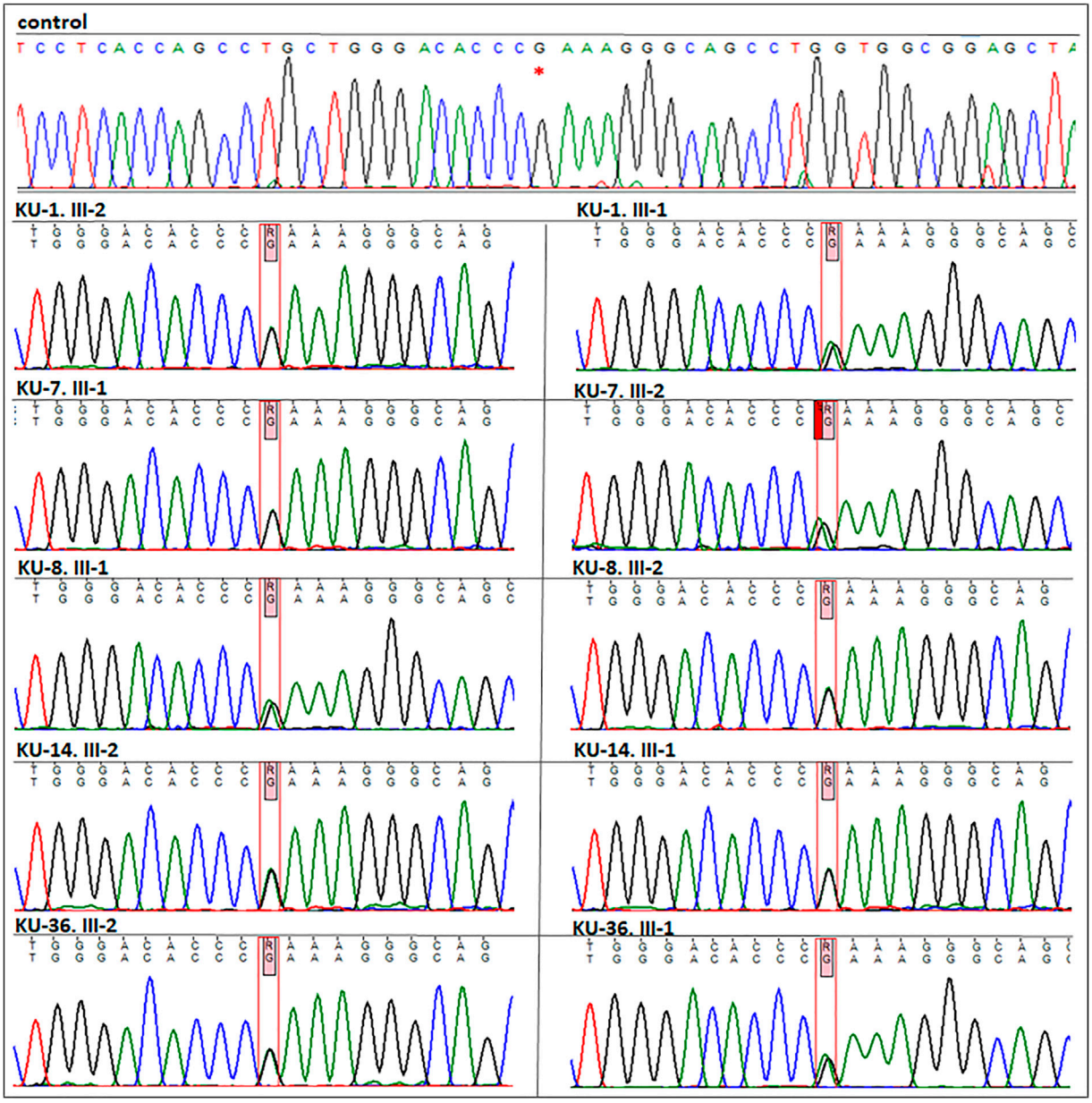

FIGURE 4
Segregation analysis for the parents of the five families. As seen in this figure the chromatographs for the sequencing results for the five parents, which demonstrate that all the parents are carriers for the missense variant (*DNAI2*:c.740 G>A; p.Arg247Gln) rs755060592 in exon 7. This confirms that the variant is segregated along with the disease phenotype in the seven PCD individuals.

individuals than in closely related individuals, such as affected siblings or cousins, especially in an inbred population, such as the Kuwaiti population. Since patients in multiplex families have multiple IBD intervals, sometimes in multiple chromosomes as frequently seen in our patients, mapping of the disease-gene can be challenging, especially considering the huge volume of sequence variant data generated from next generation sequencing experiments (Williams and Hegde, 2013; Johansen Taber et al., 2014). Autozygosity mapping is also the most efficient strategy for mapping the deleterious founder variants in patients with rare autosomal recessive disorders (Lander and Botstein, 1987; Abecasis et al., 2002; Carr et al., 2011a). Here, we successfully applied AgileMultiIdeogram and AgileVCFMapper software, the latter enabling to visualize small ROH intervals that could not be visualized with other software solutions, to identify a founder variant in *DNAI2* inherited within a single Arabic tribe

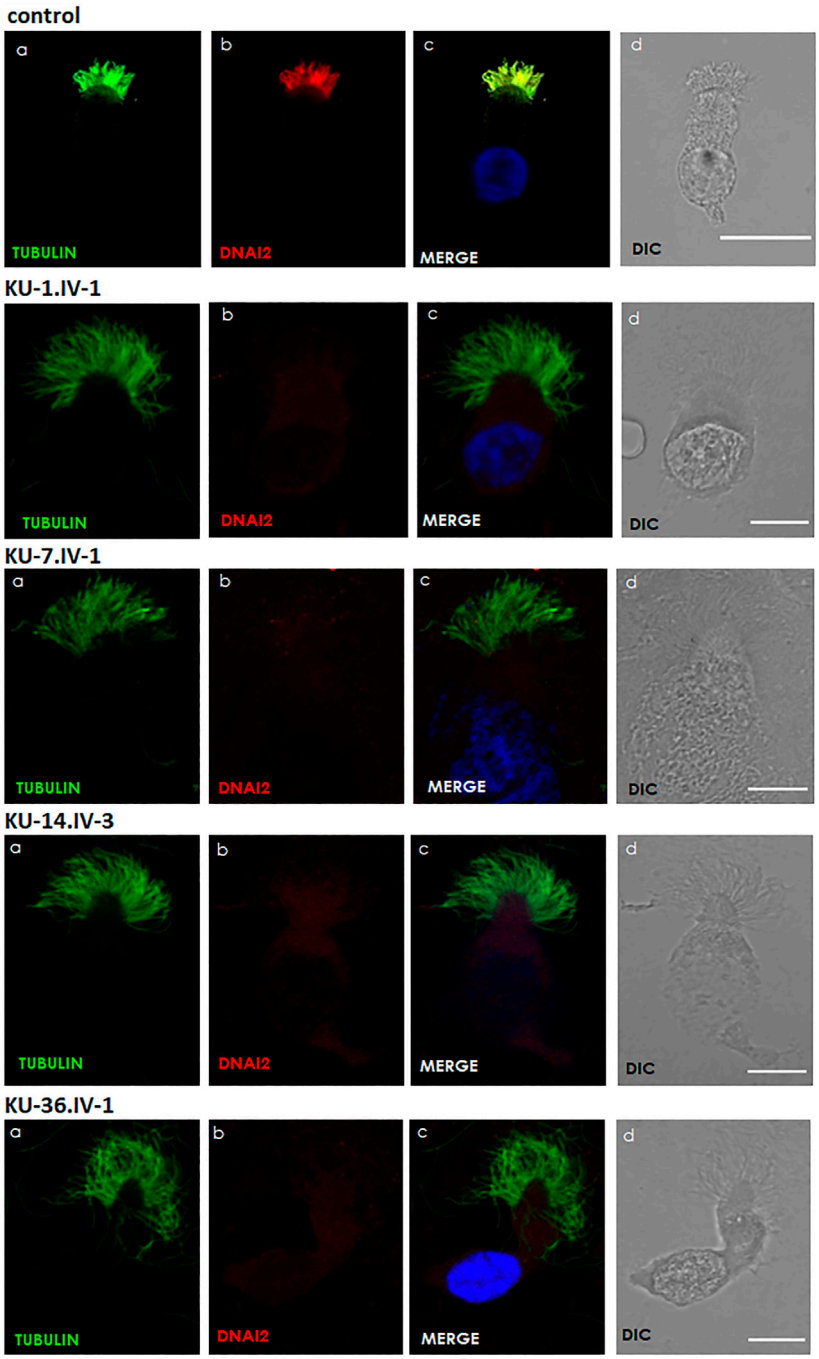

FIGURE 5
Immunofluorescence images of primary respiratory epithelial cells for PCD individuals. The IF was performed using monoclonal anti-acetylated α tubulin: panel **(A)** and polyclonal anti-DNAI2: panel **(B)** antibody for selected PCD individuals *vs.* healthy controls. As seen in the control, the merged images: panel **(C)** show a yellow co-staining within the ciliary axoneme which indicates that both proteins co-localized within respiratory cilia compared with the images for PCD individuals that demonstrate an absence of anti-DNAI2 staining. Scale bar is 10 μm. **(D)** shows differential interference contrast figures (DIC) for analyzed cells.

in Kuwait. This strategy was previously successful in the identification of two novel PCD-loci *CCDC103* and *LRRC6* genes in UK-Pakistani populations (Panizzi et al., 2012; Zariwala et al., 2013) and *CCNO* causing oligocilia with *situs solitus* in a multiplex Kuwaiti family having four PCD individuals (Wallmeier et al., 2014).

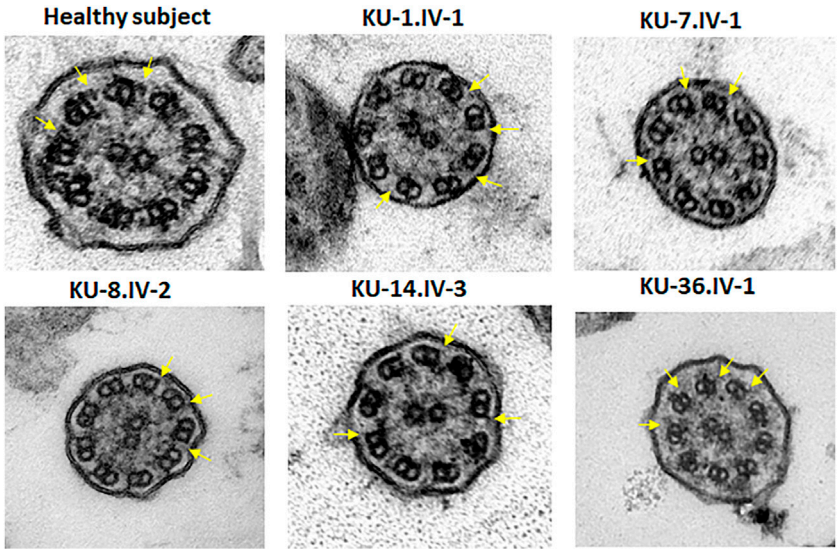

FIGURE 6
TEM sections of the ciliary axoneme for PCD individuals versus control. TEM results for ciliary axoneme of the ciliated epithelial cells of respiratory system indicate that the PCD patients have an absence of ODAs compared with control, which is mainly seen in patients with defects in genes encoding dynein arm components, consistent with their genotypes.

Using this strategy we identified novel homozygous missense variant (*DNAI2*:c.740G>A; p.Arg247Gln)) in exon 7 of *DNAI2*. We mapped this *DNAI2* variant in five unrelated consanguineous Arab families, most of them having a family history of the disease. Although this variant is annotated with rs755060592, it is still considered to be a novel variant since the allele frequency of G (normal allele) is 100% in all ethnic backgrounds. All patients harbouring this variant in *DNAI2* (*DNAI2*:c.740G>A) belong to the same tribe, despite samples of these families have been obtained from different hospitals in Kuwait. This suggests that the abovementioned variant in *DNAI2* is a founder hereditary variant running in one tribe that has practiced consanguineous marriages among the members of the tribe over generations and is considered to be particularly isolated, i.e., never married outside the tribe due to historical issues. Immunofluorescence analyses indicates that axonemal assembly of both proximal and distal localized ODA types 1 and 2 does not take place, demonstrated by complete absence of DNAI2, DNAH5, and DNAI1 in ciliary axonemes of affected individuals. TEM analysis on cilia cross-sections confirms lack of ODAs as ultrastructural defect in these individuals.

Previously published data about DNAI2 function characterized DNAI2 as relevant component of ODA type 1 and ODA type 2 in human (Fowkes and Mitchell, 1998): ODAs are the driving force for generation of the ciliary beats. ODAs and IDAs are composed of multimeric protein complexes that are pre-assembled in the cytoplasm prior to transport into and docking onto the axonemes (Fowkes and Mitchell, 1998). The human respiratory cilia have two different ODA heavy chains (HCs): ODA type 1 in the proximal part of the axoneme, composed of γ-HC DNAH5 and β-HC DNAH11, and ODA type 2 in the distal part of the axoneme, composed of β-HC DNAH9 and γ-HC DNAH5 (Loges et al., 2018). IF studies on respiratory cilia show subcellular localization of DNAI2 throughout the entire length of ciliary axonemes, demonstrating that DNAI2 is a component of both ODA type 1 and ODA type 2 complexes. In addition, previous IF analyses of respiratory cilia of PCD individuals with bi-allelic pathogenic nonsense and frameshift *DNAI2* variants showed a complete absence of not only DNAI2, but also of DNAH5, component of both ODA type 1 and ODA type 2 and of DNAH9, component of ODA type 2, demonstrating that DNAI2 is necessary for the correct ODA assembly of both ODA types. In contrast to DNAI2, the Dynein Axonemal Intermediate Chain 1 (DNAI1) is relevant for the assembly of especially ODA type 2 as shown by restriction of both DNAH5 and DNAI2 to the proximal part of the axoneme and lack of DNAH5 and DNAI2 in the distal part of the axoneme in DNAI1 mutant respiratory epithelial cells (Fliegauf et al., 2005; Loges et al., 2008). Thus, DNAI2 is only partially dependent on DNAI1 as it can be assembled in proximal ODAs.

Here, we showed by immunofluorescence analysis complete absence of DNAI2, DNAH5. and DNAI1 in axonemes of affected *DNAI2* individuals identified in this study, demonstrating that this missense variant completely abrogates preassembly of both ODA type 1 and ODA type 2. Electron microscopy analyses confirmed loss of ODAs in these affected individuals. According

to ACMG criteria, the *DNAI2* missense variant identified in this study (*DNAI2*:c.740G>A; p.Arg247Gln) has so far been classified as Variant of Uncertain Significance despite high pathogenicity scores. Using these two well-established *in vitro* functional tests, immunofluorescence analysis and electron microscopy, we now provide functional evidence, that this missense variant is pathogenic according to ACMG criteria and cause of PCD in the families presented here.

The identification of this founder variant (*DNAI2*: c.740G>A; p.Arg247Gln) in this Arabic tribe and functional evidence of pathogenicity presented in this manuscript will impact and improve genetic analysis of the Kuwaiti population suspected for PCD, especially from this Arabic tribe.

Data availability statement

The datasets presented in this article are not readily available because ethical, legal and privacy issues prevent deposition in public community supported repositories as they contain data that would allow re-identification of individuals. Requests to access the datasets should be directed to Dalal A. Al-Mutairi (dalal.almutairi@ku.edu.kw).

Ethics statement

The studies involving human participants were reviewed and approved by Chair of medical and Health research coordination committee, Ministry of Health, Kuwait. Written informed consent to participate in this study was provided by the participants' legal guardian/next of kin. Written informed consent was obtained from the individual(s), and minor(s)' legal guardian/next of kin, for the publication of any potentially identifiable images or data included in this article.

Author contributions

DA-M designed the study, collected the blood samples for the patients and the parents, obtained the informed consent, performed autozygosity mapping, mutations screening, segregation analyses, IF staining, prepared all the figures and wrote the manuscript. BHA performed nasal biopsies for all the patients under study. DA-M and BHA provided the clinical data for families; KU-7, KU-8, KU-14 and KU-36. BAA provided the clinical data for Family KU-1. PP provided the TEM data that was performed in Germany and reviewed the manuscript. HO has reviewed the manuscript.

Funding

This work was funded by Kuwait Foundation for the Advancement of Sciences (KFAS); Grant No. P114-13MG-01. General Facility Grant SRUL02/13 by the Health Science Center, Kuwait University.

Acknowledgments

We are grateful to the PCD families for their participation in the study. We would like to thank the radiologist Wasif Mohammed at the Sabah hospital, Kuwait, for his help with the radiological data that shows the pathogenesis of PCD. We thank Heike Olbrich and Rim Hjeij at University Hospital Muenster, Germany, for their training in exome analysis and IF technique. We also would like to thank Professor Trevor Batten at University of Leeds, United Kingdom, for editing the manuscript.

Conflict of interest

The authors declare that the research was conducted in the absence of any commercial or financial relationships that could be construed as a potential conflict of interest.

Publisher's note

Supplementary material

The Supplementary Material for this article can be found online at: https://www.frontiersin.org/articles/10.3389/fgene.2022.1017280/full#supplementary-material

SUPPLEMENTARY FIGURE S1
Immunofluorescence images of primary respiratory epithelial cells for PCD patients. The IF was performed using monoclonal anti-acetylated α tubulin: panel **(A)** and polyclonal anti- DNAI1: panel **(B)** antibody for selected PCD patients versus healthy controls. As seen in the control, the merged images: panel **(C)** show a yellow co-staining within the ciliary axoneme which indicates that both proteins co-localized within respiratory cilia compared with the images for PCD patients that demonstrate an absence of anti-DNAI2 staining. Scale bar is 10 μm: panel **(D)**.

SUPPLEMENTARY FIGURE S2
Immunofluorescence images of primary respiratory epithelial cells for PCD patients. The IF was performed using monoclonal anti-acetylated α tubulin: panel **(A)** and polyclonal anti- DNAH5: panel **(B)** antibody for selected PCD patients versus healthy controls. As seen in the control, the merged images: panel **(C)** show a yellow co-staining within the ciliary axoneme which indicates that both proteins co-localized within respiratory cilia compared with the images for PCD patients that demonstrate an absence of anti-DNAI2 staining. Scale bar is 10 μm: panel **(D)**.

SUPPLEMENTARY FIGURE S3
Allelic discrimination Plot for DNAI2 Mutation. The six patients showed homozygous mutant type pattern (AA; red dots) while their parents showed heterozygous mutant and normal alleles pattern (GA; green dots) consistent with Sanger sequencing data. A control DNA panel composed of 100 DNA samples collected randomly from healthy Arab individuals from different areas in Kuwait were run in the assay and the results showed all the control samples carry the wild type allele in homozygous pattern (GG; blue dots). This indicates that this mutation is very rare and even the carriers are not existing in Arabs.

References

Abecasis, G. R., Cherny, S. S., Cookson, W. O., and Cardon, L. R. (2002). Merlin-rapid analysis of dense genetic maps using sparse gene flow trees. *Nat. Genet.* 30, 97–101. doi:10.1038/ng786

Adzhubei, I., Jordan, D. M., and Sunyaev, S. R. (2013). Predicting functional effect of human missense mutations using PolyPhen-2. *Curr. Protoc. Hum. Genet.* 7, Unit7.20. Unit7 20. doi:10.1002/0471142905.hg0720s76

Carr, I. M., Bhaskar, S., Sullivan, O. J., Aldahmesh, M. A., Shamseldin, H. E., Markham, A. F., et al. (2012). Autozygosity mapping with exome sequence data. *Hum. Mutat.* 34, 50–56. doi:10.1002/humu.22220

Carr, I. M., Camm, N., Taylor, G. R., Charlton, R., Ellard, S., Sheridan, E. G., et al. (2011). GeneScreen: A program for high-throughput mutation detection in DNA sequence electropherograms. *J. Med. Genet.* 48, 123–130. doi:10.1136/jmg.2010.082081

Carr, I. M., Markham, S. A., and Pena, S. D. (2011). Estimating the degree of identity by descent in consanguineous couples. *Hum. Mutat.* 32, 1350–1358. doi:10.1002/humu.21584

Carr, I. M., Morgan, J., Watson, C., Melnik, S., Diggle, C. P., Logan, C. V., et al. (2013). Simple and efficient identification of rare recessive pathologically important sequence variants from next generation exome sequence data. *Hum. Mutat.* 34, 945–952. doi:10.1002/humu.22322

Carr, I. M., Robinson, J. I., Dimitriou, R., Markham, A. F., Morgan, A. W., and Bonthron, D. T. (2009). Inferring relative proportions of DNA variants from sequencing electropherograms. *Bioinformatics* 25, 3244–3250. doi:10.1093/bioinformatics/btp583

Dalrymple, R. A., and Kenia, P. (2019). European respiratory society guidelines for the diagnosis of primary ciliary dyskinesia: A guideline review. *Arch. Dis. Child. Educ. Pract. Ed.* 104, 265–269. doi:10.1136/archdischild-2017-312902

Davis, S. D., Rosenfeld, M., Lee, H. S., Ferkol, T. W., Sagel, S. D., Dell, S. D., et al. (2019). Primary ciliary dyskinesia: Longitudinal study of lung disease by ultrastructure defect and genotype. *Am. J. Respir. Crit. Care Med.* 199, 190–198. doi:10.1164/rccm.201803-0548OC

Failly, M., Bartoloni, L., Letourneau, A., Munoz, A., Falconnet, E., Rossier, C., et al. (2009). Mutations in DNAH5 account for only 15% of a non-preselected cohort of patients with primary ciliary dyskinesia. *J. Med. Genet.* 46, 281–286. doi:10.1136/jmg.2008.061176

Fliegauf, M., Olbrich, H., Horvath, J., Wildhaber, J. H., Zariwala, M. A., Kennedy, M., et al. (2005). Mislocalization of DNAH5 and DNAH9 in respiratory cells from patients with primary ciliary dyskinesia. *Am. J. Respir. Crit. Care Med.* 171, 1343–1349. doi:10.1164/rccm.200411-1583OC

Fowkes, M. E., and Mitchell, D. R. (1998). The role of preassembled cytoplasmic complexes in assembly of flagellar dynein subunits. *Mol. Biol. Cell.* 9, 2337–2347. doi:10.1091/mbc.9.9.2337

Hornef, N., Olbrich, H., Horvath, J., Zariwala, M. A., Fliegauf, M., Loges, N. T., et al. (2006). DNAH5 mutations are a common cause of primary ciliary dyskinesia with outer dynein arm defects. *Am. J. Respir. Crit. Care Med.* 174, 120–126. doi:10.1164/rccm.200601-084OC

Johansen Taber, K. A., Dickinson, B. D., and Wilson, M. (2014). The promise and challenges of next-generation genome sequencing for clinical care. *JAMA Intern. Med.* 174, 275–280. doi:10.1001/jamainternmed.2013.12048

Knowles, M. R., Leigh, M. W., Carson, J. L., Davis, S. D., Dell, S. D., Ferkol, T. W., et al. (2012). Mutations of DNAH11 in patients with primary ciliary dyskinesia with normal ciliary ultrastructure. *Thorax* 67, 433–441. doi:10.1136/thoraxjnl-2011-200301

Lander, E. S., and Botstein, D. (1987). Homozygosity mapping: A way to map human recessive traits with the DNA of inbred children. *Science* 236, 1567–1570. doi:10.1126/science.2884728

Leigh, M. W., Pittman, J. E., Carson, J. L., Ferkol, T. W., Dell, S. D., Davis, S. D., et al. (2009). Clinical and genetic aspects of primary ciliary dyskinesia/Kartagener syndrome. *Genet. Med.* 11, 473–487. doi:10.1097/GIM.0b013e3181a53562

Loges, N. T., Antony, D., Maver, A., Deardorff, M. A., Gulec, E. Y., Gezdirici, A., et al. (2018). Recessive DNAH9 loss-of-function mutations cause laterality defects and subtle respiratory ciliary-beating defects. *Am. J. Hum. Genet.* 103, 995–1008. doi:10.1016/j.ajhg.2018.10.020

Loges, N. T., Olbrich, H., Fenske, L., Mussaffi, H., Horvath, J., Fliegauf, M., et al. (2008). DNAI2 mutations cause primary ciliary dyskinesia with defects in the outer dynein arm. *Am. J. Hum. Genet.* 83, 547–558. doi:10.1016/j.ajhg.2008.10.001

Lucas, J. S., Burgess, A., Mitchison, H. M., Moya, E., Williamson, M., and Hogg, C.U.K. National Pcd Service (2014). Diagnosis and management of primary ciliary dyskinesia. *Arch. Dis. Child.* 99, 850–856. doi:10.1136/archdischild-2013-304831

Magnin, M. L., Cros, P., Beydon, N., Mahloul, M., Tamalet, A., Escudier, E., et al. (2012). Longitudinal lung function and structural changes in children with primary ciliary dyskinesia. *Pediatr. Pulmonol.* 47, 816–825. doi:10.1002/ppul.22577

Mazor, M., Alkrinawi, S., Chalifa-Caspi, V., Manor, E., Sheffield, V. C., Aviram, M., et al. (2011). Primary ciliary dyskinesia caused by homozygous mutation in DNAL1, encoding dynein light chain 1. *Am. J. Hum. Genet.* 88, 599–607. doi:10.1016/j.ajhg.2011.03.018

Mitchell, D. R., and Rosenbaum, J. L. (1985). A motile Chlamydomonas flagellar mutant that lacks outer dynein arms. *J. Cell. Biol.* 100, 1228–1234. doi:10.1083/jcb.100.4.1228

Nonaka, S., Tanaka, Y., Okada, Y., Takeda, S., Harada, A., Kanai, Y., et al. (1998). Randomization of left-right asymmetry due to loss of nodal cilia generating leftward flow of extraembryonic fluid in mice lacking KIF3B motor protein. *Cell.* 95, 829–837. doi:10.1016/s0092-8674(00)81705-5

O'Callaghan, C., Chetcuti, P., and Moya, E. (2010). High prevalence of primary ciliary dyskinesia in a British Asian population. *Arch. Dis. Child.* 95, 51–52. doi:10.1136/adc.2009.158493

Olbrich, H., Haffner, K., Kispert, A., Volkel, A., Volz, A., Sasmaz, G., et al. (2002). Mutations in DNAH5 cause primary ciliary dyskinesia and randomization of left-right asymmetry. *Nat. Genet.* 30, 143–144. doi:10.1038/ng817

Panizzi, J. R., Becker-Heck, A., Castleman, V. H., Al-Mutairi, D. A., Liu, Y., Loges, N. T., et al. (2012). CCDC103 mutations cause primary ciliary dyskinesia by disrupting assembly of ciliary dynein arms. *Nat. Genet.* 44, 714–719. doi:10.1038/ng.2277

Pazour, G. J., Agrin, N., Walker, B. L., and Witman, G. B. (2006). Identification of predicted human outer dynein arm genes: Candidates for primary ciliary dyskinesia genes. *J. Med. Genet.* 43, 62–73. doi:10.1136/jmg.2005.033001

Pennarun, G., Chapelin, C., Escudier, E., Bridoux, A. M., Dastot, F., Cacheux, V., et al. (2000). The human dynein intermediate chain 2 gene (DNAI2): Cloning, mapping, expression pattern, and evaluation as a candidate for primary ciliary dyskinesia. *Hum. Genet.* 107, 642–649. doi:10.1007/s004390000427

Petrovski, S., Wang, Q., Heinzen, E. L., Allen, A. S., and Goldstein, D. B. (2013). Genic intolerance to functional variation and the interpretation of personal genomes. *PLoS Genet.* 9, e1003709. doi:10.1371/journal.pgen.1003709

Pifferi, M., Michelucci, A., Conidi, M. E., Cangiotti, A. M., Simi, P., Macchia, P., et al. (2010). New DNAH11 mutations in primary ciliary dyskinesia with normal axonemal ultrastructure. *Eur. Respir. J.* 35, 1413–1416. doi:10.1183/09031936.00186209

Ratjen, F., Waters, V., Klingel, M., McDonald, N., Dell, S., Leahy, T. R., et al. (2016). Changes in airway inflammation during pulmonary exacerbations in patients with cystic fibrosis and primary ciliary dyskinesia. *Eur. Respir. J.* 47, 829–836. doi:10.1183/13993003.01390-2015

Schwabe, G. C., Hoffmann, K., Loges, N. T., Birker, D., Rossier, C., de Santi, M. M., et al. (2008). Primary ciliary dyskinesia associated with normal axoneme ultrastructure is caused by DNAH11 mutations. *Hum. Mutat.* 29, 289–298. doi:10.1002/humu.20656

Shah, A., Shoemark, A., MacNeill, S. J., Bhaludin, B., Rogers, A., Bilton, D., et al. (2016). A longitudinal study characterising a large adult primary ciliary dyskinesia population. *Eur. Respir. J.* 48, 441–450. doi:10.1183/13993003.00209-2016

Shapiro, A. J., Davis, S. D., Polineni, D., Manion, M., Rosenfeld, M., Dell, S. D., et al. (2018). Diagnosis of primary ciliary dyskinesia. An official American thoracic society clinical practice guideline. *Am. J. Respir. Crit. Care Med.* 197, e24–e39. doi:10.1164/rccm.201805-0819ST

Wallmeier, J., Al-Mutairi, D. A., Chen, C. T., Loges, N. T., Pennekamp, P., Menchen, T., et al. (2014). Mutations in CCNO result in congenital mucociliary clearance disorder with reduced generation of multiple motile cilia. *Nat. Genet.* 46, 646–651. doi:10.1038/ng.2961

Watson, C. M., Crinnion, L. A., Gurgel-Gianetti, J., Harrison, S. M., Daly, C., Antanavicuite, A., et al. (2015). Rapid detection of rare deleterious variants by next generation sequencing with optional microarray SNP genotype data. *Hum. Mutat.* 36, 823–830. doi:10.1002/humu.22818

Williams, E. S., and Hegde, M. (2013). Implementing genomic medicine in pathology. *Adv. Anat. Pathol.* 20, 238–244. doi:10.1097/PAP.0b013e3182977199

Zariwala, M. A., Gee, H. Y., Kurkowiak, M., Al-Mutairi, D. A., Leigh, M. W., Hurd, T. W., et al. (2013). ZMYND10 is mutated in primary ciliary dyskinesia and interacts with LRRC6. *Am. J. Hum. Genet.* 93, 336–345. doi:10.1016/j.ajhg.2013.06.007

Zariwala, M. A., Knowles, M. R., and Omran, H. (2007). Genetic defects in ciliary structure and function. *Annu. Rev. Physiol.* 69, 423–450. doi:10.1146/annurev.physiol.69.040705.141301

Zariwala, M. A., Leigh, M. W., Ceppa, F., Kennedy, M. P., Noone, P. G., Carson, J. L., et al. (2006). Mutations of DNAI1 in primary ciliary dyskinesia: Evidence of founder effect in a common mutation. *Am. J. Respir. Crit. Care Med.* 174, 858–866. doi:10.1164/rccm.200603-370OC

Zariwala, M. A., Omran, H., and Ferkol, T. W. (2011). The emerging genetics of primary ciliary dyskinesia. *Proc. Am. Thorac. Soc.* 8, 430–433. doi:10.1513/pats.201103-023SD

Advantages of publishing in Frontiers

OPEN ACCESS
Articles are free to read for greatest visibility and readership

FAST PUBLICATION
Around 90 days from submission to decision

HIGH QUALITY PEER-REVIEW
Rigorous, collaborative, and constructive peer-review

TRANSPARENT PEER-REVIEW
Editors and reviewers acknowledged by name on published articles

Frontiers
Avenue du Tribunal-Fédéral 34
1005 Lausanne | Switzerland

Visit us: www.frontiersin.org
Contact us: frontiersin.org/about/contact

REPRODUCIBILITY OF RESEARCH
Support open data and methods to enhance research reproducibility

DIGITAL PUBLISHING
Articles designed for optimal readership across devices

FOLLOW US
@frontiersin

IMPACT METRICS
Advanced article metrics track visibility across digital media

EXTENSIVE PROMOTION
Marketing and promotion of impactful research

LOOP RESEARCH NETWORK
Our network increases your article's readership